The Role of *Arabidopsis thaliana* Annexins 1, 2 and 4 in Extracellular ATP Signalling

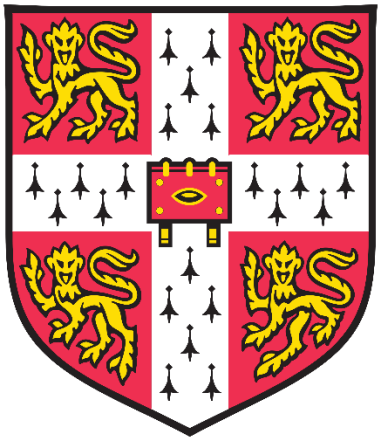

A thesis submitted for the degree of Doctor of Philosophy

by

Amirah binti Mohammad Sidik

Newnham College

Department of Plant Sciences

University of Cambridge

September 2019

Declaration

This dissertation is the result of my own work and includes nothing which is the outcome of work done in collaboration except as specified in the text.

It is not substantially the same as any that I have submitted, or, is being concurrently submitted for a degree or diploma or other qualification at the University of Cambridge or any other University or similar institution except as declared in the Preface and specified in the text. I further state that no substantial part of my dissertation has already been submitted, or, is being concurrently submitted for any such degree, diploma or other qualification at the University of Cambridge or any other University or similar institution except as specified in the text.

Amirah Mohammad Sidik

September 2019

Abstract

Amirah Binti Mohammad Sidik

The Role of *Arabidopsis thaliana* Annexins 1, 2 and 4 in Extracellular ATP Signalling

Extracellular ATP (eATP) is an important signalling molecule in animals but its importance is less understood in plants. Accumulation of eATP in plants occurs in response to biotic and abiotic stresses. eATP causes downstream responses such as increase in cytosolic free calcium ($[Ca^{2+}]_{cyt}$), reactive oxygen species (ROS), nitric oxide (NO) and phosphatidic acid (PA). The identification of *Arabidopsis thaliana* AtDORN1 (Does Not Respond to Nucleotides) as the first higher plant purinoreceptor has confirmed eATP in plant signalling systems. AtDORN1 is a plasma membrane receptor kinase that appears to command the eATP-induced transient increase in $[Ca^{2+}]_{cyt}$ and directs the translational response to wounding. The identity of the plasma membrane Ca^{2+}-permeable channels involved in eATP-induced $[Ca^{2+}]_{cyt}$ increases remain unknown. Patch clamp electrophysiology has shown that a plasma membrane Ca^{2+} influx conductance lies downstream of the AtRBOHC NADPH oxidase in the response to eATP. As *Arabidopsis thaliana* ANNEXIN 1 (AtANN1) underpins ROS-activated plasma membrane Ca^{2+} influx conductance, it has been considered here as operating downstream of AtDORN1 in the eATP-induced increase in $[Ca^{2+}]_{cyt}$. In this thesis, the role of AtANN1, AtANN2 and AtANN4 in eATP signalling was tested in *A. thaliana.*

Using (apo)aequorin, AtANN1 and ANNEXIN 2 (AtANN2) have been found to be involved in the root's $[Ca^{2+}]_{cyt}$ response to both eATP and eADP whereas ANNEXIN 4 (AtANN4) might be acting as a negative regulator of AtANN1 (Chapters 3 and 4). Application of Gd^{3+} as a plasma membrane Ca^{2+} channel blocker indicated the possibility of the release of Ca^{2+} from intracellular stores (Chapters 3 and 4). AtANN1 is confirmed to be downstream of the AtDORN1 receptor and also possibly downstream of AtRBOH NADPH Oxidase based on $[Ca^{2+}]_{cyt}$ measurement and ROS assays (Chapter 3). Loss-of-function mutants of AtANN1, AtANN2 and AtANN4 altered the eATP-induced gene expression of *AtACS6* but not *AtWRKY40* demonstrating a possible link between eATP signalling and hormone responses in plants (Chapters 3 and 4). Unlike AtANN1 and AtANN4, fewer studies regarding the involvement of AtANN2 in salinity stress and biotic stress were reported. In Chapter 5, results suggest that AtANN2 might not be part of the components mediating salinity stress and biotic stress in plants.

Acknowledgements

I would like to express my utmost appreciation to my supervisor Dr. Julia Davies for giving me the opportunity to learn, for the patient guidance, encouragement, and tremendous support for me to grow to be a good researcher. Thank you so much for everything. I am grateful to Cambridge Trust, Yayasan Daya Diri, Newnham College and Tom ap Rees funding for the financial support over the past four years. Also thank you to my second supervisor Prof. Alex Webb for his support and guidance.

This PhD study would not have been possible without other members of the Ion Transport group; thank you Elsa, Katie, Limin, Adeeba, Stéphanie and Zhi Zhong for being the best colleagues and always willing to share skills and knowledge. To other members of Lab 201; Carmen, Tim, Hyunju, Jun, Lukas, Gareth, Laura and Matt, thank you so much for being very helpful and making this PhD journey much more exciting both inside and outside of the lab. I would also like to thank Barbara, Dick, Simon and Nigel for the technical help. Also thank you Dr. Birgitta Olofsson for the encouragement and advice as a mentor.

Thank you to my furry companion Coco for the comforting purr, all fellow Newnhamites and friends for making my experience in Cambridge richer and memorable. I would also like to say a heartfelt thank you to mom and dad for always believing in me from the beginning, and my family for the endless support. And finally and especially to my husband Hazwan, thank you so much for always being by my side.

Table of Contents

List of Figures

List of Tables

List of Abbreviations

ABA	Abscisic Acid
ABC	ATP Binding Casette
ACA	Autoinhibited Ca^{2+}-ATPase
ACS	1-aminocyclopropane-1-carboxylate synthase
ADP	Adenosine 5'-diphosphate
AMP	Adenosine 5'-monophosphate
ANOVA	Analysis of variance
AQP	Aquaporin
AtANN1-AtANN8	*Arabidopsis thaliana* Annexins 1 - 8
ATP	Adenosine 5'-triphosphate
BICAT	Bivalent Cation Transporter
BIFC	Bimolecular Fluorescence Complementation
BLAST	Basic local alignment search tool
bp	base pair
$[Ca^{2+}]_{cyt}$	Cytosolic free calcium ion
Ca^{2+}	Calcium ion
CAM	Calmodulin
CAMV35S	Cauliflower mosaic virus 35S
CBL	Calcineurin B-like protein
CDPK	Calcium-dependent protein kinase
CMH_2DCFDA	2',7'-dichlorodihydrofluorescein diacetate
CNGC	Cyclic nucleotide gated channel

CUC	Cup-shaped cotyledon
DACC	Depolarisation activated calcium channel
DAMP	Damage associated molecular pattern
K_d	Equilibrium dissociation constant
DMSO	Dimethyl Sulphoxide
DNA	Deoxyribonucleic acid
DORN1	Does not Respond to Nucleotides1
DP	Depolarisation buffer
DPI	Diphenyleneiodonium
eATP	Extracellular adenosine 5'-triphosphate
ECM	Extracellular matrix
EMS	Ethyl methanesulfonate
ER	Endoplasmic reticulum
ETC	Electron Transport Chain
FRET	Förster resonance energy transfer
gDNA	genomic DNA
GFP	Green fluorescent protein
GCaMP3	GFP Calmodulin-M13-peptide 3
GLR	Glutamate-like receptor
HACC	Hyperpolarisation activated calcium channel
HGI	Horizontal growth Index
H_2O_2	Hydrogen peroxide
HP	Hyperpolarisation buffer
HRP	Horseradish peroxidase

HSP	Heat shock protein
HSR	Hypersensitive response
IAA	Indole-3-acetic acid
IP	Immuno precipitation
JA	Jasmonic acid
LB	Lysogeny broth
LSM	Low salt medium
MAMP	Microbe associated molecular pattern
MAPK	Mitogen-activated protein kinase
MDA	Malondialdehyde
MES	2-(N-morpholino) ethanesulfonic
MS	Murashige and Skoog nutrient medium
MSL	MscS-like gene family
NaCl	Sodium chloride
NADPH	Nicotinamide adenine dinucleotide phosphate
NAM	No apical meristem
NMR	Nuclear magnetic resonance
NO	Nitric oxide
NOS	Nitric oxide synthase
NSCC	Non-selective cation channel
OH•	Hydroxyl radical
OSCA	Reduced hyperosmolality-induced $[Ca^{2+}]_{cyt}$ increase
PA	Phosphatidic acid
PAMP	Pathogen associated molecular pattern

PCR	Polymerase chain reaction
PEG	Polyethylene glycol
PPADS	Pyridoxalphosphate-6-azophenyl-2',4'-disulfonic acid tetrasodium salt
PTI	PAMP triggered immunity
qRT-PCR	Quantitative reverse transcription-polymerase chain reaction
RBOH	Respiratory burst homologue
RLU	Relative light unit
RNA	Ribonucleic acid
ROS	Reactive oxygen species
RSA	Root system architecture
SA	Salicylic acid
SDW	Sterilised distilled water
SEM	Standard error of mean
SOC	Super optimal broth with catabolite repression
SOD	Superoxide dismutase
SOS	Salt overly sensitive
TDNA	Transfer DNA
Tris	Tris base, 2-amino-2-(hydroxymethyl)-1,3-propanediol
VDAC	Voltage dependent anion channel
VDACL	Volume dependent ATP-conductive large conductance
VDCC	Voltage dependent calcium channel
VICC	Voltage independent calcium channel
YC3.6	Yellow Cameleon 3.6 reporter

Chapter 1

Introduction

1.1 Environmental stresses: Reduction in crop yield

According to Lewandowski (2015), the total population of the world will continue to rise to 8.5 billion in 2030 and 9.7 billion in 2050. To feed this growing population (Figure 1.1) around the globe by 2050, it was estimated an increase of as much as 70% to 100% of food production will be needed (Godfray *et al.*, 2010). In recent years, crop production has been facing many challenges especially from climate change. Dramatic climate change around the globe has imposed environmental stresses on plants such as drought stress, osmotic stress and ozone stress causing reduction in crop yield (Assmann, 2013). For instance, drought stress alone has been the cause of 45% and 46% drop in wheat production in Africa and Australia respectively and 2 billion Yuan (317 million USD) loss in agriculture in China (FAO Land and Water, 2013). At the worldwide scale, drought stress caused national cereal production loss by 9% to 10%. In order to overcome this problem, fundamental understanding of the mechanisms lying behind plant signalling systems and responses towards environmental stimuli must be achieved.

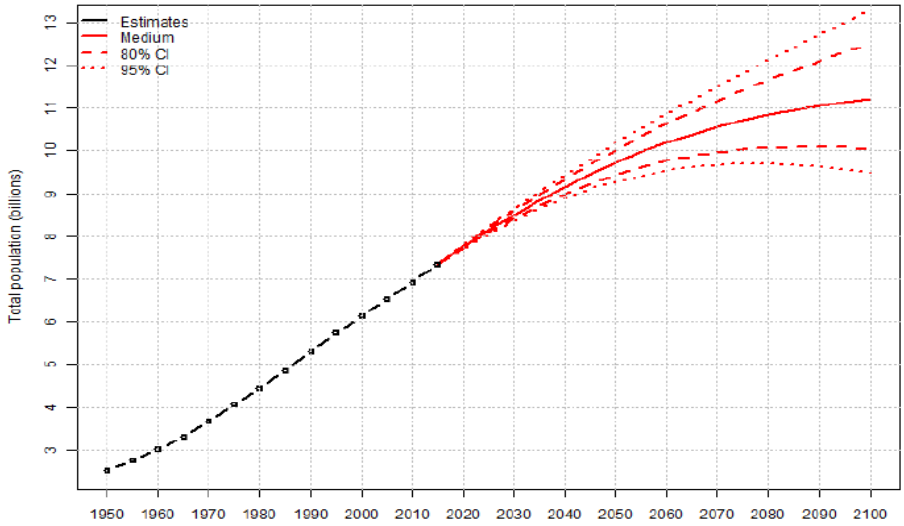

Figure 1.1: **Estimation (1950-2015), medium variant projection and prediction (80% and 95% projection) of the world population from 2015 to 2100.** The population was predicted to increase over the years (Source: United Nations, Department of Economic and Social Affairs, Population Division (2015). *World Population Prospects: The 2015 Revision*. New York: United Nations.)

1.2 Salinity stress

Soil salinity has been causing reduction in crops yield worldwide. Saline conditions in soil could be due to natural causes such as from mineral rocks or deposition from oceanic salt. However, most of the increase in soil salinity is due to the anthropogenic activities such as wrong management of agricultural land, water logging and excessive use of fertilisers (Kumar *et al.*, 2017). High salinity could affect plants by increasing the influx of Na^+, which could cause ionic stress in turn causing water deprivation due to hyperosmotic stress. In addition, high Na^+ content in plants could cause oxidative stress due to increase in reactive oxygen species (ROS) production and also altering Ca^{2+} and K^+ homeostasis.

Plants generally require only low amounts of Na^+. Although high amounts of Na^+ could cause toxicity, Na^+ has been shown to be able to enhance K^+ deficiency thus suggesting that the balance between these two is important (Mäser *et al.*, 2002). To date, the identity of the transporter that mediates Na^+ uptake is still under study. Duan *et al.*, (2013) showed that the Na^+ is perceived at the endodermis of the *Arabidopsis thaliana* root. Demidchik and Tester (2002) proposed that plasma membrane Non-Selective Cation Channel (NSCC) activity would mediate Na^+ uptake under high saline conditions. A review by Mäser *et al.* (2002) suggested more candidates for Na^+ uptake such as KUP (K^+ uptake) /HAK (High-

affinity K^+) /KTs (K^+ Transporters), HKTs (High-affinity K^+ Transporters), CNGCs (Cyclic Nucleotide-Gated Channels) and LCT1 (Low-affinity Cation Transporter 1).

Besides the mechanism of Na^+ uptake, Na^+ sensor mechanisms have been hotly contested. Cation-H^+ exchanger (CHX) is suggested as one of the mechanisms of detecting Na^+ entry in plant cells (Shabala *et al.*, 2015). Shi *et al.* (2000) reported the possibility of the plasma membrane Salt-Overly-Sensitive (AtSOS1) Na^+/H^+ antiporter as the Na^+ sensor. Recently, *AtMOCA1* (Monocation-induced $[Ca^{2+}]_i$ Increase 1) which encodes for glucoronosyl transferase for glycosylinositol phosphorylceramide sphingolipids (GIPC) was discovered as the Na^+ sensor. Tests done on the mutant of this gene showed that it is needed for the NaCl-induced changes in *A. thaliana* such as accumulation of cytosolic free Ca^{2+} ($[Ca^{2+}]_{cyt}$) as a second messenger and that the mutant was vulnerable to high salt conditions (Jiang *et al.*, 2019).

Most studies carried out on plants regarding high salinity stress would use NaCl for the Na^+ donor. Treatment with high concentration of NaCl generally from 100 - 300 mM NaCl would result in increase in $[Ca^{2+}]_{cyt}$, production of ROS and activation of salt-stress induced genes (Huh *et al.*, 2010; Sun *et al.*, 2012; Choi *et al.*, 2014a). The NaCl-induced $[Ca^{2+}]_{cyt}$ increase was found to be mostly at the root level compared to the shoot and the Ca^{2+} could originally be from the apoplast or the intracellular stores (Tracy *et al.*, 2008). The same study also found the oscillatory nature of the $[Ca^{2+}]_{cyt}$ increase to be specific for NaCl treatment. The $[Ca^{2+}]_{cyt}$ accumulation however depends on the ecotype as the C24 background of *A. thaliana* lacks the $[Ca^{2+}]_{cyt}$ response compared to the Col-0 (Schmöckel *et al.*, 2015). Although in nature roots are highly likely to be exposed to the high salinity conditions, the effect of salinity could traversed across the plants towards the shoot. This is achieved through signal propagation *via* $[Ca^{2+}]_{cyt}$ waves. Choi *et al.*, (2014a) and Evans *et al.* (2016) reported systemic signalling involving Ca^{2+} which was aided by the vacuolar channel AtTPC1 (Two Pore Channel1) to produce waves from the spot of initial exposure (root tips) towards the shoot through cortex and endodermis at a rate of ~400 μm/s. Besides the $[Ca^{2+}]_{cyt}$ response, salt-induced gene expression was altered at the shoot although the stress was applied at the root tips.

AtTPC1 was shown to be involved in propagating the $[Ca^{2+}]_{cyt}$ waves, most probably by permitting Ca^{2+} efflux from the vacuole (Evans *et al.*, 2016). The current model is that $[Ca^{2+}]_{cyt}$ causes activation of the plasma membrane NADPH oxidase AtRBOHD (Respiratory

Burst Oxidase Homologue D) to produce ROS and that these activate a plasma membrane Ca^{2+}-permeable channel. There are a few channel candidates thought to be involved in mediating $[Ca^{2+}]_{cyt}$ accumulation under salinity stress. One of the candidates is *A. thaliana* ANNEXIN 1 (AtANN1). NaCl has been shown to be able to induce H_2O_2 accumulation (Sun *et al.*, 2012). Laohavisit *et al.* (2013), demonstrated through the patch-clamping technique that under NaCl treatment, AtANN1 is the ROS-activated plasma membrane Ca^{2+} channel that helps mediate the $[Ca^{2+}]_{cyt}$ increase. Mutation of *AtANN1* caused hypersensitivity towards NaCl with stunted growth and reduction in $[Ca^{2+}]_{cyt}$ accumulation (Laohavisit *et al.*, 2013). Apart from AtANN1, another member of the annexin family ANNEXIN 4 (AtANN4) proved to be involved in regulating growth and viability under saline and drought conditions (Huh *et al.*, 2010). The same study showed physical interaction between AtANN1 and AtANN4 in NaCl treatment suggesting the possibility of both annexins in the salt stress response in *A. thaliana*. Annexins are considered further in section 1.8.5.

Salinity stress results immediately in osmotic stress and over time, the Na^+ ionic stress. Both stresses induce transcription factors that are crucial for activation of stress-induced genes in order for the plants to survive. Transcription factors such as NACs (NAM, ATAF and CUC), MYBs, bZIPs (Basic Leucine Zipper Domain), DREBs (Dehydration Responsive Element Binding factor) and WRKY have been regarded as the salinity and osmotic stress transcription factors (Kumar *et al.*, 2017). Stress-induced NAC (SNAC) overexpression in rice showed improved tolerance towards salinity stress and osmotic stress in germination and growth (Hu *et al.*, 2008). An RNAi line of OsNAC5 (rice) on the other hand showed decreased tolerance towards salt stress due to reduction in proline content and high Na^+/K^+ ratio (Song *et al.*, 2011). Enhanced salt stress tolerance could also be observed in overexpression of *OsMYB2* transcription factor with higher gene expression of proline synthase and stress-related genes (Yang *et al.*, 2012a). Another member of the MYB transcription factor family, AtMYB2 is needed for ABA-induced (abscisic acid) gene expression under water-deprivation conditions with overexpression enhancing the gene expression whereas mutants showed lower gene expression (Abe *et al.*, 2003). Constitutive expression of bZIP transcription factor in *Poncirus trifoliata* enhanced tolerance towards drought stress (Huang *et al.*, 2010). OsDREB transcription factor (Dubouzet *et al.*, 2003) as well as WRKY33 and WRKY25 transcription factor overexpression also caused higher tolerance towards salt and dehydration (Jiang and Deyholos 2009).

The SOS (Salt-Overly-Sensitive) signalling pathway is the most studied mechanism of salt tolerance in plants. The working model of the SOS pathway suggested so far begins with the perception of the $[Ca^{2+}]_{cyt}$ signal by AtSOS3 (AtCBL4; Calcineurin B-Like protein 4) calcium binding protein, which then forms a complex with AtSOS2 (AtCIPK24; CBL-interacting serine/threonine-protein kinase 24). This complex then phosphorylates AtSOS1 increasing the activity of that Na^+/H^+ antiporter for removal of Na^+ from the cytosol (Shabala *et al.*, 2015). Other than Na^+/H^+ antiporters, plants are also equipped with Na^+/H^+ NHX exchangers at the tonoplast for the sequestration of Na^+ into the vacuole (Qiu *et al.*, 2004). Besides compartmentalisation of excess Na^+, protein degradations or senescence is also applied by plants in parts of the survival response (Luo *et al.*, 2017). In terms of the osmotic stress component of high saline conditions, resistance in the form of production of osmolytes and antioxidants to balance the water status in plants is a common feature (Munns, 2005). There are however differences in terms of salt tolerance mechanism by plants that are susceptible to salt stress (glycophytes) and plants that are resistant towards salt stress (halophytes). A detailed review by Kosová *et al.* (2013) considered changes in both glycophytes and halophytes due to salt ionic and osmotic stress at protein level. It was suggested in a study by Oh *et al.* (2009) that SOS1 activity is centrally important for the ability of the halophyte *Thellungiella salsuginea* to thrive in saline conditions. Other than that, factors such as the size of vacuole could play an important role for halophytes to exclude Na^+ from the cytosol.

Phytohormones (especially ABA) are heavily involved in mediating salt stress responses due to the disruption of water status. Studies have found increases in ABA production in plants under salt stress. In salt-stressed roots, this can affect primary and lateral root growth (Duan *et al.*, 2013) whilst the best-studied effect is the promotion of guard cell closure to limit water loss (Jeon *et al.*, 2019). IAA (Indole Acetic Acid) as one of the auxin class of hormones is also affected by salinity stress. IAA levels showed reduction when plants were exposed to salinity stress and this is in line with the observation that salt could cause growth arrest. Application of exogenous IAA in plants treated with salt stress alleviates the growth impairment phenotype by salt (Fu *et al.*, 2019). Besides ABA and IAA, other phytohormone such as jasmonic acid and salicylic acid might also played some role in salinity stress in plants (Ahmad *et al.*, 2013).

The significant impact of salinity stress on agriculture coupled with the gaps in knowledge of how salinity stress signalling is achieved in plants will make it a focal point for study in this thesis.

1.3 Pathogen-induced stress and signalling

Plants are at risk not only from environmental abiotic stress such as salinity but also from the pathogenic microbes they encounter in their environment. Plants are constantly exposed to microorganisms both from the air and mostly in the soil. Pathogens cause reduction in growth and destroy crops. It has been estimated that pathogens and pest have caused global reduction in crops of approximately 21% in wheat, 30% in rice, 22% in maize, 17% in potato and 21% in soybean (Savary *et al.*, 2019). Although plants have physical barriers such as cuticles, these can be breached by fungal appressoria with the rice blast fungus *Magnaporthe oryzae* as a notable example (Foster *et al.*, 2017). Natural pores such as stomata can become an entry point for bacterial pathogens such as *Pseudomonas* or for hyphae (Melotto *et al.*, 2006; Schulze-Lefert and Robatzek 2006). Besides pores, wounding could also expose plant cells to infection.

Upon entry, pathogenic microorganisms release peptides known as Pathogen Associated Molecular Patterns (PAMPs) or Microbe Associated Molecular Patterns (MAMPs) to refer to non-pathogenic microorganisms, which are recognised by plants *via* Pattern Recognition Receptors (PRRs). Wounding caused by injuries or due to pathogen attacks (including herbivory) could induce the production of Damage Associated Molecular Patterns (DAMPs), which are derived from the plant itself in contrast to PAMPs/MAMPs. The perception of PAMP peptides then activates the PAMP-Triggered Immunity (PTI) as a basal resistance (Boller and Felix 2009). One of the earliest PTI by plants is stomatal closure. Stomatal closure is an effective effort in preventing further entry of pathogen and halting the spread of the disease (Sawinski *et al.*, 2013). Reducing the flow of nutrients into the apoplast of infected cells also helps plants against pathogens. A study on *Nicotiana benthamiana* revealed this process to be involved in the biosynthesis of phytosterol where mutation of the gene responsible caused increase in nutrients released into the apoplast thus leading to bacterial growth (Wang *et al.*, 2012). Other than that, secondary metabolites with antimicrobial functions are also produced in plants to restrict pathogens (Bednarek, 2012).

Most of the studies on PAMPs use either the conserved 22-amino acid peptide flg22 from the N-terminus of bacterial flagellin or the N-terminus of EF-Tu peptide called elf18

(Boller and Felix 2009). Flg22 treatment in plants has shown phenotypic effects such as callose deposition, reduction in growth and accumulation of defence proteins (Boller and Felix 2009). In 2000, FLS2 (Flagellin Sensing 2) was first discovered in *A. thaliana* by Gómez-Gómez and Boller (2000) as the putative receptor kinase recognising the flg22 peptide. Upon binding with flg22, AtFLS2 was found to form a heteromer with AtBAK1 (Brassinosteroid Insensitive I-associated Kinase 1). The activated AtBAK1-FLS2 complex then leads to the downstream PTI response. Direct interaction between AtBAK1 and AtFLS2 is needed in the perception of flg22 thus making AtBAK1 a co-receptor of flg22 elicitor (Sun *et al.*, 2013). The AtBAK1-FLS2 complex also activated both protein's intercellular kinase domain suggesting its function in signalling pathways downstream of the perception, possibly in phosphorylation (Boller and Felix 2009).

The earliest downstream responses of flg22 perception are increases in $[Ca^{2+}]_{cyt}$ accumulation, ROS burst and production of nitric oxide (NO) and phosphatidic acid (PA). The co-receptor AtBIK1 has been shown to be involved in the induction of $[Ca^{2+}]_{cyt}$ increase as the mutant *Atbik1* showed impaired $[Ca^{2+}]_{cyt}$ accumulation compared to wild type upon flg22 treatment (Li *et al.*, 2014). Recently, it has been shown that upon flg22 treatment AtBIK1 phosphorylates a channel complex formed by AtCNGC2 and AtCNGC4 to affect Ca^{2+} influx across the plasma membrane (Tian *et al.*, 2019). Besides AtBIK1, *Arabidopsis* Autoinhibited Ca^{2+}-ATPase 8 (AtACA8) and 10 (AtACA10) might also be involve in regulating the Ca^{2+} influx in the presence of flg22 as the double mutant *Ataca8 Ataca10* showed decreased $[Ca^{2+}]_{cyt}$ elevation (Frei Dit Frey *et al.*, 2012). This appears counter-intuitive as ACAs export Ca^{2+} from the cytosol (considered in more detail in section 1.8.1). The same study showed interaction between AtACA8 and AtFLS2 *in planta* suggesting its role in regulating plasma membrane receptor kinases thus affecting the downstream response. An electrophysiological approach was used in a study by Jeworutzki *et al.* (2010) that reported that flg22 caused plasma membrane depolarisation dependent on AtFLS2 perception and involved the activation of an anion channel.

The ROS burst in response to flg22 was found to be synthesised by AtRBOHD and the interplay between ROS and Ca^{2+} influx was evidenced as the mutant *Atrbohd* showed an impaired second peak of $[Ca^{2+}]_{cyt}$ increase (Ranf *et al.*, 2011). This relation between $[Ca^{2+}]_{cyt}$ increase and ROS burst was also reported by Ogasawara *et al.* (2008) as they discovered the ROS production by AtRBOHD is dependent on Ca^{2+}. These authors also revealed the presence of an EF-hand motif in AtRBOHD and binding of Ca^{2+} could change the

conformation of AtRBOHD. Other than that, AtRBOHD activation in ROS production also involves direct phosphorylation. Interestingly, the AtFLS2-BIK1 complex upon flg22 binding showed direct phosphorylation of AtRBOHD protein in a Ca^{2+} independent manner, which evoked the ROS burst (Li *et al.*, 2014). As previously mentioned, the flg22 elicitation caused depolarisation of the plasma membrane. The *Atrbohd/Atrbohf* mutant showed similar depolarisation of plasma membrane as in wild type suggesting it is not involved in the ion flux (Jeworutzki *et al.*, 2010). These studies suggest the possibility of ROS production in Ca^{2+}-dependent and -independent pathways in the flg22 response possibly governed by the AtFLS2-BIK1 complex.

Whilst the signalling pathways of immune responses are being elucidated, it has become clear in recent years that *extracellular* ATP must now also be considered as part of the system. It must also be considered in abiotic stress responses such as salinity.

1.4 Extracellular ATP as a signalling molecule

Adenosine Triphosphate (ATP) is well known for its role as the cell's immediate energy currency through its hydrolysis releasing the terminal phosphate group and at the same time liberating energy required for cellular function (Prieß *et al.*, 2018). Its use to phosphorylate is also pivotal to post-translational modifications. This view of ATP largely as fuel was challenged when Burnstock *et al.* (1970) discovered that ATP was also released out of cells (hence known as extracellular ATP) and hypothesised for it to possibly be a different type of chemical neurotransmitter. The concept of eATP signalling or "purinergic" signalling in animal cells however was not fully embraced until Burnstock *et al.*, (1978) discovered a purinergic receptor (considered in greater detail in section 1.7). From this point, more studies discovered that purinergic signalling was important in various animal biological processes. In animal cells, purinergic signalling is important in mediating the central nervous system, cardiovascular activities, reproduction and growth. The components of purinergic signalling are conserved throughout evolution. It was thought to be one of the earliest signalling systems in multicellular organisms (Verkhratsky and Burnstock, 2014). Thus, it is not impossible that this purinergic signalling is also employed by the plant kingdom in responses to various environmental stimuli. Recently, studies have begun in earnest to explore the possibility of eATP being a signal molecule in the plant kingdom.

Earlier research found that eATP could cause an array of growth changes in plants. In 2000, Lew and Dearnaley (2000) in an effort to look at electrophysiological changes in

Arabidopsis thaliana root hairs upon eATP or eADP (adenosine diphosphate) treatment found that the extracellular nucleotides caused depolarisation of the plasma membrane potential and increased root hair growth. In terms of growth, eATP also rescued the inhibition of hypocotyl growth (Tonón *et al.*, 2010) and root hair growth by glutathione (GSH) reducing agent (Terrile *et al.*, 2010). Extracellullar ATP was found to be localised in the actively growing region of root hair tips where ROS production is abundant (Kim *et al.*, 2006). Other than promoting growth, exogenously applied 1 mM or higher concentrations of eATP could regulate root gravitropism by possibly altering auxin transport in *A. thaliana* roots (Tang *et al.*, 2003). Apyrases, which possibly control the amount of eATP in the apoplast through hydrolysis, could regulate auxin transport, which eventually regulates growth and gravitropism (Liu *et al.*, 2012a; Yang *et al.*, 2015)

Similar to the animal counterparts, exposure to eATP has been proven to be able to induce production of ROS, possibly through plasma membrane NADPH Oxidases (Song *et al.*, 2006). Increase $[Ca^{2+}]_{cyt}$ was also part of the eATP-induced change in plants (Demidchik *et al.*, 2003a; Jeter *et al.*, 2004). In line with this, both Demidchik *et al.* (2009) and Shang *et al.* (2009) found that eATP evoked a plasma membrane hyperpolarisation-activated calcium conductance in *Arabidopsis* root epidermis that could contribute to $[Ca^{2+}]_{cyt}$ elevation. Changes in $[Ca^{2+}]_{cyt}$ as a second messenger drive specific transcriptional changes in *Arabidopsis* (Short *et al.*, 2012), which imply a link between eATP and transcriptional response *via* $[Ca^{2+}]_{cyt}$. eATP also regulates stomatal aperture (Clark *et al.*, 2011) and plasma membrane repair (Deng *et al.*, 2015).

The existance of apyrases and plant adenosine nucleotidases in the apoplast (Riewe *et al.*, 2008a,b) could serve as negative feedback control for the accumulation of eATP, affirming the role of eATP as a signal molecule. Plant apyrases break down eATP into eADP, AMP and Pi which could add another layer of complexity to plant purinergic signalling as eADP alone has the potential to have its own signalling pathway (Demidchik *et al.*, 2011). It too can activate a plasma membrane Ca^{2+} influx and elevate $[Ca^{2+}]_{cyt}$ in *Arabidopsis* (Demidchik *et al.*, 2011). Keeping an optimum amount of eATP in the apoplast is crucial for the growth and viability of plants. Depleting eATP could reduce cell viability in suspension culture and *in planta* (Chivasa *et al.*, 2005) and too high of a concentration could also cause cell death in *Populus euphratica* cell culture (Sun *et al.*, 2012). Thus the presence of apyrases and nucleotidases in the apoplast could regulate and terminate the stimulus signal, which is an important component of any signalling system.

1.5 Accumulation of eATP

Extracellular ATP (eATP) accumulation has been recorded not just in *A. thaliana* (Jeter *et al.*, 2004; Song *et al.*, 2006; Weerasinghe *et al.*, 2009; Dark *et al.*, 2011) but also in other plants. *Populus euphratica* (Salicaceae family) cell suspension cells transiently accumulated eATP under high salinity stress (Sun *et al.*, 2012). *In vivo* visualisation of *Medicago truncatula* (Fabaceae) roots found eATP accumulation in actively growing regions (Kim *et al.*, 2006). Yeast extract elicitor evoked accumulation of eATP in *Salvia miltiorrhiza* hairy root cultures (Lamiaceae; Wu *et al.*, 2008). Copper stress was found to induce the accumulation of eATP in tobacco suspension cells (*Nicotiana tabacum,* solanaceae) and in wheat roots (*Triticum aestivum*, poaceae; Jia *et al.* 2019). Thus eATP accumulation is not specific to *Arabidopsis* and the Brassicaceae family but occurs and could be utilised by other families in the plant kingdom, including monocots.

ATP is a reactive molecule, which in the apoplast may be kept at minimum level possibly by plant apyrases and nucleotidases. Previously it was found that the average concentration of cytoplasmic ATP is in the mM range (Gout *et al.*, 1992; Roux and Steinebrunner, 2007). This approximation of cytoplasmic concentration however did not take into account the ATP concentration in different organelles and the possibility of ATP (which is anionic) complexing with Mg^{2+}. A recent study that was done by Gout *et al.* (2014) using NMR (Nuclear Magnetic Resonance) to measure the concentration of ATP in different compartments of sycamore cells discovered that cytosol and mitochondria contained approximately 54 μM and 10 μM free ATP concentration respectively. The concentration of eATP could vary according to the stimulus that the plants were exposed to. Song *et al.* (2006) reported that an average of 40 μM of eATP accumulated at the wound site of *A. thaliana* leaves. A touch stimulus (198 mN) was found to cause a lower concentration of eATP than wounding in the range of 10 to 15 nM but still managed to induce downstream responses (Weerasinghe *et al.*, 2009). The same authors suggested the possibility of lower eATP concentration detected might be due to the dilution of the eATP outside of the cells and the overwhelming concentration of nucleotidases that quickly catalyse the eATP turnover. Other stimuli also showed transient accumulation of eATP in *A. thaliana* roots with 300 mM sorbitol's effecting a maximum of 40 nM, 200 mM NaCl effecting 70 nM, 10 μM ABA (abscisic acid) 25 nM, 1 μM L-Glutamate 25 nM and wounding 80 nM (Dark *et al.*, 2011). Other than stress stimuli, eATP monitored through a CBD-luciferase (Cellulose Binding Domain-luciferase) reporter found hotspots at the apices of rapidly growing region of root

hairs, indicating the importance of eATP in growth, although the exact quantification of the eATP concentration was not possible (Kim *et al.*, 2006).

1.6 The release of ATP into the extracellular matrix

The mechanism of ATP release from the cytosol into the extracellular matrix in plants however is not yet elucidated. There are some potential mechanisms such as transport through an ATP-Binding Cassette (ABC) transporter across the plasma membrane as in animal cells or through vesicular trafficking. ABC proteins in animals consist of two cytoplasmic domains that could bind to ATP and two hydrophobic domains inserted in the plasma membrane that could form the ATP carrier (Bodin and Burnstock, 2001). Some ATP was also found released together with other neurotransmitters in animal studies through exocytosis, making it one of the possible mechanisms of ATP release in plants (Bodin and Burnstock, 2001). Another study carried out in mouse mammary cells under hypotonic conditions proposed swelling-induced ATP release through an anion channel known as the Volume Dependent ATP-Conductive Large Conductance (VDACL) (Dutta *et al.*, 2002). Others have mentioned the possibility of mechano-sensitive anion channels (Sauer *et al.*, 2000). Voltage Dependent Anion Channel (VDAC) and connexin hemichannels operating in ATP release (Lazarowski *et al.*, 2003). These findings show that the mechanism of ATP release could vary depending on the process or the stimulus.

In plant cells, ATP could be released through wounding or injury where the content of cells is released into the extracellular matrix (Jeter *et al.*, 2004). A study done by Thomas *et al.* (2000) demonstrated that yeast transformed with the plant homologue of the ABC transporter protein (P-Glycoprotein) gene known as *AtPGP1* showed ability to translocate ATP into the extracellular medium. This study suggests that the homologue of the ABC transporter in plant cells could also be the mechanism which releases ATP (Thomas *et al.*, 2000; Demidchik *et al.*, 2003a). Exocytotic ATP release is also possible in plant cells as treatment with Brefeldin A, which is a vesicular trafficking inhibitor, reduces the eATP accumulated by *Medicago truncatula* roots (Kim *et al.*, 2006). Another study employed both Brefeldin A and an ABC transporter inhibitor known as 1-naphthylphthalamic acid (NPA), showing that the release mechanism is more likely exocytosis than the transporter (Tanaka *et al.*, 2010), which would be in contrast to the previous publication on AtPGP1 (Thomas *et al.*, 2000). ATP release through mechanical stimulated anion channels (as in animal cells) is feasible as eATP accumulated in touch-induced roots (Weerasinghe *et al.*, 2009). As in

animal cell studies, various ATP release mechanisms are likely to occur in plant cells to cater for the exposure to different type of stimuli.

A large number of studies as stated have observed the accumulation of eATP and the cellular and developmental changes caused by challenging with eATP. These changes however could only take place with the perception of the eATP signal. A study by Demidchik *et al.* (2009) demonstrated that the perception of eATP was at the plasma membrane instead of cell wall in *Arabidopsis*, bringing the search for the plant purinoreceptor to focus on plasma membrane proteins. In 2014, the first plant purinoreceptor known as *DORN1* (*Does not response to nucleotides 1*) was discovered by Choi *et al.* (2014b) through forward genetic screening.

1.7 DORN1: L-type Lectin Receptor-like Kinase as a purinoreceptor

The first animal purinoreceptor was discovered by Burnstock (1978). Since then, more animal purinoreceptors were found forming different groups of animal purinoreceptor. A detailed review was written by Burnstock (2018) regarding different subtypes of purinoreceptor, their localisation and the biological processes in which these purinoreceptors are involved. In animal cells, there are 2 groups of purinoreceptor known as P1 and P2 receptors. P1 receptors perceive adenine, which forms from the breakdown of ATP whereas P2 receptors could bind to either ATP or ADP. Divergence of P2 receptors into P2X and P2Y receptors was later discovered. Each of the P1, P2X and P2Y receptors consists of more than one subtype. P1 is involved in different physiological processes in animal cells and is made up of 4 different subtypes known as A_1, A_{2A}, A_{2B}, and A_3. P2X receptors on the other hand, consist of 7 different subtypes P2X1 - P2X7 and these are mainly involved in diseases. It is interesting that these subtypes could form heterotrimers. The other P2Y receptor has 8 different subtypes namely $P2Y_1$, $P2Y_2$, $P2Y_4$, $P2Y_6$, $P2Y_{11}$, $P2Y_{12}$, $P2Y_{13}$, and $P2Y_{14}$. P2X purinoreceptors in general are a non-selective cation channels that bind to a specific ligand (mainly ATP) causing alteration in membrane potential and regulating the intracellular Ca^{2+} concentration (Kaczmarek-Hájek *et al.*, 2012) while P2Y receptors are membrane-spanning proteins that activate heterotrimeric G proteins.

However, there are no equivalent of P2X or P2Y purinoreceptors found in higher plants in terms of the amino acid sequence (Demidchik *et al.*, 2003a). The role of eATP as an important signalling molecule in plants has been confirmed by the discovery of the plant purinoreceptor, an *Arabidopsis thaliana* L-type Lectin Receptor-like Kinase-I.9 (LecRK-I.9)

protein encoded by the gene *DORN1* (*Does Not Respond to Nucleotide1*; Choi *et al.* 2014b). With this, a new family of purinoreceptor was created called P2K in which the K represents the kinase domain of the receptor and with AtDORN1 listed as the first member of the family (Choi *et al.*, 2014b). There are 45 members of the LecRK family in *Arabidopsis* and the expression of each of the members is regulated by different abiotic and biotic stresses (Bouwmeester and Govers, 2009). Deng *et al.* (2009) demonstrated the role of LecRK (*LecRK-b2)* in salt stress and osmotic stress, as the germination rate of the mutant of *LecRK* was insensitive to both of the stresses. *LecRK1.9* gene was found to be highly up-regulated by methyl jasmonate, wounding, dark, ozone, salinity, osmotic and some biotic stresses (Bouwmeester and Govers, 2009).

Extracellular ATP triggered a transient $[Ca^{2+}]_{cyt}$ biphasic increase in *Arabidopsis thaliana* seedlings but not in the loss of function *dorn1* mutant. This indicates that AtDORN1 is the receptor that perceives the eATP stimulus (Choi *et al.*, 2014b) and allows the downstream consequences of eATP signalling such as release of Ca^{2+} into the cytosol, NO and ROS production that lead to MAPK phosphorylation, gene activation and transcriptional changes (Tanaka *et al.*, 2014). Choi *et al.* (2014b) also listed several characteristics of the AtDORN1 purinoreceptor. AtDORN1 was found to be specific to nucleotide agonists as it was not responsive towards other biotic or abiotic treatments. AtDORN1 also has the ability to bind to a broad range of nucleotides but has the highest affinity for ATP in a concentration-dependent manner, followed by ADP. *In vitro* tests with the extracellular domain of AtDORN1 found ATP to be able to bind to AtDORN1 with a K_d of 45.7 nM. *In vivo* tests with *A. thaliana* protoplasts confirmed AtDORN1-eATP binding at the extracellular surface (Choi *et al.*, 2014b). The same study also suggested eATP was acting as a danger signal as most of the eATP-induced genes overlapped with wound-induced genes and were differentially regulated in *Atdorn1* loss of function mutant or the ectopically expressed *oxDORN1*.

An in-depth review was written on the protein domains of AtDORN1 by Choi *et al.* (2014c) as shown in Figure 1.2. The L-type lectin extracellular domain which usually served as a carbohydrate-binding domain instead served as an ATP-binding domain due to the substitution of amino acid Asp^{79} to histidine (Choi *et al.*, 2014c). The same review showed the localisation of *AtDORN1* at the plasma membrane of 10-day-old *A. thaliana* roots which was in agreement with the previous study by Demidchik *et al.* (2009) on eATP-induced $[Ca^{2+}]_{cyt}$ elevation mentioned earlier. The intracellular domain on the other hand is a

serine/threonine kinase domain, which was found to play an important role in mediating the eATP signal. *Atdorn1-1* (which is an EMS mutant at the kinase site) failed to show kinase activity in *in vitro* phosphorylation assay that eventually affected the eATP-induced response of plants. All loss-of-function mutants at different domains of DORN1 (Figure 1.2) isolated by Choi *et al.*, (2014c) failed to produce transient $[Ca^{2+}]_{cyt}$ increase upon ATP treatment.

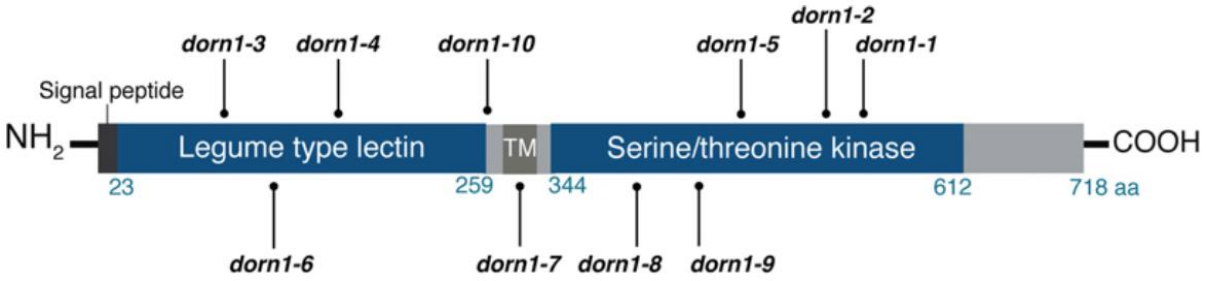

Figure 1.2: Different loss-of-function mutant alleles affecting different domains of the AtDORN1. EMS mutation of *dorn1-1* (kinase domain X), *dorn1-2* (kinase domain IX; DxxWxG motif), *dorn1-5* (kinase domain VII activation loop), *dorn1-6* (extracellular domain), *dorn1-7* (transmembrane domain; TM), *dorn1-8* (kinase domain V), *dorn1-9* (kinase domain VIb), *dorn1-10* (juxta-membrane region) and T-DNA insertion mutants of *dorn1-3* (extraellular domain) and *dorn1-4* (extracellular domain) were identified by Choi *et al*., (2014c). Source: Choi *et al.,* (2014c). *Extracellular ATP, a danger signal, is recognised by DORN1 in Arabidopsis.*

Since the function of the intracellular kinase domain of AtDORN1 was found to be important in eATP signal mediation, a further study was done to determine the phosphorylation activity and the targets of the AtDORN1 protein. There were 13 autophosphorylation sites found in the AtDORN1 protein. *In vitro* kinase client assay (KiC) revealed that AtRBOHD is one of the targeted proteins of DORN1. An interaction study was also done through co-immuno precipitation (Co-IP) that confirmed that eATP intensified the interaction between AtDORN1 and AtRBOHD (Chen *et al.*, 2017). AtRBOHD is the plasma membrane NADPH Oxidase homolog D that produced ROS. *Atdorn1* and *Atrbohd* mutants each showed reduction in the ROS burst evoked by eATP proving that the interaction between AtDORN1 and AtRBOHD in the presence of eATP is important in the ROS production (Chen *et al.*, 2017). An *in planta* BiFC (Bimolecular Fluorescence Complement) assay was performed and confirmed that the interaction between AtDORN1 and AtRBOHD occurred in the presence of eATP at the plasma membrane regardless of the kinase activity of AtDORN1 (Chen *et al.*, 2017). This again was in agreement with the previous studies suggesting the perception of eATP at the plasma membrane (Demidchik *et al.*, 2009; Choi *et*

al., 2014c). Chen *et al.* (2017) also showed AtDORN1 could phosphorylate AtRBOHD *in vivo* and the phosphorylation could promote ROS production in the presence of eATP.

Choi *et al.* (2014b) demonstrated that the eATP-induced biphasic $[Ca^{2+}]_{cyt}$ increase observed at whole seedling level depends on AtDORN1 as the eATP receptor. A study by Matthus *et al.* (2019a) however showed that the leaves of *Atdorn1-1* and *Atdorn1-3* mutant could still produce a $[Ca^{2+}]_{cyt}$ response to eATP treatment albeit lower than the Col-0 wild type. This suggests the presence of another eATP receptor. The $[Ca^{2+}]_{cyt}$ increase depends on the organs tested. The Col-0 leaves tested with eATP supported a monophasic $[Ca^{2+}]_{cyt}$ response which differs from the biphasic $[Ca^{2+}]_{cyt}$ of excised roots (Demidchik *et al.*, 2003a; Matthus *et al.*, 2019a,b). The biphasic root $[Ca^{2+}]_{cyt}$ response was completely dependent on AtDORN1 (Matthus *et al.*, 2019a). This is in accordance to the localisation of AtDORN1, which was found to be most abundant within 1 mm of the root apex and declined as the cells mature (Cho *et al.*, 2017; Matthus *et al.*, 2019a). The same study also showed the possibility of AtDORN1's involvement in the generation of a $[Ca^{2+}]_{cyt}$ "wave" along the root starting from the apical tissues and moving distally (Matthus *et al.*, 2019a).

Previously it was shown that exogenous application of ATP could depolarise the plasma membrane (Lew and Dearnaley, 2000) and could also activate Ca^{2+} influx through a Hyperpolarisation Activated Calcium Channel (HACC) conductance (Demidchik *et al.*, 2009, 2011; Wang *et al.*, 2019). A study was later done on *Atdorn1* mutants to determine whether AtDORN1 is involved in activating the HACC conductance. ATP treatment of root apical protoplasts of Col-0 wild type produced inward Ca^{2+} currents at hyperpolarised voltage, which could be the Ca^{2+} influx through the HACC as treatment with $GdCl_3$ (as a calcium channel blocker) reduced the conductance. This current however was absent in *Atdorn1-1* (EMS mutant at the kinase domain) and the *Atdorn1-3* mutant (T-DNA insert mutant of the eATP-binding site) (Wang *et al.* 2018a).

eATP is implicated in root growth, gravitropism and is regarded as a danger signal. Zhu *et al.* (2017) reported that growing Col-0 roots avoid ATP when present in the growth medium and this was also phenocopied by the *Atdorn1* mutant suggesting that AtDORN1 might not be involved in modulating the root avoidance mechanism. However, AtDORN1 might be heavily involved in biotic stress resistance and in the wounding response. *LecRK-I.9* from *A. thaliana* expressed in potato and tobacco plants exhibited resistance towards the *Phytophthora infestans* pathogen (Bouwmeester *et al.*, 2014). Another study also showed the

lecrk-I.9 T-DNA insertion mutant in *A. thaliana* to be vulnerable towards *Phytophthora brassicae* whereas the gain-of-function mutant showed enhanced resistance (Bouwmeester *et al.*, 2011). Exogenous ATP treatment caused *A. thaliana* resistance towards the fungus *Botrytis cinerea* but this resistance ceased in the *Atdorn1* mutant, which shows the requirement of AtDORN1 in the biotic response (Tripathi *et al.*, 2017). Extracellular ATP-induced genes were found to be overlapping with the pathogen-induced genes (Cao *et al.*, 2014). Extracellular ATP could also regulate stomatal aperture, promoting closure, which depended on the phosphorylation of AtRBOHD by AtDORN1 and was independent of ABA (Chen *et al.*, 2017). This is in line with the notion of eATP and AtDORN1 acting in pathogen resistance as the stomata could be an entry point of a pathogen.

1.8 Downstream responses of eATP signalling

Extracellular ATP was envisaged as a signalling molecule, thus the perception of eATP by a purinoreceptor should cause an array of downstream responses at the molecular level and physiological level. Exogenous application of eATP often results in production of ROS (Song *et al.*, 2006), increase in $[Ca^{2+}]_{cyt}$ (Demidchik *et al.*, 2009; Matthus *et al.*, 2019a,b), production of NO (Foresi *et al.*, 2007) and PA (Sueldo *et al.*, 2010). These molecules themselves could act as a secondary messenger, which will drive different signalling pathways leading to the changes at molecular level such as changes in stress-related gene expression. In this subchapter, we will discuss each of the components of this eATP-induced response.

1.8.1 Cytosolic free calcium ion as a secondary messenger

Ca^{2+} is one of the main macronutrients needed for plants to grow and function normally. Plants obtain their Ca^{2+} supply from the soil *via* root plasma membrane Ca^{2+} channels especially from the root tips (McGonigle and Grant, 2015) and transport it systemically to avoid Ca^{2+} deprivation. Although rare, some vegetables can suffer from Ca^{2+} deficiency and exhibit symptoms such as injury, necrosis, black-heart and tip-burn confirming the importance of Ca^{2+} in plants (Olle and Bender 2009). Ca^{2+} is involved in fundamental processes in plants such as maintaining the structure of cell wall and plasma membrane and to balance the ratio of cations and anions in the cells (White and Broadley, 2003). Ca^{2+} is transported from the root to the shoot *via* xylem (White *et al.*, 2001) and could enter plant cells across the plasma membrane through calcium permeable channels. However, too high a Ca^{2+} concentration in the cytosol could cause toxicity through anion chelation

(particularly phosphate) that would be detrimental to the plant. Furthermore excess Ca^{2+} causes biomineralisation in plants, which could reduce viability (De Kreij *et al.*, 1992). Thus, the mechanism of Ca^{2+} efflux and sequestration is important in keeping a low cytosolic Ca^{2+} concentration in plant cells. Ca^{2+} is stored mainly in vacuoles (Cheng *et al.*, 2005) or endoplasmic reticulum (ER) (Navazio *et al.*, 2001). The process of removing Ca^{2+} from the cytosol would be against the electrochemical potential gradient thus making necessary the use of a protein pump energized by ATP or an antiporter energized by a H^+ gradient.

The removal of Ca^{2+} from the cytosol to the intracellular Ca^{2+} stores or to the apoplast is mediated primarily by either Ca^{2+}-ATPases or by Ca^{2+}/H^+ antiporters (Cation Exchanger; CAX) (Dodd *et al.*, 2010). The accumulation of Ca^{2+} in the stores however varies depending on the type of cells (Storey and Leigh, 2004). Both Ca^{2+}-ATPases and Ca^{2+}/H^+ antiporters can be found residing at the plasma membrane such as found in corn leaves (Kasai and Muto, 1999). There are two types of Ca^{2+}-ATPases known as ER type Ca^{2+}-ATPases (ECA) or the Auto Inhibition Ca^{2+}-ATPases (ACA). An *in vivo* study of ER Ca^{2+}-ATPase pump (AtECA1) found it localised at the ER of *A. thaliana* and contributed to 70% of the Ca^{2+} transported to the ER (Wu *et al.*, 2002). The same study suggested the importance of ECA in *A. thaliana* Ca^{2+} distribution and homeostasis. Another ECA in *A. thaliana* known as AtECA3 plays an important role in the transport of Ca^{2+} and Mn^{2+} to the Golgi and Ca^{2+} homeostasis (Mills *et al.*, 2008). In *A. thaliana*, Bonza *et al.* (2000) discovered Ca^{2+}-ATPase 8 (AtACA8), localised to the plasma membrane and is a member of a multi-gene family that includes ACA2, which localises to the vacuole (Harper *et al.*, 1998). CAX are also from multi-gene families. In *A. thaliana*, the *AtCAX3* Ca^{2+}/H^+ antiporter transcript was found expressed in all tissues and is important in Ca^{2+} homeostasis (Shigaki and Hirschi, 2000). Since then, it has become clear that AtCAX3 can form a heterodimer with AtCAX1 at the vacuolar membrane, which is important for their operation in controlling stomatal aperture (Hocking *et al.*, 2017). ATPases and antiporters would move Ca^{2+} against its electrochemical gradient and so require energy. However, uptake of Ca^{2+} from the cytosol by mitochondria involves the Mitochondrial Calcium Uniporter (MCU), which has a subunit that acts as a channel (Teardo *et al.*, 2017). As channels are passive transporters, this complex could operate when $[Ca^{2+}]_{cyt}$ is high.

Chloroplasts may also play a role in removing Ca^{2+} from the cytosol, as Ca^{2+} is required for correct function of Photosystem II (PSII) and this organelle appears to use changes in its own Ca^{2+} for signalling (Loro *et al.*, 2016). AtACA1 may play a role in uptake at the chloroplast envelope (Huang *et al.*, 1993) and recently a new type of Ca^{2+} transporter

AtBICAT2 (Bivalent Cation Transporter2) has been shown to be involved (Frank *et al.*, 2019). Chloroplasts also have a member of the Mitochondrial Calcium Uniporter family for uptake from the cytosol (Teardo *et al.*, 2019). Within the chloroplast, AtBICAT1 or another protein unrelated to CAX termed AtCCHA1 (Chloroplast Calcium H^+ Antiporter1) may underpin the thylakoid Ca^{2+}/H^+ antiporter activity (Ettinger *et al.*, 1999; Wang *et al.*, 2016; Frank *et al.*, 2019). The localisation of these varied Ca^{2+} transporters in both plasma membrane and intracellular membranes implies tight regulation of Ca^{2+} concentration in the cytosol.

The importance of keeping $[Ca^{2+}]_{cyt}$ low links to another pivotal role of Ca^{2+} that will be the main focus of this study, which is the role of Ca^{2+} as a secondary messenger for the plant to receive and respond accordingly to any stimulus from the environment, particularly the eATP signal. At resting level, $[Ca^{2+}]_{cyt}$ is kept at 100-200 nM by the presence of Ca^{2+} transporters as mentioned before. When a plant receives a cue from the environment, it is envisaged that a receptor or sensor protein that perceives this stimulus activates certain processes that eventually lead to the influx of Ca^{2+} into the cytosol through Ca^{2+} channels in the plasma membrane and/or endomembranes. This influx causes transient increase in $[Ca^{2+}]_{cyt}$ (monophasic, biphasic or oscillatory) that is known as the "calcium signature" as different stimuli are found to produce different Ca^{2+} influx patterns in terms of the period and the magnitude of the accumulation (McAinsh and Pittman, 2009). The mechanism of Ca^{2+} influx will be discussed later in section 1.8.4.

The increase in $[Ca^{2+}]_{cyt}$ has been reported numerously upon wounding (León *et al.*, 2001), touch or wind (Knight *et al.*, 1992) salinity stress (Sun *et al.*, 2012; Laohavisit *et al.*, 2013; Choi *et al.*, 2014c), osmotic stress (Knight *et al.*, 1997), drought stress (Huh *et al.*, 2010) heat stress (Larkindale and Knight 2002; Finka *et al.*, 2012; Wang *et al.*, 2015), ozone stress (Evans *et al.*, 2005), oxidative stress (Rentel, Knight and Kingdom, 2004), pathogen attack (Cheval *et al.*, 2013), flg22 elicitor (Li *et al.*, 2014; Beck *et al.*, 2014), glutamate (Meyerhoff *et al.*, 2005), sugar (Furuichi *et al.*, 2001) and growth (Demidchik *et al.*, 2002). Nucleotides such as eATP (Demidchik *et al.*, 2009; Tanaka *et al.*, 2010; Choi *et al.*, 2014b; Matthus *et al.*, 2019a,b) or eADP (Demidchik *et al.*, 2011) and other secondary messengers such as NO (Abdul-Awal *et al.*, 2016) and PA (Cao *et al.*, 2014) that were previously found to be danger signals under different stresses were also able to generate $[Ca^{2+}]_{cyt}$ accumulation.

A study by Tracy *et al.* (2008) found that the $[Ca^{2+}]_{cyt}$ signature under salt stimulus could differ based on the background solution used during measurement such as water, Murashige-Skoog (MS) medium, membrane hyperpolarising solution or membrane depolarising solution. The $[Ca^{2+}]_{cyt}$ signature when tested with salt stress, sorbitol or cold stress could also be influenced by the ecotype of the plant used for example between Col-0 background and C24 background (Schmöckel *et al.*, 2015). Another factor influencing the $[Ca^{2+}]_{cyt}$ signature is the organ that is used during measurement. Extracellular ATP-induced $[Ca^{2+}]_{cyt}$ accumulation showed a monophasic pattern when measured in leaves but produced a biphasic pattern when tested at root tips (Matthus *et al.*, 2019a).

Another characteristic of $[Ca^{2+}]_{cyt}$ change is the presence of a refractory period for every stimulus. Repetitive exposure to one type of stimulus would cause desensitization for a certain refractory period where continuous $[Ca^{2+}]_{cyt}$ increase as response does not occur. This was found when repetitive wind stimulus (Knight *et al.*, 1992), gravitational force (Plieth and Trewavas, 2002) or eATP (Matthus *et al.*, 2019a) was applied to *A. thaliana* and showed a lesser $[Ca^{2+}]_{cyt}$ response compared to the initial exposure.

Ca^{2+} increase as a secondary messenger would be highly dependent on the Ca^{2+} sensor protein as it can sense Ca^{2+} that accumulated in the cytosol to begin decoding the signature by eATP or other stimuli. These proteins usually have EF-binding motifs as a domain to be able to bind to the Ca^{2+}. In plants, there are three main groups of Ca^{2+} sensor, which are the calmodulin (CaM)-binding proteins, the CDPKs (Calcium-Dependent Protein Kinases) and the Calcineurin B-Like proteins. Through binding, Ca^{2+} could induce change in the conformation of the sensor protein that eventually triggers the downstream responses (Kim *et al.*, 2009). Kim and Kim (2006) found the transcription factor in *Arabidopsis thaliana*, AtNIG1 that is assumed to be a Ca^{2+} sensor protein as it has the EF hand motif and is able to regulate the expression of salinity-responsive genes. Other than directly influencing the Ca^{2+} sensor, Ca^{2+} could also influence CaM-binding kinases or phosphatases that could also cause modification to target proteins. In plant thermotolerance, CaM-binding protein kinase was found to regulate the heat shock signal transduction through regulating the expression of heat-shock protein (HSP) (Liu *et al.*, 2008).

Another example would be the crucial role of Ca^{2+} in plant tolerance towards cold stress. Calmodulin-binding Transcription Activator (CAMTA) that depends on the transient increase of $[Ca^{2+}]_{cyt}$ is one of the key players that is responsible in activating transcription of

the *AtCBF2* gene in response to cold stress (Doherty *et al.*, 2009). Thus, systemic signalling involving Ca^{2+} is important for the effective communication for survival. Other pivotal players in this systemic signalling process are the Ca^{2+} transporters that allow the Ca^{2+} influx to occur in the first place. These Ca^{2+} transporters are categorised as Ca^{2+} channels and the activation of these channels depends on ligand gating and/or the potential difference across the plasma membrane of the cell or endomembrane.

1.8.2 Reactive Oxygen Species (ROS) production

AtDORN1 was found to be phosphorylating AtRBOHD, which could affect the production of ROS in the presence of eATP (Chen *et al.*, 2017). AtDORN1 interacting with AtRBOHD when treated with eATP (Chen *et al.*, 2017) showed the importance of the ROS component as one of the secondary messengers in the eATP signalling.

ROS comprise non-radical singlet oxygen (O_2) and hydrogen peroxide (H_2O_2) which is more stable than the free radical forms such as superoxide radical or superoxide anion ($O_2^{\bullet -}$), and hydroxyl radical ($OH^{\bullet -}$). ROS are generally produced by plants as part of being phototrophs where oxygen in excess is the byproduct of photosynthesis. ROS generated through this process however play important roles in growth and development, stress response and viability. The major ROS that is produced during photosynthesis is the singlet oxygen O_2. Under high light absorption by chloroplasts but low energy dissipation in PSII, the chlorophyll will be transformed into chlorophyll triplet state where it could react with ground state O_2 to become singlet oxygen O_2 (Krieger-Liszkay *et al.*, 2008). $O_2^{\bullet -}$ is mainly formed in the PSI by photoreduction of oxygen during photosynthesis (Asada, 2006). It could also formed due to electron leakage in PSII. Other than chloroplasts, $O_2^{\bullet -}$ can be produce in plant mitochondria (Turrens, 2003) rich with oxygen and also in peroxisomes during metabolic processes (Noctor *et al.*, 2002). At the plasma membrane, $O_2^{\bullet -}$ is generated by NADPH oxidases (Foreman *et al.*, 2003). Similar to $O_2^{\bullet -}$, H_2O_2 is one of the by-products of photosynthesis. It can be produced through a non-enzymatic pathway, which involves the electron transport chain (ETC) (Niu and Liao, 2016). It can also be produced extracellularly by superoxide dismutases acting on $O_2^{\bullet -}$ from plasma membrane NADPH oxidase activity (Richards *et al.*, 2015). H_2O_2 could react with transition metal ions such as Fe^{2+} and create the hydroxyl radical $OH^{\bullet -}$ through the Fenton reaction (Halliwell, 2006)

Through evolution, plants as aerobic organisms evolved to utilise the excess oxygen in the form of ROS to serve some important biological processes. ROS are found to be

important secondary messengers in response to growth and stress. In a study by Foreman *et al* (2003), ROS were accumulated in the wild type of growing *Arabidopsis thaliana* root hairs. This accumulation however was impaired in the *Atrhd2* mutant, which has lost the function of a plasma membrane NADPH Oxidase (encoded by *Respiratory Burst Oxidase Homologue C*) and has a short root and root hair phenotype. Inhibition of the NADPH Oxidase through the treatment with DPI (Diphenyleneiodonium) also phenocopied the *Atrhd2* mutant response. This observation proved that NADPH Oxidase synthesised the ROS production during development of root hairs. NADPH oxidase activity is also implicated in salinity stress, where it is required for the adaptive transcriptional response (Chung *et al.*, 2007). Superoxide radical, hydroxyl radical and hydrogen peroxide play some roles in growth regulation. These ROS species were found accumulating at the growing zone of maize roots (Liszkay *et al.*, 2004). Applications of these ROS species help break seed dormancy in *Bidens pilosa* L. seeds (Whitaker *et al.*, 2010).

Different ROS species however might serve disparate roles depending on the membrane permeability, reactivity with other molecules, rate of diffusion and the half-life of each ROS species. Superoxide anion has a short lifetime (Gardner, 2002) and is regarded as an intermediate ROS. It is important in plant immune response (Hyodo *et al.*, 2017), activating metabolic pathways (Tsukagoshi *et al.*, 2010), regulating growth (Dunand *et al.*, 2007), inducing lignification (Ogawa *et al.*, 1997), activating response to pathogen, wounding (Miller *et al.*, 2009) salinity stress (Li *et al.*, 2018) and could serve as a signalling molecule (Buetler *et al.*, 2004).

Hydrogen peroxide (H_2O_2) synthesised from the superoxide radical is the most extensively studied ROS as it is more stable than the radical species. H_2O_2 is thought to be produced in the apoplast downstream of NADPH Oxidase activity or through apoplastic peroxidases (Laloi *et al.*, 2004; Richards *et al.*, 2015). H_2O_2 has been implicated as an important secondary messenger downstream of ABA signalling. It was found to activate Ca^{2+} influx in the protoplast and guard cell of *A. thaliana* (Pei *et al.*, 2000). The same study suggested that H_2O_2 is involved in mediating stomatal aperture regulation under ABA signalling as the ABA-insensitive mutant *Atgca2* failed to induce H_2O_2 production and stomatal closure. Kwak *et al.* (2003) discovered *in vivo* the expression of *AtRBOHD* and *AtRBOHF* genes (encoding the NADPH Oxidases that lead to H_2O_2 production) that were important in ABA signalling. Mutants of these genes failed to show hallmarks of ABA treatment such as production of H_2O_2, $[Ca^{2+}]_{cyt}$ increase, induction of stomatal closure,

inhibition of seed germination and root elongation thus showing the importance of H_2O_2 in mediating ABA responses. In relation to the ABA-induced stomatal regulation, optimum H_2O_2 concentration production proved to increase resistance towards water deprivation as it could lower malondialdehye (MDA) level and increase antioxidant enzyme activity in maize seedlings (Ashraf *et al.*, 2015). In the ABA-independent pathway, H_2O_2 works together with NO in CO_2 -induced stomatal closure (García-Mata and Lamattina, 2013; Shi *et al.*, 2015). Besides stomatal regulation, H_2O_2 is heavily involved in mediating pathogen response. The presence of the fungal pathogens *Monilinia fructiola* and *Penicillium digitatum* in peach flower petals induced the gene expression and activity of NADPH Oxidase and cell wall peroxidases leading to increase in H_2O_2 production (Liu *et al.*, 2013). Other than fungal pathogens, both *AtRBOHD* and *AtRBOHF* are needed for H_2O_2 production in the resistance to bacterial pathogens (Torres *et al.*, 2002). H_2O_2 in turn activates mitogen-activated protein kinase kinase kinase AtANP1, which could phosphorylate Mitogen-activated Protein Kinase 3 (AtMPK3) and Mitogen-activated Protein Kinase 6 (AtMPK6). The orthologue of this ANP1 in tobacco, NPK1 showed resistance towards a variety of stresses when expressed continuously (Kovtun *et al.*, 2000). This was also reported by Li *et al.* (2015) where H_2O_2 is involved in resistance towards heat stress in maize seedlings. Other than abiotic and biotic stresses, some studies suggest the involvement of H_2O_2 in growth and development. H_2O_2-induced activation of AtMPK3 and AtMPK6 inhibited auxin action, which could tie pathogen perception and growth inhibition (Kovtun *et al.*, 2000). Furthermore, both H_2O_2 and $OH^{\bullet -}$ could modify the cell wall of tobacco pollen although inversely with each other. H_2O_2 impeded pollen germination by strengthening the cell wall whereas $OH^{\bullet -}$ promoted germination by causing cell wall loosening (Smirnova *et al.*, 2014)

Hydroxyl radicals produced *in vivo* in the apoplast of germinating cress seeds help in inducing endosperm breaking (Müller *et al.*, 2009). Hydroxyl radicals targeted to cell wall polysaccharides help loosen the cell wall for cell elongation during cress seeds radicle formation and during elongation of maize coleoptile (Müller *et al.*, 2009). A study *in vivo* confirmed the role of $OH^{\bullet -}$ converted from auxin-induced $O_2^{\bullet -}$ production and that the $OH^{\bullet -}$ generated was important in promoting elongation growth in maize coleoptile (Schopfer *et al.*, 2002). In maize roots, $OH^{\bullet -}$ possibly produced by cell wall peroxidase causes cell wall loosening especially in the growing zone (Liszkay *et al.*, 2004). Another study discovered in pea root cell wall that the $OH^{\bullet -}$ generated during cell wall loosening was from the action of peroxidase and Mn-superoxide dismutase towards H_2O_2 (Kukavica *et al.*, 2009). Extracellular

$OH^{\bullet -}$ are also implicated in promoting root hair elongation, possibly by increasing apical $[Ca^{2+}]_{cyt}$ (Foreman *et al.*, 2003).

Singlet oxygen O_2's short life makes it hard to be monitored in plant cells but method development has led to the discovery of the roles of this ROS. Singlet O_2 is a byproduct of high light illumination that failed to be quenched in PSII. This excess generation of singlet O_2 by triplet chlorophyll can cause protein damage as shown in spinach chloroplasts (Rinalducci *et al.*, 2004). The discovery of the *Atflu* mutant, which could generate singlet O_2 in the presence of light, has enabled the study of the role or effect of singlet O_2 production (op den Camp, 2003). The same study found that the singlet O_2 generated led to inhibition of growth, occurrence of necrotic lesions, peroxidation of chloroplast membrane lipid and activation of a different set of genes from the radical species or H_2O_2. These findings suggest that the singlet O_2 potentially acted as a stress signal on top of being a toxic molecule itself. Another studies supporting this notion showed that mutation of the *AtEXECUTER1* gene (that is responsible for cell death and growth inhibition under oxidative stress) evaded stress response caused by singlet O_2 (Wagner *et al.*, 2004). Singlet O_2 is also implicated in photooxidative stress where high light intensity treatment on PSII showed production of excess singlet O_2 causing changes in gene expression related to resistance towards photooxidative stress (Krieger-Liszkay *et al.*, 2008). Overexpression of two singlet O_2-induced genes (glutathione peroxidase and glutathione S-transferase) improved resistance towards singlet O_2 under high light conditions (Ledford *et al.*, 2007). Other than photooxidative stress, singlet O_2 is also involved in osmotic stress as treatment with polyethylene glycol (PEG) generated singlet O_2. The production of singlet O_2 and not other ROS species leads to cell death, change in the gene expression and alters vacuolar rigidity in the PEG treatment (Chen and Fluhr, 2018). Singlet O_2 is implicated in retrograde signalling where singlet O_2 activates a signalling system outside of the thylakoid that leads to the expression of nuclear *AtGPXH* (glutathione peroxidase homologous gene) (Fischer *et al.*, 2007).

Based on these studies, it is important for plant cells to keep the balance between the production of ROS and the scavenging of ROS as it determines the downstream process of either a systemic signalling or if in excess, oxidative stress that could lead to senescence and cell death (Das and Roychoudhury, 2014). This is where the action of antioxidant enzymes plays an important role to keep a balanced ROS level in plant cells under various circumstances. Copper for example serve as micronutrient in plants but in excess, as a transition metal, could form high levels of $OH^{\bullet -}$ from H_2O_2 leading to oxidative stress-

induced growth arrest and chlorosis in *A. thaliana*. As a counter mechanism, copper induced-oxidative stress in *A. thaliana* causes elevation of antioxidants peroxidase and superoxide dismutase (Drązkiewicz *et al.*, 2004). Another study carried out on carrizo plants found that their ability to persevere in both drought and heat stresses was through the action of superoxide dismutase (SOD), ascorbate peroxidase (APX), catalase (CAT), and glutathione reductase (GR) in ROS detoxification (Zandalinas *et al.*, 2017).

Oxidative chemical stress and light stress during photosynthesis in *A. thaliana* showed increase in ROS leading to the antioxidants such as APX, monodehydroascorbate reductase (NADH) and GR to be targeted to both chloroplast and mitochondria as the organelles that produce ROS (Chew *et al.*, 2003). Another form of antioxidant peroxiredoxins (Prx) in animals has been discovered in *A. thaliana* as At-PrxII is also targeted to mitochondria. Mutants of this antioxidant exhibited root growth inhibition and alteration in nuclear and mitochondrial gene expression under cadmium metal stress (Finkemeier *et al.*, 2005). Another organelle that is responsible for ROS production (intracellular H_2O_2 and $O_2^{\bullet -}$) is the peroxisome. ROS scavengers for peroxisomal ROS are either enzymatic or non-enzymatic antioxidants such as CAT, SODs, ascorbate-glutathione cycle, GR, glutathione S-transferase (GST), NADPH generating dehydrogenase and Prx (Del Río and López-Huertas, 2016). Antioxidants such as catalase 2 (AtCAT2) and ascorbate peroxidase 1 (AtAPX1) also protect plant DNA from damage by excess of H_2O_2 (Vanderauwera *et al.*, 2011). Some antioxidants are specific towards certain species of ROS. Carotenoids for example are the major singlet O_2 scavenger in the chloroplast. Under photooxidative stress, oxidation of β-carotene caused accumulation of β-cyclocitral which could lead to changes in gene expression corresponding to the O_2-induced gene expression (Ramel *et al.*, 2012a). Another study on antioxidant action was done on *A. thaliana* leaves where scavenging of O_2 occurs by oxidation of β-carotene, leutein, and zeaxanthin forming aldehyde and enderoperoxidases under high light conditions (Ramel *et al.*, 2012b). Other than carotenoids, tocopherol is also one of the O_2 scavengers in the chloroplast under high light stress (Krieger-Liszkay and Trebst, 2006). Besides photooxidative stress, an overall review was done listing all the drought-induced antioxidants and their targets (Laxa *et al.*, 2019).

eATP is envisaged to be the danger signal upon stresses that triggered the synthesis of ROS *via* NADPH Oxidase (Chen *et al.*, 2017). In *A. thaliana* roots, this reaction depends on the accumulation of $[Ca^{2+}]_{cyt}$ (Demidchik *et al.*, 2009). Song *et al.* (2006) showed eATP and eADP possibly as danger or wound signals evoked $O_2^{\bullet -}$ accumulation in *A. thaliana* leaves.

Besides wounding, ABA and light induction could be one of the triggers for eATP accumulation (Clark and Roux, 2011). As previously mentioned, H_2O_2 played an important function in mediating ABA responses (Pei *et al.*, 2000) which could put H_2O_2 downstream of eATP and ABA.

Most of the studies done on ROS involved biotic stresses. Extracellular ATP treatment has been shown to induce H_2O_2 production and both eATP and H_2O_2 managed to induce stomatal closure and resistance towards *Pseudomonas syringae* (Chen *et al.*, 2017). The same study showed AtDORN1 as the receptor of eATP directly phosphorylating AtRBOHD, which is responsible ultimately for the H_2O_2 production. Another study with biotic stress involving yeast extract found eATP accumulated due to chitin treatment caused Ca^{2+} influx, which H_2O_2 production relied on (Wu *et al.*, 2008). Kim *et al.* (2006) in addition reported the ability of chitin to trigger eATP accumulation and evoked an intracellular ROS burst. These studies could put ROS production downstream of eATP production in biotic stresses. Apart from biotic stresses, NaCl-induced eATP accumulation by *Populus euphratica* cells also evoked H_2O_2 production. Inhibition of eATP perception by the purinoreceptor blockers suramin and PPADS (pyridoxalphosphate-6-azophenyl-2',4'-disulfonic acid) reduced the production of antioxidant APX, CAT and GR which put redox regulation in salinity stress under the eATP signalling pathway (Sun *et al.*, 2012). Clark *et al.* (2010) also showed ability of the non-hydrolysable analogue of ATP (ATPϒS) to cause H_2O_2 production and the optimum concentration of H_2O_2 proved to be important in regulating root hair growth of *A. thaliana*.

Gilroy *et al.* (2014) and Demidchik *et al.* (2009) suggested the possibility of Ca^{2+} and ROS integration in long distance signalling. Stimuli cause opening of plasma membrane calcium channels thus allowing Ca^{2+} influx in the cytosol leading to induction of ROS released in the apoplast and the ROS produced can in turn directly activate another Ca^{2+} channel releasing another wave of $[Ca^{2+}]_{cyt}$. Previously, free oxygen radicals managed to activate Ca^{2+} permeable channels in root cells (Demidchik *et al.*, 2003b). A study by Matthus *et al.* (2019a) reported the possibility of eATP inducing calcium waves in *A. thaliana* from the root tips towards the mature zone downstream of the AtDORN1 receptor. This accumulation or waves of $[Ca^{2+}]_{cyt}$ triggered by eATP and ROS decoded by Ca^{2+} sensors could eventually cause changes at the molecular level such as the *AtMAPKinase3* gene expression that is involved in stress responses. Another study on salinity stress in *Populus*

euphratica (Sun *et al.*, 2012) also suggested that ROS downstream of eATP directs a MAP Kinase cascade.

1.8.3 Nitric Oxide and Phosphatidic Acid

NO (Nitric Oxide) is regarded as one of the second messengers involved in signalling pathways in plant cells. Production of NO downstream of a signal is tightly related to the signalling pathway in abiotic and biotic response of plants. According to Boudain *et al.* (2010), NO could be operating by modifying stress-related proteins at cysteine residues that eventually has an impact on gene expression and overall response. In ozone stress conditions, NO was first produced in the guard cell and spread to the epidermal and mesophyll cells. This NO production happened concurrently with lesions observed on the leaves of plants tested (Ahlfors *et al.*, 2009). Besides NO, in animal cells Phosphatidic Acid (PA) has been implicated in the purinergic signalling pathway thus making it another possible secondary messenger in the plant system. Increased production of PA *via* Phospholipase C has been shown in response to PAMP (Pathogen Activated Molecular Pattern) by xylanase and flg22 (Van der Luit *et al.*, 2000). Another study done to test for specificity used chitosan instead of xylanase and also showed increase in the production of PA in tomato cells (Raho *et al.*, 2011). Besides pathogen response, PA production has been reported caused by wounding in soybean seedlings (Lee *et al.*, 2001) and hypoosmotic stress but not in hyperosmotic stress of tobacco pollen tube (Zonia and Munnik 2004).

The role of PA in plants might be related to NO as guard cells of an *A. thaliana* mutant that was impaired in producing PA failed to produce NO and induce stomatal closure when treated with ABA, suggesting that NO is dependent on PA (Zhang *et al.*, 2009). Furthermore, both NO and PA were found to play an important role in causing cell death of tomato cell suspension in xylanase treatment (Laxalt *et al.*, 2007). This was again supported by a study done by Sueldo *et al.* (2010) where they discovered that exogenous ATP was able to generate NO, dependent on the presence of PA and the accumulation of $[Ca^{2+}]_{cyt.}$ The production of PA however is not affected by the inhibition of $[Ca^{2+}]_{cyt}$ accumulation pointing to the synthesis of NO downstream of PA. Although the plant purinoreceptor can bind to both eATP and eADP, eADP was unable to activate the production of PA in a tomato cell suspension culture study (Sueldo *et al.*, 2010) supporting the notion of eADP having a disparate signalling pathway to eATP. Wu and Wu (2008) again emphasised the importance

of Ca^{2+} influx as application of Ca^{2+} chelators or Ca^{2+} channel blockers inhibited accumulation of NO during eATP signalling (Wu and Wu, 2008).

Given the importance of NO as one of the downstream responses of the eATP signal, there is no established knowledge on the synthesis of NO in plant cells. In mammals, where NO also plays an important role in signal transduction, NO is synthesised by the enzyme Nitric Oxide Synthase (NOS). An NOS with functional NO synthesising domain however was not found in plant cells yet. Based on the study carried out by Foresi *et al.* (2007), NO could be synthesised from both NOS and Nitrite Reductase (NR) triggered by eATP, non-hydrolysable eATP or eADP. Another study provided evidence of NR involvement in production of NO where the mutation of *AtNIA1* and *AtNIA2* (genes that code for the NR) in *A. thaliana* caused impairment of NO accumulation following ABA treatment and failure in guard cell closure (Chen *et al.*, 2015).

1.8.4 Ca^{2+} Channels

The influx of Ca^{2+} from the apoplast or intracellular Ca^{2+} stores causing increase in $[Ca^{2+}]_{cyt}$ serves to generate a secondary messenger in transducing various stimuli. Ca^{2+} influx to the cytosol across membranes is mediated by Ca^{2+}-permeable channels. The Ca^{2+} channels identified in plant cells by electrophysiology can be categorised according to their voltage response. There are voltage-dependent channels (VDCC), which can be further divided into depolarisation- (DACC) and hyperpolarisation-activated calcium channels (HACC) and the voltage-independent Ca^{2+} channels (VICC). These VDCC and VICC can occur in the same membrane thus making it possible for a $[Ca^{2+}]_{cyt}$ response to occur over a wide range of plasma membrane voltage (Miedema *et al.*, 2001). Upstream components that determine the changes of the plasma membrane voltage such as H^+-ATPases, K^+ channels and anion channels are also important in the signalling system.

Demidchik *et al.* (2009) reported that upon application of 20 μM eATP, an *A. thaliana* root mature epidermal plasma membrane Ca^{2+} influx conductance occurred at hyperpolarised voltage and thus suggesting that the HACC activation caused the $[Ca^{2+}]_{cyt}$ increase. An eATP-activated HACC and smaller HACC-like conductance have since been described in *A. thaliana* root epidermal plasma membrane from apical/elongation zone (Wang *et al.*, 2018a, 2019). Plasma membrane HACCs were also found to regulate stomatal aperture (Hamilton *et al.*, 2000) and are also receptive towards Ca^{2+}, ROS and actin. These may be relevant to effects of eATP on stomatal closure. In *Vicia faba* guard cells, plasma

membrane HACC activity was enhanced by eATP (Wang *et al.*, 2014). Thus in this subchapter, the focus will be on the calcium channels categorised in the HACC group.

1.8.5 Annexins

In 1989, Boustead *et al.* (1989) discovered the first plant annexin in tomato. Annexins are soluble proteins with a size of 32 - 36 kDa and are among the most abundant proteins in plant cells. Annexins also constitute a large multigene family with 8 annexins in *Arabidopsis thaliana* (Cantero *et al.*, 2006) and 9 annexins in rice (Jami *et al.*, 2012). The presence of annexin protein has been found in *A. thaliana* (Lee *et al.*, 2004) barley (Clarke *et al.*, 2008). *M. truncatula* (Kovács *et al.*, 1998) rice (Hashimoto *et al.*, 2009), potato (Riewe *et al.*, 2008a,b), tobacco (Tang *et al.*, 2003) and wheat (Breton *et al.*, 2000). In terms of phylogenetics, plant annexins are quite distinct from their animal counterparts with less than 45% identity (Moss and Morgan, 2004). However the common feature that both plant and animal annexins still retain is the four endonexin repeats that are made up of five alpha helices.

Based on the conserved domains of annexins that could also be found in AtANN1 protein as shown in figure 1.3, annexins could be multifunctional proteins. The most prominent feature of the protein is the Ca^{2+}-binding domain in the first and the fourth endonexin repeats. Another feature of plant annexins that is also found in animal annexins is the salt-bridges that are responsible for the formation of Ca^{2+} channels by these proteins (Liemann *et al.*, 1996; Laohavisit *et al.*, 2009). Annexin A5 in animal cells was found to be able to transport Ca^{2+} into matrix vesicles in a planar lipid bilayer experiment suggesting its ability to form a calcium channel (Arispe *et al.*, 1996). The phosphatidylserine motif of annexin, the conserved tryptophan (TRP) motif and the diacidic motif could give the protein the ability to bind to the phospholipid bilayer of plasma membranes or internal membranes. Although annexins are well known for an ability to bind to membranes with Ca^{2+} binding involvement, annexins also have the potential to bind to membranes independently of Ca^{2+} (Dabitz *et al.*, 2005; Hofmann *et al.*, 2002). Other potential functions also involve the presence of a putative haem-binding site, actin-binding site, GTP- binding site and a domain that encodes for peroxidase activity. The long N-termini of animal annexins serve as a site for a post-translational modification that leads to different behaviour of the protein. In comparison to animal annexins, plant annexins have shorter N-termini. Thus, the differences in the function of plant annexins could be in regards to the changes in the core protein instead

of the N-terminal (Laohavisit and Davies, 2011; Clark *et al.*, 2012). For example, in *A. thaliana* annexin1 (AtANN1), S-glutathionylation due to ABA treatment caused reduced Ca^{2+} binding ability of AtANN1 which could affect its function in mediating stress response (Konopka-Postupolska *et al.*, 2009).

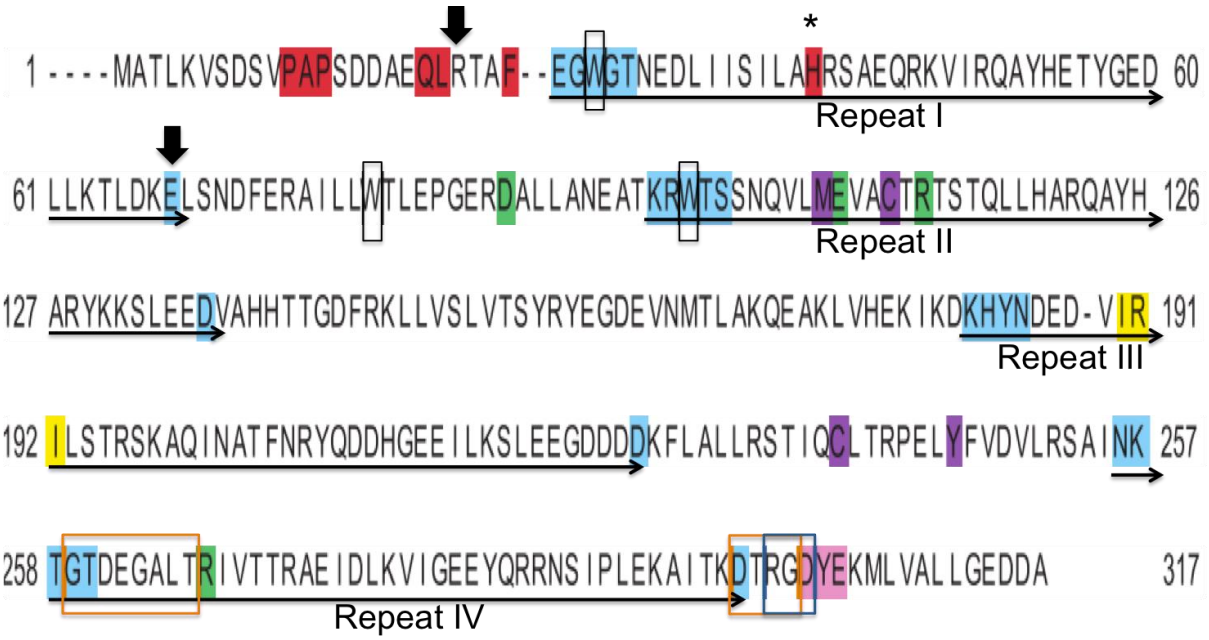

Figure 1.3: Amino acid sequence of AtANN1 with its four endonexin repeats and putative domains. The putative domains of AtANN1 highlighted are as follows: red; putative haem-binding motifs, teal; Ca^{2+}- binding sequences, black arrow; phosphatidylserine-binding motif (PS), black box; conserved trytophan residue, black star; conserved Histidine residue, green; salt-bridges motif, purple; putative S3 cluster for redox reaction, yellow; IRI motif for actin binding, orange box; putative GTP binding motif and blue box; RGD motif to bind to C2 domain proteins. Alignment diagram was reproduced from Laohavisit and Davies, 2011.

Localisation of annexins protein could also shed light on the possible function of these proteins. Annexins were found to be localised or expressed in pollen and seeds during germination (Yang *et al.*, 2007), in roots during primary and lateral root formation, in the vasculature (Clark *et al.*, 2005a) and during elongation of cotton fibre (Yang *et al.*, 2008). This study focused on the function of annexins possibly as calcium channels specifically in the model organism *A. thaliana.*

AtANN1 is the most extensively studied annexin as it is the most abundant of the *A. thaliana* annexin proteins. AtANN1 has been implicated in mediating Ca^{2+} signalling during abiotic stress such as osmotic stress, abscisic acid (ABA) response (Lee *et al.*, 2004), salt stress (Laohavisit *et al.*, 2013), H_2O_2 (Richards *et al.*, 2014), heat stress (Wang *et al.*, 2015)

and drought stress (Huh *et al.*, 2010). AtANN1 can be cytosolic, membrane-bound or extracellular. A detailed review by Laohavisit and Davies (2011) regarding the localisation of AtANN1 in the plasma membrane or endomembrane suggested the possible function of this protein in calcium signalling. Critically, it contains the salt bridges needed for the channel activity of animal annexin A5. In 2010, a planar lipid bilayer study done with maize annexin (ZmANN33/35, structurally similar to AtANN1) showed it could form a HACC-like conductance when the bilayer was exposed to malondialdehyde (MDA), which is released during oxidative stress and causes lipid peroxidation. This links annexins to ROS production possibly during stress conditions (Laohavisit *et al.*, 2010). The role of AtANN1 as a ROS-activated plasma membrane HACC has been studied by Laohavisit *et al.* (2012). *Arabidopsis thaliana annexin1* loss-of-function mutant (*Atann1*) was unable to sustain a root plasma membrane Ca^{2+}- and K^{+}-permeable conductance in the presence of extracellular hydroxyl radicals, $OH^{\bullet -}$, while the recombinant protein in phospholipid bilayers was able to recapitulate the wild type conductance. AtANN1 is also implicated in mediating Ca^{2+} signalling during oxidative stress by H_2O_2 (Richards *et al.*, 2014). As a ROS-activated channel, AtANN1 is likely to lie downstream of NADPH oxidase activity. Although NADPH oxidase activity depends on Ca^{2+} influx (Demidchik *et al.*, 2009) and calmodulin (CaM) (Hu *et al.*, 2007), no Ca^{2+} channels upstream of NADPH oxidase have been found.

A. thaliana Annexin 2 (AtANN2) has the most similar amino acid sequence and protein structure to AtANN1 and is the second most abundant annexin in *A. thaliana* (Clark *et al.*, 2001). However, there are fewer reports in the literature regarding AtANN2 either in model or crop species. In a previous study, both AtANN1 and AtANN2 localised to highly secretory cell types; this suggests these two functions in growth and development (Clark *et al.*, 2005a). *Atann2* previously showed impaired hypocotyl growth, which was linked to probable function in exocytosis of oligosaccharides (Clark *et al.*, 2001). Clark *et al* (2001) found that both *AtANN1* and *AtANN2* genes were highly expressed in stem and roots respectively of young seedlings suggesting importance in growth and development. Both AtANN1 and AtANN2 also played a role in distribution of sugar in the phloem in seedlings supporting the notion of a role in plant growth (Wang *et al.*, 2018b).

Amino acid alignment by Laohavisit and Davies (2011) showed that AtANN2 contains the salt bridge residues that are crucial for ion transport ability and the diacidic motif for association with the plasma membrane. This could suggest the function of AtANN2 as a calcium channel although no Ca^{2+} conductance study has been done with AtANN2. In a gene

expression study conducted by Cantero *et al.* (2006) however, showing that in almost all abiotic stresses, *AtANN1* was highly up-regulated but *AtANN2* was down-regulated except for when the plant was challenged with heat stress which could be linked to a possible function as a protein regulator.

A. thaliana Annexin 4 (AtANN4) is the most distinct annexin protein compared to AtANN1 and AtANN2. Unlike other annexins, AtANN4 does not have a Ca^{2+} binding motif in its fourth repeat. The protein also lacks the TRP residues and haem binding site that other *A. thaliana* annexins have (Clark *et al.*, 2012). Nonetheless, an expression study showed that *Atann4* is up-regulated under oxidative stress induced by H_2O_2 (Richards *et al.*, 2014). In addition, AtANN4 was found to be operating together with AtANN1 in mediating salt and drought stress despite the differences in the protein structure (Huh *et al.*, 2010). It is also interesting that under heat and oxidative stress, both AtANN1 and AtANN4 shared the same transcriptional regulator AtMYB30 that negatively regulates elevation of $[Ca^{2+}]_{cyt}$ under these stresses (Liao *et al.*, 2017). Recently, AtANN4 was found to be involved in the generation of the salt-induced $[Ca^{2+}]_{cyt}$ signature, raising the possibility of its working as a channel (Ma *et al.*, 2019).

Another member of the *A. thaliana* annexin family, AtANN5 is envisaged to be important in regulating pollen growth and development. According to Zhu *et al.* (2014a), AtANN5 is responsible for endomembrane trafficking that depends on Ca^{2+} influx during pollen germination. Another study also showed that the RNAi lines of AtANN5 plants have impaired male pollen grain compared to the wild type and this is related to the down-regulation of *AtANN5* expression. The complemented line displayed a better pollen growth and recovers the normal phenotype (Zhu *et al.*, 2014b). Subcellular localisation by Lichochka *et al.*, (2018) found AtANN5 to be localised mostly in the nucleus, nucleolus, cytoplasm and plastid nucleoids suggesting possible roles for AtANN5 in the network between plastid and nucleus during reproduction. Similar to AtANN1, *A. thaliana* Annexin 8 (AtANN8) was implicated in salt and osmotic stress. Yadav *et al.* (2016) reported that overexpression of *AtANN8* enhanced seed germination under saline and osmotic conditions as well as increasing the proline content and lowering MDA content in the seedlings. The same study found AtANN8 to localised mostly at the periphery of epidermal cells suggesting possible function in vesicle trafficking and growth.

1.8.6 Candidate putative plasma membrane calcium channels in *Arabidopsis* eATP signalling

The search for encoding genes has revealed that there are plant homologues for animal Cyclic Nucleotide Gated Channels (CNGCs; Talke *et al.*, 2003; Dietrich *et al.*, 2010) and the Glutamate-Like Receptors (GLRs; Lam *et al.* 1998; Kim *et al.* 2001). There are 20 *CNGC* genes in *Arabidopsis thaliana*. CNGCs contain the Cyclic Nucleotide Binding Domain (CNBD) and CaM Binding site. The widely accepted working mechanism of CNGC as a calcium channel is that upon a certain stimulus which increases cGMP or cAMP, the cyclic nucleotide binds to CNBD and causes channel opening for conduction of Ca^{2+} which leads to increase in the $[Ca^{2+}]_{cyt}$. Calmodulin (CaM) as a Ca^{2+} sensor in turn accommodates this Ca^{2+} and binds to the CaM Binding site of CNGC, promoting channel closure and thus terminating the signal. In line with this probable CNGC working mechanism, Fischer *et al.* (2013) mapped the CaM binding site of AtCNGC20 and found it to be at the isoleucine glutamine (IQ) motif. The study found that the binding is specific for CaM and in a Ca^{2+}-dependent manner. A Bimolecular Fluorescence Complementation (BiFC) study also found this interaction occurred at the plasma membrane. However, this model has recently been challenged by the finding that Ca^{2+}-free CaM2 binds to an AtCNGC8/18 complex to promote channel opening but once Ca^{2+} binds CaM2 it dissociates to close the channel (Pan *et al.*, 2019).

CNGCs are implicated in growth, development, abiotic and biotic stress responses. AtCNGC14 is involved in root $[Ca^{2+}]_{cyt}$ increases caused by auxin (Shih *et al.*, 2015) and may underpin the HACC at the apex of root hairs (Zhang *et al.*, 2017a). AtCNGC7 and AtCNGC8 are both expressed in pollen and are needed in order to maintain pollen fertility and this function relies on the cGMP and CaM binding sites (Tunc-Ozdemir *et al.*, 2013a). The same study reported localisation of these two CNGCs at the plasma membrane of the growing pollen tube tip. Another study by Tunc-Ozdemir *et al.* (2013b) reported that AtCNGC16 is important in pollen productivity and germination. Loss-of-function mutant of *Atcngc16* has reduced pollen viability. In the same study, the *Atcngc16* pollen when challenged with thermal stress showed alteration in heat-stress induced gene expression. AtCNGC18 was found also to regulate pollen tube growth (Frietsch *et al.*, 2007). More recently, AtCNGC18 and AtCNGC8 were reported to form a CaM-regulated heterotetramer for pollen tube Ca^{2+} influx (Pan *et al.*, 2019).

AtCNGC6 was discovered to function as a Ca^{2+} channel activated by cAMP under heat stress. Gao *et al.* (2012) demonstrated *via* patch clamping that AtCNGC6 mediates Ca^{2+} influx in heat stress conditions. The authors also showed that the level of cAMP rose under heat stress leading to the increase in Heat Shock Response (HSR) related gene expression. A localisation study done in root tissue showed AtCNGC6 resided at the plasma membrane (Gao *et al.*, 2012). In relation to heat stress, AtCNGC2 and its orthologue in moss CNGCb also play an important role in mediating heat stress responses. Mutants of these CNGCs showed hypersensitivity towards thermal stimulation where the HSR was activated even at tolerable temperature (Finka *et al.*, 2012). Patch clamping done on the CNGCb in moss protoplasts confirmed that three Ca^{2+} channels were involved in conducting Ca^{2+} influx and CNGCb was one of the identified channels (Finka *et al.*, 2012). AtCNGC3 on the other hand might aid Na^+ and K^+ uptake. Expression of *AtCNGC3* in yeast showed the ability to take up Na^+ and K^+. The *Atngc3* mutant also showed higher resistance towards toxic concentrations of NaCl and KCl during germination probably due to inability of the mutant to absorb the ions (Gobert *et al.*, 2006). The same study reported that *AtCNGC3* is mainly expressed at the plasma membrane of the epidermal and cortical cells of root.

Besides heat stress, AtCNGC2 was implicated as the working channel in Pathogen-Activated Molecular Pattern (PAMP) response. Receptor-mediated PAMP recognition triggered the AtCNGC2 to transport Ca^{2+} into the cytosol (Ali *et al.*, 2007). Another study supporting this by Qi *et al.* (2010) showed the peptide elicitor Atpep1 could generate cGMP and caused increase in $[Ca^{2+}]_{cyt}$ depending on AtCNGC2 and the peptide receptor AtPepR1. Recently, AtCNGC2 and AtCNGC4 have been shown to interact to mediate PAMP-induced $[Ca^{2+}]_{cyt}$ elevation (Tian *et al.*, 2019) and AtCNGC19 has been found to be involved in herbivory-induced $[Ca^{2+}]$ increase (Meena *et al.*, 2019).

Ionotropic Glutamate Receptors (iGLR) in mammals are one of the important components in the nervous system. Twenty AtGLR members were first reported by Lam *et al.* (1998). Since then, studies were done on the possible function of these GLRs in signalling systems. Dennison and Spalding (2000) reported that glutamate application could cause membrane depolarisation in wild type of *A. thaliana* and this depolarisation leads to Ca^{2+} influx requiring the GLRs. In an effort to determine whether AtGLRs could permeate ions, Tapken and Holmann (2008) transplanted the ion pore of AtGLR1.1 and AtGLR1.4 into a rat GLR. They reported that both AtGLRs could conduct Na^+, K^+ and Ca^{2+} suggesting the AtGLRs as possible non-selective cation channels. Another member of the 20 GLRs found in

Arabidopsis thaliana is AtGLR3.4. In a loss-of-function study, AtGLR3.4 was demonstrated to have the ability to mediate Ca^{2+} influx and have a high Ca^{2+} permeability. It is also responsive towards glutamate, and its expression was up-regulated by cold and touch stimuli (Meyerhoff *et al.*, 2005). Vincill *et al.* (2012) demonstrated that AtGLR3.4 also could respond to amino acids Asn, Gly and Ser as agonists and produce a conductance in a patch clamp experiment. The same study also found AtGLR3.4 to be expressed mainly in the plasma membrane. Vincill *et al.* (2013) again reported that both AtGLR3.4 and AtGLR3.2 interacted with each other and the proteins mainly localised at the phloem in the sieve plate. The mutant of these *Atglr3.2* and *Atglr3.4* showed disruption in lateral root formation possibly due to inability to perceive amino acids in the apoplast of the phloem (Vincill *et al.*, 2013). GLRs are important in the formation of the pollen tube as the mutant of *A. thaliana Atglr1.2*-1 plants have aberrant tips and tube growth whereas *Atglr3.7-1* plants experienced slower pollen tube growth compared to the wild type (Michard *et al.*, 2011).

flg22, elf18 and chitin as Pathogen Associated Molecular Pattern (PAMP) were reported to be able to cause Ca^{2+} influx possibly involving GLRs in *A. thaliana*. Inhibition of the glutamate binding site impaired the Ca^{2+} influx from the apoplast. One of the downstream responses of these MAMPs perception was the Mitogen Activated Protein Kinase (MAPK) activation, also was affected by the inhibition of glutamate binding site in the study (Kwaaitaal *et al.*, 2011). This reflects findings from tobacco suspension cells challenged with Cryptogein (which is an elicitor of defence responses in plants). This elicitor induced exocytotic release of glutamate and activation of NO production. Glutamate caused $[Ca^{2+}]_{cyt}$ elevation and NO production that could be inhibited by antagonists of animal GLRs, suggesting the role of GLRs in defence response (Vatsa *et al.*, 2011). Stronger evidence has come from the *Atglr3.3* mutant which may be involved in $[Ca^{2+}]_{cyt}$ elevation and NO production in response to challenge with oligogalacturonides which are cell wall break down products associated with pathogen attack (Manzoor *et al.*, 2013).

Leaf wounding (which can include herbivory) releases glutamate and causes a local $[Ca^{2+}]_{cyt}$ elevation (Kiep *et al.*, 2015; Vincent *et al.*, 2017) and a vascular $[Ca^{2+}]_{cyt}$ wave that signals to other leaves to evoke a transcriptional response (Kiep *et al.*, 2015; Nguyen *et al.*, 2018; Toyota *et al.*, 2018). The local $[Ca^{2+}]_{cyt}$ increase and wave involve AtGLR 3.3 and AtGLR3.6 (Kiep *et al.*, 2015; Vincent *et al.*, 2017; Nguyen *et al.*, 2018; Toyota *et al.*, 2018). However, it is unclear whether the GLRs work at the plasma membrane (Toyota *et al.*, 2018) or in endomembranes (Nguyen *et al.*, 2018).

1.9 Aims and experimental approaches

AtDORN1 was firmly implicated as the receptor that is responsible for the elevation of $[Ca^{2+}]_{cyt}$ by the eATP signal (Choi *et al.*, 2014b). Figure 1.4 showed the current eATP signalling pathway under the DORN1 purinoreceptor based on the studies published to date. Chen *et al* (2017) demonstrated the direct interaction and phosphorylation between AtDORN1 and AtRBOHD, showing that AtDORN1 might be the receptor that mediates the increased ROS during eATP signalling in roots. Previous work by Foresi *et al.* (2007) showed that NO synthesis downstream of eATP required the increase of $[Ca^{2+}]_{cyt}$. Similar to NO, NADPH Oxidase also needs $[Ca^{2+}]_{cyt}$ (Demidchik *et al.*, 2009) to generate extracellular ROS in the signalling pathway. However, $[Ca^{2+}]_{cyt}$ accumulation could also be induced by ROS and NO making the relationship between these early eATP signalling components more complex. The identities of the Ca^{2+} channels upstream or downstream of ROS production and during eATP signalling are unknown.

Besides being a DAMP signal, eATP was also released into the extracellular matrix upon touch or wind stimulus, salinity stress, osmotic stress, oxidative stress and PAMP elicitation. These results suggest the possibility of eATP as an early signal molecule upstream that governs the plant stress response. The main questions behind this PhD thesis are: 1. What are the Ca^{2+} channels that help mediate the $[Ca^{2+}]_{cyt}$ accumulation after the eATP signal? 2. Is the Ca^{2+} channel involved in mediating eATP $[Ca^{2+}]_{cyt}$ increase also involved in abiotic or biotic stress responses?

In relation to the first question of this project, AtANN1 is hypothesised as the probable Ca^{2+} transporter possibly acting downstream of AtDORN1 receptor and the ROS production. Unpublished work by the Davies laboratory has shown that AtANN1 could be operating with other Ca^{2+} channel proteins to elevate free Ca^{2+} during eATP signalling (Shang *et al.*, unpublished). Demidchik *et al.* (2009) and Wang *et al.* (2019) showed the eATP induced $[Ca^{2+}]_{cyt}$ increase involved the action of HACC and AtANN1 was found to be a ROS-activated HACC under salinity stress (Laohavisit *et al.*, 2012). Previously, AtANN1 protein was found to have the ability to interact with AtANN4 in response to osmotic and drought stress (Huh *et al.*, 2010). Other than AtANN4, AtANN2 is a putative plasma membrane channel protein as it has structural similarities to AtANN1. Both AtANN1 and AtANN2 were down-regulated during oxidative stress (Richards *et al.*, 2014) and are involved in mediating heat stress (Wang *et al.*, 2015). Thus, this study will also look into the

probability of AtANN2 and AtANN4 alongside AtANN1 in mediating the $[Ca^{2+}]_{cyt}$ increase under eATP signalling. As for the second aim to look at possible relationship between eATP signalling and stress signalling in *A. thaliana*, we hypothesised that AtANN2 might be involved in stress responses particularly salinity stress and PAMP-elicitation that is envisaged to be governed by eATP, given that AtANN2 may play a role in mediating the $[Ca^{2+}]_{cyt}$ increase in the eATP signalling pathway. To date, not many studies were done on AtANN2's role in stress responses in plants.

Overall, the working hypothesis of this PhD thesis is as shown in Figure 1.4: eATP released upon exposure towards stimuli is perceived by the AtDORN1 purinoreceptor, which could directly interact with and phosphorylate AtRBOHD leading to the production of ROS at the intercellular space. AtRBOHD could also be activated by $[Ca^{2+}]_{cyt}$ influx through unknown Ca^{2+} channels. ROS produced would then activate another Ca^{2+} channel possibly AtANN1 that might form an oligomer or work together with AtANN2 and AtANN4 as Ca^{2+} channels that mediate the $[Ca^{2+}]_{cyt}$ accumulation. Jewell *et al*. (2019) found that most of the eATP-induced genes contain the CAM-box motif which suggests that CAMTA is an important component that connects Ca^{2+} as a secondary messenger to the changes in transcription due to eATP. Decoding of this $[Ca^{2+}]_{cyt}$ increase would then lead to downstream responses such as activation of eATP-induced gene expression and alteration in growth and development.

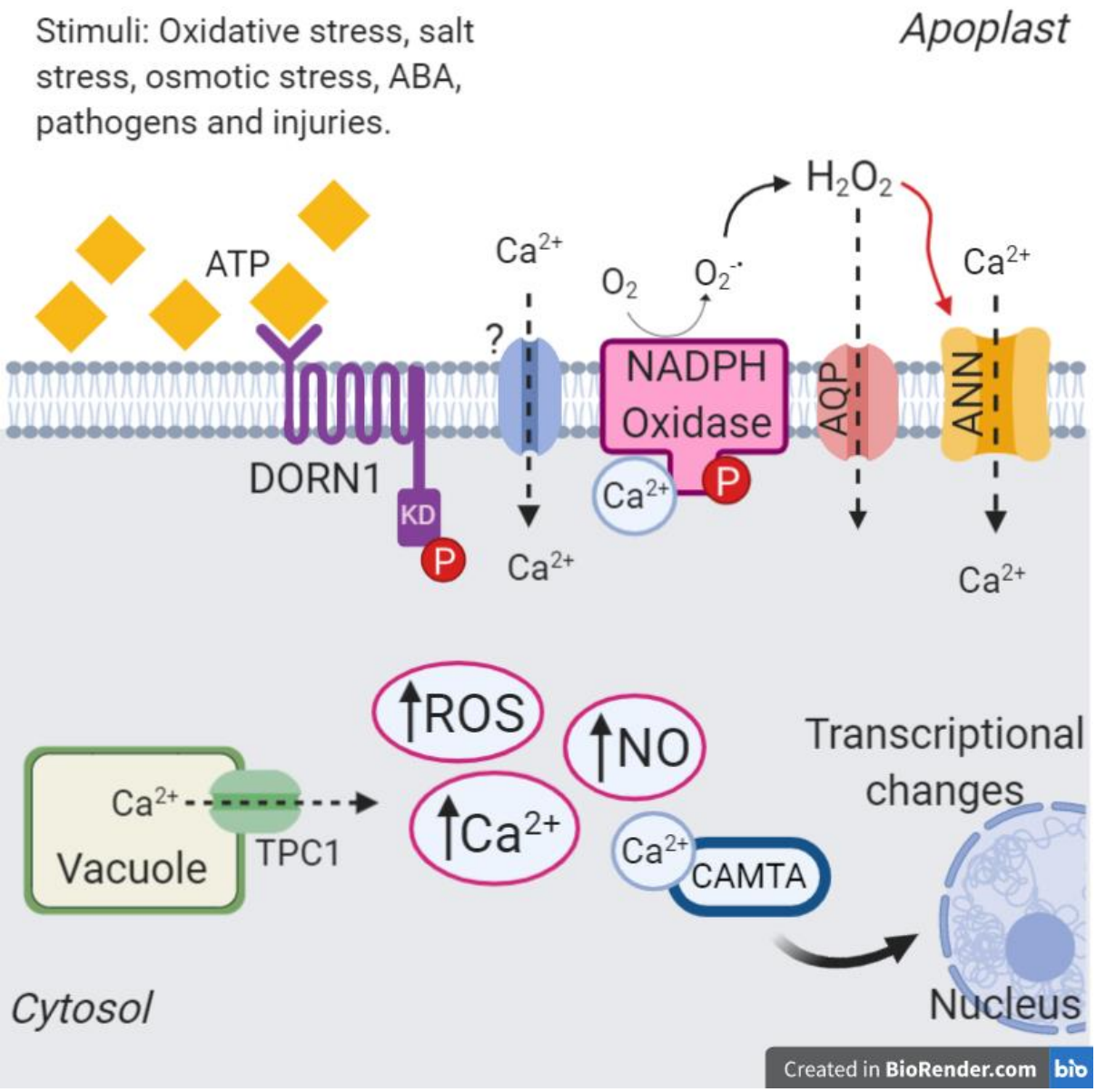

Figure 1.4: Extracellular ATP signalling pathway with AtANNs as the candidates for the Ca^{2+} channels involved. This model is based on previous studies when plants are exposed to different environmental stimuli. AtDORN1 as the purinoreceptor received the ATP at the extracellular domain. Kinased domain (KD) of AtDORN1 is important in the activation of downstream responses such as ROS production by NADPH Oxidase (encoded by AtRBOHD), NO production, accumulation of $[Ca^{2+}]_{cyt}$ by unknown Ca^{2+} channels (upstream of ROS production) and accumulation of $[Ca^{2+}]_{cyt}$ downstream of ROS hypothesised to be by AtANNs. These eventually lead to the changes in transcriptional response mediated possibly by CAMTA.

Chapter 2

Materials and Methods

2.1 Plant materials and growth conditions

The *annexin 1* (*Atann1*) knock-out mutant was from the Columbia (Col-0) wild type line where it was mutated *via* T-DNA insertion at the third exon; complementation using the 35S promoter generated the *Atann1/ANN1* line (Lee *et al.*, 2004). Both lines were obtained from Dr. Ohkmae Park (Korea University, Seoul). The *Atann1* line expressing the (apo)aequorin protein cytosolically under the 35S promoter was as described by Laohavisit *et al.* (2012). The *Atdorn1-1* (single point mutation) and *Atdorn1-3* (SALK 042209) containing aequorin construct were a gift from Prof. Gary Stacey (University of Missouri). Seeds of the *Atann2, Atann1,2*, *Atann1,4*, and *Atann1,2,4* putative homozygous mutant plants expressing (apo) aequorin protein in the cytosol under the 35S promoter were produced by Siân Richards and Dr. Katie Wilkins, University of Cambridge, UK. The *Atfls2* mutant seeds were the progeny of the generous donation from Prof. Dr. Silke Robatzek (Ludwig-Maximilian University of Munich). All of the mutants were of the ecotype Columbia (Col-0) background and mutations were via *Agrobacterium*-mediated T-DNA insertion except for the *Atdorn1-1*.

Seeds were first washed in 1 ml of 70 % (v/v) EtOH and 1 ml distilled water before further sterilization was carried out by shaking the seeds in seed sterilising solution (10 % (v/v) sodium hypochlorite; 0.05 % (v/v) Triton-X; sterilised distilled water) for 5 minutes at

1250 rpm (20°C). After the seed sterilising solution was discarded, the seeds were rinsed thoroughly with sterilised distilled water for 5 times. Seeds were then sown on a half-strength Murashige-Skoog (MS; Duchefa Biochemie) medium (0.8 % (w/v) Bactoagar, BD Diagnostics VWR; pH 5.6 with 0.1 M KOH) in square petri dishes (12 cm x 12 cm, Greiner Bio-One) and incubated in the dark at 4 °C for stratification. After 2 days of stratification, the seeds were transferred into a 23 °C growth chamber (PERCIVAL, CLF Plant Climatics) with 16 hours photoperiod (80 μmol m^{-2} s^{-1}) and were left to grow in a vertical position (for excised root experiments) or horizontal position (for whole leaves or seedlings experiments) for a certain period of growth depending on the experiment.

2.1.1 Seed production and plant propagation

For seed production and propagation, selected 10 to 14-day-old seedlings were transferred into and grown in Levington's F2 compost containing vermiculite and 0.2 g/l fungicide (Intercept 70 WG) for 8 to 10 weeks at the Plant Growth Facility (16 hours photoperiod, 200 μmol m^{-2} s^{-1} light level). The mature plants were then left to dry without watering for approximately 2 weeks before the seeds were harvested.

2.2 Bacterial transformation by using heat shock

Transformation was done by mixing bacteria and desired solution (DNA construct) before being cooled down on ice for 30 minutes. The mixture was then applied to heat treatment by incubating at 42°C for 45 s. Then 900 μL of SOC media solution (Super Optimal broth with Catabolite repression) (0.5% Yeast extract,Oxoid; 2% Tryptone, Oxoid; 10 mM NaCl, Sigma-Aldrich; 2.5 mM KCl, VWR Chemicals BDH; 10 mM $MgCl_2$, VWR Chemicals BDH; 10 mM $MgSO_4$, Fisher Scientific; 20 mM glucose, Sigma-Aldrich) was immediately added into the mixture. The mixture was quickly put on ice and incubated for another 2 minutes. Finally the mixture was left to further incubate at 37°C for 1 hour with shaking. After the incubation was done, the mixture was plated onto LB media (1% Tryptone, Oxoid; 0.5% Yeast extract, Oxoid; 1% NaCl, Sigma-Aldrich) with the appropriate antibiotic for selection of successful transformants.

2.3 Floral dip transformation with 35S::Aequorin

Floral dip transformations of *Atann1*, *Atann2*, *Atann1/2*, *Atann1/4* and *Atann1/2/4* were previously carried out by Dr. Katie Wilkins, University of Cambridge. The plants (*Atann2.2*, *Atann4* and the Col-0 pair) that were going to be used for the floral dipping were

grown at the plant growth facility in the soil (type of soil as described in section 2.1.1) until the first primary bolt emerged (about 4 -5 weeks). The primary bolt was cut and the plants were left to grow the secondary bolt for 5 days. The *Agrobacterium* culture containing the CaMV 35S aequorin construct was acquired from Prof. Alex Webb, University of Cambridge. The CaMV 35S aequorin-containing *Agrobacterium* was prepared by growing 200 µL of the culture in 5 mL LB medium (1% Tryptone, Oxoid; 0.5% Yeast extract, Oxoid; 1% NaCl, Sigma-Aldrich) containing antibiotics (50 µg/mL Kanamycin; Sigma-Aldrich, USA and 50 µg/mL Gentamycin; Melford, UK) overnight at 30°C with shaking (150 rpm). The next day, 500 µL of the culture were inoculated into 200 mL LB medium containing 50 µg/mL Kanamycin and 50 µg/mL Gentamycin in a 1000 mL flask and left to grow overnight (30 °C, 150 rpm). The culture was then centrifuged at 3000 rpm for 20 minutes (18 °C). Pellets formed were air-dried and re-suspended in 1 mL 5 % (w/v) sucrose, 0.05 % (v/v) silwet L-77 (Lehle Seeds, USA) in sterilised distilled water. The re-suspended solution (400 µL) was then dissolved into 50 mL of the sucrose/silwet solution.

Before the dipping process was carried out, fertilised flowers and siliques that were already developing were cut from the plants. Then, the plants were carefully dipped into the sucrose/silwet solution containing the *Agrobacterium* carrying the aequorin construct for at least 5 minutes. A brush was also used to paint some parts of the plants with the *Agrobacterium* solution that were not covered during the dipping, especially the base of the plants and the flowering organs. The plants were then covered with plastic and sealed to maintain humidity. The seal was opened after two days. The plants were irrigated once a week and left to grow until the seeds matured for harvesting.

2.4 Genomic DNA Extraction for mutant screening

Samples for DNA extraction (healthy leaves) were taken from each of the mutant (7 - 14-day-old) plants and were immediately flash frozen in liquid Nitrogen. The samples were quickly ground to a powder by using a micro pestle. Extraction buffer (400 µl of 1 M Tris; 1 M NaCl; 0.5 M EDTA; 10 % (w/v) SDS) was added to each sample followed by vigorous vortexing to break the cells further. The DNA was then separated from the proteins and other components through centrifugation at full speed (13000 rpm) for 7.5 minutes. Ice-cold isopropanol (300 µL) was added to 300 µL supernatant from each sample in a clean Eppendorf tube and was centrifuged again at full speed for 5 minutes to precipitate the DNA. The DNA pellet formed was air-dried and re-suspended with 25 µL sterilised distilled water. The entire extracted DNA was stored at -20 °C.

2.5 Screening for homozygous mutant plants

Screening for the successful T-DNA insertion mutation for each mutant (single, double or triple mutant) was carried out to make sure that the T_3 progeny of the mutant plants (both aequorin and non-aequorin containing) were homozygous before further experiments were conducted. A simple way of screening is genotyping through Polymerase Chain Reaction (PCR). This method uses two sets of primers, in which the first set is designed to complement with *Arabidopsis thaliana* wild-type plant (native gene-specific forward and reverse primer) whereas the second set matches with the sequence of the T-DNA insert in the mutant plant (native gene-specific forward primer and T-DNA insert LB1.3 reverse primer) as in Table 2.1. Annexins native gene-specific primers were designed by Sian Richards, University of Cambridge whereas the DORN1 native gene primer sequence were obtained from Choi *et al.* (2014b). LB1.3 reverse primer sequence was obtained from the SALK institute. Specificity and the approximate size of PCR product from each primer pair was assessed by using the NCBI Primer-BLAST (https://www.ncbi.nlm.nih.gov/tools/primer-blast/).

Each of the 25 μL PCR reaction mix consisted of forward and reverse primers (2.0 μL), genomic DNA template (2.0 μL), dNTPs mix (0.4 μL), Reaction Buffer (Taq Buffer containing NH_4SO_4 and $MgCl_2$; 2.0 μL) and Taq DNA Polymerase (Bioline; 0.5 units). The PCR was carried out for 30 cycles and each pair of primers used was assigned to different optimum annealing temperature (Table 2.2). The genotyping PCR products were visualised through gel electrophoresis (1% (w/v) Agarose gel, 1 X TAE buffer) at 100 V (400 mA) for 50 minutes and the size of DNA on all gels was determined by using 100 bp HyperLadder DNA ladder (100 bp - 1013 bp range; Bioline).

Atdorn1-1/ann1 double mutant plants contain point-mutation at the kinase site of the *AtDORN1* gene and also contain the T-DNA insert at the *AtANN1* gene. Screening for homozygous mutation at both of the genes were carried out by amplifying the point-mutation containing sequence of the *AtDORN1* gene through PCR by using the KW13 primer pair (obtained from Dr. Katie Wilkins, University of Cambridge). The PCR products was then purified by using the QIAquick PCR purification kit (Qiagen) before being sent for Sanger sequencing. The sequencing was done at the Source BioScience sequencing service (U.K). Kinase site sequence obtained then subjected to sequence alignment and comparison between Col-0 wild type plants and the *Atdorn1-1/ann1* mutant plants kinase site was done to confirm

the point mutation. Alignment was carried out by using the Pairwise Sequence Alignment tool provided by the EMBL-EBI (https://www.ebi.ac.uk/Tools/psa/)

Table 2.1: The different pairs of primer sequence used for mutant screening. *AtANN1, AtANN2, AtANN2.2, AtANN4, AtDORN1* gene-specific forward primers paired with T-DNA insert LB1.3 reverse primer were used to detect homozygous mutants for *Atann1, Atann1/2, Atann1/4, Atann1/2/4, Atdorn1-1/ann1* and *Atdorn1-3/ann1*. KW13 forward and reverse primers were used to amplify specific sequence of *AtDORN1* gene, which contain the kinase component of the gene. Gene-specific forward and reverse primers were used to screen for wild-type plants.

Gene	Forward (5' – 3')	Reverse (3' – 5')
AtANN1	TGAGCGTGATGCTTTATTGG	TGCTCCTTCATCAGTTCCAG
AtANN2	CACACATCTGGTGACCTTCG	TTGCAGAACCAGTTTCACAAC
AtANN2.2	GTTTTTTGGGTTTGGTCTGA AACAGG	TTGCAGAACCAGTTTCACAAC
AtANN4	ACTGCGGTGGTGATGTGGGC	CGGATTTGGAGAGAAGTGTGAGC AA
AtDORN1	TCCATGCAACAGTTGCGTTG TCT	CTGCAATACCCAAACAGTGGTA
AtDORN1 (KW13)	TTCATGAGCACGGAGGCAAT	ATTGTCTGTCCCCATGGCTG
Lb1.3		ATTTTGCCGATTTCGGAAC

Table 2.2: The PCR parameters used for the genotyping of T3 homozygous mutants of *Atann1/2, Atann1/4* and *Atann1/2/4*. Different optimum annealing temperature was used for *AtANN1*, *AtANN2* and *AtANN4* gene-specific primers.

PCR Steps		Temperature (°C)	Time (minutes)
Initial		94.0	2.0
Denaturation		94.0	0.5
Annealing	*AtANN1*	61.0	0.5
	AtANN2	64.0	
	AtANN2.2	64.0	
	AtANN4	61.0	
	AtDORN1	61.0	
	AtDORN1 (KW13)	61.0	
Extension		72.0	2.0
Final		72.0	11.0

Aequorin-containing seedlings (*Atann1, Atann2, Atann1/2, Atann1/4, Atann1/2/4, Atdorn1-1/ann1* and *Atdorn1-3/ann1)* that were confirmed to be homozygous mutants from the genotyping were screened again for the ability to produce a clear luminescence signal

from aequorin upon stimulation with calcium discharge solution as in section 2.6.2 by using leaf samples. Selected seedlings that were confirmed to be homozygous mutants and had a good luminescence signal (above 2 million counts) were then grown for seed production as described in section 2.1.1. Confirmed homozygous mutant seedlings that were not yet transformed with (apo)aequorin reporter (*Atann2.2* and *Atann4* with Col-0 pair) were grown at the Plant Growth Facility and assigned to floral dip transformation with 35S::aequorin as explained in section 2.3.

2.6 Measurement of $[Ca^{2+}]_{cyt}$ by using a plate reader

2.6.1 Coelanterazine incubation of samples and recording of luminescence

A. thaliana aequorin-expressing samples (individual whole seedlings, whole leaves, whole roots or 1 cm excised root tips; age of sample depends on the type of experiments as in chapter 2.6.3, 2.6.4, 2.6.5, 2.6.6, 2.6.7) were first incubated in 100 µL of control solution (2 mM Bis-Tris Propane; 10 mM $CaCl_2$; 0.1 mM KCl, pH 5.8 adjusted by using 1 M Bis-Tris Propane and 0.5 M MES) containing 10 µL coelanterazine (10 µM; Nanolight Technology) overnight in the dark at room temperature in a 96-well plate (Greiner Bio-One). All the samples were washed with coelanterazine-free control solution before any luminescence measurement was taken and then placed (as individual samples) into a 96-well plate containing 100 µL fresh control solution. Luminescence (as an output of free cytosolic calcium ion, $[Ca^{2+}]_{cyt}$) upon different treatments and control was measured by using a FLUOstar OPTIMA (BMG Labtech) plate reader. All the treatment solutions were prepared with the control solution and adjusted to pH 5.8 (1 M Bis-Tris Propane and 0.5 M MES) prior to measurement. After 35 seconds of initial background measurement, 100 µL of treatment solution was injected and the luminescence signals produced were continuously measured. Period of measurement varies according to the setup of the experiments (refer to section 2.6.3, 2.6.4, 2.6.5, 2.6.6 and 2.6.7). At the end of each measurement, 100 µL discharge solution (10% (v/v) ethanol; 1 M $CaCl_2$) was added to quench the total (apo)aequorin luminescence in each sample.

2.6.2 Aequorin luminescence discharge screening

Discharge screening was carried out to make sure that the total (apo)aequorin discharge from the seeds used would be comparable to each other during experiments. This screening method was also used to make sure the plants that were transformed with 35S CAMV aequorin construct produced high luminescence signal before being propagated into

the next generation for stable line production. Excised leaves (10 - 12 days old) were incubated with coelanterazine as in section 2.6.1. Discharge solution (100 µL of 10% (v/v) ethanol; 1 M $CaCl_2$) was added after the first 15 seconds of luminescence recording followed by continuous measurement for another 60 seconds. The sum of all luminescence from each line of seed was calculated and the mean of the total luminescence was used for comparison with other lines of seeds. For propagation purpose, seedlings that were confirmed to have good discharge values were grown in the soil at the PGF as described in chapter 2.1.1.

2.6.3 Tests of response to ATP, ATPγS, ADP, ADPβS

ATP (Adenosine-5'-triphosphate, disodium salt trihydrate) and ADP (Adenosine-5'-diphosphate, disodium salt dihydrate) were purchased from Melford Laboratories Ltd whereas non-hydrolysable analogues ATPγS (Adenosine 5'-[γ-thio] triphosphate tetralithium salt and ADPβS (Adenosine 5'-[β-thio] diphosphate trilithium salt) were purchased from Sigma-Aldrich. The ATP, ADP and the non-hydrolysable analogues treatment solutions were prepared with the control solution (2 mM Bis-Tris Propane; 10 mM $CaCl_2$; 0. 1mM KCl, pH 5.8) freshly on the day of the experiment. Addition of 4 mM LiCl or 3 mM LiCl (Sigma-Aldrich) (prepared in control solution) was carried out as a control for the LiCl salt present in the ATPγS and ADPβS salts respectively. Samples (7-day-old whole roots or 1 cm excised root tips) were incubated with coelanterazine a day before as explained in 2.6.1. Measurements for each treatment were taken for 200 seconds where the first 35 seconds were the background measurement and the discharge solution was added at the 155th second.

2.6.4 Gadolinium chloride ($GdCl_3$), suramin, and PPADS inhibitor tests

Samples (7-day-old root tips) were prepared and incubated in coelanterazine solution overnight as explained in 2.6.1. Thirty minutes prior to measurement, the samples were soaked in control solution (2 mM Bis-Tris Propane; 10 mM $CaCl_2$; 0.1 mM KCl, pH 5.8), 0.5 mM $GdCl_3$ solution (Sigma-Aldrich, prepared in control solution) or 1.5 mM suramin (Sodium salt; Cayman chemical, prepared in control solution) in the 96-well plate. After the 30 minutes incubation, luminescence recordings were taken for 200 s with addition of 0.5 mM ATP or ADP (prepared in control solution) treatment at the 35th second and the discharge solution was added at the 155th second.

2.6.5 Sodium chloride (NaCl) and sorbitol test

400 mM NaCl stock (Sigma-Aldrich) was prepared in control solution (2 mM Bis-Tris Propane; 10 mM $CaCl_2$; 0.1 mM KCl, pH 5.8). Samples (7-day-old whole seedlings or whole roots) were incubated a day before the $[Ca^{2+}]_{cyt}$ measurements carried out (section 2.6.1). 800 mM sorbitol stock (Sigma-Aldrich) in control solution was used as an osmotic control for the NaCl tests. Treatment (100 µL) was added at the 35th second into individual well already containing 100 µL control solution making the final concentration of NaCl and sorbitol to be 200 mM and 400 mM respectively. Measurements were taken for 200 seconds with discharge solution injected after 155 seconds.

2.6.6 Hydrogen peroxide (H_2O_2) test

Hydrogen Peroxide (10 mM; H_2O_2, Sigma-Aldrich) treatment was prepared in the control solution, pH 5.8. Coelanterazine incubation of the samples (7-day-old whole roots) was carried out as explained in section 2.6.1. After 35 s of background measurement of luminescence (1 s per interval), 100 µL of the 10 mM H_2O_2 treatment was added (5 mM final concentration). The luminescence recordings were taken for 1290 s (6 s per interval). Discharge solution (100 µL) was added after 1290 s to obtain the total (apo)aequorin luminescence.

2.6.7 Flagellin 22 (flg22) test

Flagellin22 (flg22) was obtained from EZBiolab (Amino acid sequence: QRLSTGSRINSAKDDAAGLQIA). Seven-day-old whole seedlings were incubated in coelantrazine as described in section 2.6.1. Stock solution of flg22 (2 µM) was prepared freshly with control solution (pH 5.8). After 35 s of background measurement of luminescence (1 s per interval), flg22 (100 µL of 2 µM stock, 1 µM final concentration) was added at the 35th second of measurement and the discharge was carried out at the end of the measurement. Recordings were carried out for another 1290 seconds (6 s per interval). Loss-of-function mutant of the flg22 receptor in *A. thaliana Atfls2* was also used as a sample alongside the sample of interest and the wild type Col-0 as a control for the flg22 perception.

2.6.8 Determination of $[Ca^{2+}]_{cyt}$

Concentration of $[Ca^{2+}]_{cyt}$ was determined by subtracting the background luminescence signal and then dividing by the overall luminescence signal according to the calibration formula of Knight *et al.* (1997):

$$-log[Ca^{2+}]_{cyt} = 0.3326 \times (-log\ k) + 5.5593$$

where k is the luminescence count minus the background divided by the total luminescence of the recording.

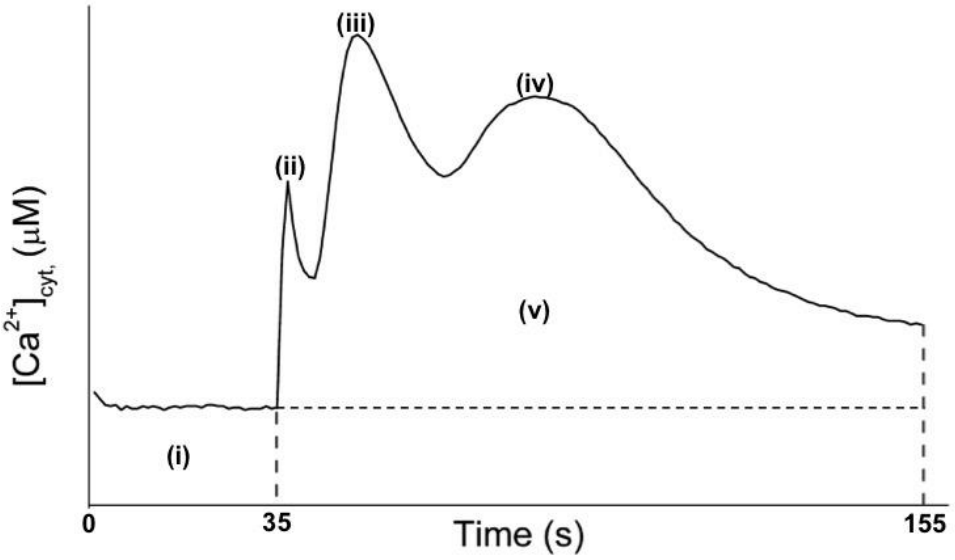

Figure 2.1: **Different section of data analysis of the time course of $[Ca^{2+}]_{cyt}$ changes.** Each section is calculated with the average baseline value (i) subtracted. Touch peak is the highest value of the touch response due to the mechanical stimulus from the treatment injection (ii). First peak (iii) and the second peak (iv) are the highest value of each peak. Total $[Ca^{2+}]_{cyt}$ accumulation (v) is obtained from the area under the curve.

The time course data for a biphasic $[Ca^{2+}]_{cyt}$ signature was analysed after subtraction of the pre-stimulus baseline (i), then split into touch peak (ii) caused by mechanical disturbance, first peak (iii), second peak (iv) and the overall area under the curve (v) (Figure 2.1). The first peak and the second peak are the highest points of the peaks formed after the touch peak. The total $[Ca^{2+}]_{cyt}$ measured was represented by the area under the curve minus the $[Ca^{2+}]_{cyt}$ basal level (v).

2.7 Germination assays

Germination assay was performed by assessing the germinated seeds grown on either control medium or treatment-containing medium. The seeds were observed everyday under a Leica M165 FC stereomicroscope and the percentage of germinated seeds was calculated every day for 9 days. The formula that was used to calculate the percentage of germinated seeds was as follows:

$$Percentage\ of\ germination\ (\%) = \frac{Number\ of\ germinated\ seeds}{Total\ number\ of\ seeds\ tested}\ per\ day$$

2.7.1 Germination on ATP-containing medium

The test was carried out on three different types of media; ½ MS control medium, ½ MS medium containing 1 mM ATP or ½ MS medium containing 2 mM NaCl (as a control for the Na^+ in the ATP test). Half MS medium (780 mL, see section 2.1) with 0.8 % (w/v) bactoagar (pH 5.6) was prepared and autoclaved as the base of all the three treatments. For the ATP-containing medium, 20 mL of 40 mM ATP prepared in autoclaved ½ MS solution (pH 5.6 with 0.5 M MES without agar) was added to slightly cooled base medium prepared earlier. The ATP containing growth medium was stirred slowly before being poured into square plates. For control medium, 20 mL ½ MS solution without ATP was added to 780 ml of the growth medium, whereas 20 mL of 80 mM NaCl solution prepared in ½ MS solution was added to the base medium to prepare the 2 mM NaCl growth medium. The seeds tested were sterilised as explained in section 2.1.

2.7.2 Germination on high salinity growth medium

This test was carried out to determine the effect of high salinity on the germination rate of the seeds. NaCl-containing growth medium was prepared (200 mM NaCl, ½ MS, 0.8 % (w/v) bactoagar, pH 5.6) and autoclaved. Medium with 400 mM Sorbitol (½ MS, 0.8 % (w/v) bactoagar, pH 5.6) was also prepared as an osmotic control to the NaCl treatment. Control growth medium (½ MS, 0.8 % (w/v) bactoagar, pH 5.6) was prepared for comparison of germination percentage. Sterilisation and sowing of the seeds was carried out as in section 2.1.

2.8 Root System Architecture measurements and fresh mass

2.8.1 Growth media and sample preparation

All seeds were sterilised as explained in section 2.1. Seeds were first germinated on control growth medium (½ MS, 0.8 % (w/v) bactoagar, pH 5.6) and stratified for 2 days in the dark before moving to the growth cabinet (16 hours photoperiod ; 80 μmol m^{-2} s^{-1}). After three days, each seedling was carefully transferred onto the assigned treatment plates and left to grow vertically in the growth cabinet for 6 more days. The ATP- and NaCl-containing growth media were prepared as in section 2.7.1 and 2.7.2 respectively. flg22-containing growth medium (1 µM flg22 final concentration) without sucrose was prepared with ½ MS,

0.8% (w/v) bactoagar (BD Diagnostics VWR) (pH 5.6). flg22 (EZBiolab) was added (181 µL of 2.2 mM flg22 stock to 398.2 ml medium) after autoclaved medium had cooled and then the medium was mixed slowly with a magnetic stirrer.

2.8.2 Primary root length and lateral root density

The plates containing seedlings from different genotypes were scanned by using an Epson Perfection V300 Photo scanner with 300 dpi resolutions. Image J programme was first used to convert the scanned picture from coloured (.tif) file into gray-scale (8bit.tif) format (Meijering *et al.*, 2004). The new format images were then uploaded into Neuron J, a plugin of Image J (Abràmofff *et al.*, 2005). Traces of the primary root length of all the seedlings were measured in cm by using the Neuron J programme. Then, the number of lateral roots formed for each seedling was counted and the density was calculated as:

$$Lateral\ root\ density\ = \frac{Number\ of\ lateral\ root}{Primary\ root\ length\ (cm)}$$

2.8.3 Horizontal growth index (HGI) and degree of root skewing

Horizontal growth index (HGI) was used to determine the direction of root skewing either to the right or to the left from the initial point and calculated by using the formula:

$$Horizontal\ Growth\ Index = \frac{L_x}{L},$$

where L_x is the horizontal displacement of the root tips (abscissa value) and L is the primary root length in pixel (Grabov *et al.*, 2005). L_x was obtained from the vertex value generated by the ImageJ software.

The degree of skewing was determined through measuring the angle of root growing horizontally away from the ideally straightened root:

$$cos\ \beta = \frac{L_y}{L_c}$$

$$\beta = (\cos^{-1})\frac{L_y}{L_c}$$

where L_y is the vertical displacement of the straightened root (ordinate value) obtained from the y-vertex value generated by ImageJ software. L_c is a straight-line length from initial point

of measurement towards the end of the root tips. L_c is obtained from the vertices measurement of both x and y using the formula $L_c = \sqrt{(L_y^2 + L_x^2)}$ (Grabov *et al.*, 2005).

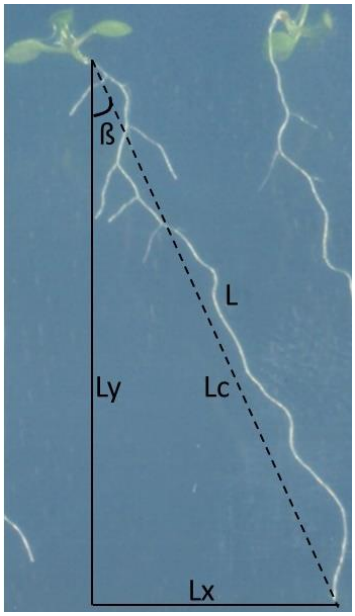

Figure 2.2*:* **Measurement of root skewing**. Primary root length, L is the length of the whole root whereas L_c is a straight line between the initial points of measurement to the end of the root tip. L_y and L_x are the ordinate and the abscissa values of the root respectively. β is the degree of the root skewing away from the vertical line.

2.9 Quantification of Reactive Oxygen Species (ROS)

2.9.1 eATP-induced intracellular ROS measurement

Intracellular ROS measurement was carried out by using the intracellular ROS probe CMH_2DCFDA (chloromethyl-2',7'-dichlorodihydrofluorescein diacetate; Invitrogen), dissolved in dimethysulphoxide (DMSO) to give a stock solution of 10 mM. Seven-day-old Col-0 and *Atann1* (5 - 8) whole roots were incubated in 100 µL Low Salt Medium (LSM) solution (Table 2.3) (Hong *et al.*, 2013), containing 20 µM CMH_2DCFDA in a 6-well plate (Greiner Bio-One) for 1 hour at 4°C. The plate was covered with aluminium foil to ensure that the roots were not exposed to light during the probe loading as the dye is light sensitive. After 1 hour, the roots were placed onto growth medium (½ MS, 0.8 % (w/v) bactoagar, pH 5.6) and were left to acclimatise at room temperature for another hour in the light.

Roots were then observed under a Leica Stereo M205FA microscope with both bright field and GFP filter (excitation 450 - 490 nm; emission 500 - 550 nm) under the Z stacks option which allowed the roots to be observed under bright field and GFP filter over a period of time continuously. Control treatment (LSM) or 1 mM ATP treatment (prepared with LSM

as background solution) was added after the first 35 seconds and the measurements of the fluorescence intensity were carried out for 12 minutes with 6 seconds interval for each image taken. The images were subjected to the Fiji ImageJ image processing package where fluorescence intensity value for each root was measured and generated. Measurement of fluorescence intensity from each root images obtained was carried out by tracing the length of each root zone along the centre of the root (line width = 10), the upper part and the lower part of the root highlighting the overall zone using ImageJ software. Then, the 'Plot Profile' function in ImageJ (Reyt *et al.*, 2015) was used to generate the fluorescence intensity values based on the tracing.

Table 2.3: Composition of Low Salt Medium (LSM). The macro and micro elements contained in the LSM with the final concentration used in the experiment.

Macro elements	**Final concentration**
Potassium nitrate, KNO_3	1.25 mM
Calcium nitrate, $Ca(NO_3)_2$	2 mM
Magnesium sulphate, $MgSO_4$	0.75 mM
Potassium dihydrogen phosphate, KH_2PO_4	0.5 mM
Micro elements	**Final concentration**
Boric acid, H_3BO_3	50 μM
Manganese (II) chloride, $MnCl_2$	10 μM
Zinc sulphate, $ZnSO_4$	2 μM
Copper sulphate, $CuSO_4$	1.5 μM
Ferric EDTA, FeEDTA	75 μM
Ammonium molybdate, $(NH_4)_6Mo_7O_{24}$	0.075 μM

2.9.2 flg22-treated extracellular ROS measurement

Leaf discs from 3-week-old Col-0, *Atann2* and *Atfls2* were prepared a day before by using a small puncher. The leaf discs were incubated in 8 mL sterilised distilled water (SDW) in small petri dishes for 2 hours with the SDW replaced every 30 minutes. After 2 hours, each disc was placed in a 96-well plate containing 200 μL SDW, covered with aluminium foil and left overnight at room temperature. The next day, the SDW in the 96-well plate was replaced

with 200 µL 1.25X final concentration Luminol (Sigma-Aldrich) and 1.25X final concentration Horseradish Peroxidase (HRP; Sigma-Aldrich) mixture prepared in SDW and left to rest in the plate reader for 20 minutes. This was done carefully using forceps to make sure the leaf discs were not injured during the process. The first 35 seconds of ROS measurement was regarded as the background (1 second per interval). Control solution (SDW) or the 1 µM flg22 treatment (prepared in SDW) was added at the 35th second and the luminescence recordings were taken for another 1290 s (6 s per interval).

2.10 RNA extraction of ATP-treated samples

Seven-day old Col-0, *Atann1, Atann2, Atann1/2, Atann1/4* and *Atann1/2/4* seedlings were acclimatised for 1 hour in 8 mL buffer solution (2 mM Bis-Tris Propane; 10 mM $CaCl_2$; 0.1 mM KCl) in separate small petri dishes (Thermo Scientific). Then, 8 mL of either buffer solution (as control) or 1 mM ATP solution (2 mM stock prepared in buffer solution) was added into each assigned petri dish. After the assigned period of treatment (10 or 30 minutes), all the seedlings were then quickly put into separate test tubes containing 10 mL RNAlater solution (25 mM sodium citrate; 10 mM EDTA; 70 g ammonium sulphate/100 mL solution; pH 5.2). The root from each seedling was excised (in the RNAlater solution), dried on a filter paper to remove excess RNAlater solution and put into separate microcentrifuge tubes quickly before being frozen in liquid nitrogen.

Whole root frozen samples were ground by using a sterilised micro pestle before being subjected to the RNA extraction. RNA extraction was carried out by using the RNAeasy Plant Mini Kit (QIAGEN) with DNAse treatment additional step (RNAse free DNAse kit,QIAGEN). The method used followed the manufacturer's protocol. After the RNA extraction was completed, LiCl precipitation of the total RNA was performed to purify the RNA. A quarter of LiCl solution (2 M final concentration) was added to each RNA sample and then incubated at -20 °C for 1 hour. After 1 hour the RNA samples were centrifuged at 4 °C for 5 minutes (16,000 x *g*). Remaining supernatant was removed making sure not to disrupt the RNA pellets formed. The RNA was resuspended in 25 µL SDW after the pellets were air-dried at room temperature. Concentration and purity of the RNA samples were then measured by using a Nanodrop spectrophotometer (Nanodrop 2000;Thermo Scientific).

2.11 Quantification of ATP-induced gene expression

RNA was extracted from the whole root samples as explained in section 2.10. Complementary DNA (cDNA) was synthesised from each of the RNA samples (starting 500 ng RNA concentration) by using the Quantitect Reverse Transcription kit (QIAGEN). The protocol used was as given by the manufacturer with slight modifications. Genomic DNA elimination reactions were prolonged for 3 minutes instead of 2 minutes and the reverse-transcription reaction incubation time at 42 °C was also prolonged to 25 minutes instead of 15 minutes. cDNA obtained from this kit were then diluted in 1:100 dilution with SDW and aliquoted into smaller tubes for use.

Quantitative Polymerase Chain Reaction (qPCR) was done with a Rotor-Gene 3000 thermocycler with the Rotor-Gene™ SYBR® Green PCR Kit (QIAGEN) according to the manufacturer's protocol. cDNA material final concentration used was 5 ng with 0.25 μM final primer concentration. The programme that was used to run the qPCR was as follow: Initial stage 95°C for 5 minutes, 40 cycles of 95°C for 5 s, 60°C for 10 s. Melting curves were used to check for specific amplification (ramping from 55°C to 95°C with 1°C rise each step and 5 s delay between steps).The primer pairs used in the qPCR reaction were as shown in the Table 2.4.

Table 2.4: Primer sequences used for the qPCR reactions. Forward 5' - 3' and reverse 3' - 5' orientation sequence of primer used for each gene in the qPCR experiments.

Gene	Forward (5' - 3')	Reverse (3' - 5')
AtANN1	TGTTCTTCGTTCAGCAATCAAC	GTACTCCTCTCCAATGACCTTC
AtANN2	GGCGTCTCTCAAAGTCCCAAGCA	CAAGCTGCGTTGTGCTGCGT
AtANN4	TCATGCACACGCTCTGCTGAGG	AAGCACTCACGAGCCCCACA
AtUBQ10	CCGACTACAACATTCAGAAGGA	TCAGAACTCTCCACCTCCAAA
AtTUB4	AGGGAAACGAAGACAGCAAG	GCTCGCTAATCCTACCTTTGG
AtRBOHD	ATGATCAAGGTGGCTGTTTACCC	ATCCTTGTGGCTTCGTCATGTG
AtWRKY40	AGCTTCTGACACTACCCTCGTTG	TTGACAGAACAGCTTGGAGCAC
AtACS6	TATCCAGGGTTTGATAGAGA	TCCACCGTAATCTTGAACC

Three technical replicates were carried out for each sample. Raw data obtained were loaded into R software and by using the 'modlist' and the 'getPar' function in R (qpcR package) (Andrej-Nikolai Spiess, 2018), a list of Ct and efficiency coefficient values was generated. Ct values generated with less than 0.5 cycles apart were chosen for further calculation. Quantification of gene (R value) was performed by using the average of the selected Ct and efficiency values through the formula R_{sample} = Efficiency $^{(-Ct)}$. Data normalisation was done by obtaining the R value from two different housekeeping genes *UBQ10* (R_{UBQ10}) and *TUB4* (R_{TUB4}).

Normalised value of gene expression relative to the housekeeping genes for each sample was obtained from the formula:

$$Final\ R\ value, R_{final} = R_{sample} / \sqrt{(R_{UBQ10}) \times (R_{TUB4})}$$

2.12 Production of stable *Atann2/AtANN2* mutant complementary lines

The complemented mutant line *Atann2/AtANN2* was created by reinserting a functional *AtANN2* gene construct with its native promoter into the *Atann2* loss-of-function mutant plant. This was achieved by using the Gateway cloning technology. Gateway cloning works by using BP (bacteria attB site - phage attP site) cloning reaction to insert the *AtANN2* gene with its promoter construct into an entry vector (pDONR221) before being subjected to LR (attL;left site - attR;right site) cloning reaction to finally get the *AtANN2* gene construct into a destination vector (impGWB604). *Atann2* mutant plants transformed with the *AtANN2*-containing destination vector will carry the *AtANN2* construct thus forming the *Atann2/AtANN2* complemented mutant line.

2.12.1 Primer design and AtANN2 gene amplification

The primers were designed to include the native promoter of the *AtANN2* gene 2 kb upstream of the start codon of the *AtANN2* sequence (Pann2_ANN2). Another primer pair was designed to amplify the coding sequence of *AtANN2* without the native promoter for the purpose of an overexpression study (CDSann2_ANN2). Since the amplified *AtANN2* gene will later be subjected to BP cloning reaction for insertion into an entry vector, the sequence of the primers were designed to include the *att*B1 site with 4 G's (forward primer) and *att*B2 site with 4 G's (reverse primer). The expected *AtANN2* gene construct will be flanked by the *att*B sites which would help in the BP reaction into the entry vector as the entry vector

contained the *att*P sites. Table 2.5 shows the sequence of the primers to obtain the *AtANN2* gene construct. DNA sequence with highlight is the *att*B site with 4 G's adaptor. Specificity of the primers was examined by using the NCBI Primer-BLAST program (https://www.ncbi.nlm.nih.gov/tools/primer-blast/).

Table 2.5: Primer sequence used for amplification of *AtANN2* gene for BP Reaction. *att*B1 site with 4 G adaptor and the *att*B2 site with 4 G was added in front of every forward primer and reverse primer respectively to stabilize and make sure correct orientation of PCR product was cloned during the Gateway cloning. The primers were purified by using PAGE purification by the manufacturer of the oligos.

Primer	Forward primer (5' - 3')	Reverse primer (3' - 5')
Pann2_ANN2	GGGGACAAGTTTGTACAAAAAAGCAGGCTGGTCTCTGATACTATGCTGTCAAA	GGGGACCACTTTGTACAAGAAAGCTGGGTAGTTTCAAGCATCGCCATGTC
CSDann2_ANN2	GGGGACAAGTTTGTACAAAAAAGCAGGCTATGGCGTCTCTCAAAGTCCCAAGCA	GGGGACCACTTTGTACAAGAAAGCTGGGTAGTTTCAAGCATCGCCATGTCCGAGAA

Before the amplification was carried out, genomic DNA (gDNA) extraction from Col-0 wild type was done by using DNeasy Plant Mini kit (Qiagen). This gDNA will serve as the DNA template for the amplification of the *AtANN2* gene. Crude extraction of DNA is not suitable to be used for cloning, as there is the possibility of contaminations and chemical carry over from the extraction process. The usage of the filter in the extraction kit is useful in making sure the high purity of the gDNA was extracted. The method of extraction was as instructed by the manufacturer. Amplification of *AtANN2* gene was done via Polymerase Chain Reaction (PCR) method by using Phusion High Fidelity DNA Polymerase (Thermo Scientific) in order to obtain blunt-end PCR product required for the Gateway cloning. The reagents and parameters used during the PCR reaction are as in Table 2.6 and Table 2.7. PCR product formed was then subjected to gel electrophoresis to determine whether the correct size of gene was amplified before subsequent cloning process.

Table 2.6: Reagents used during *AtANN2* gene amplification by using Phusion High Fidelity DNA Polymerase kit.

Reagents	Volume (µL)	Final concentration
5X Phusion HF Buffer	4.0	1X
10 mM dNTPs	0.4	200 µM

10 µM Forward primer	1.0	0.5 µM
10 µM Reverse Primer	1.0	0.5 µM
Template DNA	2.0	64 ng/µL
Phusion DNA Polymerase	0.2	0.02U/µL
Distilled H_2O	11.4	-

Table 2.7: The parameters used for the amplification process via PCR.

Step	Temperature	Time	Cycle
Initial	98°C	30 s	1 x
Denaturion	98°C	10 s	35 x
Annealing	64°C	30 s	35 x
Extension`	72°C	2 min.	35 x
Final	72°C	10 min.	1 x

2.12.2 BP Cloning of AtANN2 construct into pDONR221 entry vector

Purified *AtANN2* construct obtained from the amplification step was inserted into entry vector pDONR221 via BP reaction. Gateway BP Clonase II Enzyme Mix (Thermofisher) was used in this process. The process involved integration between *att*B sites carrying the *AtANN2* construct with *attP* sites in the entry vector by the enzyme mentioned to produce entry clone containing *att*L sites with *AtANN2* construct.

Fifty femtomoles (fmol) of *att*B PCR product was required for the BP reaction (as suggested by the manufacturer). A formula was used to determine the right concentration in ng to be used by taking into account the size of the DNA construct and the desired femtomoles. The formula that was used is as follows:

$$ng\ PCR\ product = \frac{(y\ fmoles) \times (N) \times ((660\ fmol \times 1\ ng))}{1\ fmol \times 10^6\ fg},$$

where y = number of femtomoles desired

N = Size of DNA construct

Based on the formula, the concentration of *att*B PCR product used for the BP reaction was 121.8 ng. The reagents as in Table 2.8 were mixed together in a tube and left for incubation overnight at 25°C. After an overnight incubation, the BP reaction was then halted by incubating the reaction with 1.0 µL Proteinase K (2µg/µL) for 10 minutes at 37°C.

Table 2.8: Reagents used for the BP clonase reaction. attB PCR product was introduced into the pDONR221 entry vector with the help of BP Clonase II Enzyme Mix.

Reagents	Volume	Final concentration
***att*B PCR product (17.4 ng/µL)**	7.0 µL	121.8 ng
pDONR 221 (150 ng/µL)	1.0 µL	150 ng
BP Clonase II Enzyme Mix	2.0 µL	-

2.12.3 Screening of the successful BP cloning of AtANN2 construct

The recombinant entry vector pDONR221 was then inserted into DH5α *E. coli* via heat shock method (as described in Chapter 2.2). Fifty mg/mL kanamycin antibiotic was added into LB medium used to grow transformed *E. coli* and left to grow overnight at 27°C as a selection method for successful transformation. In order to check whether the colonies formed carried the correct construct, colony PCR was carried out to determine the presence of M13 sequence from the pDONR221 vector (M13 forward primer) and part of the *AtANN2* construct (Part_1 reverse primer). The reagents and parameters used for the colony PCR were as described in Table 2.9, 2.10 below.

Table 2.9: Reagents and the concentration used in colony PCR for screening of successful transformants.

Reagents	**Volume**	**Final concentration**
10X PCR Buffer	2.0 µL	1X
10 mM dNTPs	1.0 µL	0.5 µM
10 µM M13 forward primer	1.0 µL	0.5 µM

10 μM Part_1 reverse primer	1.0 μL	0.5 μM
Taq DNA Polymerase	0.2 μL	0.5 unit
Template DNA	1 colony	-
Distilled H_2O	13.8 μL	-

Table 2.10: The parameters used for the colony PCR.

Step	Temperature	Time	Cycle
Initial	94°C	5 min.	1 x
Denaturion	94°C	30 s	35 x
Annealing	62°C	30 s	35 x
Extension`	72°C	2 min.	35 x
Final	72°C	10 min.	1 x

Successful colonies of *E. coli* formed (Figure 5.12; Chapter 5.2.8) containing the insert were grown again overnight in the presence of antibiotic (50 mg/mL Kanamycin) as a stock and also for plasmid extraction. Plasmids were extracted from 6 mL of overnight *E.coli* culture by using Qiaprep Spin Miniprep kit (Qiagen) as in manufacturer's protocol. Further screening of the plasmid carrying the correct construct was done by using plasmid PCR before being sent to sequencing service. Since the size of *AtANN2* construct with its promoter is too big for sequencing, we designed a few primers to split up the sequencing of *AtANN2* construct into 6 parts. Table 2.11 lists the primers used for plasmid PCR and sequencing and the expected PCR product size. Reagents used for plasmid PCR was shown in Table 2.12. Parameters used for the plasmid PCR were as described in Table 2.10 but with different annealing temperature for each primer (M13 and Part_1 = 62 °C, Part_2 = 62°C, Part_3 = 62°C, Part_4 = 64°C, Part 5 = 64°C, Part 6 = 65°C). The results of the plasmid PCR and alignment from sequencing were as shown in Figure 5.13 (Chapter 5.2.8) and Appendix III respectively.

Table 2.11: List of primers used for plasmid PCR and sequencing. Part_x, where x refers to the number of part where the *AtANN2* construct were split-up to get smaller PCR product size.

Primer	Forward primer (5' - 3')	Reverse primer (3' -	Expected

		5')	**size**
M13 and Part_1 (for BP reaction)	GTAAAACGACGGCCAG (M13 forward primer)	GTAGACAACGTGTATCACTTGCAC (Part_1 reverse primer)	683 bp
*att*B1 and Part_1 (for LR reaction)	GGGGACAAGTTTGTACAAAAAAGCAGGCT (*att*B1 forward primer)	GTAGACAACGTGTATCACTTGCAC (Part_1 reverse primer)	664 bp
Part_2	AGTGCAAGTGATACACGTTGTCTACA	GACTTCACGTGGTTGGCTCT	568 bp
Part_3	GAATCCTCTCTGTCGTTTTCGTAT	CTTAAGTAATGTAACGGGAATCCC	840 bp
Part_4	GGGATTCCCGTTACATTACTTAAG	CCCATCCTGTTTCAGACCAAAC	603 bp
Part_5	GTTTGGTCTGAAACAGGATGGG	GTCAGAAACATGTGTCCCAAATAC	557 bp
Part_6	GTATTTGGGACACATGTTTCTGAC	AAGCATCGCCATGTCCGAG	646 bp

Table 2.12: Reagents and the concentration used in plasmid PCR for screening of successful transformants.

Reagents	**Volume**	**Final concentration**
10X PCR Buffer	2.0 µL	1X
10 mM dNTPs	1.0 µL	0.5 µM
10 µM Part_x forward primer	1.0 µL	0.5 µM
10 µM Part_x reverse primer	1.0 µL	0.5 µM
Taq DNA Polymerase	0.2 µL	0.5 unit
Template DNA (from plasmid extraction)	1.0 µL	-
Distilled H_2O	13.8 µL	-

2.12.4 LR Cloning of AtANN2 construct into destination vector impGWB604

The next step in producing the *Atann2/AtANN2* complemented mutant lines was to transfer the *AtANN2* construct into the destination vector. After BP cloning reaction, we

managed to obtain transformed pDONR221 containing *AtANN2* construct with the *att*L site. The *AtANN2* construct flanked by *att*L sites was then transferred into destination vector impGWB604 with the help of the LR clonase enzyme in the LR reaction. The impGWB604 destination vector stock was obtained from Dr. Tsuyoshi Nakagawa (Shimane University, Japan). The specificity of this process is guaranteed as the impGWB604 vector carried the *att*R sites that were important for LR reaction and can only match with the *att*L sites. The impGWB604 destination vector contained no promoter sequence thus allowing the native 2 kb *AtANN2* promoter to function and required BASTA selection for screening. The sequences contained in the destination vector impGWB604 are as explained in Appendix IV.

Before the LR reaction was carried out, the purity and the concentration of the destination vector was determined. LR reaction was done by using the Gateway LR Clonase II Enzyme Mix kit (Thermo Fisher) following the manufacturer's protocol. The reagents that were used during the reaction were as described in Table 2.13. LR reaction was left for overnight incubation at 25°C (~ 18 hours). The reaction was terminated by high temperature (75°C) the next day for 10 minutes. Competent *E.coli* DH5α cells were then transformed with 3.0 µL product from the LR reaction via heat shock method as explained in Chapter 2.2. Transformed *E.coli* were left to grow on LB medium containing 50 mg/mL spectinomycin antibiotic for screening at 37°C for approximately 13 hours.

Table 2.13: Reagents used for the LR clonase reaction. *AtANN2* construct contained in the transformed pDONR221 entry vector was integrated into the impGWB604 destination vector with the help of LR Clonase II Enzyme Mix.

Reagents	Volume	Final concentration
Transformed entry clone (pDONR221)	0.5 µL	100 ng
Destination vector impGWB604	1.0 µL	100 ng
BP Clonase II Enzyme Mix	0.5 µL	-
Sterilised distilled H_2O	2.0 µL	-

After the incubation step, some colonies formed on the medium indicating possible insertion of the *AtANN2* construct in the impGWB604 vector. Colony PCR was carried out to

confirm this based on the size of PCR product from forward primer *att*B (previously tagged on the *AtANN2* construct) and the Part_1 reverse primer (first part of the *AtANN2* construct). The sequence of the primers used is as shown in Table 2.11. The reagents that were used for colony PCR and the programme were as previously described in Table 2.9 and Table 2.10 respectively with slight modification on the annealing temperature (*att*B1 - Part_1 primer pair annealing temperature = 62°C). The results of the colony PCR were as shown in Chapter 5.2.8 (Figure 5.14). After the colony PCR, further screenings to confirm the correct *AtANN2* sequence has been inserted into the destination vector were done via plamid PCR (results in Chapter 5.2.8; Figure 5.15) and sequencing (results in Appendix V) as explained in Chapter 2.12.3.

2.12.5 Agrobacterium transformation of Atann2 with AtANN2 with its native promoter construct.

Competent agrobacterium cells (GV1031) were obtained from the Webb laboratory (University of Cambridge). Agrobacterium cells were transformed with the purified plasmid extracted from the LR reaction by using heat shock method as describe in Chapter 2.2. Transformed agrobacterium cells were grown on LB medium containing 10 mg/mL gentamycin, 50 mg/mL streptomycin and 50 mg/mL rifampicin for screening purpose. The cells were left to grow at 30°C for 2 days. Agrobacterium colonies formed in the antibiotic-selection medium were re-grown to extract the plasmid for subsequent plasmid PCR and Sanger sequencing as described in subchapter 2.12.3 as a final check.

Agrobacterium transformation of Col-0 with the desired *AtANN2* construct was done by using the floral dipping method. Healthy 5-weeks-old Col-0 plants were used for the transformation. The method of floral dipping was as described in Chapter 2.3 with *impGWB604-AtANN2* containing agrobacterium instead of agrobacterium containing *35S::CAMV::aequorin* construct. Transformed plants were left to grow at the Plant Growth Facilities (University of Cambridge) before the seeds were harvested after about 8 - 10 weeks. Harvested seeds were screened for successful *Atann2/AtANN2* production via 20 µg/mL BASTA screening on normal ½ MS medium. Seeds that survived the BASTA screening were bulked-up and reproduced until the third generation with BASTA screening carried out for each generation.

2.13 Statistical analyses

All the data collected were analysed with the R statistical programme (https://www.r-project.org). One-Way ANOVA or Welch Two Sample *t*-Test were used for parametric tests whereas for non-parametric tests, Wilcoxon rank-sum test was applied. The *p*-value outcomes of <0.05 from these two statistical tests indicated significant difference between any two groups compared. Further comparison between each element of each two groups from the ANOVA test was analysed with Tukey's HSD *post-hoc* test. A 95% confidence interval was used for the comparison of all tests carried out.

Chapter 3

AtANN1 in eATP and eADP Signalling

3.1 Introduction

Extracellular ATP (eATP) is thought to be acting as a signal molecule that is involved in mediating biotic and abiotic responses. In the event of these stresses, in *Arabidopsis thaliana* ATP released into the extracellular matrix could trigger downstream effects through the plasma membrane purinoreceptor AtDORN1 (Choi *et al.*, 2014b), such as the accumulation of $[Ca^{2+}]_{cyt}$ that leads to the production of Reactive Oxygen Species (ROS) at the root hair tips (Kim *et al.*, 2006) and mature whole root (Demidchik *et al.*, 2009), plus the production of Nitric Oxide (NO) in *A. thaliana* root hair cells (Clark *et al.*, 2010), tomato cell (Foresi *et al.*, 2007) and Salvia hairy root culture (Wu & Wu, 2008). AtDORN1's second highest affinity is for eADP (Choi *et al.*, 2014b). Lew and Dearnaley (2000) found that both eATP and eADP have the ability to depolarise the plasma membrane of *A. thaliana* root hairs. In a previous study, eATP evoked ROS accumulation in whole roots of *A. thaliana* (Demidchik *et al.*, 2009) wheareas eADP failed to do so (Demidchik *et al.*, 2011). Tonón *et al.* (2009) also found that eADP does not induce formation of Phosphatidic Acid (PA) as eATP does. These findings might suggest diversification in the signalling pathway between eATP and eADP. Demidchik *et al.* (2009) found that the plasma membrane calcium channel that could be involved in elevation of free cytsosolic Ca^{2+} ($[Ca^{2+}]_{cyt}$) in response to eATP is hyperpolarisation-activated. However, the genetic identities of the calcium channels that are

responsible for the $[Ca^{2+}]_{cyt}$ accumulation in the eATP and eADP signalling pathways are not yet discovered. This chapter will shed light on the role of AtANN1 in the eATP signalling pathway, possibly as a plasma membrane calcium channel.

Arabidopsis thaliana AtANN1 (Annexin 1) has previously been suggested to act as the plasma membrane calcium channel that works in the root $[Ca^{2+}]_{cyt}$ response to salinity stress, hyperosmotic stress, and oxidative stress (Laohavisit *et al.*, 2012, 2013; Richards *et al.*, 2014). There are also past studies that showed accumulation of extracellular ATP under salinity and osmotic stresses (Dark *et al.*, 2011), suggesting that eATP could be involved in their signalling pathways. As increase in $[Ca^{2+}]_{cyt}$ is also one of the downstream responses to the eATP signal (Demidchik *et al.*, 2003a; Demidchik *et al.*, 2009; Choi *et al.*, 2014b), AtANN1 is implicated as the plasma membrane calcium channel that mediates the $[Ca^{2+}]_{cyt}$ response due to the eATP signal released during abiotic stresses. Diminishing extracellular calcium causes reduction in the $[Ca^{2+}]_{cyt}$ accumulation in eATP treatment, showing that the calcium might be originating from the extracellular matrix (Demidchik *et al.*, 2003a; Jeter *et al.*, 2004). In this case, calcium channels in the plasma membrane might be involved in the calcium influx. AtANN1 is localised to the plasma membrane (Laohavisit *et al.*, 2009) making it a suitable candidate as a calcium channel. Furthermore, a study by Lee *et al.* (2004) showed the ability of AtANN1 to relocate from the cytosol to the plasma membrane in salt stress conditions.

The AtDORN1 purinoreceptor can directly interact with the AtRBOHD (Respiratory Burst Oxidase Homologue D) NADPH Oxidase in the presence of eATP, which induces the production of ROS (Chen *et al.*, 2017). The *AtRBOHD* gene was stated to be one of the few genes that is regulated by eATP (Choi *et al.*, 2014b). Laohavisit *et al.* (2012) showed that AtANN1 acts as a plasma membrane calcium channel activated by ROS, which is one of the components of eATP signalling as mentioned before. These findings sparked the idea of AtANN1 as a possible calcium channel that works downstream of the eATP perception by AtDORN1, most likely downstream of AtDORN1-dependent ROS production.

Other than stress and immune responses, eATP is important in regulating growth and viability of plants. Optimum eATP concentration is crucial as high eATP concentration could be detrimental and too low a concentration would impede the growth of plants (Chivasa *et al.*, 2005; Clark *et al.*, 2010; Sun *et al.*, 2012). eATP is also directly linked with normal root hair growth where actively growing cells have higher levels of eATP at their apex (Kim *et*

al., 2006). Root curling (which is a response to mechanosensing) was observed when plants are grown in the presence of eATP. High ATP concentration supplied above 3 mM could inhibit gravitropism of roots, which indicates involvement of eATP signalling in auxin transport (Tang *et al*, 2003). The mechanism and the components involved in eATP-related growth however are not yet fully understood. Gene expression studies tied eATP to stress responses. Some of the genes that were regulated by eATP were *Arabidopsis thaliana* Mitogen Activated Protein Kinase Kinase Kinase (*AtMEKK*), Mitogen-Activated Protein Kinase 3 (*AtMPK3*), Calcium-Dependent Protein Kinase 19 (*AtCPK19*), and 1-Aminocyclopropane-1-carboxylic Acid Synthase (*AtACS6*) (Jeter *et al.*, 2004). Some of the genes that are up-regulated in wounding stress are also found to be eATP-induced genes such as *A. thaliana* WRKY DNA-Binding Protein 40 (*AtWRKY40*), Calcium Dependent Protein Kinase 28 (*AtCPK28*) and NADPH/Respiratory Burst Oxidase Protein D (*AtRBOHD*) (Choi *et al.*, 2014b).

In this chapter, the possibility that AtANN1 might be in the eATP signalling pathway has been tested using an *Atann1* loss of function mutant constitutively expressing cytosolic (apo)aequorin as a luminescent $[Ca^{2+}]_{cyt}$ reporter (Laohavisit *et al.*, 2012). Additionally, double mutants of *Atann1* and *Atdorn1* expressing (apo)aequorin were used to confirm whether AtANN1 lies downstream of AtDORN1. Based on this study, we found that AtANN1 might be acting in the AtDORN1 pathway and is required for the normal $[Ca^{2+}]_{cyt}$ response towards eATP and eADP at whole roots and root tips level. A gene expression study was carried out that also suggests the involvement of AtANN1 in the eATP signalling pathway related to the ethylene defence system in plants. Finally, a growth assay experiment carried out indicates that AtANN1 might not be involved in eATP-modulated root formation.

3.2 Results

3.2.1 Homozygous mutant screening: *Atann1, Atdorn1-1/ann1* and *Atdorn1-3/ann1*

The Col-0, *Atann1, Atdorn1-1/ann1* and *Atdorn1-3/ann1* mutant seedlings expressing cytosolic (apo)aequorin were tested for homozygosity by genotyping using Polymerase Chain Reaction (PCR) with different primers or through Sanger sequencing (Chapter 2). Based on the primer design, PCR results of *Atann1, Atdorn1-1/ann1* and *Atdorn1-3/ann1* homozygous mutant seedlings with annexin gene-specific primers were expected to show no PCR product at all whereas pairing the annexin gene-specific forward primer with T-DNA insert LB1.3 reverse primer was expected to produce a single band of PCR product. Gene-specific forward

primer (FP) and reverse primer (RP) are able to bind to their complementary sites of the gene. If the T-DNA sequence was successfully inserted into both of the alleles and disrupted the gene sequence, both annexin gene native FP and RP would be unable to bind to the gene thus no amplification could be observed. On the other hand, the gene-specific primer paired with T-DNA insert LB1.3 reverse primer could bind to its complementary site at the T-DNA insert sequence in both alleles, producing a single PCR product.

The PCR products were subjected to gel electrophoresis as explained in Chapter 2. Figures 3.1 A and 3.1 B depict the outcomes of PCR to check for the 600 bp *AtDORN1* gene product and *Atann1* homozygous mutation respectively. Based on the gel diagram in Figure 3.1 A, the wells that were loaded with PCR product of *AtDORN1* KW13 primer pair from Col-0 and *Atdorn1-1/ann1* samples showed a single band with a size of around ~600 bp. The KW13 primer pairs were designed to make sure that the PCR product was specific and contained the site where the point mutation of AtDORN1 kinase domain occurred (Choi *et al*, 2014b). The 600 bp PCR product samples were then purified before being subjected to Sanger sequencing (Source Bioscience) (Chapter 2). DNA sequence alignment between Col-0 wild type and the *Atdorn1-1/ann1* showed that all the *Atdorn1-1/ann1* samples contained a single point mutation where the G base was switched with A (Appendix I) which converts the amino acid Asp to Asn (Choi *et al.*, 2014b). Based on Figure 3.1 B, the wells loaded with PCR product of the *ANN1*-T-DNA LB1.3 primer pairs (lane 2, 4, 6, 8, 10, 12) and *AtANN1* gene native primers (lane 1, 3, 5, 7, 9, 11) displayed a band with a size between 400 bp - 500 bp (as 494 bp product expected from *AtANN1* homozygous mutation) and no bands respectively. These findings validate that the *Atdorn1-1/ann1* seedlings were mutated at both *AtDORN1* (as single-point mutation) and *AtANN1* genes (as T- DNA insertion mutation).

Figure 3.2 shows the results from four *Atdorn1-3/ann1* genomic DNA samples tested for *AtDORN1* homozygous mutation (Figure 3.2 A) and *AtANN1* homozygous mutation (Figure 3.2 B). Based on Figure 3.2 A, the wells loaded with PCR product from the *AtDORN1*-T-DNA LB1.3 primer pair (lane 2, 4, 6, 8) displayed ~800 bp bands (agreeing with the predicted 639 - 939 bp product for successful T-DNA insertion) whereas the wells loaded with PCR product from the *AtDORN1* gene native primers (lane 1, 3, 5, 7) exhibited no bands. This is consistent with the expected results for homozygous mutation. Col-0 control sample (lane 9) showed the product from *AtDORN1* gene native primer (~1424 bp) whereas lane 10 showed no band as a result of *AtDORN1*-TDNA LB1.3 primer pair from Col-0 sample. This was repeated in PCR by using *AtANN1* gene native primers or the

AtANN1-T-DNA LB1.3 primer pairs. The lane containing PCR product from the *AtANN1* gene native primers showed no bands (lane 1, 3, 5, 7) whereas a single band at ~500 bp was visible in lanes 2, 4, 6 and 8 containing PCR product from *AtANN1*-T-DNA LB1.3 primer pairs (Figure 3.2 B). The predicted PCR product size for the *AtANN1*-T-DNA LB1.3 primer pair with *AtANN1* was 494 bp, which is close to the value shown in the gel image based on the DNA size marker.

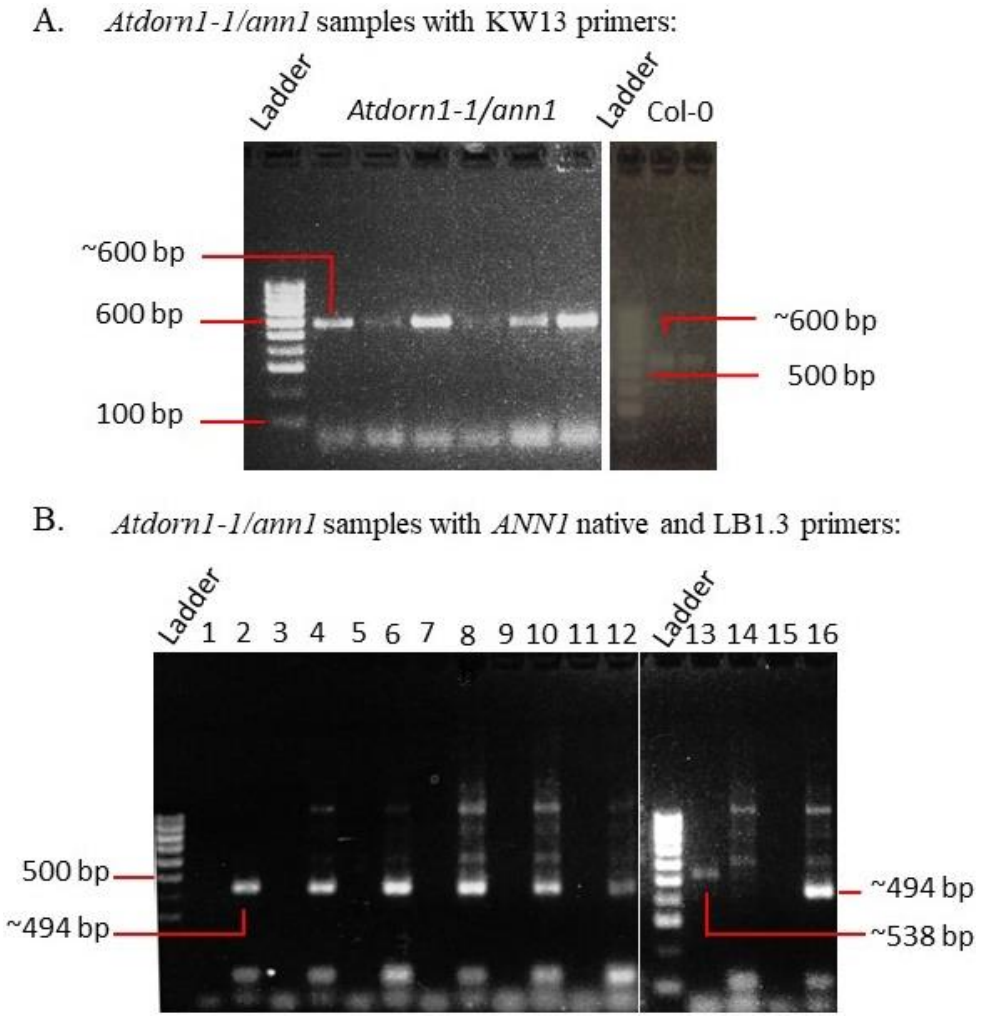

Figure 3.1: Verification of *Atdorn1-1/ann1* homozygous mutants. Image (A) shows KW13 specific primers used to amplify the sequence containing the point mutation for AtDORN1 kinase site in both *Atdorn1-1/ann1* samples and Col-0 samples. The PCR product was subjected to sequencing to confirm the point mutation in the *AtDORN1* gene. Image (B) shows the PCR product from the *AtANN1* native primers (lane 1, 3, 5, 7, 9, 11) and *AtANN1-T-DNA* LB1.3 primer pair (lane 2, 4, 6, 8, 10, 12) of the *Atdorn1-1/ann1* sample. Col-0 samples (lane 13, *AtANN1* native primers; lane 14, LB1.3 primers) and *Atann1* samples (lane 15, *AtANN1* native primers; lane 16, *AtANN1*-LB1.3 primers) acted as a control for the PCR reaction. DNA size marker used for each gel electrophoresis run was the 100 bp hyperladder.

A. *Atdorn1-3/ann1* samples with *DORN1* native and LB1.3 primers:

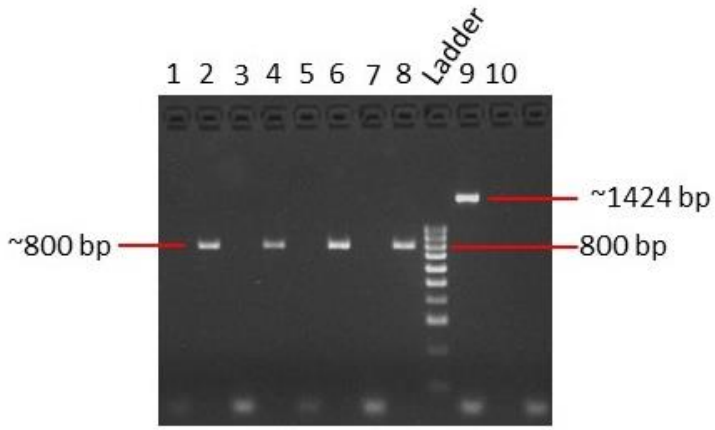

B. *Atdorn1-3/ann1* samples with *ANN1* native and LB1.3 primers:

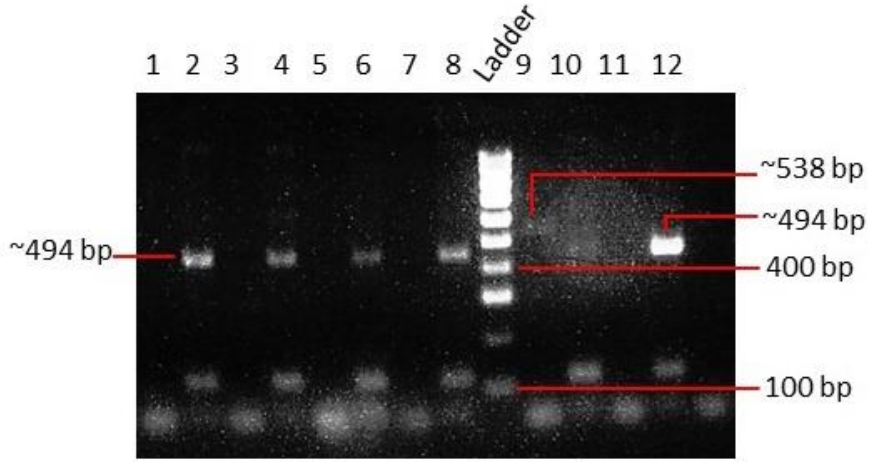

Figure 3.2*:* Verification of *Atdorn1-3/ann1* homozygous mutants. Image (A) shows genotyping by using *AtDORN1* native gene primer (lane 1, 3, 5, 7) and the *AtDORN1*-LB1.3 primer pair (lane 2, 4, 6, 8) for the *Atdorn1-3/ann1* samples. Col-0 samples (lane 9, *AtANN1* native primer; lane 10, *AtANN1*-LB1.3 primer pair) acted as the positive control for the PCR reaction. Gel image (B) is the PCR product from the *AtANN1* native primer (lane 1, 3, 5, 7) and the *AtANN1*-LB1.3 primer pair (lane 2, 4, 6, 8) for the *Atdorn1-3/ann1* samples. Col-0 samples (lane 9, *AtANN1* native primer; lane 10, *AtANN1*-LB1.3 primer pair) and *Atann1* samples (lane 11, *AtANN1* native primer; lane 12, *AtANN1*-LB1.3 primer pair) acted as a control for the PCR reaction. DNA size marker used for each gel electrophoresis run is the 100 bp hyperladder.

Four Col-0 and *Atann1* genomic DNA samples from leaves were subjected to PCR to check for the *AtANN1* homozygous mutation (seeds were produced by Dr Jenny Mortimer, University of Cambridge). Figure 3.3 shows the gel image from the PCR genotyping. *AtANN1* native primers produced a single band with the size ~538 bp (lane 1, 3, 5, 7) and the

AtANN1-T-DNA LB1.3 primer pairs did not produce any bands (lane 2, 4, 6, 8) for Col-0 samples. In the *Atann1* gDNA samples, the *AtANN1*-T-DNA LB1.3 primer pairs generated a single band with an expected size of approximately 494 bp (lane 10, 12, 14, 16) whereas the *AtANN1* native gene primers showed no bands (lane 9, 11, 13, 15). This confirmed the *Atann1* seedlings used in this chapter were homozygous mutants for the *AtANN1* gene.

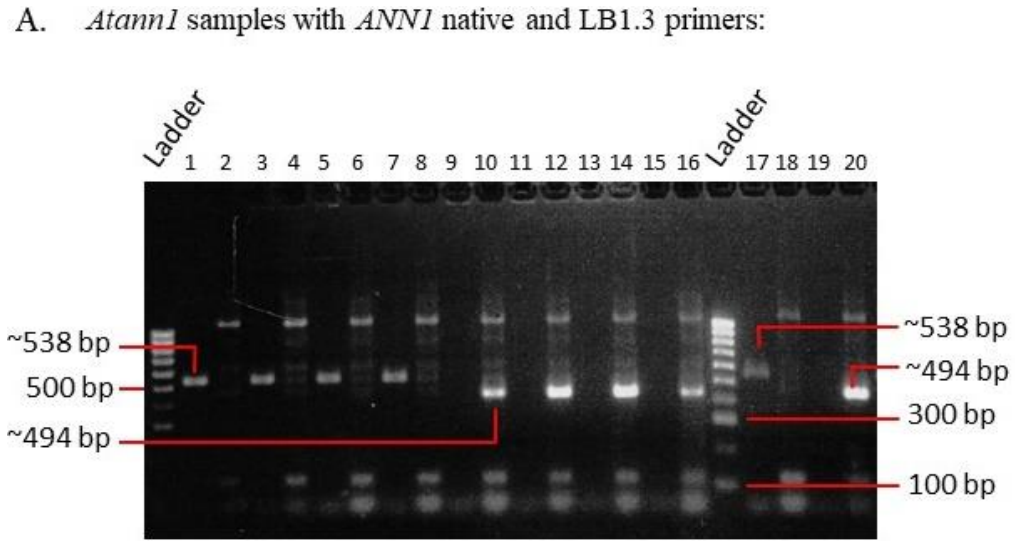

Figure 3.3*:* Confirmation of *Atann1* homozygous mutant. The gel electrophoresis of the PCR product from Col-0 (lane 1 - 8) and *Atann1* (lane 9 - 16) whole leaves genomic DNA samples. *AtANN1* gene native primer (lane 1, 3, 5, 7, 9, 11, 13, 15, 16) and *AtANN1*-T-DNA LB1.3 primer pair (lane 2, 4, 6, 8, 10, 12, 14, 16) were used for the PCR reaction. Col-0 samples (lane 17, *AtANN1* native primers; lane 18, *AtANN1*-LB1.3 primer pair) and *Atann1* samples (lane 19, *AtANN1* native primers; lane 20, *AtANN1*-LB1.3 primer pair) acted as a control for the PCR reaction. DNA size marker used for each gel electrophoresis run was the 100 bp hyperladder.

3.2.2 *Atann1* is impaired in $[Ca^{2+}]_{cyt}$ elevation by eATP and eADP at whole root level

Seven-day-old whole roots of both *Atann1* and Col-0 wild type (harbouring apoaequorin protein produced under the 35S CaMV promoter; propagated by Dr. Jenny Mortimer, University of Cambridge) were excised and assayed to measure the changes in $[Ca^{2+}]_{cyt}$ in the presence of eATP. Addition of control solution (2 mM Bis-Tris Propane; 10 mM $CaCl_2$; 0.1 mM KCl) after 35 seconds of measurement evoked a single peak of $[Ca^{2+}]_{cyt}$ accumulation known as the "touch response" (response due to mechanical disturbance) for approximately 15 seconds before $[Ca^{2+}]_{cyt}$ returned to the basal level (Figure 3.4 A). Mean ± SEM basal $[Ca^{2+}]_{cyt}$ of *Atann1* excised roots in the control buffer (0.06±0.0009 μM) was lower than the Col-0 wild type (0.07±0.002 μM) (Figure 3.4 A) but the touch response was similar (Col-0 0.17±0.04 μM; *Atann1* 0.17±0.01 μM) (Figure 3.4 B). This dissimilarity

between the Col-0 and *Atann1* mutant in resting $[Ca^{2+}]_{cyt}$ was mentioned by Laohavisit *et al.* (2013) and by removing the baseline value during analysis, the $[Ca^{2+}]_{cyt}$ response between the two genotypes is comparable. Comparison between the total accumulation of $[Ca^{2+}]_{cyt}$ (Figure 3.4 C) of both Col-0 (2.36±0.67 μM) and *Atann1* mutant (2.17±0.38 μM) confirmed that the control treatment had no effect on the test.

Time course measurement of $[Ca^{2+}]_{cyt}$ in response to 1 mM ATP treatment showed a biphasic response comprising the first peak (T = 50 s) and the second peak (T = 83 s) after the initial touch response (Figure 3.4 D). The touch response for both Col-0 (0.14±0.03 μM) and *Atann1* (0.11±0.01 μM) were not significantly different (Figure 3.4 E) but the following biphasic response of *Atann1* exhibited a significantly lower $[Ca^{2+}]_{cyt}$ response than the Col-0 specifically at the second peak (Col-0 0.30 ±0.009 μM; *Atann1* 0.23±0.01 μM, T = 83 s) (Figure 3.4 F; Figure 3.4 G). This was highlighted again as the total $[Ca^{2+}]_{cyt}$ accumulated due to eATP treatment in *Atann1* (16.42±0.56 μM) roots was significantly lower compared to Col-0 (20.92±0.67 μM) (Figure 3.4 H).

As ADP was also found to be able to bind to the purinoreceptor AtDORN1 (Choi *et al.*, 2014b) and can elevate root $[Ca^{2+}]_{cyt}$ (Demidchik *et al.*, 2009), a similar test with ADP on 7-day-old excised roots was carried out for both Col-0 and the *Atann1* mutant. Control treatment ensured that differences between *Atann1* mutant and Col-0 in the test were due to the ADP treatment applied as the $[Ca^{2+}]_{cyt}$ touch peak response (Col-0 0.16±0.02 μM; *Atann1* 0.13±0.01 μM; Figure 3.5 A, B) and the overall $[Ca^{2+}]_{cyt}$ (Col-0 2.17±0.39 μM; *Atann1* 1.83±0.36 μM) (Figure 3.5 C) were not significantly different between genotypes.

The test showed that under the 1 mM ADP treatment, both Col-0 and *Atann1* produced a similar biphasic calcium signature as in the ATP treatment with *Atann1* having a lower response in the first peak (T = 50 s) and the second peak (Col-0 T = 82 s; *Atann1* T = 86 s) (Figure 3.5 D). Unlike ATP treatment, 1 mM ADP revealed significantly impaired *Atann1* ability to produce both the first peak (0.16±0.008 μM) (Figure 3.5 F) and the second peak (0.22±0.01 μM) (Figure 3.5 G) compared to the Col-0 (first peak 0.26±0.01 μM; second peak 0.29±0.009 μM). Overall, the loss of functional AtANN1 protein led to less total accumulation of $[Ca^{2+}]_{cyt}$ of *Atann1* compared to the Col-0 (Col-0 21.0±0.61 μM; *Atann1* 15.10±0.58 μM) (Figure 3.5 H). *Atann1*'s inability to accumulate similar levels of $[Ca^{2+}]_{cyt}$ as the wild type shows that it is required in both eATP and eADP signalling pathways, possibly as a calcium channel at whole root level.

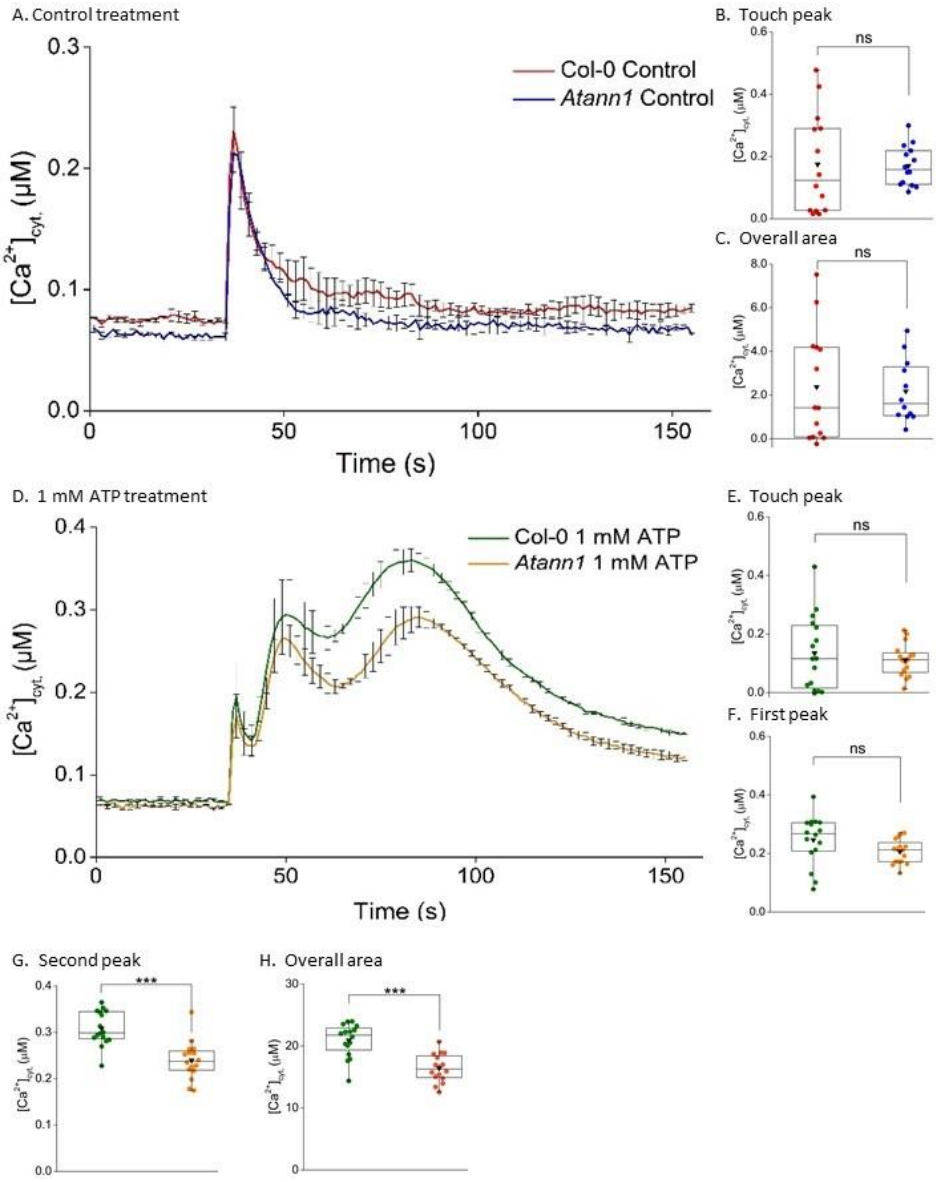

Figure 3.4: **eATP causes $[Ca^{2+}]_{cyt}$ elevation at whole root level as a downstream response through AtANN1**. Both Col-0 and *Atann1* 7-day-old roots expressed apo-aequorin cytosolically. The $[Ca^{2+}]_{cyt}$ response for the control treatment (A) and 1 mM ATP (D) were recorded for 155 s and each treatment was added at the 35th second. These time course data were from the means ± SEM of 3 independent trials, with n = 15 - 16 roots per genotype and treatment. Touch peak (B) represents the highest value of the touch response (35 - 50 s) whereas the overall area (C) is the total area under the curve extracted from the time course data of the control treatment (35 - 155 s). Time course analysis of the 1 mM ATP treatment is split up into the first peak (F) and the second peak (G) responses, which are the highest value of the peaks that emerged after the touch response (E). The total accumulation of $[Ca^{2+}]_{cyt}$ of Col-0 and *Atann1* was determined through the overall area under the curve (H). All calculations were carried out with the baseline (the first 35 s of measurement) subtracted. Middle line of the boxplot represents the median whereas the inverted triangle represents the mean. p-values: ns (not significant $p > 0.05$), *** ($p < 0.001$), Welch's t-test.

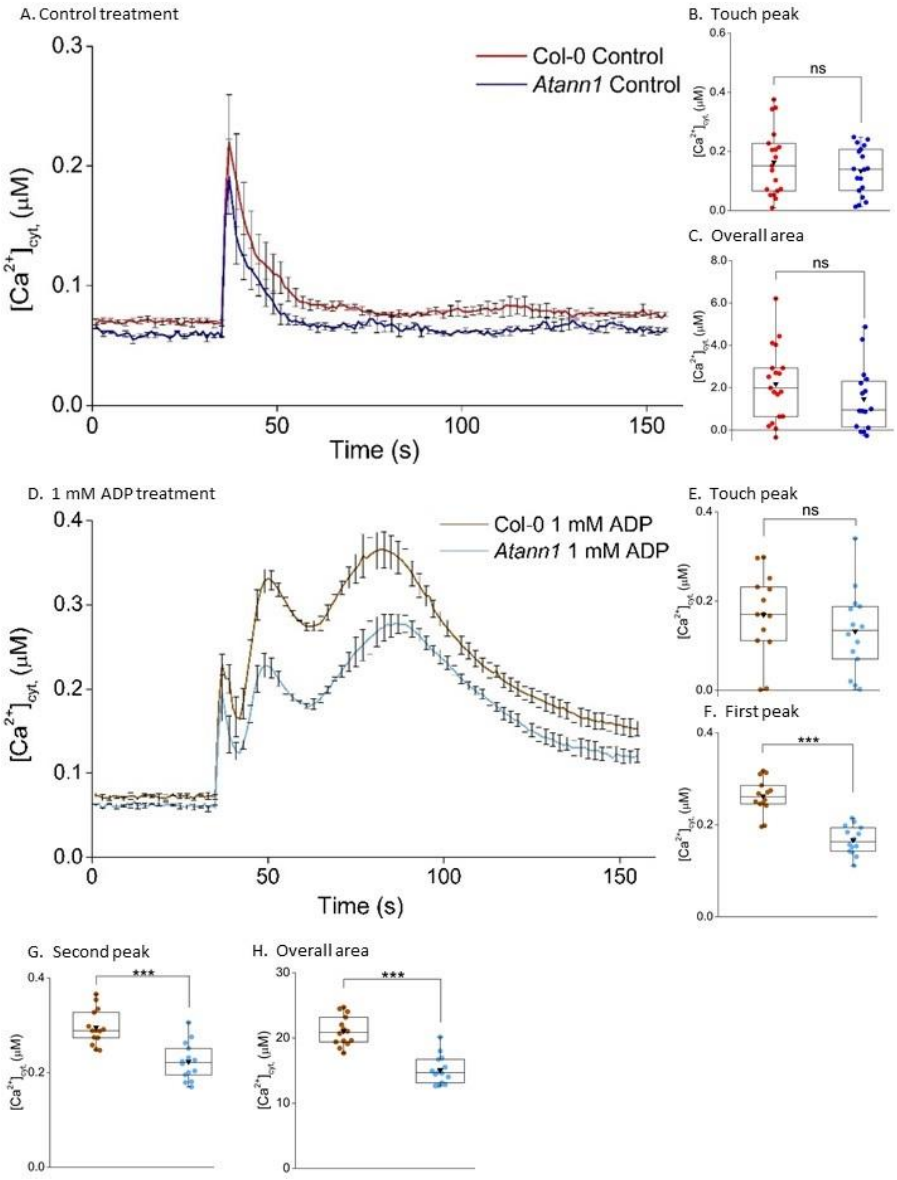

Figure 3.5*:* eADP causes $[Ca^{2+}]_{cyt}$ elevation at whole root level as a downstream response through AtANN1. Both Col-0 and *Atann1* 7-day-old roots expressed apo-aequorin cytosolically. The $[Ca^{2+}]_{cyt}$ response for the control treatment (A) and 1 mM ADP (D) were recorded for 155 s and each treatment was added at the 35th second. These time course data were from the means ± SEM of 3 independent trials, with n = 14 - 19 roots per genotype and treatment. Touch peak (B) represents the highest value of the touch response whereas the overall area (C) is the total area under the curve extracted from the time course data of the control treatment. Time course analysis of the 1 mM ADP treatment is split up into the first peak (F) and the second peak (G) responses which were the highest value of the peaks that emerged after the touch response (E). The total accumulation of $[Ca^{2+}]_{cyt}$ of Col-0 and *Atann1* was determined through the overall area under the curve (H). All calculations were carried out with the baseline (the first 35 s of measurement) subtracted. Middle line of the boxplot represents the median whereas the inverted triangle represents the mean *p*-values: ns (not significant $p > 0.05$), *** ($p < 0.001$), Welch's *t*-test.

3.2.3 *Atann1* supported less $[Ca^{2+}]_{cyt}$ elevation by eATP and eADP at root tip level

Using only root tips would make the experimental results more relevant to sensing environmental change and elongative growth. It would also minimise any effect of differences in gross root system architecture between genotypes. Therefore, $[Ca^{2+}]_{cyt}$ measurement at root tip level was carried out. Instead of the whole roots, the apical 1 cm tip of 7-day-old roots of Col-0 and *Atann1* were excised and used in this experiment. $[Ca^{2+}]_{cyt}$ changes in the control and ATP- or ADP-treated individual root tips were monitored by measuring the bioluminescence produced by the root tips carrying the (apo)aequorin reporter across time.

The $[Ca^{2+}]_{cyt}$ time course shows baseline measurement for both Col-0 (0.08±0.02 μM) and *Atann1* (0.07±0.001 μM) followed by the touch response (after the addition of the control solution at the 35th second) that lasted approximately 15 s before declining towards the basal level (Figure 3.6 A). The touch peak (Col-0 0.19±0.02 μM; *Atann1* 0.18±0.01 μM) (Figure 3.6 B) and the total $[Ca^{2+}]_{cyt}$ measurement (Col-0 2.5±0.25 μMs; *Atann1* 2.8±0.27 μM) (Figure 3.6 C) in the control treatment were not significantly different between Col-0 and *Atann1* mutant.

A lower concentration (0.5 mM) of ATP was used instead of 1 mM ATP to find out whether AtANN1 is involved in mediating the $[Ca^{2+}]_{cyt}$ accumulation at root tip level. Based on the time course of the $[Ca^{2+}]_{cyt}$ measurement, both Col-0 and *Atann1* produced $[Ca^{2+}]_{cyt}$ accumulation in a biphasic manner with *Atann1* showing lower amplitude after the touch response until the end of recording (Figure 3.6 D). ATP (0.5 mM) treatment had no effect on the touch response as the touch peak between Col-0 (0.16±0.01 μM) and the *Atann1* mutant (0.13±0.02 μM) was not significantly different (Figure 3.6 E). The first peak was higher than the second peak for both genotypes with *Atann1* (first peak 0.24±0.008 μM; second peak 0.19±0.005 μM) constantly having lower amplitude than Col-0 (first peak 0.29±0.007 μM; second peak 0.25±0.006 μM; Figure 3.6 F, G). Overall area under the curve of *Atann1* (14.84±0.40 μM) was also significantly less than Col-0 (19.16±0.35 μM) showing that AtANN1 is involved in mediating the $[Ca^{2+}]_{cyt}$ accumulation under 0.5 mM ATP treatment at the root tip level (Figure 3.6 H).

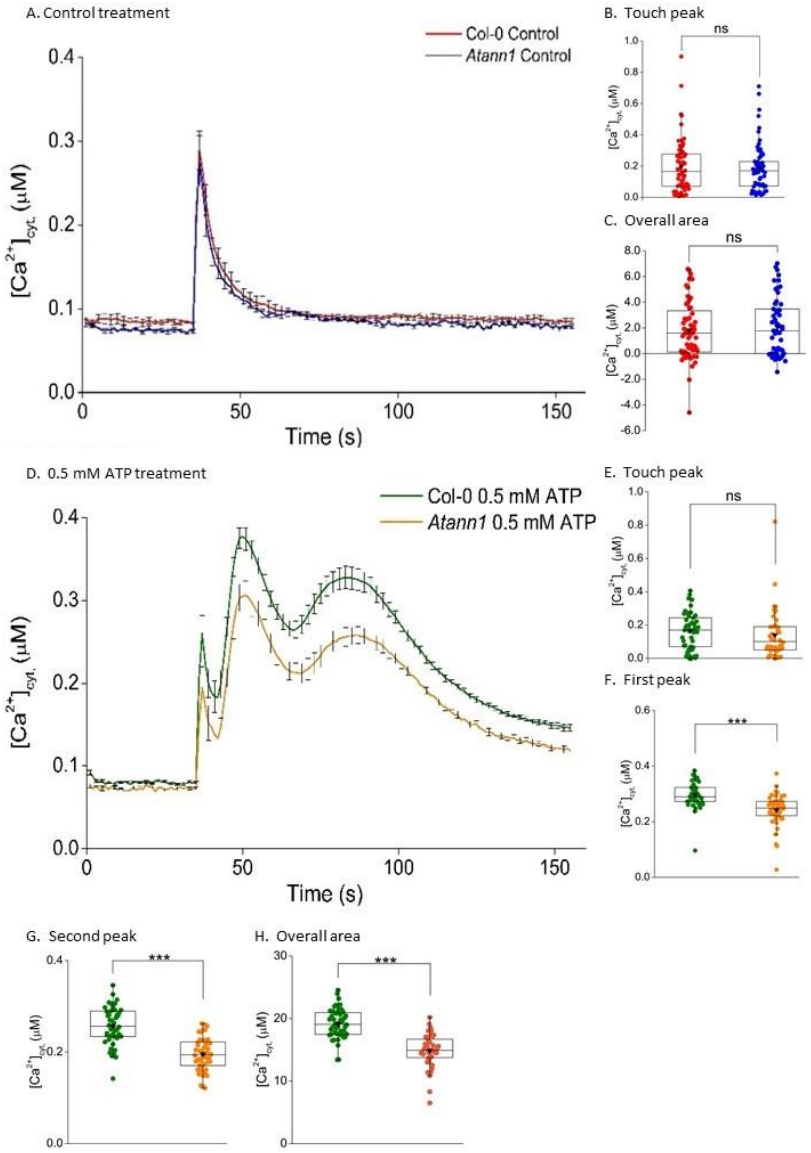

Figure 3.6: **$[Ca^{2+}]_{cyt}$ accumulation in the root tip caused by 0.5 mM eATP requires AtANN1.** The apical 1 cm of 7-day-old root tips expressing (apo)aequorin were excised and used for the test. The $[Ca^{2+}]_{cyt}$ response for the control treatment (A) and 0.5 mM ATP (D) were recorded for 155 s and treatment was added at the 35th second. Time course data were from the means ± SEM of 3 independent trials, with n = 45 root tips per genotype and treatment. Touch peak (B) represents the highest value of the touch response (35 - 53 s) whereas the overall area (C) is the total area under the curve extracted from the time course data of the control treatment (35 - 155 s). Time course analysis of the 0.5 mM ATP treatment is split up into the first peak (F) and the second peak (G) responses, which were the highest values of the peaks that emerged after the touch response (E) . The total accumulation of $[Ca^{2+}]_{cyt}$ of Col-0 and *Atann1* were determined through the overall area under the curve (H) (35 - 155 s). All calculations carried out were with the baseline (the first 35 s of measurement) subtracted. Middle line of the boxplot represents the median whereas the inverted triangle represents the mean. *p*-values: ns (not significant $p > 0.05$), *** ($p < 0.001$), Welch's *t*-test for parametric test and Wilcoxon rank sum test for non-parametric test.

This test was also carried out for 0.5 mM ADP treatment. In the control treatment, the baseline for both Col-0 (0.08±0.0009 μM) and *Atann1* mutant (0.07±0.001 μM) was at a similar level (Figure 3.7 A). After the addition of the control solution at the 35th second, Col-0 and *Atann1* generated touch responses that were not significantly different from each other (Col-0 0.17±0.01 μM; *Atann1* 0.14±0.01 μM; Figure 3.7 B). There was also no significant difference in the overall accumulation of $[Ca^{2+}]_{cyt}$ by Col-0 (2.06±0.30 μM) and *Atann1* (1.63±0.25 μM) (Figure 3.7 C) due to the control solution.

With 0.5 mM ADP treatment, recordings for 155 seconds showed a biphasic pattern of $[Ca^{2+}]_{cyt}$ response after the touch response for both Col-0 and *Atann1*, with the first peak having slightly higher amplitude than the second peak (Figure 3.7 D). The touch response was not affected by the 0.5 mM ADP treatment, as there was no difference in the touch peak value between Col-0 (0.14±0.01 μM) and *Atann1* (0.14±0.02 μM) (Figure 3.7 E). However, *Atann1* had significantly lower amplitude of $[Ca^{2+}]_{cyt}$ in contrast to Col-0 in the first peak (Col-0 0.25±0.01 μM; *Atann1* 0.20±0.015 μM; Figure 3.7 F) and the second peak (Col-0 0.24±0.011 μM; *Atann1* 0.18±0.008 μM; Figure 3.7 G). Overall accumulation of $[Ca^{2+}]_{cyt}$ in *Atann1* (13.56±0.96 μM) was reduced compared to Col-0 (17.49±0.87 μM), confirming the role of AtANN1 in mediating the $[Ca^{2+}]_{cyt}$ response due to 0.5 mM ADP treatment at the root tip level (Figure 3.7 H).

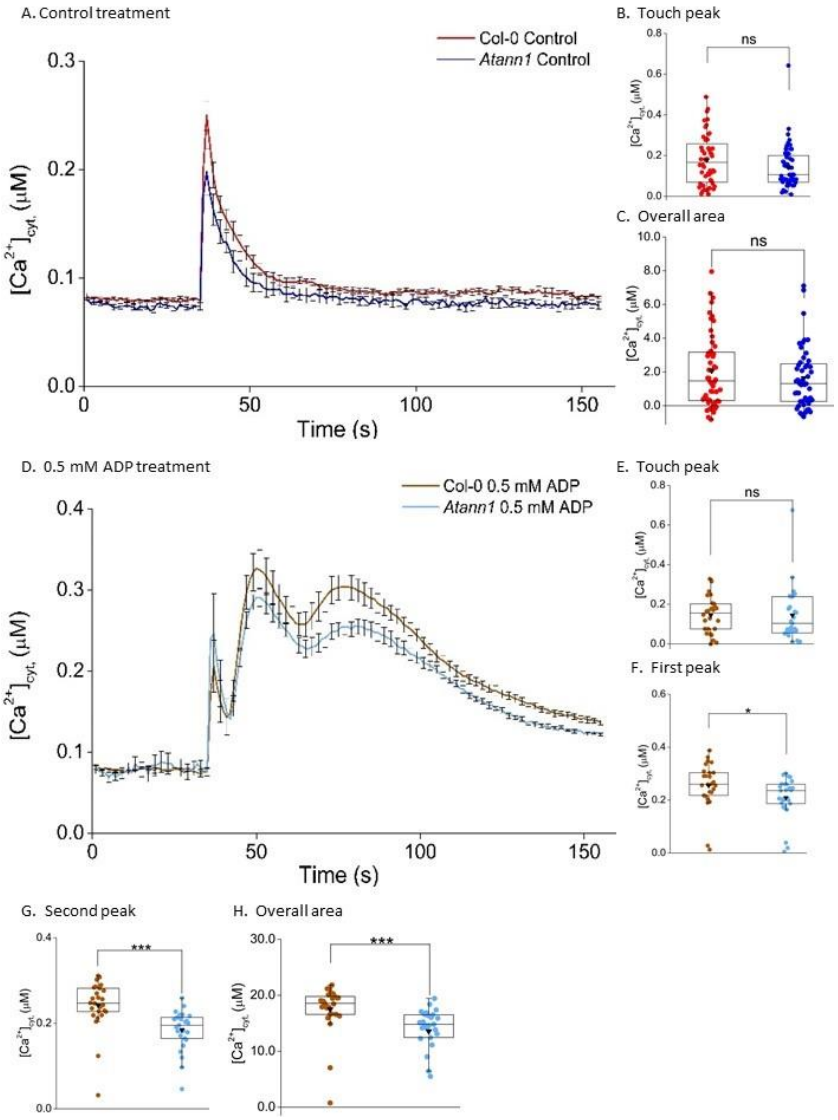

Figure 3.7*:* $[Ca^{2+}]_{cyt}$ accumulation in the root tips caused by 0.5 mM eADP requires AtANN1. The apical 1 cm of 7-day-old root tips were excised and used for the test. The $[Ca^{2+}]_{cyt}$ response for the control treatment (A) and 0.5 mM ADP (D) were recorded for 155 s and each treatment was added at the 35th second. Time course data were from the means ± SEM of 6 independent trials, with n = 25 root tips per genotype and treatment. Touch peak (B) represents the highest value of the touch response (35 - 55 s) whereas the overall area (C) is the total area under the curve extracted from the time course data of the control treatment (35 - 155 s). Time course analysis of the 0.5 mM ADP treatment is split up into the first peak (F) and the second peak (G) responses, which were the highest values of the peaks that emerged after the touch response (E). The total accumulation of $[Ca^{2+}]_{cyt}$ of Col-0 and *Atann1* were determined through the overall area under the curve (H) (35 - 155 s). All calculations carried out were with the baseline (the first 35 s of measurement) subtracted. Middle line of the boxplot represents the median whereas the inverted triangle represents the mean. *p*-values: ns (not significant $p > 0.05$), * ($p<0.05$), ** ($p<0.01$), *** ($p< 0.001$); Welch's *t*-test for parametric test and Wilcoxon rank sum test for non-parametric test.

In order to complete the assessment of function of AtANN1, the complemented mutant line of *Atann1* (*Atann1/ANN1*) was put to the test. The Col-0, *Atann1* and *Atann1/ANN1* seeds containing aequorin reporter used in this experiment were prepared and genotyped by Dr Katie Wilkins (University of Cambridge). Excised root tips (apical 1 cm) of *Atann1/ANN1* were challenged with 1 mM ATP solution alongside the Col-0 wild type and *Atann1* mutant for comparison. Figure 3.8 A shows the time course of the $[Ca^{2+}]_{cyt}$ responses of each genotype when treated with control solution, which evoked a single touch response for 10 s (35 - 45 seconds) before going back to the basal level. Statistical analysis confirmed no significant differences in the touch peak (Col-0 0.52±0.08 μM; *Atann1* 0.53±0.09 μM; *Atann1/ANN1* 0.53±0.09 μM) (Figure 3.8 B) and the overall $[Ca^{2+}]_{cyt}$ accumulation due to control treatment (Col-0 3.29±0.53 μM; *Atann1* 3.52±055 μM; *Atann1/ANN1* 3.37±0.59 μM) (Figure 3.8 C) between all genotypes.

When exposed to 1 mM ATP solution at the 35th second, Col-0, *Atann1* and *Atann1/ANN1* sustained a biphasic $[Ca^{2+}]_{cyt}$ response after the touch response (Figure 3.8 D). In-depth analysis confirmed that there were no significant differences in the touch response between all the genotypes due to the treatment injection (Col-0 0.20±0.03 μM; *Atann1* 0.21±0.03 μM; *Atann1/ANN1* 0.22±0.04 μM) (Figure 3.8 E). *Atann1* (0.19±0.007 μM) was significantly impaired in the $[Ca^{2+}]_{cyt}$ response first peak compaired to Col-0 (0.28±0.008 μM) in the 1 mM ATP treatment test. The complemented line of the *Atann1* mutant, *Atann1/ANN1* (0.24±0.006 μM) however managed to only partially rescue the $[Ca^{2+}]_{cyt}$ response in the first peak (Figure 3.8 F). In the second peak, *Atann1* again showed significant difference in $[Ca^{2+}]_{cyt}$ compared to Col-0 (Col-0 0.30±0.007 μM; *Atann1* 0.27±0.01 μM). Unlike in the first peak, *Atann1/ANN1* showed ability to complement the mutant phenotype as in the second peak the $[Ca^{2+}]_{cyt}$ was not significantly different from the Col-0 (*Atann1/ANN1* 0.28±0.008 μM) (Figure 3.8 G). The total $[Ca^{2+}]_{cyt}$ accumulated under 1 mM ATP treatment in the *Atann1* mutant (16.80±0.52 μM) is lower compared to the Col-0 (20.73±0.47 μM), however the *Atann1/ANN1* (18.71 ±0.38 μMs) unexpectedly showed slightly lower $[Ca^{2+}]_{cyt}$ than Col-0 (Figure 3.8 H).

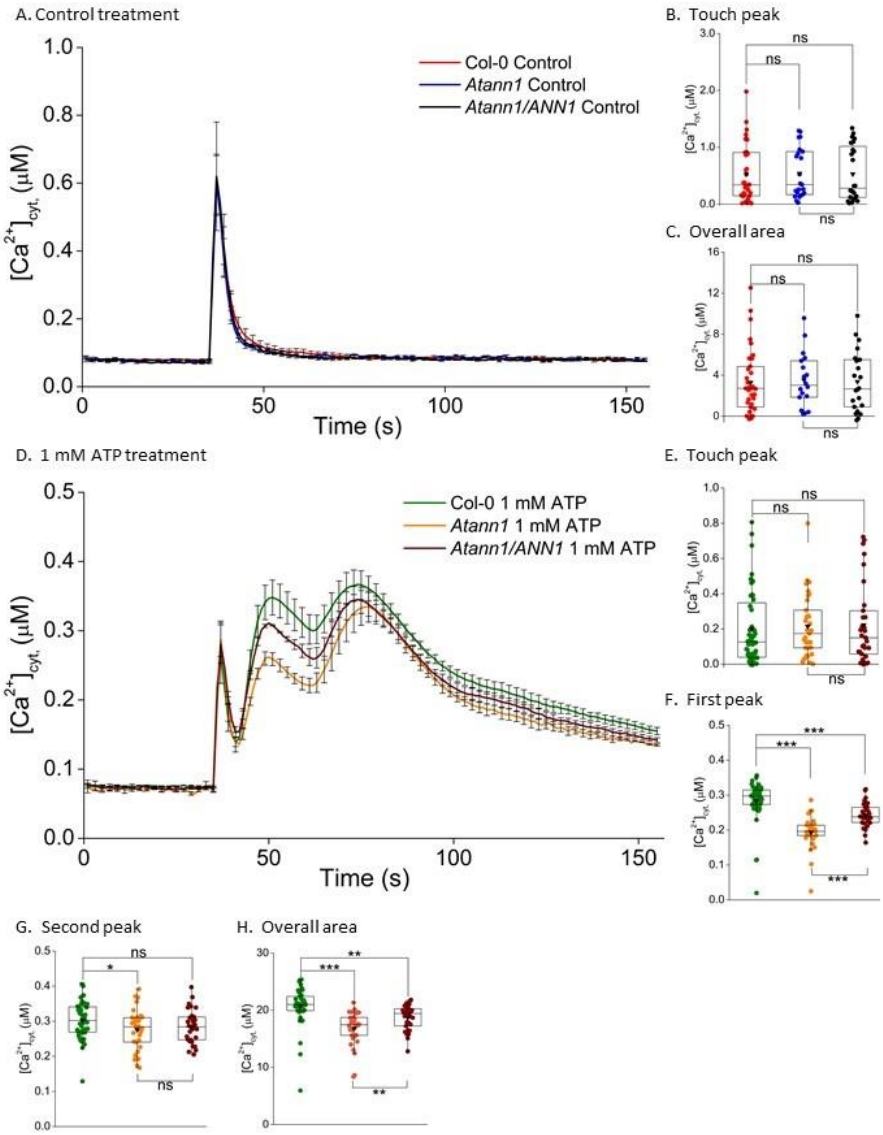

Figure 3.8*: Atann1* **complemented line rescued the second peak $[Ca^{2+}]_{cyt}$ accumulation due to 1 mM ATP treatment.** Seven-day-old 1 cm root tips were challenged with control solution (A) or 1mM ATP (B) at the 35th second and the $[Ca^{2+}]_{cyt}$ measurement was taken for 155 seconds. Time course data are from the means ± SEM of 3 independent trials, with *n* = 25 - 34 root tips per genotype and treatment. Touch peak (B) represents the highest value of the touch response (35 - 55 s) whereas the overall area (C) is the total area under the curve extracted from the time course data of the control treatment (35 - 155 s). Time course analysis of the 1 mM ATP treatment is split up into the first peak (F) and the second peak (G) responses, which were the highest values of the peaks that emerged after the touch response (E). The total accumulation of $[Ca^{2+}]_{cyt}$ of Col-0, *Atann1* and *Atann1/ANN1* were determined through the overall area under the curve (H) (35 - 155 s). All calculations carried out were with the baseline (the first 35 seconds of measurement) subtracted. Middle line of the boxplot represents the median whereas the inverted triangle represents the mean. *p*-values: ns (not significant $p>0.05$), * ($p<0.05$), ** ($p<0.01$), *** ($p< 0.001$); Welch's *t*-test for parametric test and Wilcoxon rank sum test for non-parametric test.

3.2.4 eATP and eADP act as signals rather than energy sources

In order to confirm that eATP acted as a signal instead of an energy source in producing the $[Ca^{2+}]_{cyt}$ response, a non-hydrolysable ATP analogue (ATPγS) was also tested as a function of concentration. The ATPγS used in this study was a tetralithium salt and lithium was previously found to inhibit the action of free Ca^{2+} in the cytoplasm (Allender *et al.*, 1997). Seven-day-old whole roots of the wild type Col-0 with (apo)aequorin were subjected to the $[Ca^{2+}]_{cyt}$ assay with control treatment, 1 mM ATP treatment (sodium salt), 1 mM ATPγS treatment and 1 mM ATP in 4 mM LiCl treatment solution (as a lithium control).

$[Ca^{2+}]_{cyt}$ measurements taken for 155 s showed the familiar biphasic $[Ca^{2+}]_{cyt}$ response in Col-0 in all treatments after the touch response (Figure 3.9 A). Based on the overall $[Ca^{2+}]_{cyt}$ accumulation, treatment with 1 mM ATPγS (21.84±1.53 μM) evoked a similar $[Ca^{2+}]_{cyt}$ response to 1mM ATP (20.92±0.67 μM) (Figure 3.9 B). LiCl (4 mM) and 1 mM ATP treatment added as a control proved that the lithium salt did not interfere with Ca^{2+} transport as the overall $[Ca^{2+}]_{cyt}$ in this combined treatment (22.91±0.58 μM) did not differ significantly from the 1 mM ATP treatment alone (Figure 3.9 B).

Tests with the *Atann1* mutant also showed the biphasic pattern of $[Ca^{2+}]_{cyt}$ response towards all the treatments albeit with lower amplitude compared to Col-0 (Figure 3.9 C). The overall $[Ca^{2+}]_{cyt}$ accumulation of *Atann1* in the 1 mM ATP treatment (16.42±0.56 μM) was similar to the 1 mM ATPγS (15.79±0.64 μM) treatment as well as the 4 mM LiCl and 1 mM ATP treatment (16.19±0.72 μM; Figure 3.9 D). This confirmed that the ATP acted as a signal molecule and hydrolysis of this molecule to provide an energy source is not needed to drive the $[Ca^{2+}]_{cyt}$ response.

A test with the non-hydrolysable analogue of ADP (ADPβS) as the agonist was also carried out to see whether ADP hydrolysis at the plasma membrane was necessary. Col-0 whole roots produced the biphasic pattern of $[Ca^{2+}]_{cyt}$ response in all treatments except for the control (Figure 3.10 A). The overall area under the curve between Col-0 treated with 1 mM ADP (21.08±0.61 μM) was similar to the 1 mM ADPβS treatment (21.59±0.47 μM), indicating that the hydrolysis of ADP was not needed to produce the $[Ca^{2+}]_{cyt}$ response (Figure 3.10 B).

In the *Atann1* whole root samples, lower amplitude of the $[Ca^{2+}]_{cyt}$ biphasic response was seen with all of the treatments compared with Col-0 except for the control treatment (Figure 3.10 C). Total accumulation of *Atann1* $[Ca^{2+}]_{cyt}$ in the presence of ADPβS

(17.15±0.55 µM) was not significantly different from ADP (15.10±0.58 µM) proving that ADP did not need to be hydrolysed to produce the $[Ca^{2+}]_{cyt}$ response (Figure 3.10 D). The ADPβS obtained was a trilithium salt thus 3 mM LiCl salt together with 1 mM ADP served as a control to ensure that the LiCl salt did not influence the outcome of the experiment. Both Col-0 and *Atann1* whole roots showed no significant difference between the LiCl/ADP treatment (Col-0 23.27±0.69 µM; *Atann1* 16.20±0.75 µM) and the 1 mM ADP treatment (Figure 3.10 B; Figure 3.10 D).

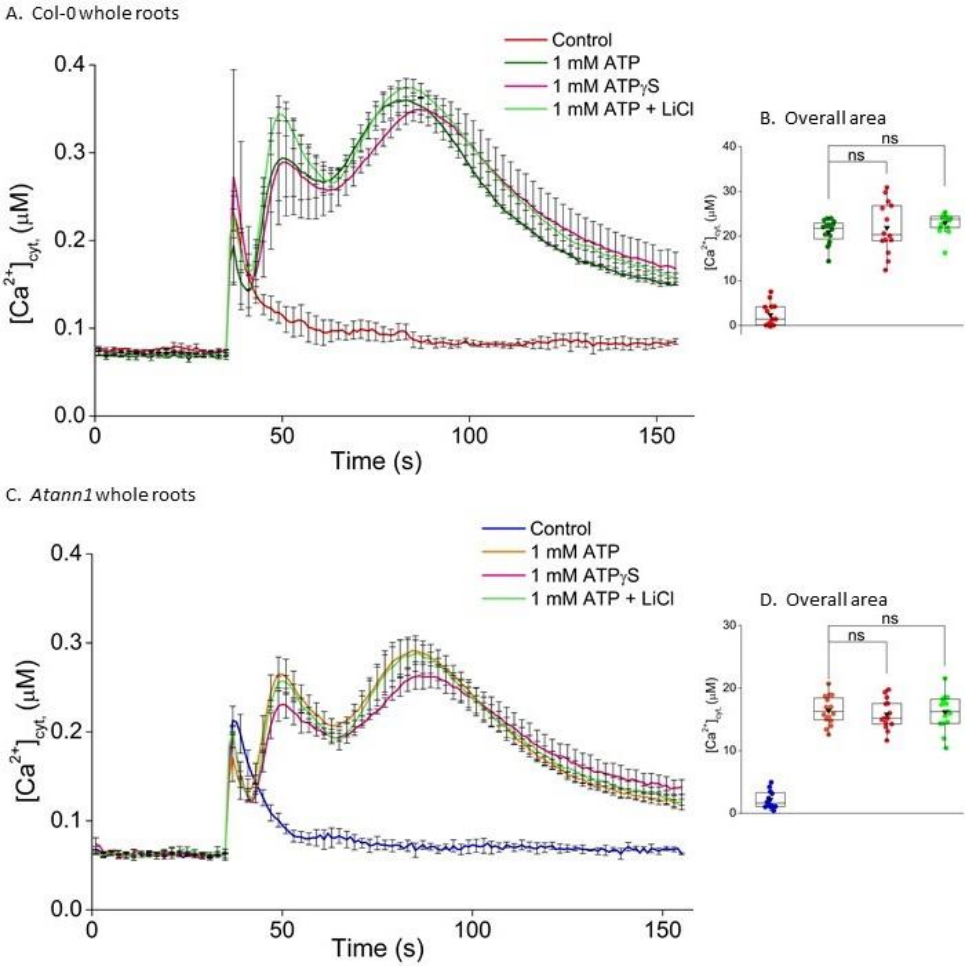

Figure 3.9*:* eATP is not hydrolysed and acts as a signal molecule. Seven-day-old whole roots of Col-0 (A) and *Atann1* (C) were treated with 1 mM ATP or the non-hydrolysable ATP analogue (ATPγS). ATP treatment (1 mM) with 4 mM $LiCl_2$ acted as a control for the tetralithium salt contained in the ATPγS. The $[Ca^{2+}]_{cyt}$ responses were recorded for 155 s and each treatment was added at the 35th second. These time course data were from the means ± SEM of 3 independent trials, with n = 13 - 15 roots per genotype and treatment. Overall area which indicates the total accumulation of $[Ca^{2+}]_{cyt}$ in (B) and (D) was the total area under the curve extracted from the time course data of Col-0 and *Atann1* respectively (35 - 155 s). All calculations carried out were with the baseline (the first 35 s of measurement) subtracted. Middle line of the boxplot represents the median whereas the inverted triangle represents the mean p-values: ns (not significant $p > 0.05$), Welch's t-test.

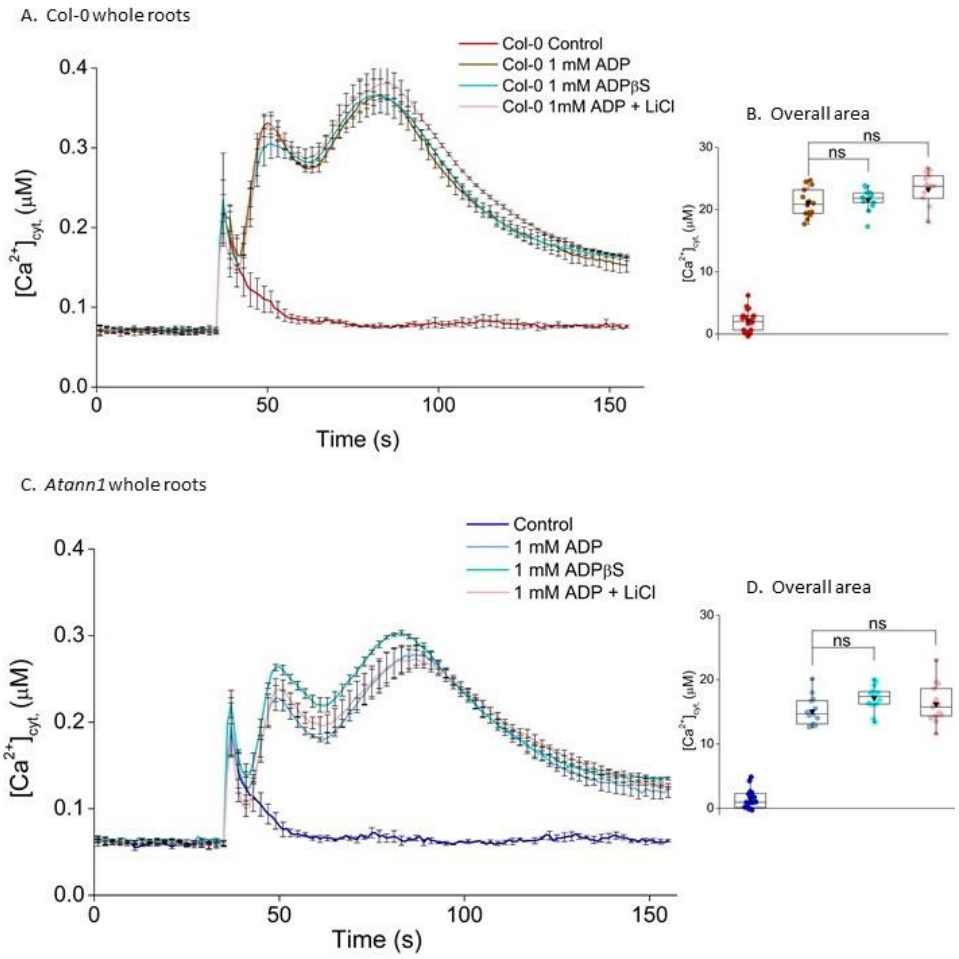

Figure 3.10*:* eADP acts as a signal not an energy source. Seven-day-old whole roots of Col-0 (A) and *Atann1* (C) were treated with 1 mM ADP or the non-hydrolysable ADP analogue (ADP*β*S). ADP treatment (1 mM) with 3 mM $LiCl_2$ acted as a control for the trilithium salt contained in the ADP*β*S. The $[Ca^{2+}]_{cyt}$ responses were recorded for 155 s and each treatment was added at the 35th second. These time course data were from the means ± SEM of 3 independent trials, with n = 12 - 13 roots per genotype and treatment. Overall area which indicates the total accumulation of $[Ca^{2+}]_{cyt}$ in (B) and (D) was the total area under the curve extracted from the time course data of Col-0 and *Atann1* respectively (35 - 155 s). All calculations carried out were with the baseline (the first 35 s of measurement) subtracted. Middle line of the boxplot represents the median whereas the inverted triangle represents the mean. p-values: ns (not significant $p > 0.05$), * ($p<0.05$); Welch's t-test.

3.2.5 Comparison between $[Ca^{2+}]_{cyt}$ accumulation in eATP and eADP signalling

Previous studies found that intracellular ROS are produced by *Arabidopsis* roots in the presence of eATP but not eADP (Demidchik *et al.*, 2009, 2011), suggesting the possibility of disparate pathways between eATP and eADP. In this test, comparison of the $[Ca^{2+}]_{cyt}$ changes in seven-day-old whole roots of Col-0 between 1 mM ATP and 1 mM ADP was carried out. This was to observe whether there were any differences in terms of the

calcium signature or amplitude between 1 mM ATP and 1 mM ADP treatment to further investigate the idea of eATP and eADP as separate signalling mechanisms.

Both 1 mM ATP and 1 mM ADP evoked a biphasic $[Ca^{2+}]_{cyt}$ response after the touch response with almost similar amplitude in the first peak (ATP 0.24±0.02 μM; ADP 0.26±0.01 μM) and the second peak (ATP 0.30±0.09 μM; ADP 0.29±0.009 μM; Figure 3.11 A). Based on the overall area under the curve, Col-0 challenged with 1 mM ATP and 1 mM ADP accumulated the same amount of $[Ca^{2+}]_{cyt}$ (ATP 20.92±0.67 μM; ADP 21.08 ±0.61 μM; Figure 3.11 B).

In 0.1 mM ATP or 0.1 mM ADP treatments, Col-0 produced almost similar amplitudes of the first peak (ATP 0.24±0.014 μM; ADP 0.21±0.011 μM) and the second peak (ATP 0.24±0.018 μM; ADP 0.23±0.015 μM) after the touch response (ATP 0.64±0.11 μM; ADP 0.51±0.08 μM; Figure 3.11 C) as well. The total accumulation of $[Ca^{2+}]_{cyt}$ also showed no significant difference between 0.1 mM ATP (19.31±1.56 μM) and 0.1 mM ADP treatment (18.67±1.06 μM; Figure 3.11 D). There were no differences in terms of $[Ca^{2+}]_{cyt}$ response between eATP and eADP signal at whole root level.

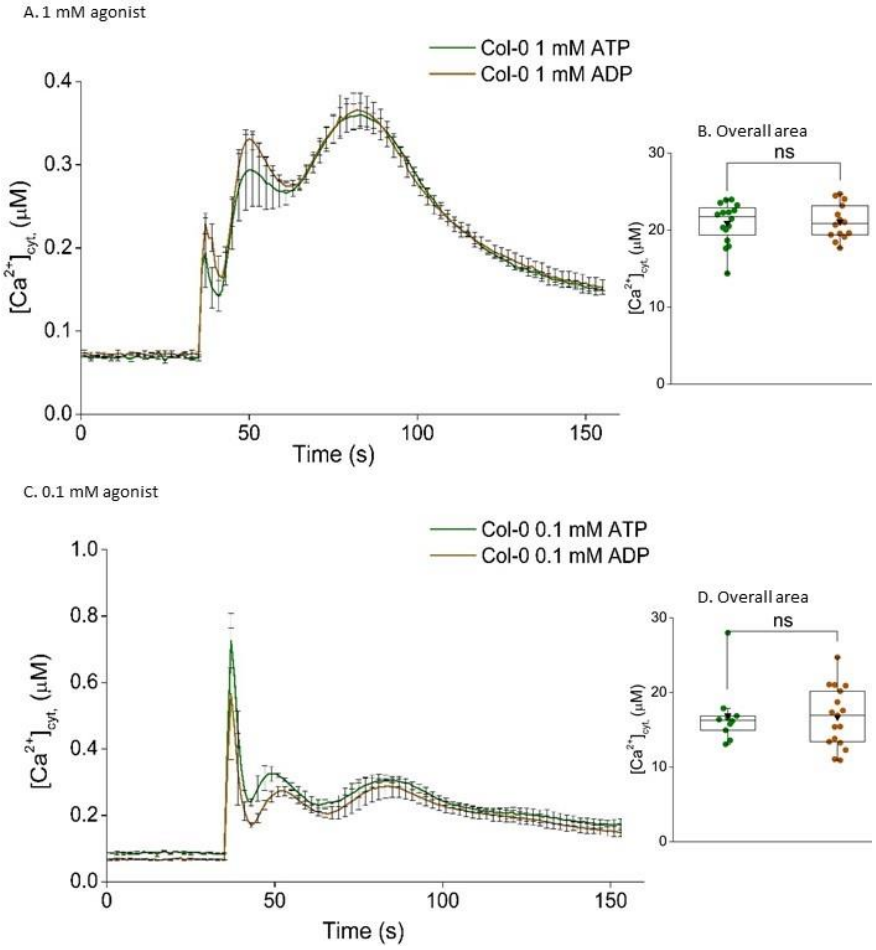

Figure 3.11: **eATP and eADP evoke similar $[Ca^{2+}]_{cyt}$ signatures in whole roots.** Time course data show 7-day-old Col-0 whole root response towards 1 mM ATP or 1 mM ADP (A); and 0.1 mM ATP or 0.1 mM ADP (B). The $[Ca^{2+}]_{cyt}$ responses were recorded for 155 s and each treatment was added at the 35th second. Time course data were from the means ± SEM of 3 independent trials, with n = 25 whole roots for (A) and means ± SEM of 3 independent trials, with n = 12 – 13 whole roots for (C). Analysis was carried out by comparing the total accumulation of $[Ca^{2+}]_{cyt}$ (overall area under the curve) between eATP and eADP at 1 mM (B) (35 - 155 s) and 0.1 mM (D) (35 - 155 s). All calculations carried out are with the baseline (the first 35 seconds of measurement) subtracted. Middle line of the boxplot represents the median whereas the inverted triangle represents the mean. p-values: ns (not significant p>0.05); Welch's t-test.

3.2.6 $GdCl_3$ partially blocked the $[Ca^{2+}]_{cyt}$ increase by 0.5 mM ATP

In order to understand the mechanism of the $[Ca^{2+}]_{cyt}$ increase, a test using the voltage-sensitive calcium channel blocker $GdCl_3$ was carried out to identify the source of the calcium ion. Gd^{3+}, as a trivalent, can effectively remain bound to calcium channels and compete with the calcium ion thus acting as a calcium channel blocker (Malasics *et al.*, 2010). In this test, 7-day-old 1 cm root tips of Col-0 and *Atann1* were incubated with 0.5 mM

Gd^{3+} for 30 minutes prior to the $[Ca^{2+}]_{cyt}$ measurement with 0.5 mM ATP or ADP added at the 35th second as a treatment.

Control treatment only produced a single touch response in roots that were not incubated with $GdCl_3$ and roots that were incubated with $GdCl_3$ prior to measurement (Figure 3.12 A). In *Atann1*, the touch peak did not differ significantly between control (0.20±0.03 μM) and the $GdCl_3$ pre-treatment (0.13±0.02 μM), but was lowered by the treatment. The touch response of Col-0 however was affected by the $GdCl_3$ treatment as the peak value differed significantly between the control (0.20±0.02 μM) and the $GdCl_3$ pre-treatment (0.11±0.02 μM). The overall $[Ca^{2+}]_{cyt}$ accumulation in control conditions (Col-0 2.67±0.42 μM; *Atann1* 2.32±0.49 μM) and $GdCl_3$ pre-treatment (Col-0 1.52±0.74 μM; *Atann1* 3.36±0.61 μM) was not significantly different between Col-0 and *Atann1*, confirming that the Gd^{3+} incubation has no effect on the overall touch response of $[Ca^{2+}]_{cyt}$ (Figure 3.12 B).

Upon challenge with 0.5 mM ATP, both Col-0 and *Atann1* with or without the $GdCl_3$ produced the signature biphasic pattern of $[Ca^{2+}]_{cyt}$. However, a delayed $[Ca^{2+}]_{cyt}$ response in the first peak followed by a less pronounced second peak for $GdCl_3$-treated samples was observed (Figure 3.12 C). Detailed analysis of the first peak showed that the $GdCl_3$ significantly inhibited the full $[Ca^{2+}]_{cyt}$ response of both Col-0 (with $GdCl_3$ 0.18±0.01 μM) and *Atann1* (with $GdCl_3$ 0.16±0.01 μM) compared to the treatment without $GdCl_3$ (Col-0 0.29±0.01 μM; *Atann1* 0.24±0.01 μM; Figure 3.12 D). Unlike the 0.5 mM ATP treatment alone, the first peak $[Ca^{2+}]_{cyt}$ response of Col-0 and *Atann1* of 0.5 mM ATP treatment with $GdCl_3$ was not significantly different from each other (Figure 3.12 D).

A similar observation was seen in the second peak where $GdCl_3$ severely impeded the $[Ca^{2+}]_{cyt}$ increase for both Col-0 (with $GdCl_3$ 0.14±0.01 μM; without $GdCl_3$ 0.25±0.01 μM) and *Atann1* (with $GdCl_3$ 0.12±0.007 μM; without $GdCl_3$ 0.19±0.009 μM) in 0.5 mM ATP treatment. Statistical analysis showed no significant difference between Col-0 and *Atann1* in $GdCl_3$-treated samples whereas there was a significantly lower second peak value of *Atann1* compared to Col-0 in 0.5 mM ATP treatment without $GdCl_3$ (Figure 3.12 E)

The total $[Ca^{2+}]_{cyt}$ accumulation confirmed the ability of $GdCl_3$ to partially block the normal $[Ca^{2+}]_{cyt}$ increase as the $GdCl_3$-treated root tips of both Col-0 (13.34±1.23 μM) and *Atann1* (12.04±0.89 μM) was significantly impaired compared to the non $GdCl_3$-treated root tips (Col-0 19.10±0.60 μM; *Atann1* 15.19±0.81 μM; Figure 3.12 F). As shown in the previous section, *Atann1* root tips significantly accumulated less $[Ca^{2+}]_{cyt}$ compared to Col-0

in response to eATP. However, in $GdCl_3$-treated samples, there was no significant difference between Col-0 and *Atann1* in the total $[Ca^{2+}]_{cyt}$ accumulation.

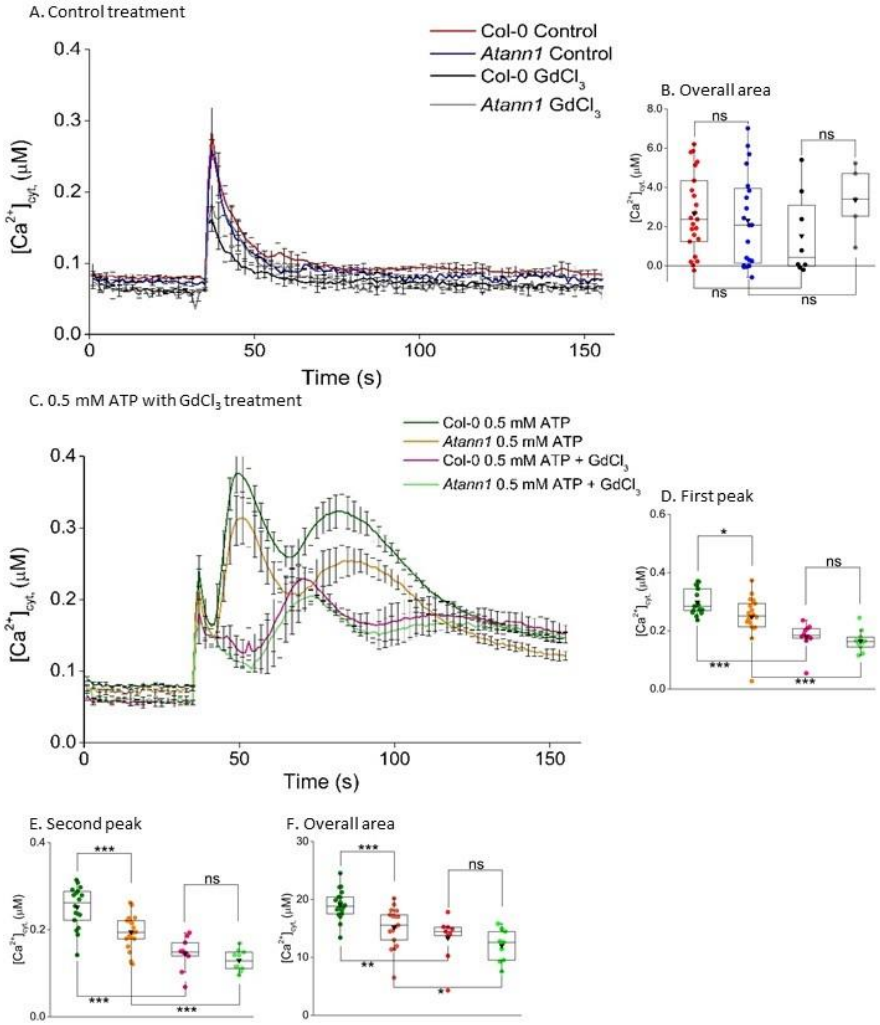

Figure 3.12: **$GdCl_3$ treatment inhibits $[Ca^{2+}]_{cyt}$ accumulation by eATP in root tips.** The $[Ca^{2+}]_{cyt}$ responses were recorded for 155 s for both the control treatment (A) and the 0.5 mM ATP treatment (C) and each treatment was added at the 35th second. Seven-day-old Col-0 and *Atann1* 1 cm root tips were incubated with 0.5 mM $GdCl_3$ for 30 minutes prior to the treatment. These time course data were from the means ± SEM of 3 independent trials, with a total of 10 – 23 root tips per genotype and treatment. The overall area (B) (35 - 155 s) was the total area under the curve for the control treatment. Time course analysis of the 0.5 mM ATP treatment (C) is split up into the first peak (D) (without $GdCl_3$ 41 - 66 s; with $GdCl_3$ 51 - 93 s) and the second peak (E) (without $GdCl_3$ 66 - 155 s; with $GdCl_3$ 93 - 155 s) response, which is the highest value of the peaks that emerge after the touch response. The total accumulation of $[Ca^{2+}]_{cyt}$ by both genotypes was determined through the overall area under the curve (F) (35 - 155 s). All of the calculations carried out were with the baseline (the first 35 s of measurement) subtracted. Middle line of the boxplot represents the median whereas the inverted triangle represents the mean. *p*-values: ns (not significant $p>0.05$), *($p<0.05$), **($p<0.01$),***($p<0.001$); Analysis of Variance (ANOVA) with Tukey's test.

As eADP could potentially direct a different signalling pathway to eATP, a similar test with $GdCl_3$ was executed to determine whether the $[Ca^{2+}]_{cyt}$ accumulated under an eADP signal was from the intracellular or extracellular calcium store. Time courses of $[Ca^{2+}]_{cyt}$ measurements shown in Figure 3.13 A indicate that the $GdCl_3$ pre-treatment (Col-0 0.06±0.001 μM; *Atann1* 0.006±0.001 μM) caused a lower $[Ca^{2+}]_{cyt}$ baseline compared to the control incubation solution (Col-0 0.08±00009; *Atann1* 0.07±0.001 μM). However, both conditions supported a single touch response in response to control solution, with $GdCl_3$-treated root tips having a lower $[Ca^{2+}]_{cyt}$ touch response compared to those pre-treated with control solution alone in Col-0 ($GdCl_3$ 0.15±0.03 μM; control 0.19±0.02 μM) but not in *Atann1* ($GdCl_3$ 0.15±0.02 μM; control 0.11±0.015 μM). This again showed that $GdCl_3$ might be affecting the touch response of the Col-0 root tips tested. As the control response of *Atann1* was lower than previously found (Figure 3.12 A) and lower than with $GdCl_3$ pre-treatment, it is not possible to speculate on the effect of this blocker. The touch-induced total accumulation of $[Ca^{2+}]_{cyt}$ showed no significant difference between control solution pre-treatment of Col-0 (1.75±0.34 μM) and $GdCl_3$ pre-treatment (1.69±0.55 μM). However total accumulation of $[Ca^{2+}]_{cyt}$ by $GdCl_3$ pre-treated *Atann1* (2.33±0.45 μM) was significantly greater than control solution pre-treated root tips of *Atann1* (1.01±0.27 μM; Figure 3.13 B), in disagreement with the analogous control experiment shown in Figure 3.12 B.

$[Ca^{2+}]_{cyt}$ measurements showed the familiar biphasic response due to 0.5 mM ADP after the touch response regardless of pre-treatment. Col-0 and *Atann1* root tips that were treated with $GdCl_3$ however showed dampened and delayed $[Ca^{2+}]_{cyt}$ increase after the touch response (first peak 55s - 104s; second peak 104s - 155s) compared to the tips that were not treated with $GdCl_3$ (first peak 41s - 62s; second peak 62s - 155s; Figure 3.13 C). Based on statistical analysis, $GdCl_3$-treated Col-0 (0.15±0.004 μM) and *Atann1* (0.11±0.007 μM) root tips had lower $[Ca^{2+}]_{cyt}$ compared to the control-treated root tips (Col-0 0.21±0.02 μM; *Atann1* 0.18±0.02 μM) at the first peak (Figure 3.13 D).

Figure 3.13 E shows the second peak $[Ca^{2+}]_{cyt}$ value comparison between $GdCl_3$-treated and control-treated Col-0 and *Atann1* root tips when subjected to 0.5 mM ADP solution. $GdCl_3$ managed to partially block the $[Ca^{2+}]_{cyt}$ accumulation in both Col-0 (with $GdCl_3$ 0.09±0.004 μM; without $GdCl_3$ 0.23±0.02 μM) and *Atann1* (with $GdCl_3$ 0.07±0.005 μM; without $GdCl_3$ 0.17±0.01 μM). In both control-treated root tips and $GdCl_3$-treated root tips, the second peak value of Col-0 was significantly higher compared to *Atann1* (Figure 3.13 E). Overall area under the curve analysis confirmed that the $GdCl_3$ was capable of

partially blocking $[Ca^{2+}]_{cyt}$ accumulation in the presence of 0.5 mM ADP as shown in Figure 3.13 F. Total accumulated $[Ca^{2+}]_{cyt}$ in $GdCl_3$-treated Col-0 (9.82±0.44 µM) and *Atann1* (6.90±0.47 µM) root tips was lower compared to control pre-treatment (Col-0 16.07±1.49 µM; *Atann1* 12.09±1.56 µM). In the absence or presence of $GdCl_3$, Col-0 accumulated higher total $[Ca^{2+}]_{cyt}$ compared to *Atann1* (Figure 3.13 F).

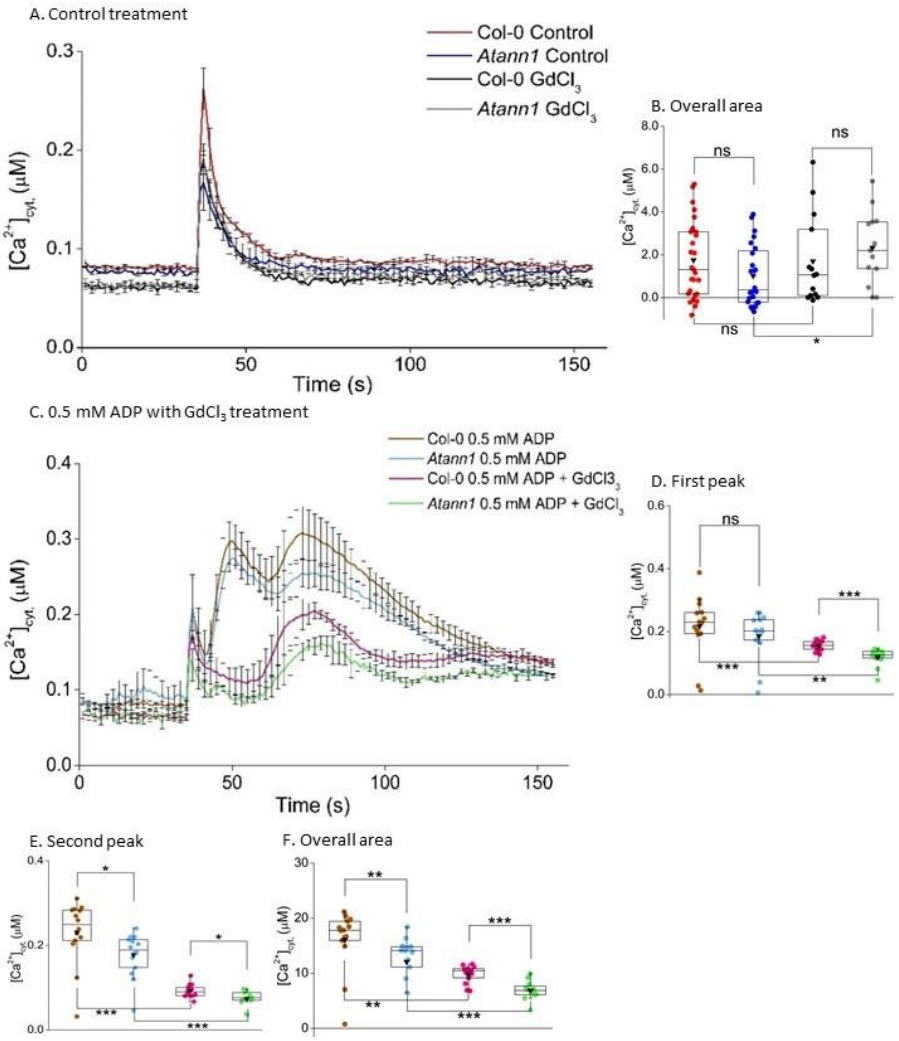

Figure 3.13*: GdCl₃ treatment inhibits $[Ca^{2+}]_{cyt}$ accumulation by eADP in root tips. The $[Ca^{2+}]_{cyt}$ responses were recorded for 155 s for both the control treatment (A) and the 0.5 mM ADP treatment (C) and each treatment was added at the 35th second. Seven-day-old Col-0 and *Atann1* 1 cm root tips were incubated with 0.5 mM $GdCl_3$ for 30 minutes prior to treatment. This time course data were from the means ± SEM of 3 independent trials, with a total of 13 – 27 root tips per genotype and treatment. The overall area (B) (55 - 155 s) was the total area under the curve for the control treatment. Time course analysis of the 0.5 mM ADP treatment (C) is split up into the first peak (D) (without $GdCl_3$ 41 - 62 s; with $GdCl_3$ 55 - 104 s) and the second peak (E) (without $GdCl_3$ 62 - 155 s; with $GdCl_3$ 104 - 155 s) response, which was the highest value of the peaks that emerged after the touch response. The total accumulation of $[Ca^{2+}]_{cyt}$ by both genotypes was determined through the

overall area under the curve (F) (35 - 155 s). All calculations were carried out with the baseline (the first 35 s of measurement) subtracted. Middle line of the boxplot represents the median whereas the inverted triangle represents the mean. *p*-values: ns (not significant $p>0.05$), *($p<0.05$), **($p<0.01$),***($p<0.001$); Analysis of Variance (ANOVA) with Tukey's test.

3.2.7 Suramin partially inhibited the $[Ca^{2+}]_{cyt}$ response to both eATP and eADP

In animal cell studies, suramin was found to have the ability to become a P2 purinoreceptor inhibitor (Hoyle *et al.*, 1990). Here, suramin was tested to implicate the involvement of purinoreceptors in producing the $[Ca^{2+}]_{cyt}$ response to eATP and eADP. Seven-day-old 1 cm root tips of Col-0 and *Atann1* were incubated with 1.5 mM suramin or control solution for 30 minutes before the $[Ca^{2+}]_{cyt}$ measurements were taken.

The baselines for Col-0 (Control 0.09±0.008 μM; suramin 0.08±0.001 μM) and *Atann1* (Control 0.07±0.001 μM; suramin 0.06±0.001 μM) were equivalent for the first 35 s of $[Ca^{2+}]_{cyt}$ measurement and were then followed by a single touch response upon addition of the control solution (Figure 3.14 A). The touch peak values were similar between Col-0 and *Atann1* in control pre-treated root tips (Col-0 0.22±0.05 μM; *Atann1* 0.22±0.03 μM) and the suramin pre-treated root tips (Col-0 0.12±0.02 μM; *Atann1* 0.11±0.02 μM) but the suramin pre-treatment caused significantly lower touch peak response for both genotypes compared to the control pre-treatment. Despite this, based on the overall $[Ca^{2+}]_{cyt}$ accumulated upon the addition of the control solution, there were no significant differences between control pre-treatment (Col-0 1.08±0.46 μM; *Atann1* 2.38±0.51 μM) and the suramin pre-treatment (Col-0 1.23±0.39 μM; *Atann1* 1.63±0.60 μM; Figure 3.14 B).

Upon the addition of 0.5 mM ATP treatment at the 35th second, both the Col-0 and *Atann1* root tips sustained the $[Ca^{2+}]_{cyt}$ biphasic pattern after the touch response until the end of recordings (Figure 3.14 C). Analysis of the first peak from the time course showed that the first peak value of Col-0 was significantly higher compared to *Atann1* in both suramin pre-treated (Col-0 0.22±0.01 μM; *Atann1* 0.18±0.006 μM) and control pre-treated (Col-0 0.29±0.006 μM; *Atann1* 0.23±0.009 μM) root tips. Suramin inhibited some $[Ca^{2+}]_{cyt}$ response to 0.5 mM ATP as both the Col-0 and *Atann1* root tips that were pre-treated with suramin had significantly lower $[Ca^{2+}]_{cyt}$ in the first peak than the root tips that were not pre-treated with suramin (Figure 3.14 D).

Unlike the first peak, the second peak $[Ca^{2+}]_{cyt}$ values for both Col-0 and *Atann1* root tips that were pre-treated with suramin were similar to the root tips that were not pre-treated.

However in both groups, *Atann1* root tips (suramin 0.20±0.005 μM; control 0.20±0.008 μM) accumulated less $[Ca^{2+}]_{cyt}$ than Col-0 (suramin 0.25±0.008 μM; control 0.26±0.008 μM) (Figure 3.14 E).

Based on the overall accumulation of $[Ca^{2+}]_{cyt}$, 1.5 mM suramin seemed not to be effective in inhibiting the 0.5 mM ATP $[Ca^{2+}]_{cyt}$ response. Total $[Ca^{2+}]_{cyt}$ accumulated in suramin pre-treated Col-0 (19.40±0.52 μM) and *Atann1* (15.12±0.33 μM) root tips was not significantly different from the Col-0 (19.92±0.49 μM) and *Atann1* (15.05±0.50 μM) that were not pre-treated with suramin. Total $[Ca^{2+}]_{cyt}$ accumulated due to 0.5 mM ATP in *Atann1* mutant root tips was less than Col-0 in both suramin and control pre-treated samples (Figure 3.14 F).

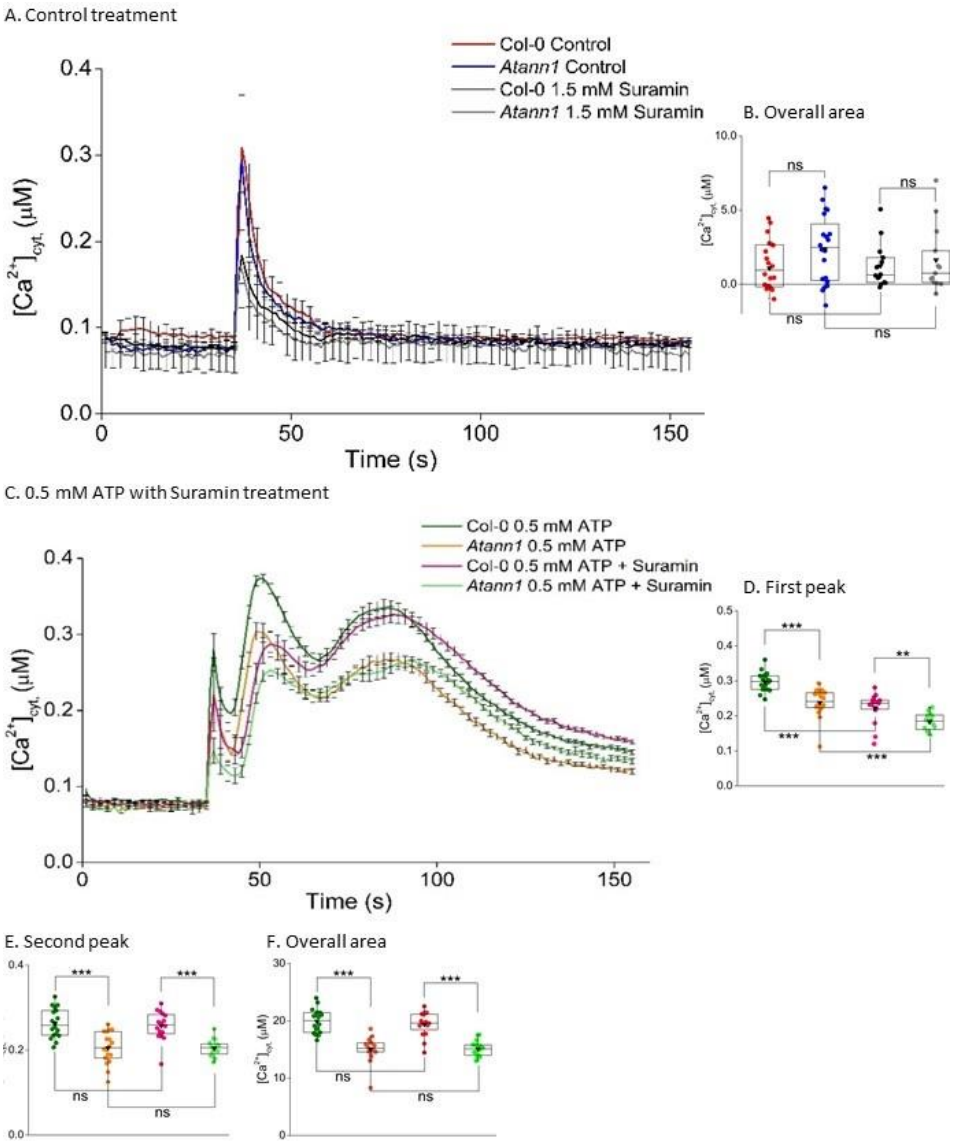

Figure 3.14: **Suramin impaired the first peak $[Ca^{2+}]_{cyt}$ response to eATP.** The $[Ca^{2+}]_{cyt}$ responses were recorded for 155 s for both the control treatment (A) and the 0.5 mM ATP treatment (C) and each treatment was added at the 35th second. Seven-day-old Col-0 and *Atann1* 1 cm root tips were incubated with 1.5 mM suramin or control solution for 30 minutes prior to treatment. These time course data were from the means ± SEM of 3 independent trials, with a total of 15 - 19 root tips per genotype and treatment. The overall area (B) (35 - 155 s) was the total area under the curve for the control treatment. Analysis of the 0.5 mM ATP treatment (C) time course was done with the first peak (D) (41 - 64 s) and the second peak (E) (64 - 155 s) response, which was the highest value of the peaks that emerged after the touch response. The total accumulation of $[Ca^{2+}]_{cyt}$ by both genotypes in 0.5 mM ATP treatment was determined through the overall area under the curve (F) (35 - 155 s). All calculations were carried out with the baseline (the first 35 s of measurement) subtracted. Middle line of the boxplot represents the median whereas the inverted triangle represents the mean. *p*-values: ns (not significant $p>0.05$), *($p<0.05$), **($p<0.01$),***($p<0.001$); Analysis of Variance (ANOVA) with Tukey's test.

A similar test was carried out for 0.5 mM ADP as an agonist on the root tips of Col-0 and *Atann1*. The baseline of both Col-0 and *Atann1* pre-treated with control solution (Col-0 0.07±0.001 μM; *Atann1* 0.07±0.002 μM) or pre-treated with suramin (Col-0 0.07±0.002 μM; *Atann1* 0.07±0.004 μM) were similar and both genotypes produced a single touch peak upon addition of control solution (Figure 3.15 A). There were no significant differences between touch-induced $[Ca^{2+}]_{cyt}$ increases. The total $[Ca^{2+}]_{cyt}$ accumulated by control pre-treated tips (Col-0 2.44±0.50 μM; *Atann1* 2.41±0.48 μM) and the suramin pre-treated tips (Col-0 1.68±0.44 μM; *Atann1* 2.29±0.78 μM) were not significantly different from each other (Figure 3.15 B). This confirmed that suramin pre-treatment did not have an effect on the touch-induced $[Ca^{2+}]_{cyt}$ response of the root tips.

ADP treatment (0.5 mM) evoked a $[Ca^{2+}]_{cyt}$ biphasic response after the touch response in Col-0 and *Atann1* regardless of pre-treatment. The first peak of the $[Ca^{2+}]_{cyt}$ produced in all samples was slightly higher than the second peak (Figure 3.15 C). Detailed analysis of the first peak value indicated that suramin pre-treatment was able to slightly inhibit the $[Ca^{2+}]_{cyt}$ response. Col-0 root tips that were not incubated with 1.5 mM suramin triggered significantly higher $[Ca^{2+}]_{cyt}$ increase (0.28±0.01 μM) compared to Col-0 pre-treated with 1.5 mM suramin (0.23±0.008 μM). This is also true for *Atann1* root tips samples as the 1.5 mM suramin pre-treatment (0.18±0.02 μM) caused significantly lower $[Ca^{2+}]_{cyt}$ released compared to the control-treated *Atann1* root tips (0.24±0.01 μM) (Figure 3.15 D).

Analysis of the second peak of the 0.5 mM ADP treatment showed that suramin pre-treatment was not fully effective in blocking $[Ca^{2+}]_{cyt}$ increase as the second peak value in suramin pre-treated Col-0 (0.22±0.006 μM) and *Atann1* (0.17±0.008 μM) root tips was not significantly impaired compared to the control pre-treated Col-0 (0.24±0.01 μM) and *Atann1* (0.20±0.007 μM) root tips. However, the *Atann1* root tips showed consistently lower $[Ca^{2+}]_{cyt}$ second peak values compared to the Col-0 regardless of whether the root tips were pre-treated with suramin or not (Figure 3.15 E).

As in the ATP treatment, suramin pre-treatment failed to inhibit the total $[Ca^{2+}]_{cyt}$ accumulation caused by 0.5 mM ADP. Total $[Ca^{2+}]_{cyt}$ accumulation in Col-0 (17.43±0.39 μM) and *Atann1* (13.2±0.75 μM) root tips incubated with suramin was not significantly different from the Col-0 (17.86±0.83 μM) and *Atann1* (15.29±0.43 μM) roots tips pre-treated with control solution. *Atann1* root tips consistently accumulated significantly lower $[Ca^{2+}]_{cyt}$ than Col-0 regardless of pre-treatment when challenged with 0.5 mM ADP (Figure 3.15 F).

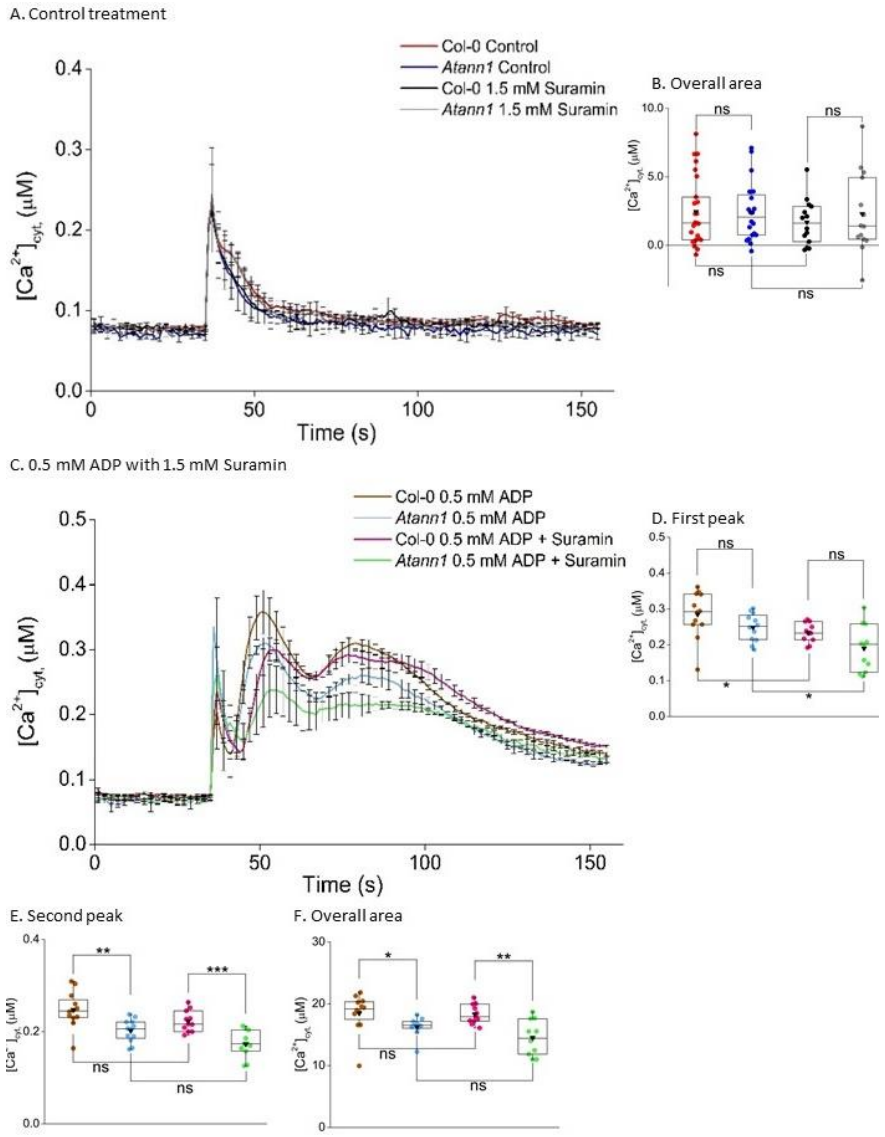

Figure 3.15: **Suramin causes impaired first peak $[Ca^{2+}]_{cyt}$ response to eADP.** The $[Ca^{2+}]_{cyt}$ responses were recorded for 155 s for both the control treatment (A) and the 0.5 mM ADP treatment (C) and each treatment was added at the 35th second. Seven-day-old Col-0 and *Atann1* 1 cm root tips were incubated with 1.5 mM suramin or control solution for 30 minutes prior to the treatment. These time course data were from the means ± SEM of 3 independent trials, with a total of 12 - 25 root tips per genotype and treatment. The overall area (B) (35 - 155 s) was the total area under the curve for the control treatment. Analysis of the 0.5 mM ADP treatment (C) time course was done with the first peak (D) (41 - 64 s) and the second peak (E) (64 - 155 s) response, which was the highest value of the peaks that emerged after the touch response. The total accumulation of $[Ca^{2+}]_{cyt}$ by both genotypes in 0.5 mM ADP treatment was determined through the overall area under the curve (F) (35 - 155 s). All calculations were carried out with the baseline (the first 35 s of measurement) subtracted. Middle line of the boxplot represents the median whereas the inverted triangle represents the mean. *p*-values: ns (not significant $p>0.05$), *($p<0.05$), **($p<0.01$),***($p<0.001$); Analysis of Variance (ANOVA) with Tukey's test.

3.2.8 AtANN1 has the potential to be in the AtDORN1 pathway

AtDORN1 has been established as the purinoreceptor that perceives the eATP and eADP signals but the calcium channels that mediate the downstream responses are not yet known. As AtANN1 is required for the full $[Ca^{2+}]_{cyt}$ response to eATP and eADP, it is important to determine the relation between AtDORN1 and AtANN1 in the eATP and eADP signalling pathways. Here, $[Ca^{2+}]_{cyt}$ measurement of *Atdorn1-1/ann1* (single point mutation in *AtDORN1* and T-DNA insertion in *ANN1*) and *Atdorn1-3/ann1* (T-DNA insertions in *AtDORN1* and *AtANN1*) double mutants (1 cm root tips) when challenged with ATP and ADP were used as a tool to shed some light on this matter. The *Atdorn1-1* mutant is defective in kinase activity and the *Atdorn1-3* mutant is defective in eATP binding (Choi *et al.*, 2014b).

Figure 3.16 A shows that the baseline $[Ca^{2+}]_{cyt}$ was similar between the Col-0 (0.07±0.001 μM), *Atdorn1-1/ann1* (0.06±0.001 μM) and *Atdorn1-1* (0.08±0.001 μM) and that all three genotypes sustained a single touch response upon addition of the control solution with similar amplitude (Col-0 0.27±0.04 μM; *Atdorn1-1/ann1* 0.14±0.01 μM; *Atdorn1-1* 0.34±0.07 μM). $[Ca^{2+}]_{cyt}$ accumulation proved not to be affected by the mutations as the overall $[Ca^{2+}]_{cyt}$ changes due to the control solution between Col-0 (3.05±0.52 μM) *Atdorn1-1/ann1* (1.22±0.32 μM) and *Atdorn1-1* (4.35±0.91 μM) were not significantly different. However, *Atdorn1-1/ann1* accumulated significantly lower total $[Ca^{2+}]_{cyt}$ compared to *Atdorn1-1* due to the control solution (Figure 3.16 B). Replacing the control solution with 1 mM ATP treatment evoked a biphasic $[Ca^{2+}]_{cyt}$ pattern after the touch response in Col-0 (first peak 0.25±0.01 μM; second peak 0.27±0.01 μM) but not in the *Atdorn1-1/ann1* and the *Atdorn1-1* mutants (Figure 3.16 C). Analysis of the overall area under the curve proved that the mutation in both *AtDORN1* and *AtANN1* (*Atdorn1-1/ann1* 2.07±0.44 μM; *Atdorn1-1* 4.30±0.85 μM) almost completely abolished the total $[Ca^{2+}]_{cyt}$ accumulation compared to Col-0 (19.64±0.98 μM) at the root tip level (Figure 3.16 D). However, similar to the control treatment, the total $[Ca^{2+}]_{cyt}$ accumulated by *Atdorn1-1/ann1* was significantly less than *Atdorn1-1* in the 1 mM ATP treatment.

Lower concentrations of eATP have been found to able to also induce physiological change such as stomatal regulation and hypocotyl growth (Clark and Roux, 2011; Jeter and Roux, 2006) thus it is relevant to use a lower concentration of eATP to evoke the $[Ca^{2+}]_{cyt}$ changes. The same experiment was replicated with 0.1 mM instead of 1 mM ATP concentration on 7-day-old 1 cm root tips. At 0.1 mM, ATP elicited a $[Ca^{2+}]_{cyt}$ biphasic

response with lower amplitude in Col-0 root tips (first peak 0.22±0.01 μM; second peak 0.19±0.008 μM) but this response was missing in the *Atdorn1-1/ann1* and *Atdorn1-1* mutants (Figure 3.16 E). The total $[Ca^{2+}]_{cyt}$ accumulated by 0.1 mM ATP treatment in both *Atdorn1-1/ann1* (1.54±0.32 μM) and *Atdorn1-1* (2.17±0.50 μM) were significantly impaired compared to Col-0 (15.43±0.55 μM) but not significantly different to each other (Figure 3.16 F).

Figure 3.17 shows the comparison between the control treatment and the 1 mM ATP treatment or 0.1 mM ATP treatment for each mutant. As shown previously, both *Atdorn1-1/ann1* and *Atdorn1-1* in control treatment and 1 mM ATP treatment or 0.1 mM ATP treatment did not induce the $[Ca^{2+}]_{cyt}$ biphasic response as in Col-0 and showed almost a flat $[Ca^{2+}]_{cyt}$ trace (Figure 3.17 A, C). Detailed analysis was carried out to observe any differences between control treatment and the ATP treatment for each mutant. Based on the overall area under the curve, there were no significant differences between control treatment and the 1 mM ATP for both *Atdorn1-1/ann1* (control 1.22±0.32 μM; 1 mM ATP 2.07±0.44 μM) and *Atdorn1-1* (control 4.35±0.91 μM; 1 mM ATP 4.30±0.85 μM) (Figure 3.17 B). A similar observation was found with 0.1 mM ATP treatment which in both *Atdorn1-1/ann1* and *Atdorn1-1*, there were no statistically significant contrasts in the total accumulation of $[Ca^{2+}]_{cyt}$ between the control treatment (*Atdorn1-1/ann1* 1.22±0.32 μM; *Atdorn1-1* 4.35±0.91 μM) and the 0.1 mM ATP treatment (*Atdorn1-1/ann1* 1.54±0.32 μM; *Atdorn1-1* 2.17±0.50 μM) (Figure 3.17 D).

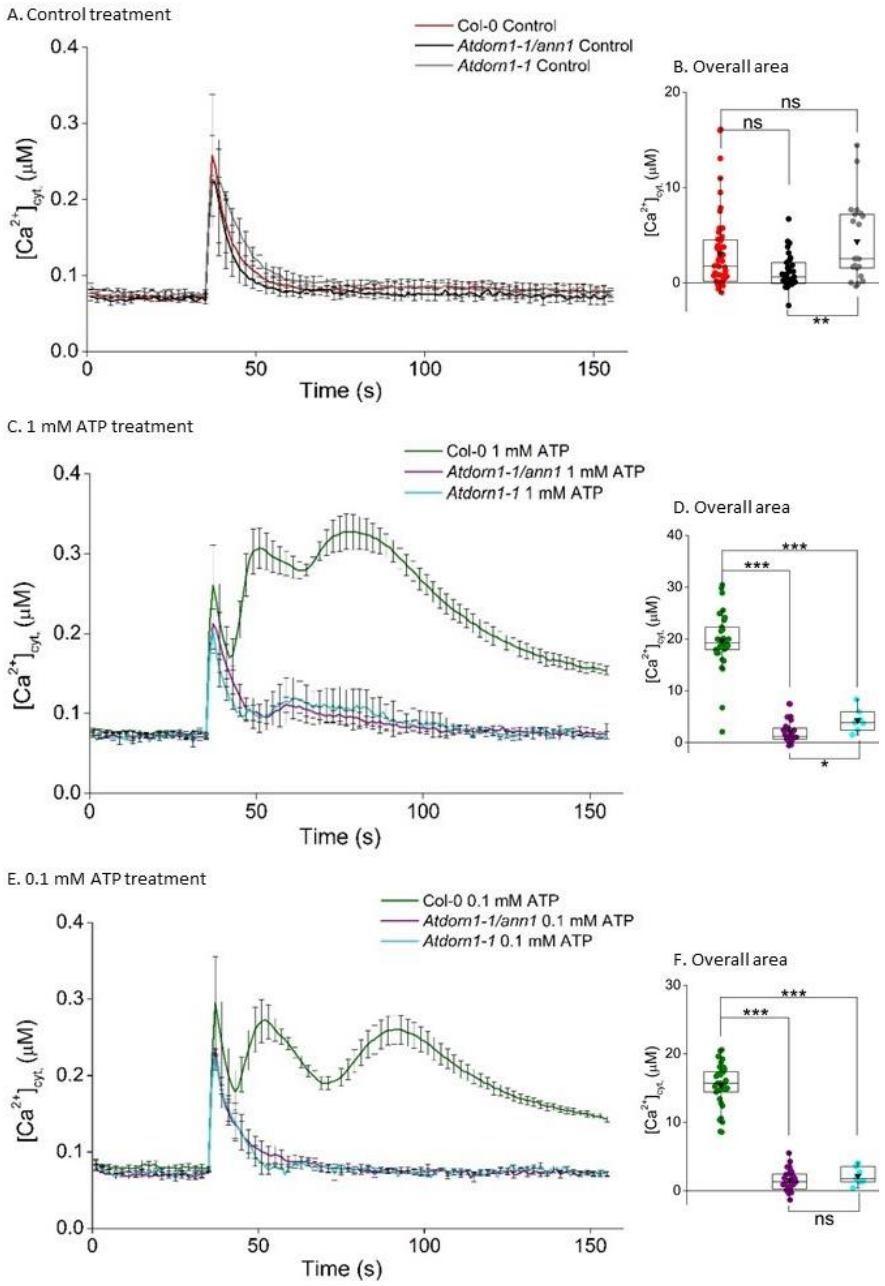

Figure 3.16: **AtANN1 might in the DORN1 pathway in eATP signalling.** Seven-day-old 1 cm root tips of Col-0, *Atdorn1-1*, *Atdorn1-1/ann1* were treated with control buffer (2 mM MES/Tris-HCl; 10 mM $CaCl_2$; 0.1 mM KCl) (A), 1 mM ATP (C) or 0.1 mM ATP (E). The $[Ca^{2+}]_{cyt}$ responses were recorded for 155 s and each treatment was added at the 35th second. These time course data were from the means ± SEM of 6 independent trials, with n = 8 – 36 roots per genotype and treatment. Overall area which indicates the total accumulation of $[Ca^{2+}]_{cyt}$ was the total area under the curve extracted from the time course data from the control (B), 1 mM ATP treatment (D) and 0.1 mM ATP (F) (35 - 155 s). All calculations carried out were with the baseline (the first 35 s of measurement) subtracted. Middle line of the boxplot represents the median whereas the inverted triangle represents the mean. p-values: ns (not significant p>0.05), * (p<0.05), **(p<0.01), ***(p<0.001); Welch's t-test for parametric test and Wilcoxon rank sum test for non-parametric test.

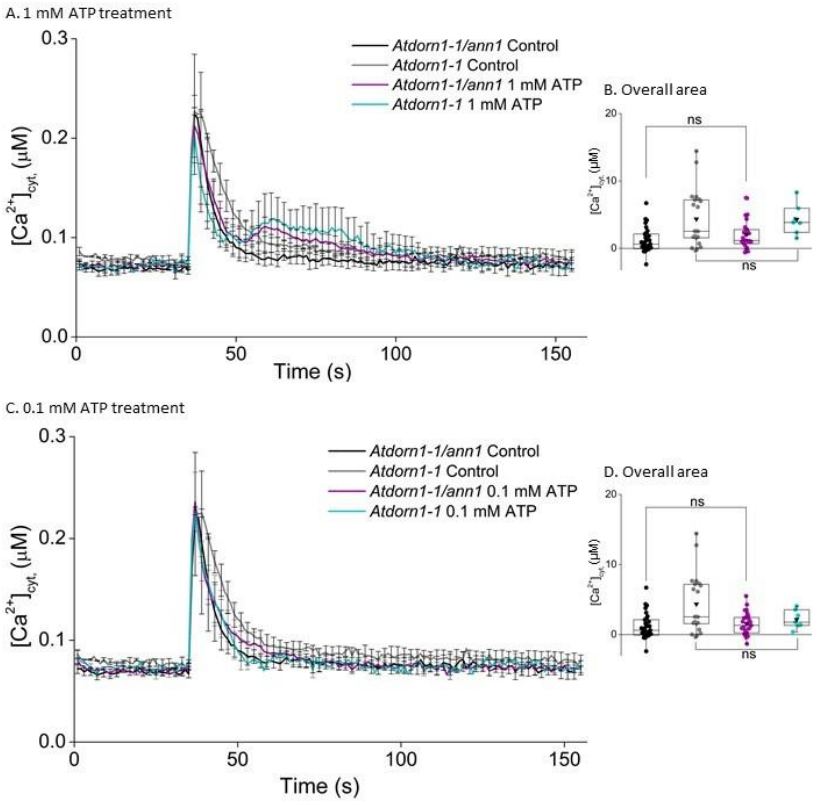

Figure 3.17: **Kinase mutation of AtDORN1 and AtANN1 knock-out eliminates response to ATP.** Seven-day-old 1 cm root tips of *Atdorn1-1* and *Atdorn1-1/ann1* were treated with control buffer (2 mM MES/Tris-HCl; 10 mM $CaCl_2$; 0.1 mM KCl) or 1 mM ATP (A), or control buffer and 0.1 mM ATP (C). The $[Ca^{2+}]_{cyt}$ responses were recorded for 155 s and each treatment was added at the 35th second. These time course data were from the means ± SEM of 6 independent trials, with n = 8 – 36 roots per genotype and treatment. Overall area which indicates the total accumulation of $[Ca^{2+}]_{cyt}$ was the total area under the curve extracted from the time course data of control treatment and 1 mM ATP (A) or 0.1 mM ATP (C) (35 - 155 s). All calculations carried out were with the baseline (the first 35 s of measurement) subtracted. Middle line of the boxplot represents the median whereas the inverted triangle represents the mean. p-values: ns (not significant p>0.05), * (p<0.05), **(p<0.01), ***(p<0.001); Welch's t-test for parametric test and Wilcoxon rank sum test for non-parametric test.

The changes in $[Ca^{2+}]_{cyt}$ response due to the mutation in *AtDORN1* and *AtANN1* when challenged with eADP were also observed. Control treatment confirmed that the changes in $[Ca^{2+}]_{cyt}$ were solely due to eADP treatment as only a single touch response was produced upon addition of control solution for each genotype (Col-0 0.50±0.05 µM; *Atdorn1-1/ann1* 0.46±0.06 µM; *Atdorn1-1* 0.44±0.07 µM) (Figure 3.18 A). Total changes in $[Ca^{2+}]_{cyt}$ accumulated were not significantly different between Col-0 (5.33±0.53 µM), *Atdorn1-1/ann1* (3.24±0.74 µMs), and *Atdorn1-1* (4.81±0.62 µM) supporting the notion that mutation in both *AtDORN1* and *AtANN1* does not alter the touch $[Ca^{2+}]_{cyt}$ response (Figure 3.18 B). After the

addition of 1 mM ADP at the 35th second, Col-0 sustained a touch response followed by the first peak (0.31±0.01 μM) and the second peak (0.35±0.009 μM) of $[Ca^{2+}]_{cyt}$ elevation. Both *Atdorn1-1/ann1* and *Atdorn1-1* failed to produce these $[Ca^{2+}]_{cyt}$ responses over the whole 155 s of measurement (Figure 3.18 C). Detailed analysis of the area under the curve showed that total $[Ca^{2+}]_{cyt}$ accumulated under 1 mM ADP treatment in Col-0 (24.04±0.77 μM) was far higher than the total $[Ca^{2+}]_{cyt}$ of both *Atdorn1-1/ann1* (3.70±0.60 μM) and *Atdorn1-1* (4.32±0.48 μM) (Figure 3.18 D).

When the root tips were challenged with 0.1 mM ADP, Col-0 produced a distinct first peak (0.22±0.03 μM) and second peak (0.27±0.04 μM) after the touch response whereas the *Atdorn1-1/ann1* and *Atdorn1-1* mutants did not respond in the same way (Figure 3.18 E). Touch responses in 0.1mM ADP treatment produced by all genotypes Col-0 (0.26±0.001 μM), *Atdorn1-1/ann1* (0.37±0.07 μM), and *Atdorn1-1* (0.30±0.08 μM) were not significantly different from each other, thus proving that the biphasic response in Col-0 was due to the eADP treatment alone. Based on the overall area under the curve, the total $[Ca^{2+}]_{cyt}$ produced by Col-0 was 19.77±3.27 μM, which was significantly higher than the mutants *Atdorn1-1/ann1* (3.35±0.63 μM) and *Atdorn1-1* (3.12±0.93 μM) (Figure 3.18 F).

Comparison between control treatment and 1 mM ADP or 0.1 mM ADP for each mutant was also carried out in detailed analysis. In the $[Ca^{2+}]_{cyt}$ traces produced by each single and double mutant, 1 mM ADP treatment but not the control treatment induced a small peak (Figure 3.19 A). However, based on the total $[Ca^{2+}]_{cyt}$ derived from the area under the curve, there were no significant differences between the two treatments for each *Atdorn1-1/ann1* (control 3.24±0.74 μM; 1 mM ADP 3.70±0.60 μM) and *Atdorn1-1* (control 4.81±0.62 μM; 1 mM ADP 4.32±0.48 μM) (Figure 3.19 B). Similar analysis was carried out for 0.1 mM ADP concentration (Figure 3.19 C) where no significant differences were found between control treatment and 0.1 mM ADP treatment in both *Atdorn1-1/ann1* (control 3.24±0.74 μM; 0.1 mM ADP 3.35±0.63 μM) and *Atdorn1-1* samples (control 4.81±0.62 μM; 0.1 mM ADP 3.12±0.93 μM) (Figure 3.19 D).

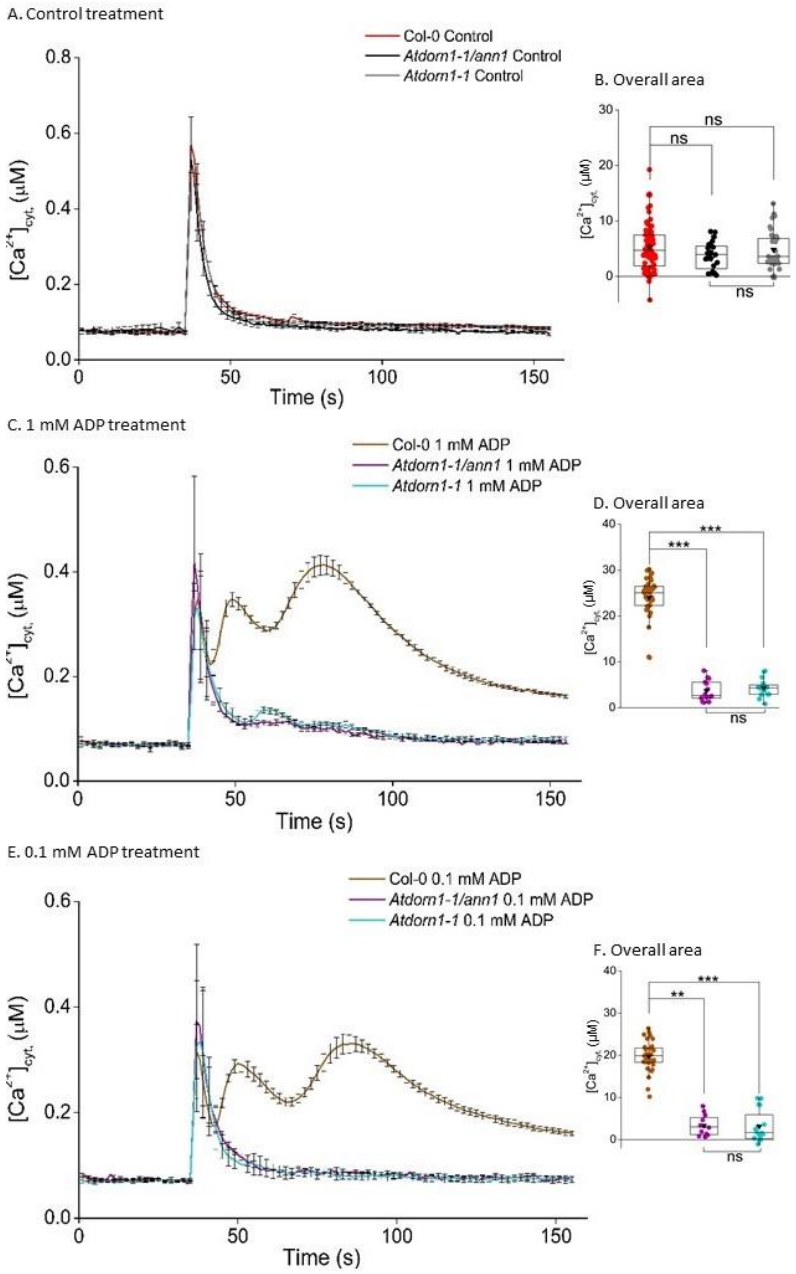

Figure 3.18: **AtANN1 might in the AtDORN1 pathway for eADP signalling.** Seven-day-old 1 cm root tips of Col-0, *Atdorn1-1*, *Atdorn1-1/ann1* were treated with control buffer (2 mM MES/Tris-HCl; 10 mM $CaCl_2$; 0.1 mM KCl) (A), 1 mM ADP (C) and 0.1 mM ADP (E). The $[Ca^{2+}]_{cyt}$ responses were recorded for 155 s and each treatment was added at the 35th second. These time course data were from the means ± SEM of 5 independent trials, with n = 13 – 65 roots. Overall area which indicates the total accumulation of $[Ca^{2+}]_{cyt}$ was the total area under the curve extracted from the time course data from the control (B), 1 mM ADP treatment (D) and 0.1 mM ADP (F) (35 - 155 s). All calculations carried out were with the baseline (the first 35 s of measurement) subtracted. Middle line of the boxplot represents the median whereas the inverted triangle represents the mean. p-values: ns (not significant p>0.05), * (p<0.05), **(p<0.01), ***(p<0.001); Welch's t-test for parametric test and Wilcoxon rank sum test for non-parametric test.

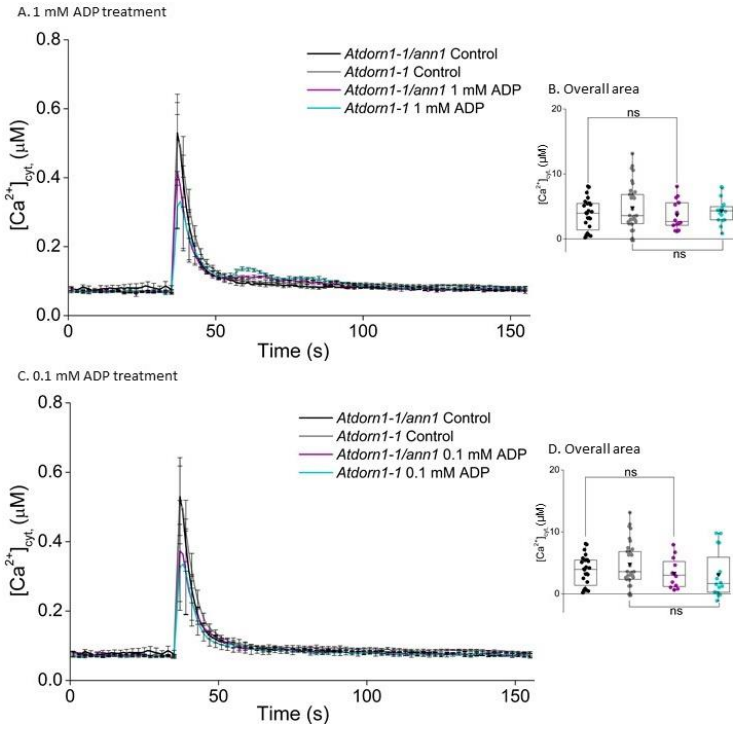

Figure 3.19: **Kinase mutation of AtDORN1 and AtANN1 eliminates response to ADP.** Seven-day-old 1 cm root tips of *Atdorn1-1* and *Atdorn1-1/ann1* were treated with control buffer (2 mM MES/Tris-HCl; 10 mM $CaCl_2$; 0.1 mM KCl) or 1 mM ADP (A), or control buffer and 0.1 mM ADP (C). The $[Ca^{2+}]_{cyt}$ responses were recorded for 155 s and each treatment was added at the 35th second. These time course data were from the means ± SEM of 6 independent trials, with n = 8 – 36 roots per genotype and treatment. Overall area which indicates the total accumulation of $[Ca^{2+}]_{cyt}$ was the total area under the curve extracted from the time course data of control treatment and 1 mM ADP (B) or 0.1 mM ADP (D) (35 - 155 s). All calculations carried out were with the baseline (the first 35 s of measurement) subtracted. Middle line of the boxplot represents the median whereas the inverted triangle represents the mean. p-values: ns (not significant p>0.05), * (p<0.05), **(p<0.01), ***(p<0.001); Welch's t-test for parametric test and Wilcoxon rank sum test for non-parametric test.

Atdorn1-3 is a mutant line where the *AtDORN1* gene is completely knocked-out by a T-DNA insertion (Choi *et al.*, 2014b). Here, the role of AtANN1 in the AtDORN1-mediated eATP signalling pathway was tested by using the *Atdorn1-3/ann1* T-DNA insertion double mutant. $[Ca^{2+}]_{cyt}$ measurements of *Atdorn1-3/ann1* and *Atdorn1-3* 1 cm excised root tips were taken upon treatment with 1 mM ATP or 0.1 mM ATP. Control treatment was carried out to make sure that the background solution (2 mM MES/Tris-HCl; 10 mM $CaCl_2$; 0.1 mM KCl) had no effect on the outcome of the experiments. Based on the time courses of the $[Ca^{2+}]_{cyt}$ measurements, the $[Ca^{2+}]_{cyt}$ baseline of Col-0 (0.07±0.002 μM), *Atdorn1-3/ann1* (0.09±0.01 μM), and *Atdorn1-3* (0.07±0.001 μM) were not significantly different from each other. After

the addition of the control treatment at the 35th second, all three genotypes produced almost similar single touch response (Col-0 0.28±0.06 μM; *Atdorn1-3/ann1* 0.35±0.10 μM; *Atdorn1-3* 0.26±0.08 μM) before going back to basal level (Figure 3.20 A). The total $[Ca^{2+}]_{cyt}$ measured for Col-0 (3.45±0.66 μM), *Atdorn1-3/ann1* (1.34±1.50 μM) and *Atdorn1-3* (2.39±0.80 μM) in the control treatment were not significantly different from each other (Figure 3.20 B).

ATP treatment (1 mM) caused a $[Ca^{2+}]_{cyt}$ biphasic pattern in Col-0 (first peak 0.28±0.01 μM; second peak 0.32±0.01 μM) but not in the *Atdorn1-3/ann1* and *Atdorn1-3* mutants after the touch response (Figure 3.20 C). Analysis of the overall area under the curve showed that the Col-0 (21.2±0.74 μM) accumulated significantly higher $[Ca^{2+}]_{cyt}$ compared to *Atdorn1-3/ann1* (2.38±1.89 μM) and *Atdorn1-3* (1.62±0.41 μM) (Figure 3.20 D). When challenged with a lower concentration of 0.1 mM ATP, the Col-0 sustained the familiar $[Ca^{2+}]_{cyt}$ biphasic response but with lower amplitude (first peak 0.23±0.02 μM; second peak 0.22±0.009 μM) compared to the 1 mM ATP treatment. Unlike Col-0, both the *Atdorn1-3/ann1* and *Atdorn1-3* mutants failed to produce the $[Ca^{2+}]_{cyt}$ biphasic response after the touch response (Figure 3.20 E). Based on the total $[Ca^{2+}]_{cyt}$ accumulation, *Atdorn1-3/ann1* (0.74±0.40 μM) and *Atdorn1-3* (2.05±0.72 μM) were almost non-responsive towards 0.1 mM ATP and were completely impaired compared to Col-0 (16.77±0.96 μM) (Figure 3.20 F). This proved that DORN1 is crucial in eATP signal perception while ANN1 could also be involved in the pathway.

Comparison between control treatment and 1 mM ATP or 0.1 mM ATP was also carried out to confirm whether each mutant was responsive towards ATP treatment. $[Ca^{2+}]_{cyt}$ traces as shown in Figure 3.21 A and 3.21 C showed a touch response after addition of either control treatment, 1 mM ATP or 0.1 mM ATP which later declined to basal $[Ca^{2+}]_{cyt}$ levels. Based on the area under the curve from the $[Ca^{2+}]_{cyt}$ traces, there were no significant differences between control treatment and 1 mM ATP or 0.1 mM ATP in both *Atdorn1-3/ann1* (control 1.34±1.50 μM; 1 mM ATP 2.38±1.89 μM; 0.1 mM ATP 0.74±0.40 μM) and *Atdorn1-3* (control 2.39±0.80 μM; 1 mM ATP 1.62±0.41 μM ; 0.1 mM ATP 2.05±0.72 μM) (Figure 3.21 B, D).

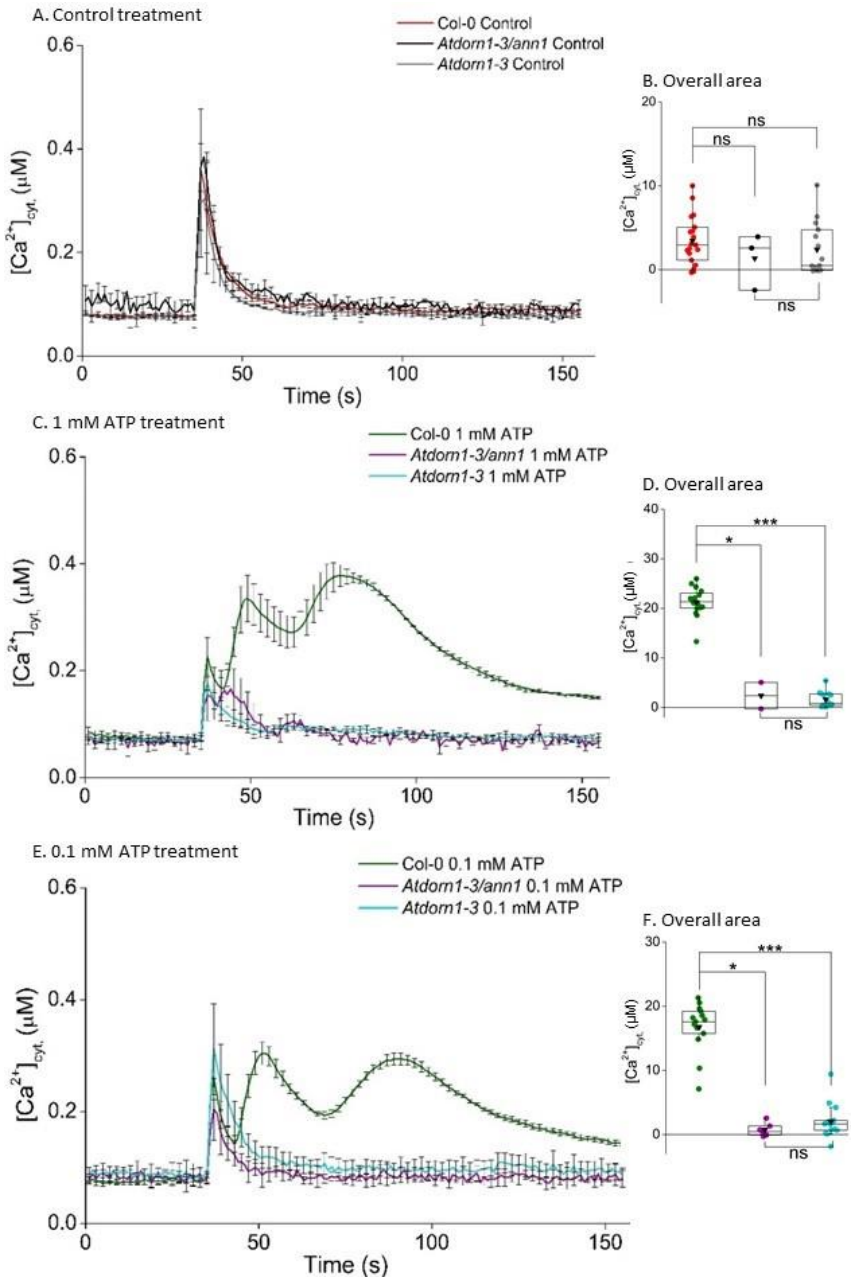

Figure 3.20*:* **AtANN1 might be in the AtDORN1 pathway in response to eATP.** Seven-day-old 1 cm root tips of Col-0, *Atdorn1-3*, *Atdorn1-3/ann1* were treated with control buffer (A), 1 mM ATP (C) or 0.1 mM ATP (E). The $[Ca^{2+}]_{cyt}$ responses were recorded for 155 s and each treatment was added at the 35th second. These time course data were from the means ± SEM of 4 independent trials, with n = 7 – 12 root tips. Overall area which indicates the total accumulation of $[Ca^{2+}]_{cyt}$ was the total area under the curve extracted from the time course data from the control treatment (B), 1 mM ATP treatment (D) and 0.1 mM ATP treatment (F) (35 - 155 s). All calculations carried out were with the baseline (the first 35 s of measurement) subtracted. Middle line of the boxplot represents the median whereas the inverted triangle represents the mean. p-values: ns (not significant p>0.05), * (p<0.05), **(p<0.01), ***(p<0.001); Welch's t-test for parametric test and Wilcoxon rank sum test for non-parametric test.

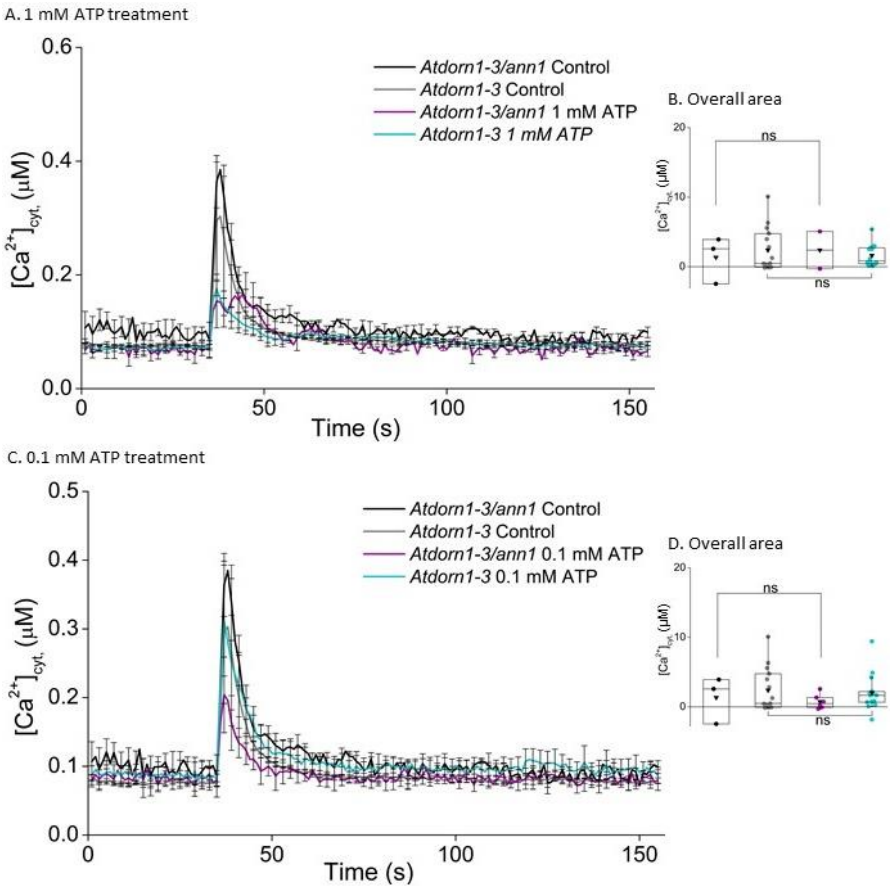

Figure 3.21*:* AtDORN1 and AtANN1 knock-out mutation eliminates response to ATP. Seven-day-old 1 cm root tips of *Atdorn1-3* and *Atdorn1-3/ann1* were treated with control buffer (2 mM MES/Tris-HCl; 10 mM $CaCl_2$; 0.1 mM KCl) or 1 mM ATP (A), or control buffer and 0.1 mM ATP (C). The $[Ca^{2+}]_{cyt}$ responses were recorded for 155 s and each treatment was added at the 35th second. These time course data were from the means ± SEM of 6 independent trials, with n = 8 – 36 roots per genotype and treatment. Overall area which indicates the total accumulation of $[Ca^{2+}]_{cyt}$ was the total area under the curve extracted from the time course data of control treatment and 1 mM ATP (B) or 0.1 mM ATP (D) (35 - 155 s). All calculations carried out were with the baseline (the first 35 s of measurement) subtracted. Middle line of the boxplot represents the median whereas the inverted triangle represents the mean. p-values: ns (not significant p>0.05), * (p<0.05), **(p<0.01), ***(p<0.001); Welch's t-test for parametric test and Wilcoxon rank sum test for non-parametric test.

In order to see whether both AtDORN1 and AtANN1 are involved in mediating eADP signalling possibly in the same pathway, the same experiment was carried out with 1 mM ADP and 0.1 mM ADP. Col-0, *Atdorn1-3/ann1* and *Atdorn1-3* excised root tips that were treated with control solution at the 35th second of $[Ca^{2+}]_{cyt}$ measurement produced only a single touch response (Col-0 0.47±0.10 μM; *Atdorn1-3/ann1* 0.28±0.07 μM; *Atdorn1-3* 0.45±0.11 μM) (Figure 3.22 A). The overall area under the curve analysis showed that the total $[Ca^{2+}]_{cyt}$ produced by Col-0 (1.58±0.55 μM), *Atdorn1-3/ann1* (0.55±0.64 μM) and

Atdorn1-3 (1.01±0.48 μM) were not significant to each other in the control treatment (Figure 3.22 B).

When challenged with 1 mM ADP, Col-0 increased $[Ca^{2+}]_{cyt}$ (first peak 0.32±0.01 μM; second peak 0.38±0.02 μM) but not the *Atdorn1-3/ann1* and the *Atdorn1-3* mutants (Figure 3.22 C). Based on the overall area under the curve analysis, *Atdorn1-3/ann1* (0.65±0.18 μM) and *Atdorn1-3* (0.54±0.16 μM) failed to accumulate high $[Ca^{2+}]_{cyt}$ as in Col-0 (22.19±0.90 μM) (Figure 3.22 D). As with eATP, a lower concentration of eADP also managed to induce calcium increase in the cytosol. ADP (0.1 mM) evoked a lower $[Ca^{2+}]_{cyt}$ biphasic response in Col-0 (first peak 0.22±0.02 μM; second peak 0.23±0.02 μM) whereas *Atdorn1-3/ann1* and *Atdorn1-3* $[Ca^{2+}]_{cyt}$ fell to basal level after the touch response (Figure 3.22 E). Failure of the mutants to accumulate $[Ca^{2+}]_{cyt}$ was confirmed when the total $[Ca^{2+}]_{cyt}$ accumulated by the Col-0 (15.44±1.89 μM) was found to be significantly higher compared to *Atdorn1-3/ann1* (0.66±0.29 μM) and *Atdorn1-3* (1.81±0.61 μM) (Figure 3.22 F).

Another analysis of the data was carried out to look into the comparison between control treatment and 1 mM ADP or 0.1 mM ADP treatment in both *Atdorn1-3/ann1* and *Atdorn1-3.* Both genotypes seems to be non-responsive towards either 1 mM ADP or 0.1 mM ADP based on the $[Ca^{2+}]_{cyt}$ traces when compared to the control treatment (Figure 3.23 A, C). In order to confirm this, total changes in $[Ca^{2+}]_{cyt}$ from control treatment were compared with 1 mM ADP or 0.1 mM ADP treatment in both *Atdorn1-3/ann1* and *Atdorn1-3.* Statistical analysis showed that there were no significant differences between control treatment (*Atdorn1-3/ann1* 0.55±0.64 μM; *Atdorn1-3* 1.01±0.48 μM) and 1 mM ADP treatment (*Atdorn1-3/ann1* 0.65±0.18 μM; *Atdorn1-3* 0.54±0.16 μM) (Figure 3.23 B) or 0.1 mM ADP treatment (*Atdorn1-3/ann1* 0.66±0.29 μM ; *Atdorn1-3* 1.81±0.61 μM) (Figure 3.23 D) in both mutants.

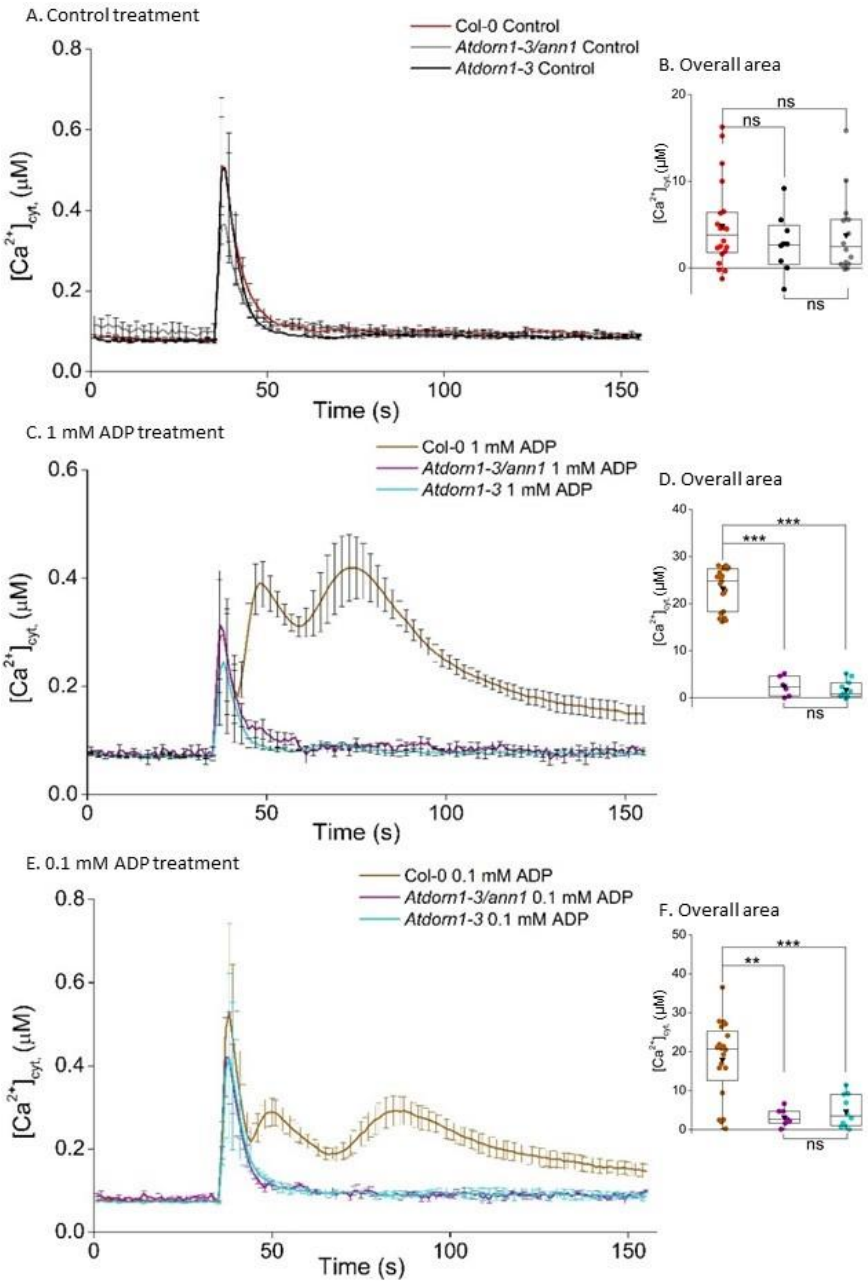

Figure 3.22: **AtANN1 might be in the AtDORN1 pathway in eADP signalling.** Seven-day-old 1 cm root tips of Col-0, *Atdorn1-3*, *Atdorn1-3/ann1* were treated with control buffer (A), 1 mM ADP (C) and 0.1 mM ADP (E). The $[Ca^{2+}]_{cyt}$ responses were recorded for 155 s and each treatment was added at the 35th second. These time course data were from the means ± SEM of 3 independent trials, with n = 10 – 20 root tips. Overall area which indicates the total accumulation of $[Ca^{2+}]_{cyt}$ was the total area under the curve extracted from the time course data from the control treatment (B) ,1 mM ADP treatment (D) and 0.1 mM ADP treatment (F) (35 - 155 s). All calculations carried out were with the baseline (the first 35 s of measurement) subtracted. Middle line of the boxplot represents the median whereas the inverted triangle represents the mean. *p*-values: ns (not significant p>0.05), * (p<0.05), **(p<0.01), ***(p<0.001); Welch's *t*-test for parametric test and Wilcoxon rank sum test for non-parametric test.

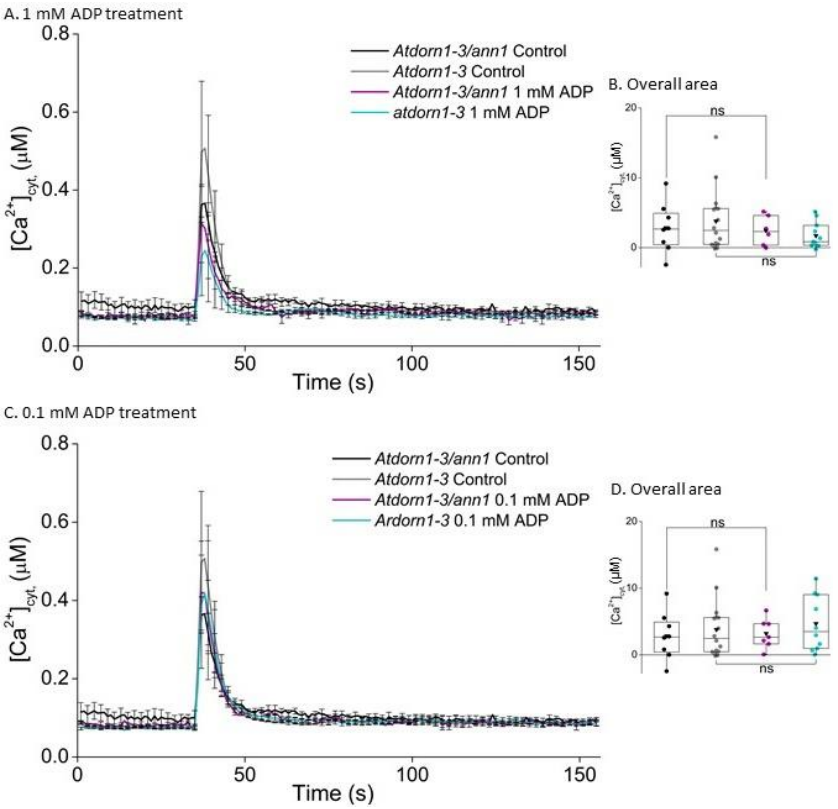

Figure 3.23: **AtDORN1 and AtANN1 knock-out mutant does not respond to ADP.** Seven-day-old 1 cm root tips of *Atdorn1-3* and *Atdorn1-3/ann1* were treated with control buffer (2 mM MES/Tris-HCl; 10 mM $CaCl_2$; 0.1 mM KCl) or 1 mM ADP (A), or control buffer and 0.1 mM ADP (C). The $[Ca^{2+}]_{cyt}$ responses were recorded for 155 s and each treatment was added at the 35th second. These time course data were from the means ± SEM of 6 independent trials, with n = 8 – 36 roots per genotype and treatment. Overall area which indicates the total accumulation of $[Ca^{2+}]_{cyt}$ was the total area under the curve extracted from the time course data of control treatment and 1 mM ADP (B) or 0.1 mM ADP (D) (35 - 155 s). All calculations carried out were with the baseline (the first 35 s of measurement) subtracted. Middle line of the boxplot represents the median whereas the inverted triangle represents the mean. *p*-values: ns (not significant p>0.05), * (p<0.05), **(p<0.01), ***(p<0.001); Welch's *t*-test for parametric test and Wilcoxon rank sum test for non-parametric test.

3.2.9 $[Ca^{2+}]_{cyt}$ accumulation in hyperpolarisation and depolarisation conditions

Arabidopsis root epidermal plasma membrane calcium channels mediating the eATP-induced calcium influx were voltage dependent as eATP induced a hyperpolarisation-activated Ca^{2+} conductance (Demidchik *et al.*, 2009; Shang *et al.*, 2009). The background solution that is used during measurement of $[Ca^{2+}]_{cyt}$ increase due to eATP is crucial as it can affect the plasma membrane voltage, thus affecting the opening of the voltage-dependent calcium channels. A previous study showed that root epidermal plasma membrane voltage can be manipulated by regulating the K^+ concentration of the background solution

(Demidchik *et al.*, 2002). In this study, two different conditions were tested; a hyperpolarising (HP) solution with 0.1 mM K^+ concentration (2 mM MES/Tris-HCl; 10 mM $CaCl_2$; 0.1 mM KCl) and a depolarising solution (DP) with 10 mM K^+ concentration (2 mM MES/Tris-HCl; 10 mM $CaCl_2$; 10 mM KCl). Seven-day-old whole roots of Col-0 and *Atann1* mutants carrying the (apo)aequorin construct were subjected to $[Ca^{2+}]_{cyt}$ measurement in these two different conditions and then challenged with either ATP or ADP agonists.

HP control solution and DP control solution were first tested to see whether varying the K^+ concentration would affect the basal level of the $[Ca^{2+}]_{cyt}$. Based on the 155 s time course measurement of $[Ca^{2+}]_{cyt,}$ there were no significant differences of the baseline values between HP control and DP control treatment in both Col-0 (HP 0.08±0.01 μM; DP 0.08±0.04 μM) and *Atann1* (HP 0.08±0.06 μM; DP 0.07±0.04 μM) samples. At the 35th second of measurement, both HP and DP control solutions produced a single touch response with slight variability but not significant in Col-0 (HP 0.25±0.05 μM; DP 0.38±0.08 μM) and *Atann1* (HP 0.15±0.03 μM; DP 0.33±0.07 μM) (Figure 3.24 A). The overall accumulation of $[Ca^{2+}]_{cyt}$ shows that there were no significant differences between HP (Col-0 2.44±0.48 μM; *Atann1* 0.41±0.32 μM) and DP (Col-0 2.68±0.63 μM; *Atann1* 1.06±0.61 μM) control solution in both Col-0 and *Atann1* whole roots. Comparison between genotypes in HP condition showed that *Atann1* induced significantly lower total $[Ca^{2+}]_{cyt}$ than the Col-0 in control treatment. This is however not true for the DP condition where no significant differences were found between Col-0 and *Atann1* due to control treatment (Figure 3.24 B).

Both Col-0 (first peak 0.24±0.01 μM; second peak 0.28±0.01 μM) and *Atann1* (first peak 0.17±0.01 μM; second peak 0.19±0.005 μM) whole roots challenged with 1 mM ATP in HP solution produced a $[Ca^{2+}]_{cyt}$ biphasic response. Putatively lowering the plasma membrane voltage did not change this pattern as both Col-0 (first peak 0.24±0.006 μM; second peak 0.27±0.004 μM) and *Atann1* (first peak 0.16±0.007 μM; second peak 0.18±0.004 μM) in DP solution treated with 1 mM ATP also produced the familiar biphasic pattern. In both conditions, the $[Ca^{2+}]_{cyt}$ traces of *Atann1* were impaired compared to the Col-0 (Figure 3.24 C). To look at the total $[Ca^{2+}]_{cyt}$ accumulated by the whole roots in these two conditions, the overall area under curve analysis was carried out. Based on the analysis, $[Ca^{2+}]_{cyt}$ accumulated in Col-0 (18.90±1.18 μM) and *Atann1* (12.66±0.38 μM) in HP solution was not significantly different from the $[Ca^{2+}]_{cyt}$ accumulated in DP (Col-0 20.71±0.36 μM; *Atann1* 13.07±0.39 μM). However, *Atann1* consistently accumulated less $[Ca^{2+}]_{cyt}$ than Col-0 in both conditions (Figure 3.24 D).

To find out whether a different concentration of eATP would have a different outcome, 0.1 mM ATP treatment was also tested. Both HP and DP conditions evoked similar $[Ca^{2+}]_{cyt}$ biphasic responses as in 1 mM ATP treatment. The *Atann1* $[Ca^{2+}]_{cyt}$ traces in HP (first peak 0.14±0.02 µM; second peak 0.13±0.01 µM) and DP (first peak 0.13±0.007 µM; second peak 0.13±0.005 µM) conditions were lower compared to Col-0 in HP (first peak 0.24±0.01 µM; second peak 0.24±0.01 µM) and DP (first peak 0.23±0.01 µM; second peak 0.21±0.007 µM; Figure 3.24 E). Analysis of the overall area under the $[Ca^{2+}]_{cyt}$ trace showed that HP and DP supported a similar amount of $[Ca^{2+}]_{cyt}$ accumulation in both Col-0 (HP 19.31±1.56 µM; DP 19.16±0.82 µM) and *Atann1* (HP 10.27±1.15 µM; DP 11.15±0.50 µM) with *Atann1* having significantly lower $[Ca^{2+}]_{cyt}$ accumulation (Figure 3.24 F).

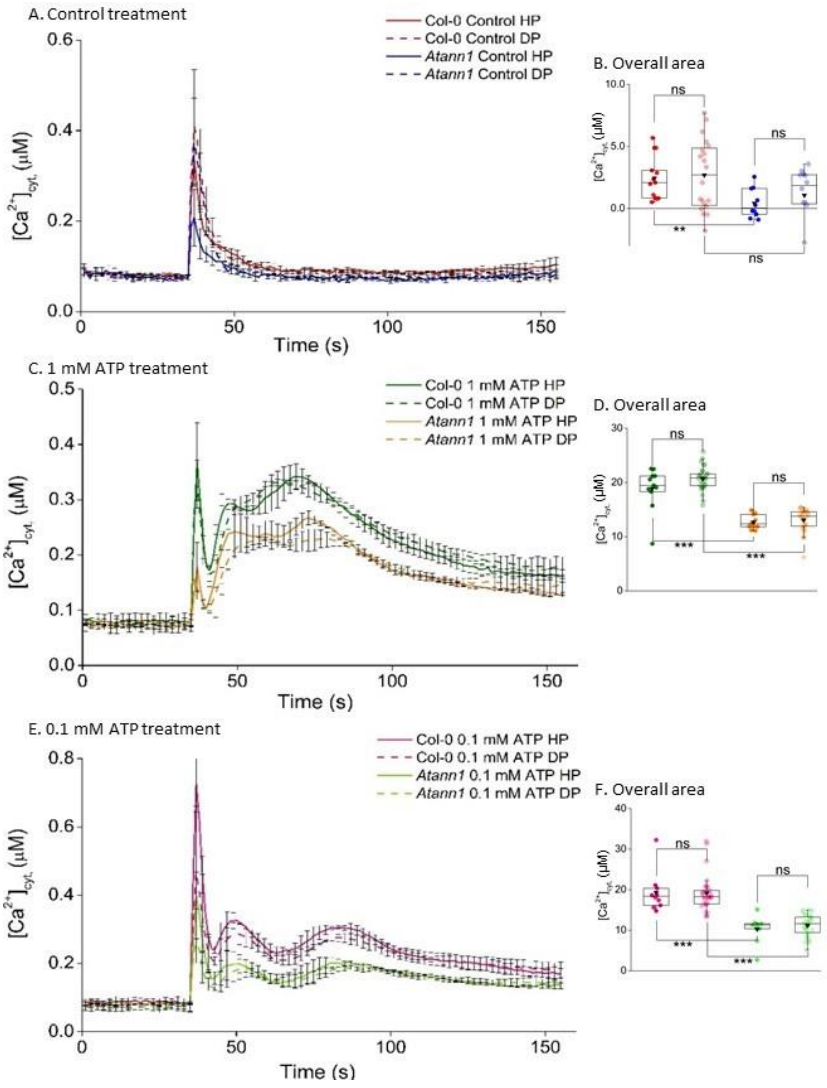

Figure 3.24*:* An effect of depolarising conditions on $[Ca^{2+}]_{cyt}$ response to eATP was not found in whole roots . Seven- day-old whole roots of Col-0 and *Atann1* were treated with control buffer (A), 1 mM ATP (C) or 0.1 mM ATP (E) in either hyperpolarising (HP) conditions (solid line -) or

depolarising (DP) conditions (dash line - -). Depolarisation conditions were achieved by increasing the K^+ concentration in the background solution to 10 mM. The $[Ca^{2+}]_{cyt}$ responses were recorded for 155 s and each treatment was added at the 35th second. These time course data were from the means ± SEM of 3 independent trials, with n = 12 – 19 whole roots. Overall area which indicates the total accumulation of $[Ca^{2+}]_{cyt}$ was the total area under the curve extracted from the time course data from the control treatment (B) ,1 mM ATP treatment (D) and 0.1 mM ATP treatment (F) (35 - 155 s) (HP, solid circle; DP, cross circle). All calculations carried out were with the baseline (the first 35 s of measurement) subtracted. Middle line of the boxplot represents the median whereas the inverted triangle represents the mean. *p*-values: ns (not significant $p>0.05$), * ($p<0.05$), **($p<0.01$), ***($p<0.001$); Welch's *t*-test for parametric test and Wilcoxon rank sum test for non-parametric test.

The same test was carried out with 1 mM ADP treatment. In the control treatment, both HP (Col-0 0.22±0.05 μM; *Atann1* 0.29±0.05 μM) and DP conditions (Col-0 0.55±0.08 μM; *Atann1* 0.44±0.07 μM) induced a single $[Ca^{2+}]_{cyt}$ touch response that lasted approximately 40 seconds before going back to the basal level (Figure 3.25 A). The overall $[Ca^{2+}]_{cyt}$ accumulation due to HP control solution in Col-0 (Col-0 1.86±0.47 μM) was significantly lower than the Col-0 in DP control solution (Col-0 3.64±0.56 μM). Unlike Col-0, *Atann1* in HP condition (2.66±0.39 μM) was not significantly different to that of *Atann1* with the DP control solution (3.69±0.47 μM) proving that the control solution did not have any effect on the $[Ca^{2+}]_{cyt}$ touch response in *Atann1* but might influence the touch response in Col-0 (Figure 3.25 B).

In the 1 mM ADP $[Ca^{2+}]_{cyt}$ measurements, the Col-0 in both HP (first peak 0.28±0.01 μM; second peak 0.33±0.01 μM) and DP solution (first peak 0.23±0.01 μM; second peak 0.26±0.01 μM) gave rise to higher $[Ca^{2+}]_{cyt}$ responses compared to *Atann1* in HP (first peak 0.17±0.01 μM; second peak 0.22±0.01 μM) and DP solution (first peak 0.21±0.01 μM; second peak 0.20±0.01 μM) after the touch response (Figure 3.25 C). This was also reflected in the overall area under the curve as the total $[Ca^{2+}]_{cyt}$ accumulated due to 1 mM ADP in Col-0 HP (23.96±0.70 μM) and DP solution (20.75±1.35 μM) were significantly higher compared to *Atann1* in HP (15.22±0.88 μM) and DP (15.87±1.13 μM) solution. There were however no significant differences in total $[Ca^{2+}]_{cyt}$ accumulated between HP solution and DP solution in an individual genotype (Figure 3.25 D).

A lower concentration of eADP was also tested to see if this revealed any differences between genotype responses. When treated with 0.1 mM ADP solution, a first peak was produced by Col-0 (HP 0.21±0.01 μM; DP 0.20±0.01 μM) and *Atann1* (HP 0.17±0.009 μM;

DP 0.16±0.006 µM) followed by the second peak in Col-0 (HP 0.23±0.01 µM; DP 0.19±0.01 µM) and *Atann1* (HP 0.16±0.01 µM; 0.15±0.006 µM) with consistently lower $[Ca^{2+}]_{cyt}$ values from *Atann1* (Figure 3.25 E). Analysis of the overall area under the $[Ca^{2+}]_{cyt}$ curve revealed that the total $[Ca^{2+}]_{cyt}$ accumulated due to 0.1 mM ADP was not significantly different between HP (Col-0 18.67±1.06 µM; *Atann1* 13.99±0.68 µM) and DP conditions (Col-0 18.68±1.22 µM; *Atann1* 13.57±0.70 µM). However in either condition, *Atann1* failed significantly to accumulate a similar amount of $[Ca^{2+}]_{cyt}$ as in Col-0 (Figure 3.25 F).

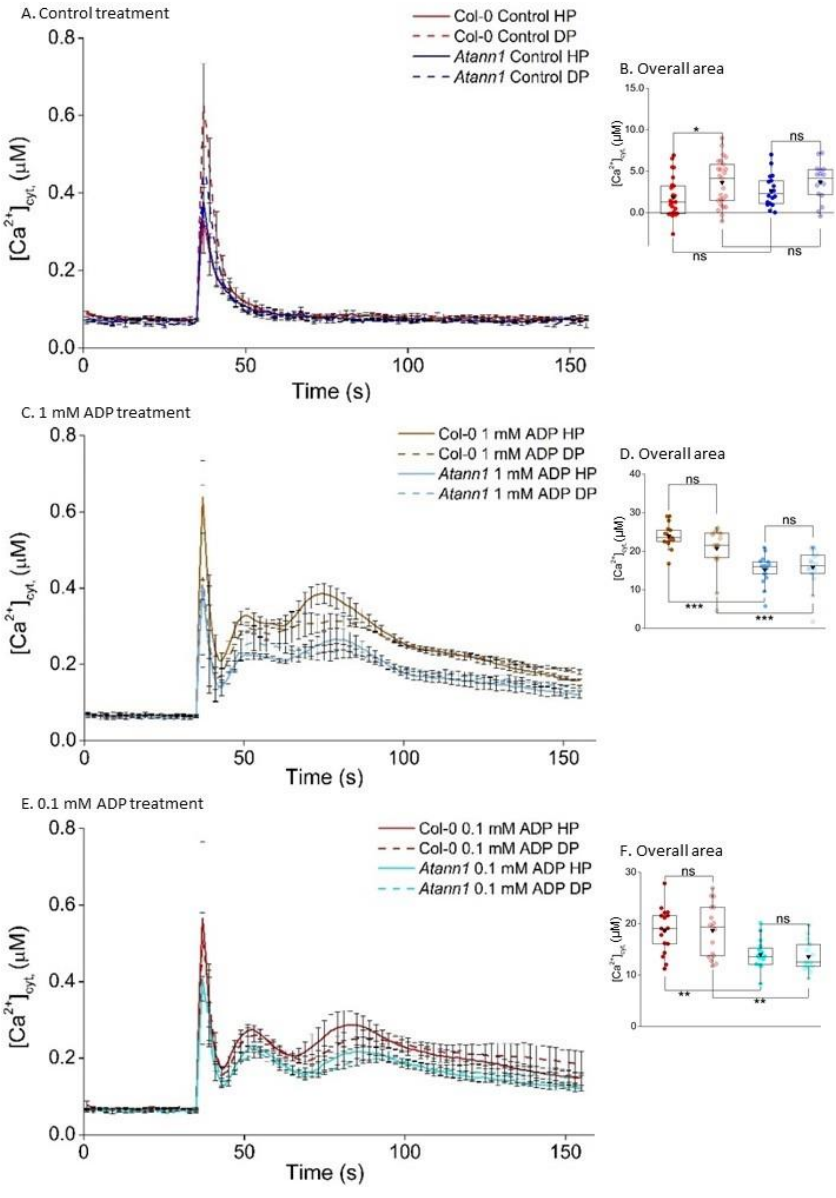

Figure 3.25*:* **An effect of depolarisation conditions on $[Ca^{2+}]_{cyt}$ response to eADP signal could not be seen in whole roots.** Seven-day-old whole roots of Col-0 and *Atann1* were treated with control buffer (A), 1 mM ADP (C) or 0.1 mM ADP (E) in either hyperpolarising (HP solid line -) or depolarising (DP dash line - -) conditions. Depolarisation conditions werw achieved by increasing the K^+ concentration in the background solution to 10 mM. The $[Ca^{2+}]_{cyt}$ responses were recorded for 155

s and each treatment was added at the 35th second. These time course data were from the means ± SEM of 3 independent trials, with n = 16 – 25 whole roots. Overall area which indicates the total accumulation of $[Ca^{2+}]_{cyt}$ was the total area under the curve extracted from the time course data from the control treatment (B),1 mM ADP treatment (D) and 0.1 mM ADP treatment (F) (35 - 155 s) (HP, solid circle; DP, cross circle). All calculations carried out were with the baseline (the first 35 s of measurement) subtracted. Middle line of the boxplot represents the median whereas the inverted triangle represents the mean. p-values: ns (not significant $p>0.05$) * ($p<0.05$), **($p<0.01$), ***($p<0.001$); Welch's t-test for parametric test and Wilcoxon rank sum test for non-parametric test.

3.2.10 eATP-induced ROS production in Col-0 and *Atann1* whole roots

Another immediate response in the event of eATP signalling other than increase in $[Ca^{2+}]_{cyt}$ is the production of Reactive Oxygen Species (ROS). Previously it was shown that 0.1 mM ATP evoked intracellular ROS production in wild type *A. thaliana* roots (Demidchik *et al.*, 2009). This could be inhibited (but not completely) by $GdCl_3$, suggesting that Ca^{2+} influx alone was not sufficient for the response. In 2017, Chen *et al.* showed that AtDORN1 directly interacts with and phosphorylates AtRBOHD, which leads to the production of ROS. This eATP-induced ROS burst also was shown to be dependent on the presence of extracellular Ca^{2+} as chelating calcium and overexpression of apyrases caused reduction in eATP-induced ROS production in leaves (Song *et al.*, 2006). Thus whether production of ROS is upstream or downstream of the accumulation of $[Ca^{2+}]_{cyt}$ triggered by eATP is not yet confirmed.

AtANN1 (as shown in sections 3.2.2 and 3.2.8) is involved in mediating $[Ca^{2+}]_{cyt}$ possibly downstream of AtDORN1 purinoreceptor in eATP signalling. Whether AtANN1 is involved in the production of ROS in the presence of eATP was tested here by comparing the ROS production between Col-0 wild type and the *Atann1* knock-out mutant. CMH_2DCFDA dye is used as a probe to detect a variety of intracellular ROS species in the cytosol, as CMH_2DCFDA is able to diffuse across plasma membrane (Jakubowski and Bartosz, 2000). Intracellular esterases already available in the cell will then cleave the probe producing a different form of the probe retained in the cell that will emit fluorescence during oxidation. The measurements are taken as fluorescence intensity or F value (F).

Figure 3.26 (A-H) shows microscopy images of roots that were taken three minutes after the control solution treatment or 1 mM ATP treatment. The Col-0 root treated with eATP (Figure 3.26 A, B) seems to show more intense fluorescence than the Col-0 treated with control solution (Figure 3.27 C, D). *Atann1* roots however showed higher intensity in

control treatment (Figure 3.26 E, F) than the eATP treatment (Figure 3.26 G, H). It was also observed that the ROS production centred mostly at the mature zone of the roots away from the root tips. Further analysis of the intracellular ROS production across the length of the roots starting from the root tips was then carried out.

In the analysis, the roots were divided into three different growth stages: apex zone (~500 μm from root tips), the elongation/transition zone (~1000 μm from root tips) and the mature or differentiation zone (~1500 μm from root tips) (Dolan and Davies, 2004; Verbelen *et al.,* 2006). Analysis was done as explained in chapter 2.9.1. Figure 3.27 shows the fluorescence intensity representing the intracellular ROS level across the length of the root when treated with either control solution or 1 mM ATP for 3 minutes. Based on the line graph, intracellular ROS accumulation was higher in the mature zone compared to the younger meristem stage. This notion is true for both Col-0 and *Atann1*, with *Atann1* having higher ROS accumulation than Col-0 especially starting from the elongation zone towards the mature zone in both treatments.

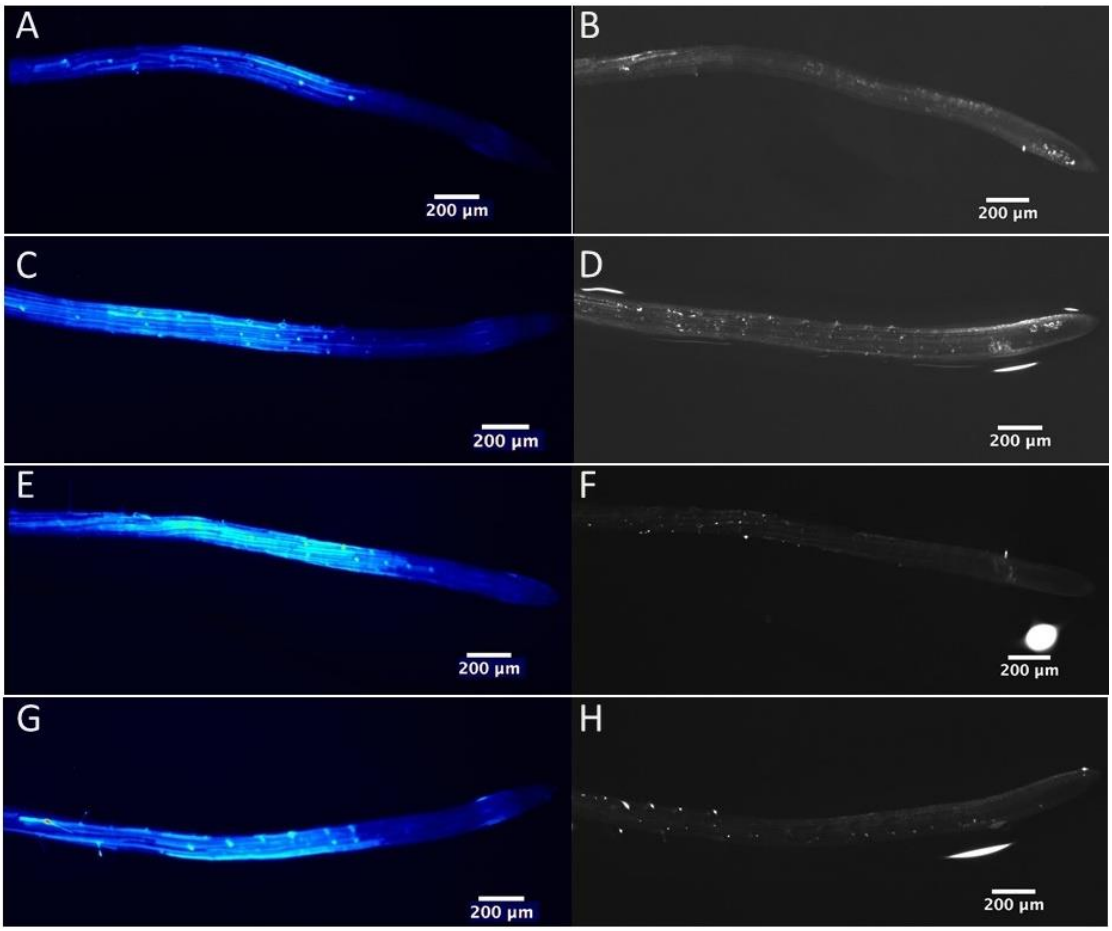

Figure 3.26: **Microscopy images of Col-0 and *Atann1* roots after 3 minutes of eATP treatment.** ATP treatment (1 mM) was added at the 35th second of measurement. Images of the roots were taken after 3 minutes of the treatment. Col-0 root treated with Low Salt Medium (LSM) as control under GFP filter (A); bright field (B), Col-0 root treated with 1 mM ATP under GFP filter (C); bright field (D), *Atann1* root treated with LSM control under GFP filter (E); bright field (F) and *Atann1* root treated with 1 mM ATP under GFP filter (G); bright field (H).

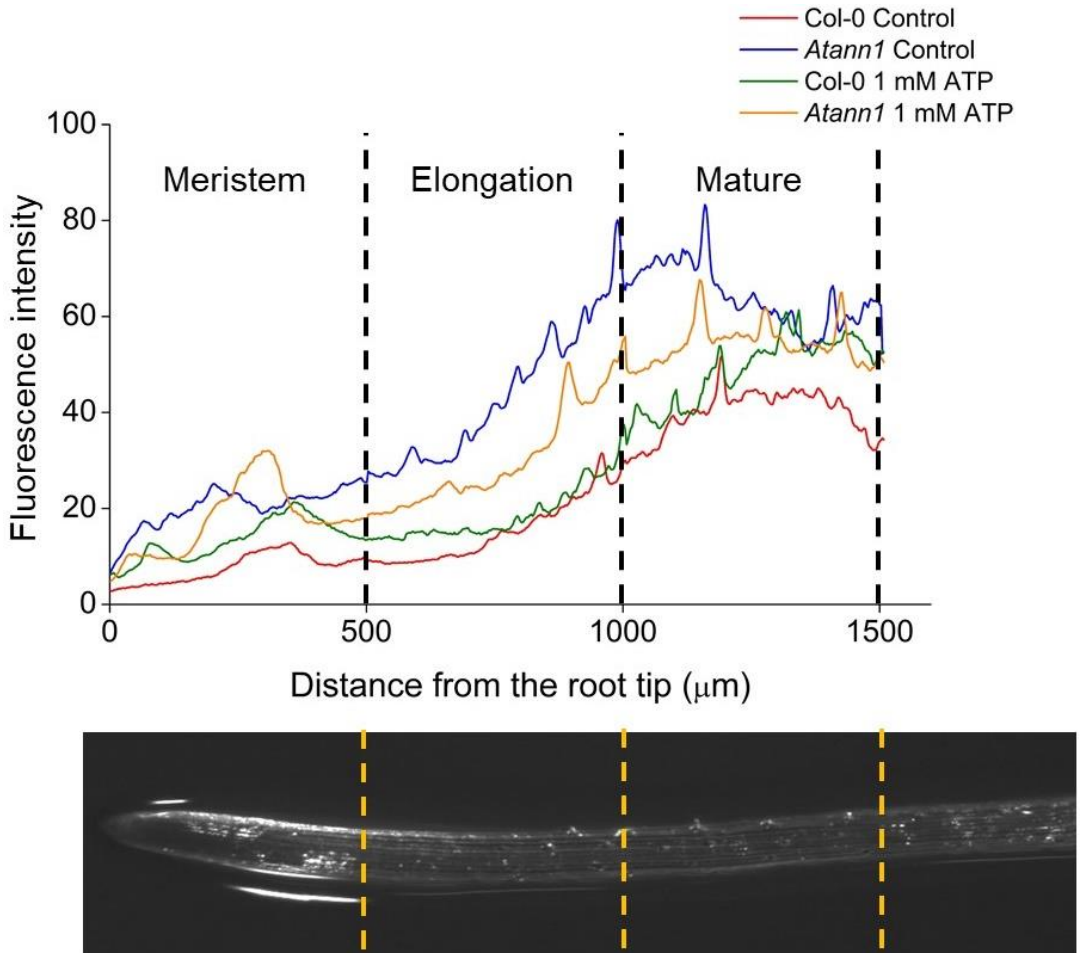

Figure 3.27*: Atann1* has higher ROS content compared to Col-0 across the length of the roots. Line graph shows traces of fluorescent intensity across the length of the roots including the meristem (~500 μm from the root tip), the elongation zone (~1000 μm from the root tip), and the mature zone (~1500 μm from the root tip) after 3 minutes of 1 mM ATP treatment. Data are from 1 trial with one root per genotype and treatment.

Further analysis of the eATP treatment was carried out by comparing the mean fluorescence intensity value for each root zone across time (Figure 3.28 A-C). At the meristem level (Figure 3.28 A), the ROS value of the Col-0 root assigned to control treatment slightly decreased across the 3 minutes measurement from the baseline value (F = 9.32, 0 minute control; F= 7.55, 3 minutes control). *Atann1* root however started off with higher baseline value (F = 21.44, 0 minute control) compared to the Col-0 and also slightly reduced in the ROS value after 3 minutes of the control treatment (F = 20.27, 3 minutes control). The Col-0 root that was assigned to 1 mM ATP treatment also induced higher baseline ROS value (F = 12.82, 0 minute ATP) than the Col-0 control root at 0 minute and only slightly increased after 3 minutes of 1 mM ATP treatment (F = 13.42, 3 minutes ATP). Similar to Col-0, *Atann1* also only slightly increased the ROS value after 3 minutes of 1 mM ATP treatment (F

= 17.17, 0 minute ATP; F = 17.45, 3 minutes ATP). The *Atann1* assigned for ATP treatment however continuously produced higher ROS value than the Col-0 assigned for ATP treatment across the 3 minutes period.

Baseline value of ROS at the elongation zone (Figure 3.28 B) for Col-0 (F = 19.24, 0 minute control) was lower than the *Atann1* root (F = 28.24, 0 minute control) assigned for the control treatment. After 3 minutes of control treatment, Col-0 (F = 15.38, 3 minutes control) slightly reduced in its ROS production but *Atann1* (F = 43.50, 3 minutes control) induced higher ROS production compared to the baseline. In the 1 mM ATP treatment, the ROS baseline value for both Col-0 (F = 17.66, 0 minute ATP) and *Atann1* (F = 19.15, 0 minute ATP) roots were not distinctly different from each other. Three minutes of 1 mM ATP treatment was found to be not effective in altering the ROS value in Col-0 root (F = 18.92, 3 minutes ATP) but was effective in increasing the ROS production in *Atann1* root (F = 30.30, 3 minutes ATP).

Mature root zone of *Atann1* root (F = 50.48, 0 minute control) exhibited higher ROS baseline value compared to the ROS baseline value of the Col-0 root (F = 37.01, 0 minute control) assigned for control treatment. The ROS production in Col-0 root (F = 39.64, 3 minutes control) however remained almost the same as the baseline value whereas the *Atann1* root (F = 64.23, 3 minutes control) has increased in its ROS production after 3 minutes of control treatment. Similar as in the control treatment, Col-0 root (F = 30.13, 0 minute ATP) ROS baseline value assigned for 1 mM ATP treatment was slightly lower compared to the *Atann1* root (F = 35.02, 0 minute ATP) ROS baseline value. Three minutes of 1 mM ATP caused increase in accumulation of ROS in both Col-0 (F = 48.84, 3 minutes ATP) and *Atann1* root (F = 54.15, 3 minutes ATP) with *Atann1* having higher ROS value than the Col-0 (Figure 3.28 C).

Since the ROS baseline value for each root and treatment was not at the same level, comparison in terms of changes in the fluorescence intensity across 3 minutes period was done to clearly distinguish the effect of genotypes and treatments on the ROS production at different stages of root growth (Figure 3.29 A, B). At the meristem level, changes in fluorescence intensity showed 1 mM ATP managed to induce ROS production compared to the control treatment (negative F value) in both Col-0 ($\Delta F = 0.59$) and *Atann1* ($\Delta F = 0.28$) with Col-0 having higher increase in fluorescence intensity than *Atann1*. At the elongation zone however, only Col-0 was found to be inducing more ROS production in 1 mM ATP

treatment (ΔF = 1.25) compared to the control treatment (negative F value). At this growth stage, 1 mM ATP might be reducing the ROS production in *Atann1* compared to the control treatment as the increase in fluorescence intensity for *Atann1* in control treatment (ΔF = 15.26) is higher compared to the ATP treatment (ΔF = 11.15). Mature root zone of both Col-0 and *Atann1* roots were more reactive towards 1 mM ATP (Col-0 ΔF = 18.70, *Atann1* ΔF = 19.12) compared to the control treatment (Col-0 ΔF = 2.63, *Atann1* ΔF = 13.75) and induced higher ROS production compared to the other growth stages. *Atann1* root was also much more sensitive than the Col-0 wild type in the control treatment but not in the 1 mM ATP treatment at this growth stage.

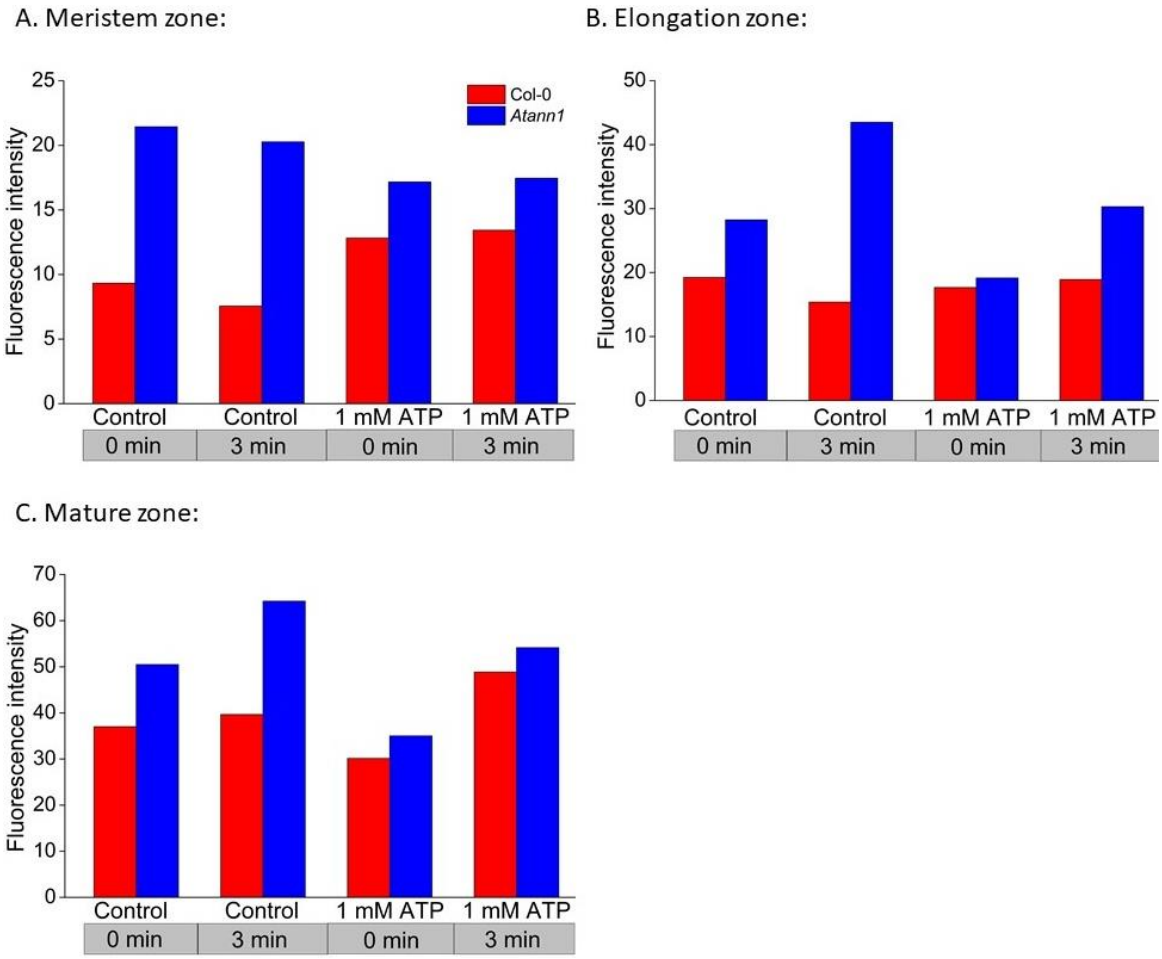

Figure 3.28*:* ROS production is higher in *Atann1* compared to Col-0 in control and 1 mM ATP treatment. Col-0 and *Atann1* roots were observed under a stereomicroscope with GFP filter (excitation 440 - 470 nm, emission 525 - 550 nm). ATP treatment (1 mM) or control treatment was started at the 35th second of measurement. The roots were analysed according to the growth stage: Meristem (~500 µm from the root tip) (A), the elongation zone (~1000 µm from the root tip) (B) and the mature zone (~1500 µm from the root tip) (C). Analysis was carried out at two different time

points; 0 minute (the baseline of measurement) and 3 minutes after the addition of the treatment. These data are from 1 trial with 1 root per genotype per treatment.

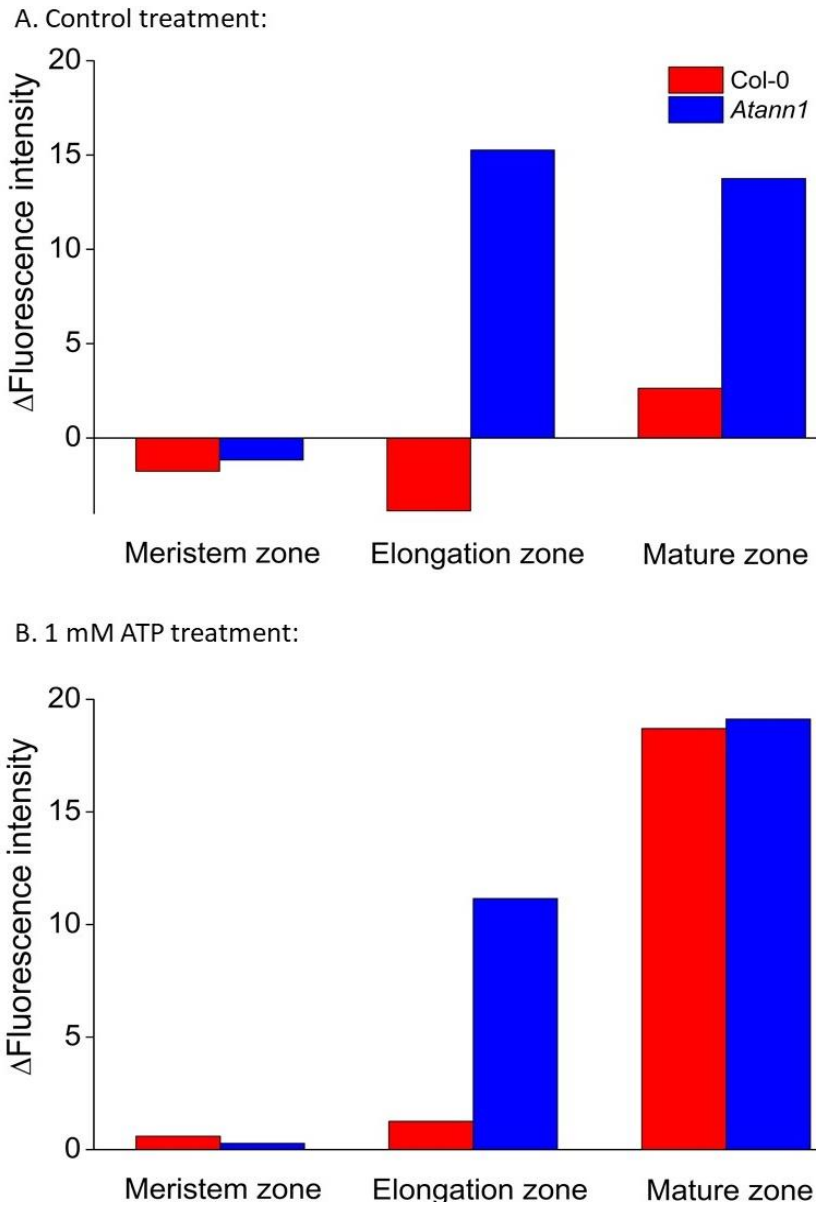

Figure 3.29*:* ATP-induced ROS production is higher in mature zone compared to meristem and elongation zone. Col-0 and *Atann1* roots were observed under a stereomicroscope with GFP filter (excitation 440 - 470 nm, emission 525 - 550 nm). ATP treatment (1 mM) or control treatment was added at the 35th second of measurement. Analysis was done by subtracting the value of fluorescence intensity at 3 minutes from the baseline value at 0 minute (Δ fluorescence intensity) for each genotype and root zone in control treatment (A) and 1 mM ATP treatment (B). These data are from 1 trial with one root per genotype and treatment.

3.2.11 eATP has no effect on the rate of germination or the root system architecture

eATP has been proven to be able to regulate root growth and gravitropism (Tang *et al.*, 2003; Clark *et al.*, 2010) but the mechanism is not yet fully understood. Since AtANN1 has been shown to be involved in mediating eATP signalling, possibly as a calcium channel, it would be essential to investigate whether AtANN1 has any effects on eATP-regulated root growth. Germination tests were carried out with Col-0, *Atann1* and *Atann1/ANN1* complemented mutant seeds. The seeds were germinated onto three different growth media, which were the control medium, medium containing 1 mM ATP and medium containing 2 mM NaCl (as a control for the Na-ATP salt). The rate of germination for the seeds in each type of growth medium was determined over 9 days.

All the Col-0 wild type seeds that were assigned to control medium were fully germinated (100%) on the second day of observation (Figure 3.30 A). However, this was only achieved by the third day for the Col-0 seeds that were grown on the 1 mM ATP-containing growth medium (Figure 3.30 B). The eATP that was used in this test was a disodium-ATP, thus the presence of 2 mM NaCl in the growth medium acted as a control to make sure that the NaCl content in the ATP did not interfere with the rate of germination. This was largely confirmed as the seeds grown on the 2 mM NaCl-containing growth medium achieved total germination (100%) on the second day of observation as for the control medium, after a lower germination rate on control at day 1 (Figure 3.30 C).

Unlike the Col-0, *Atann1* mutant seeds achieved 91% germination rate on day 1 which did not improve over the 9 days of observation in the control condition (Figure 3.30 A). The presence of 1 mM ATP however caused a slight delay, as only 40% of all the seeds germinated on the first day (compared to 91.7 % of Col-0) and 95% of seeds germinated on the second day of observation. This did not increase further as some of the seeds failed to germinate at all (Figure 3.30 B). This is also true for the 2 mM NaCl containing medium as only 45% of all seeds germinated on the first day (compared to 100% of Col-0 seeds) but with larger delay as 87% of the seeds germinated on the second day of observation. On the third day, 91% of all *Atann1* seeds fully germinated on the NaCl-containing medium and this did not increase as some of the *Atann1* seeds failed to germinate at all (Figure 3.30 C).

Of the *AtANN1/ann1* complemented seeds, 87% grown on the control medium germinated on day 1 (Figure 3.30 A) but only 37% and 58% of the seeds fully germinated in the presence of 1 mM ATP and 2 mM NaCl respectively (Figure 3.30 B, C). The

Atann1/ANN1 thus only partially complemented the germination phenotype in 2 mM NaCl conditions as 75% of all the Col-0 seeds germinated on day 1 whereas only 58% of *Atann1/ANN1* seeds germinated on day 1. The second day of observation showed that 95% of all the seeds on control medium and ATP-containing medium were fully germinated whereas only 91% of the total seeds were germinated when grown on the 2 mM NaCl growth medium. These values did not increase as the remaining *Atann1*/ANN1 seeds did not germinate at all. This proved that the *Atann1/ANN1* has the ability to complement the effect of salt and ATP on the germination rate of *Atann1* seeds.

Comparison done in terms of genotype showed that in a control condition, *Atann1* has better germination rate as it achieved full germination on Day 1 compared to Col-0 and *Atann1/ANN1* (Figure 3.30 A). All the genotypes showed similar pattern of germination in 1 mM ATP growth condition (Figure 3.30 B). In 2 mM NaCl condition however, *Atann1* was the most sensitive towards salt as it could only achieved full germination on the third day wheareas Col-0 and the complemented mutant line managed to reach full germination on Day 2 (Figure 3.30 C). This suggests that eATP could slightly affect the rate of germination but this might not involve the action of AtANN1.

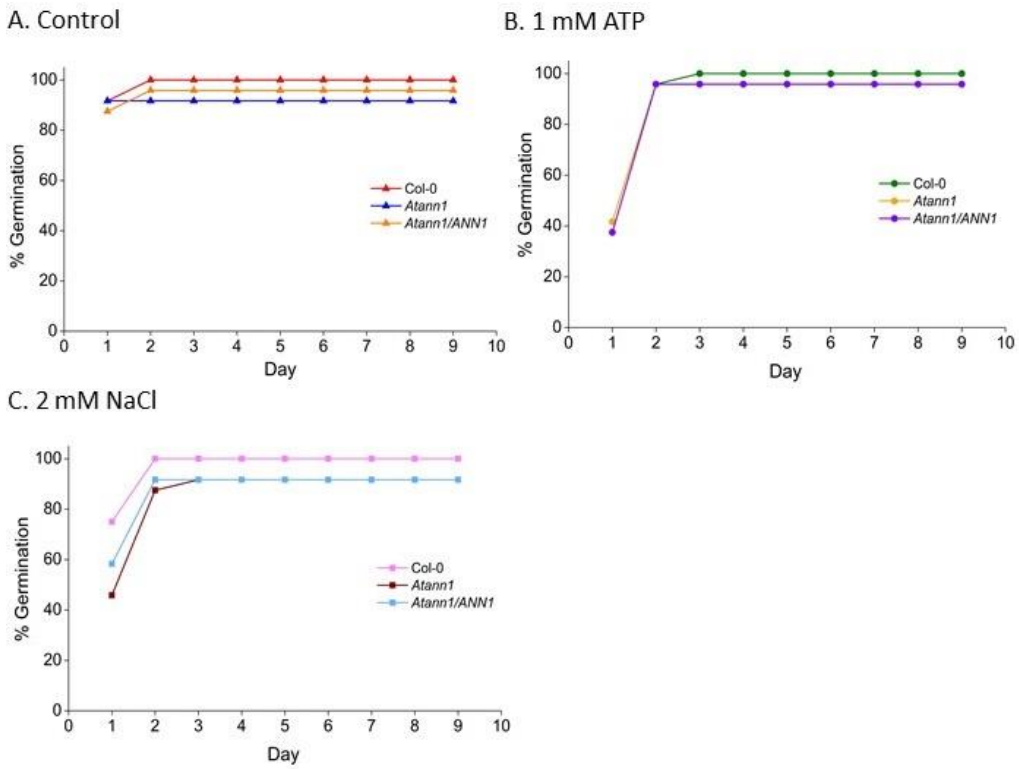

Figure 3.30: **ATP in growth medium slightly delays the germination rate of seeds.** Germination of Col-0 seeds (A), *Atann1* seeds (B), and *Atann1/ANN1* seeds (C) were observed for 9 days. All the seeds were germinated on ½ MS medium with 0.8% (w/v) bactoagar (pH 5.6) as control, or

containing 1 mM ATP or 2 mM NaCl. These data were from 1 trial, with n = 30 seeds per genotype and treatment. Percentage germination was obtained from the number of germinated seeds over the total number of seeds tested.

The germination rate test was carried out as an initial experiment for the root growth assay to examine the root system architecture of the Col-0, *Atann1* mutant and the *Atann1/ANN1* complemented mutant. Since the different genotypes and eATP could influence germination rate, the seedlings that were subjected to the root growth assay were germinated on control growth medium before being transferred to the assigned treatment medium after 3 days of germination. This was to make sure that all the seeds would germinate at the same time. Nine-day-old Col-0, *Atann1* and *Atann1/ANN1* seedlings that were grown on either control medium, 1 mM ATP medium or 2 mM NaCl medium were scanned and analysis of the primary root length, lateral root density, horizontal growth index and the degree of root skewness was carried out. Figure 3.31 shows representatives of Col-0, *Atann1* and *Atann1/ANN1* 9-day-old seedlings grown on either control medium (Figure 3.31 A-C), 1 mM ATP-containing medium (Figure 3.31 D-F) or 2 mM NaCl containing medium (Figure 3.31 G-I).

eATP treatment (1 mM) seemed not to be affecting the length of primary root as the Col-0 (3.8±0.48 cm), *Atann1* (4.0±0.3 cm) and *Atann1/ANN1* (4.2±0.4 cm) primary root lengths in ATP-containing medium were not significantly different from the control medium (Col-0 4.01±0.4 cm; *Atann1* 4.19±0.25 cm; *Atann1/ANN1* 4.24±0.24 cm). The 2 mM NaCl growth medium acted as a control to make sure the disodium content in the ATP had no effect on the experiment and this was confirmed as the primary root growth of all the genotypes in 2 mM NaCl growth medium (Col-0 4.0±0.5 cm; *Atann1* 4.1±0.3 cm; *Atann1/ANN1* 3.8±0.4 cm) were indistinct from the control medium (Figure 3.32 A).

Density of the lateral roots is the number of lateral roots formed over the length of the primary root. Lateral root density showed slight variations between seedlings grown in control medium (Col-0 0.8±0.2; *Atann1* 1.0±0.04; *Atann1/ANN1* 0.96±0.13) compared to the 1 mM ATP growth medium (Col-0 1.1±0.2; *Atann1* 1.1±0.3; *Atann1/ANN1* 1.2±0.2) but it was not significantly different. NaCl medium (Col-0 1.0±0.2; *Atann1* 0.8±0.1; *Atann1/ANN1* 0.6±0.2) showed no effect on the lateral root density, as it was almost similar to the seedlings grown in the control medium. There were also no significant differences between Col-0, *Atann1* and *Atann1/ANN1* lateral root density in all three different growth media (Figure 3.32 B).

According to Grabov *et al*. (2005) measuring the horizontal growth index (HGI) is much more accurate in determining root skewing. HGI with a positive value indicates that the roots are growing towards the right direction and negative value indicates growing towards the left direction. Based on the HGI analysis, it was obvious that roots growing on the 1 mM ATP growth medium showed higher positive values that suggest the roots were skewing to the right (Col-0 0.24±0.003; *Atann1* 0.32±0.12; *Atann1/ANN1* 0.16±0.02). This was not true for the HGI values in control medium (Col-0 -0.01±0.01; *Atann1* 0.007±0.01; *Atann1/ANN1* -0.02±0.007) and the 2 mM NaCl medium (Col-0 0.002±0.02; *Atann1* -0.01±0.013; *Atann1/ANN1* 0.04±0.03). Both the control medium and the 2 mM NaCl medium supported HGI values closer to zero compared to positive or negative values, indicating that the roots were growing straight. AtANN1 however might not be involved in the root skewing regulated by eATP as there were no significant differences between the HGI value of Col-0, *Atann1* and *Atann1/ANN1* roots (Figure 3.32 C).

HGI provides the direction of the skewing but the degree of skewing shows the degree of the root diversion from vertical growth. As shown in the high positive HGI values, the degree of root skewing was larger in 1 mM ATP growth medium (Col-0 15.7±0.4 °; *Atann1* 15.2±2.3 °; *Atann1/ANN1* 11.3±1.3 °) compared to the control medium (Col-0 4.0±0.1 °; *Atann1* 3.6±0.5 °; *Atann1/ANN1* 5.1±0.7 °) or the 2 mM NaCl medium (Col-0 3.3±0.1 °; *Atann1* 3.8±0.2 °; *Atann1/ANN1* 4.5±1.0 °). This was however not related to the function of AtANN1 in eATP signalling as the loss of function mutant *Atann1* degree of skewing was not significantly distinct from the Col-0 and the *Atann1/ANN1* complemented mutant (Figure 3.32 D).

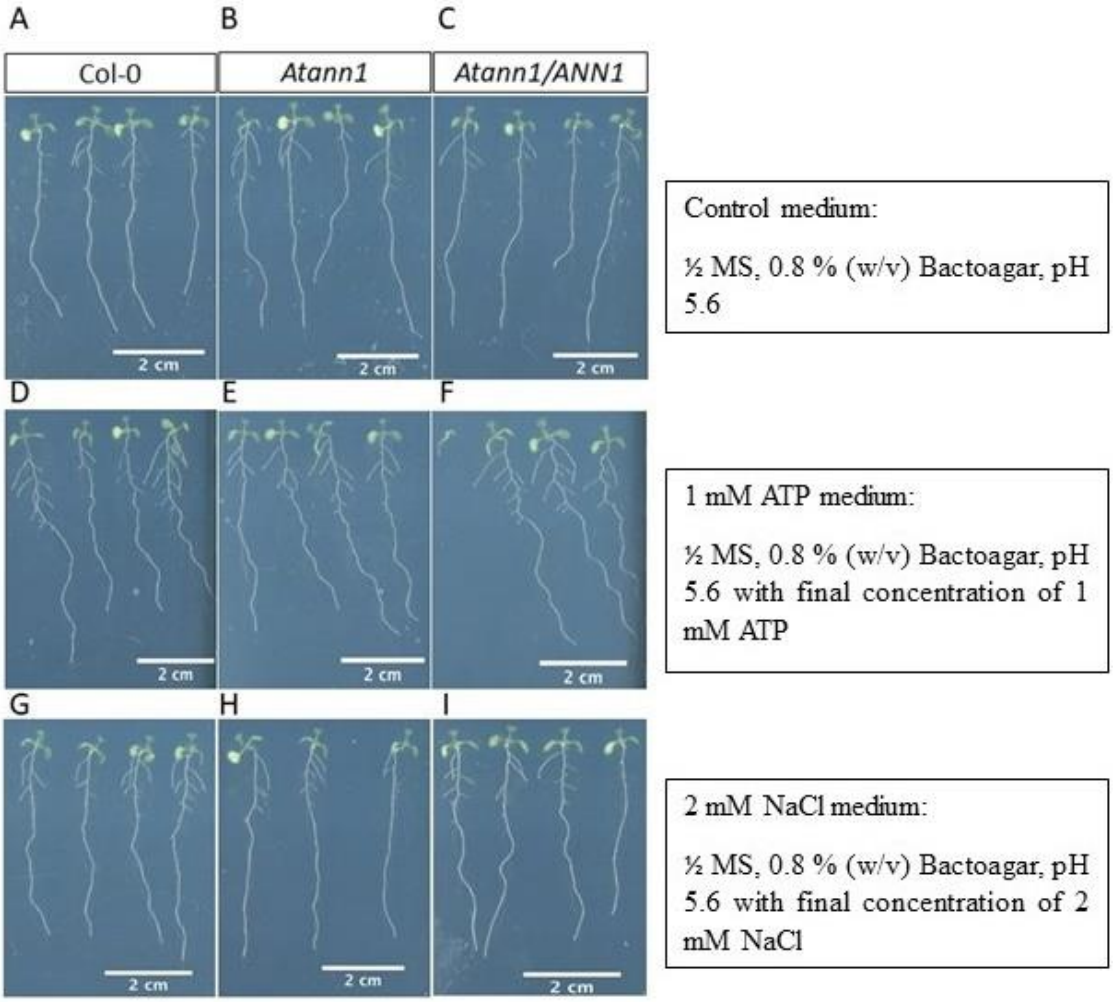

Figure 3.31: ***A. thaliana*** **seedlings grown on 1 mM ATP showed right skewing of roots.** Col-0, *Atann1* and *Atann1/ANN1* were grown on normal control medium (A, B, C), 1 mM ATP-containing medium (D, E, F) or 2 mM NaCl-containing medium (G, H, I) after being germinated on normal control medium for 3 days. Images were taken on day 9 of growing (6 days after transfer). Images shown are the representative of each treatment.

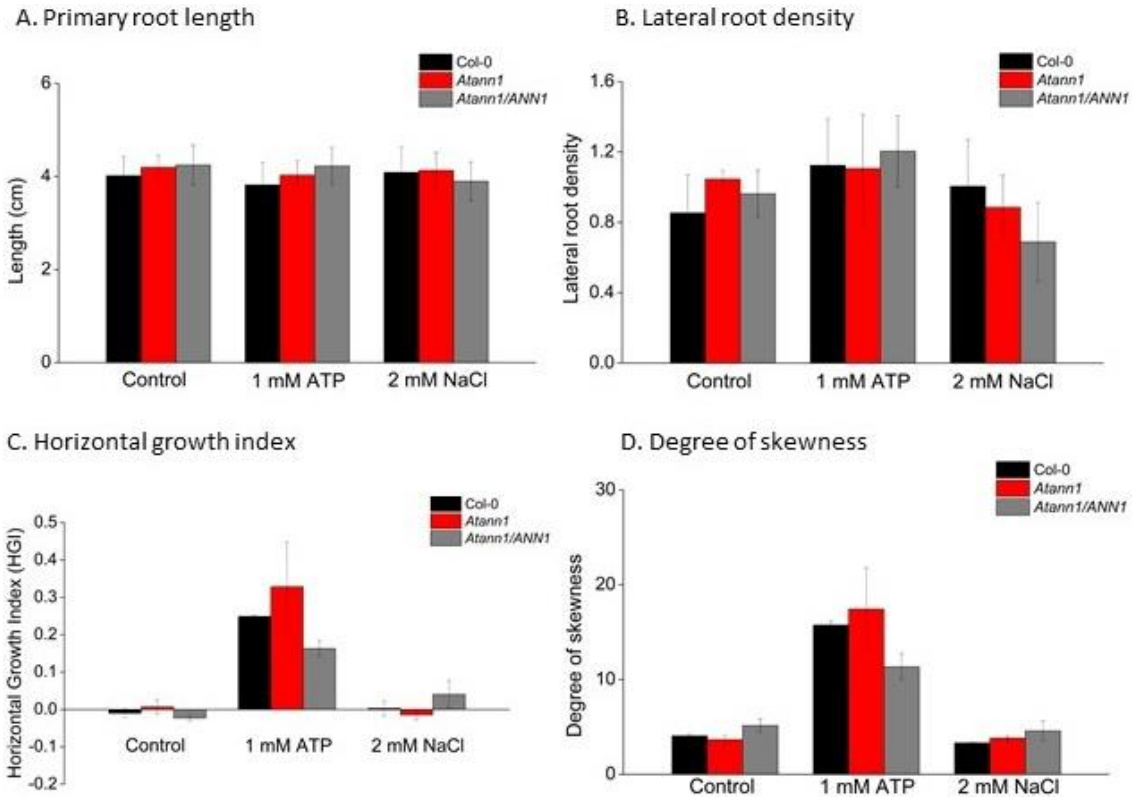

Figure 3.32*:* **eATP causes right skewing of primary root growth.** All Col-0, *Atann1* and *Atann1/ANN1* seeds were germinated on control medium (½ MS with 0.8% (w/v) Bactoagar, pH 5.6) and transferred to control or treatment medium containing 1 mM ATP or 2 mM NaCl after 3 days of germination. Measurement of primary root length (A), lateral root density (B), horizontal growth index (C) and the degree of skewing (D) were carried out after 9 days. Data were from the means ± SEM of 3 independent trials, with n = 16 – 25 seedlings.

3.2.12 AtANN1 plays a role in eATP-induced *AtACS6* gene expression

eATP previously has been shown to be able to induce a group of genes particularly those involved in stress responses (Chivasa *et al.*, 2009; Tanaka *et al.*, 2014; Choi *et al.*, 2014; Jewell *et al.*, 2019). Some of the genes found to be eATP-induced are *AtRBOHD*, *AtWRKY40* and *AtACS6*. Here these genes were tested for regulation by eATP and the possibility of AtANN1's affecting the regulation of these genes. Whole roots of Col-0 and *Atann1* mutant were treated with either control solution (2 mM MES/Tris-HCl; 10 mM $CaCl_2$; 0.1 mM KCl) or 1 mM ATP solution for two different periods; 10 minutes or 30 minutes. RNA was then extracted from these roots before being subjected to qRT-PCR to quantify the gene expression. Two housekeeping genes that were used as a baseline for comparison were *AtTUB4* and *AtUBQ10.*

Before quantifying the eATP-induced gene candidates, it is crucial to look at the expression of *AtANN1* to make sure that the *AtANN1* gene is knocked-out or down in the *Atann1* mutant RNA samples and to discover whether *AtANN1* gene expression is affected by the eATP treatment. In control treatment for 10 or 30 minutes, the transcript abundance value of *AtANN1* gene for Col-0 was (17.50±9) and (13.84±6.4) respectively whereas it was almost completely knocked-down in the *Atann1* sample (10 mins 0.003±0.001; 30 mins 0.001±0.0005). Similar observations can be made for the 1 mM ATP treated samples where Col-0 (10 mins 14.4±2.4; 30 mins 18.6±14) had higher *AtANN1* transcript abundance compared to the *Atann1* sample (10 mins 0.003±0.003; 30 mins 0.009±0.007). *AtANN1* expression might not be affected by the 1 mM ATP particularly after 10 minutes or 30 minutes of treatment as there was no significant difference in the *AtANN1* gene expression between the control treatment and the 1 mM ATP treatment for both Col-0 and *Atann1* samples (Figure 3.33 A).

AtRBOHD transcript abundance seemed to be higher especially after 30 minutes in 1 mM ATP treatment compared to the control treatment for both Col-0 (0.055±0.01) and *Atann1* (0.037±0.022) samples but it was not significant based on statistical analysis. *AtRBOHD* transcript abundance value for the control treatment after 10 minutes (Col-0 0.035±0.01; *Atann1* 0.031±0.01) and 30 minutes (Col-0 0.024±0.006; *Atann1* 0.009±0.004) as well as 10 minutes in 1 mM ATP treatment (Col-0 0.029±0.005; *Atann1* 0.033±0.01) was very low and not distinctly different from each other in all Col-0 and *Atann1* whole root samples (Figure 3.33 B).

AtWRKY40 is known to be up-regulated under stress stimulus. Transcript abundance of this gene was clearly up-regulated by eATP as shown in Figure 3.20 C. Col-0 and *Atann1* samples treated with 1 mM ATP either for 10 minutes (Col-0 0.25±0.09; *Atann1* 0.45±0.12) or 30 minutes (Col-0 1.43±0.75; *Atann1* 1.04±0.4) had significantly higher *AtWRKY40* transcript abundance compared to the samples in 10 minutes control treatment (Col-0 0.035±0.01; *Atann1* 0.047±0.02) or 30 minutes control treatment (Col-0 0.076±0.026; *Atann1* 0.05±0.02). *AtWRKY40* gene expression also seemed to be time-dependent as the transcript abundance increased in both Col-0 and *Atann1* samples as the period of 1 mM ATP treatment extended from 10 minutes to 30 minutes. However, AtANN1 might not be involved in this *AtWRKY40* eATP-induced up-regulation as there was no significant difference in the transcript abundance value between Col-0 and *Atann1* mutant samples either in 10 minutes or 30 minutes eATP treatment (Figure 3.33 C).

Another gene that was tested was *AtACS6*. Based on the quantified transcript, *AtACS6* was significantly up-regulated when the Col-0 samples were treated with 1 mM ATP treatment for 10 minutes (0.36±0.02). The *Atann1* mutant samples in the same 10 minutes 1 mM ATP treatment (0.21±0.04) however failed to show increase in *AtACS6* expression. This shows the possibility of AtANN1's involvement in the eATP-induced *AtACS6* gene expression at whole root level. Temporal regulation of eATP-induced *AtACS6* gene expression was also revealed here as the *AtACS6* transcript abundance value in samples exposed to 1 mM ATP for 30 minutes (Col-0 0.14±0.03; *Atann1* 0.12±0.02) return to the basal level similar to the control treatment in Col-0 (10 minutes 0.065±0.03; 30 minutes 0.069±0.02) and *Atann1* (10 minutes 0.085±0.02; 30 minutes 0.16±0.08) (Figure 3.33 D).

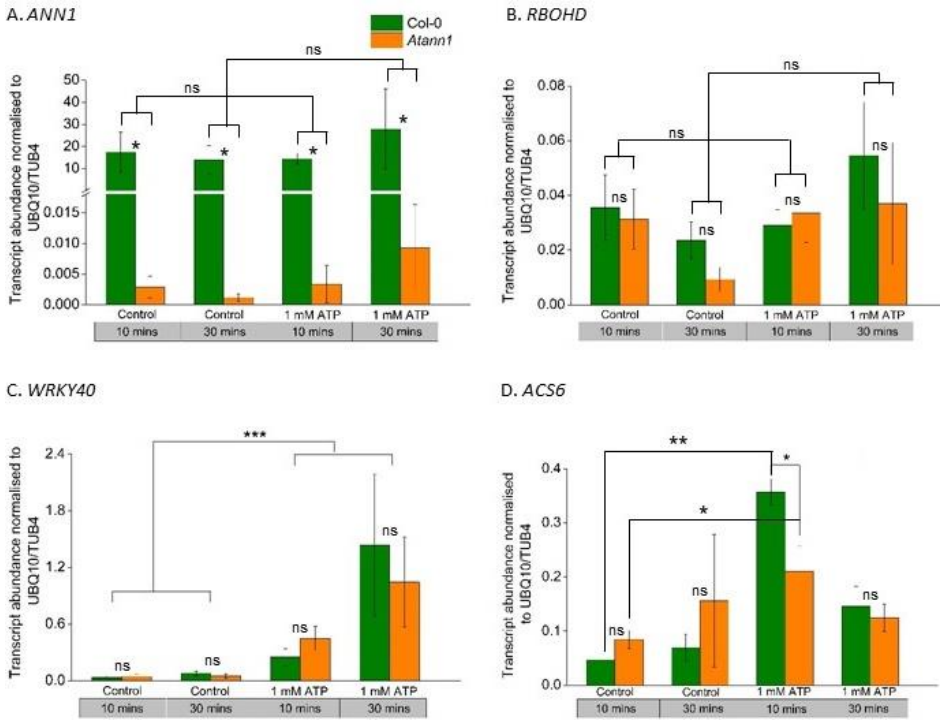

Figure 3.33: **AtANN1 is involved in eATP-induced *AtACS6* up-regulation.** Seven-day-old Col-0 and *Atann1* seedlings were treated with control solution or 1 mM ATP for 10 minutes or 30 minutes. RNA was extracted from excised whole roots. Transcript abundance of *AtANN1* (A), *AtRBOHD* (B), *AtWRKY40* (C) and *AtACS6* (D) in Col-0 and *Atann1* whole root samples was normalised to two housekeeping genes; *AtUBQ10* and *AtTUB4*. Data were from the means ± SEM of 4 independent trials. *p*-values: * (p<0.05), **(p<0.01), ***(p<0.001); Welch's *t*-test for parametric test and Wilcoxon rank sum test for non-parametric test.

3.3 Discussion

3.3.1 AtANN1 is involved in mediating $[Ca^{2+}]_{cyt}$ in 1 mM ATP and ADP treatment

Extracellular ATP (eATP) together with its cognate receptor was proposed as a mechanism of stress signalling that is fundamental to most abiotic and biotic stresses (Demidchik *et al.*, 2003a; Cao *et al.* 2014) and also plant cell death (Chivasa *et al.*, 2005). This signalling system couples with apyrases and possibly purple acid phosphatases, enzymes that have the ability to hydrolyse ATP as a negative feedback to bring the eATP back to a normal level to complete the regulation of this ATP signal. Downstream events caused by the eATP signal such as Ca^{2+} influx into the cytosol, production of ROS (Demidchik *et al.*, 2009) and NO (Foresi *et al.*, 2007; Wu and Wu, 2008) could lead to activation of certain stress-response pathways. The key question in the eATP signalling pathway is the identity of the Ca^{2+} channels that mediate the eATP-induced $[Ca^{2+}]_{cyt}$ accumulation. Identifying the calcium channels that are involved would fill in the gap between the eATP signal perception and the downstream responses such as changes in gene expression and activation of defence mechanism. In this study, $[Ca^{2+}]_{cyt}$ accumulation occurred in the Col-0 whole roots when treated with exogenous ATP (Figure 3.3) as found in previous studies (Demidchik *et al.*, 2003a; Jeter *et al.*, 2004). AtDORN1, discovered by Choi *et al.* (2014b), is believed to be the receptor that governs this eATP signal that triggers the $[Ca^{2+}]_{cyt}$ accumulation. In the same study, AtDORN1 was also found to have the ability to perceive an eADP signal. Here AtANN1 is hypothesised to be the calcium channel that is responsible for the increase in $[Ca^{2+}]_{cyt}$ triggered by nucleotide treatment via the AtDORN1 receptor.

The approach that is used to test the role of AtANN1 in the eATP and eADP signalling pathway is by monitoring the changes in $[Ca^{2+}]_{cyt}$ through the (apo)aequorin reporter specifically in roots. In the environment, the root is the organ that is mainly exposed to a variety of stimuli such as microorganisms, physical obstacles, high saline condition and water deprivation thus making it an apropriate sample to be tested for stress responses. Aequorin is a bioluminescent protein that consists of a calcium binding site that will emit blue light fluorescence upon binding of calcium ion and its ligand coelanterazine (Knight *et al.*, 1992). Although this reporter is excellent at monitoring the changes in $[Ca^{2+}]_{cyt}$ in real time and in a non-invasive manner, there are some limitations that should be taken into consideration when it comes to data analysis.

(Apo)aequorin is constitutively expressed with the 35SCAMV promoter in the Col-0 and *Atann1* whole roots tested in this study. Monitoring the $[Ca^{2+}]_{cyt}$ at whole roots level would be useful to look at the total $[Ca^{2+}]_{cyt}$ accumulated over the time recorded but might not be specific in terms of the calcium signature. As shown in Figure 3.3 D and 3.4 D, Col-0 and *Atann1* treated with 1 mM ATP or 1 mM ADP produced biphasic $[Ca^{2+}]_{cyt}$ traces in 155 seconds measurement. The sources of the fluorescence signal in the first peak and the second peak could not be resolved as whole roots were used as samples. A possible way to look at it is that the calcium burst in the first peak could be produced at the very root tips and the $[Ca^{2+}]_{cyt}$ eventually moves along the roots and triggers another calcium burst or the second peak at the upper elongation zone of the roots. This is because as the root apex contains younger cells and possibly more receptors, root tips would respond faster compared to the more mature cells in the elongation zone. It is also possible that the first peak Ca^{2+} signal is from the outer epidermis layer of the roots and the second peak of Ca^{2+} is produced as the ATP or ADP seeped through the inner layer of the roots. Apart from this inability to resolve the $[Ca^{2+}]_{cyt}$ pattern, the test carried out at whole roots level provides useful information in terms of the total $[Ca^{2+}]_{cyt}$ accumulated due to the eATP or eADP agonist.

$[Ca^{2+}]_{cyt}$ changes were monitored by using a plate reader that could measure the wavelength of fluorescence produced by the sample upon addition of treatment. The addition of treatment however was carried out through pump injection that would induce physical stimulus towards the sample. The touch peak that could be seen in all experiments carried out by using this method is the $[Ca^{2+}]_{cyt}$ response due to the physical stimulus. Although there is no proof that this injection method affects the outcomes of the experiments, a perfusion system where root samples placed in a stream of background solution to avoid the touch stimulus upon addition of eATP or eADP treatment would eliminate the possibility of the touch response affecting the eATP-induced $[Ca^{2+}]_{cyt}$ response. In this study, the pump injection was automated and set to 150µL/sec for all the treatments thus making the outcome of each sample consistent and comparable to each other.

Despite the limitations of using (apo)aequorin at whole roots level, this method is efficient in identifying the possibility of AtANN1 as a component of the eATP signalling pathway. We predicted that *Atann1* mutants will have impaired $[Ca^{2+}]_{cyt}$ response compared to the wild type Col-0 when challenged with eATP or eADP. Inability of *Atann1* to accumulate $[Ca^{2+}]_{cyt}$ as in Col-0 wild type suggests that AtANN1 is required in mediating $[Ca^{2+}]_{cyt}$ increase in the presence of 1 mM ATP (Figure 3.3), 1mM ADP (Figure 3.4) at whole

root level and 0.5 mM ATP (Figure 3.5), 0.5 mM ADP (Figure 3.6), 1 mM ATP (Figure 3.7) or 0.1mM ATP (Figure 3.8) at the root tips level. AtANN1 contains the conserved salt bridges that have the potential to form calcium channels (Liemann *et al.*, 1996; Laohavisit *et al.*, 2009). This is supported by the electrophysiological patch clamping test carried out in the past demonstrating the ability of AtANN1 to form a Ca^{2+}-permeable conductance (Laohavisit *et al.*, 2012). Exogenous ATP supplied to *Arabidopsis* in this study mimics the eATP accumulated under abiotic stresses (Dark *et al.*, 2011) although in a much higher concentration that causes transient elevation of $[Ca^{2+}]_{cyt}$ (Demidchik *et al.*, 2003a).

Tests with the complementation line 1 cm excised root tip were carried out to confirm the AtANN1 function in eATP and eADP signalling. In the 1 mM ATP test, the complemented line of AtANN1 managed to restore the full $[Ca^{2+}]_{cyt}$ response in the second $[Ca^{2+}]_{cyt}$ peak, but only partially in the overall $[Ca^{2+}]_{cyt}$ released. This might be because the *Atann1/ANN1* complementation was under the 35S CAMV promoter thus it might not completely phenocopy the wild type under the native *AtANN1* promoter. Although the (apo)aequorin is under the 35S CAMV promoter and (apo)aequorin discharge screening was carried out to make sure that the aequorin discharge is similar between all the genotypes tested, there is a possibility that slight differences in the (apo)aequorin expression in different seedlings line affected the outcome of this test. A higher number of samples tested with the complemented line might resolve this issue and confirm the phenotype complementation.

A previous study found *Atann1* exhibited shorter primary root length compared to Col-0 (Clark *et al.*, 2005b). This arguably could be causing lower fluorescent signal as there would be a fewer cells in shorter roots. A similar test with eATP and eADP as agonist carried out on 1 cm root tips shows the impairment of *Atann1* in accumulating $[Ca^{2+}]_{cyt}$ compared to Col-0 (Figure 3.5, Figure 3.6). This demonstrates that the lower signals from *Atann1* whole roots or root tips were not due to differences in the number of cells but due to the absence of AtANN1 to mediate the $[Ca^{2+}]_{cyt}$ response.

As the length of primary root could also be determined by the elongation of each cell and the number of cells making up the whole roots, it would be more accurate to weigh the whole roots instead of measuring the root length. This however could introduce physical stress or possibly injury while handling the roots. Another possible approach with high resolution is by using protoplasts. Protoplasts would be more specific in terms of the $[Ca^{2+}]_{cyt}$ pattern as shown in a previous study where mature epidermal protoplast evoked a single $[Ca^{2+}]_{cyt}$ peak in eATP (Demidchik *et al.*, 2009) and eADP treatment (Demidchik *et al.*,

2011). The disadvantages however would be that the population of protoplasts should be cell-specific and similar in the total number of protoplasts in each genotype. Whole roots consist mainly of mature developed cells compared to root tips that are made up of young proliferating cells. The outcome of the test using whole roots would likely link eATP as environmental stimulus instead of the function of eATP in growth and development.

A different argument regarding eATP-induced $[Ca^{2+}]_{cyt}$ is that the hydrolysis of eATP acts as a source of energy that drives the influx of Ca^{2+} ion through the plasma membrane thus revoking the notion of eATP as a signal molecule. Whole roots exposed to non-hydrolysable eATP or non-hydrolysable eADP gave a similar $[Ca^{2+}]_{cyt}$ signature and overall accumulation to the hydrolysable eATP (Figure 3.9) and eADP (Figure 3.10). This observation is true for both Col-0 and *Atann1* thus confirming that hydrolysis of eATP or eADP is not needed for the $[Ca^{2+}]_{cyt}$ response.

As previously mentioned, the AtDORN1 receptor can bind both eATP and eADP (Choi *et al.*, 2014b). In a study by Demidchik *et al.* (2011), eADP-treated whole roots failed to produce intracellular ROS accumulation as seen in eATP-treated whole roots. This suggests eADP as a potential signal molecule with a different pathway than the eATP signal. Comparison between the $[Ca^{2+}]_{cyt}$ signature produced by 1 mM eATP and 1 mM eADP was carried out to see any differences in the outcomes from both agonists. Based on Figure 3.11, both 1 mM eATP and 1 mM eADP agonists produced a similar pattern and total $[Ca^{2+}]_{cyt}$ accumulation in Col-0 whole roots. A similar instance was also observed with 0.1 mM eATP and 0.1 mM eADP treatment. This might indicate that the possible divergence in the signalling pathway between eATP and eADP signal is downstream of the $[Ca^{2+}]_{cyt}$ response. Another possibility is that the differences in the $[Ca^{2+}]_{cyt}$ between eATP and eADP signal is too subtle and could not be seen especially at whole roots level. In this case, a different experimental approach with better resolution is needed.

In this chapter, the involvement of AtANN1 in eATP and eADP signalling is hypothesised to be the calcium channel that mediates $[Ca^{2+}]_{cyt}$ accumulation mainly due to previous studies showing its ability to transport Ca^{2+} and the presence of the conserved salt bridges motif that is important in forming Ca^{2+} channel in animal studies. However, based on the protein motifs studies carried out previously as shown in Figure 1.3 (Chapter 1.8.5), AtANN1 is a multifunctional protein and have the possibility to play different roles than as the Ca^{2+} channel in the eATP and eADP signalling. The heme-binding motif suggests the potential of AtANN1 as a peroxidase enzyme (Laohavisit and Davies, 2011). Gorecka *et al*.

(2005) reported that AtANN1 has an active peroxidase activity that could be contributed by its heme-binding domain. It is possible that peroxidase activity of AtANN1 reacting with the ROS burst that occurs downstream of eATP perception, which could control possible ROS signalling (Evans *et al.*, 2016). AtANN1 also has the possiblity to bind to the eATP that caused the downstream responses as it contains the ATP/GTP binding motif. This AtANN1 binding with ATP/ADP however is not yet tested *in vivo*. It is also interesting that the ATP/GTP binding motif of AtANN1 overlaps with the Ca^{2+} binding motif in its fourth endonexin repeat which could suggest potential regulation of ATP/GTP binding by Ca^{2+}. Since knocked-out mutant of AtANN1 still could response to the ATP and ADP treatment at whole root level, the role of AtANN1 to perceive ATP signal based on its ATP/GTP motif might not be the case. However, this needs to be tested at different parts of the plants and at different growth stages. More discussion on AtANN1, AtDORN1 and ATP perception is presented in Chapter 3.3.3.

3.3.2 $[Ca^{2+}]_{cyt}$ accumulation might be originating from the intracellular and extracellular calcium store

Gd^{3+} is one of the components in the lanthanide series that is commonly used as a channel blocker in this field. Gd^{3+} ionic radius is very similar to that of Ca^{2+} making it easy to displace Ca^{2+} thus acting as a competitive inhibitor of Ca^{2+} (Hamill and Mcbride, 1996). Unlike Ca^{2+}, Gd^{3+} is non-permeable to the channel presumably at the plasma membrane, as it is unable to pass through the channel thus blocking Ca^{2+} conductance (Malasics *et al.*, 2010). As Gd^{3+} could potentially block Ca^{2+} influx from the apoplast, we tested the Col-0 and *Atann1* root tips with 0.5 mM ATP in the presence of $GdCl_3$ to delineate the origin of the calcium ion during influx.

Figure 3.12 and Figure 3.13 demonstrated that Gd^{3+} managed to only partially inhibit the total accumulation of $[Ca^{2+}]_{cyt}$ in both Col-0 and *Atann1* when treated with 0.5 mM eATP or 0.5 mM eADP respectively. Another study with Col-0 and *Atann1* also showed partial inhibition of Gd^{3+} in root epidermal protoplasts when challenged with NaCl treatment in the presence of 0.3 mM $GdCl_3$ (Laohavisit *et al.*, 2013). As *Atann1* pre-treated with Gd^{3+} accumulated the same $[Ca^{2+}]_{cyt}$ as the Col-0 pre-treated with Gd^{3+}, it could be that the AtANN1 is the component of the plasma membrane that mediates the calcium influx. This is however not true because in the absence of Gd^{3+}, *Atann1* does not phenocopy Col-0 that was pre-treated with $GdCl_3$ (Figure 3.12 F, 3.13 F). Thus, another possible explanation could be

that the $[Ca^{2+}]_{cyt}$ increase due to eATP originated from both the extracellular matrix and the intracellular calcium stores.

The vacuole is one of the intracellular calcium stores that plays an important part in maintaining ion homoestasis (Cheng *et al.*, 2005) by storing a large amount of Ca^{2+} making sure that the level of Ca^{2+} in the cytosol remains low. In *A. thaliana,* AtTPC1 (Two Pore Channel1) encodes the Slow Vacuolar (SV) channel that mediates calcium efflux from the vacuole (Peiter *et al.*, 2005). Another study carried out on beetroots showed that a different range of cytosolic ATP concentrations managed to produce Ca^{2+} flux from the vacuole and mediated calcium conductance through patch clamp experiments (Pottosin *et al.*, 2009). Navazio *et al.* (2001) identified ER other than the vacuole as one of the Ca^{2+} stores that released Ca^{2+} induced by cADPR in cauliflower. This suggests possible involvement of ER in calcium signalling as an intracellular calcium store. The channels that are responsible for the release of Ca^{2+} from the plant ER however remain obscure.

An earlier study in human gingival fibrolasts found that a 1 minute $GdCl_3$ incubation completely blocked intracellular calcium increase but the cells in 30 minutes incubation time managed to produce small intracellular calcium increase (Arora *et al.*, 1994). In a planar lipid bilayer experiment using maize annexins, calcium conductance through the bilayer was completely blocked after 5 minutes of Gd^{3+} treatment (Laohavisit *et al.*, 2009). Another study using whole *Arabidopsis* roots showed that $[Ca^{2+}]_{cyt}$ increase was almost completely blocked when the roots underwent 10 minutes $GdCl_3$ pre-treatment prior to the addition of 0.1 mM αβmeATP (slowly hydrolysable ATP analogue) (Demidchik *et al.*, 2003a). Gd^{3+} incubation for 30 minutes used in tests here failed to completely block the $[Ca^{2+}]_{cyt}$ increase by 0.5 mM eATP agonist. This shows the possibility of Gd^{3+} acting differently depends on the time of exposure and the type of stimulus used.

Other than partially inhibiting, 0.5 mM $GdCl_3$ caused delay in the $[Ca^{2+}]_{cyt}$ increase in the first peak (without Gd^{3+} 41-66 seconds; with Gd^{3+} 54-93 seconds) and second peak (without Gd^{3+} 66-155 seconds; with Gd^{3+} 93-155 seconds) for both Col-0 and *Atann1* when challenged with eATP or eADP (Figure 3.12 C, 3.13 C). Another possible way to interpret these data is that Gd^{3+} managed to completely block the first peak (41 - 66 seconds) but not the second peak (66 - 155 seconds). A similar observation can be seen in a previous study by Tanaka *et al.* (2010), where whole seedlings of Col-0 showed delayed $[Ca^{2+}]_{cyt}$ eATP response or missing first peak (10 - 60 seconds) when pre-treated with either 0.1 mM or 0.2 mM $GdCl_3$ for 30 minutes. The same study also discovered that higher concentration of Gd^{3+}

(~ 0.5 mM) is needed to block the proposed second peak (60 - 120 seconds). Extensive studies have been carried out to understand the mechanism of Gd^{3+} as a stretch-activated channel blocker (Ermakov *et al.*, 2010). However the detailed mechanism of how Gd^{3+} acts as cation channel inhibitor is not yet solved apart from potential competitive inhibition. The remaining possible calcium channels other than AtANN1 that help mediate the eATP signal are Gd^{3+} sensitive, which could help enable their future identification.

Suramin is a non-specific P2X receptor inhibitor that is widely used especially in animal studies. Previously AtANN1 was found to be one of the ATP-binding proteins in vitro thus making it possible that AtANN1-eATP binding triggered the downstream response (Ito *et al.*, 2006). Here we tested the Col-0 and *Atann1* excised root tips with 0.5 mM eATP and eADP pre-treated with 1.5 mM suramin. This concentration of suramin seems to be effective in impeding the $[Ca^{2+}]_{cyt}$ response in the first peak (Figure 3.14 C, D) but not the second peak and eventually the total $[Ca^{2+}]_{cyt}$ accumulation (Figure 3.14 E, F). Since the test was carried out at the root tips, it is not clear where the signal from the first peak originates in terms of the type of tissue. However, it is interesting that in the first peak of $[Ca^{2+}]_{cyt}$ response towards ATP, the Col-0 pre-treated with suramin phenocopied the *Atann1* that is not treated with suramin (Figure 3.14 D). This could suggest AtANN1 binding to ATP triggered the downstream $[Ca^{2+}]_{cyt}$ response. This notion is however not possible as we have proven that root tips are responsive towards eATP although impaired in the absence of AtANN1 (Figure 3.5 D, F). Some possible explanations are suramin could partially inhibit ATP binding to AtANN1 or inhibit AtANN1 function involved in mediating ATP-binding to a purinoreceptor most probably AtDORN1.

Based on Figure 3.14 E, suramin is ineffective at inhibiting the eATP $[Ca^{2+}]_{cyt}$ response at the second peak in both Col-0 and *Atann1* root tips. Based on previous studies (Matthus *et al.*, 2019b), the second peak signal might originate from the elongation zone of the roots and as it contains denser tissues, a higher concentration of suramin is probably required to cause total inhibition of eATP response in the second peak phase. The ability of suramin to block purinoreceptor activity could also depend on the type of cells tested. Suramin severely impaired eATP-induced Ca^{2+} conductance and $[Ca^{2+}]_{cyt}$ accumulation in mature root epidermal protoplasts (Demidchik *et al.*, 2009) but not at the root tips as shown in this study.

Low concentration of suramin could be effective at blocking the purinoreceptor present at mature epidermal cells. However, excised root tips used in this study consist of

different layers of tissues and cells and it is possible that suramin does not affect a population of purinoreceptor in the root tips. Jacobson *et al.* (2002) stated that suramin has multiple selectivity thus can have different effects on different type of receptors. Other than that, the technical approach used in different studies might led to different outcomes. Sun *et al.* (2012) found that 1 hour suramin pre-treatment managed to dampen Ca^{2+} response by *Populus euphratica* when challenged with salt and eATP treatment whereas shorter incubation time (30 minutes) was used in this study. A similar observation can be seen in 0.5 mM eADP-treated root tips where suramin managed to partially inhibit $[Ca^{2+}]_{cyt}$ response in the first peak but not in the second peak (Figure 3.15 C, D, E). This is expected as both eATP and eADP induced similar $[Ca^{2+}]_{cyt}$ response at root tips level as previously shown indicating that both are perceived by similar purinoreceptor system.

Another well-known P2X receptor inhibitor is PPADS (Pyridoxalphosphate-6-azophenyl-2',4'-disulfonic acid). PPADS is a non-specific receptor inhibitor that is selective towards P2X2 receptor in animal cells (North and Jarvis, 2013). PPADS that is commercially available has a bright red colour and initial tests with a spectrophotometer showed that at high concentration, the red colour of PPADS solution could interfere with the wavelength of blue luminescence released by (apo)aequorin reporter (Appendix II). Thus, PPADS is not a suitable antagonist to be used with the (apo)aequorin reporter in this study.

3.3.3 AtANN1 possibility to be in the AtDORN1-mediated ATP signalling pathway requires further tests

In 2014(b), Choi *et al.* discovered the first plant purinoreceptor, AtDORN1. Since AtANN1 is required for the plant's normal eATP response, it is crucial to know whether AtANN1 is in the same pathway as the AtDORN1 receptor. By using a similar approach with the (apo)aequorin reporter, we monitored changes in $[Ca^{2+}]_{cyt}$ in both *Atdorn1-1/ann1* double mutant and the *Atdorn1-1* single mutant in the presence of eATP and eADP. *Atdorn1-1* is a single point mutation that changes the amino acid make up of the kinase function in At DORN1.

Figure 3.16 and Figure 3.17 showed *Atdorn1-1/ann1* double mutants remain impaired in producing $[Ca^{2+}]_{cyt}$ increase similar to the *Atdorn1-1* single mutant compared to Col-0 in 1 mM or 0.1 mM eATP and eADP treatment respectively. Here it is shown that the kinase domain of the AtDORN1 is important in the eATP perception as the mutation causes reduced downstream responses. In the $[Ca^{2+}]_{cyt}$ traces shown in both 1 mM eATP and 1 mM eADP

treatment (Figure 3.16C and 3.17C respectively), small peaks of $[Ca^{2+}]_{cyt}$ are formed in both *Atdorn1-1/ann1* and *Atdorn1-1* roughly around the 56 - 84 seconds of measurement. Although the small peaks are not significant, it might suggest that in the kinase mutation seedlings, other domains of the AtDORN1 protein might still be active especially when treated with 1 mM eATP or eADP as these peaks are not visible in lower 0.1 mM eATP or eADP concentration.

Knock down of both AtDORN1 and AtANN1 root tips in T-DNA mutants *Atdorn1-3/ann1* and *Atdorn1-3* shows abolished $[Ca^{2+}]_{cyt}$ response towards eATP and eADP either in 1 mM or 0.1 mM concentration compared to the Col-0 wild type (Figure 3.18 and Figure 3.19). There are no small peaks of $[Ca^{2+}]_{cyt}$ formed in these mutants when challenged with 1 mM eATP or eADP treatment as found in the kinase point mutation previously. Since the knock-out of AtANN1 in the *Atdorn1-3/ann1* genotype constantly showed no response towards both ATP and ADP treatment, these show that AtANN1 could be in the same pathway as AtDORN1 in response to eATP or eADP. The confirmation of whether AtANN1 is upstream or downstream of AtDORN1 could not be resolved here. However, the $[Ca^{2+}]_{cyt}$ traces found from the test of *Atann1* single mutant with eATP and eADP were different compared to the *Atdorn1-3* and *Atdorn1-3/ann1*. This could also point out the possibility of AtANN1 working in a different pathway than AtDORN1 in both eATP and eADP signalling. Since the initial knock-out of AtDORN1 completely unresponsive in terms of $[Ca^{2+}]_{cyt}$ accumulation towards eATP or eADP, the effect of *Atann1* mutant and the relationship between AtDORN1 and AtANN1 could not be resolved here. Further tests such as co-expression test and protein interactions between AtDORN1 and AtANN1 is needed to confirm the relationship between these two components.

Looking at AtANN1 in the perspective of it acting solely as calcium channel protein, one might interpret AtANN1 to be working downstream of the AtDORN1 purinoreceptor. In animal cells, a P2X receptor is a ligand gated ion channel that is able to produce calcium response upon eATP perception (Burnstock, 2006). Plant annexin protein structure, for example in maize, consists of a potential ATPase (McClung *et al.*, 1994) and a study published by Ito *et al.* (2006) listed AtANN1 as one of the ATP-binding proteins in vitro. AtANN1 can occur extracellularly (Davies, 2014). It is also possible in another scenario that AtANN1 acting as an eATP-binding protein triggers the downstream responses in a redundant interaction with AtDORN1. The loss of AtANN1 would lower the

$[Ca^{2+}]_{cyt}$ response to eATP and eADP, but this would only be abolished if AtDORN1 were absent.

3.3.4 eATP-induced $[Ca^{2+}]_{cyt}$ accumulation might involve voltage-independent calcium channel activation at a depolarised plasma membrane

Demidchik *et al*. (2002) showed that varying the concentration of K^+ in the background solution could change the plasma membrane potential of the *Arabidopsis* root epidermal cells and potentially affect the opening and closing of ion channels. In this study, the background solution that is used during $[Ca^{2+}]_{cyt}$ measurement consists of a low concentration of K^+ (0.1 mM KCl) thus creating a hyperpolarising (HP) condition for the plasma membrane. However, seedlings are grown in half strength MS medium, which contains a very high K^+ concentration and also includes calcium chelator Ethylenediaminetetraacetic acid (EDTA) creating a depolarising (DP) condition for the plasma membrane. We tested two different K^+ concentrations (0.1mM KCl and 10 mM KCl) to test whether plasma membrane potential could have any effect on the $[Ca^{2+}]_{cyt}$ accumulation under eATP or eADP signalling and the role of AtANN1 in these varying conditions.

We hypothesised that by measuring the $[Ca^{2+}]_{cyt}$ in depolarising conditions, the resting plasma membrane potential of the whole roots would shift to a more positive value thus deactivating the hyperpolarised-activated calcium channel (HACC) that is implicated as the calcium channel responsible for mediating the eATP response. Figures 3.20 and 3.21 showed that $[Ca^{2+}]_{cyt}$ measured in HP or DP conditions does not significantly differ either in the presence of eATP or eADP in both Col-0 and *Atann1*. Since the measurement is carried out at whole roots level, it is possible that the changes that occurred between HP and DP conditions is very subtle and it is not manifested at whole roots level. Other than that, the K^+ concentration used might not be high enough to depolarise the plasma membrane of the whole roots. It might also be that there are possible calcium channels that work at slightly more positive membrane potential than HACC such as non-selective cation channel (NSCC) or voltage-independent calcium channel (VICC). These calcium channels could compensate the deactivated HACC and help mediate the $[Ca^{2+}]_{cyt}$ increase when challenged with eATP or eADP.

3.3.5 AtANN1 might be functioning downstream of eATP-induced ROS production

Another hallmark of the eATP signalling perception is the almost immediate intracellular ROS burst (Demidchik *et al.*, 2009, 2011). Here we found that 1 mM eATP treatment managed to induce intracellular ROS in Col-0 after 3 minutes at the root mature zone. In the *Atann1* root, the level of intracellular ROS increased upon addition of 1 mM eATP compared to the baseline. This might suggest that the involvement of *Atann1* is downstream of the ROS production, therefore the absence of the AtANN1 does not interfere with the intracellular ROS production. This is also supported by a previous study carried out by Laohavisit *et al.* (2012) showing that AtANN1 can be activated by ROS, thus it should be downstream of the ROS production.

The basal level of ROS in *Atann1* roots assigned for control treatment was very high from the beginning. This could be due to several reasons such as injury to the root while handling it during measurement and the possibility of the probe CMH_2DCFDA bleaching, as it is sensitive to light (Invitrogen). Other than that, the baseline level of intracellular ROS in *Atann1* roots assigned for both control and eATP treatment is higher compared to the Col-0 thus making direct comparison between different genotypes to be less accurate. The amino acid sequence of AtANN1 revealed the presence of a haem-binding domain thus raising the possibility of AtANN1 acting as peroxidase enzyme (Clark *et al.*, 2012). In-vitro studies carried out proved that AtANN1 has peroxidase activity, which depends on the phosphorylation of the protein (Gorecka *et al.*, 2005). These findings also might explain the high ROS baseline in the absence of AtANN1.

Another interesting observation is that the increase in the intracellular ROS level due to the eATP treatment is pronounced only in the mature part of the roots. The eATP treatment was applied from the tip of the roots thus the treatment reached the younger part of the roots before the mature zone. The NADPH oxidase AtRBOHC loss of function mutant, *rhd2* is unable to accumulate ROS at whole roots level when exposed to eATP (Demidchik *et al.*, 2009) making it one of the possible ROS components in eATP signalling. The same study also observed the accumulation of ROS at the mature zone of the *A. thaliana* root. Another candidate for the ROS production enzyme is AtRBOHD, which is a target of AtDORN1 (Choi *et al.*, 2014b; Chen *et al.*, 2017). Both AtRBOHC and AtRBOHD genes are mainly expressed at the mature part of *A. thaliana* root (Brady *et al.*, 2007), thus this might explain the concentration of ROS burst at the maturation zone of the roots tested.

3.3.6 AtANN1 is not involved in root skewing in the presence of 1 mM eATP

eATP is also known for its effect on growth and development of plants. In *M. trancatula*, eATP seems to be accumulated at the actively growing regions of the plants (Kim *et al.*, 2006) suggesting its involvement in growth regulation. A different study focusing on apyrases (an enzyme that hydrolyses eATP) found that suppression of apyrases leads to reduction in primary root growth (Liu *et al.*, 2012a). The same study also discovered the ability of eATP to inhibit root gravitropism. This tied eATP well into growth regulation and viability as in the absence of apyrases, eATP concentration would rise and Sun *et al.* (2012) found that high eATP concentration (0.5 mM - 2 mM) manage to induce programmed cell death in *Populus euphratica* cells.

Extracellular ATP's ability to regulate growth has been shown many times in previous studies and although AtANN1 is involved in mediating eATP-induced $[Ca^{2+}]_{cyt}$ response, we found that AtANN1 might not be related to eATP-regulated root growth. Germination rate of Col-0, *Atann1* and *Atann1/ANN1* observed over 9 days showed that 1 mM eATP and 2 mM NaCl media causes slight delay in germination compared to the control medium (Figure 3.25) for all genotypes. Based on this observation, we then decided to carry out a growth assay to compare the root system architecture of seedlings growing on 1 mM eATP medium with the control medium.

Although germination was affected by eATP, the primary root length of seedlings grown on ATP-containing medium is not significantly different to control medium for all the genotypes tested (Figure 3.27 A). This was also observed by Tang *et al.* (2003) where the primary root lengths of seedlings grown on 2 mM ATP medium were similar to those grown on control medium although it also induced root curling. Here root curling or root waviness is not pronounced in eATP-grown seedlings compared to the control medium (Figure 3.27 C). This could be due to slightly lower eATP concentration (1 mM) used instead of 2 mM ATP in the previous study mentioned. In the same study, 2 mM eATP promoted lateral root formation but Figure 3.19 B showed no significant difference in terms of lateral root density between control medium and the 1 mM eATP medium. Another characteristic of seedlings grown in ATP-containing media is root skewing. Root skewing in the presence of eATP might be related to the altered distribution of auxin. Tang *et al.* (2003) proved that addition of ATP managed to disrupt the distribution of auxin and thus inhibit gravitropism. A similar observation was also made by Liu *et al.* (2012a) where exogenous ATP inhibited root gravitropism. Based on horizontal growth index calculations, Col-0, *Atann1* and

Atann1/ANN1 roots that were grown on eATP-containing medium are skewed to the right compared to the control medium or the NaCl control medium (Figure 3.27 C). Degree of skewing was also measured to see if *Atann1* would have significantly more or less skewing compared to the Col-0. Figure 3.27 D suggests AtANN1 might not be participating in the eATP-regulated root skewing as there are no differences between *Atann1* mutant and the Col-0.

3.3.7 AtANN1 is required for the eATP-induced *AtACS6* gene expression

Changes at the gene expression level were also examined to further investigate the role of AtANN1 in eATP signalling. Here we looked at the eATP-induced genes *AtRBOHD, AtWRKY40* and *AtACS6.* Previously the *Atdorn1-3* mutant showed reduced level of *AtRBOHD* gene expression compared to Col-0, confirming the role of this receptor in the initial perception of the eATP signal (Choi *et al.*, 2014b). In the Choi *et al.* (2014b) paper, *AtRBOHD* is listed as one of the eATP-induced gene that was also up-regulated in a wounding response. This was however not replicated here as the level of *AtRBOHD* transcript in eATP-treated Col-0 and *Atann1* were not distinct from the control treatment (Figure 3.28 B). Since whole seedlings were used in the experiment carried out by Choi *et al.* (2014b), it could be that the effect of eATP treatment on *AtRBOHD* gene expression is more pronounced in leaves compared to whole roots.

AtWRKY40 is a transcription factor that is heavily involved in biotic and abiotic stresses. Both Col-0 and *Atann1* in eATP treated samples showed up-regulation of *AtWRKY40* gene expression especially at 30 minutes compared to control treatment (Figure 3.28 C). AtWRKY40 has been shown to be involved in the activation of immune response towards *P. syringae* infection (Schön *et al.*, 2013). This could relate eATP to AtWRKY40 function as eATP was found to be activating pathogen-related gene expression (Chivasa *et al.*, 2009). Both AtWRKY40 and AtANN1 are also involved in the ABA response pathway (Chen *et al.*, 2010; Lee *et al.*, 2004) and eATP is important in mediating ABA-induced stomatal closure. The absence of AtANN1 however does not affect the level of *AtWRKY40* genes in both eATP and control treatment (Figure 3.28 C). Based in these findings, AtANN1 might be downstream of the activation of *AtWRKY40* expression and thus has no effect on its expression level.

The gene expression experiment carried out in this study reveals potential regulation by eATP of ethylene production. AtACS6 is one of the many isoforms of 1-

aminocyclopropane-1-carboxylix acid synthase (ACS) that is an important enzyme in the biosynthesis of ethylene. Figure 3.28 D shows the *AtACS6* gene is up-regulated in Col-0 whole roots especially at 10 minutes eATP treatment before going down at the 30 minutes time-point compared to the control treatment. This is also supported by a previous study showing *AtACS6* gene expression was the highest at 15 minutes eATPγS treatment before decreasing after 30 minutes (Jeter *et al.*, 2004). Another study by Song *et al.* (2006) also observed high expression of *AtACS6* transcript in eATP-treated samples using Northern blot analysis. The *Atann1* mutant however failed to up-regulate *AtACS6* gene expression in either 10 minutes or 30 minutes of eATP treatment (Figure 3.28 D) indicating the requirement of AtANN1 in the *AtACS6* gene expression in eATP signalling. Luo *et al.* (2014) found that ABA activates phosphorylation of *ACS6* leading to increase production of ethylene that eventually leads to phenotypic changes such as root growth inhibition. Previously it was discovered that S-glutathionylation of AtANN1 occurs in the presence of ABA (Konopka-Postupolska *et al.*, 2009). ATP was also found to be released into the extracellular space under osmotic stress which can activate accumulation of ABA (Dark *et al.* 2011; Hartung, 1983). These might indicate the possible connection between AtANN1 and ethylene as different components of stress response in eATP signalling pathway.

3.4 Summary and future work

This study has identified the important role of AtANN1 in mediating the increase of $[Ca^{2+}]_{cyt}$ possibly as one of the calcium channels responding to both eATP and eADP signal at whole roots or root tips level. Since the knock-out mutant of *Atann1* does not completely abolish the $[Ca^{2+}]_{cyt}$ increase, there are other channels that work together with AtANN1. Complementation of the *Atann1* mutant managed to restore the full $[Ca^{2+}]_{cyt}$ response as in wild type especially at the 0.1 mM ATP concentration confirming the role of AtANN1. A higher number of samples is needed however to confirm this complementation at 1 mM eATP concentration.

We also discovered the potential disparate signalling pathway between eATP and eADP might be downstream of the $[Ca^{2+}]_{cyt}$ response as the comparison done between $[Ca^{2+}]_{cyt}$ response towards eATP and eADP at whole roots level exhibits similarity. Since the (apo)aequorin experiments here utilised whole organs, it would be interesting to carry out further investigation at the cellular level to fully understand the movement of Ca^{2+} in different tissues when challenged with eATP or eADP. Greater spatial resolution could be afforded by genetically encoded $[Ca^{2+}]_{cyt}$ reporters such as YC3.6 which could be targeted to

the plasma membrane (Krebs *et al.* 2012; Matthus *et al.*, 2019b) or GCaMP3 that could capture low intensity signals with a fluorescence microscope (Defalco *et al.*, 2017; Vincent *et al.*, 2017). Inhibitor tests carried out with calcium channel blockers indicate the possibility of the release of Ca^{2+} from the intracellular calcium stores. Recent years have seen the development of calcium reporters that could be targeted to organellar membrane or lumen such as the mitochondrial matrix (Loro *et al.*, 2012), the chloroplast to monitor stromal calcium status (Loro *et al.*, 2016), tonoplast and nucleoplasm (Krebs *et al.*, 2012) which might shed light on the possibility of calcium ion release from intracellular calcium stores.

AtANN1 is also confirmed to be in the same signalling pathway as the AtDORN1 receptor however whether AtANN1 is acting upstream or downstream of AtDORN1 in eATP signalling remains elusive. It would be useful to determine whether AtANN1 is a phosphorylation target of AtDORN1. This could be achieved by using KiC assay (Kinase client assay) which utilise a library of peptides that could be screened for potential of AtANN1 phosphorylation by AtDORN1 in the presence of ATP as previously shown with RBOHD in a study conducted by Chen *et al.*, (2017). Further comparison of ROS production in the *Atann1* loss-of-function mutant when challenged with eATP or eADP would be helpful to see if AtANN1 is upstream of the ROS production. Since AtDORN1 was found to be directly interacting with the AtRBOHD NADPH Oxidase enzyme (Chen *et al.*, 2017), this would help fit AtANN1 function in the AtDORN1 signalling pathway. In the preliminary test of measuring the intracellular ROS, we found that AtANN1 might be working downstream of the eATP-induced ROS release. This is however based on one biological replicate. More replicates need to be carried out with bigger sample size to confirm this. It would also be useful to determine whether eATP-induced extracellular ROS production is impaired in the *Atann1* mutant. Testing for extracellular superoxide anion (as the product of NADPH Oxidase activity) could be done with the XTT assay (Demidchik *et al.*, 2009). We also discovered addition of ATP in the growth assay resulted in primary root skewing is not regulated by AtANN1. It would be useful to extend this study by testing lower concentrations, in case AtANN1 was redundant at the high eATP concentration used here. At the gene expression level, AtANN1 is not involved in the eATP-induced up-regulation of *AtWRKY40* gene expression at the whole root level. However we identified AtANN1 as one of the components that regulates the increase of *AtACS6* gene expression in eATP signalling. As the eATP signal has been implicated in a myriad of biotic and abiotic stress responses,

this would help the future experimental direction to focus on the AtANN1-mediated eATP signalling pathway related to ethylene responses.

Chapter 4

AtANN2 and *AtANN4* in eATP and eADP Signalling

4.1 Introduction

Extracellular ATP (eATP) is a signal which acts as a stress signal in plants to impose its effects through the elevation of $[Ca^{2+}]_{cyt,}$ productions of reactive oxygen species (ROS) and nitric oxide (NO) which will eventually lead to changes at the transcriptional level of stress-related genes as a downstream response. In the previous chapter, we have shown the involvement of AtANN1 in this signalling pathway possibly as a calcium channel with the help of other unknown calcium channels. *A. thaliana* has 8 members of the annexin gene family. A study by Cantero *et al.*, (2006) found that the expression of the annexin gene family was highly regulated by stress stimuli. *A. thaliana* annexin 2 (AtANN2) and *A. thaliana* annexin 4 (AtANN4) are the most studied annexin members after AtANN1, although their main functions *in planta* are not yet fully understood.

A study on structural analysis and motifs showed highly conserved sequences between AtANN1 and AtANN2. Amino acid sequence alignment revealed that AtANN2 has 64% identity and 74% similarity to the AtANN1 amino acid sequence. AtANN4 on the other hand is quite different from both (Clark *et al.*, 2001). AtANN1 (as well as AtANN2) has the conserved type-II calcium binding sites in both the first and the fourth endonexin repeats

whereas AtANN4 lacks the calcium binding site in its fourth repeat (Clark *et al.*, 2001). Laohavisit *et al.* (2009) found both AtANN1 and AtANN2 maintained the conserved salt bridge motif as in animal annexin AnxA5 that was thought to form a calcium channel (Liemann *et al.*, 1996). Based on the alignment carried out in Figure 4.1, AtANN4 also conserved the salt bridge motif.

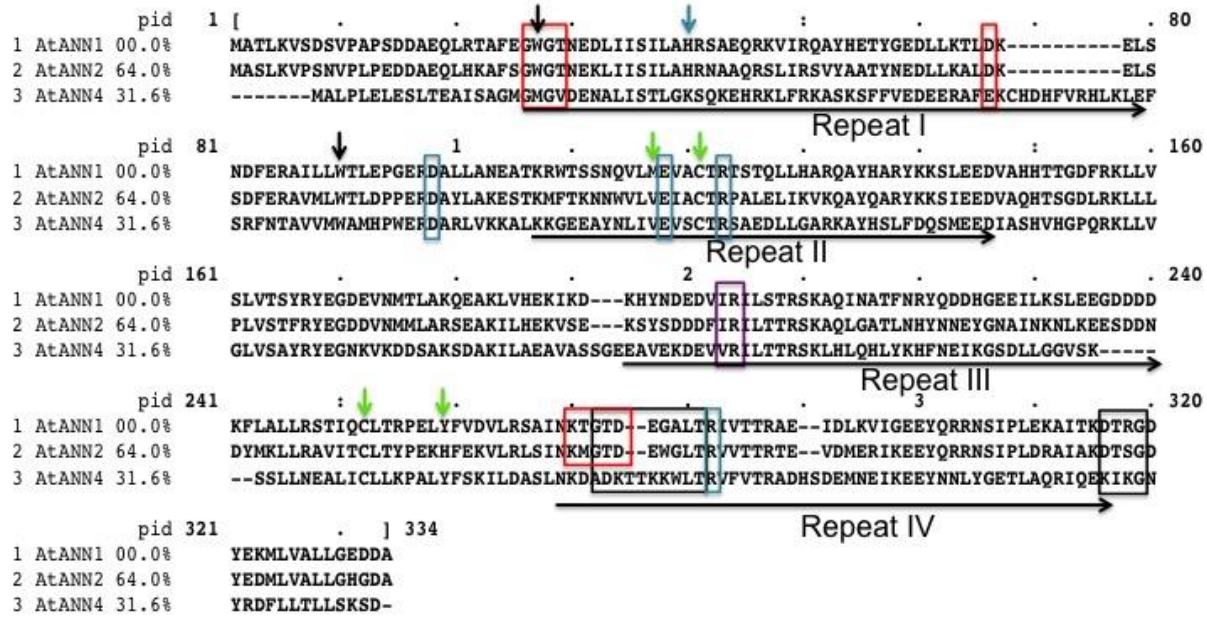

Figure 4.1: Amino acid alignment between AtANN1, AtANN2 and AtANN4. The sequence highlighted shows the protein motifs as follows: red box; Ca^{2+} binding motif GXGT--38 residues--D/E, black arrow; trytophan residue (phosphatidylserine) for membrane binding, blue arrow; His40 peroxidase residue, blue box; salt-bridges motif, green arrow; putative S3 cluster for redox activities, purple box; IRI actin binding motif and black box; putative GTP binding motif. The 'pid' column shows the percentage of identity between sequences. Alignment was done by using Clustal Omega (1.2.4).

Other than structural analysis, knowledge of the localisation of the AtANN2 protein would help discover its function. Clark *et al.* (2005a) implicated AtANN2 in regulation of growth and development in young seedlings as it was shown that the localisation of AtANN2 overlaps with secretory cells, similar to AtANN1. AtANN2 was also shows to be localised mostly in the epidermal surface of root apex, root cap, hypocotyl and cotyledon regions based on immunolocalisation. In contrast, AtANN1 was found to be strongly localised to root hair tips, epidermal cells of root apex, internal cells of elongation zone and growing sieve elements (Clark *et al.*, 2005a). Based on an RNA localisation study, AtANN2 was found heavily localised in roots and almost absent in flowers and leaves (Clark *et al.*, 2001). The

same study also found expression profile of *AtANN4* from RNA showed high expression at the root and flower but quite low expression in stem and leaves. Another study by Wang *et al.* (2018b) discovered *AtANN1* and *AtANN2* working together in post-phloem sugar transport in root tips. Huh *et al.* (2010) found both *AtANN1* and *AtANN4* are needed in mediating drought and salt stress response in *A. thaliana* seedlings. These studies showed the possibility of AtANN2 and AtANN4 working with AtANN1 in different tissues.

A study on transcription factor AtMYB30 found that it could bind to the promoter region of *AtANN1* and *AtANN4,* which caused down-regulation of expression of these genes (Liao *et al.*, 2017). Although no promoter study was carried out on *AtANN2*, the same study revealed that loss-of-function of AtMYB30 induced the expression of *AtANN2* that might hint at MYB30 negative regulation of *AtANN2*. It was proposed in the study that AtMYB30 transcription factor regulates the expression of *AtANN1*, *AtANN2* and *AtANN4* which leads to changes in $[Ca^{2+}]_{cyt}$ and eventually resistance or hypersensitive response towards heat and oxidative stress. It is known that eATP accumulates under stress conditions (Dark *et al.*, 2011) and induces the production of ROS (Demidchik *et al.*, 2009). ROS in turn regulate transcription factor AtMYB30 under light stress (Zandalinas *et al.*, 2019). Based on these studies, we speculated that eATP has the possibility to govern the activity of the MYB30 transcription factor and eventually the function of AtANN1, AtANN2 and AtANN4. Thus, we hypothesised AtANN2 and AtANN4 as the potential candidates for calcium channel activity that might work alongside AtANN1 in the eATP-signalling pathway.

In this chapter we tested the effect of *AtANN1*, *AtANN2* and *AtANN4* loss-of-function mutants on $[Ca^{2+}]_{cyt}$ elevation under the eATP signal as a test of the possibility of these annexins as calcium channels. Changes at the transcription level of eATP-induced genes in these mutants were also monitored to relate the $[Ca^{2+}]_{cyt}$ changes to the downstream responses. We discovered that AtANN2 and AtANN4 could work together with AtANN1 in mediating the eATP or eADP-induced $[Ca^{2+}]_{cyt}$ response with AtANN4 potentially as a negative regulator. There is the possibility of other unknown calcium channels involved and the possible calcium influx from the intracellular calcium store. Study at the gene expression level carried out in this chapter also highlighted the role of AtANN1, AtANN2 and AtANN4 in the regulation of the *AtACS6* gene under the influence of eATP, which is important in ethylene biosynthesis. This could tie AtANN1, AtANN2 and AtANN4 in mediating stress responses involving an eATP signal and the production of ethylene that leads to activation of ethylene signalling as a downstream responses.

4.2 Results

4.2.1 Homozygous mutant plant screening of *Atann2*

The *Atann2* T-DNA insertion mutant (SALK_054223) used in this chapter was propagated by Dr. Siân Richards (University of Cambridge) and was originally obtained from Dr Ohkmae K. Park before being transformed with the cytosolic (apo)aequorin reporter for calcium assay by Dr. Katie Wilkins (University of Cambridge). The T-DNA insert is located at nucleotide position 1605 (Lee *et al.,* 2004). Figure 4.1 shows the gel images of the Polymerase Chain Reaction (PCR) product for the screening of stable *Atann2* mutant (B) and Col-0 pair (A) containing the (apo)aequorin reporter. The genomic DNA extraction and PCR method used to genotype the seeds were as previously described in Chapter 2 (Chapter 2.4 and Chapter 2.5).

Four lanes (1, 3, 5, 7) in Figure 4.2(A) show the PCR product of Col-0 samples with *AtANN2* native gene primer pairs whereas the four lanes (2, 4, 6, 8) are Col-0 samples with *AtANN2-LB1.3* primer pairs. *AtANN2* native primers yielded a PCR product with the expected size of around 792 bp in lanes 1, 3, 5, and 7. Col-0 pair was confirmed as wild type as it did not contain a T-DNA insertion based on the absence of PCR product in lanes 2, 4, 6, and 8. Positive control showed the expected size of about 792bp from *AtANN2* native primer pairs and no expected bands were formed from the negative control (lanes 9, 11 and 10, 12 respectively).

Atann2 homozygous mutation is confirmed as lanes 1, 3, 5, and 7 containing *Atann2* samples with *AtANN2* native primers showed no band but lanes 2, 4, 6, and 8; which was assigned to *Atann2* samples with *AtANN2-LB1.3* primer pairs generated a PCR product with the size of around 854 bp (Figure 4.2 B). Col-0 samples as a positive control produced a PCR product of about 792 bp with *AtANN2* native primer pairs (lane 9) and no product of similar size with *AtANN2-LB1.3* primer pairs (lane 10). The sample in lane 9 (*AtANN2* native primer pairs) and lane 10 (*AtANN2-LB1.3* primer pairs) acted as positive controls with confirmed Col-0 samples (Figure 4. 2A, B). Lane 11 (*AtANN2* native primers) and lane 12 (*AtANN2-LB1.3* primer pairs) were assigned as negative controls containing sterilised distilled water as samples (Figure 4.2 A, B).

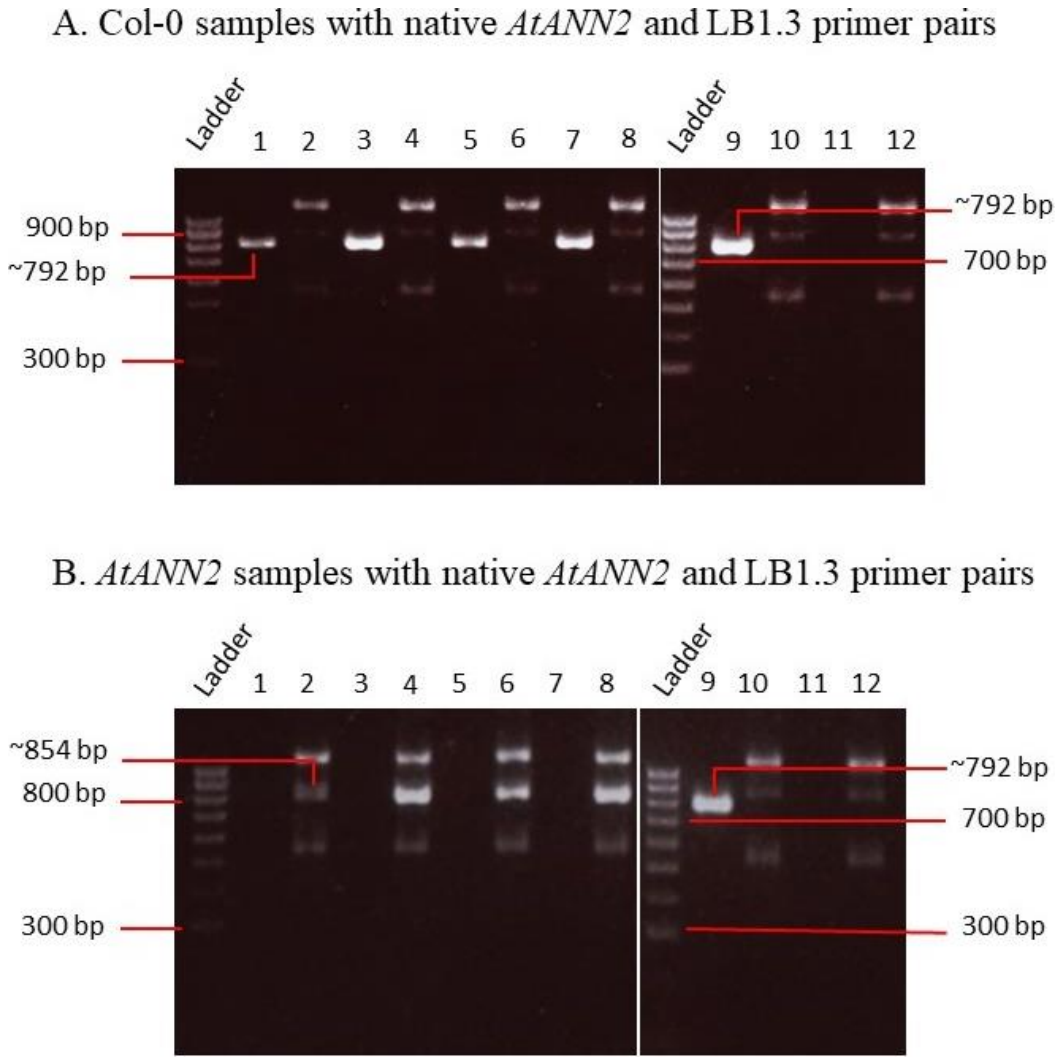

Figure 4.2: **Verification of Col-0 control and *Atann2* homozygous mutation.** Image (A) shows PCR product of Col-0 samples with *AtANN2* native primers (lane 1, 3, 5, 7) and *AtANN2*-T-DNA LB1.3 primer pairs (lane 2, 4, 6, 8). Col-0 samples (lane 9, *AtANN2* native primers; lane 10, *AtANN2*-TDNA LB1.3 primers) and sterilised water samples (lane 11, *AtANN2* native primers; lane 12, *AtANN2*-TDNA LB1.3 primers) acted as controls for the PCR reaction. DNA size marker used for each gel electrophoresis run was the 100 bp hyperladder (Bioline).

4.2.2 *Atann2* is required in mediating eATP and eADP signalling at whole seedling and whole root level

The previous chapter discovered the possibility of other calcium channels operating with AtANN1 in mediating the $[Ca^{2+}]_{cyt}$ increase in response to extracellular nucleotide treatment. As the annexin protein with the least divergence in terms of amino acid sequence and structure to AtANN1 (Clark *et al.*, 2001), AtANN2 (Annexin 2) was thought to be a suitable candidate to be tested for its ability to mediate Ca^{2+} influx under a nucleotide signal in this study.

To assess the possibility of AtANN2's operation in $[Ca^{2+}]_{cyt}$ elevation, the *Atann2* T-DNA insertion mutant expressing cytosolic (apo)aequorin was tested with nucleotide treatment at whole seedling level and whole root level. Seven-day-old whole seedlings of Col-0 and *Atann2* (both carrying (apo)aequorin reporter under the 35S CAMV promoter) were incubated with coelanterazine before being subjected to $[Ca^{2+}]_{cyt}$ measurement assay as explained in Chapter 2.6. Each measurement was recorded for 200 seconds. Control treatment (2 mM MES/Tris-HCl; 10 mM $CaCl_2$; 0.1 mM KCl) applied to Col-0 and *Atann2* at the 35th second produced a single peak that lasted about 15 seconds before going back to the basal level (Figure 4.3A). The single peak that is known as the touch response did not differ significantly between Col-0 (0.15±0.02 μM) and *Atann2* (0.13±0.02 μM) (Figure 4.3 B). Overall area under the calcium traces revealed that the control solution did not have any differential effect between genotypes as there was no significant difference between the total $[Ca^{2+}]_{cyt}$ accumulated by Col-0 (1.77±0.67 μM) and *Atann2* (1.21±0.31 μM) (Figure 4.3 C).

Replacing the control treatment with 1 mM eATP treatment at the 35th second produced a calcium biphasic response after the touch response (Figure 4.3 D). The touch peak produced by 1 mM eATP treatment did not differ significantly between Col-0 (0.1±0.01 μM) and *Atann2* (0.07±0.01 μM) confirming that the absence of AtANN2 did not affect the touch response (Figure 4.3E). *Atann2* whole seedlings however exhibited a significantly lower first peak (Col-0 0.13±0.01 μM; *Atann2* 0.08 ±0.09 μM) and second peak (Col-0 0.18±0.07 μM; *Atann2* 0.15±0.01 μM) in response to eATP compared to the Col-0 (Figure 4.3 F, G). AtANN2 is required to produce a normal eATP-induced $[Ca^{2+}]_{cyt}$ accumulation as the *Atann2* mutant (7.97±0.24 μM) induced lower overall $[Ca^{2+}]_{cyt}$ increase compared to Col-0 (10.66±0.36 μM) (Figure 4.3H).

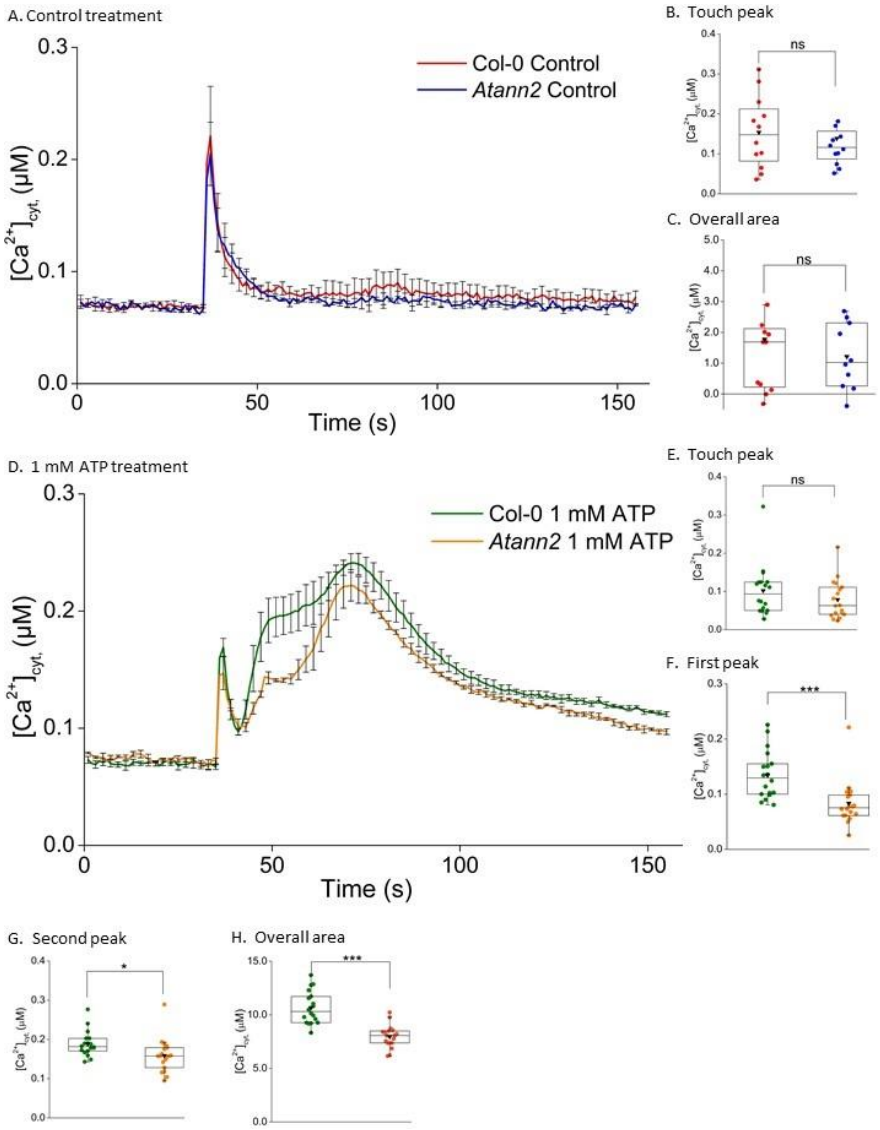

Figure 4.3: **AtANN2 is involved in eATP-induced $[Ca^{2+}]_{cyt}$ elevation at whole seedling level.** Both Col-0 and *Atann2* 7-day-old seedlings contained cytosolic apo-aequorin. The $[Ca^{2+}]_{cyt}$ response for the control treatment (A) and 1 mM eATP (D) were recorded for 155 seconds where each treatment was added at the 35th second. These time course data are from the means ± SEM of 3 independent trials, with n = 12 - 18 roots per genotype and treatment. Touch peak (B) represents the highest value of the touch response (35 - 50 s) whereas the overall area (C) is the total area under the curve extracted from the time course data of the control treatment (35 - 155 s). Time course analysis of the 1 mM eATP treatment is split up into the first peak (F) (41 - 55 s) and the second peak (G) (55 - 155 s) responses, which is the highest value of the peaks that emerged after the touch response (E) (35 - 41 s). The total accumulation of $[Ca^{2+}]_{cyt}$ was determined through the overall area under the curve (H) (35 - 155 s). All calculations carried out were with the baseline (the first 35 seconds of measurement) subtracted. Middle line of the boxplot represents the median whereas the inverted triangle represents the mean. *p*-values: ns (p>0.05), * (p<0.05), ** (p<0.01), *** (p< 0.001), Welch's *t*-test for parametric test and Wilcoxon rank-sum test for non-parametric test.

As the absence of AtANN1 failed to completely abolish the calcium response towards eADP, the possible role of AtANN2 as the other calcium channel under the eADP signal was also tested. As previously shown, the control solution did not influence the calcium response as the time course for control solution showed only a single touch peak produced by both Col-0 and *Atann2* (Figure 4.4 A). Other than that, the control treatment confirmed that the calcium responses were not affected by the different genotypes tested as both Col-0 and *Atann2* mutant had a similar touch response (Col-0 0.05±0.02 μM; *Atann2* 0.13±0.02 μM) and total $[Ca^{2+}]_{cyt}$ increase by control solution (Col-0 1.77±0.67 μM; *Atann2* 1.21±0.31 μM) (Figure 4.4B, C).

Similar to eATP treatment, 1 mM eADP also generated a biphasic calcium response where *Atann2* had lower increases than Col-0 whole seedlings (Figure 4.4D). Consistent with the previous eATP test, there was no significant difference in the touch peak between Col-0 (0.12±0.02 μM) and *Atann2* (0.09±0.02 μM) but *Atann2* (0.08±0.01 μM) sustained a significantly lower first peak compared to the Col-0 (0.14±0.01 μM) due to 1 mM eADP treatment (Figure 4.4 E, F). *Atann2* also produced a lower second peak than the Col-0 but this was not statistically significant (Col-0 0.20±0.01 μM; *Atann2* 0.19±0.01 μM) (Figure 4.4 G). Mutation of *AtANN2* caused the total $[Ca^{2+}]_{cyt}$ accumulation of *Atann2* (9.76±0.52 μM) to be impaired compared to the Col-0 (11.75±0.63 μM) proving the role of AtANN2 in mediating the calcium movement under the eADP signal at whole seedling level.

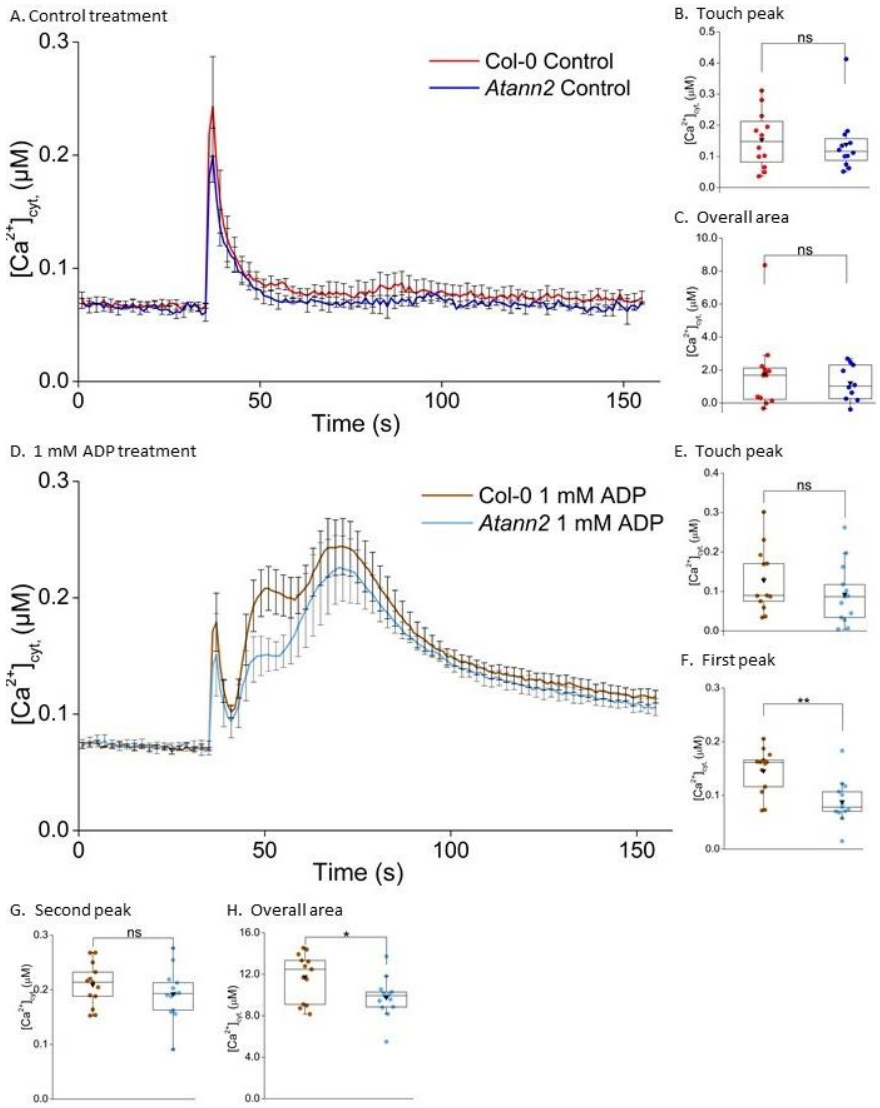

Figure 4.4: **eADP causes $[Ca^{2+}]_{cyt}$ elevation at whole seedling level as a downstream response through AtANN2.** Both Col-0 and *Atann2* 7-day-old seedlings expressed cytosolic apo-aequorin. The $[Ca^{2+}]_{cyt}$ response for the control treatment (A) and 1 mM eADP (D) were recorded for 155 seconds where each treatment was added at the 35th second. These time course data are from the means ± SEM of 3 independent trials, with n = 12 - 13 seedlings per genotype and treatment. Touch peak (B) represents the highest value of the touch response (35 - 50 seconds) whereas the overall area (C) is the total area under the curve extracted from the time course data of the control treatment (35 - 155 s). Time course analysis of the 1 mM eADP treatment is split up into the first peak (F) (41 - 53 s) and the second peak (G) (53 - 155 s) responses, which is the highest value of the peaks that emerged after the touch response (E) (35 - 41 s). The total accumulation of $[Ca^{2+}]_{cyt}$ of Col-0 and *Atann2* were determined through the overall area under the curve (H) (35 - 155 s). All calculations carried out were with the baseline (the first 35 s of measurement) subtracted. Middle line of the boxplot represents the median whereas the inverted triangle represents the mean. p-values: ns (p>0.05), * (p<0.05), **

(p<0.01),*** (p< 0.001), Welch's *t*-test for parametric test and Wilcoxon rank-sum test for non-parametric test.

Since AtANN2 is highly expressed in roots (especially at the 7-day-old stage), a similar test was done at whole root level in order to examine for a more tissue-specific response. Seven-day-old whole roots of both Col-0 and *Atann2* were carefully excised from the whole seedlings before cytosolic calcium measurement was carried out. Control treatment (2 mM MES/Tris-HCl; 10 mM $CaCl_2$; 0.1 mM KCl) used as background solution did not influence the calcium response as the addition of control treatment shown in Figure 4.5 A only produced a single touch response with Col-0 and *Atann2* whole roots having a similar touch peak (Col-0 0.27±0.04 μM; *Atann2* 0.23±0.04 μM) and overall $[Ca^{2+}]_{cyt}$ increase (Col-0 2.78±0.47 μM; *Atann2* 2.27±0.43 μM) (Figure 4.5 B, C). Application of 1 mM eATP treatment triggered higher Col-0 $[Ca^{2+}]_{cyt}$ biphasic response after the touch response compared to *Atann2* whole roots (Figure 4.5 D). This is confirmed by the statistical analysis as it shows that no significant difference was found between Col-0 (0.12±0.01 μM) and *Atann2* (0.12±0.01 μM) at the touch peak but *Atann2* whole roots evoked significantly lower first peak (Col-0 0.25±0.01 μM; *Atann2* 0.19±0.009 μM) and second peak (Col-0 0.25±0.009 μM; *Atann2* 0.22±0.007 μM) compared to the Col-0 (Figure 4.5 E, F, G). As a result, the total accumulation of $[Ca^{2+}]_{cyt}$ due to 1 mM eATP was significantly impaired in the *Atann2* mutant (16.11±0.56 μM) in comparison to the Col-0 (18.82±0.77 μM) (Figure 4.5H).

In order to complete the test, 1 mM eADP as a different nucleotide agonist was tested. Unlike the outcome of control treatment in previous tests, control solution (2 mM MES/Tris-HCl; 10 mM $CaCl_2$; 0.1 mM KCl) applied to the samples in this test showed lower *Atann2* calcium response traces compared to the Col-0 (Figure 4.6 A). Detailed statistical analysis showed that the *Atann2* whole roots samples were producing lower touch peak (Col-0 0.38±0.05 μM; *Atann2* 0.25±0.05 μM) and accumulated lower overall $[Ca^{2+}]_{cyt}$ than the Col-0 pair (Col-0 4.99±0.61 μM; *Atann2* 2.73±0.49 μM) (Figure 4.6 B, C). There was however no significant difference between the Col-0 (0.22±0.05 μM) and *Atann2* (0.15±0.03 μM) touch peak by 1 mM eADP treatment (Figure 4.6E). Figure 4.6 D also shows lower *Atann2* $[Ca^{2+}]_{cyt}$ response with statistically lower first peak (Col-0 0.29±0.02 μM; *Atann2* 0.21±0.01 μM) and second peak (Col-0 0.31±0.008 μM; *Atann2* 0.25±0.009 μM) compared to the Col-0 $[Ca^{2+}]_{cyt}$ response (Figure 4.6 F, G). AtANN2 could play an important role in eADP signalling at whole roots level as it is needed for the normal $[Ca^{2+}]_{cyt}$ response to occur based on the reduced *Atann2* (17.87±0.97 μM) total $[Ca^{2+}]_{cyt}$ accumulation compared to the Col-0

(22.03±1.06 μM) (Figure 4.6 H). However the genotype differences found in the control treatment has made the comparison between Col-0 and *Atann2* in 1 mM eADP treatment to be less accurate as any differences between Col-0 and *Atann2* could be influenced by the initial difference caused by the background control solution.

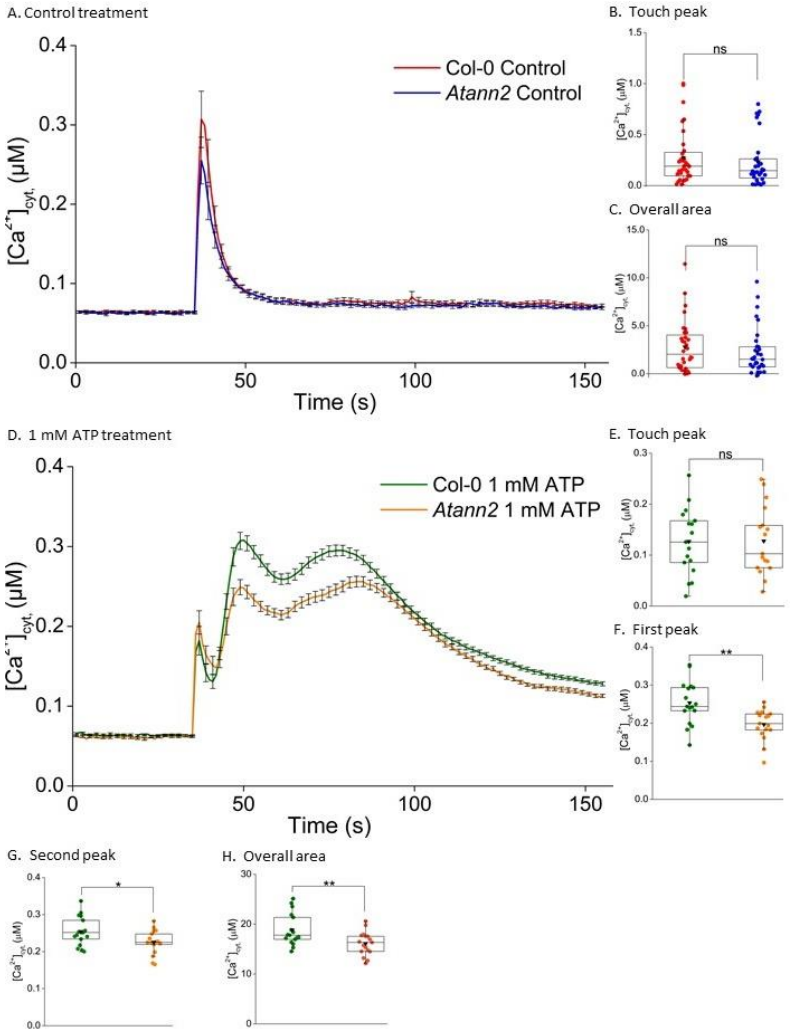

Figure 4.5: **eATP causes $[Ca^{2+}]_{cyt}$ elevation at whole root level as a downstream response through AtANN2**. Both Col-0 and *Atann2* 7-days-old whole roots contained cytosolic apo-aequorin. The $[Ca^{2+}]_{cyt}$ response for the control treatment (A) and 1 mM eATP (D) were recorded for 155 seconds where each treatment was added at the 35th second. These time course data are from the means ± SEM of 3 independent trials, with n = 17 - 32 roots per genotype and treatment. Touch peak (B) represents the highest value of the touch response (35 - 50 s) whereas the overall area (C) is the total area under the curve extracted from the time course data of the control treatment (35 - 155 s). Time course analysis of the 1 mM eATP treatment is split up into the first peak (F) (41 - 63 s) and the second peak (G) (63 - 155 s) responses, which is the highest value of the peaks that emerged after the touch response (E) (35 - 41 s). The total accumulation of $[Ca^{2+}]_{cyt}$ of Col-0 and *Atann2* were determined through the overall area under the curve (H) (35 - 155 s). All calculations carried out were with the baseline (the first 35 s of measurement) subtracted. Middle line of the boxplot represents the

median whereas the inverted triangle represents the mean. *p*-values: ns ($p>0.05$), * ($p<0.05$), ** ($p<0.01$),*** ($p< 0.001$), Welch's *t*-test for parametric test and Wilcoxon rank-sum test for non-parametric test.

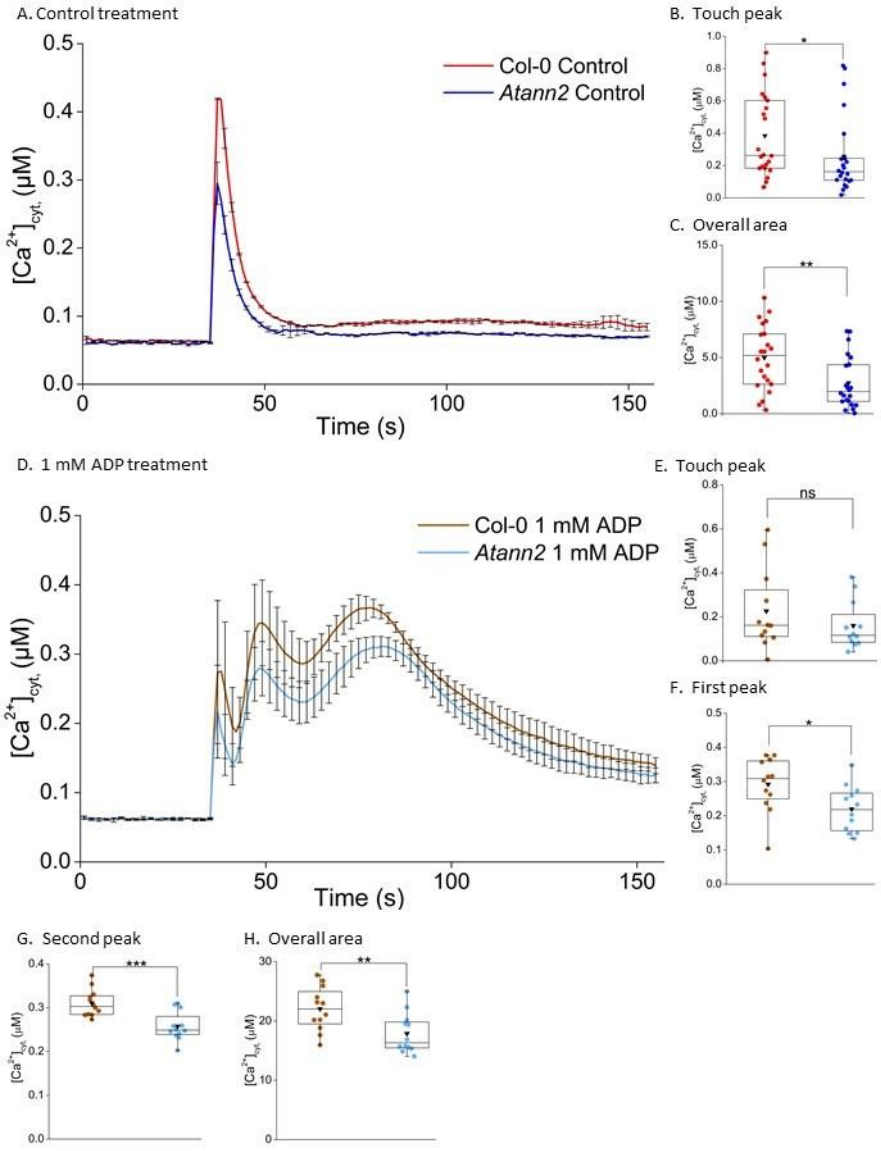

Figure 4.6: **eADP causes $[Ca^{2+}]_{cyt}$ elevation at whole root level that might depend on AtANN2.** Both Col-0 and *Atann2* 7-days-old whole roots contained cytosolic apo-aequorin. The $[Ca^{2+}]_{cyt}$ response for the control treatment (A) and 1 mM eADP (D) were recorded for 155 seconds where each treatment was added at the 35th second. These time course data are from the means ± SEM of 3 independent trials, with n = 12 - 22 roots per genotype and treatment. Touch peak (B) represents the highest value of the touch response (35 - 50 s) whereas the overall area (C) is the total area under the curve extracted from the time course data of the control treatment (35 - 155 s). Time course analysis of the 1 mM eADP treatment is split up into the first peak (F) (41 - 59 seconds) and the second peak (G) (59 - 155 seconds) responses, which is the highest value of the peaks that emerged after the touch response (E) (35 - 41 s). The total accumulation of $[Ca^{2+}]_{cyt}$ of Col-0 and *Atann2* were determined

through the overall area under the curve (H) (35 - 155 s). All calculations carried out were with the baseline (the first 35 s of measurement) subtracted. Middle line of the boxplot represents the median whereas the inverted triangle represents the mean. *p*-values: ns ($p>0.05$), * ($p<0.05$), ** ($p<0.01$), *** ($p< 0.001$), Welch's *t*-test for parametric test and Wilcoxon rank-sum test for non-parametric test.

As ATP has a variety of roles in biological processes, another test using non-hydrolysable eATP or eADP was carried out to confirm that the whole ATP or ADP molecule acts as a signalling molecule that drives the calcium movement at whole root level rather than merely an energy source. Both Col-0 and *Atann2* treated with control solution (2 mM MES/Tris-HCl; 10 mM $CaCl_2$; 0.1 mM KCl) produced the consistent touch peak before going back to basal level, confirming that the background control solution had no effect on the experiment (Figure 4.7 A, B). Col-0 and *Atann2* evoked biphasic calcium signatures upon application of 1 mM eATP or 1 mM eATPγS (non-hydrolysable ATP analogue) after the touch peak (Figure 4.7 A, C). Based on the overall $[Ca^{2+}]_{cyt}$ accumulation, there were no significant differences between 1 mM eATP treatment and the non-hydrolysable ATP analogue in both Col-0 (ATP 18.82±0.77 μM; ATPγS 20.18±0.51 μM) and *Atann2* (ATP 16.11±0.56 μM; ATPγS 16.41±0.53 μM) whole roots which proved that the whole ATP molecule is important in inducing the calcium response (Figure 4.7 B, D). eATP (1 mM) together with 4 mM LiCl solution treatment acted as a control as the non-hydrolysable ATP was added as its Li salt. The overall $[Ca^{2+}]_{cyt}$ accumulated in the 1 mM eATP treatment and the 1 mM eATP treatment with 4 mM LiCl were similar for both Col-0 (ATP 18.82±0.77 μM; ATP+ LiCl 20.03±0.87 μM) and *Atann2* (ATP 16.11±0.56 μM; ATP+ LiCl 16.99±0.75 μM), confirming that the LiCl had no influence in the outcome of the assay (Figure 4.7 B, D).

The experiment was repeated with 1 mM eADP, 1 mM eADPβS (non-hydrolysable ADP analogue) and 1 mM eADP with 3 mM LiCl treatment. Similar to the previous test, the control solution produced a single touch response whereas eADP, eADPβS and eADP with LiCl treatments invoked a biphasic pattern of $[Ca^{2+}]_{cyt}$ increase in both Col-0 and *Atann2* (Figure 4.8 A, C). Analysis of the total $[Ca^{2+}]_{cyt}$ accumulation showed that there were no significant differences between 1 mM eADP and the non-hydrolysable analogue for both Col-0 (ADP 22.03±1.06 μM; ADPβS 18.05±1.41 μM) and *Atann2* (ADP 17.87±0.97 μM; ADPβS 16.30±1.37 μM) indicating that the eADP molecule does not need to be hydrolysed in producing the $[Ca^{2+}]_{cyt}$ response (Figure 4.8 B, D). The 1 mM eADP with 3 mM LiCl treatment applied to both Col-0 (ADP 22.03±1.06 μM; ADP+ LiCl 20.75±0.93 μM) and *Atann2* (ADP 17.87±0.97 μM; ADP+ LiCl 18.48±0.71 μM) also showed no significant

difference with eADP treatment alone. This result again confirmed that the Li contained in the 1 mM eADPβS did not interfere with the $[Ca^{2+}]_{cyt}$ response (Figure 4.8 B, D).

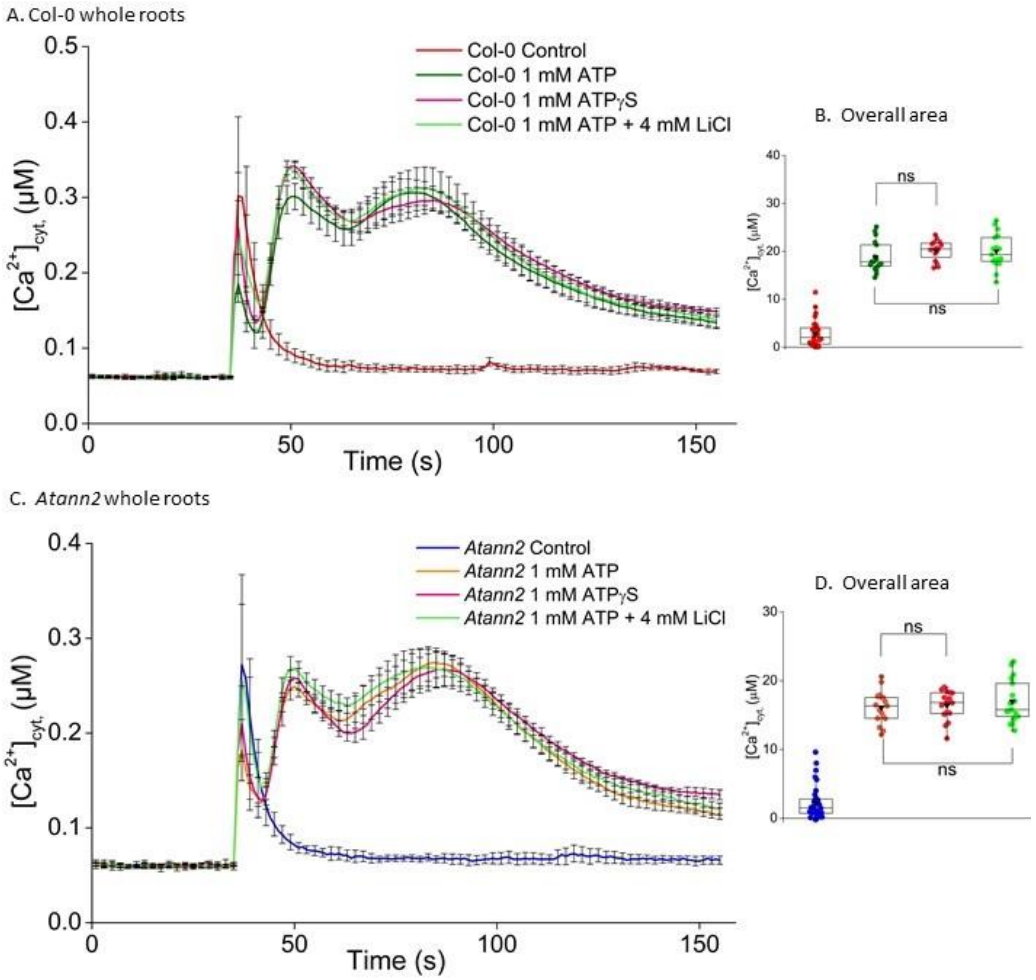

Figure 4.7: **eATP acts as a signalling molecule rather than as an energy source**. Seven-day-old whole roots of Col-0 (A) and *Atann2* (C) were treated with 1 mM eATP or the non-hydrolysable ATP analogue (ATPyS). eATP treatment (1 mM) with 4 mM $LiCl_2$ acted as a control for the tetralithium contained in the ATPyS. The $[Ca^{2+}]_{cyt}$ responses were recorded for 155 s and each treatment was added at the 35th second. These time course data were from the means ± SEM of 3 independent trials, with n = 16 - 17 roots per genotype and treatment. Overall area which indicates the total accumulation of $[Ca^{2+}]_{cyt}$ in (B) and (D) was the total area under the curve extracted from the time course data of Col-0 and *Atann2* respectively (35 - 155 s). All calculations carried out were with the baseline (the first 35 s of measurement) subtracted. Middle line of the boxplot represents the median whereas the inverted triangle represents the mean *p*-values: ns (not significant $p > 0.05$), Welch's *t*-test.

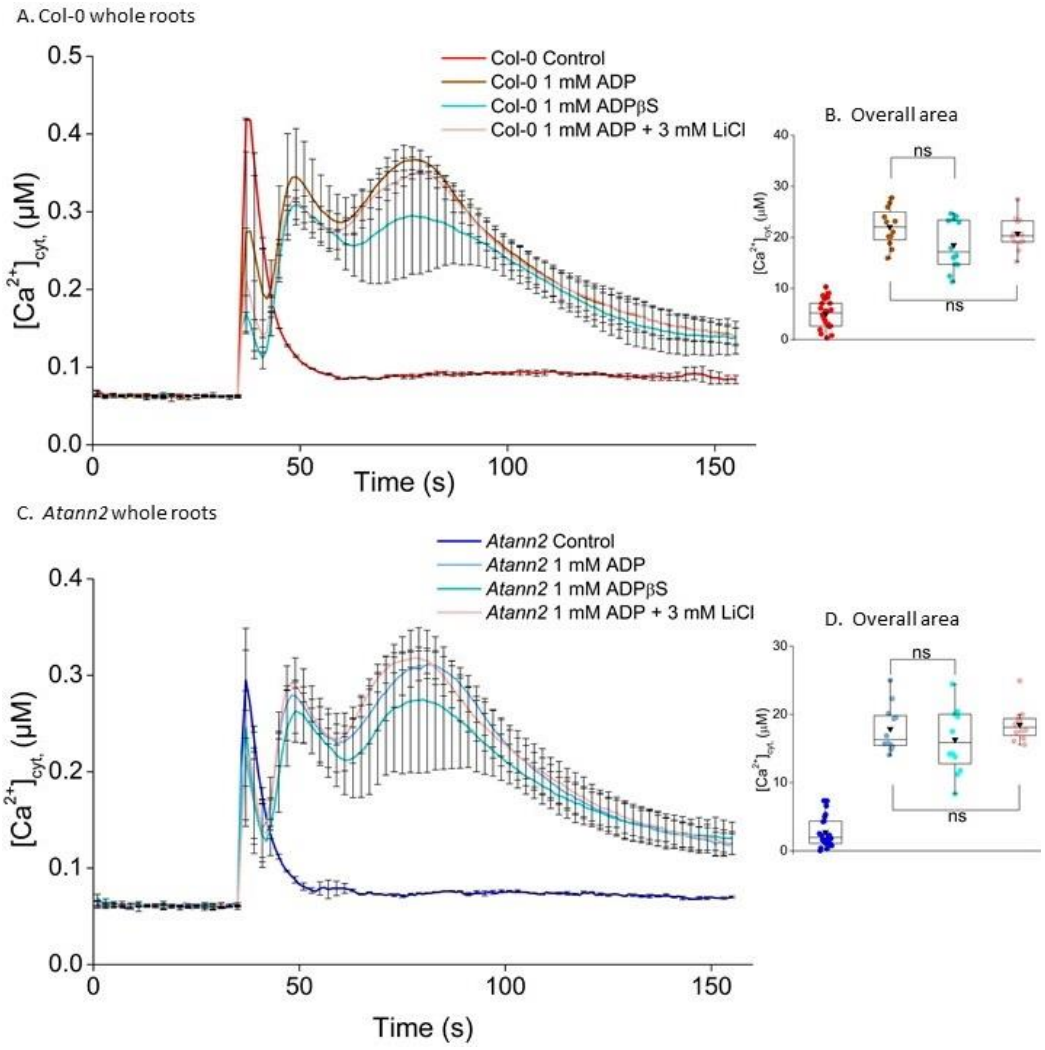

Figure 4.8: **Non-hydrolysable eADP analogue causes similar $[Ca^{2+}]_{cyt}$ accumulation to that with hydrolysable eADP treatment.** Seven-day-old whole roots of Col-0 (A) and *Atann2* (C) were treated with 1 mM eADP or the non-hydrolysable eADP analogue (ADPβS). ADP treatment (1 mM) with 3 mM $LiCl_2$ acted as a control for the trilithium contained in the ADPβS. The $[Ca^{2+}]_{cyt}$ responses were recorded for 155 s and each treatment was added at the 35th second. These time course data were from the means ± SEM of 3 independent trials, with n = 12 roots per genotype and treatment. Overall area which indicates the total accumulation of $[Ca^{2+}]_{cyt}$ in (B) and (D) was the total area under the curve extracted from the time course data of Col-0 and *Atann2* respectively (35 - 155 s). All calculations carried out were with the baseline (the first 35 s of measurement) subtracted. Middle line of the boxplot represents the median whereas the inverted triangle represents the mean. p-values: ns (not significant $p > 0.05$), Welch's t-test.

Previously (Chapter 3.2.6), we have shown that the calcium accumulating in the cytosol might be originating from the apoplast or the intracellular calcium store. Here, we tested both Col-0 and *Atann2* with the calcium channel blocker $GdCl_3$ to monitor any

differences caused by the absence of AtANN2 which might indicate its possible localisation to the plasma membrane under eATP or eADP signal. The test with $GdCl_3$ was carried out on 7-day-old 1 cm root tips where the excised root tips were incubated for 30 minutes with either 1.5 mM $GdCl_3$ or control solution prior to $[Ca^{2+}]_{cyt}$ measurement (refer to Chapter 2.6.4 for method). Control solution (2 mM MES/Tris-HCl; 10 mM $CaCl_2$; 0.1 mM KCl) with or without $GdCl_3$ pre-treatment produced a single touch response consistently in both Col-0 and *Atann2* (Figure 4.9 A). The overall area under the curve verified that the $GdCl_3$ pre-treatment alone had no effect on the outcome of the experiment as there were no significant differences in the overall $[Ca^{2+}]_{cyt}$ increase between the two treatments in both Col-0 (Control 0.8±0.24 μM; $GdCl_3$ 2.31±0.72 μM) and *Atann2* (Control 1.96±0.43 μM; $GdCl_3$ 2.82±0.75 μM) (Figure 4.9 B).

In 0.5 mM eATP treatment, both Col-0 and *Atann2* root tips produced a $[Ca^{2+}]_{cyt}$ biphasic pattern regardless of control or $GdCl_3$ pre-treatment (Figure 4.9 C). At the first peak after the touch response, control pre-treated *Atann2* (0.23±0.008 μM) showed significantly lower $[Ca^{2+}]_{cyt}$ increase than the Col-0 (0.27±0.01 μM). In contrast, $GdCl_3$ pre-treated *Atann2* (0.15±0.009 μM) root tips were not significantly different from the $GdCl_3$ pre-treated Col-0 (0.16±0.01 μM) (Figure 4.9 D). The second peak of the 0.5 mM eATP treatment however showed no significant differences between Col-0 and *Atann2* in both control (Col-0 0.22±0.007 μM; *Atann2* 0.20±0.01 μM) and $GdCl_3$ (Col-0 0.01±0.003 μM; *Atann2* 0.10±0.007 μM) pre-treated whole roots (Figure 4.9 E). Based on the area under the curve, *Atann2* (14.64±0.57 μM) accumulated significantly lower overall $[Ca^{2+}]_{cyt}$ than Col-0 (16.61±0.55 μM) in the non $GdCl_3$ pre-treated root tips. Col-0 (11.18±0.65 μM) was not significantly different compared to *Atann2* (10.56±0.66 μM) in accumulating total $[Ca^{2+}]_{cyt}$ caused by 0.5 mM eATP in $GdCl_3$ pre-treated root tips (Figure 4.9 F). Overall, both Col-0 and *Atann2* treated with $GdCl_3$ induced lower $[Ca^{2+}]_{cyt}$ accumulation compared to the non-$GdCl_3$ pre-treated root tips in the first peak, second peak and overall $[Ca^{2+}]_{cyt.}$

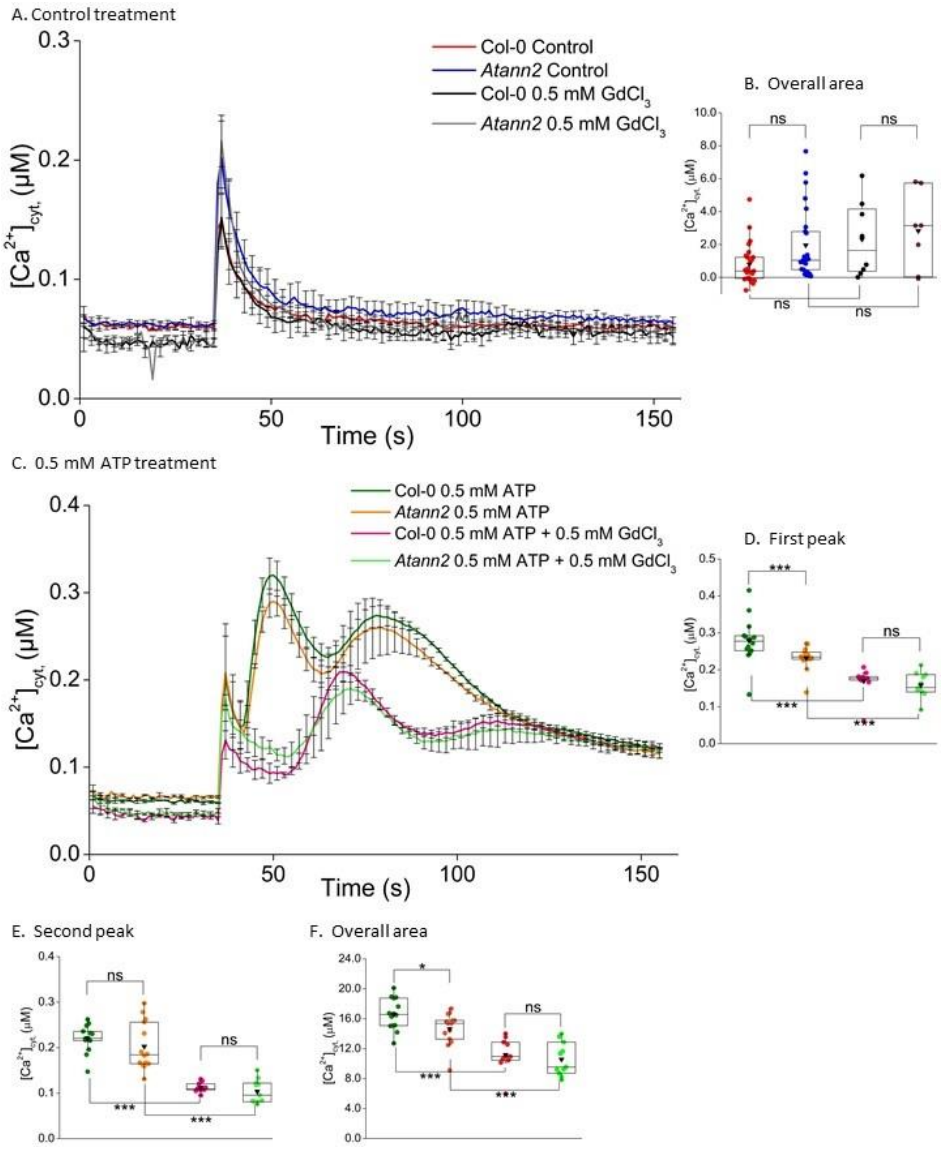

Figure 4.9: **$GdCl_3$ partially blocked eATP induced $[Ca^{2+}]_{cyt}$ accumulation.** The $[Ca^{2+}]_{cyt}$ responses were recorded for 155 s for both the control treatment (A) and the 0.5 mM eATP treatment (C) and each treatment was added at the 35th second. Seven-day-old Col-0 and *Atann2* 1 cm root tips were incubated with either control or 0.5 mM $GdCl_3$ for 30 minutes prior to the treatment. These time course data were from the means ± SEM of 3 independent trials, with a total of 11 – 25 root tips per genotype and treatment. The overall area (B) (35 - 155 s) was the total area under the curve for the control treatment. Time course analysis of the 0.5 mM eATP treatment (C) is split up into the first peak (D) (without $GdCl_3$ 41 - 63 s; with $GdCl_3$ 53 - 90 s) and the second peak (E) (without $GdCl_3$ 63 - 155 s; with $GdCl_3$ 90 - 155 s) response, which is the highest value of the peaks that emerge after the touch response. The total accumulation of $[Ca^{2+}]_{cyt}$ by both genotypes was determined through the overall area under the curve (F) (35 - 155 s). All of the calculations carried out were with the baseline (the first 35 s of measurement) subtracted. Middle line of the boxplot represents the median whereas the inverted triangle represents the mean. *p*-values: ns (p>0.05), * (p<0.05), ** (p<0.01), *** (p< 0.001), Welch's *t*-test for parametric test and Wilcoxon rank-sum test for non-parametric test.

The test was replicated by replacing 0.5 mM eATP with 0.5 mM eADP in order to see any possible difference as eADP is implicated as a different signalling molecule to eATP. Control solution applied to Col-0 and *Atann2* either with or without $GdCl_3$ pre-treatment produced a single touch response before going back to the basal level (Figure 4.10 A). Statistical analysis confirmed that the $GdCl_3$ alone did not interfere with the $[Ca^{2+}]_{cyt}$ accumulation as the overall $[Ca^{2+}]_{cyt}$ accumulated by $GdCl_3$ pre-treated root tips were not significantly different from the control pre-treated root tips for both Col-0 (control 1.93±0.33 μM; $GdCl_3$ 1.62±0.33 μM) and *Atann2* (control 1.94±0.44 μM; $GdCl_3$ 1.28±0.38 μM) (Figure 4.10 B).

eADP treatment (0.5 mM) showed a biphasic pattern in both control and $GdCl_3$ pre-treated Col-0 and *Atann2* root tips (Figure 4.10 C). The first $[Ca^{2+}]_{cyt}$ peak produced by Col-0 (control 0.26±0.007 μM; $GdCl_3$ 0.14±0.01 μM) was not significantly different from *Atann2* (control 0.22±0.009 μM; $GdCl_3$ 0.11±0.008 μM) regardless of $GdCl_3$ incubation (Figure 4.10 D). A similar observation was made for the second peak where both Col-0 (control 0.24±0.01 μM; $GdCl_3$ 0.08±0.006 μM) and *Atann2* (control 0.22±0.01 μM; $GdCl_3$ 0.08±0.007 μM) sustained similar $[Ca^{2+}]_{cyt}$ elevation with or without $GdCl_3$ pre-treatment (Figure 4.10 E). These lead to similar values between Col-0 (control 16.89±0.49 μM; $GdCl_3$ 8.43±0.88 μM) and *Atann2* (control 15.88±0.50 μM; $GdCl_3$ 7.51±0.77 μM) in the total $[Ca^{2+}]_{cyt}$ accumulated for control or $GdCl_3$ pre-treated root tips (Figure 4.10 F). Both Col-0 and *Atann2* incubated with $GdCl_3$ showed consistent lower $[Ca^{2+}]_{cyt}$ increase in the first peak, second peak and total $[Ca^{2+}]_{cyt}$ compared to the control pre-treatment.

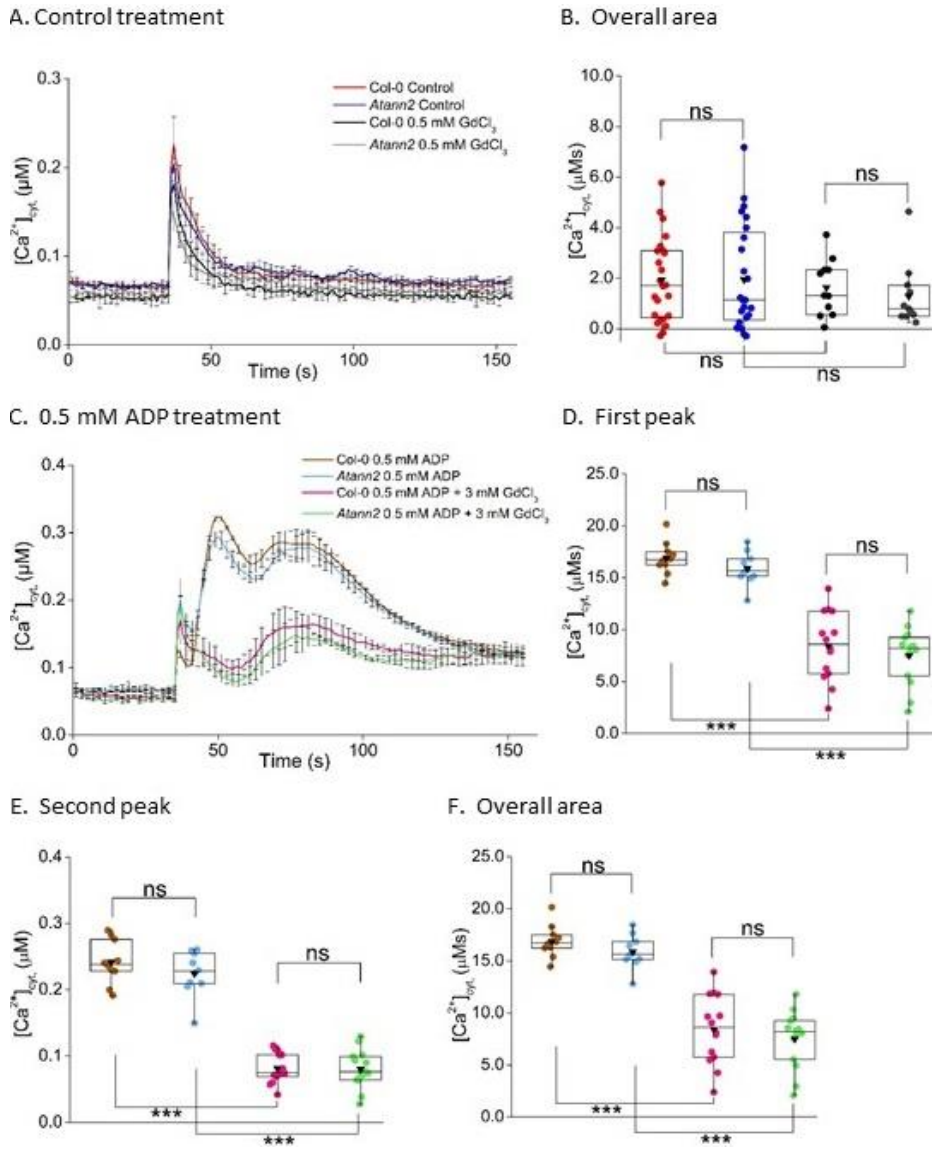

Figure 4.10: **$GdCl_3$ partially inhibits eADP induced $[Ca^{2+}]_{cyt}$ accumulation.** The $[Ca^{2+}]_{cyt}$ responses were recorded for 155 s for both the control treatment (A) and the 0.5 mM ADP treatment (C) and each treatment was added at the 35th second. Seven-day-old Col-0 and *Atann2* 1 cm root tips were incubated with 0.5 mM $GdCl_3$ for 30 minutes prior to the treatment. These time course data were from the means ± SEM of 3 independent trials, with a total of 11 – 24 root tips per genotype and treatment. The overall area (B) (35 - 155 s) was the total area under the curve for the control treatment. Time course analysis of the 0.5 mM eADP treatment (C) is split up into the first peak (D) (without $GdCl_3$ 41 - 63 s; with $GdCl_3$ 53 - 110 s) and the second peak (E) (without $GdCl_3$ 63 - 155 s; with $GdCl_3$ 110 - 155 s) response, which is the highest value of the peaks that emerge after the touch response. The total accumulation of $[Ca^{2+}]_{cyt}$ by both genotypes was determined through the overall area under the curve (F) (35 - 155 s). All of the calculations carried out were with the baseline (the first 35 s of measurement) subtracted. Middle line of the boxplot represents the median whereas the inverted triangle represents the mean. *p*-values: ns (p>0.05), * (p<0.05), ** (p<0.01), *** (p< 0.001), Welch's *t*-test for parametric test and Wilcoxon rank-sum test for non-parametric test.

The purinoreceptor blocker suramin was used in this study to test whether mutation of *AtANN2* would have any effect on the role of eATP and eADP in driving the calcium response through a receptor. Seven-day-old 1 cm root tips of both Col-0 and *Atann2* that were incubated in 1.5 mM suramin for 30 minutes were subjected to $[Ca^{2+}]_{cyt}$ measurement upon treatment with 0.5 mM eATP or 0.5 mM eADP. Control solution (2 mM MES/Tris-HCl; 10 mM $CaCl_2$; 0.1 mM KCl) added at the 35th second in the time-course analysis showed a single touch peak before going down to basal level (Figure 4.11 A). Total $[Ca^{2+}]_{cyt}$ accumulated over the time course showed no significant differences between Col-0 and *Atann2* in both control solution (Col-0 1.80±0.50 μM; *Atann2* 2.30±0.66 μM) and 1.5 mM suramin treatment (Col-0 0.81±0.29 μM; *Atann2* 1.71±0.69 μM) alone (Figure 4.11 B).

eATP treatment (0.5 mM) evoked the familiar $[Ca^{2+}]_{cyt}$ biphasic pattern in both suramin and non-suramin treated Col-0 and *Atann2* (Figure 4.11 C) after the touch response. The first $[Ca^{2+}]_{cyt}$ peak analysis showed higher Col-0 (0.28±0.01 μM) $[Ca^{2+}]_{cyt}$ increase than the *Atann2* (0.22±0.01 μM) in non-suramin treated samples but no significance was found in the suramin treated samples (Col-0 0.21±0.02 μM; *Atann2* 0.19±0.008 μM) (Figure 4.11 D). Suramin is effective in inhibiting the $[Ca^{2+}]_{cyt}$ response in the first peak for the Col-0 but not for the *Atann2* (Figure 4.11 D). The second peak displayed lower *Atann2* (0.19±0.006 μM) $[Ca^{2+}]_{cyt}$ accumulation compared to the Col-0 (0.21±0.006 μM) in non-suramin treated samples but not in suramin treated samples (Col-0 0.18±0.007 μM; *Atann2* 0.20±0.009 μM). Similar to the first peak, the second $[Ca^{2+}]_{cyt}$ peak showed partially effective inhibition of Col-0 and not *Atann2* by suramin (Figure 4.11 E). Col-0 (16.80±0.50 μM) showed significantly higher total $[Ca^{2+}]_{cyt}$ increase compared to *Atann2* (14.18±0.48 μM) over the time course in the non-suramin treated root tips. In the suramin-treated root tips, no significant difference in the total $[Ca^{2+}]_{cyt}$ was found between Col-0 (14.73±0.82 μM) and *Atann2* (14.99±0.46 μM). Although suramin managed to inhibit the peak responses, overall $[Ca^{2+}]_{cyt}$ accumulation showed no significant differences between suramin and non-suramin treated root tips for both Col-0 and *Atann2* (Figure 4.11 F).

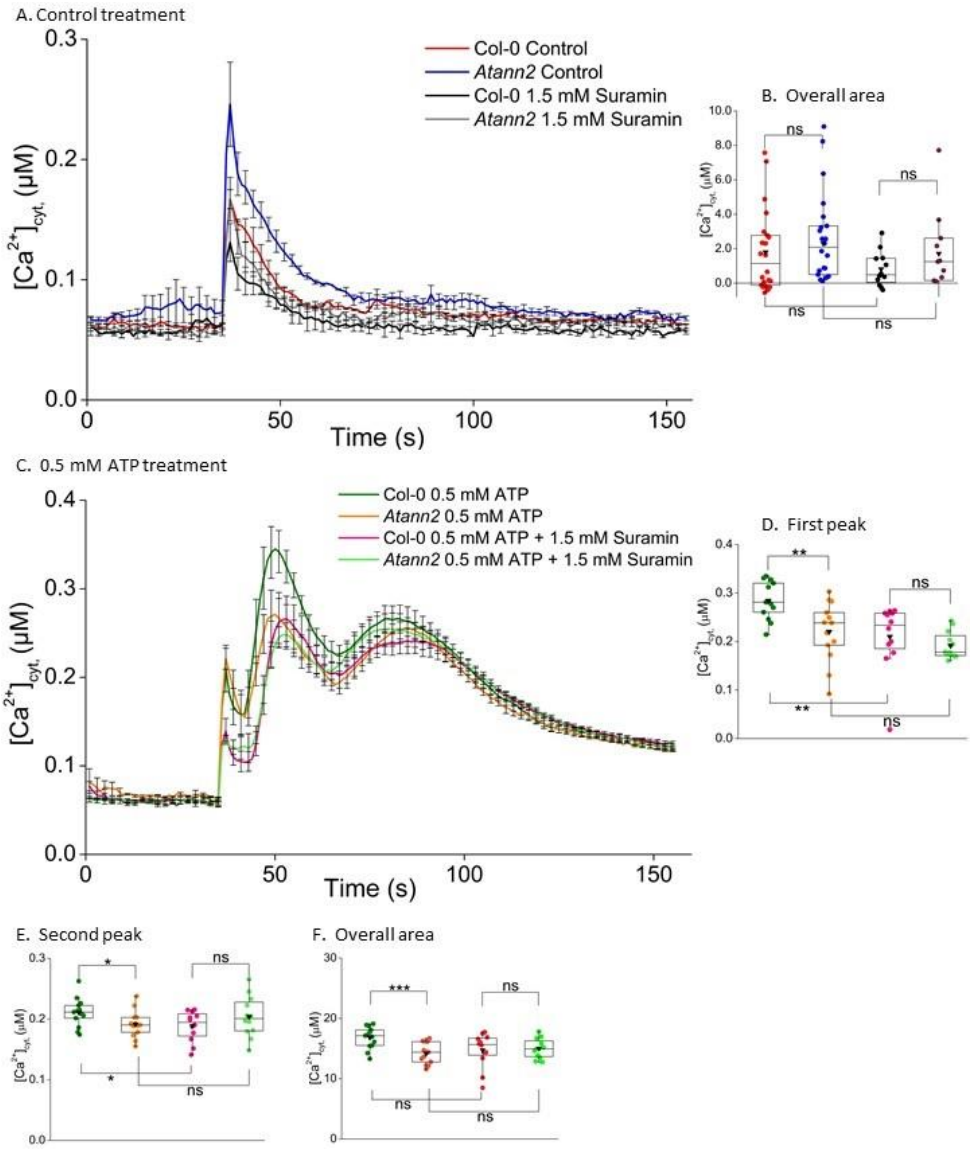

Figure 4.11: **Suramin impaired the Col-0 first and second peak $[Ca^{2+}]_{cyt}$ response to eATP.** The $[Ca^{2+}]_{cyt}$ responses were recorded for 155 s for both the control treatment (A) and the 0.5 mM ATP treatment (C) and each treatment was added at the 35th second. Seven-day-old Col-0 and *Atann2* 1 cm root tips were incubated with 1.5 mM suramin or control solution for 30 minutes prior to treatment. These time course data were from the means ± SEM of 3 independent trials, with a total of 12 - 22 root tips per genotype and treatment. The overall area (B) (35 - 155 s) was the total area under the curve for the control treatment. Analysis of the 0.5 mM ATP treatment (C) time course was done with the first peak (D) (41 - 63 s) and the second peak (E) (63 - 155 s) response, which was the highest value of the peaks that emerged after the touch response. The total accumulation of $[Ca^{2+}]_{cyt}$ by both genotypes in 0.5 mM ATP treatment was determined through the overall area under the curve (F) (35 - 155 s). All calculations were carried out with the baseline (the first 35 s of measurement) subtracted. Middle line of the boxplot represents the median whereas the inverted triangle represents the mean. *p*-values: ns (p>0.05), * (p<0.05), ** (p<0.01), *** (p< 0.001), Welch's *t*-test for parametric test and Wilcoxon rank-sum test for non-parametric test.

Figure 4.12 A shows the single touch $[Ca^{2+}]_{cyt}$ response after the control treatment and suramin treatment addition. Based on the overall area under the curve, the 1.5 mM suramin solution did not alter the result of the assay as there were no significant differences between the control treatment and the suramin treatment alone for both Col-0 (control 2.08±0.38 μM; suramin 0.53±0.50 μM) and *Atann2* samples (control 2.47±0.57 μM; suramin 1.44±0.50 μM) (Figure 4.12 B). Addition of 0.5 mM eADP showed production of the $[Ca^{2+}]_{cyt}$ biphasic curves by both Col-0 and *Atann2* preceded by the touch response (Figure 4.12 C). Analysis of the first peak found no significant differences between Col-0 (0.23±0.01 μM) and *Atann2* (0.21±0.01 μM) in non-suramin treated root tips but lower *Atann2* (0.15±0.01 μM) $[Ca^{2+}]_{cyt}$ accumulation than the Col-0 (0.21±0.007 μM) in the suramin treated root tips (Figure 4.12 D). Suramin managed to inhibit the $[Ca^{2+}]_{cyt}$ increase of *Atann2* as it was significantly lower in suramin treated than non-suramin treated root tips. This is however not true for the Col-0 root tips (Figure 4.12 D). Analysis of the second peak showed similar $[Ca^{2+}]_{cyt}$ increase between Col-0 and *Atann2* in both suramin (Col-0 0.22±0.004 μM; *Atann2* 0.21±0.01 μM) and non-suramin treated (Col-0 0.29±0.006 μM; *Atann2* 0.21±0.01 μM) root tips. The suramin treatments failed to inhibit the second $[Ca^{2+}]_{cyt}$ peak in both Col-0 and *Atann2* (Figure 4.12 E). *Atann2* (14.30±103 μM) total $[Ca^{2+}]_{cyt}$ accumulation in suramin-treated sample was lower than the Col-0 (16.99±0.52 μM). Suramin however was unsuccessful in completely blocking the putative receptor as no significant differences were found between suramin and non-suramin treated root tips for both Col-0 (control 15.99±0.58 μM; suramin 16.99±0.52 μM) and *Atann2* (control 15.29±0.42 μM; suramin 14.30±1.03 μM) (Figure 4.12 F).

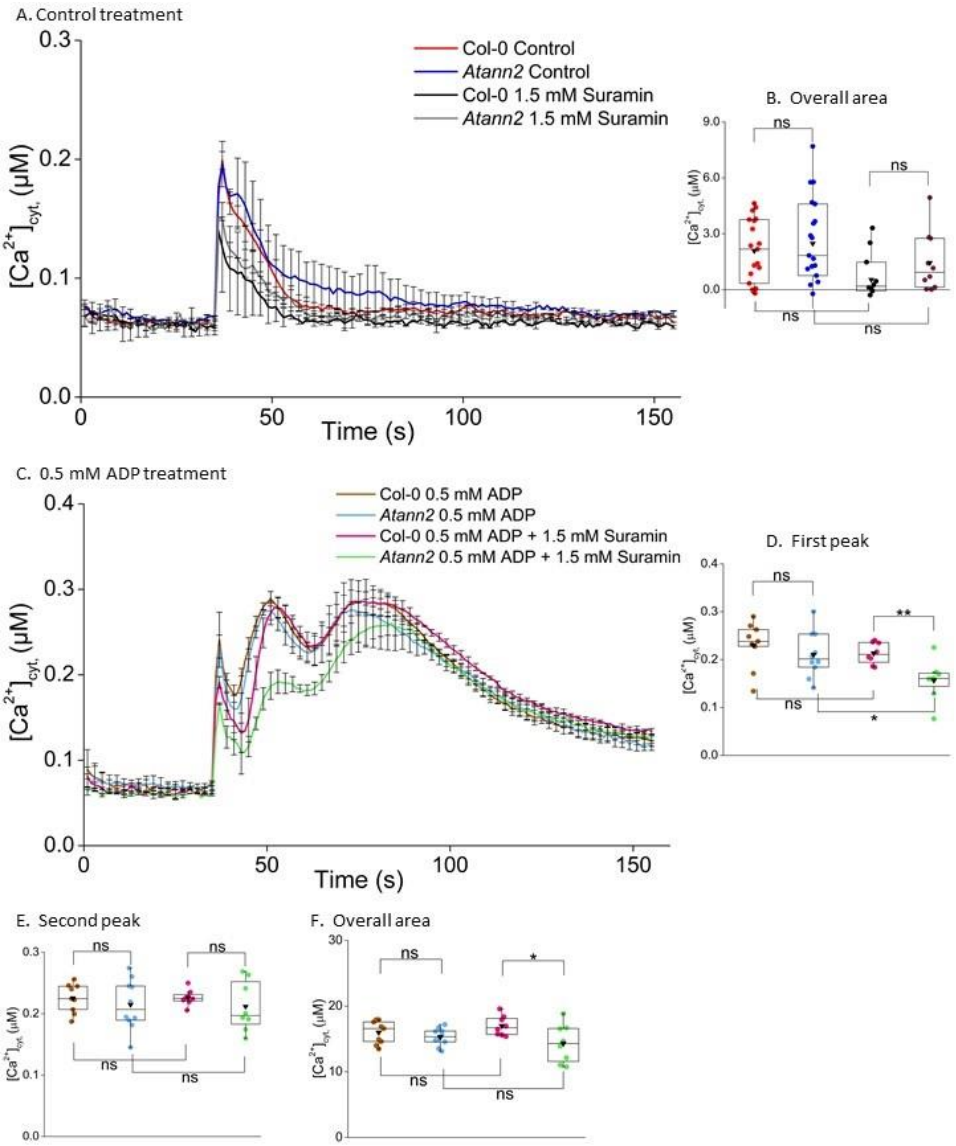

Figure 4.12: **Suramin causes impaired *Atann2* first peak $[Ca^{2+}]_{cyt}$ response to eADP**. The $[Ca^{2+}]_{cyt}$ responses were recorded for 155 s for both the control treatment (A) and the 0.5 mM eADP treatment (C) and each treatment was added at the 35th second. Seven-day-old Col-0 and *Atann2* 1 cm root tips were incubated with 1.5 mM suramin or control solution for 30 minutes prior to the treatment. These time course data were from the means ± SEM of 3 independent trials, with a total of 10 - 19 root tips per genotype and treatment. The overall area (B) (35 - 155 s) was the total area under the curve for the control treatment. Analysis of the 0.5 mM eADP treatment (C) time course was done with the first peak (D) (41 - 63 s) and the second peak (E) (63 - 155 s) response, which was the highest value of the peaks that emerged after the touch response. The total accumulation of $[Ca^{2+}]_{cyt}$ by both genotypes in 0.5 mM eADP treatment was determined through the overall area under the curve (F) (35 - 155 s). All calculations were carried out with the baseline (the first 35 s of measurement) subtracted. Middle line of the boxplot represents the median whereas the inverted triangle represents the mean. p-values: ns (p>0.05), * (p<0.05), ** (p<0.01), *** (p< 0.001), Welch's *t*-test for parametric test and Wilcoxon rank-sum test for non-parametric test.

4.2.3 The role of AtANN1 and AtANN2 together in mediating eATP and eADP-induced $[Ca^{2+}]_{cyt}$ accumulation at whole root level

In Chapter 3.2.2 and 4.2.2, we have shown that both individual AtANN1 and individual AtANN2 is required for the complete $[Ca^{2+}]_{cyt}$ response to the eATP and eADP signal. In this section, we compare the Col-0 and *Atann1/2* double mutant to examine the phenotypic effect of the absence of the two genes together in terms of $[Ca^{2+}]_{cyt}$ measurement. Production of the *Atann1/2* double mutant lines was done through crossing (*Atann1* SALK_015426 and *Atann2* SALK_054223) by Dr. Siân Richards (University of Cambridge). Genotyping and transformation of the mutant lines with 35S CAMV (apo)aequorin were carried out by Dr. Katie Wilkins (University of Cambridge).

Excised whole roots of 7-day-old Col-0 and *Atann1/2* were incubated with coelenterazine before the $[Ca^{2+}]_{cyt}$ measurement was done as explained in Chapter 2.6.1. Control solution (2 mM MES/Tris-HCl; 10 mM $CaCl_2$; 0.1 mM KCl) tested on both genotypes revealed a single touch peak that lasted for approximately 15 seconds followed by a basal level $[Ca^{2+}]_{cyt}$ response over the remaining time (Figure 4.13 A). Statistical analysis showed no significant difference between Col-0 (0.28±0.03 μM) and *Atann1/2* (0.23±0.04 μM) whole roots in the touch peak response (Figure 4.13 B). Overall $[Ca^{2+}]_{cyt}$ produced by the control solution was similar for both Col-0 (3.03±0.32 μM) and *Atann1/2* (2.82±0.71 μM) confirming that the mutation did not influence the basal $[Ca^{2+}]_{cyt}$ level and the touch response of both genotypes (Figure 4.13 C).

Upon addition of 1 mM eATP as agonist, both Col-0 and *Atann1/2* produced a single touch peak followed by the first and second peak over the course of 155 s (Figure 4.13 D). Col-0 (0.12±0.01 μM) $[Ca^{2+}]_{cyt}$ touch response was not significantly different compared to *Atann1/2* (0.06±0.01 μM) (Figure 4.13 E). *Atann1/2* (0.10±0.02 μM) evoked a significantly lower first peak $[Ca^{2+}]_{cyt}$ compared to the Col-0 (0.22±0.01 μM) (Figure 4.13 F). A similar result was found for the second peak where *Atann1/2* (0.19±0.02 μM) second peak $[Ca^{2+}]_{cyt}$ was significantly impaired compared to the Col-0 (0.30±0.01 μM) (Figure 4.13 G). Overall, the total $[Ca^{2+}]_{cyt}$ accumulated by Col-0 (18.73±0.70 μM) was significantly higher than the *Atann1/2* (10.90±1.47 μM) indicating that both AtANN1 and AtANN2 are needed for the normal $[Ca^{2+}]_{cyt}$ increase (Figure 4.13 H).

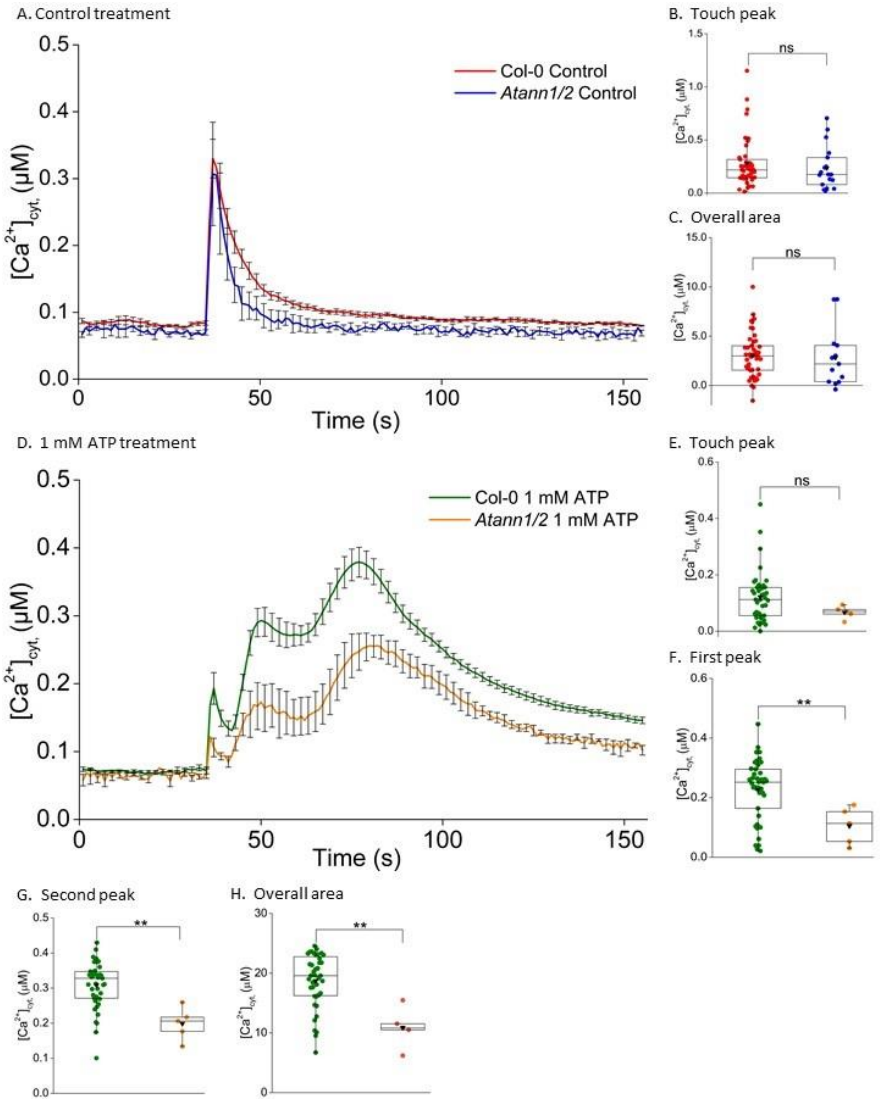

Figure 4.13: **Both AtANN1 and AtANN2 are needed for eATP-induced $[Ca^{2+}]_{cyt}$ elevation at whole roots level**. Both Col-0 and *Atann1/2* double mutant 7-day-old whole roots used were transformed to express cytosolic apo-aequorin. The $[Ca^{2+}]_{cyt}$ response for the control treatment (A) and 1 mM ATP (D) were recorded for 155 s where each treatment was added at the 35th second. This time course data are from the means ± SEM of 3 independent trials, with n = 7 - 41 roots per genotype and treatment. Touch peak (B) represents the highest value of the touch response (35 - 50 s) whereas the overall area (C) is the total area under the curve extracted from the time course data of the control treatment (35 - 155 s). Time course analysis of the 1 mM ATP treatment is split up into the first peak (F) (41 - 63 s) and the second peak (G) (63 - 155 s) responses, which is the highest value of the peaks that emerged after the touch response (E) (35 - 41 seconds). The total accumulation of $[Ca^{2+}]_{cyt}$ of Col-0 and *Atann1/2* were determined through the overall area under the curve (H) (35 - 155 s). All calculations carried out were with the baseline (the first 35 seconds of measurement) subtracted. Middle line of the boxplot represents the median whereas the inverted triangle represents the mean. p-values: ns(p>0.05), *(p<0.05), **(p<0.01),*** (p< 0.001), Welch's t-test for parametric test and Wilcoxon rank-sum test for non-parametric test.

Previous results with *Atann1* (Chapter 3.2.2; Figure 3.4) and *Atann2* (Chapter 4.4.2; Figure 4.4) tests at whole root level showed the impairment compared to Col-0 when treated with 1 mM eATP. Statistical analysis was done to compare the $[Ca^{2+}]_{cyt}$ response between single mutants *Atann1* and *Atann2* with the double mutant *Atann1/2* as shown in Figure 4.14. In control treatment, both *Atann1* and *Atann2* single mutants produced similar level of $[Ca^{2+}]_{cyt}$ increase to the *Atann1/2* double mutant at the touch peak value (*Atann1* 0.17±0.01 μM; *Atann2* 0.23±0.04 μM; *Atann1/2* 0.23±0.04 μM) and the total $[Ca^{2+}]_{cyt}$ accumulated (*Atann1* 2.17±0.4 μM; *Atann2* 2.27±0.43 μM; *Atann1/2* 2.82±0.6 μM). This confirmed that the mutations did not influence the mechanical response of the roots (Figure 4.14 A, B).

When we look at the 1 mM eATP treatment, the touch peak value of the double mutant *Atann1/2* (0.06±0.01 μM) was significantly lower than either single mutant of *Atann1* (0.11±0.01 μM; Figure 3.4) and *Atann2* (0.12±0.01 μM; Figure 4.4) (Figure 4.14 C). This is also true for the first peak value (*Atann1* 0.20±0.01 μM; *Atann2* 0.19±0.009 μM; *Atann12* 0.10±0.02 μM) (Figure 4.14 D) and the total accumulated $[Ca^{2+}]_{cyt}$ (*Atann1* 16.42±0.57 μM; *Atann2* 16.11±0.56 μM; *Atann12* 10.9±1.47 μM) (Figure 4.14 F). It is however intriguing as *Atann1/2* double mutant (0.19±0.02 μM) produced similar $[Ca^{2+}]_{cyt}$ increase as in single mutant *Atann1* (0.23±0.01 μM) and *Atann2* (0.22±0.007 μM) at the second peak value, which indicates that the mutation of both *AtANN1* and *AtANN2* was not effective in producing effect at the second peak of the 1 mM eATP $[Ca^{2+}]_{cyt}$ response (Figure 4.14 E).

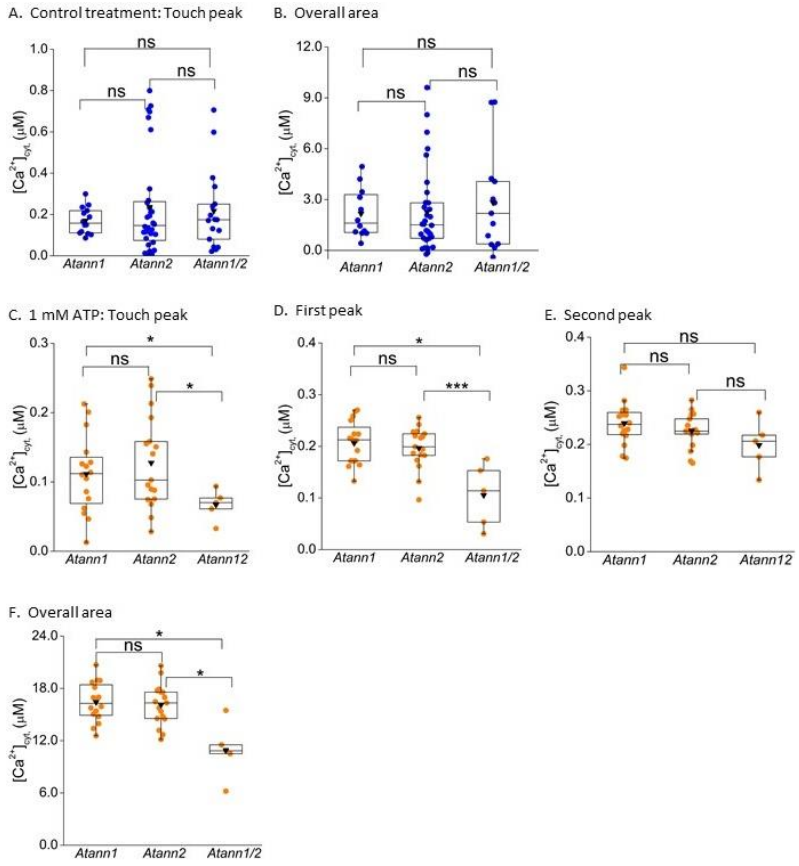

Figure 4.14: *Atann1/2* double mutant eATP-induced $[Ca^{2+}]_{cyt}$ accumulation is impaired compared to single mutants. Comparisons of $[Ca^{2+}]_{cyt}$ accumulation were done between *Atann1*, *Atann2* and *Atann1/2* for both control and 1 mM ATP treatment. Touch peak (A; control, C; 1 mM ATP) represents the highest value of the touch response. First peak (D; 1 mM ATP) and the second peak (E; 1 mM ATP) responses are the highest value of the peaks that emerged after the touch response. The total accumulation of $[Ca^{2+}]_{cyt}$ of all the genotypes were determined through the overall area under the curve from the time course analysis done previously (B; control, F; 1 mM ATP). Middle line of the boxplot represents the median whereas the inverted triangle represents the mean. *p*-values: ns(p>0.05), *(p<0.05), **(p<0.01),*** (p< 0.001), Welch's *t*-test for parametric test and Wilcoxon rank-sum test for non-parametric test.

This experiment was replicated with a lower eATP concentration as agonist (0.1 mM) to look at the function of concentration. Figure 4.15 A shows the biphasic $[Ca^{2+}]_{cyt}$ pattern after the touch response produced by both Col-0 and *Atann1/2* upon addition of 0.1 mM eATP. In contrast to the previous results, *Atann1/2* (0.10±0.02 µM) touch peak was significantly lower compared to the Col-0 (0.20±0.03 µM) when challenged with 0.1 mM eATP (Figure 4.15 B). Statistical analysis done on the first peak showed a similar pattern with *Atann1/2* (0.09±0.01 µM) having an impaired first peak compared to the Col-0 (0.19±0.01 µM) (Figure 4.15C). This is also true for the second peak where *Atann1/2*

(0.13±0.01 µM) was significantly impaired in comparison to the Col-0 (0.22±0.009 µM) (Figure 4.15 D). Analysis of the overall $[Ca^{2+}]_{cyt}$ accumulated confirmed that the absence of AtANN1 and AtANN2 caused reduction in the normal $[Ca^{2+}]_{cyt}$ response (Col-0 14.39±0.66 µM; *Atann1/2* 7.56±0.73 µM) by 0.1 mM eATP (Figure 4.15 E).

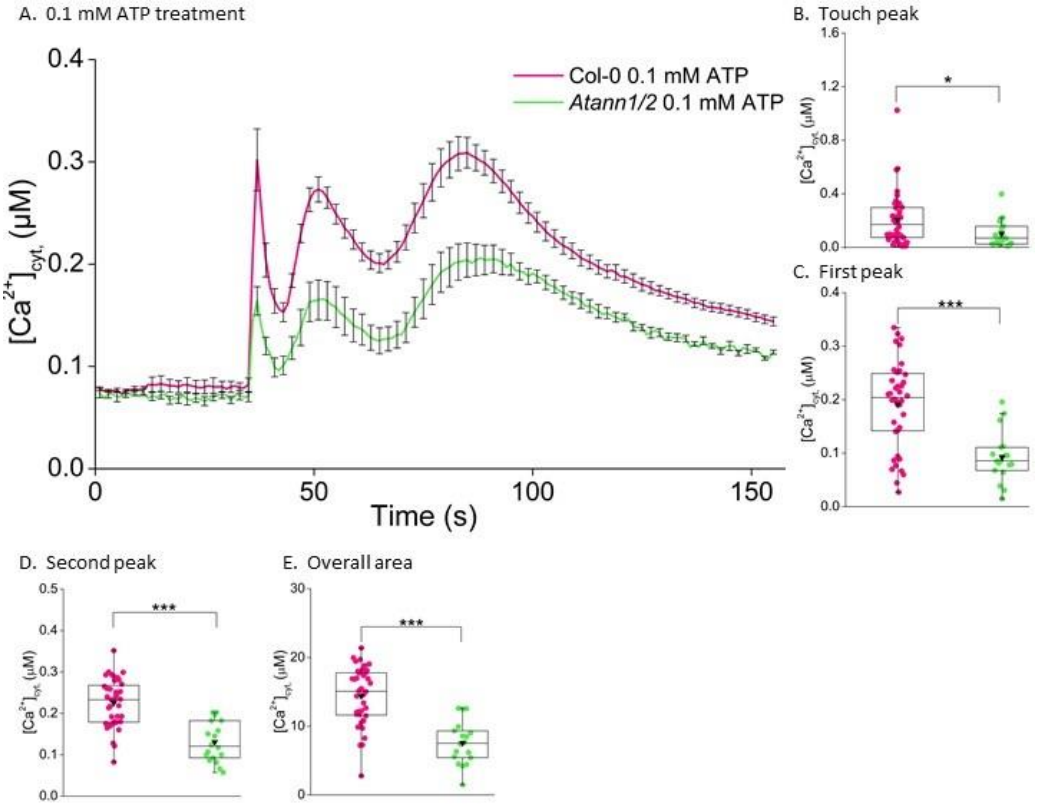

Figure 4.15: **A lower concentration eATP evokes $[Ca^{2+}]_{cyt}$ signatures in whole roots that depend on both AtANN1 and AtANN2.** Time course data show 7-day-old Col-0 and *Atann1/2* double mutant whole roots response towards 0.1 mM eATP (A). The $[Ca^{2+}]_{cyt}$ responses were recorded for 155 s and treatment was added at the 35th second. Time course data were from the means ± SEM of 3 independent trials, with n = 18 - 40. Time course analysis of the 0.1 mM eATP treatment is split up into the first peak (C) (42 - 65 s) and the second peak (D) (65 - 155 s) responses, which is the highest value of the peaks that emerged after the touch response (B) (35 - 41 s). The total accumulation of $[Ca^{2+}]_{cyt}$ of Col-0 and *Atann1/2* were determined through the overall area under the curve (H) (35 - 155 s). All calculations carried out were with the baseline (the first 35 seconds of measurement) subtracted. Middle line of the boxplot represents the median whereas the inverted triangle represents the mean. p-values: ns (p>0.05), * (p<0.05), ** (p<0.01), *** (p< 0.001), Welch's t-test for parametric test and Wilcoxon rank-sum test for non-parametric test.

Comparison between single mutant *Atann1* (data as shown in Chapter 3.2.9; Figure 3.24) and double mutant *Atann1/2* was also carried out at the lower 0.1 mM eATP concentration. The results from the control treatment showed no significant difference

between *Atann1* and *Atann1/2* in terms of the touch peak value (*Atann1* 0.15±0.03 μM*; Atann1/2* 0.23±0.04 μM) but *Atann1/2* (2.82±0.71 μM) produced significantly higher total $[Ca^{2+}]_{cyt}$ compared to the *Atann1*(0.41±0.32 μM) (Figure 4.16 A, B). This contrasting result with the control treatment carried out in 1 mM eATP test could be caused by low number of *Atann1* samples. Comparison done for the 0.1 mM eATP test results showed *Atann1/2* to be significantly impaired compared to the *Atann1* at the touch peak value (*Atann1* 0.32±0.08 μM; *Atann1/2* 0.10±0.02 μM) (Figure 4.16 C) and the first peak value (*Atann1* 0.14±0.02 μM;*Atann1/2* 0.09±0.01 μM) (Figure 4.16 D). Similar to the 1 mM eATP test, mutation of both *Atann1* and *Atann2* proved not to be effective at lower concentration as the double mutant *Atann1/2* (0.13±0.01 μM) produced a similar level of second peak value as the *Atann1* (0.13±0.01 μM) single mutant (Figure 4.16 E). This is also true for the total $[Ca^{2+}]_{cyt}$ accumulated as *Atann1/2* (7.56±0.73 μM) was not significantly different from *Atann1* (10.27±1.15 μM) (Figure 4.16 F).

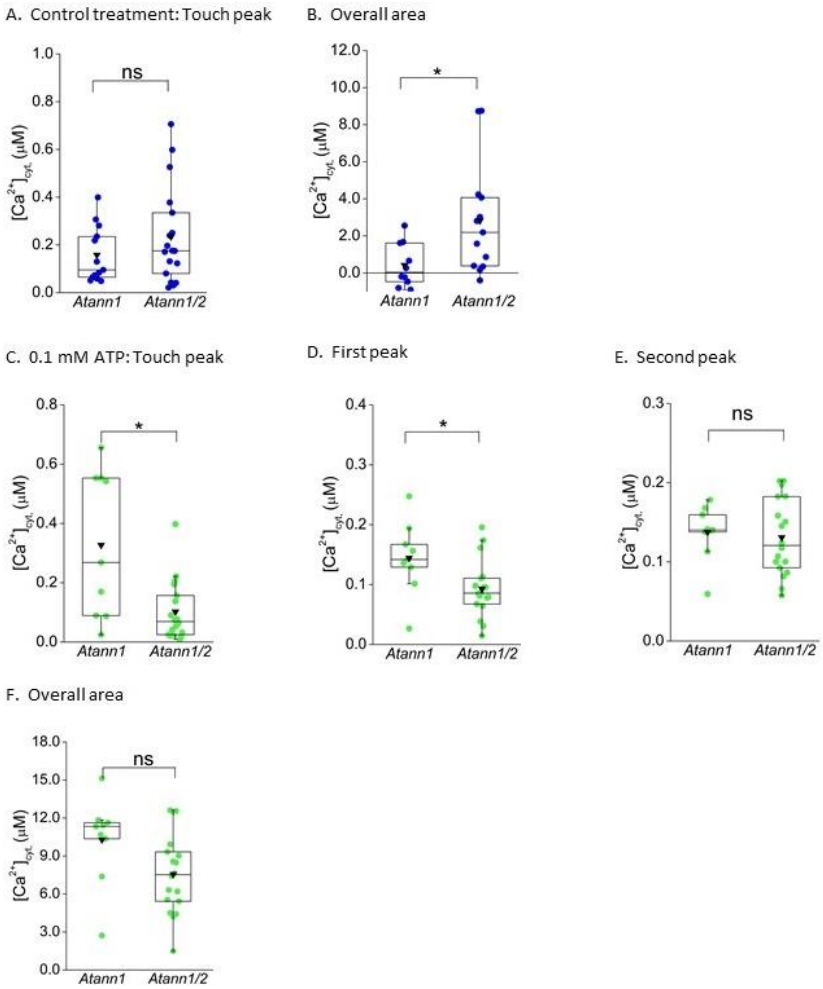

Figure 4.16: ***Atann1/2* significantly reduced than *Atann1* at the first peak $[Ca^{2+}]_{cyt}$ value in lower 0.1 mM ATP treatment.** Comparisons of $[Ca^{2+}]_{cyt}$ accumulation were done between *Atann1* and *Atann1/2* for both control and 0.1 mM ATP treatment. Touch peak (A; control, C; 0.1 mM ATP) represents the highest value of the touch response. First peak (D; 0.1 mM ATP) and the second peak (E; 0.1 mM ATP) responses are the highest value of the peaks that emerged after the touch response. The total accumulation of $[Ca^{2+}]_{cyt}$ of all the genotypes were determined through the overall area under the curve from the time course analysis done previously (B; control, F; 0.1 mM ATP). Middle line of the boxplot represents the median whereas the inverted triangle represents the mean. *p*-values: ns(p>0.05), *(p<0.05), **(p<0.01),*** (p< 0.001), Welch's *t*-test for parametric test and Wilcoxon rank-sum test for non-parametric test.

Col-0 and *Atann1/2* 7-day-old whole roots were also tested with eADP treatment as agonist to determine whether AtANN1 and AtANN2 involvement is specific for eATP signalling. In Figure 4.17 A, control treatment produced a single touch response before going back to the basal level for both Col-0 and *Atann1/2*. Analysis of the touch peak (Col-0 0.48±0.07 µM; *Atann1/2* 0.45±0.08 µM) and overall $[Ca^{2+}]_{cyt}$ accumulated (Col-0 2.30±0.43

μM; *Atann1/2* 4.33±0.72 μM) showed consistency with previous control results where no significant differences were found between Col-0 and *Atann1/2* (Figure 4.17 B, C).

Upon application of 1 mM eADP, both Col-0 and *Atann1/2* were consistent in generating the touch response with the subsequent first peak and the second peak $[Ca^{2+}]_{cyt}$ response (Figure 4.17 D). Statistical analysis displayed equivalent touch peak between Col-0 (0.33±0.04 μM) and *Atann1/2* (0.26±0.05 μM) (Figure 4.17 E). This is however not true for the first peak as the Col-0 (0.22±0.01 μM) first peak was significantly higher compared to the *Atann1/2* (0.16±0.01 μM) (Figure 4.17 F). The same instance was found at the second peak $[Ca^{2+}]_{cyt}$ response where *Atann1/2* mutant (0.19±0.01 μM) evoked less $[Ca^{2+}]_{cyt}$ than the Col-0 (0.28±0.008 μM) (Figure 4.17 G). The total $[Ca^{2+}]_{cyt}$ accumulated confirmed that both AtANN1 and AtANN2 are needed for the full eADP-induced $[Ca^{2+}]_{cyt}$ response as the mutation (*Atann1/2* 13.24±0.58 μM) was impaired in comparison to the Col-0 (18.89±0.60 μM) (Figure 4.17 H).

Statistical analysis was done between the *Atann1* outcomes (Chapter 3.2.2; Figure 3.5) and *Atann2* outcomes (Chapter 4.2.2; Figure 4.5) with the *Atann1/2* when tested with 1 mM eADP in order to see the additive effect of either *AtANN1* or *AtANN2* mutation (comparison in Figure 4.18). In the control treatment, *Atann1* showed lower $[Ca^{2+}]_{cyt}$ response compared to the *Atann1/2* in both touch peak response (*Atann1* 0.13±0.01 μM; *Atann1/2* 0.45±0.08 μM) and the total $[Ca^{2+}]_{cyt}$ production (*Atann1* 1.46±0.36 μM; *Atann1/2* 4.33±0.72 μM) whereas *Atann2* showed significantly lower touch peak response (*Atann2* 0.25±0.05 μM) but not the total $[Ca^{2+}]_{cyt}$ accumulation (*Atann2* 2.73±0.49 μM) (Figure 4.18 A, B). *Atann1* produced significantly lower touch peak $[Ca^{2+}]_{cyt}$ value (0.13±0.02 μM) compared to the *Atann1/2* (0.26±0.05 μM) in 1 mM eADP treatment in contrast to *Atann2* (0.15±0.03 μM) where it produced similar touch peak value as in *Atann1/2* double mutant (Figure 4.18 C). Comparison between *Atann1* and *Atann1/2* showed no significant differences in the first peak (*Atann1* 0.16±0.008 μM; *Atann1/2* 0.16±0.01 μM) (Figure 4.18 D) and the second peak (*Atann1* 0.22±0.01 μM; *Atann1/2* 0.19±0.01 μM) (Figure 4.18 E). This was however not true for *Atann2* in the first peak (*Atann2* 0.21±0.01 μM) and the second peak value (*Atann2* 0.25±0.009 μM) which showed significantly higher $[Ca^{2+}]_{cyt}$ response compared to the *Atann1/2*. Regardless, mutation of *AtANN2* proved to have an additive effect as the total $[Ca^{2+}]_{cyt}$ accumulated in *Atann1/2* (13.23±0.58 μM) was significantly lower compared to both *Atann1* (15.10±0.58 μM) and *Atann2* (17.87±0.97 μM) when treated with 1 mM eADP (Figure 4.18 F).

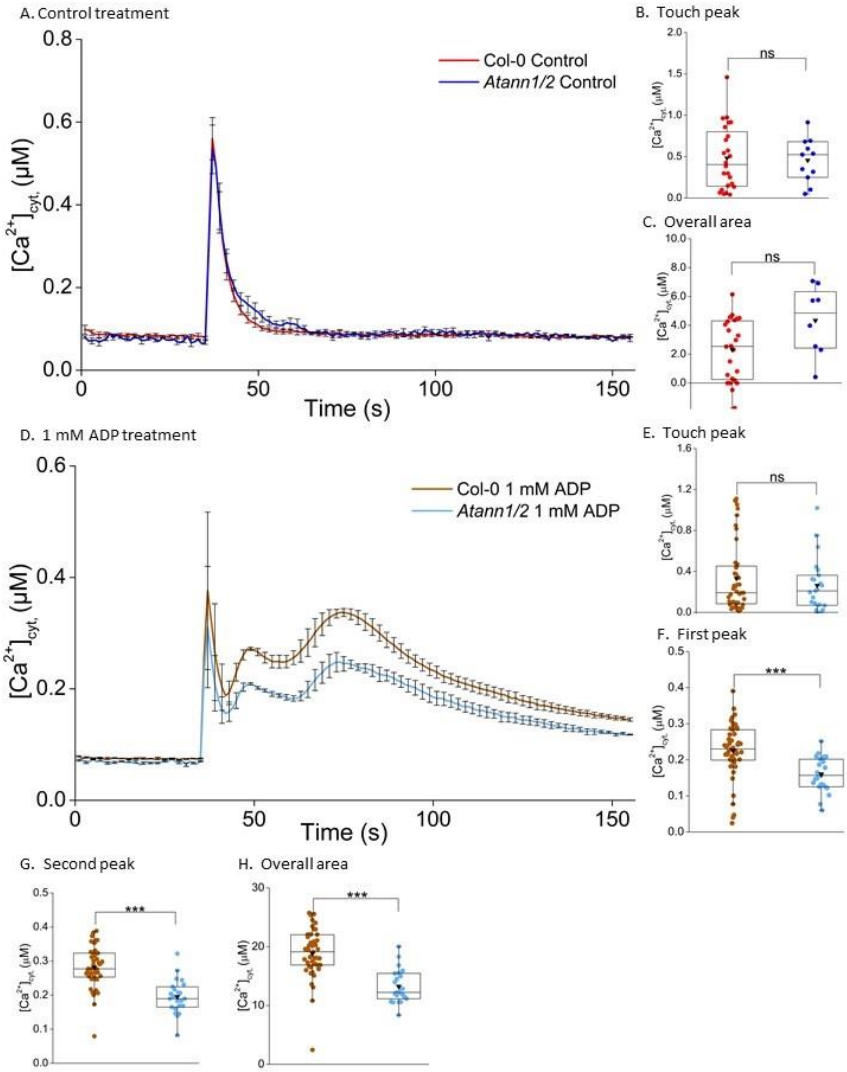

Figure 4.17: **eADP causes $[Ca^{2+}]_{cyt}$ elevation at whole roots level as a downstream response through AtANN1 and AtANN2.** Both Col-0 and *Atann1/2* 7-day-old whole roots contain apo-aequorin protein marker. The $[Ca^{2+}]_{cyt}$ response for the control treatment (A) and 1 mM ADP (D) were recorded for 155 seconds where each treatment was added at the 35th second. This time course data are from the means ± SEM of 3 independent trials, with n = 12 - 47 roots per genotype and treatment. Touch peak (B) represents the highest value of the touch response (35 - 50 s) whereas the overall area (C) is the total area under the curve extracted from the time course data of the control treatment (35 - 155 s). Time course analysis of the 1 mM ATP treatment is split up into the first peak (F) (41 - 59 s) and the second peak (G) (59 - 155 s) responses, which is the highest value of the peaks that emerged after the touch response (E) (35 - 41 s). The total accumulation of $[Ca^{2+}]_{cyt}$ of Col-0 and *Atann1/2* were determined through the overall area under the curve (H) (35 - 155 s). All calculations carried out are with the baseline (the first 35 seconds of measurement) subtracted. Middle line of the boxplot represents the median whereas the inverted triangle represents the mean. *p*-values: ns (p>0.05), *(p<0.05), **(p<0.01),*** (p< 0.001), Welch's *t*-test for parametric test and Wilcoxon rank-sum test for non-parametric test.

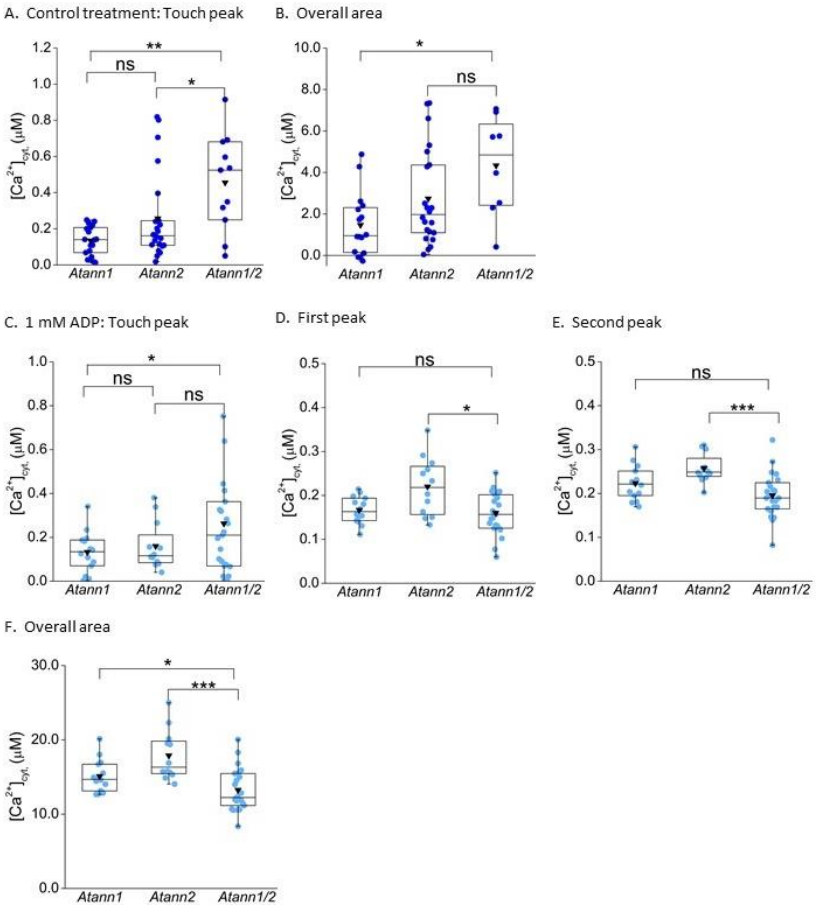

Figure 4.18: Comparison with single mutants showed absence of both *AtANN1* and *AtANN2* significantly reduced eADP-induced $[Ca^{2+}]_{cyt}$. Comparisons of $[Ca^{2+}]_{cyt}$ accumulation were done between *Atann1, Atann2* and *Atann1/2* for both control and 1 mM ADP treatment. Touch peak (A; control, C; 1 mM ATP) represents the highest value of the touch response. First peak (D; 1 mM ADP) and the second peak (E; 1 mM ADP) responses are the highest value of the peaks that emerged after the touch response. The total accumulation of $[Ca^{2+}]_{cyt}$ of all the genotypes were determined through the overall area under the curve from the time course analysis done previously (B; control, F; 1 mM ADP). Middle line of the boxplot represents the median whereas the inverted triangle represents the mean. *p*-values: ns(p>0.05), *(p<0.05), **(p<0.01),*** (p< 0.001), Welch's *t*-test for parametric test and Wilcoxon rank-sum test for non-parametric test.

Lowering the eADP treatment concentration to 0.1 mM did not change the $[Ca^{2+}]_{cyt}$ biphasic pattern as shown in Figure 4.19 A. In contrast to the 0.1 mM eATP test, the touch $[Ca^{2+}]_{cyt}$ showed statistically insignificant response between Col-0 (0.21±0.02 µM) and *Atann1/2* (0.26±0.03 µM) in the 0.1 mM eADP test (Figure 4.19 B). Similar to the 1 mM eADP test, Col-0 whole roots displayed significantly higher $[Ca^{2+}]_{cyt}$ than the *Atann1/2* in both the first peak (Col-0 0.18±0.01 µM; *Atann1/2* 0.15±0.01 µM) and the second peak (Col-0 0.19±0.007 µM; 0.15±0.005 µM) (Figure 4.19 C, D). The absence of both AtANN1 and

AtANN2 has caused significant reduction in total $[Ca^{2+}]_{cyt}$ (*Atann1/2* 11.65±0.61 μM) compared to the Col-0 (13.72±0.64 μM) again confirming that both AtANN1 and AtANN2 are important in mediating the eADP signalling response (Figure 4.19 E).

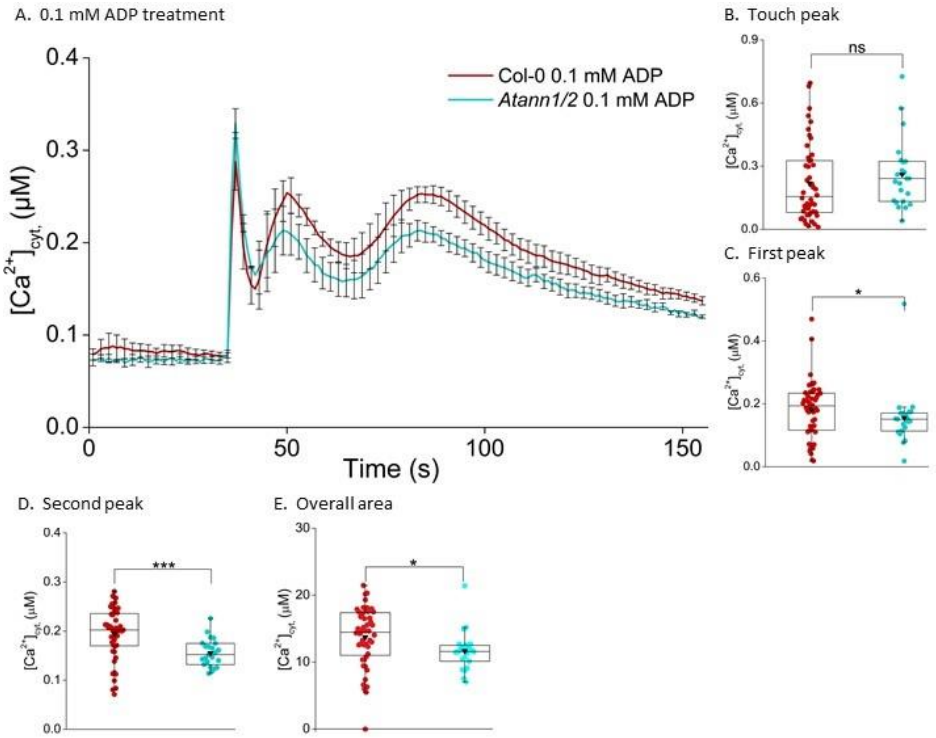

Figure 4.19: **A lower concentration of eADP induced accumulation of $[Ca^{2+}]_{cyt}$ in whole roots that depended on both AtANN1 and AtANN2**. Time course data show 7-day-old Col-0 and *Atann1/2* double mutant whole roots response towards 0.1 mM ADP (A). The $[Ca^{2+}]_{cyt}$ responses were recorded for 155 s and treatment was added at the 35th second. Time course data were from the means ± SEM of 3 independent trials, with n = 23 - 48. Time course analysis of the 0.1 mM eADP treatment is split up into the first peak (C) (42 - 66 s) and the second peak (D) (66 - 155 s) responses, which is the highest value of the peaks that emerged after the touch response (B) (35 - 41 s). The total accumulation of $[Ca^{2+}]_{cyt}$ of Col-0 and *Atann1/2* were determined through the overall area under the curve (H) (35 - 155 s). All calculations carried out are with the baseline (the first 35 seconds of measurement) subtracted. Middle line of the boxplot represents the median whereas the inverted triangle represents the mean. p-values: ns (p>0.05), * (p<0.05), ** (p<0.01), *** (p< 0.001), Welch's t-test for parametric test and Wilcoxon rank-sum test for non-parametric test.

In order to see the additive effect of *AtANN2* mutation, comparison between the results obtained in the *Atann1* test with 0.1 mM eADP treatment (Chapter 3.2.9; Figure 3.25) with *Atann1/2* was done. Both *Atann1* and *Atann1/2* whole roots produced similar $[Ca^{2+}]_{cyt}$ response at the touch peak (*Atann1* 0.29±0.05 μM; *Atann1/2* 0.45±0.08 μM) and the total $[Ca^{2+}]_{cyt}$ accumulation (*Atann1* 2.66±0.39; *Atann1/2* 4.33±0.72 μM) when treated with

control solution (Figure 4.20 A, B). In 0.1 mM eADP treatment, both *Atann1* (0.33±0.07 μM) and *Atann1/2* (0.26±0.03) produced similar level of touch peak response (Figure 4.20 C). In the first peak response however *Atann1/2* (0.15±0.01 μM) evoked lower $[Ca^{2+}]_{cyt}$ value compared to the *Atann1* (0.17±0.009 μM) (Figure 4.20 D). This is not true for the second peak where *Atann1* (0.16±0.01 μM) had similar second peak value with *Atann1/2* (0.15±0.005 μM) (Figure 4.20 E). Overall, the mutation of *AtANN2* proved to have an effect as the total $[Ca^{2+}]_{cyt}$ accumulation by *Atann1/2* (11.65±0.61 μM) was significantly lower compared to the *Atann1* (13.99±0.68 μM) (Figure 4.20 F).

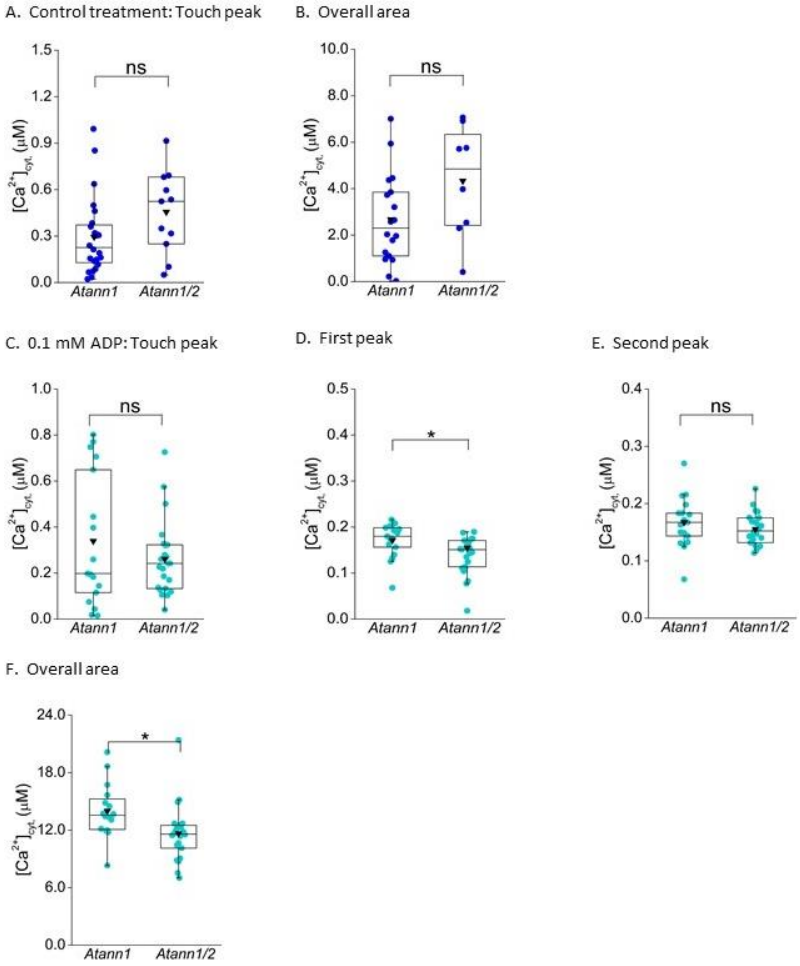

Figure 4.20: 0.1 mM ADP evoked lower $[Ca^{2+}]_{cyt}$ in *Atann1/2* compared to single *Atann1* mutant. Comparisons of $[Ca^{2+}]_{cyt}$ accumulation were done between *Atann1* and *Atann1/2* for both control and 0.1 mM ADP treatment. Touch peak (A; control, C; 0.1 mM ADP) represents the highest value of the touch response. First peak (D; 0.1 mM ADP) and the second peak (E; 0.1 mM ADP) responses are the highest value of the peaks that emerged after the touch response. The total accumulation of $[Ca^{2+}]_{cyt}$ of all the genotypes were determined through the overall area under the curve from the time course analysis done previously (B; control, F; 0.1 mM ADP). Middle line of the boxplot represents the median whereas the inverted triangle represents the mean. *p*-values: ns(p>0.05), *(p<0.05),

(p<0.01),* (p< 0.001), Welch's *t*-test for parametric test and Wilcoxon rank-sum test for non-parametric test.

4.2.4 *AtANN1* and *AtANN4* mutations failed to reduce $[Ca^{2+}]_{cyt}$ accumulation under eATP and eADP signal

Both AtANN1 and AtANN2 proved to be involved in mediating eATP and eADP response based on the findings of this and the previous chapter. However, there are potentially other candidates for calcium channels as knocking out *AtANN1* and *AtANN2* together still failed to completely abolish the calcium response. Expression of *AtANN1* and *AtANN2* in the *Atann1/2* line was confirmed to be knocked-down based on the gene expression study as shown in Chapter 4.2.5 (Figure 4.38). A study has discovered the ability of AtANN4 to bind to AtANN1 in response to salt stress (Huh *et al.*, 2010) making it a good protein candidate that might work with AtANN1 in eATP and eADP signalling. To test this hypothesis, comparison between Col-0 and *Atann1/4* double mutant 7-day-old whole roots when challenged with eATP and eADP in terms of $[Ca^{2+}]_{cyt}$ measurement was carried out. *Atann1/4* was prepared by Dr. Siân Richards (University of Cambridge) through crossing of *Atann1* and *Atann4* (SALK_019725). T-DNA insertion of *Atann4* is located at nucleotide 1670 (Lee *et al.*, 2004). Transformation to express (apo)aequorin cytosolically was done by Dr. Katie Wilkins (University of Cambridge).

Figure 4.21 A shows a single touch peak response by Col-0 and *Atann1/4* upon addition of control treatment (2 mM MES/Tris-HCl; 10 mM $CaCl_2$; 0.1 mM KCl). Statistical analysis confirmed that the mutation did not alter the $[Ca^{2+}]_{cyt}$ response as there were no significant differences between Col-0 and *Atann1/4* in the peak value (Col-0 0.55±0.09 μM; *Atann1/4* 0.68±0.09 μM) and the total $[Ca^{2+}]_{cyt}$ (Col-0 3.92±0.70 μM; *Atann1/4* 3.90±0.49 μM) of the touch response by control treatment (Figure 4.21 A, B). eATP treatment (1 mM) applied to the Col-0 and *Atann1/4* displayed the signature biphasic $[Ca^{2+}]_{cyt}$ release pattern after the touch response (Figure 4.21 C). Similar to the control treatment, the touch response caused by 1 mM eATP agonist held no significant difference between Col-0 (0.23±0.05 μM) and *Atann1/4* (0.32±0.04 μM) (Figure 4.21 D). This however was changed at the first peak value as the Col-0 (0.21±0.01 μM) whole roots produced statistically lower $[Ca^{2+}]_{cyt}$ response than the *Atann1/4* (0.26±0.01 μM) (Figure 4.21 E). Further analysis of the second peak value (Col-0 0.26±0.01 μM; *Atann1/4* 0.26±0.008 μM) and the total $[Ca^{2+}]_{cyt}$ accumulated (Col-0

18.51±1.03 μM; *Atann1/4* 20.32±0.67 μM) over the course of the measurement showed no significant differences between Col-0 and *Atann1/4* (Figure 4.21 F, G).

Since no tests on *Atann4* could be done due to technical problems and time constraint, comparison between *Atann1* results (Chapter 3.2.2; Figure 3.4) and *Atann1/4* results under the influence of 1 mM eATP treatment was done to get an insight into possible additive effect of mutation of *AtANN4*. Comparison in the initial control treatment results revealed that the mutation of *AtANN4* alone proved to enhance calcium response as the *Atann1/4* double mutant evoked higher $[Ca^{2+}]_{cyt}$ response compared to *Atann1* single mutant at both touch peak (*Atann1* 0.17±0.01 μM; *Atann1/4* 0.68±0.09 μM) and overall $[Ca^{2+}]_{cyt}$ accumulated (*Atann1* 2.17±0.38 μM; *Atann1/4* 3.90±0.49 μM) (Figure 4.22 A, B). Similar pattern was shown in the 1 mM eATP treatment where *Atann1/4* again produced significantly higher $[Ca^{2+}]_{cyt}$ response compared to the *Atann1* single mutant in the touch peak (*Atann1* 0.11±0.01 μM; *Atann1/4* 0.32±0.04 μM) (Figure 4.22 C), first peak (*Atann1* 0.20±0.01 μM; *Atann1/4* 0.26±0.01 μM) (Figure 4.22 D) and the total $[Ca^{2+}]_{cyt}$ accumulated (*Atann1* 16.42±0.56 μM; *Atann1/4* 20.32±0.67 μM) (Figure 4.22 F). Exception of this occurrence was at the second peak value where no significant difference was found between *Atann1* single mutant (0.23±0.01 μM) and the *Atann1/4* double mutant (0.26±0.008 μM) (Figure 4.22 E).

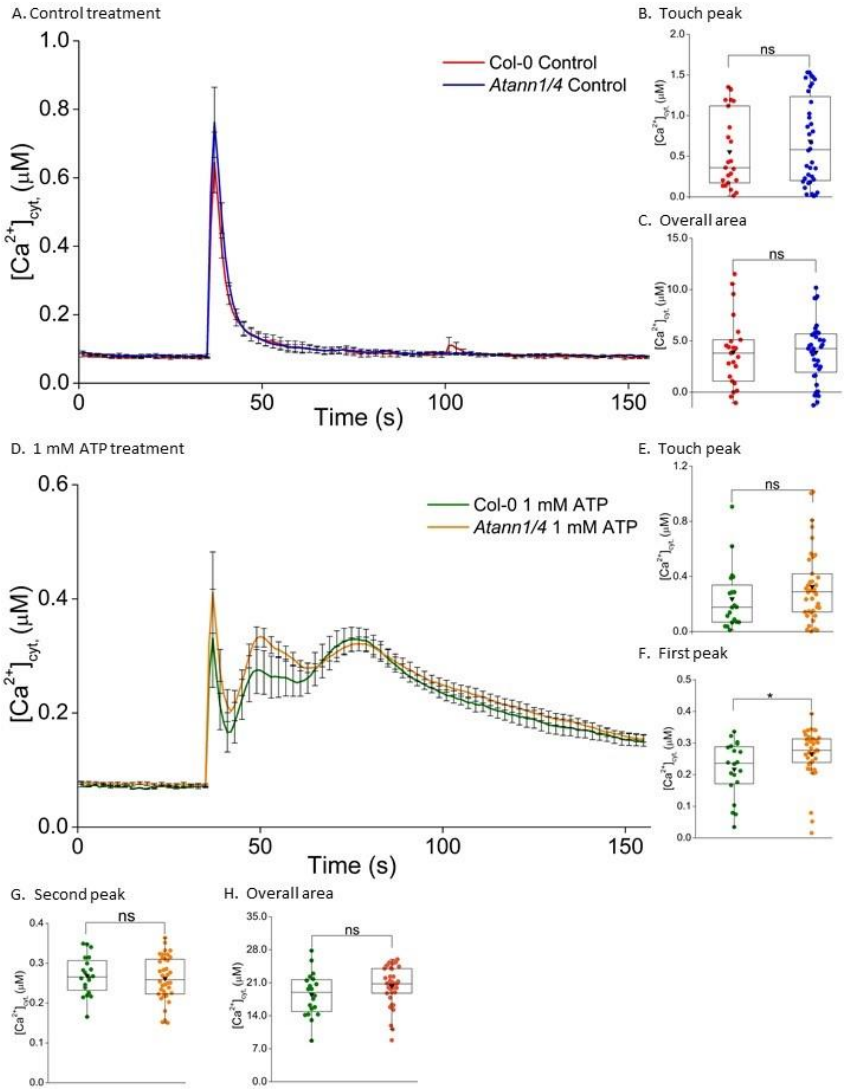

Figure 4.21: **AtANN4 might negatively regulate eATP-induced $[Ca^{2+}]_{cyt}$ elevation at whole root level in the first peak.** Both Col-0 and *Atann1/4* double mutant 7-day-old whole roots contained cytosolic apo-aequorin. The $[Ca^{2+}]_{cyt}$ response for the control treatment (A) and 1 mM eATP (D) were recorded for 155 seconds where each treatment was added at the 35th second. These time course data are from the means ± SEM of 3 independent trials, with n = 20 - 38 roots per genotype and treatment. Touch peak (B) represents the highest value of the touch response (35 - 50 s) whereas the overall area (C) is the total area under the curve extracted from the time course data of the control treatment (35 - 155 s). Time course analysis of the 1 mM eATP treatment is split up into the first peak (F) (41 - 63 s) and the second peak (G) (63 - 155 s) responses, which is the highest value of the peaks that emerged after the touch response (E) (35 - 41 s). The total accumulation of $[Ca^{2+}]_{cyt}$ of Col-0 and *Atann1/4* were determined through the overall area under the curve (H) (35 - 155 s). All calculations carried out were with the baseline (the first 35 seconds of measurement) subtracted. Middle line of the boxplot represents the median whereas the inverted triangle represents the mean. p-values: ns (p>0.05), * (p<0.05), ** (p<0.01) ,*** (p< 0.001), Welch's t-test for parametric test and Wilcoxon rank-sum test for non-parametric test.

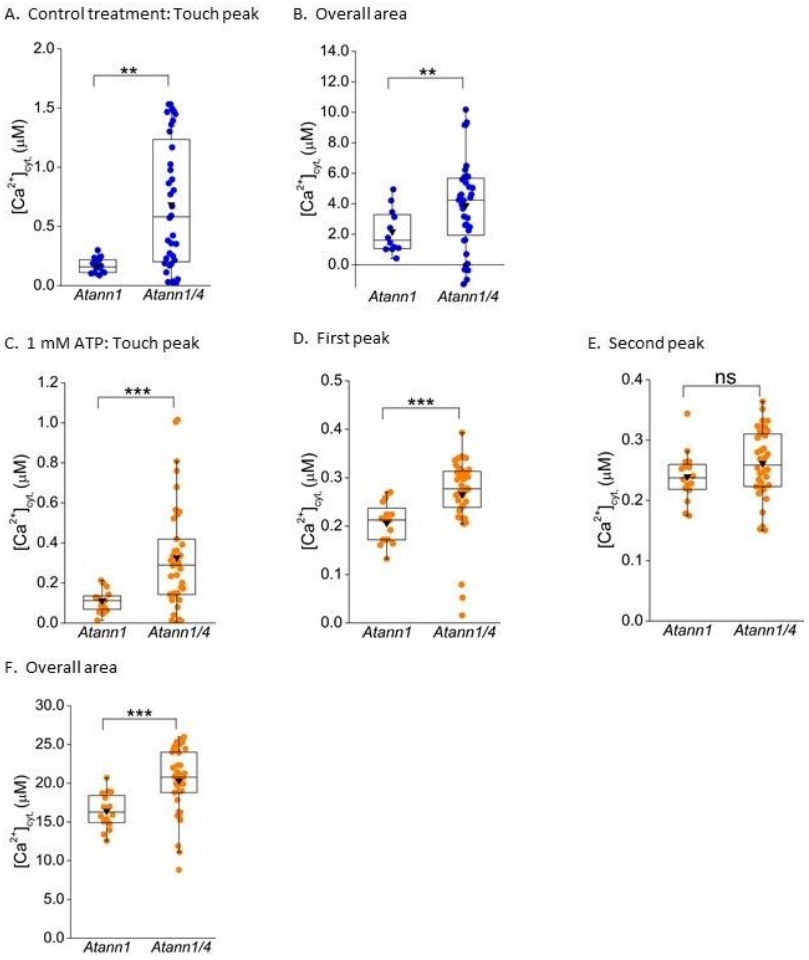

Figure 4.22: ***Atann1/4* enhanced $[Ca^{2+}]_{cyt}$ elevation compared to single *Atann1* mutant in 1 mM ATP treatment.** Comparisons of $[Ca^{2+}]_{cyt}$ accumulation were done between *Atann1* and *Atann1/4* for both control and 1 mM ATP treatment. Touch peak (A; control, C; 1 mM ATP) represents the highest value of the touch response. First peak (D; 1 mM ATP) and the second peak (E; 1 mM ATP) responses are the highest value of the peaks that emerged after the touch response. The total accumulation of $[Ca^{2+}]_{cyt}$ of all the genotypes were determined through the overall area under the curve from the time course analysis done previously (B; control, F; 1 mM ATP). Middle line of the boxplot represents the median whereas the inverted triangle represents the mean. *p*-values: ns(p>0.05), *(p<0.05), **(p<0.01),*** (p< 0.001), Welch's *t*-test for parametric test and Wilcoxon rank-sum test for non-parametric test.

Past studies found that the eATP and eADP response were concentration-dependent. Here we tested a lower concentration of 0.1 mM eATP as an agonist to detect any changes in the $[Ca^{2+}]_{cyt}$ response. The biphasic $[Ca^{2+}]_{cyt}$ pattern remained similar to the 1 mM eATP test albeit with a lower $[Ca^{2+}]_{cyt}$ amplitude (Figure 4.23 A). The touch peak response upon application of 0.1 mM eATP treatment showed consistent similarity between Col-0 (0.50±0.06 µM) and *Atann1/4* (0.56±0.06 µM) as in previous tests (Figure 4.23 B). The first

peak response also remained consistent with Col-0 (0.16±0.01 μM) having statistically lower $[Ca^{2+}]_{cyt}$ response than the *Atann1/4* (0.22±0.01 μM) (Figure 4.23 C). Analysis of the second peak (Col-0 0.18±0.005 μM; *Atann1/4* 0.18±0.005 μM) and the total $[Ca^{2+}]_{cyt}$ increased (Col-0 12.94±0.51 μM; *Atann1/4* 14.22±0.52 μM) found insignificant differences between Col-0 and *Atann1/4* (Figure 4.23 D, E).

Comparison of *Atann1/4* double mutant results with *Atann1* results in 0.1 mM eATP treatment (Chapter 3.2.9; Figure 3.24) was carried out to see the effect of *AtANN4* mutation. Mutation of *AtANN4* alone might have an effect as in control treatment, *Atann1/4* double mutant produced touch peak value (*Atann1* 0.15±0.03 μM; *Atann1/4* 0.68±0.09 μM) and total $[Ca^{2+}]_{cyt}$ increase (*Atann1* 0.41±0.32 μM; *Atann1/4* 3.9±0.49 μM) that were significantly higher than the *Atann1* single mutant (Figure 4.24 A, B). This notion is supported by the comparison done in 0.1 mM eATP treatment where *Atann1/4* again showed significantly higher $[Ca^{2+}]_{cyt}$ response in the touch peak value (*Atann1* 0.32±0.08 μM; *Atann1/4* 0.56±0.06 μM) (Figure 4.24 C), the first peak (*Atann1* 0.14±0.02 μM; *Atann1/4* 0.22±0.01 μM) (Figure 4.24 D), second peak (*Atann1* 0.13±0.01 μM; *Atann1/4* 0.18±0.005 μM) (Figure 4.24 E) and the total $[Ca^{2+}]_{cyt}$ accumulated (*Atann1* 10.27±1.15 μM; *Atann1/4* 14.22±0.52 μM) (Figure 4.24F).

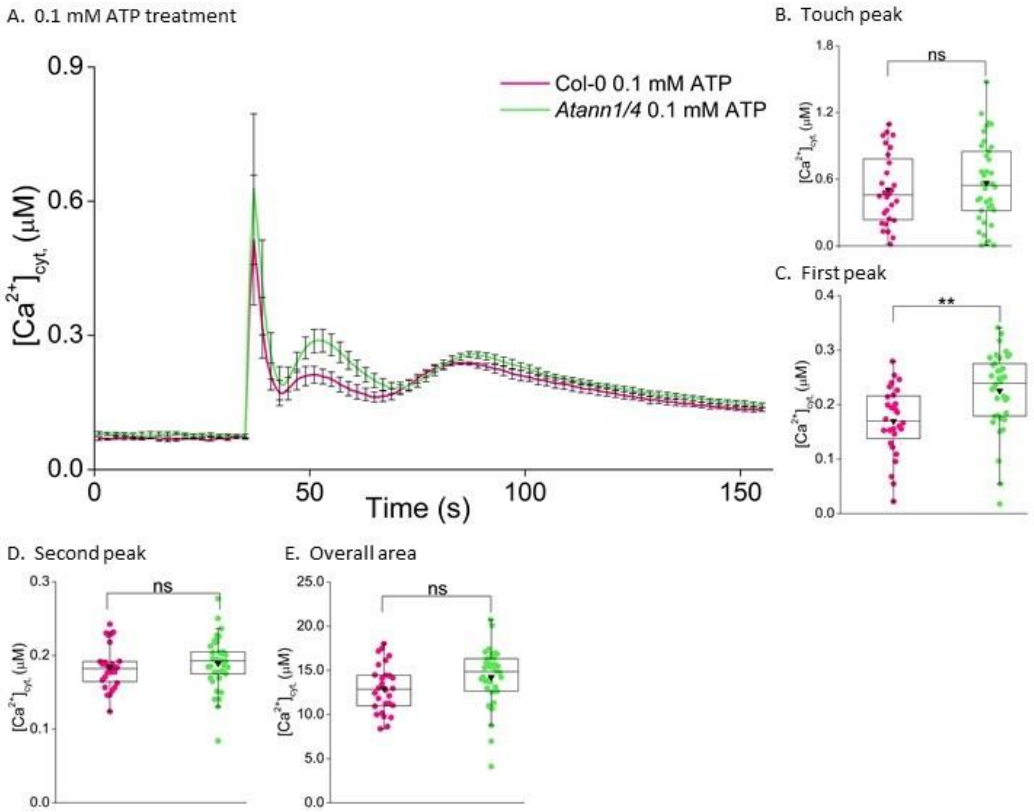

Figure 4.23: **A lower concentration of eATP evokes $[Ca^{2+}]_{cyt}$ signatures in whole roots that are negatively regulated by AtANN4 at the first peak.** Time course data show 7-day-old Col-0 and *Atann1/4* double mutant whole roots response towards 0.1 mM eATP (A). The $[Ca^{2+}]_{cyt}$ responses were recorded for 155 s and treatment was added at the 35th second. Time course data were from the means ± SEM of 3 independent trials, with n = 23 - 36. Time course analysis of the 0.1 mM eATP treatment is split up into the first peak (C) (42 - 65 s) and the second peak (D) (65 - 155 s) responses, which is the highest value of the peaks that emerged after the touch response (B) (35 - 41 s). The total accumulation of $[Ca^{2+}]_{cyt}$ of Col-0 and *Atann1/4* were determined through the overall area under the curve (H) (35 - 155 s). All calculations carried out were with the baseline (the first 35 seconds of measurement) subtracted. Middle line of the boxplot represents the median whereas the inverted triangle represents the mean. p-values: ns (p>0.05), * (p<0.05), ** (p<0.01), *** (p< 0.001), Welch's t-test for parametric test and Wilcoxon rank-sum test for non-parametric test.

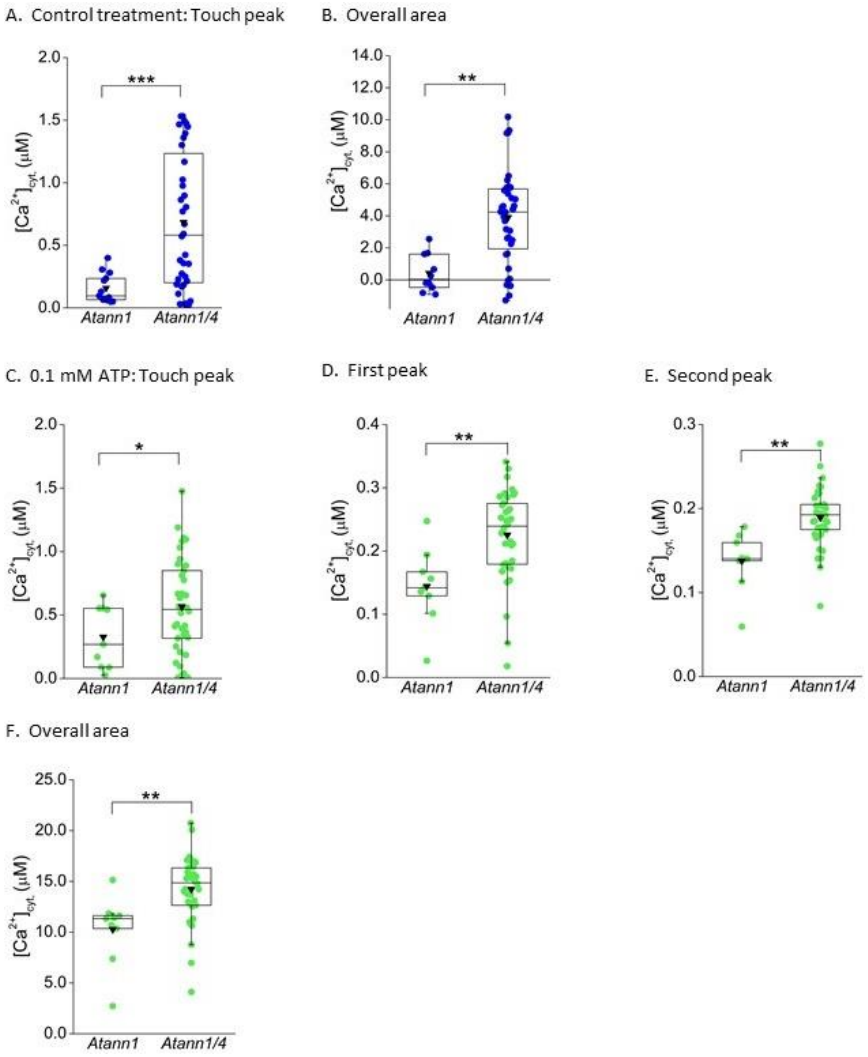

Figure 4.24: ***Atann1/4*** **enhanced $[Ca^{2+}]_{cyt}$ elevation compared to single** ***Atann1*** **mutant in 0.1 mM ATP treatment.** Comparisons of $[Ca^{2+}]_{cyt}$ accumulation were done between *Atann1* and *Atann1/4* for both control and 0.1 mM ATP treatment. Touch peak (A; control, C; 0.1 mM ATP) represents the highest value of the touch response. First peak (D; 0.1 mM ATP) and the second peak (E; 0.1 mM ATP) responses are the highest value of the peaks that emerged after the touch response. The total accumulation of $[Ca^{2+}]_{cyt}$ of all the genotypes were determined through the overall area under the curve from the time course analysis done previously (B; control, F; 0.1 mM ATP). Middle line of the boxplot represents the median whereas the inverted triangle represents the mean. *p*-values: ns($p>0.05$), *($p<0.05$), **($p<0.01$),*** ($p< 0.001$), Welch's *t*-test for parametric test and Wilcoxon rank-sum test for non-parametric test.

The *Atann1/4* mutant in the eATP treatment tests earlier showed opposite results from mutants in *AtANN1* and *AtANN2*. This raised the question of whether this response is also true for the eADP agonist. A similar set of experiments with 1 mM and 0.1 mM eADP was carried out to elucidate this matter. Application of control treatment (2 mM MES/Tris-HCl; 10 mM $CaCl_2$; 0.1 mM KCl) produced a single touch response that lasted for about 15 seconds followed by basal level $[Ca^{2+}]_{cyt}$ response for both Col-0 and *Atann1/4* (Figure 4.25A). The touch peak value (Col-0 0.51±0.09 μM; *Atann1/4* 0.47±0.08 μM) and the total $[Ca^{2+}]_{cyt}$ released proved that the mutation did not interfere with the touch response as both Col-0 (2.30±0.44 μM) and *Atann1/4* (2.05±0.47 μM) showed no significant response from each other in the control treatment (Figure 4.25 B, C).

When challenged with 1 mM eADP treatment, both Col-0 and *Atann1/4* retained the biphasic $[Ca^{2+}]_{cyt}$ signature of nucleotide response after the touch response (Figure 4.25 D). *Atann1/4* (0.50±0.08 μM) whole roots displayed similar touch response as the Col-0 (0.43±0.09) again proved that the mutation did not affect the touch response in eADP treatment (Figure 4.25 E). Analysis of the peaks found that *Atann1/4* supported a statistically higher $[Ca^{2+}]_{cyt}$ response than the Col-0 in both the first peak (Col-0 0.20±0.01 μM; *Atann1/4* 0.25±0.01 μM) and the second peak (Col-0 0.27±0.01 μM; *Atann1/4* 0.31±0.009 μM) (Figure 4.25 F, G). The enhanced $[Ca^{2+}]_{cyt}$ response in *Atann1/4* whole roots again showed when total $[Ca^{2+}]_{cyt}$ of *Atann1/4* (21.58±0.70 μM) accumulated over the recording time was found to be significantly higher than the Col-0 (17.98±0.71 μM) (Figure 4.25 H).

When comparing with the *Atann1* single mutant (Chapter 3.2.2; Figure 3.5), no significant difference was found between *Atann1* single mutant (1.46±0.36 μM) and *Atann1/4* double mutant (2.05±0.47 μM) in the total $[Ca^{2+}]_{cyt}$ accumulation of the control treatment although the touch peak value of *Atann1/4* (0.47±0.08 μM) was significantly higher than the *Atann1* (0.13±0.01 μM) (Figure 4.26 A, B). In the 1 mM eADP treatment however, *AtANN4* mutation proved to produce reductive effect towards *AtANN1* mutation as the *Atann1/4* double mutant evoked statistically higher touch peak value (*Atann1* 0.13±0.02 μM; *Atann1/4* 0.50±0.08 μM) (Figure 4.36 C), first peak value (*Atann1* 0.16±0.008 μM; *Atann1/4* 0.25±0.01 μM) (Figure 4.26 D), second peak value (*Atann1* 0.22±0.01 μM; *Atann1/4* 0.31±0.009 μM) (Figure 4.26 E) and the overall $[Ca^{2+}]_{cyt}$ accumulation (*Atann1* 15.10±0.58 μM; *Atann1/4* 21.58±0.70 μM) than the *Atann1* single mutant (Figure 4.26 F).

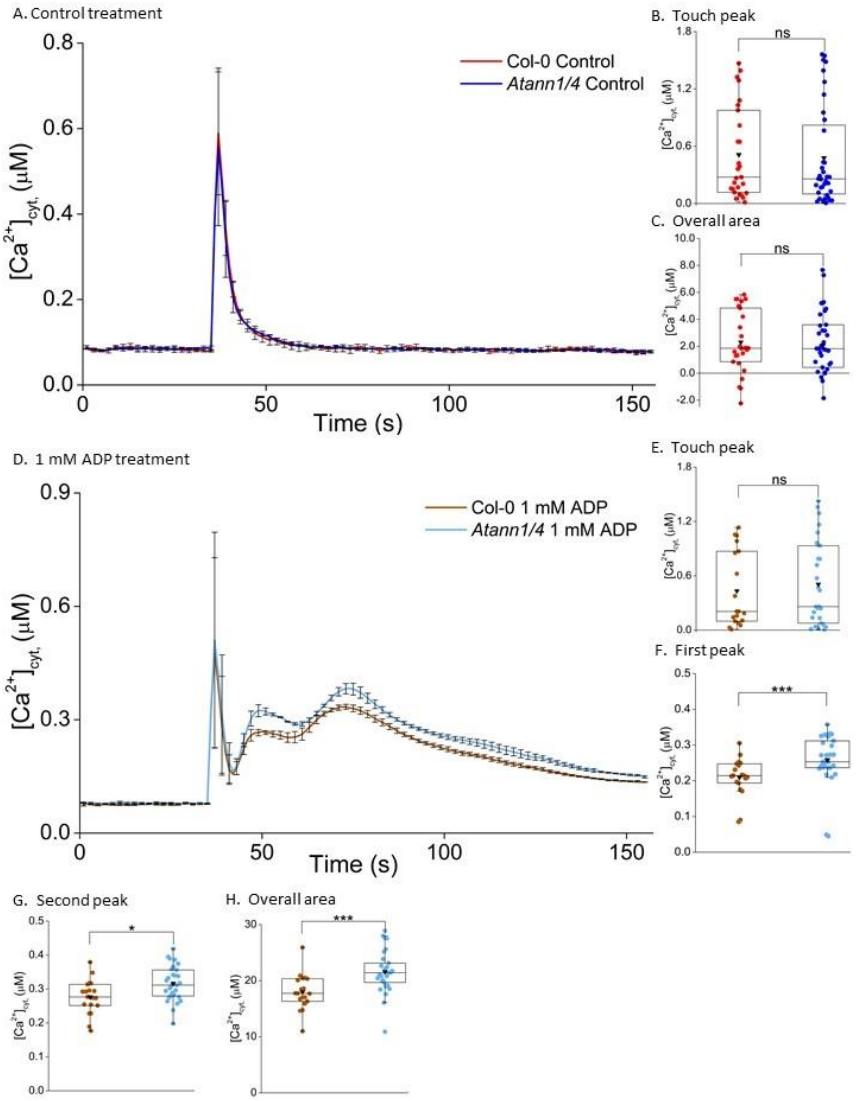

Figure 4.25: **AtANN4 might negatively regulate eADP-induced $[Ca^{2+}]_{cyt}$ elevation at whole roots.** Both Col-0 and *Atann1/4* double mutant 7-day-old whole roots used contain the apo-aequorin protein marker. The $[Ca^{2+}]_{cyt}$ response for the control treatment (A) and 1 mM ADP (D) were recorded for 155 seconds where each treatment was added at the 35th second. This time course data are from the means ± SEM of 3 independent trials, with n = 19 - 36 roots per genotype and treatment. Touch peak (B) represents the highest value of the touch response (35 - 50 s) whereas the overall area (C) is the total area under the curve extracted from the time course data of the control treatment (35 - 155 s). Time course analysis of the 1 mM ADP treatment is split up into the first peak (F) (41 - 59 s) and the second peak (G) (59 - 155 s) responses, which is the highest value of the peaks that emerged after the touch response (E) (35 - 41 s). The total accumulation of $[Ca^{2+}]_{cyt}$ of Col-0 and *Atann1/4* were determined through the overall area under the curve (H) (35 - 155 seconds). All calculations carried out are with the baseline (the first 35 seconds of measurement) subtracted. Middle line of the boxplot represents the median whereas the inverted triangle represents the mean. p-values: ns(p>0.05), *(p<0.05), **(p<0.01),*** (p< 0.001), Welch's t-test for parametric test and Wilcoxon rank-sum test for non-parametric test.

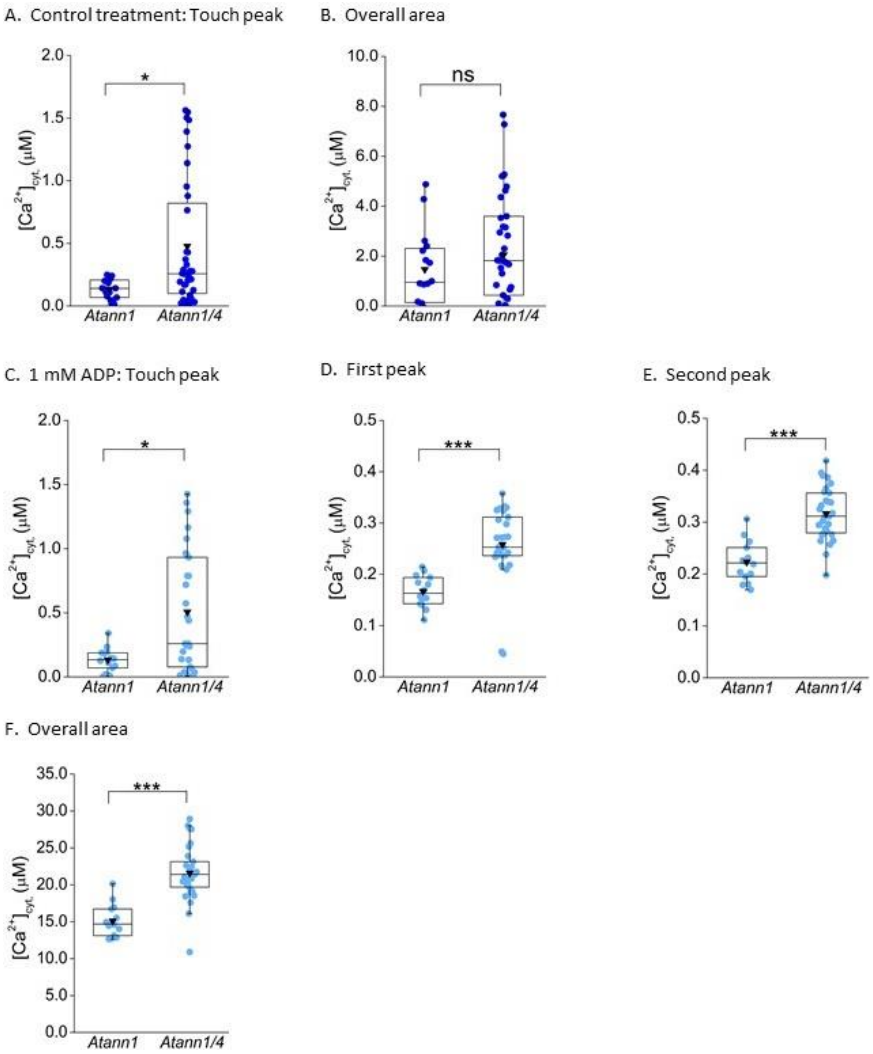

Figure 4.26: Absence of both AtANN1 and AtANN4 enhanced $[Ca^{2+}]_{cyt}$ elevation compared to single *Atann1* mutant in 1 mM ADP treatment. Comparisons of $[Ca^{2+}]_{cyt}$ accumulation were done between *Atann1* and *Atann1/4* for both control and 1 mM ADP treatment. Touch peak (A; control, C; 1 mM ATP) represents the highest value of the touch response. First peak (D; 1 mM ADP) and the second peak (E; 1 mM ADP) responses are the highest value of the peaks that emerged after the touch response. The total accumulation of $[Ca^{2+}]_{cyt}$ of all the genotypes were determined through the overall area under the curve from the time course analysis done previously (B; control, F; 1 mM ADP). Middle line of the boxplot represents the median whereas the inverted triangle represents the mean. *p*-values: ns(p>0.05), *(p<0.05), **(p<0.01),*** (p< 0.001), Welch's *t*-test for parametric test and Wilcoxon rank-sum test for non-parametric test.

The experiment was repeated with a lower concentration of eADP (0.1 mM) to determine the effect of concentration. Comparable to the 1 mM eADP treatment test, both Col-0 and *Atann1/4* whole roots exhibited the $[Ca^{2+}]_{cyt}$ biphasic pattern after the touch response with Col-0 showing lower amplitude (Figure 4.27 A). The touch peak $[Ca^{2+}]_{cyt}$ response remained insignificant between Col-0 (0.25±0.05 µM) and *Atann1/4* (0.26±0.04

μM) (Figure 4.27 B). Contrary to the 1 mM concentration test, Col-0 whole roots $[Ca^{2+}]_{cyt}$ response in the first peak (Col-0 0.17±0.01 μM; *Atann1/4* 0.19±0.01 μM) and the second peak (Col-0 0.22±0.01 μM; *Atann1/4* 0.23±0.008 μM) were not significantly different from the *Atann1/4* when challenged with 0.1 mM eADP (Figure 4.27 C, D). Although over the time course the $[Ca^{2+}]_{cyt}$ of *Atann1/4* (16.80±0.65 μM) seems to be higher than the Col-0 (15.34±0.78 μM), analysis on the total $[Ca^{2+}]_{cyt}$ accumulated showed no significant difference between the two genotypes (Figure 4.27 E).

Previously we have tested *Atann1* whole roots with lower 0.1 mM eADP treatment (Chapter 3.2.9; Figure 3.25). Here we compare the results of *Atann1* with *Atann1/4* in the control and 0.1 mM eADP treatment in order to look at the effect of *AtANN4* mutation. Control treatment showed no significant difference between *Atann1* and *Atann1/4* in the touch peak value (*Atann1* 0.29±0.05 μM; *Atann1/4* 0.47±0.08 μM) and the overall $[Ca^{2+}]_{cyt}$ accumulated (*Atann1* 2.6±0.39 μM; *Atann1/4* 2.05±0.47 μM) confirming that the mutations and the background solution has no effect on the $[Ca^{2+}]_{cyt}$ response (Figure 4.28 A, B). Touch peak response in the 0.1 mM eADP treatment also showed similar $[Ca^{2+}]_{cyt}$ value between *Atann1* (0.33±0.07 μM) and *Atann1/4* (0.26±0.04 μM) (Figure 4.28 C). Mutation of *AtANN4* however showed an effect in 0.1 mM eADP treatment as the *Atann1/4* double mutant produced significantly higher first peak (*Atann1* 0.17±0.009 μM; *Atann1/4* 0.19±0.01 μM) (Figure 4.28 D), second peak (*Atann1* 0.16±0.01 μM; *Atann1/4* 0.23±0.008 μM) (Figure 4.28 E), and the total $[Ca^{2+}]_{cyt}$ accumulation (*Atann1* 13.99±0.68 μM; *Atann1/4* 16.8±0.65 μM) compared to the single *Atann1* mutant (Figure 4.28 F).

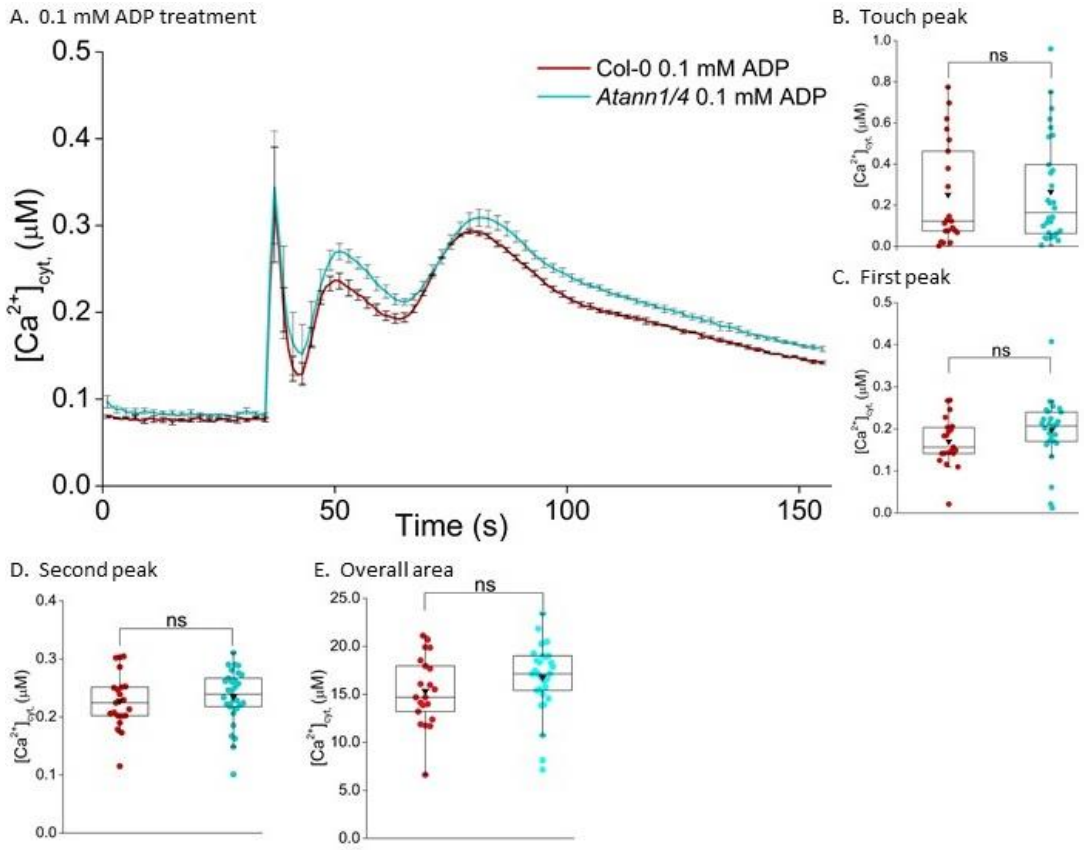

Figure 4.27: **A lower concentration eADP causes accumulationof $[Ca^{2+}]_{cyt}$ in whole roots that is slightly impaired by AtANN4.** Time course data show 7-day-old Col-0 and *Atann1/4* double mutant whole roots response towards 0.1 mM eADP (A). The $[Ca^{2+}]_{cyt}$ responses were recorded for 155 s and treatment was added at the 35th second. Time course data were from the means ± SEM of 3 independent trials, with n = 21 - 36. Time course analysis of the 0.1 mM eADP treatment is split up into the first peak (C) (42 - 66 s) and the second peak (D) (66 - 155 s) responses, which is the highest value of the peaks that emerged after the touch response (B) (35 - 42 s). The total accumulation of $[Ca^{2+}]_{cyt}$ of Col-0 and *Atann1/4* were determined through the overall area under the curve (H) (35 - 155 s). All calculations carried out were with the baseline (the first 35 seconds of measurement) subtracted. Middle line of the boxplot represents the median whereas the inverted triangle represents the mean. p-values: ns (p>0.05), * (p<0.05), ** (p<0.01), *** (p< 0.001), Welch's t-test for parametric test and Wilcoxon rank-sum test for non-parametric test.

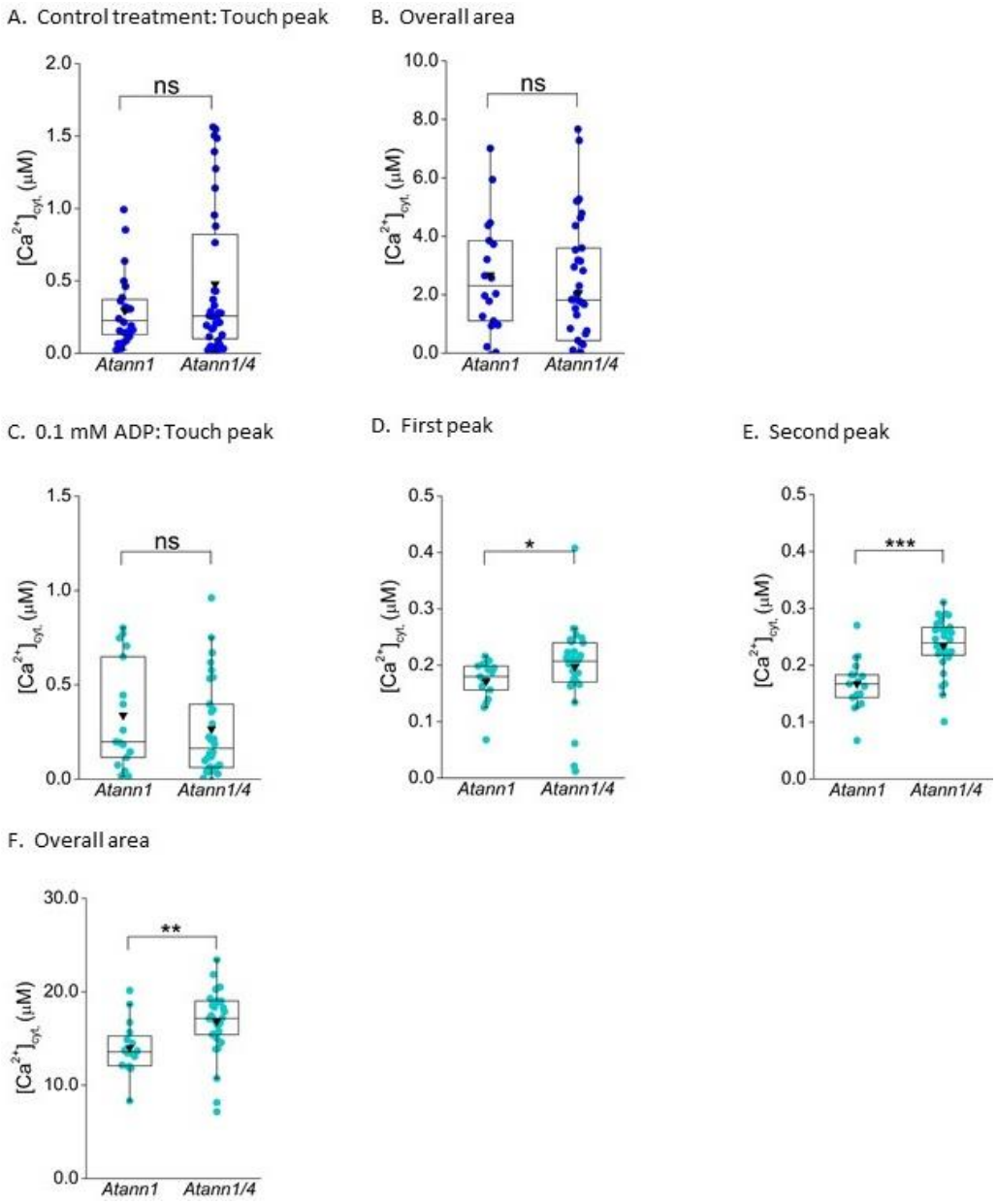

Figure 4.28: *Atann1/4* produced significantly higher $[Ca^{2+}]_{cyt}$ compared to single *Atann1* mutant in 0.1 mM ADP treatment. Comparisons of $[Ca^{2+}]_{cyt}$ accumulation were done between *Atann1* and *Atann1/4* for both control and 0.1 mM ADP treatment. Touch peak (A; control, C; 0.1 mM ADP) represents the highest value of the touch response. First peak (D; 0.1 mM ADP) and the second peak (E; 0.1 mM ADP) responses are the highest value of the peaks that emerged after the touch response. The total accumulation of $[Ca^{2+}]_{cyt}$ of all the genotypes were determined through the overall area under the curve from the time course analysis done previously (B; control, F; 0.1 mM ADP). Middle line of the boxplot represents the median whereas the inverted triangle represents the mean. *p*-values: ns(p>0.05), *(p<0.05), **(p<0.01),*** (p< 0.001), Welch's *t*-test for parametric test and Wilcoxon rank-sum test for non-parametric test.

4.2.5 AtANN1, AtANN2 and AtANN4 together are important in mediating eATP and eADP-induced $[Ca^{2+}]_{cyt}$ accumulation at whole root level

The tests carried out so far have shown AtANN1, AtANN2 and AtANN4 have a role in mediating the eATP and eADP response although the mechanisms are still unclear. AtANN1 and AtANN2 might be the channels that drive the $[Ca^{2+}]_{cyt}$ increase but it was also clear that the absence of both AtANN1 and AtANN4 acted as an enhancer to the $[Ca^{2+}]_{cyt}$ accumulation especially under the eADP signal which might suggest negative regulation. Due to some technical problems, we were not yet able to test a *Atann4* single mutant in the previous tests. In order to get a clearer picture of the role of these annexin genes, we tested *Atann1/2/4* triple T-DNA insertion knock-out mutant with eATP and eADP agonists to look into the changes in $[Ca^{2+}]_{cyt}$. The mutant plants were generated through crossing by Dr. Siân Richards (University of Cambridge). Genotyping and transformation to express (apo)aequorin was done by Dr. Katie Wilkins (University of Cambridge).

Seven-day-old excised whole roots of Col-0 and *Atann1/2/4* were incubated with coelenterazine overnight before $[Ca^{2+}]_{cyt}$ measurement was carried out as explained in Chapter 2.6.1. Control solution (2 mM MES/Tris-HCl; 10 mM $CaCl_2$; 0.1 mM KCl) tested showed a single touch response by each genotype (Figure 4.29 A). There were no significant differences between Col-0 and *Atann1/2/4* triple mutants in the touch peak value (Col-0 0.50±0.009 μM; *Atann1/2/4* 0.36±0.05 μM) and the total $[Ca^{2+}]_{cyt}$ released (Col-0 4.74±0.81 μM; *Atann1/2/4* 2.58±0.41 μM) in the control treatment (Figure 4.29 B). This ensured that the mutation of *AtANN1*, *AtANN2* and *AtANN4* did not have any influence on the initial touch response. Upon addition of 1 mM eATP treatment, Col-0 and *Atann1/2/4* samples maintained the biphasic $[Ca^{2+}]_{cyt}$ signature after the touch peak as found in previous tests (Figure 4.12 C; Figure 4.21 C). In contrast to the control solution test, *Atann1/2/4* (0.21±0.02 μM) produced significantly lower touch peak than the Col-0 (0.34±0.05 μM) indicating the possible involvement of these annexins in mechanical stimulation (Figure 4.29 D). Detailed analysis of the peaks revealed that the *Atann1/2/4* samples were significantly impaired in driving the $[Ca^{2+}]_{cyt}$ increase in the first peak (Col-0 0.21±0.01 μM; *Atann1/2/4* 0.12±0.009 μM) and the second peak (Col-0 0.22±0.009 μM; *Atann1/2/4* 0.13±0.006 μM) (Figure 4.29 E, F). Similarly, the total $[Ca^{2+}]_{cyt}$ accumulated by *Atann1/2/4* (8.88±0.44 μM) was significantly impaired compared to the Col-0 (16.43±0.79 μM) (Figure 4.29 G).

Since we have previously done an experiment on *Atann1/2* (Chapter 4.2.3; Figure 4.12) and *Atann1/4* (Chapter 4.2.4; Figure 4.21) double mutant whole roots with 1 mM eATP, we compared the results between the double mutants with the *Atann1/2/4* triple mutant to see the effect of both *AtANN2* and *AtANN4* mutations. Control treatment showed no significant difference in the touch peak response between *Atann1/2* (0.23±0.04 μM) and *Atann1/2/4* (0.36±0.05 μM) but *Atann1/4* (0.68±0.09 μM) showed significantly higher touch peak response than the *Atann1/2/4* mutant (Figure 4.30 A). Both *Atann1/2* (2.82±0.7 μM) and *Atann1/4* (3.90±0.49 μM) double mutant however evoked no significant difference compared to the *Atann1/2/4* (2.58±0.41 μM) in the overall accumulated $[Ca^{2+}]_{cyt}$ by the control treatment (Figure 4.30 B). Touch response in the 1 mM eATP treatment showed significantly lower touch peak by *Atann1/2* (0.06±0.01 μM) than the *Atann1/2/4* (0.21±0.02 μM) but *Atann1/4* (0.32±0.04) showed significantly higher touch peak than the *Atann1/2/4* (Figure 4.30 C). *Atann1/2* double mutant revealed similar level of $[Ca^{2+}]_{cyt}$ with *Atann1/2/4* in the first peak (*Atann1/2* 0.10±0.02 μM; *Atann124* 0.12±0.009 μM) (Figure 4.30 D) and the total $[Ca^{2+}]_{cyt}$ accumulation (*Atann1/2* 10.9±1.47 μM; *Atann1/2/4* 8.88±0.44 μM) (Figure 4.30 F). The second peak value however showed significantly higher *Atann1/2* (0.19±0.02) $[Ca^{2+}]_{cyt}$ production than the *Atann1/2/4* (0.13±0.006 μM) (Figure 4.30 E). *AtANN4* mutation however exhibited a contrasting effect as the *Atann1/4* double mutant produced significantly higher first peak (0.26±0.01 μM), second peak (0.26±0.008 μM) and the total $[Ca^{2+}]_{cyt}$ accumulation (20.32±0.67 μM) compared to the *Atann1/2/4* triple mutant.

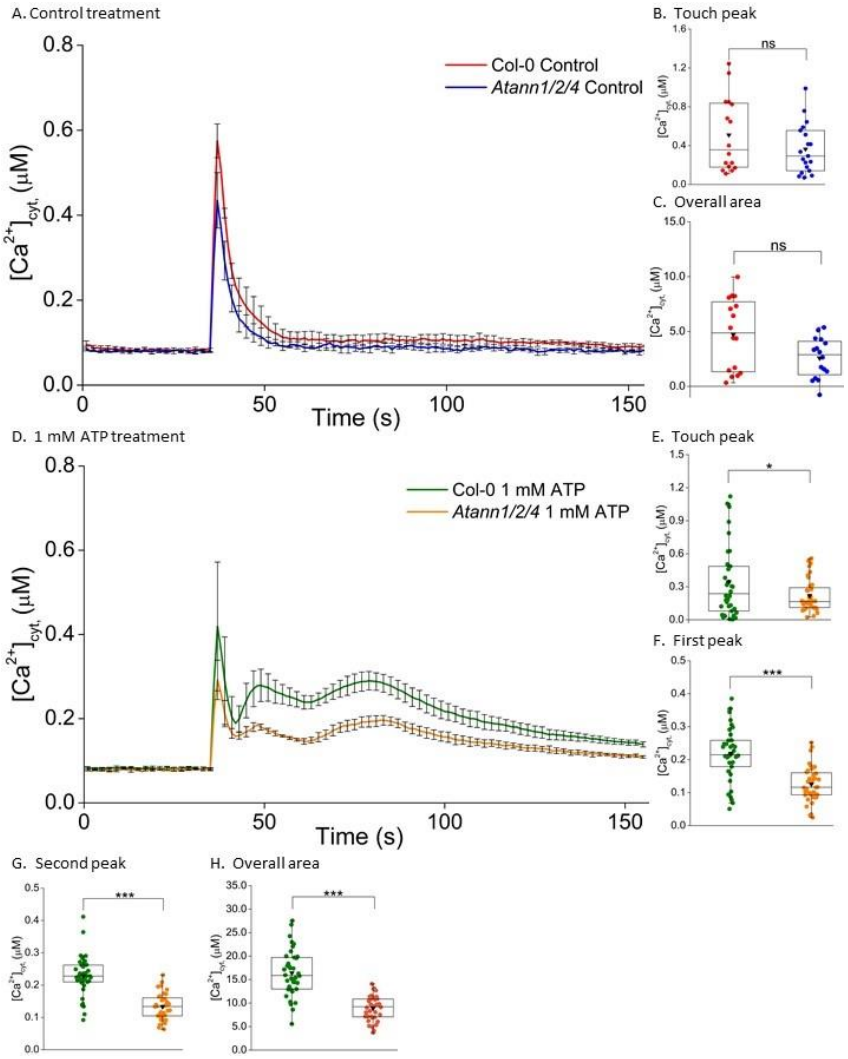

Figure 4.29: **The mutation of AtANN1, AtANN2 and AtANN4 impairs the $[Ca^{2+}]_{cyt}$ elevation by 1 mM eATP at whole root level.** Both Col-0 and *Atann1/2/4* triple mutant 7-day-old whole roots contained cytosolic apo-aequorin. The $[Ca^{2+}]_{cyt}$ response for the control treatment (A) and 1 mM eATP (D) were recorded for 155 seconds where each treatment was added at the 35th second. These time course data are from the means ± SEM of 3 independent trials, with n = 16 - 38 roots per genotype and treatment. Touch peak (B) represents the highest value of the touch response (35 - 50 s) whereas the overall area (C) is the total area under the curve extracted from the time course data of the control treatment (35 - 155 s). Time course analysis of the 1 mM eATP treatment is split up into the first peak (F) (41 - 63 s) and the second peak (G) (63 - 155 s) responses, which is the highest value of the peaks that emerged after the touch response (E) (35 - 41 s). The total accumulation of $[Ca^{2+}]_{cyt}$ of Col-0 and *Atann1/2/4* were determined through the overall area under the curve (H) (35 - 155 s). All calculations carried out are with the baseline (the first 35 s of measurement) subtracted. Middle line of the boxplot represents the median whereas the inverted triangle represents the mean. p-values: ns (p>0.05), * (p<0.05), ** (p<0.01), *** (p< 0.001), Welch's t-test for parametric test and Wilcoxon rank-sum test for non-parametric test.

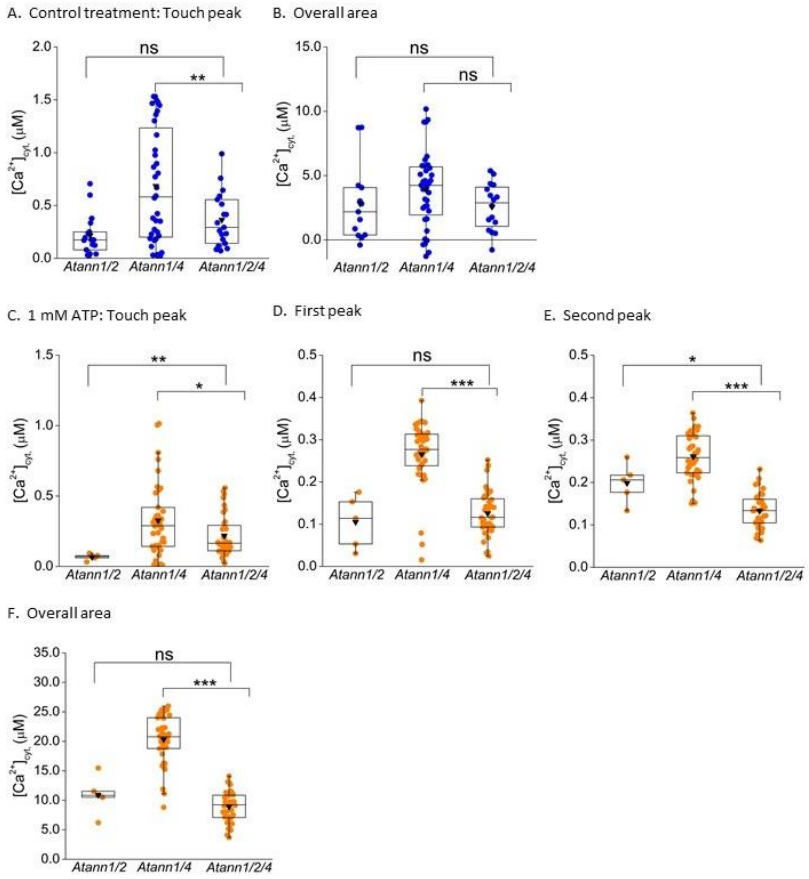

Figure 4.30: ***Atann1/2/4* $[Ca^{2+}]_{cyt}$ elevation is impaired compared to *Atann1/4* mutant in 1 mM ATP treatment.** Comparisons of $[Ca^{2+}]_{cyt}$ accumulation were done between *Atann1/2*, *Atann1/4* and *Atann1/2/4* for both control and 1 mM ATP treatment. Touch peak (A; control, C; 1 mM ATP) represents the highest value of the touch response. First peak (D; 1 mM ATP) and the second peak (E; 1 mM ATP) responses are the highest value of the peaks that emerged after the touch response. The total accumulation of $[Ca^{2+}]_{cyt}$ of all the genotypes were determined through the overall area under the curve from the time course analysis done previously (B; control, F; 1 mM ATP). Middle line of the boxplot represents the median whereas the inverted triangle represents the mean. *p*-values: ns(p>0.05), *(p<0.05), **(p<0.01),*** (p< 0.001), Welch's *t*-test for parametric test and Wilcoxon rank-sum test for non-parametric test.

With the lower eATP concentration tested (0.1 mM), Col-0 and *Atann1/2/4* retained the $[Ca^{2+}]_{cyt}$ biphasic signature after the touch response with lower amplitude than the 1 mM eATP test (Figure 4.31 A). The touch peak analysis showed significantly lower touch $[Ca^{2+}]_{cyt}$ response of the *Atann1/2/4* (0.22±0.02 µM) compared to the Col-0 (0.36±0.04 µM) as previously found with the 1 mM eATP test (Figure 4.31 B). Similar observations were found with the first peak (Col-0 0.15±0.01 µM; *Atann1/2/4* 0.08±0.007 µM) and the second peak (Col-0 0.13±0.009 µM; *Atann1/2/4* 0.07±0.003 µM) where *Atann1/2/4* was significantly

impaired compared to the Col-0 (Figure 4.31 C, D). Overall, *AtANN1*, *AtANN2* and *AtANN4* are required in mediating the eATP-induced $[Ca^{2+}]_{cyt}$ response as the absence of these annexin genes caused significant reduction in total $[Ca^{2+}]_{cyt}$ accumulation (Col-0 4.35±0.29 μM; *Atann1/2/4* 9.40±0.72 μM) (Figure 4.31 E).

Comparison with the results from *Atann1/2* (Chapter 4.2.3; Figure 4.13) and *Atann1/4* (Chapter 4.2.4; Figure 4.23) double mutant in 0.1 mM eATP tests were done in other to confirm the effect of the mutations. Comparison in the initial control treatment showed *Atann1/2* to produce similar touch peak (0.23±0.04 μM) and overall $[Ca^{2+}]_{cyt}$ accumulation (2.82±0.71 μM) with *Atann1/2/4* (touch peak 0.36±0.05 μM; total $[Ca^{2+}]_{cyt}$ 2.58±0.41 μM) whereas *Atann1/4* produced significantly higher touch peak response (0.68±0.09 μM) but similar level of total $[Ca^{2+}]_{cyt}$ accumulation (3.9±0.49 μM) (Figure 4.32 A, B). In the 0.1 mM eATP treatment, *Atann1/2* showed mixed results as it evoked significantly lower touch peak response (*Atann1/2* 0.10±0.02 μM; *Atann1/2/4* 0.22±0.02 μM) (Figure 4.32 C) but significantly higher second peak value (*Atann1/2* 0.13±0.01 μM; *Atann1/2/4* 0.07±0.003 μM) (Figure 4.32 E) and the total $[Ca^{2+}]_{cyt}$ increase (*Atann1/2* 7.56±0.73 μM; *Atann1/2/4* 4.35±0.29 μM) (Figure 4.32 F) compared to the *Atann1/2/4* triple mutant. First peak value of *Atann1/2* (0.09±0.01 μM) showed no significant difference with the *Atann1/2/4* (0.08±0.007 μM) (Figure 4.32 D). *Atann1/4* on the other hand produced consistent results with significantly higher production of $[Ca^{2+}]_{cyt}$ accumulation at the touch peak (*Atann1/4* 0.56±0.06 μM; *Atann1/2/4* 0.22±0.02 μM), first peak (*Atann1/4* 0.22±0.01 μM; *Atann1/2/4* 0.08±0.007 μM), second peak (*Atann1/4* 0.18±0.005 μM; *Atann1/2/4* 0.07±0.003 μM) and the overall $[Ca^{2+}]_{cyt}$ increase (*Atann1/4* 14.22±0.52 μM; *Atann1/2/4* 4.35±0.29 μM) in comparison to the *Atann1/2/4* triple mutant.

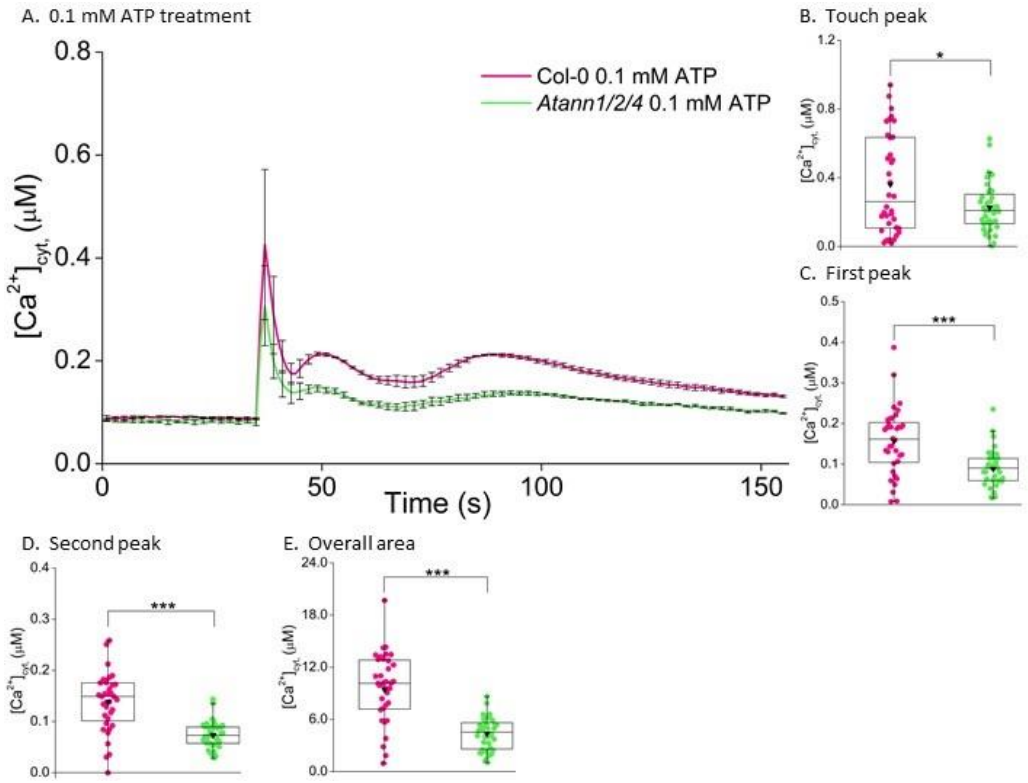

Figure 4.31: **A lower concentration of eATP evoked $[Ca^{2+}]_{cyt}$ signatures in whole roots regulated by AtANN1, AtANN2 and AtANN4.** Time course data show 7-day-old Col-0 and *Atann1/2/4* triple mutant whole roots response towards 0.1 mM eATP (A). The $[Ca^{2+}]_{cyt}$ responses were recorded for 155 s and treatment was added at the 35th second. Time course data were from the means ± SEM of 3 independent trials, with *n* =16 - 40. Time course analysis of the 0.1 mM eATP treatment is split up into the first peak (C) (42 - 65 s) and the second peak (D) (65 - 155 s) responses, which is the highest value of the peaks that emerged after the touch response (B) (35 - 41 s). The total accumulation of $[Ca^{2+}]_{cyt}$ of Col-0 and *Atann1/2/4* were determined through the overall area under the curve (H) (35 - 155 s). All calculations carried out were with the baseline (the first 35 seconds of measurement) subtracted. Middle line of the boxplot represents the median whereas the inverted triangle represents the mean. *p*-values: ns (p>0.05), * (p<0.05), ** (p<0.01), *** (p< 0.001), Welch's *t*-test for parametric test and Wilcoxon rank-sum test for non-parametric test.

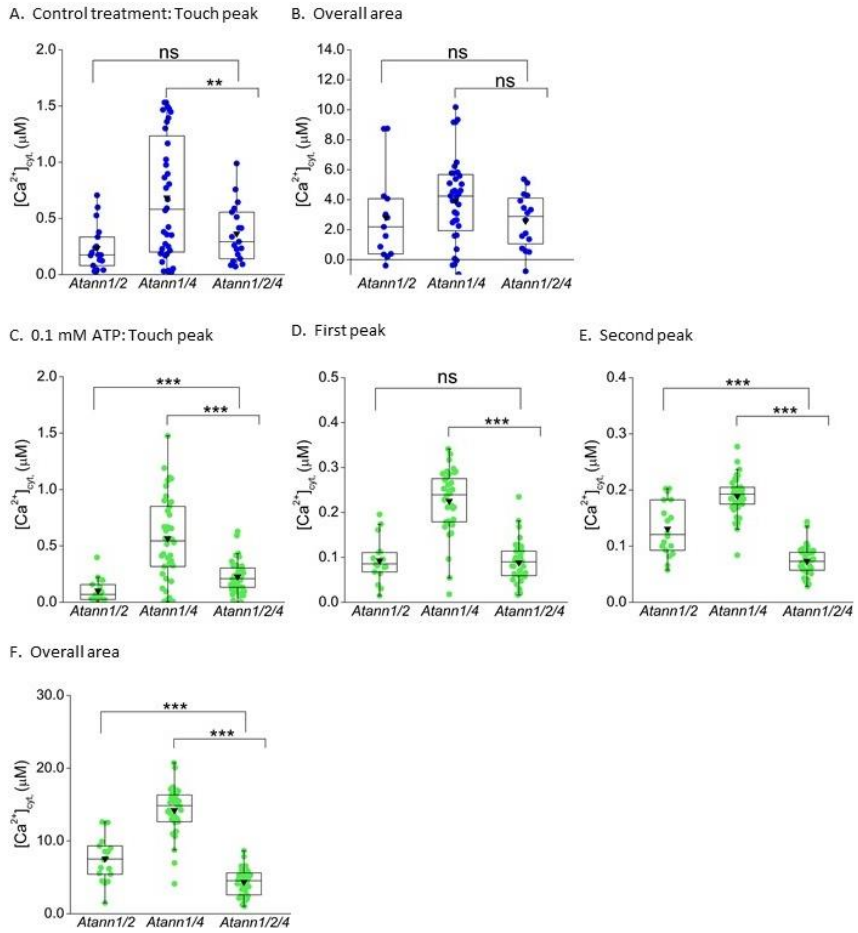

Figure 4.32: ***Atann1/2/4* showed significant reduction in $[Ca^{2+}]_{cyt}$ elevation compared to *Atann1/2* and *Atann1/4* mutant in 0.1 mM ATP treatment.** Comparisons of $[Ca^{2+}]_{cyt}$ accumulation were done between *Atann1/2*, *Atann1/4* and *Atann1/2/4* for both control and 0.1 mM ATP treatment. Touch peak (A; control, C; 0.1 mM ATP) represents the highest value of the touch response. First peak (D; 0.1 mM ATP) and the second peak (E; 0.1 mM ATP) responses are the highest value of the peaks that emerged after the touch response. The total accumulation of $[Ca^{2+}]_{cyt}$ of all the genotypes were determined through the overall area under the curve from the time course analysis done previously (B; control, F; 0.1 mM ATP). Middle line of the boxplot represents the median whereas the inverted triangle represents the mean. *p*-values: ns($p>0.05$), *($p<0.05$), **($p<0.01$),*** ($p< 0.001$), Welch's *t*-test for parametric test and Wilcoxon rank-sum test for non-parametric test.

In order to test for the effect of the *AtANN1*, *AtANN2* and *AtANN4* mutations on the eADP-induced response, the test with 7-day-old whole roots was replicated with 1 mM and 0.1 mM eADP. The first control treatment (2 mM MES/Tris-HCl; 10 mM $CaCl_2$; 0.1 mM KCl) application exhibited a single touch response by Col-0 and *Atann1/2/4* before going back to the basal level (Figure 4.33 A). Detailed analysis revealed that Col-0 (0.32±0.07 µM) and *Atann1/2/4* (0.49±0.10 µM) was not significantly different at the touch peak value (Figure 4.33 B). However, *Atann1/2/4* (2.98±0.60 µM) samples showed higher control

solution induced $[Ca^{2+}]_{cyt}$ accumulation compared to the Col-0 (1.72±0.44 μM) which contradicted the result in previous control treatment test (Figure 4.33 C).

Replacing the control with 1 mM eADP treatment exhibited a single touch response followed by the first and the second peak (biphasic) by both Col-0 and *Atann1/2/4* (Figure 4.33 D). Similar to the control treatment, Col-0 (0.48±0.07 μM) and *Atann1/2/4* (0.44±0.05 μM) produced similar touch peak values (Figure 4.33 E). Statistical analysis revealed that *Atann1/2/4* elevation of $[Ca^{2+}]_{cyt}$ was significantly reduced compared to the Col-0 at the first peak (Col-0 0.21±0.01 μM; *Atann1/2/4* 0.12±0.006 μM) and the second peak value (Col-0 0.23±0.01 μM; *Atann1/2/4* 0.16±0.009 μM) (Figure 4.33 F, G). This is also true for the total $[Ca^{2+}]_{cyt}$ accumulated as there was significant difference between the two genotypes tested (Col-0 15.63±0.95 μM, *Atann1/2/4* 10.58±0.51 μM) (Figure 4.33 H).

In the 1 mM eADP test with *Atann1/2* (Chapter 4.2.3; Figure 4.17) and *Atann1/4* (Chapter 4.2.4; Figure 4.25) double mutant whole roots also produced the familiar biphasic pattern. Comparison of these results with the *Atann1/2/4* in 1 mM eADP treatment was done to look at the effect of mutations of *AtANN2* and *AtANN4*. In the control treatment, both *Atann1/2* and *Atann1/4* double mutant showed no significant differences in the touch peak value (*Atann1/2* 0.45±0.08 μM; *Atann1/4* 0.47±0.04 μM; *Atann1/2/4* 0.42±0.10 μM) and the overall $[Ca^{2+}]_{cyt}$ accumulated (*Atann1/2* 4.33±0.72 μM; *Atann1/4* 2.05±0.47 μM; *Atann1/2/4* 2.98±0.60 μM) compared to the *Atann1/2/4* triple mutant (Figure 4.34 A, B). In 1 mM eADP treatment, *Atann1/2* (0.26±0.05 μM) showed significantly lower touch peak response than the *Atann1/2/4* (0.44±0.05 μM) (Figure 4.34 C). In contrast, *Atann1/2* showed significantly higher first peak value (*Atann1/2* 0.16±0.01 μM; *Atann1/2/4* 0.12±0.006 μM) (Figure 4.34 D) and the total $[Ca^{2+}]_{cyt}$ increase (*Atann1/2* 13.23±0.58 μM; *Atann1/2/4* 10.58±0.51 μM) (Figure 4.34 F). No significant between *Atann1/2* (0.19±0.01 μM) and *Atann1/2/4* (0.16±0.009 μM) was found at the second peak value (Figure 4.34 E). Comparison done between *Atann1/4* and *Atann1/2/4* revealed that *Atann1/4* produced significantly higher first peak (0.25±0.01 μM), second peak (0.31±0.009 μM) and the total $[Ca^{2+}]_{cyt}$ accumulation (21.58±0.70 μM) although the touch peak response (0.50±0.08 μM) was not significantly different from the *Atann1/2/4*.

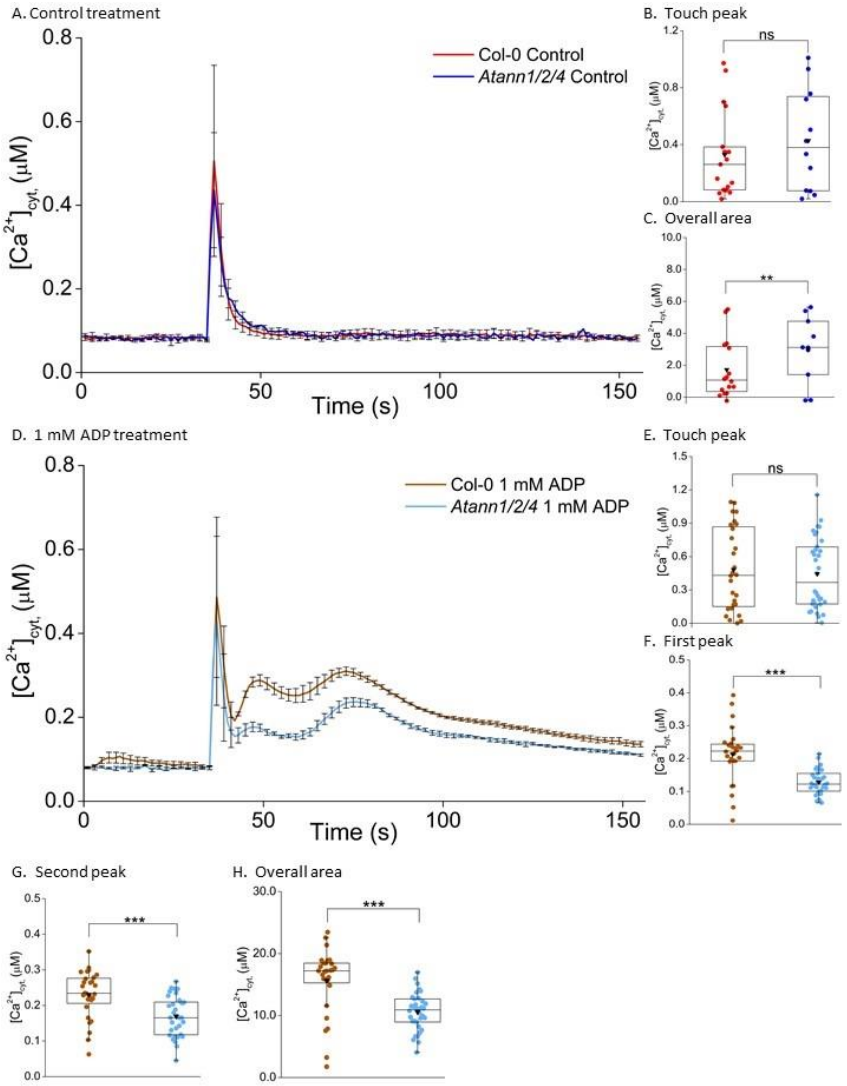

Figure 4.33: **AtANN1, AtANN2 and AtANN4 working together might involved in elevating the $[Ca^{2+}]_{cyt}$ at whole root level by eADP.** Both Col-0 and *Atann1/2/4* triple mutant 7-day-old whole roots used were transformed to be able to express cytosolic apo-aequorin. The $[Ca^{2+}]_{cyt}$ response for the control treatment (A) and 1 mM eADP (D) were recorded for 155 seconds where each treatment was added at the 35th second. This time course data are from the means ± SEM of 3 independent trials, with n = 12 - 34 roots per genotype and treatment. Touch peak (B) represents the highest value of the touch response (35 - 50 s) whereas the overall area (C) is the total area under the curve extracted from the time course data of the control treatment (35 - 155 s). Time course analysis of the 1 mM eADP treatment is split up into the first peak (F) (41 - 59 seconds) and the second peak (G) (59 - 155 seconds) responses, which is the highest value of the peaks that emerged after the touch response (E) (35 - 41 s). The total accumulation of $[Ca^{2+}]_{cyt}$ of Col-0 and *Atann1/2/4* were determined through the overall area under the curve (H) (35 - 155 s). All calculations carried out were with the baseline (the first 35 s of measurement) subtracted. Middle line of the boxplot represents the median whereas the inverted triangle represents the mean. p-values: ns (p>0.05), * (p<0.05), ** (p<0.01),*** (p< 0.001), Welch's t-test for parametric test.

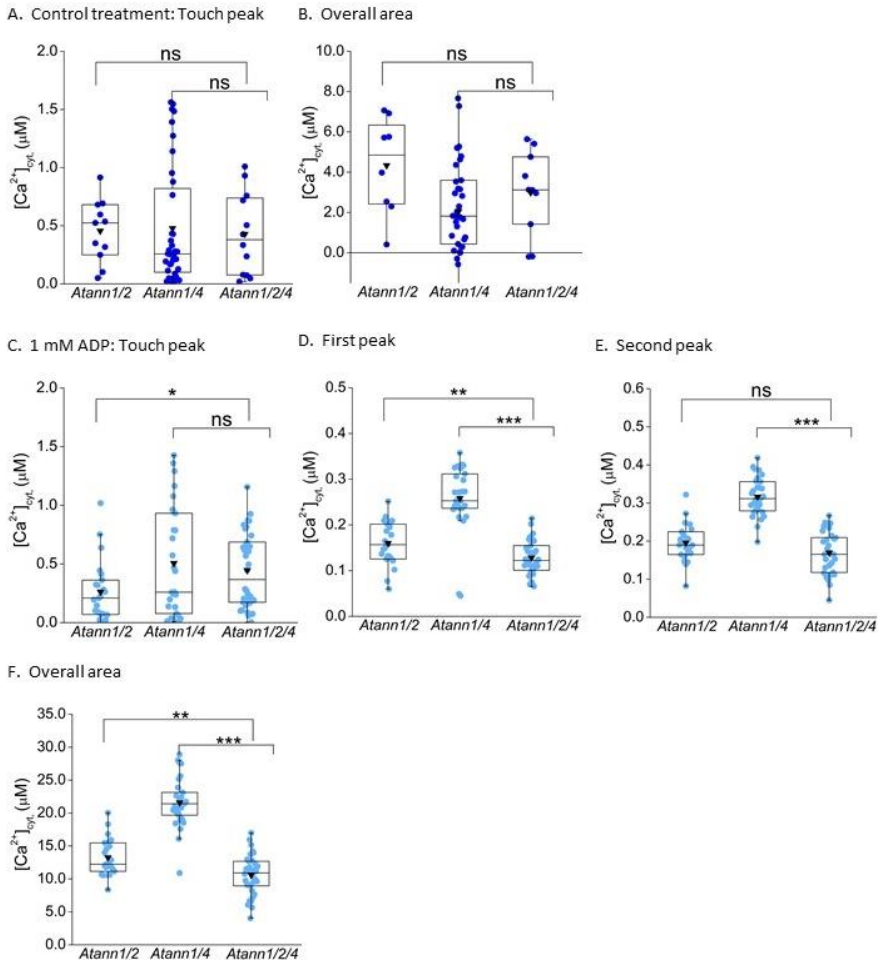

Figure 4.34: **0.1 mM ADP-induced $[Ca^{2+}]_{cyt}$ elevation is lower in *Atann1/2/4* compared to *Atann1/2* and *Atann1/4* mutant in 1 mM ADP treatment.** Comparisons of $[Ca^{2+}]_{cyt}$ accumulation were done between *Atann1/2, Atann1/4* and *Atann1/2/4* for both control and 1 mM ADP treatment. Touch peak (A; control, C; 1 mM ADP) represents the highest value of the touch response. First peak (D; 1 mM ADP) and the second peak (E; 1 mM ADP) responses are the highest value of the peaks that emerged after the touch response. The total accumulation of $[Ca^{2+}]_{cyt}$ of all the genotypes were determined through the overall area under the curve from the time course analysis done previously (B; control, F; 1 mM ADP). Middle line of the boxplot represents the median whereas the inverted triangle represents the mean. *p*-values: ns(p>0.05), *(p<0.05), **(p<0.01),*** (p< 0.001), Welch's *t*-test for parametric test and Wilcoxon rank-sum test for non-parametric test.

Tests with 0.1 mM eADP were also carried out to examine the effect of concentration on the $[Ca^{2+}]_{cyt}$ response. Col-0 and *Atann1/2/4* maintained the eADP-induced biphasic $[Ca^{2+}]_{cyt}$ response in 0.1 mM eADP treatment (Figure 4.35 A). Comparable to the 1 mM eADP test, the touch peak $[Ca^{2+}]_{cyt}$ value evoked by Col-0 (0.26±0.03 µM) was not significantly different from the *Atann1/2/4* mutant (0.21±0.02 µM) in the 0.1 mM eADP treatment (Figure 4.35 B). The first peak (Col-0 0.15±0.01 µM; *Atann1/2/4* 0.08±0.005 µM)

and the second peak (Col-0 0.14±0.006 μM; *Atann1/2/4* 0.08±0.004 μM) value of the *Atann1/2/4* samples however were statistically impaired compared to the Col-0 (Figure 4.35 C,D). Overall, the total $[Ca^{2+}]_{cyt}$ triggered by 0.1 mM eADP showed significant difference between Col-0 (10.69±0.59 μM) and *Atann1/2/4* (5.97±0.27 μM) (Figure 4.35 E). These results with 1 mM and 0.1 mM eADP treatment might suggest that AtANN1, AtANN2 and AtANN4 have important roles in the $[Ca^{2+}]_{cyt}$ responses but this could not be confirmed as there is a possible effect of the control solution.

Comparison with the *Atann1/2* (Chapter 4.2.3; Figure 4.19) and *Atann1/4* (Chapter 4.2.4; Figure 4.27) results was also done at the lower 0.1 mM eADP concentration to determine the effect of *AtANN2* and *AtANN4* mutations at lower agonist concentration. Comparison of the control treatment results showed both *Atann1/2* and *Atann1/4* having similar touch peak value (*Atann1/2* 0.45±0.08 μM; *Atann1/4* 0.47±0.08 μM; *Atann1/2/4* 0.42±0.10 μM) and total $[Ca^{2+}]_{cyt}$ increase (*Atann1/2* 4.22±0.72 μM; *Atann1/4* 2.05±0.47 μM; *Atann1/2/4* 2.98±0.60 μM) with the *Atann1/2/4* triple mutant (Figure 4.36 A, B). This is also true for the touch peak response in the 0.1 mM eADP treatment where both *Atann1/2* (0.26±0.03 μM) and *Atann1/4* (0.26±0.04 μM) double mutant have no significant differences with the *Atann1/2/4* (0.21±0.02 μM) triple mutant (Figure 4.36 C). However, *Atann1/2* and *Atann1/4* produced significantly higher first peak (*Atann1/2* 0.15±0.01 μM; *Atann1/4* 0.19±0.01 μM; *Atann1/2/4* 0.08±0.005 μM) (Figure 4.36 D), second peak (*Atann1/2* 0.15±0.005 μM; *Atann1/4* 0.23±0.008 μM; *Atann1/2/4* 0.08±0.004 μM) (Figure 4.36 E) and total $[Ca^{2+}]_{cyt}$ accumulation (*Atann1/2* 11.66±0.61 μM; *Atann1/4* 16.8±0.65 μM; *Atann1/2/4* 5.97±0.27 μM) compared to the *Atann1/2/4* triple mutant (Figure 4.36 F).

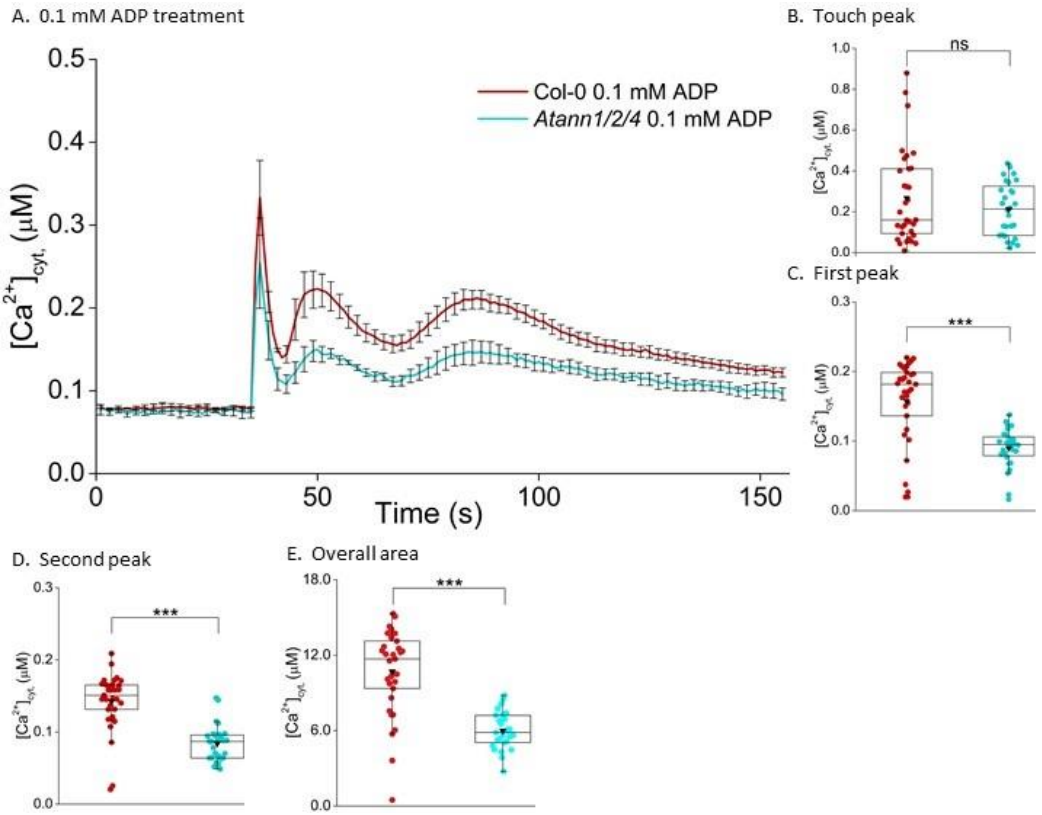

Figure 4.35: **A lower concentration eADP causes accumulation of $[Ca^{2+}]_{cyt}$ in whole roots that might depend on AtANN1, AtANN2 and AtANN4.** Time course data show 7-day-old Col-0 and *Atann1/2/4* triple mutant whole roots response towards 0.1 mM eADP (A). Both Col-0 and *Atann1/2/4* triple mutant 7-day-old whole roots used were transformed to be able to express apo-aequorin protein marker. The $[Ca^{2+}]_{cyt}$ responses were recorded for 155 s and treatment was added at the 35th second. Time course data were from the means ± SEM of 3 independent trials, with n = 12 - 33. Time course analysis of the 0.1 mM ADP treatment is split up into the first peak (C) (42 - 66 s) and the second peak (D) (66 - 155 s) responses, which is the highest value of the peaks that emerged after the touch response (B) (35 - 42 s). The total accumulation of $[Ca^{2+}]_{cyt}$ of Col-0 and *Atann1/2/4* were determined through the overall area under the curve (H) (35 - 155 s). All calculations carried out were with the baseline (the first 35 s of measurement) subtracted. Middle line of the boxplot represents the median whereas the inverted triangle represents the mean. p-values: ns (p>0.05), * (p<0.05), ** (p<0.01), *** (p< 0.001), Welch's t-test for parametric test and Wilcoxon rank-sum test for non-parametric test.

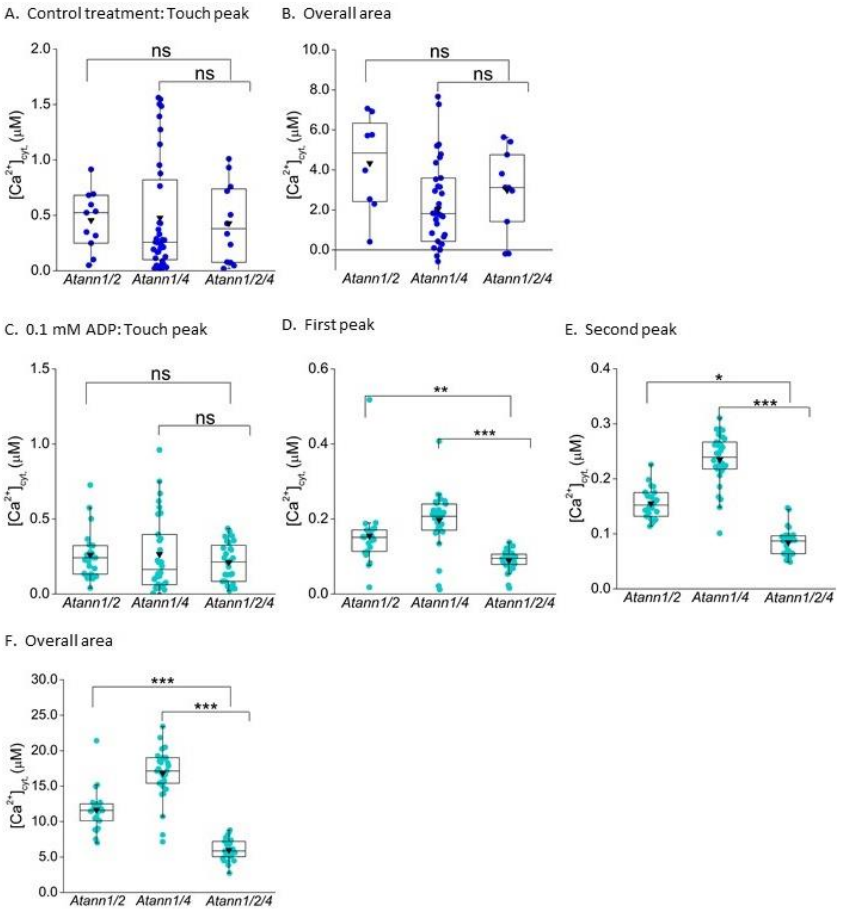

Figure 4.36: **Lower 0.1 mM ADP agonist showed enhanced $[Ca^{2+}]_{cyt}$ reduction in *Atann1/2/4* compared to *Atann1/2* and *Atann1/4* mutant.** Comparisons of $[Ca^{2+}]_{cyt}$ accumulation were done between *Atann1/2*, *Atann1/4* and *Atann1/2/4* for both control and 0.1 mM ADP treatment. Touch peak (A; control, C; 0.1 mM ADP) represents the highest value of the touch response. First peak (D; 0.1 mM ADP) and the second peak (E; 0.1 mM ADP) responses are the highest value of the peaks that emerged after the touch response. The total accumulation of $[Ca^{2+}]_{cyt}$ of all the genotypes were determined through the overall area under the curve from the time course analysis done previously (B; control, F; 0.1 mM ADP). Middle line of the boxplot represents the median whereas the inverted triangle represents the mean. *p*-values: ns(p>0.05), *(p<0.05), **(p<0.01),*** (p< 0.001), Welch's *t*-test for parametric test and Wilcoxon rank-sum test for non-parametric test.

4.2.6 AtANN1, AtANN2 and AtANN4 have roles in regulating the expression of eATP-induced genes *AtRBOHD* and *AtACS6*

Cytosolic calcium accumulation acts as a secondary messenger that conveys the information from the environment especially stress responses or during growth and development to the transcription level (Whalley and Knight, 2013). This is carried out *via* calcium binding proteins that might be regulating transcription factors that eventually

regulate the level of certain genes (Takahashi *et al.*, 2011; Coca and San Segundo, 2010). These lead to the specific response from the plants towards the stimuli. In order to further investigate the involvement of AtANN1, AtANN2 and AtANN4 in mediating the eATP signalling in plants, changes at the transcription level of eATP-induced genes (*AtRBOHD, AtWRKY40, AtACS6*; Choi *et al.*, 2014b; Jeter *et al.*, 2004) were examined in Col-0, *Atann2*, *Atann1/2*, *Atann1/4* and *Atann1/2/4* mutant whole roots. As a control, the expression of *AtANN1*, *AtANN2* and *AtANN4* genes were also quantified. Seven-day-old whole roots were treated with either control solution (2 mM MES/Tris-HCl; 10 mM $CaCl_2$; 0.1 mM KCl) or 1 mM eATP solution for 10 minutes or 30 minutes. The whole roots were then quickly excised in RNAlater solution before being subjected to RNA extraction and real time quantitative Reverse Transcription PCR (qRT-PCR).

Figure 4.24 shows the outcomes from the qRT-PCR carried out on Col-0 and *Atann2* mutant whole roots. *AtANN1* gene transcription was not affected by the absence of AtANN2 as there were no significant differences between Col-0 (control 10 mins 17.50±9.0; control 30 mins 13.84±6.41; ATP 10 mins 14.43±2.4; ATP 30 mins 18.59±14.0) and *Atann2* samples (control 10 mins 8.5±2.3; control 30 mins 9.8±1.7; ATP 10 mins 8.55±0.88; ATP 30 mins 21.22±7.3) in all of the treatments (Figure 4.37 A). *Atann2* samples (control 10 mins 0.06±0.02; control 30 mins 0.04±0.03; ATP 10 mins 0.08±0.03; ATP 30 mins 0.15±0.06) in all four conditions showed significant reduction in the *AtANN2* gene product quantified compared to the Col-0 (control 10 mins 0.92±0.24; control 30 mins 0.98±0.42; ATP 10 mins 0.95±0.22; ATP 30 mins 1.48±0.32). eATP treatment at both 10 minutes and 30 minutes however had no effect on the production of *AtANN2* regardless in Col-0 or *Atann2* samples (Figure 4.37 B). Similar to the test on *AtANN2* gene expression, *AtANN4* gene induction was not altered by the eATP treatment at both 10 minutes (Col-0 0.72±0.37; *Atann2* 1.02±0.13) and 30 minutes period (Col-0 0.91±0.09; *Atann2* 1.48±2.6). *AtANN4* gene production was also unscathed by the absence of AtANN2 as the *AtANN4* expression level quantified in Col-0 samples (control 10 mins 1.05±0.5; control 30 mins 1.56±0.47) was not significantly different from the *Atann2* samples (control 10 mins 0.62±0.3; control 30 mins 0.88±0.6) (Figure 4.37 C).

AtRBOHD is listed as one of the eATP-induced genes in a previous study (Choi *et al.*, 2014b). *Atann2* (control 10 mins 0.021±0.008; control 30 mins 0.010±0.002; ATP 10 mins 0.030±0.007; 0.058±0.019) samples here showed no significant difference with the Col-0

samples in control treatment (10 mins 0.035±0.01; 30 mins 0.024±0.006) and the Col-0 samples in eATP treatment (10 mins 0.029±0.005; 30 mins 0.055±0.01). In Col-0 samples, the eATP treatment for 30 minutes seemed to cause some increase in the *AtRBOHD* transcript level but statistical analysis revealed it to be insignificant. This is also true for the Col-0 samples in 10 minutes eATP treatment in which the *AtRBOHD* gene induction was similar in comparison to 10 minutes control treatment (Figure 4.37 D).

Another eATP-induced gene monitored was *AtWRKY40*. Absence of AtANN2 did not alter the quantity of *AtWRKY40* transcript in both control treatment and eATP treatment compared to the Col-0. The eATP treatment however influenced the *AtWRKY40* gene expression as both 10 minutes (Col-0 0.25±0.09; *Atann2* 0.34±0.08) and 30 minutes treatment (Col-0 1.43±0.75; *Atann2* 1.51±0.38) of eATP produced higher expression of *AtWRKY40* transcript than the 10 minutes (Col-0 0.035±0.011; *Atann2* 0.046±0.02) and 30 minutes control treatment (Col-0 0.076±0.02; *Atann2* 0.050±0.02) respectively (Figure 4.37 E).

AtACS6 is a gene that is involved in the biosynthesis of ethylene (Wang *et al.*, 2002). Here we also quantified the *AtACS6* gene transcript in Col-0 and *Atann2* samples treated with either control treatment or the eATP treatment. There were no significant differences between Col-0 and *Atann2* found in the 10 minutes control sample (Col-0 0.065±0.03; *Atann2* 0.046±0.13), 30 minutes control sample (Col-0 0.069±0.024; *Atann2* 0.026±0.065) and the 30 minutes eATP treatment sample (Col-0 0.14±0.03; *Atann2* 0.08±0.02). However, *Atann2* showed significant impairment in the expression of *AtACS6* gene compared to the Col-0 when treated with eATP treatment for 10 minutes (Col-0 0.36±0.02; *Atann2* 0.15±0.02) consistent with the result found in *Atann1* test done previously (Chapter 3.2.12; Figure 3.33). This indicated that AtANN2 is required in the regulation of *AtACS6* gene during eATP signalling. eATP treatment (1 mM) for 10 minutes managed to influence *AtACS6* gene expression as the Col-0 eATP-treated sample produced significantly higher *AtACS6* gene transcript compared to the 10 minutes Col-0 control-treated sample (Figure 4.37 F).

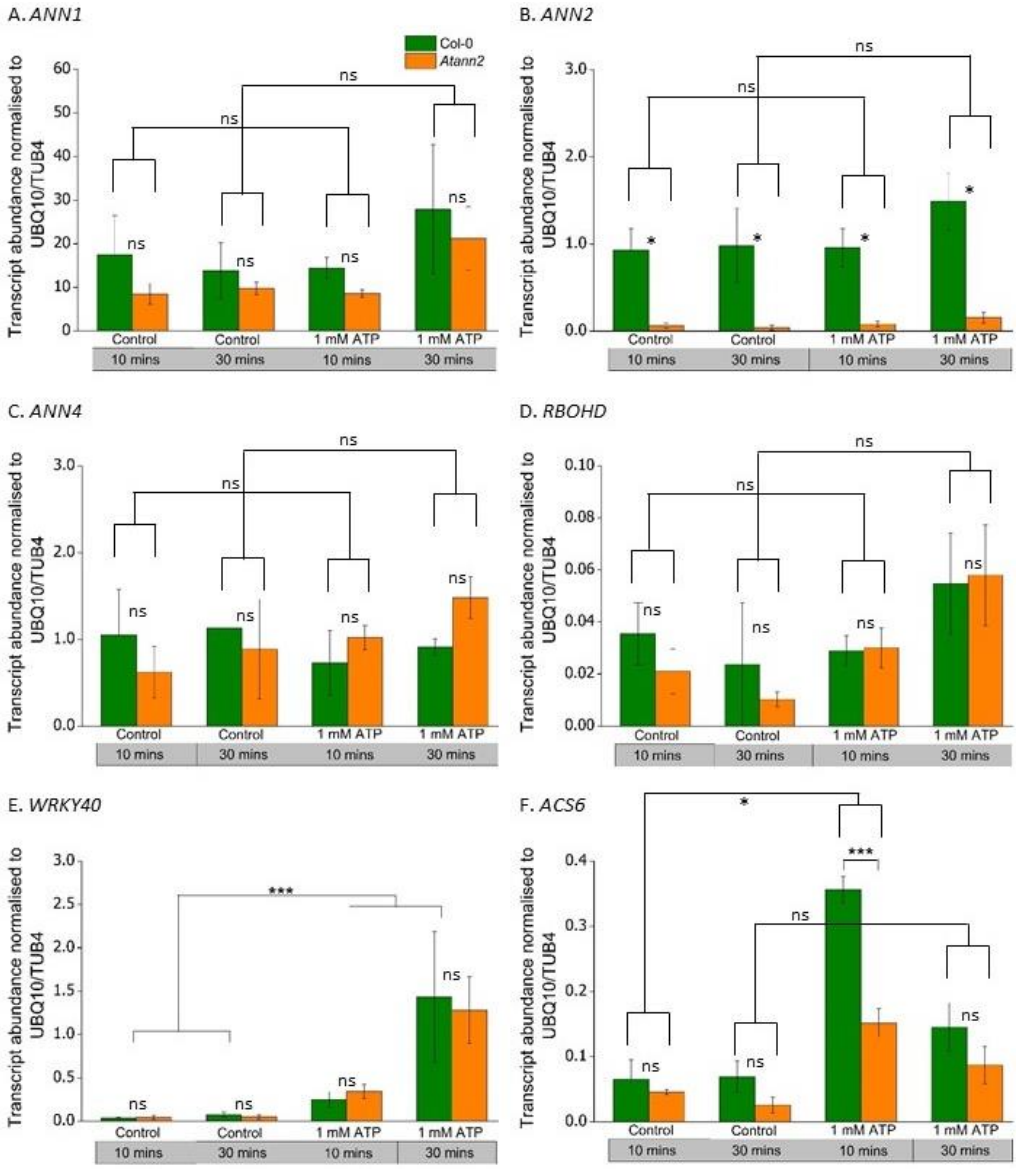

Figure 4.37: **eATP-regulated genes affected by the absence of AtANN2**. Quantification of transcripts of *AtANN1* (A), *AtANN2* (B), *AtANN4* (C), *AtRBOHD* (D), *AtWRKY40* (E) and *AtACS6* (F) was carried out for Col-0 and *Atann2* at whole roots level. Control treatment or 1 mM eATP treatment was carried out for 10 minutes or 30 minutes before RNA extraction was carried out followed by qRT-PCR. Housekeeping genes used for normalisation were *AtUBQ10* gene and *AtTUB4*. Data were from the means ± SEM of 3 independent trials, with $n = 20$ for each genotype and treatment. p-values: ns ($p>0.05$), * ($p<0.05$), ** ($p<0.01$), *** ($p< 0.001$), Welch's t-test for parametric test and Wilcoxon rank-sum test for non-parametric test.

Expression of *AtANN1* and *AtANN2* genes in the *Atann1/2* mutant was also monitored to make sure that the genes were knocked-down in the mutant samples. Figure 4.38 A showed total knock-down of *AtANN1* gene expression in *Atann1/2* samples compared to the Col-0 samples regardless of control treatment and eATP treatment. *AtANN1* gene expression

was not affected by eATP treatment since no significant difference were found in Col-0 between control treatment (10 mins 17.50±9.0; 30 mins 13.84±6.4) and eATP treatment (10 mins 14.48±2.4 ; 30 mins 18.6±14.01). Similar observations were found between control treatment (10 mins 0.005±0.001; 30 mins 0.002±0.001) and eATP treatment (10 mins 0.004±0.002; 30 mins 0.01±0.005) in *Atann1/2* samples. *Atann1/2* samples also displayed significant knock-down in the production of *AtANN2* gene transcript compared to Col-0 samples in all treatments (Figure 4.38 B). *AtANN4* gene was quantified to determine whether the mutation in *AtANN1* and *AtANN2* would have any effect on the *AtANN4* gene expression. Figure 4.38 C shows no significant differences between Col-0 and *Atann1/2* in *AtANN4* gene expression regardless of control treatment or eATP treatment. *AtANN4* gene expression also was not affected by eATP treatment as 10 minutes (Col-0 0.72±0.37; *Atann1/2* 0.80±0.26) or 30 minutes (Col-0 0.91±0.09; *Atann1/2* 1.04±0.95) eATP treatment produced similar amount of *AtANN4* gene transcript compared to 10 minutes (Col-0 0.51±0.52; *Atann1/2* 1.01±0.30) or 30 minutes (Col-0 1.50±0.47; *Atann1/2* 1.89±0.64) control treatment in both genotypes (Figure 4.38 C).

Comparable to the *Atann2* test, no significant differences were found between Col-0 (10 mins 0.035±0.01; 30 mins 0.024±0.006) and *Atann1/2* (10 mins 0.028±0.01; 30 mins 0.045±0.02) in the *AtRBOHD* gene expression assigned for control treatment. No significant difference was found between Col-0 (10 mins 0.029±0.005; 30 mins 0.055±0.019) and *Atann1/2* (10 mins 0.047±0.03; 30 mins 0.053±0.035) in eATP treatment as well. The eATP treatment also showed no effect towards the *AtRBOHD* gene expression as similar expression was found between eATP-treated Col-0 samples and control-treated Col-0 samples (Figure 4.38 D).

In contrast to *AtRBOHD* gene transcript, *AtWRKY40* gene expression proved to be altered by eATP treatment. eATP-treated Col-0 (10 mins 0.25±0.09; 30 mins 1.43±0.75) and *Atann1/2* samples (10 mins 0.28±0.10; 30 mins 1.51±0.38) showed significantly higher *AtWRKY40* gene expression compared to the control-treated Col-0 (10 mins 0.035±0.01; 30 mins 0.076±0.02) and *Atann1/2* samples (10 mins 0.070±0.026; 30 mins 0.054±0.026). Both AtANN1 and AtANN2 however might not be involved in this eATP up-regulation of *AtWRKY40* gene expression as similar expression of *AtWRKY40* was found between Col-0 and *Atann1/2* in both 10 minutes and 30 minutes eATP treatment (Figure 4.38 E).

Figure 4.38 F shows expression of *AtACS6* gene in both Col-0 and *Atann1/2*. *AtACS6* gene maintained the higher expression at 10 minutes eATP treatment than the 10 minutes

control treatment in Col-0 (control 0.065±0.03; ATP 0.357±0.020) and *Atann1/2* samples (control 0.078±0.27; ATP 0.306±0.10). However, the absence of both AtANN1 and AtANN2 did not have any influence on the gene expression of *AtACS6,* as no significant differences were found between Col-0 (10 mins 0.35±0.020; 30 mins 0.146±0.036) and *Atann1/2* (10 mins 0.306±0.10; 30 mins 0.013±0.03) in the eATP-treated samples. This observation was also true for Col-0 (10 mins 0.065±0.03; 30 mins 0.069±0.024) and *Atann1/2* (10 mins 0.078±0.27; 30 mins 0.11±0.10) in the control-treated samples (Figure 4.38 F).

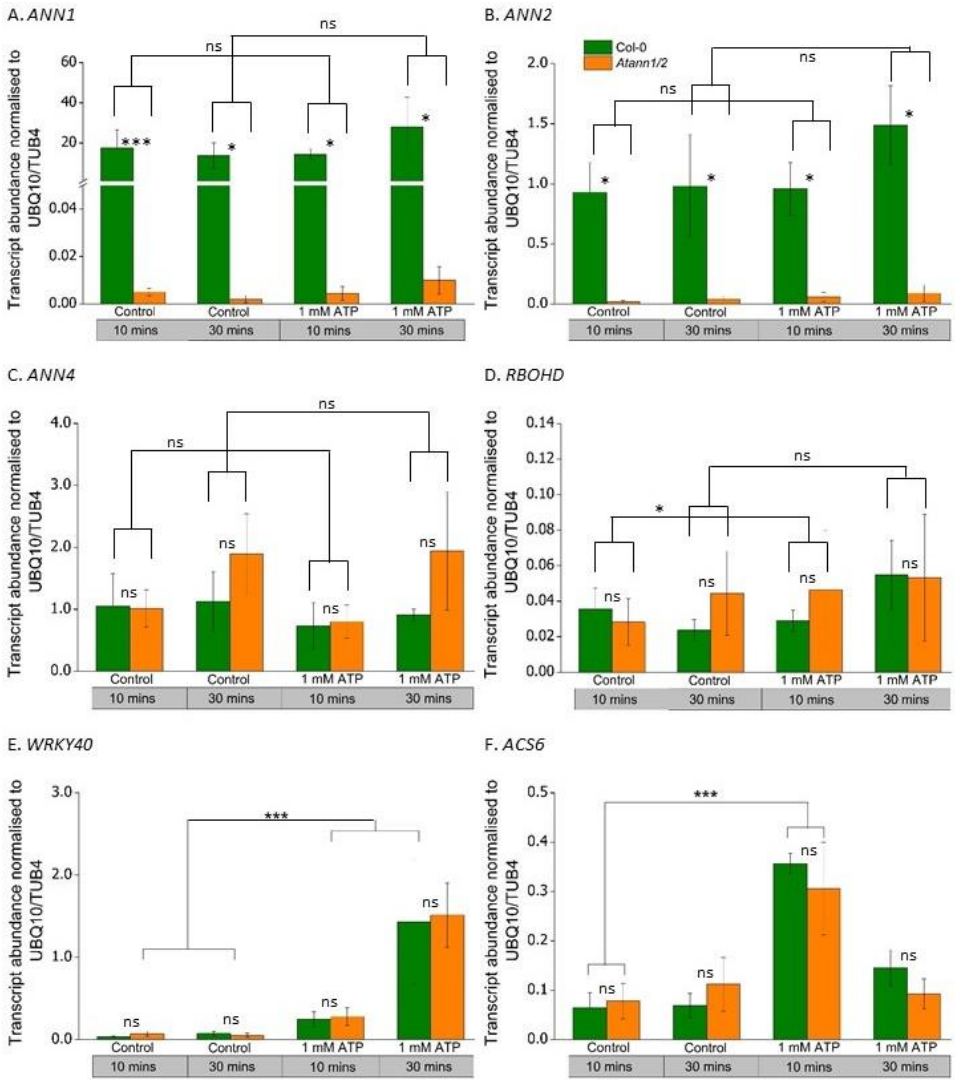

Figure 4.38: **eATP-regulated genes not affected by the absence of both AtANN1 and AtANN2.** Quantification of gene transcripts of *AtANN1* (A), *AtANN2* (B), *AtANN4* (C), *AtRBOHD* (D), *AtWRKY40* (E) and *AtACS6* (F) was carried out for Col-0 and *Atann1/2* at whole roots level. Control treatment or 1 mM eATP treatment was carried out for 10 minutes or 30 minutes before RNA extraction was carried out followed by qRT-PCR. Housekeeping genes used for normalisation were *AtUBQ10* and *AtTUB4.* Data were from the means ± SEM of 3 independent trials, with *n* = 20 for

each genotype and treatment. *p*-values: ns ($p>0.05$), * ($p<0.05$), ** ($p<0.01$), *** ($p< 0.001$), Welch's *t*-test for parametric test and Wilcoxon rank-sum test for non-parametric test.

qRT-PCR was also carried out for *Atann1/4* samples in order to find the relation with the calcium signature response. Figure 4.39 A shows the expression of *AtANN1* gene in Col-0 and *Atann1/4* samples treated with either control solution or 1 mM eATP solution. *Atann1/4* samples exhibited significantly impaired *AtANN1* gene expression compared to the Col-0 regardless of the treatments. This confirmed the mutation of *AtANN1* in the *Atann1/4* samples. In agreement with the results in previous tests, the eATP treatment showed no significant effects on the regulation of *AtANN1* gene expression for Col-0 (10 mins 14.43±2.40; 30 mins 18.59±14.01) and *Atann1/4* (10 mins 0.001±0.003; 30 mins 0.005±0.003) in comparison to the control-treated Col-0 (10 mins 17.50±9.0; 30 mins 13.84±6.41) and *Atann1/4* samples (10 mins 0.002±0.001; 30 mins 0.006±0.003) (Figure 4.39 A).

Expression of the *AtANN2* gene also was not affected by the eATP treatment as no significant differences were found between control-treated samples and eATP-treated samples in both Col-0 and *Atann1/4* mutant (Figure 4.39 B). The absence of AtANN1 and AtANN4 did not have any effects on the *AtANN2* gene transcript abundance as the gene expression in control-treated Col-0 samples (10 mins 0.92±0.24; 30 mins 0.98±0.42) and eATP-treated Col-0 samples (10 mins 0.95±0.22; 30 mins 1.48±0.32) were similar to the control-treated *Atann1/4* samples (10 mins 0.99±0.40; 30 mins 0.56±0.26) and eATP-treated *Atann1/4* samples (10 mins 1.04±0.38; 30 mins 1.21±0.73) respectively (Figure 4.39 B).

Mutation of *AtANN4* in the *Atann1/4* samples was confirmed as the *AtANN4* expression was significantly knocked-down compared to the Col-0 in both control treatment and eATP treatment (Figure 4.39 C). As previously shown, eATP treatment did not alter the expression of *AtANN4* gene as the expression of the gene was similar between 10 minutes eATP treatment (Col-0 0.729±0.37; *Atann1/4* 0.216±0.08) and 10 minutes control treatment (Col-0 1.05±0.52; *Atann1/4* 0.083±0.01) as well as between 30 minutes eATP treatment (Col-0 0.91±0.09; *Atann1/4* 0.20±0.06) and 30 minutes control treatment (Col-0 1.56±0.47; *Atann1/4* 0.042±0.08) samples (Figure 4.39 C).

Expression of the *AtRBOHD* gene was also monitored in Col-0 and *Atann1/4* samples. Figure 4.39 D showed the possibility of ATP inducing the *AtRBOHD* gene especially at the *Atann1/4* samples as the *Atann1/4* 30 minutes ATP-treated samples (0.021±0.006) were

significantly higher than the *Atann1/4* 30 minutes control-treated samples (0.002±0.0004). However, this might not be true as the *Atann1/4 AtRBOHD* gene expression was already lower than the Col-0 in the 30 minutes control-treated samples (Col-0 0.024±0.006; *Atann1/4* 0.002±0.0004). This was supported by the results of 10 minutes control treatment test where *Atann1/4* (0.009±0.002) *AtRBOHD* gene expression was also reduced compared to the Col-0 (0.035±0.01) (Figure 4.39 D).

Figure 4.38 E shows the *AtWRKY40* gene transcript abundance in the different conditions. *AtWRKY40* transcript levels in Col-0 eATP-treated samples (10 mins 0.25±0.09; 30 mins 1.43±0.75) and *Atann1/4* eATP-treated samples (10 mins 0.59±0.20; 30 mins 1.20±0.38) were significantly up-regulated compared to the Col-0 (10 mins 0.035±0.01; 30 mins 0.076±0.02) and *Atann1/4* control-treated samples (10 mins 0.15±0.04; 30 mins 0.14±0.05). No significant differences were found between Col-0 and the *Atann1/4* whole roots samples suggesting that the mutation of both *AtANN1* and *AtANN4* did not influence the regulation of the *AtWRKY40* gene (Figure 4.39 E).

AtACS6 gene expression was induced by eATP treatment in the previous tests shown. Here, we found a similar pattern of *AtACS6* gene expression where 10 minutes eATP treatment (0.36±0.020) managed to significantly up-regulate *AtACS6* gene expression compared to the 10 minutes control solution treatment (0.065±0.03) specifically in the Col-0 samples. *Atann1/4* mutant samples on the other hand failed to produce the same level of *AtACS6* gene expression at the 10 minutes eATP treatment (0.118±0.03) and was not significantly different from the *AtACS6* gene expression at 10 minutes control treatment (0.030±0.01). This indicated the possibility of both AtANN1 and AtANN4 involvement in regulating the *AtACS6* gene expression under the eATP signalling (Figure 4.39 F).

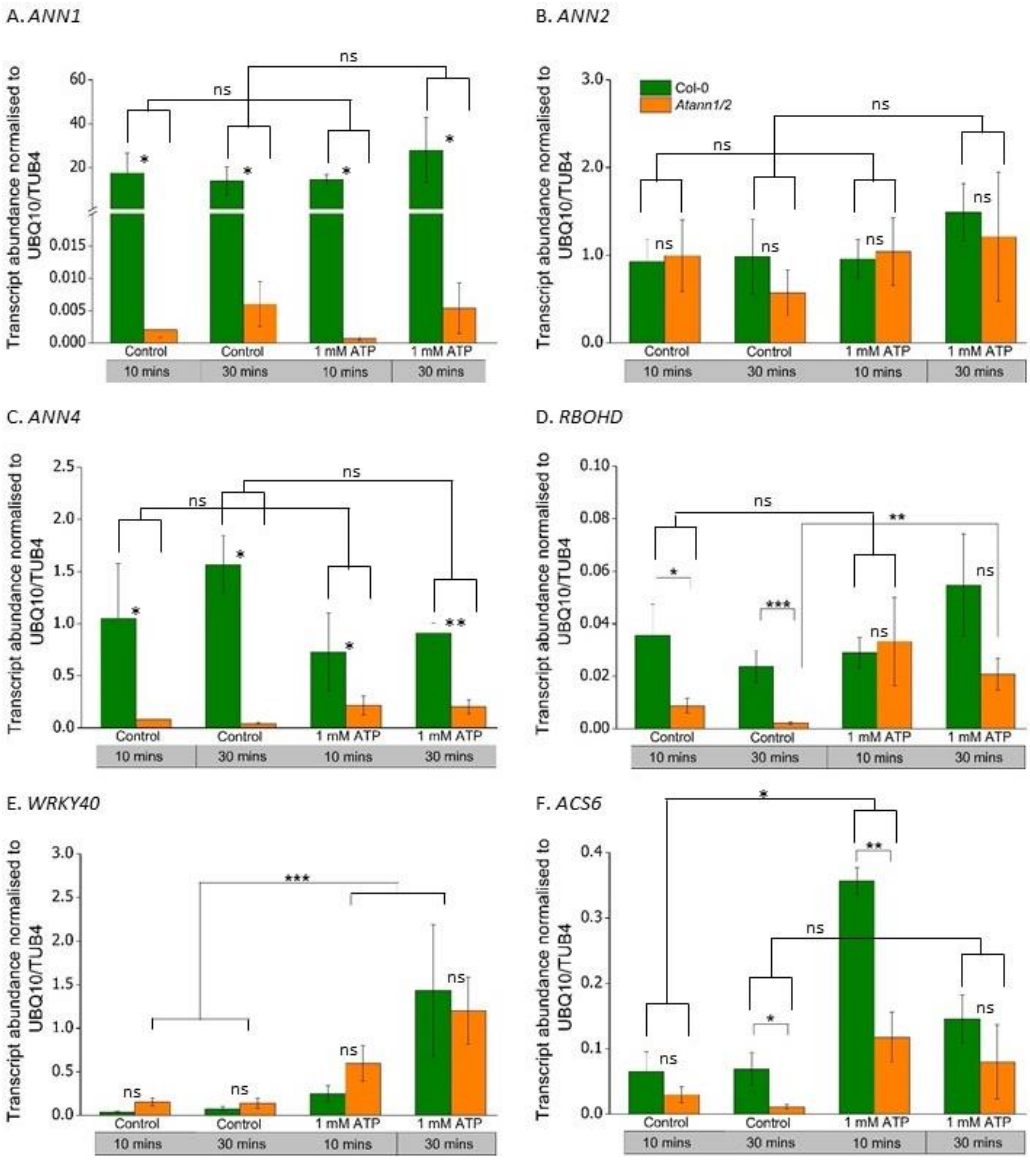

Figure 4.39: **eATP-regulated genes altered by the absence of both AtANN1 and AtANN4**. Quantification of gene transcripts of *AtANN1* (A), *AtANN2* (B), *AtANN4* (C), *AtRBOHD* (D), *AtWRKY40* (E) and *AtACS6* (F) was carried out for Col-0 and *Atann1/4* at whole roots level. Control treatment or 1 mM eATP treatment was carried out for 10 minutes or 30 minutes before RNA extraction was done followed by qRT-PCR. Housekeeping genes used for data normalisation were *AtUBQ10* and *AtTUB4*. Data were from the means ± SEM of 3 independent trials, with n = 20 for each genotype and treatment. p-values: ns (p>0.05), * (p<0.05), ** (p<0.01), *** (p< 0.001), Welch's t-test for parametric test and Wilcoxon rank-sum test for non-parametric test.

In Chapter 3.2.12 (Figure 3.33), we have done similar *AtACS6* gene test on *Atann1* mutant. Percentage of reduction between Col-0 samples and *Atann1* or *Atann1/4* was calculated in order determine whether mutation of *AtANN4* has an influence on the expression of *AtACS6* gene. *Atann1* mutant experienced reduction in *AtACS6* gene expression

by 41.67% compared to the Col-0 samples. *Atann1/4* mutant on the other hand expressed *AtACS6* gene less than the Col-0 by 66.9%. This showed that mutation of both *Atann1* and *Atann4* caused additional impairment in inducing ATP-regulated *AtACS6* gene. This is however still needed to be confirmed with gene expression study on *Atann4* single mutant sample.

Figure 4.40 shows the expression of annexin genes tested and the eATP-induced genes in Col-0 and *Atann1/2/4* triple mutant when subjected to either control treatment or eATP treatment for different periods of time. The mutation of *AtANN1* was confirmed as the expression of the *AtANN1* gene was completely impaired in *Atann1/2/4* samples compared to the Col-0 samples in all treatments tested. Consistent with previous results, no significant differences were found between 10 minutes (17.50±9.0) or 30 minutes (13.84±6.41) control treatment and 10 minutes (14.43±2.4) or 30 minutes (18.59±14.01) eATP treatment in Col-0. No significant differences were also found between 10 minutes (0.004±0.002) or 30 minutes (0.002±0.001) control treatment and 10 minutes (0.003±0.001) or 30 minutes (0.03±0.001) eATP treatment for *Atann1/2/4* samples suggesting that eATP treatment might not have had any effect on the *AtANN1* gene regulation (Figure 4.40 A). Similar observation was found with the *AtANN2* gene where 10 minutes (Col-0 0.928±0.247; *Atann1/2/4* 0.048±0.025) or 30 minutes (Col-0 0.982±0.427; *Atann1/2/4* 0.015±0.010) control-treated samples expressed a similar level of *AtANN2* gene expression compared to the 10 minutes (Col-0 0.958±0.220; *Atann1/2/4* 0.021±0.011) or 30 minutes (Col-0 1.489±0.326; *Atann1/2/4* 0.076±0.033) eATP-treated samples in both Col-0 and *Atann1/2/4* respectively (Figure 4.40 B). *AtANN2* gene expression was completely knocked-down in *Atann1/2/4* samples proving successful *AtANN2* mutation (Figure 4.39 B). The test with *AtANN4* gene also displayed insignificant difference in the *AtANN4* gene expression between 10 minutes (Col-0 1.051±0.52; *Atann1/2/4* 0.216±0.076) or 30 minutes (Col-0 1.567±0.47; *Atann1/2/4* 0.071±0.029) control treatment and 10 minutes (Col-0 0.729±0.37; *Atann1/2/4* 0.165±0.048) or 30 minutes (Col-0 0.911±0.09; *Atann1/2/4* 0.381±0.111) eATP treatment for both Col-0 and *Atann1/2/4* samples respectively (Figure 4.40 C). As expected, the expression of *AtANN4* gene was knocked-down in the *Atann1/2/4* samples in comparison to the Col-0 samples for all the treatments (Figure 4.40 C).

AtRBOHD gene expression seemed to be up-regulated in 30 minutes eATP treatment in both Col-0 (0.055±0.019) and *Atann1/2/4* (0.047±0.019) samples but it was not significantly higher than the 30 minutes control treatment (Col-0 0.029±0.005; *Atann1/2/4*

0.027±0.012) demonstrating that *AtRBOHD* expression might not be regulated by eATP at whole root level (Figure 4.40 D). Mutation in all three *AtANN1*, *AtANN2* and *AtANN4* also did not regulate the expression of *AtRBOHD* as shown by insignificant differences between Col-0 (control 10 mins 0.035±0.011; ATP 10 mins 0.029±0.005) and *Atann1/2/4* (control 10 mins 0.024±0.016; ATP 10 mins 0.027±0.012) in all treatments (Figure 4.40 D).

The expression level of *AtWRKY40* on the other hand was affected by eATP treatment as revealed by the significantly up-regulated *AtWRKY40* gene expression in 10 minutes (Col-0 0.250±0.090; *Atann1/2/4* 0.517±0.235) or 30 minutes (Col-0 1.43±0.75; *Atann1/2/4* 3.19±1.80) eATP-treated samples than the 10 minutes (Col-0 0.035±0.011; *Atann1/2/4* 0.083±0.030) or 30 minutes (Col-00.076±0.026; *Atann1/2/4* 0.065±0.019) control-treated samples (Figure 4.40 E). However, the level of *AtWRKY40* gene expressed was similar between Col-0 and *Atann1/2/4* verifiying the possibility that *AtANN1*, *AtANN2* and *AtANN4* might not involved in eATP-induced *AtWRKY40* gene up-regulation (Figure 4.40 E).

Unlike the *AtWRKY40* gene, *AtANN1*, *AtANN2* and *AtANN4* might be important in regulating eATP-induced up-regulation of the *AtACS6* gene. This was demonstrated by the significant lack of *AtACS6* gene abundance in *Atann1/2/4* samples compared to the Col-0 samples specifically at 10 minutes eATP treatment (Col-0 0.357±0.020; *Atann1/2/4* 0.128±0.031) and not at longer 30 minutes (Col-0 0.146±0.036; *Atann1/2/4* 0.234±0.152) ATP treatment (Figure 4.40 F). No significant differences were found between Col-0 and *Atann1/2/4* level of *AtACS6* expression in 10 minutes (Col-0 0.065±0.030; *Atann1/2/4* 0.070±0.018) or 30 minutes (Col-0 0.069±0.024; *Atann1/2/4* 0.044±0.025) control solution treatments.

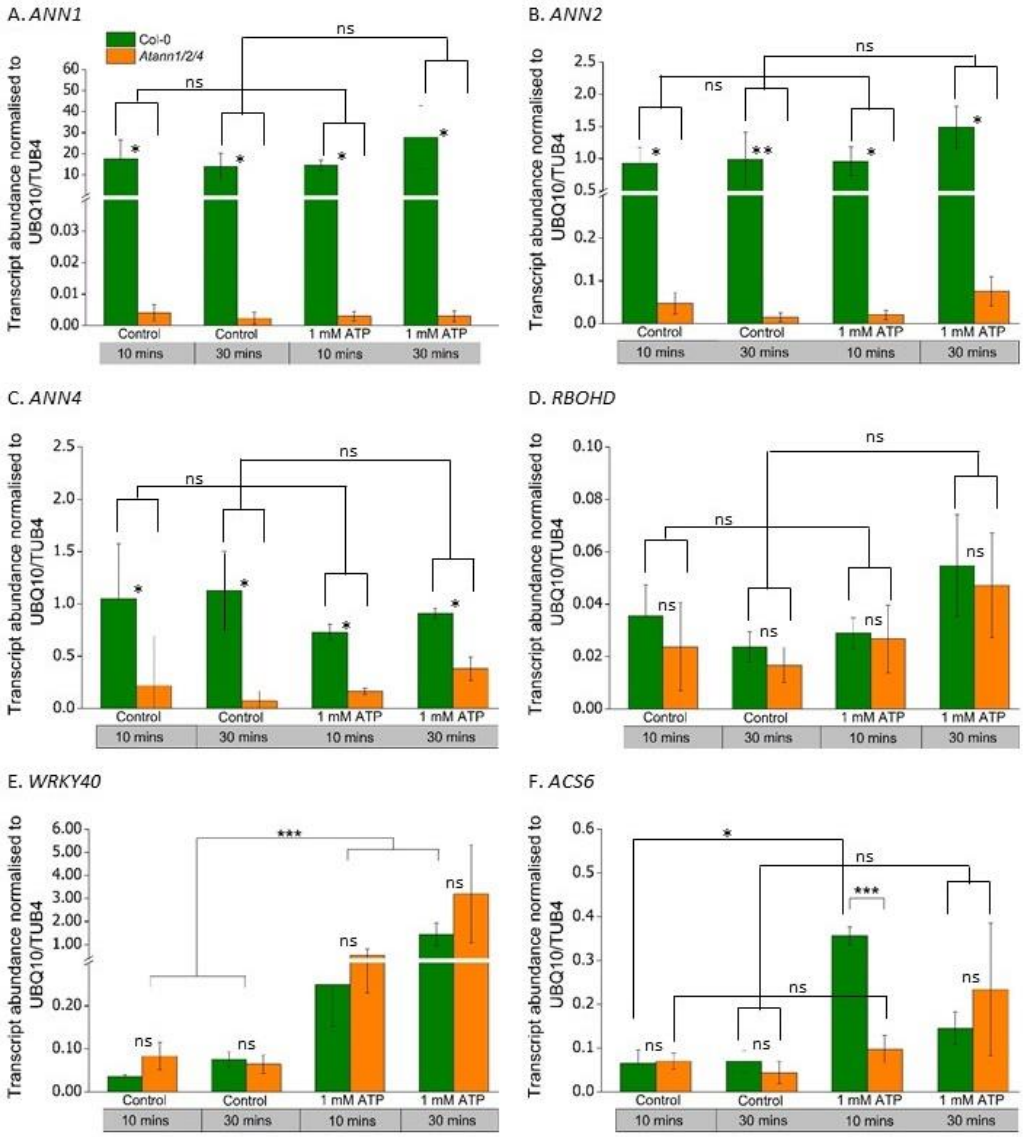

Figure 4.40: **eATP-regulated *AtACS6* expression affected by the absence ofAtANN1, AtANN2 and AtANN4.** Quantification of gene products of *AtANN1* (A), *AtANN2* (B), *AtANN4* (C), *AtRBOHD* (D), *AtWRKY40* (E) and *AtACS6* (F) were carried out for Col-0 and *Atann1/2/4* at whole roots level. Control treatment or 1 mM eATP treatment was carried out for 10 minutes or 30 minutes before RNA extraction was done followed by qRT-PCR. Housekeeping genes used for data normalisation were *AtUBQ10* and *AtTUB4*. Data were from the means ± SEM of 3 independent trials, with n = 20 for each genotype and treatment. p-values: ns (p>0.05), * (p<0.05), ** (p<0.01), *** (p< 0.001), Welch's t-test for parametric test and Wilcoxon rank-sum test for non-parametric test.

4.3 Discussion

4.3.1 AtANN2 is involved in mediating eATP-induced $[Ca^{2+}]_{cyt}$ increase at whole seedling and whole root level

In the previous chapter, we have seen the importance of AtANN1 in producing $[Ca^{2+}]_{cyt}$ response when subjected to eATP or eADP treatment. However mutation of *AtANN1* failed to completely abolish the $[Ca^{2+}]_{cyt}$ increased as expected. This showed that there are other possible calcium channels working together with AtANN1 in mediating this response. AtANN1 is one member of the annexin multigene family. In *A. thaliana,* there are 8 members of the annexin family (Clark *et al.,* 2012). AtANN2 is the closest to AtANN1 in terms of nucleotide sequence (Clark *et al.,* 2001) making it a suitable candidate for the calcium channel that might work with AtANN1. Here we tested this possibility by looking at the effect of *Atann2* loss-of-function mutant on the accumulation of $[Ca^{2+}]_{cyt}$ when subjected to eATP or eADP treatment at whole seedling and whole root level. Cytosolic (apo)aequorin (as in previous tests) was used to monitor the changes in $[Ca^{2+}]_{cyt.}$

The test was carried out at 7-day-old whole seedling level to first look at the overall response before specifically focusing at the whole root level. As shown in Figure 4.2, AtANN2 is required for the normal $[Ca^{2+}]_{cyt}$ response due to 1 mM eATP treatment and the mechanical touch response by the control treatment was not affected by the absence of AtANN2. The overall $[Ca^{2+}]_{cyt}$ accumulated during 1 mM eADP treatment also agreed with the notion above. However, the difference between *Atann2* and Col-0 second peak value caused by the eADP treatment was missing (Figure 4.3 G) unlike in the eATP treatment. Clark *et al.* (2001) found that the *AtANN2* expression was low in the stem region with almost none in the leaves thus the effect of the *AtANN2* mutation might not be pronounced at whole seedlings level. A study comparing the $[Ca^{2+}]_{cyt}$ response from 0.5 mM eADPβS demonstrated higher $[Ca^{2+}]_{cyt}$ response from the shoot region compared to the roots (Jeter *et al.,* 2004). Since the results were the average of the whole seedlings, it is possible that the differences in $[Ca^{2+}]_{cyt}$ that might occur at the root region was masked by the $[Ca^{2+}]_{cyt}$ response at the shoot. Although all the seedlings were of 7-day-old age, it is possible that slight differences in the size of the leaves influencing the outcome of the experiments. Despite the indifference at the second peak value, the overall $[Ca^{2+}]_{cyt}$ response showed a possible role of AtANN2 as the calcium channel mediating both the eATP and eADP signal.

The experiment was repeated at whole root level to look at specific AtANN2 response since *AtANN2* is highly expressed in roots compared to the shoots (Clark *et al.*, 2001). The results at whole root level support the finding at the whole seedling level where AtANN2 was needed in producing the eATP-induced $[Ca^{2+}]_{cyt}$ response (Figure 4.4). Similar observation was found in 1 mM eADP treatment. However, AtANN2's role in mediating the $[Ca^{2+}]_{cyt}$ response in eADP treatment could not be confirmed as the absence of AtANN2 seems to be affecting the touch peak and overall touch $[Ca^{2+}]_{cyt}$ response from the control treatment (Figure 4.5 B,C). *Atann2* lower touch peak response compared to the Col-0 might indicate the involvement of AtANN2 in mechanical stimulus since no significant differences were found between Col-0 and *Atann2* at the basal level (Figure 4.5 A). This is however not consistent with the control treatment results carried out with the 1 mM eATP treatment. Thus, it is also possible that this was caused by technical error where some of the roots assigned for the control treatment were injured during handling or the roots were not fully submerged in the control solution and sticking to the wall of the 96-well plate during $[Ca^{2+}]_{cyt}$ measurement.

A previous study by Matthus (2019b) discovered the root spatial biphasic $[Ca^{2+}]_{cyt}$ response by using the YC3.6 reporter which positioned the first peak $[Ca^{2+}]_{cyt}$ response at the apical root tip (1 mm) and the second $[Ca^{2+}]_{cyt}$ peak to be further up from the 1 mm apical root tip (elongation/mature zone). In the root region of 6-day-old *A. thaliana*, *AtANN2* was found to be expressed mainly at the vasculature region of the elongation and maturation zone (Brady *et al.*, 2007). *AtANN1* on the other hand can be found mostly at the epidermal and endodermal layer of the elongation zone (Brady *et al.*, 2007). Mutation of *AtANN1* (Chapter 3.2.2) and *AtANN2* reduced the $[Ca^{2+}]_{cyt}$ response of both the first peak and the second peak which indicates the possibility of AtANN1 and AtANN2 working in both apical root tip region and the elongation zone possibly in different tissues. Study on the localisation of both AtANN1 and AtANN2 under the eATP signal could help confirmed this assumption.

4.3.2 eATP and eADP were not hydrolysed in producing $[Ca^{2+}]_{cyt}$ response in Col-0 and *Atann2* whole roots

Another test with non-hydrolysable ATP or ADP analogues was carried out to test whether the agonists were hydrolysed in driving the $[Ca^{2+}]_{cyt}$ response. The overall $[Ca^{2+}]_{cyt}$ accumulated in 1 mM eATP treatment and 1 mM eATPγS were not significantly different indicating that the agonist was not hydrolysed in order to form the $[Ca^{2+}]_{cyt}$ response (Figure 4.6). It was previously found that lithium caused hypersensitive response in tobacco plants

(Naranjo *et al.*, 2003). In order to make sure that the lithium salt contained in the ATPγS used did not influence the test, another treatment of 1 mM eATP with 4 mM LiCl was carried out. LiCl proved not to have any effects as no significant difference was found with or without LiCl added (Figure 4.6). Similar observation was found in the eADP trial with non-hydrolysable ADP analogue (ADPβS). Figure 4.7 again showed that hydrolysis of eADP agonist was not needed in order to produce the $[Ca^{2+}]_{cyt}$ response. The test also demonstrated that the LiCl did not influence the $[Ca^{2+}]_{cyt}$ response. These tests with non-hydrolysable analogues proved that the whole molecule of eATP or eADP acted as a signalling molecule rather than being hydrolysed as an energy molecule to drive the response.

4.3.3 $[Ca^{2+}]_{cyt}$ accumulated in response to eATP and eADP treatment might be from both intracellular and extracellular calcium stores

In Chapter 3.2.6, we have shown that the $GdCl_3$ managed to partially block the $[Ca^{2+}]_{cyt}$ response in both eATP and eADP solution and the absence of AtANN1 brought no change to the $[Ca^{2+}]_{cyt}$ accumulation. Previously, annexin protein was found in phloem saps of several plant species and transported around *via* phloem movement (Clark *et al.*, 2012). We hypothesised that upon eATP or eADP signal, the possible free form of AtANN2 in the extracellular space would be activated and inserted to the plasma membrane. MultiLoc subcellular prediction programme predicted AtANN2 to be localised in the cytosol (Höglund *et al.*, 2006). Thus, it is also possible for the AtANN2 in the cytosol to be inserted into the membranes delimiting intracellular calcium stores (example vacuole;Yoshida *et al.* 2013; Hooper *et al.*, 2017) to help transport the calcium ion and that this would be impaired in the absence of AtANN2. Here, we monitored the production of $[Ca^{2+}]_{cyt}$ in 30 minutes $GdCl_3$ pre-treated Col-0 and *Atann2* 1 cm excised root tips with eATP or eADP treatment. Gd^{3+} as a non-permeable trivalent cation is a calcium channel blocker and was used in this test to block potential calcium channels at the plasma membrane (Malasics *et al.*, 2010).

The absence of AtANN2 caused reduction in the $[Ca^{2+}]_{cyt}$ value in the first peak and in total accumulation but not in the second peak value upon 0.5 mM ATP treatment (Figure 4.8). According to a study published by Matthus *et al.*, 2019b, the second peak $[Ca^{2+}]_{cyt}$ burst could potentially be derived from the elongation zone and initial mature zone of the roots. Since AtANN2 abundance is quite low at the elongation zone judged from an immunolocalisation study (Clark *et al.*, 2005a), it is possible that the absence of AtANN2 caused no significant change in $[Ca^{2+}]_{cyt}$ compared to the Col-0. This however contradicted

with the results showed previously with AtANN2 whole roots in 1 mM eATP treatment. Similar test on 1 cm excised root tips with 0.5 mM ADP treatment also showed contrasted results with previous 1 mM eADP test on whole roots where no significant differences were found between Col-0 and *Atann2* at the first peak value, second peak value and the total $[Ca^{2+}]_{cyt}$ accumulation (Figure 4.9). One possible explanation to these contrasted results is that the concentration of the eATP or eADP agonists played an important role in determining the $[Ca^{2+}]_{cyt}$ response. Previously, 1 mM eATP or eADP used showed AtANN2 is required to produce the normal $[Ca^{2+}]_{cyt}$ response. However, in the test with $GdCl_3$ calcium channel blocker, we used a lower 0.5 mM eATP or eADP concentration which might be the cause of the inconsistent results. Both Demidchik *et al.* (2003a) and Choi *et al.* (2014b) showed that the $[Ca^{2+}]_{cyt}$ response due to eATP is concentration-dependent. Therefore, lowering the concentration to 0.5 mM might have caused less $[Ca^{2+}]_{cyt}$ increase in Col-0 and not significantly higher than the *Atann2*.

In eATP and eADP treatment, 30 minutes $GdCl_3$ managed to partially block the full $[Ca^{2+}]_{cyt}$ response in both Col-0 and *Atann2* 1 cm root tips. Since *Atann2* with $GdCl_3$ pre-treatment did not produce lower $[Ca^{2+}]_{cyt}$ than Col-0 pre-treated with $GdCl_3$, the hypothesis that AtANN2 relocated to drive calcium ion from intracellular calcium store could not be proven. As Gd^{3+} is thought to be working at the plasma membrane and the pre-treatment failed to completely block the $[Ca^{2+}]_{cyt}$ response, it is possible that there are unknown intracellular calcium channels that might transport calcium ions from intracellular calcium stores upon addition of eATP or eADP thus causing only partial $[Ca^{2+}]_{cyt}$ inhibition. Several instances showing partial inhibition of $GdCl_3$ were mentioned in previous Chapter 3.2.6. We also mentioned the possibility of intracellular calcium stores such as the vacuole in releasing $[Ca^{2+}]_{cyt}$ through its calcium channel AtTPC1. Vacuoles contain approximately 0.2 - 5 mM free form calcium ion stored that might be involved during calcium signalling (Conn and Gilliham, 2010). Other than the vacuole, endoplasmic reticulum (ER) also contains ~0.05 - 0.5 mM free form calcium ion that could potentially be released into the cytosol. In animal cells, ER is established as one of the calcium stores that is involved in calcium signalling activated by Inositol 1,4,5-triphosphate (InsP3) (Rossi & Dirksen, 2006). Although higher plants lost their inositol triphosphate receptor (IP_3R) during evolution (Edel *et al.*, 2017), InsP3 still managed to induce intracellular $[Ca^{2+}]_{cyt}$ release possibly through a receptor different from the animal counterparts. Other than that, ER could still potentially be one of the components of calcium influx to the cytosol as there is evidence showing calcium ion flux

from the ER activated by Nicotinic Acid Adenine Dinucleotide Phosphate (NAADP) (Navazio *et al.*, 2001). Release of calcium from ER induced by eATP and eADP signalling in plants however is yet to be determined.

Based on the time course data for both eATP and eADP, $GdCl_3$ pre-treatment showed delayed first peak (without $GdCl_3$ 41 s - 63 s; with $GdCl_3$ 53 s - 90 s) followed by the second peak (without $GdCl_3$ 63 s - 155 s; with $GdCl_3$ 90 s - 155 s) for eATP and also delayed first peak (without $GdCl_3$ 41 s - 63 s; with $GdCl_3$ 53 s - 110 s) followed by second peak (without $GdCl_3$ 63 s - 155 s; with $GdCl_3$ 110 s - 155 s). A possible explanation to the delayed $[Ca^{2+}]_{cyt}$ response is that the Gd^{3+} might be blocking some of the calcium channels at the plasma membrane thus causing increase in the time taken to drive the $[Ca^{2+}]_{cyt}$ first peak and the second peak from the remaining unblocked calcium channel or from the intracellular calcium stores. As discussed in previous Chapter 3.3.2, the delayed response could also be seen in other studies done previously (Tanaka *et al.*, 2010) although the mechanism underlying the partial inhibition and the delayed $[Ca^{2+}]_{cyt}$ response is not known.

4.3.4 AtANN2-mediated eATP and eADP first peak $[Ca^{2+}]_{cyt}$ response involves activation of purinoreceptor

Perception of eATP and eADP signal that drives $[Ca^{2+}]_{cyt}$ responses requires the activation of purinoreceptors and so far the only discovered purinoreceptor in higher plants is the DORN1 purinoreceptor (Choi *et al.*, 2014b). Here we tested the involvement of purinoreceptors in producing the $[Ca^{2+}]_{cyt}$ response by using purinoreceptor inhibitor suramin in a 30 minutes pre-treatment of 1 cm excised root tips. In 0.5 mM eATP treatment, the 1.5 mM suramin pre-treatment seems to be effective in partially inhibiting the first and the second $[Ca^{2+}]_{cyt}$ peak value of Col-0 but not in *Atann2* samples. This could be due to suramin not being a specific or effective inhibitor to AtDORN1 as the possible receptor. It could also be that the concentration of suramin used was too low to cause total inhibition of the purinoreceptor. In contrast to the Col-0 samples, suramin failed to inhibit the $[Ca^{2+}]_{cyt}$ response in *Atann2* samples in both the first and the second $[Ca^{2+}]_{cyt}$ peak (Figure 4.10 D, E). It is worth noting that the Col-0 pre-treated with 1.5 mM suramin produced a similar $[Ca^{2+}]_{cyt}$ response with *Atann2* without the pre-treatment. This suggests that AtANN2 is directly or indirectly the target of suramin. This might raise the possibility of AtANN2 acting as an ATP-binding protein that drives the $[Ca^{2+}]_{cyt}$ response since AtANN2 contains the GTP-binding motif based on the analysis of its amino acid sequence (Clark *et al.*, 2001). Although

no evidence found that support the binding of AtANN2 with ATP, AtANN1 protein which is a close relative of AtANN2 was found to be able to bind to ATP (Ito *et al.*, 2006). This is however not a strong assumption as this is only true for the first and the second peak $[Ca^{2+}]_{cyt}$ value but not the overall $[Ca^{2+}]_{cyt}$ accumulated. Furthermore, the absence of AtANN2 did not completely abolish the ATP-induced $[Ca^{2+}]_{cyt}$ increased which might indicates involvement of another receptor such as AtDORN1. AtDORN1 as in the previous chapter has been proven to be the receptor for eATP and the results of *Atann2* with suramin could place *Atann2* downstream of AtDORN1 but would still be affected by suramin. In a previous study by Strattman *et al.*, (2000), suramin found to be effective in inhibiting the systemin receptor in mediating defence signal in tomato plants. A similar receptor however is not yet discovered in *A. thaliana.* Based on the results shown, suramin was effective in blocking AtANN2 that might put AtANN2 as a possible equivalent of systemin receptor in *A. thaliana.* In depth study regarding this function of AtANN2 in the future might shed some light on this matter.

Replacing the treatment with 0.5 mM eADP yielded contradicting results. In the 0.5 mM eADP test, pre-treatment with 1.5 mM suramin was efficient in blocking the $[Ca^{2+}]_{cyt}$ response in *Atann2* samples but not in Col-0 for the first peak value. *Atann2* samples pre-treated with suramin produced lower $[Ca^{2+}]_{cyt}$ accumulation than the Col-0 pre-treated with suramin in the first peak and the overall $[Ca^{2+}]_{cyt}$ accumulated (Figure 4.11 D). This could show that the suramin-sensitive pathway working under the eADP signal might be working together with AtANN2 in mediating the $[Ca^{2+}]_{cyt}$ burst. In contrast to the 0.5 mM eADP treatment carried out on 1 cm root tips, non suramin pre-treated *Atann2* samples did not induce significantly lower $[Ca^{2+}]_{cyt}$ than the Col-0 in the first peak, second peak and the overall $[Ca^{2+}]_{cyt}$ increase (Figure 4.11 D, E, F) which would be the opposite of the previous findings showing the importance of AtANN2 in mediating the $[Ca^{2+}]_{cyt}$ response. These differences in results could be attributed to technical error especially in handling 1 cm excised root tips that could get easily injured during excision and transfer that might impose wounding stress to the root tips on top of the treatment.

4.3.5 AtANN1 and AtANN2 work together in mediating eATP or eADP-induced $[Ca^{2+}]_{cyt}$ response whereas AtANN4 might act as a negative regulator for the response

Chapter 3.2.2 highlighted the importance of AtANN1 in producing the $[Ca^{2+}]_{cyt}$ response at whole roots level and in the tests carried out in this chapter (4.2.2), we have

discussed the possible role of AtANN2 in mediating the same response. In order to investigate the possibility of both AtANN1 and AtANN2 in mediating the eATP or eADP-induced $[Ca^{2+}]_{cyt}$ response, we tested Col-0 and *Atann1/2* double mutants in eATP or eADP treatment at whole root level. Since both AtANN1 and AtANN2 showed positive responses in previous tests with eATP or eADP agonists, we hypothesised that the double mutants would yield additive effect in reduction of $[Ca^{2+}]_{cyt}$ response compared to the Col-0. Figure 4.12 confirmed the results from previous tests as it demonstrated that *Atann1/2* double mutant samples were impaired in driving the $[Ca^{2+}]_{cyt}$ increased compared to the Col-0.

We have also in the results section compared between single mutant and double mutant as well as double mutant against the triple mutant. Based on this comparison, we could clearly see the pattern of positive regulation by both AtANN1 and AtANN2 and negative regulation by AtANN4. *Atann1/2* double mutant produced significantly less total $[Ca^{2+}]_{cyt}$ compared to either *Atann1* or *Atann2* single mutant in the eATP or eADP test. *Atann1/2* double mutant on the other hand showed similar total $[Ca^{2+}]_{cyt}$ accumulation as in *Atann1/2/4* in eATP test; this is however not true when carried out with eADP agonist which might suggest different components involved under eADP signalling. Furthermore, tests with *Atann1/4* double mutant showed consistently higher accumulation of total $[Ca^{2+}]_{cyt}$ compared to the *Atann1* single mutant or *Atann1/2/4* triple mutant in either eATP or eADP test.

Since the experiments of *Atann1, Atann2* and *Atann1/2* were carried out separately, it might not be completely accurate to compare the $[Ca^{2+}]_{cyt}$ measurement directly. Thus, percentage of reduction of each mutant to the Col-0 pair was calculated to help determine whether the double mutants have an additive effect on the reduction of $[Ca^{2+}]_{cyt}$ response. In 1 mM eATP test at whole root level, *Atann1* produced 21.5% less total $[Ca^{2+}]_{cyt}$ accumulation than the Col-0 pair (Chapter 3.2.2; Figure 3.4). *Atann2* in similar test showed 14.4% reduction in $[Ca^{2+}]_{cyt}$ accumulation compared to the Col-0 pair. Mutation in both of *AtANN1* and *AtANN2* proved to cause an additive effect in the reduction of $[Ca^{2+}]_{cyt}$ response due to eATP treatment by 41.8% compared to the Col-0 pair (Figure 4.12 H). Similar analysis of the 1 mM eADP tests at whole root level were carried out to see any additive effect of *Atann1/2* double mutants. *Atann1* accumulated less $[Ca^{2+}]_{cyt}$ by 28% compared to the Col-0 (Chapter 3.2.2; Figure 3.4) whereas *Atann2* accumulated less $[Ca^{2+}]_{cyt}$ by 18.8% than the Col-0 pair (Chapter 4.2.2; Figure 4.5). *Atann1/2* (13.24±0.58 μM) in 1 mM eADP treatment at whole roots level caused slight additive effect in total $[Ca^{2+}]_{cyt}$ reduction by only 30% compared to

its Col-0 pair (Chapter 4.2.3; Figure 4.17). These results confirmed that both AtANN1 and AtANN2 might be working together in the eATP and eADP signalling pathways.

Plant annexins including AtANN1 have the ability to form oligomers under oxidative stress conditions (Hofmann *et al.*, 2002; Gorecka *et al.*, 2005). Cotton annexin AnxGb5 is able to form a heterodimer with AnxGb6 according to an interaction study carried out by Huang *et al.* (2013). It could be that eATP (which might be acting as a stress signal) induced formation of ROS which possibly lead to heteromerisation between AtANN1 and AtANN2 to mediate the $[Ca^{2+}]_{cyt}$ response possibly as calcium channels. AtANN1 has the ability to transport calcium in planar lipid bilayers (Laohavisit *et al.*, 2012, 2013). Although no direct evidence showing the same ability of AtANN2 is available, AtANN2 contains the calcium-binding motif and has close similarity to AtANN1 (Clark *et al.*, 2001). This assumption of AtANN1 forming a heterodimer with AtANN2 however might need a supporting evidence of physical interaction between AtANN1 and AtANN2. Information regarding the subcellular localisation of AtANN1 and AtANN2 under eATP or eADP signalling also might be helpful in proving this assumption. Clark *et al.*, (2005a) however showed AtANN1 localised mostly at the epidermal cells of root elongation zone whereas AtANN2 mostly localised at the epidermal cells of the root apex under normal condition in younger seedlings. This could suggest the possibility of AtANN1 and AtANN2 being relocated under eATP or eADP signals to form heterodimer or they serve similar functions but in different tissues. Although *Atann1/2* double mutants caused more reduction than the single mutant, the $[Ca^{2+}]_{cyt}$ response was not completely abolished. This indicates that the remaining calcium influx might be from the plasma membrane or intracellular calcium stores through unknown channels as shown in previous tests with $GdCl_3$ calcium channel blocker; or there are other channels than AtANN1 and AtANN2 operating in eATP or eADP signalling pathways.

Another potential candidate for a calcium channel working alongside AtANN1 and AtANN2 is AtANN4. Both AtANN1 and AtANN4 expression were high in roots compared to other regions and the two annexins have been shown to interact (Huh *et al.*, 2010). Due to some unforeseen circumstances, we could not get a working loss of function mutant of *AtANN4* with cytosolic (apo)aequorin; hence we proceeded with the test on Col-0 and *Atann1/4* double mutant to determine whether the double mutant would have an additive effect compared to the *Atann1* single mutant upon eATP or eADP treatment. Here, AtANN4 was hypothesised to be the other calcium channel other than AtANN1 and AtANN2, thus the *Atann1/4* double mutant should be accumulating less $[Ca^{2+}]_{cyt}$ than the Col-0 and *Atann1*

single mutant. The $[Ca^{2+}]_{cyt}$ measurement however yielded unexpected results when in 1 mM eATP and 0.1 mM eATP treatment tests, the double mutant *Atann1/4* produced a higher first peak than Col-0 although total $[Ca^{2+}]_{cyt}$ accumulation was not affected by the mutation (Figure 4.21; Figure 4.23). This could indicate that AtANN4 is a negative regulator that could even overcome the loss of AtANN1. Interestingly, in the 1 mM eADP test carried out later, *Atann1/4* mutant accumulated higher total $[Ca^{2+}]_{cyt}$ than the Col-0. This again points to AtANN4 as a negative regulator and that not all of its function requires AtANN1.

Based on the tests carried out in eATP and eADP treatments in the previous chapter (3.2.2), the absence of AtANN1 resulted in the impairment of the $[Ca^{2+}]_{cyt}$ response. If AtANN4 negatively regulates another component of the eATP signalling pathway, its absence could trigger the activation of the component which might compensate for the loss of $[Ca^{2+}]_{cyt}$ accumulation by *Atann1* mutant thus resulting in wild type Col-0 phenocopy. Previously, it was found that under salt stress conditions, AtANN1 could physically bind to AtANN4 dependent on calcium ion binding (Huh *et al.*, 2010). AtANN4 physically interacting with AtANN1 might negatively regulate AtANN1 function under eATP or eADP signalling thus resulting in contrasting results than the previous tests with *Atann1*. AtANN4 lacks one of the canonical type II calcium-binding loop (Clark *et al.*, 2001). Instead of operating as a calcium channel, it is possible that AtANN4 also might be acting as a negative regulator of certain protein(s) other than AtANN1 downstream of the eATP and eADP signal perception. The differences in the results obtained from the eATP (Figure 4.21) and eADP test (Figure 4.25) with *Atann1/4* could be attributed to the possible different signalling pathway between eATP and eADP signalling although the mechanism is not yet known. It has to be noted however that the sample size for the double mutant test was quite low thus further tests with additional number of samples is required to confirm this.

Up to this point, we have seen contrasting results from the $[Ca^{2+}]_{cyt}$ measurement of *Atann1/2* and *Atann1/4* in eATP and eADP treatments which showed the role of AtANN1 and AtANN2 in mediating the $[Ca^{2+}]_{cyt}$ response possibly as calcium channels and AtANN4 as a negative regulator in part of this process. Further investigation was done by testing *Atann1/2/4* triple mutant whole roots with eATP or eADP treatment with $[Ca^{2+}]_{cyt}$ measurement using the same reporter as previously, which was the 35S CAMV-driven (apo)aequorin. According to the assumptions made previously, the *Atann1/2/4* mutant would accumulate total $[Ca^{2+}]_{cyt}$ less than or similar to the *Atann1/2* mutant. The *Atann1/2/4* mutant was confirmed to be impaired compared to Col-0 in the total $[Ca^{2+}]_{cyt}$ accumulation in both 1

mM eATP and 1 mM eADP tests (Figure 4.29; Figure 4.33). Calculation of the percentage of reduction compared to the Col-0 showed that *Atann1/2/4* triple mutant (Col-0 16.43±0.79 μM; *Atann1/2/4* 8.88±0.44 μM) experienced reduction in total $[Ca^{2+}]_{cyt}$ accumulation by 46% whereas the *Atann1/2* mutant (Col-0 18.73±0.70 μM; *Atann1/2* 10.90±1.47 μM) showed almost similar amount of reduction which is 41.8% reduction in total $[Ca^{2+}]_{cyt}$ accumulated during 1 mM eATP treatment. In 1 mM eADP treatment, the *Atann1/2/4* (Col-0 15.63±0.99 μM; *Atann1/2/4* 10.58±0.51 μM) whole roots sample $[Ca^{2+}]_{cyt}$ accumulation was reduced by 32.3% compared to the Col-0 which was also on par to the *Atann1/2* (Col-0 18.89±0.60 μM; *Atann2* 13.24±0.58 μM) percentage of reduction at 30%.

Assuming that AtANN4 is acting as a negative regulator of AtANN1 or other proteins in the eATP or eADP signalling pathways, mutation of *AtANN4* in the *Atann1/2/4* samples might undo the negative regulation thus activating the unknown protein or calcium channels that might compensate for the loss of AtANN1 and AtANN2. This together with the possible influx from the intracellular calcium channel could be the underlying reason why $[Ca^{2+}]_{cyt}$ accumulation was not completely abolished in the *Atann1/2/4* triple mutant.

The discussions above are mainly from the point of view of both AtANN2 and AtANN4 acting as potential calcium channels besides AtANN1 under eATP and eADP signalling. This is mainly due to the conserved salt bridges motif in both AtANN2 and AtANN4 amino acid sequence which previously found to be an important motif to for Ca^{2+} channel in animal cells (Liemann *et al.*, 1996; Laohavisit *et al.*, 2009). No studies showing the ability of both AtANN2 and AtANN4 to transport Ca^{2+} *in vivo* has been done yet. Although there are studies with abiotic stresses supported the importance of both AtANN2 and AtANN4 in producing Ca^{2+} signature (Wang *et al.*, 2015; Huh *et al.*, 2010; Ma *et al.*, 2019), these two proteins also have the potential to play other roles besides ion transport based on the motifs found in the amino acid sequence.

Both AtANN2 and AtANN4 contain the conserved Ca^{2+} binding motif although this motif is lost in the fourth repeat of AtANN4 (Figure 4.1). Besides Ca^{2+} binding motif, both AtANN2 and AtANN4 have the plasma membrane binding motif. Annexins protein has been found to be able to bind to phospholipid bilayer in Ca^{2+} or Ca^{2+}-independent manner (Dabitz *et al.*, 2005; Hofmann *et al.*, 2002). This could suggests to the potential of both AtANN2 and AtANN4 acting as a calcium sensor in the event of $[Ca^{2+}]_{cyt}$ accumulation in eATP and eADP signalling. It is also possible that the AtANN2 and AtANN4 binding of Ca^{2+} caused the

proteins to be inserted into plasma membrane or endomembranes thus changing the integrity of the membrane which could lead to the activation of other membrane proteins. AtANN2 also has the potential peroxidase motif. A study done regarding the role of AtANN1 and AtANN2 in post-phloem sugar transport suggested that similar to AtANN1, AtANN2 could also acts as peroxidase enzyme that could regulate level of ROS thus lowering the production of callose that could interfere with sugar transports to the root tips (Tan *et al.*, 2011). Based on this assumption, in the eATP and eADP signalling, AtANN2 could be a peroxidase enzyme that could detoxify excess ROS and possibly regulate ROS wave or signalling. There are however no studies regarding AtANN2 peroxidase activity that have been reported yet. Both AtANN2 and AtANN4 also have the S3 cluster motif that could be a redox reaction centre. It is also possible that AtANN2 and AtANN4 redox activity promotes oxidation or reduction of other proteins leading to change in conformation and regulation of the proteins involved (Hoffman, 2004).

4.3.6 Regulation of eATP-induced genes *AtRBOHD* and *AtACS6* by AtANN1, AtANN2 and AtANN4

Change in the transcription level of genes is one of the downstream responses of the eATP-signalling pathway (Choi *et al.*, 2014b). AtANN1, AtANN2 and AtANN4 were hypothesised to be working upstream of the changes in the gene expression, thus mutation in one of the annexin gene tested would likely affect the level of eATP-induced gene expression. qRT-PCR was carried out for 7-day-old whole root samples of *Atann2*, *Atann1/2*, *Atann1/4* and *Atann1/2/4*. The seedlings were treated with either control solution or 1 mM eATP solution for 10 minutes or 30 minutes before the qRT-PCR was done. The level of expression of the previously proven eATP-induced genes *AtRBOHD*, *AtWRKY40* (Choi *et al.*, 2014b), and *AtACS6* (Jeter *et al.*, 2004) of eATP-treated samples were predicted to be reduced or similar to the control condition in all of the mutant samples as all of the annexin genes tested were envisaged to be involved in the eATP signalling pathway. The expression level of *AtANN1*, *AtANN2* and *AtANN4* genes were also tested to make sure that the expression of these genes in the mutant samples were knocked-down to confirm the loss-of-function of these genes.

Mutation of *AtANN1* gene was confirmed when the expression level was knocked-down in the *Atann1/2*, *Atann1/4* and *Atann1/2/4* samples compared to the Col-0 samples in all conditions (Figure 4.38 A; 4.39 A; 4.40 A). *Atann1/2* (Figure 4.38 B; 4.38 C) and

Atann1/4 (Figure 4.39 B; 4.39 C) were confirmed to be mutant as the *AtANN2* and *AtANN4* gene expression in the samples were knocked-down respectively. This is also true for *Atann1/2/4* sample as *AtANN1*, *AtANN2* and *AtANN4* levels of expression were completely impaired compared to the Col-0 (Figure 4.40 A; 4.40 B; 4.40C). In the *Atann2* and *Atann1/2* samples, the expression of *AtANN4* gene was similar to the Col-0 confirming that *AtANN4* did not compensate for the absence of functional AtANN2 (Figure 4.37 C; 4.38 C). This is also true for the *Atann1/4* where AtANN2 did not compensate for the loss of *AtANN4* (Figure 4.39 B).

The *AtRBOHD* gene was previously shown to be up-regulated under eATP treatment (Choi *et al.*, 2014b). Here, we failed to obtain the same result as the *AtRBOHD* gene was not significantly up-regulated in either 10 minutes or 30 minutes eATP treatment in Col-0 or the mutant samples. This could be due to the different sampling area where we only used the whole roots whereas whole seedlings were used in the previous study mentioned. It is interesting that the expression of *AtRBOHD* in *Atann1/4* samples were significantly lower than the Col-0 samples even in control solution (Figure 4.39 D). AtANN4 as previously discussed as a potential negative regulator under the eATP-signalling pathway. In Chapter 3.2.12 (Figure 3.33B), AtANN1 absence did not affect the expression of *AtRBOHD* gene. Although in Col-0 samples treatment with eATP did not alter the *AtRBOHD* gene expression, *Atann1/4* samples showed significant up-regulation of *AtRBOHD* gene expression in eATP treatment compared to the control treatment (Figure 4.39 D). It is possible that AtANN4 negatively regulates peroxidases that might reduce the oxidative stress or the expression of genes responsible for ROS production under certain condition. Huh *et al.* (2010) proved that mutation of *AtANN4* caused resistance towards salinity stress whereas overexpressing the protein induced a hypersensitive response. This could relate AtANN4 to the production of ROS and the regulation of *AtRBOHD* gene at the whole root level as it encodes for the NADPH Oxidase that was envisaged as the enzyme that produced ROS under the eATP signal (Chen *et al.*, 2017).

AtWRKY40 expression level was highly up-regulated after 30 minutes of eATP treatment compared to the control treatment (Figure 4.37 E; 4.38 E; 4.39 E; 4.40 E). This up-regulation however occurred in all of the mutant samples and the Col-0 indicating that AtANN1, AtANN2 and AtANN4 were not involved in the regulation of this eATP-induced gene. AtWRKY40 is one of the WRKY DNA-binding transcription factors that are heavily involved in stress responses in plants especially ABA (Chen *et al.*, 2010), low temperature,

oxidative stress and wounding (Miller *et al.*, 2009). This observation proved the variation in eATP signalling pathway and that eATP might act as the initial stress signal leading to a variety of response involving different downstream responses. Here, it is confirmed that AtANN1, AtANN2 and AtANN4 are not involved in the pathway that is related to the role of AtWRKY40 under the eATP signal.

In contrast to the *AtWRKY40* gene, *AtACS6* gene expression proved to be regulated by AtANN1, AtANN2 and AtANN4. *Atann2, Atann1/4* and *Atann1/2/4* samples failed to up-regulate the expression of *AtACS6* gene as in Col-0 samples after 10 minutes eATP treatment (Figure 4.37 F; 4.39 F; 4.40 F). This result showed that AtANN1, AtANN2 and AtANN4 were needed for the normal *AtACS6* induction by eATP to occur. It is however intriguing as the *Atann1/2* samples showed no impairment of *AtACS6* up-regulation by eATP compared to the Col-0 (Figure 4.25 F). This result was in contrast to the previous statement regarding the importance of AtANN1 and AtANN2 in the *AtACS6* up-regulation. From this observation, it might be that the absence of both AtANN1 and AtANN2 would promote the up-regulation of *AtACS6* gene by eATP. Loss of function of either AtANN1 or AtANN2 would not be effective in inducing the *AtACS6* gene as shown by the *Atann1* (Chapter 3.2.12, Figure 3.33D), *Atann2* (Figure 4.37 F) single mutant and *Atann1/4* double mutant results (Figure 4.39 F). This could also hint to the possible interaction between AtANN1 and AtANN2 in mediating eATP response. It is possible that AtANN4 is required for the *AtACS6* up-regulation based on the *Atann1/4* and *Atann1/2/4* mutant results, but future tests on *Atann4* single mutant samples are needed to confirm this.

It is not possible to directly relate the outcomes from $[Ca^{2+}]_{cyt}$ measurement tests with the level of eATP-induced gene expression in order to delineate the mechanism of the eATP signalling pathway as we need to take into consideration the role of the $[Ca^{2+}]_{cyt}$ decoding machinery such as protein kinases, calmodulin and calmodulin-like kinases (CML) (Cheval *et al.*, 2013). Additionally, the time courses of eATP treatment differed between the two types of experiments. However, from these experiments we could confirm that AtANN1, AtANN2 and AtANN4 were involved in the eATP signalling pathway.

4.4 Summary and future work

In this chapter we have shown the involvement of both AtANN2 and AtANN4 in mediating the eATP response alongside AtANN1 as the mutation in *AtANN2* and *AtANN4* caused impairment in $[Ca^{2+}]_{cyt}$ accumulation. Further studies should include other alleles of

the genes. We have hypothesised that AtANN2 could possibly work as a calcium channel together with AtANN1 either through heteromerisation or working simultaneously in different tissue. The ability of AtANN1 in transporting calcium across membranes has been shown in previous studies (Laohavisit *et al.*, 2012, 2013) but the same ability has not yet been proven for AtANN2. Planar lipid bilayer experiments with AtANN2 protein would be the correct next step in order to prove the hypothesis of AtANN2 as a calcium channel. Other than that, an interaction study between AtANN1 and AtANN2 under eATP influence through pull down assay would be helpful in discovering the likelihood of AtANN1 forming heteromerisation with AtANN2 to form a calcium channel. Other than that, the ability of suramin receptor to block AtANN2 function in mediating $[Ca^{2+}]_{cyt}$ release under eATP signal might put AtANN2 as the possible systemin receptor in mediating wounding signal in *A. thaliana.* Further test in the detection of ethylene biosynthesis and quantification of ROS burst with systemin elicitor in *Atann2* mutant or the overexpressed *35S::CAMV AtANN2* might be useful in discovering this possibility.

Unlike AtANN2, we found that AtANN4 might not be working as a calcium channel but possibly as a negative regulator that might regulate the function of AtANN1 or other proteins in the eATP pathway in mediating $[Ca^{2+}]_{cyt}$ increase. Whether AtANN4 negative regulation affects the function of AtANN2 however is not yet known. Quantification of calcium accumulation with *Atann2/4* and interaction study between AtANN2 and AtANN4 under the eATP signal might answer this question.

The mechanism of AtANN1, AtANN2 and AtANN4 involvement in the eATP-signalling pathway however could not be deciphered based on the experiments carried out in this chapter as it was done mostly at whole roots level. Experiments at more specific protoplast level of *Atann2, Atann1/2, Atann1/4* and *Atann1/2/4* are needed to obtain cell specific $[Ca^{2+}]_{cyt}$ signature for each mutants. It is also important to determine which cell type to test for the experiment as AtANN1, AtANN2 and AtANN4 were localised to different tissues in previous studies (Clark *et al.*, 2001; Clark *et al.*, 2005a). However these studies were carried out on younger seedlings and with a different ecotype. Thus, it is interesting to look at cellular or subcellular localisation of AtANN1, AtANN2 and AtANN4 in either control conditions or under eATP signal to help confirm the role of AtANN1, AtANN2 and AtANN4 in the eATP-signalling pathway. Mutation of all three annexins *Atann1/2/4* still managed to produce $[Ca^{2+}]_{cyt}$ accumulation suggesting the possibility of other unknown plasma membrane calcium channels or the influx from the intracellular calcium store as

shown in the $GdCl_3$ calcium channel blocker experiments. It would be beneficial in the future to carry out another set of experiments with $GdCl_3$ calcium channel blocker on the *Atann1/2/4* to confirm the assumption. This test at protoplast level might help since the experiments carried out with $GdCl_3$ in this chapter failed to completely inhibit all calcium influx possibly due to inability of the $GdCl_3$ to reach to all root tissues.

In the previous chapter (3.2.10), AtANN1 was shown to possibly be working downstream of the ROS production. Previous studies also suggested the role of AtANN1 as the ROS-activated hyperpolarised activated calcium channel (HACC) in salinity stress conditions (Laohavisit *et al.*, 2012; Laohavisit *et al.*, 2013). Since AtANN2 is closely related to AtANN1, it could possibly serve the same purpose as AtANN1. Overexpression of AtANN4 caused hypersensitive response in *A. thaliana* under salinity stress, which could be related to the production of ROS under stress conditions (Huh *et al.*, 2010). Due to time constraint, we were unable to look at the production of ROS in *Atann2* and *Atann4* mutants. If both AtANN2 and AtANN4 work downstream of ROS production, the production of ROS due to eATP treatment would not be affected by mutation of *AtANN2* and *AtANN4*. Similar tests as in previous Chapter 3.2.10 by using the CMH_2DCFDA probe and stereomicroscope to detect intracellular ROS can be used to monitor the production of ROS by eATP treatment in *Atann2* and *Atann4* to determine whether AtANN2 and AtANN4 also work downstream of ROS production.

qRT-PCR carried out for *AtRBOHD* gene expression also revealed the possibility of AtANN4 function in ROS production as the expression of this gene is low in the *Atann1/4* mutant. Similar qRT-PCR test of *AtRBOHD* gene in *Atann4* single mutant plant however is required to confirm this assumption. Similar to the finding in the previous chapter regarding AtANN1, AtANN2 and AtANN4 were needed for the eATP-induced *AtACS6* up-regulation. It is however interesting that the mutation of both AtANN1 and AtANN2 but not in single AtANN1 or AtANN2 could phenocopy Col-0 in terms of *AtACS6* upregulation which could suggest negative regulation. Additional experiments such as quantification of ethylene production could be done in the future to confirm the role of AtANN1, AtANN2 and AtANN4 in the eATP-induced ACS6 or ethylene production.

Chapter 5

AtANN2 in biotic and abiotic stresses

5.1 Introduction

AtANN2 is one of the members of the annexin family, which has high similarity in terms of protein structure with AtANN1 (Clark *et al.*, 2001). Similar to *AtANN1*, the expression of the *AtANN2* gene was found to be highly regulated by environmental stimuli (Cantero *et al.*, 2006). Unlike AtANN1 however, not much literature has been produced on AtANN2 in terms of its function in response to different environmental stimuli.

AtANN1 was heavily implicated as the ROS-activated calcium channel that mediates calcium influx under salinity stress (Laohavisit *et al.*, 2013). In contrast to *AtANN1*, *AtANN2* gene expression was significantly down-regulated by salinity stress suggesting a possible role of negative regulator. Similar to salinity stress, *AtANN2* was also down-regulated in the presence of oxidative stress by H_2O_2 (Richards *et al.*, 2014). In the same test, it was discovered that treatment with the calcium channel blocker Gd^{3+} partially recovered the down-regulated expression suggesting that the expression of *AtANN2* depends on the calcium influx across the plasma membrane.

Information on the function of AtANN2 in biotic stress is also limited. Based on an interaction study carried out by Chen *et al.* (2012), AtANN2 was reported to be physically interacting with AtCPK1 (Calcium Dependent Protein Kinase 1). AtCPK1 in turn was

heavily associated with pathogen response in plants (Coca & Segundo, 2010). In a pathogen test, AtCPK1 was found to be phosphorylating an NADPH Oxidase, which is responsible for ROS production that could lead to programmed cell death (Gao *et al.*, 2013). Thus it might be possible that AtANN2 could be one of the components that activate AtCPK1 in the production of ROS through NADPH Oxidase.

Since eATP was found to be released under both biotic and abiotic stresses, here eATP is envisaged as the central regulator of these stress stimuli. We have discovered in Chapter 4 that both AtANN1 and AtANN2 is involved in mediating ATP-induced $[Ca^{2+}]_{cyt}$ accumulation. It is fitting that AtANN1 was found to be required in salinity stress response (Laohavisit *et al.*, 2013) as it was shown here to be a component of eATP signalling pathway (Chapter 3) that is hypothesised to be upstream of the stress responses. In order to figure out whether AtANN2, as another possible components of eATP signalling pathway, is also needed for stress responses in plants, we tested for its function in both biotic and abiotic stresses in *A.thaliana.*

In this chapter, we screened the possible function of AtANN2 in either oxidative stress, salinity stress or bacterial flagellin22 (flg22) elicitor response. All of these stimuli are known to cause an increase in $[Ca^{2+}]_{cyt}$ (Richards *et al.*, 2014; Laohavisit *et al.*, 2013; Jeworutzki *et al.*, 2010) and so the *Atann2* loss of function mutant expressing cytosolic (apo)aequorin has been used to test for a possible role for AtANN2 in the $[Ca^{2+}]_{cyt}$ increase. The effect of salinity stress on *Atann2* root growth and development has also been examined. The flg22 elicitor also induces an ROS burst (Ranf *et al.*, 2011) and this has been examined in the *Atann2* mutant, together with the effects of flg22 on root growth and development. Finally, the production of stable lines in which the *Atann2* mutant is complemented (driven by native promoter expression) is described.

5.2 Results

5.2.1 Role of AtANN2 in H_2O_2-induced calcium response at whole root level

AtANN1 was implicated to be the ROS-induced HACC under salinity stress (Laohavisit *et al.*, 2013). H_2O_2 is one of the most stable species of ROS that is produced when plants experience stress (Smirnoff and Arnaud, 2019). As AtANN2 is closely related to AtANN1 in terms of the amino acid sequence, we would like to test the possibility of AtANN2 being involved in mediating $[Ca^{2+}]_{cyt}$ elevation in the presence of H_2O_2. Seven-day-

old whole roots of Col-0 and *Atann2* loss-of-function mutant were subjected to $[Ca^{2+}]_{cyt}$ measurement assay by using apo-aequorin expressed under the 35S CAMV promoter (method as in Chapter 2.6.6). Since the $[Ca^{2+}]_{cyt}$ response to H_2O_2 required about 2000 s to show a clear $[Ca^{2+}]_{cyt}$ peak response (Richards *et al.*, 2014), the measurements were taken for every 6 seconds instead of every second due to the inability of the plate reader used to measure for more than 20 minutes (if setting is for 1 s per interval) for each well of the 96-well plate.

Before the H_2O_2 treatment was tested, both Col-0 and *Atann2* were tested with control solution (2 mM MES/Tris-HCl; 10 mM $CaCl_2$; 0.1 mM KCl) to determine the baseline $[Ca^{2+}]_{cyt}$. The time course of the control treatment in Figure 5.1 A showed a single touch peak produced by both Col-0 and *Atann2* whole roots after the addition of control treatment at the 35th second before returning to basal level. Comparison between the touch peak value of Col-0 (0.19±0.04 μM) and *Atann2* (0.21±0.04 μM) revealed no significant difference between the two genotypes (Figure 5.1 B). This is also true for the overall $[Ca^{2+}]_{cyt}$ accumulated as shown in Figure 5.1C where Col-0 (1.25±0.21 μM) was similar to *Atann2* (1.50±0.85 μM).

Unlike the control solution, 5 mM H_2O_2 treatment evoked a biphasic $[Ca^{2+}]_{cyt}$ response after the touch response (Figure 5.1 D). Under 5 mM H_2O_2 treatment, the touch peak value of the Col-0 samples (0.17±0.07 μM) was not significantly different from the *Atann2* samples (0.14±0.04 μM) confirming that mutation of *AtANN2* has no effect on the mechanical response of the roots (Figure 5.1 E). Analysis of the peak values showed no significant difference between Col-0 (first peak 0.21±0.01 μM; second peak 0.24±0.02 μM) and *Atann2* (first peak 0.20±0.04 μM; second peak 0.21±0.04 μM) (Figure 5.1 F, G). Based on the total $[Ca^{2+}]_{cyt}$ accumulated, we found that AtANN2 might not be required for the H_2O_2-induced $[Ca^{2+}]_{cyt}$ response as *Atann2* loss-of-function mutant (23.4±3.02 μM) bore no significant difference to the Col-0 (24.07 ±1.92 μM) in the overall area under the curve (Figure 5.1 H).

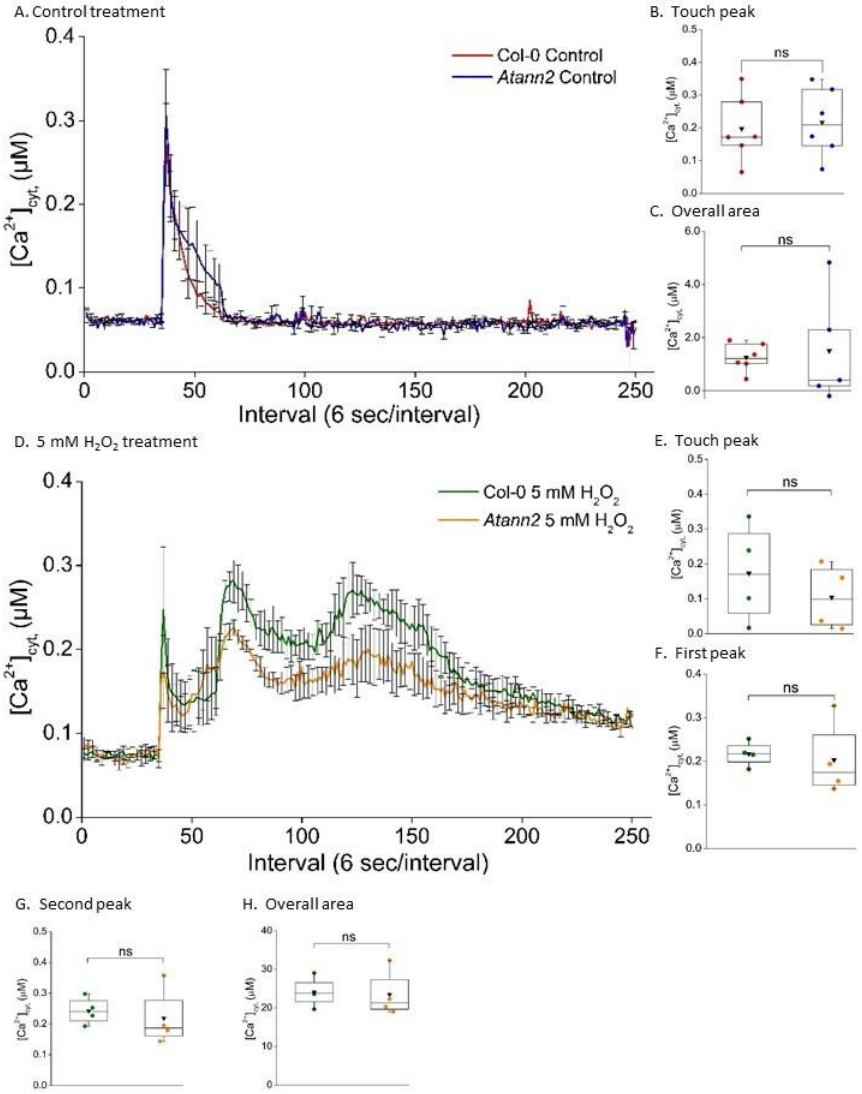

Figure 5.1: **AtANN2 might not play a role in mediating $[Ca^{2+}]_{cyt}$ elevation by H_2O_2 treatment.** Both Col-0 and *Atann2* 7-day-old whole roots expressed cytosolic apo-aequorin. The $[Ca^{2+}]_{cyt}$ response for the control treatment (A) and 5 mM H_2O_2 (D) were recorded for 250 intervals (6 seconds per interval) where each treatment was added at the 35th interval. Background measurement was taken for the first 35 intervals (1 s per interval for 35 intervals). These data are from the means ± SEM of 4 independent trials, with *n* = 4 - 6 roots per genotype and treatment. Touch peak (B) represents the highest value of the touch response (35 - 44 intervals) whereas the overall area (C) is the total area under the curve extracted from the line graph of the control treatment (35 - 250 intervals). Analysis of the 5 mM H_2O_2 treatment line graph is split up into the first peak (F) (44 - 104 intervals) and the second peak (G) (104 - 250 intervals) responses, which are the highest values of the peaks that emerged after the touch response (E) (35 - 44 intervals). The total accumulation of $[Ca^{2+}]_{cyt}$ of Col-0 and *Atann2* was determined through the overall area under the curve (H) (35 - 250 intervals). All calculations carried out are with the baseline (the first 35 s of measurement) subtracted. Middle line of the boxplot represents the median whereas the inverted triangle represents the mean. *p*-values: ns

(p>0.05), * (p<0.05), ** (p<0.01),*** (p< 0.001), Welch's t-test for parametric test and Wilcoxon rank-sum test for non-parametric test.

5.2.2 AtANN2 role in mediating calcium response due to salinity stress at whole seedling and whole root level

A previous study suggested both AtANN1 and AtANN2 might work together in mediating heat-stress response (Wang *et al.*, 2015). Since AtANN1 was highly involved in mediating salinity stress, we tested the same possibility of co-operation with AtANN2 in the $[Ca^{2+}]_{cyt}$ response due to high concentration of NaCl. Similar to previous tests, both Col-0 and *Atann2* 7-day-old whole seedlings containing cytosolic apo-aequorin were monitored for changes in $[Ca^{2+}]_{cyt}$ elevation between the two genotypes under control treatment or 200 mM NaCl treatment. Since salinity stress might impose both ionic and osmotic stress, 400 mM sorbitol treatment was added as a control to differentiate between the ionic effect of the NaCl from the osmotic effect.

We found that both Col-0 and *Atann2* whole seedlings produced oscillations of $[Ca^{2+}]_{cyt}$ elevation with different signatures and period for each individual seedling as shown in Figure 5.2 A and Figure 5.2 B when treated with 200 mM NaCl. Due to this condition, we were unable to analyse each peak value as the time range for each peak was different. Thus, analysis was only carried out on the touch response and the total $[Ca^{2+}]_{cyt}$ accumulated over the time course. Under control treatment, the touch response showed no significant difference between Col-0 (0.12±0.01 μM) and *Atann2* (0.12±0.01 μM) whole seedlings confirming that the $[Ca^{2+}]_{cyt}$ baseline between the two genotypes was similar and the mutation did not interfere with the mechanical response of the seedlings (Figure 5.2 C). This is again confirmed by the total $[Ca^{2+}]_{cyt}$ increase of both Col-0 (0.99±0.13 μM) and *Atann2* (0.44±0.13 μM) in the control treatment being statistically similar (Figure 5.2 D).

The touch peak due to 200 mM NaCl showed significantly lower Col-0 (1.0±0.01 μM) $[Ca^{2+}]_{cyt}$ value compared to the *Atann2* (1.09±0.02 μM) (Figure 5.2 E). In contrast, the total $[Ca^{2+}]_{cyt}$ accumulated by Col-0 (30.8±0.57 μM) in the presence of 200 mM NaCl was significantly higher than the *Atann2* (28.7±0.72 μM) (Figure 5.2 F). This could hint to the effect of NaCl treatment on touch mechanical response and the possible involvement of AtANN2 in mediating the NaCl-induced $[Ca^{2+}]_{cyt}$ response. Sorbitol control carried out confirmed that the majority of the $[Ca^{2+}]_{cyt}$ response was due to the ionic stress of NaCl rather than osmotic stress as the sorbitol-induced $[Ca^{2+}]_{cyt}$ touch peak (Col-0 0.82±0.02 μM; *Atann2*

0.84±0.02 μM) and total $[Ca^{2+}]_{cyt}$ accumulation (Col-0 22.12±0.85 μM; *Atann2* 20.86±0.6 μM) were significantly lower than the NaCl samples in both Col-0 and *Atann2*. No significant differences were found between the two genotypes in both touch peak value and the total $[Ca^{2+}]_{cyt}$ increase in the 400 mM sorbitol treatment (Figure 5.2 G, H).

Due to the oscillatory nature of NaCl-induced $[Ca^{2+}]_{cyt}$ response at whole seedling level, the test was repeated at whole root level to obtain a more specific response from both Col-0 and *Atann2*. Figure 5.3 A shows the single touch peak response by Col-0 and *Atann2* due to control treatment. Statistical analysis unveiled that *Atann2* touch peak value (0.16±0.01 μM) and the total $[Ca^{2+}]_{cyt}$ produced (1.95±0.26 μM) in the control treatment were not significantly different to the Col-0 samples (touch peak 0.17±0.02 μM; total $[Ca^{2+}]_{cyt}$ 2.06±0.32 μM) (Figure 5.3 B, C).

Time course $[Ca^{2+}]_{cyt}$ traces in 200 mM NaCl treatment and 400 mM sorbitol showed no $[Ca^{2+}]_{cyt}$ oscillations formed at whole root level. Col-0 and *Atann2* evoked a small peak after the touch response in 200 mM NaCl treatment whereas no peak was formed by the 400 mM sorbitol treatment (Figure 5.3 D). No significant differences were found between Col-0 and *Atann2* in the touch peak value of both 200 mM NaCl (Col-0 1.15±0.03 μM; *Atann2* 1.12±0.04 μM) and 400 mM sorbitol (Col-0 0.86±0.03 μM; *Atann2* 0.83±0.03 μM) treatment (Figure 5.3 E, F). Unlike the test carried out at whole seedling level, Col-0 whole root (37.5±1.24 μM) accumulated statistically similar total $[Ca^{2+}]_{cyt}$ compared to the *Atann2* (35.6±1.49 μM) at whole root level when exposed to 200 mM NaCl treatment. The 400 mM sorbitol treatment caused no significantly different total $[Ca^{2+}]_{cyt}$ accumulation between Col-0 (29.2±1.16 μM) and *Atann2* (27.3±0.89 μM) at whole root level (Figure 5.3 H).

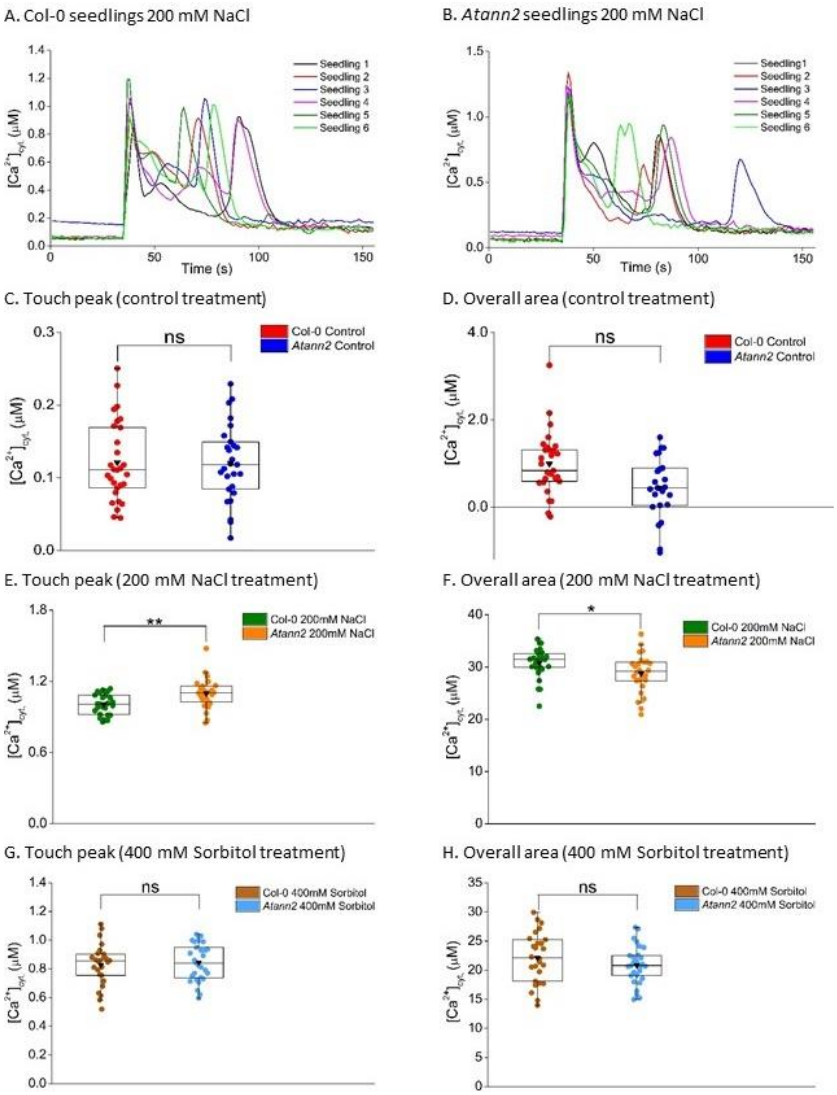

Figure 5.2: **$[Ca^{2+}]_{cyt}$ oscillation in both Col-0 and *Atann2* whole seedlings due to 200 mM NaCl treatment**. Seven-day-old Col-0 and *Atann2* whole seedlings tested expressed cytosolic apo-aequorin. The time course data show examples of $[Ca^{2+}]_{cyt}$ oscillations due to 200 mM NaCl in 6 Col-0 seedlings (A) and 6 *Atann2* seedlings (B) that were recorded for 155 seconds where the treatment was added at the 35th second. Touch peak due to control treatment (C) represents the highest value of the touch response (35 - 50 s) whereas the overall area (D) is the total area under the curve extracted from the time course data of the control treatment (35 - 155 s) (time course data for control and sorbitol treatment are not shown). Time course analysis of the 200 mM NaCl and 400 mM sorbitol treatment is split up only into the touch peak (E,G) (35 - 50 s) and the overall area (F, H) respectively due to different period of oscillation for each seedling. The total accumulation of $[Ca^{2+}]_{cyt}$ was determined through the overall area under the curve (35 - 155 s). Box plot data are from the means ± SEM of 5 independent trials, with n = 26 - 29 seedlings per genotype and treatment. All calculations carried out are with the baseline (the first 35 seconds of measurement) subtracted. Middle line of the boxplot represents the median whereas the inverted triangle represents the mean. p-values: ns (p>0.05), *

(p<0.05), ** (p<0.01), Welch's t-test for parametric test and Wilcoxon rank-sum test for non-parametric test.

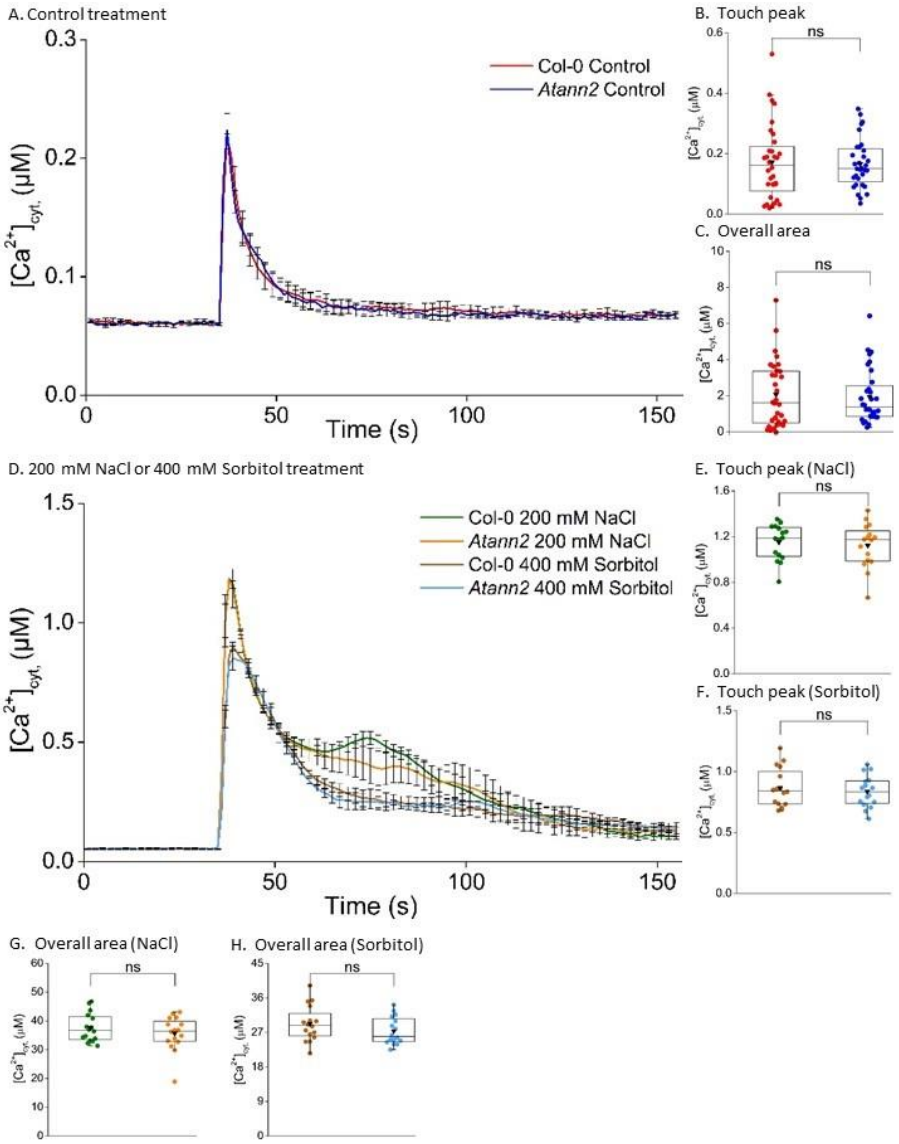

Figure 5.3: **AtANN2 mutation has no impact on the $[Ca^{2+}]_{cyt}$ elevation by 200 mM NaCl at whole root level.** Both Col-0 and *Atann2* 7-days-old whole roots expressed cytosolic apo-aequorin. The $[Ca^{2+}]_{cyt}$ response for the control treatment (A) and 200 mM NaCl or 400 mM sorbitol (D) were recorded for 155 seconds where each treatment was added at the 35th second. The time course data are from the means ± SEM of 4 independent trials, with n = 16 - 32 roots per genotype and treatment. Touch peak (B) represents the highest value of the touch response (35 - 63 s) whereas the overall area (C) is the total area under the curve extracted from the time course data of the control treatment (35 - 155 s). Time course analysis of the 200 mM NaCl or 400 mM sorbitol treatment is split up into the touch peak (E; 200 mM NaCl, D; 400 mM sorbitol) (41 - 63 s) and the overall area. The total accumulation of $[Ca^{2+}]_{cyt}$ of Col-0 and *Atann2* were determined through the overall area under the curve (G; 200 mM NaCl, H; 400 mM sorbitol) (35 - 155 s). All calculations carried out are with the

baseline (the first 35 s of measurement) subtracted. Middle line of the boxplot represents the median whereas the inverted triangle represents the mean. *p*-values: ns ($p>0.05$), * ($p<0.05$), ** ($p<0.01$),*** ($p< 0.001$), Welch's *t*-test for parametric test and Wilcoxon rank-sum test for non-parametric test.

5.2.3 Salinity stress affected seed germination of both Col-0 and *Atann2*.

Long term exposure of plants to salinity stress or exposure to salinity shock has been shown to be detrimental to growth and development of plants (Shavrukov, 2013). Stunted plant growth was linked to the high Na^+ content that activated the plasma membrane Na^+/H^+ antiporter thus diverting the plant's sources towards survival instead of focusing on vegetative growth and reproduction (Shi *et al.*, 2000). Sensing of high Na^+ content is thought to be by plasma membrane GIPC (glycosyl inositolphosphorylceramide) sphingolipid (Jiang *et al.*, 2019). The downstream process of the perception and the components that are involved which lead to the growth inhibition however are not yet known and fully understood. As AtANN2 was shown to possibly be involved in mediating the $[Ca^{2+}]_{cyt}$ under salinity stress at whole seedling level, here we tested the *Atann2* mutant alongside Col-0 in a seed germination assay to test for AtANN2's involvement in NaCl-induced growth retardation.

Both Col-0 and *Atann2* seeds were sterilised and germinated onto either ½ MS medium (control treatment), 200 mM NaCl-containing ½ MS medium or 400 mM sorbitol-containing ½ MS medium; all without sucrose (pH 5.8) (seed sterilisation as explained in Chapter 2.1). Rate of germination was observed for 9 days after 3 days of stratification. Figure 5.4 shows the percentage of germination of both Col-0 and *Atann2* seeds in 3 different conditions; control, 200 mM NaCl and 400 mM sorbitol. On day 1, some of the Col-0 (21.8±19.06 %) and *Atann2* (15.76±10.52 %) seeds in the control medium started to germinate whereas none of the seeds in NaCl or sorbitol medium did. Similar observations of no seed germination were found on day 2 and day 3 for the two genotypes in both NaCl and sorbitol medium (Figure 5.4 B, C). However, there was an exception to the Col-0 grown on sorbitol medium as 1.11±1.11 % of the total seeds started to germinate on the third day (Figure 5.4 C). Percentage of germination continued to rise for both Col-0 and *Atann2* in control medium and reached maximum percentage on day 5. Note that some of the seeds failed to germinate at all causing the maximum germination percentage to be less than 100% for the control medium. Statistical analysis carried out revealed no significant differences in the percentage of germination between Col-0 and *Atann2* in the control medium (Figure 5.4 A).

Germination of seeds in the 200 mM NaCl medium was delayed until day 5 for Col-0 where only 5.8±5.8 % of seeds started to germinate. *Atann2* on the other hand only started to germinate (2.9±1.8 %) on day 6. Both Col-0 and *Atann2* germination slowly rose from day 7 (Col-0 16.11±10.19 %; *Atann2* 7.6±1.18%) until day 9 (Col-0 41.9±2.27 %; *Atann2* 32±4.3 %). Germination of almost half of the total seeds was inhibited by the presence of 200 mM NaCl compared to the control medium in both Col-0 and *Atann2*. No significant differences were found between Col-0 and *Atann2* percentage of germination in the NaCl medium (Figure 5.4 B).

As previously mentioned, Col-0 seeds were delayed for only 2 days whereas *Atann2* seeds were delayed for 3 days when grown on 400 mM sorbitol-containing medium. On day 4, both Col-0 and *Atann2* percentage of germination was higher than the NaCl medium until day 9. Some of the seed germination was totally inhibited by the sorbitol treatment as the maximum percentage reached on day 9 in sorbitol medium was lower compared to the control treatment in both Col-0 (control 95±2.4 %; sorbitol 71.8±7.27 %) and *Atann2* (control 98.12±0.95 %; sorbitol 52±10.67 %). Col-0 and *Atann2* bore no significant difference in terms of germination percentage in the sorbitol treatment medium (Figure 5.4 C).

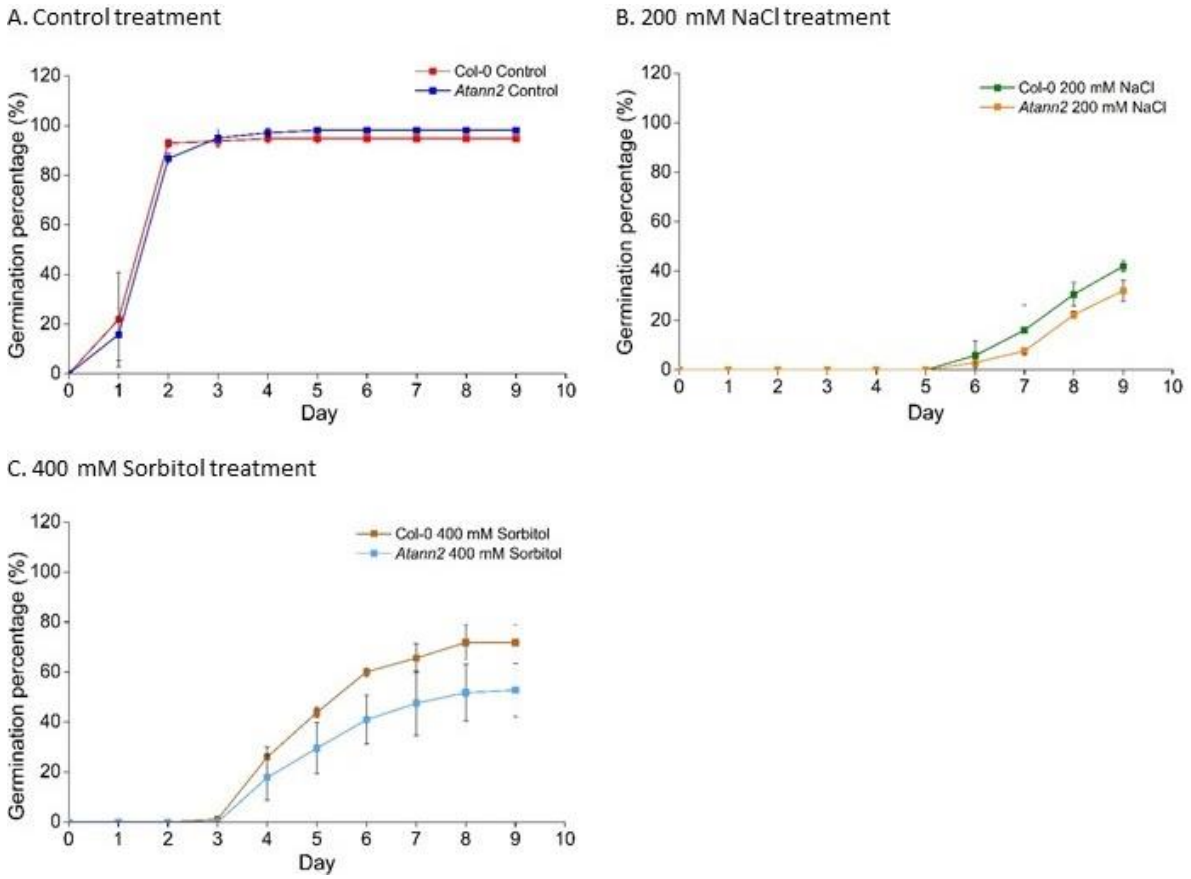

Figure 5.4: **Seed germination was impaired in 200 mM NaCl-containing medium and 400 mM sorbitol-containing medium.** Col-0 and *Atann2* seeds were germinated on ½ MS media as control treatment (A), ½ MS medium containing 200 mM NaCl (B) or ½ MS medium containing 400 mM sorbitol as osmotic control (C); all without sucrose and at pH 5.6. Seed germination was observed for 9 days for each treatment before the germination percentage was calculated. These data were from the means ± SEM of 3 independent trials, with n = 28 – 30 seeds per genotype and treatment. Welch's *t*-test was used for parametric test and Wilcoxon rank-sum test for non-parametric test.

5.2.4 Salinity-induced growth reduction and the role of AtANN2 in regulating it

High NaCl content proved to be affecting the rate of seed germination based on the findings of the previous chapter (Chapter 5.2.3) although AtANN2 seems not to be involved. A study reported *Atann1* loss-of-function mutant exhibited higher tolerance towards salinity stress in terms of growth and viability compared to the wild type (Huh *et al.*, 2010). AtANN2 was found to be highly expressed in roots (Clark *et al.*, 2001), thus it would be interesting to find out whether AtANN2 could be one of the components that affect the growth of *A. thaliana* plants in high salinity conditions. Here, we compared the growth of Col-0 and *Atann2* seedlings after 6 days when grown in either control medium (½ MS, no sucrose, pH 5.6), 200 mM NaCl medium (½ MS, 200 mM NaCl, no sucrose, pH 5.6) and 400 mM

sorbitol medium (½ MS, 400 mM sorbitol, no sucrose, pH 5.6). Growth of the seedlings was observed based on the parameters such as the primary root length, the density of lateral roots formed, possible skewing of roots via horizontal growth index and the degree of skewing, plus the fresh weight. The seeds were all germinated on control medium first for 3 days before being carefully transferred to treatment medium as high salinity proved to be affecting germination. Figure 5.5 shows the representative images of Col-0 and *Atann2* seedlings grown either in control treatment (Figure 5.5 A, B), 200 mM NaCl treatment (Figure 5.5 C, D) or the 400 mM sorbitol (Figure 5.5 E, F).

Exposure to 200 mM NaCl inhibited the growth of primary roots of Col-0 (4.75±0.12 cm) and *Atann2* (4.58±0.25 cm) compared to the control medium (Col-0 7.77±0.35 cm; *Atann2* 8.0±0.36 cm) as shown in Figure 5.6 A. These observations were also true for the seedlings grown on 400 mM sorbitol medium (Col-0 5.14±0.15 cm; *Atann2* 4.76±0.30 cm). Statistical analysis however confirmed that AtANN2 might not be involved in the regulation of the primary root growth as no significant difference in terms of primary root length was found between Col-0 and *Atann2* roots for all the three different treatments (Figure 5.6 A).

Other than primary root growth, high salinity seems to be affecting the lateral root density as the lateral root density of both Col-0 (0.08±0.01) and *Atann2* (0.10±0.01) grown in 200 mM NaCl medium were reduced compared to the roots grown in control medium (Col-0 0.50±0.06; *Atann2* 0.50±0.02) (Figure 5.6 B). Osmotic stress imposed by 400 mM sorbitol also affecting the lateral root density as Col-0 (0.29±0.11) and *Atann2* (0.25±0.01) grown in sorbitol formed less dense lateral roots than those grown in control medium. In all of the three treatment media, there were no significant differences between Col-0 and *Atann2* indicating that AtANN2 again might not be involved in the root growth regulation under normal or stress conditions (Figure 5.6 B).

Horizontal growth index (HGI) is the parameter that was used in this study to observe the direction of possible root skewing due to the different treatments. Positive value indicates that the roots were growing to the right whereas negative value indicates skewing to the left (Grabov *et al.*, 2005). Based on the HGI values shown in Figure 5.6C, 200 mM NaCl-containing medium seems to be causing a slight root skewing to the right as most of the roots have a positive HGI value. In contrast, the 400 mM sorbitol medium caused root slight skewing to the left as the HGI value of roots in this medium were mostly negative. As

expected, the control medium did not cause any root skewing and the roots were growing in a straight manner (Figure 5.6 C).

Since we already knew the direction of the root skewing based on the HGI value mentioned above, we calculated the degree of skewing to measure the magnitude of effect of the treatments. The 200 mM NaCl treatment (Col-0 14.55±2.53 °; *Atann2* 14.58±2.72 °) caused the highest degree of skewing compared to the control (Col-0 4.23±0.77 °; *Atann2* 3.81±0.09 °) and the 400 mM sorbitol (Col-0 5.76±0.33 °; *Atann2* 5.88±0.82 °) treatment in both Col-0 and *Atann2* roots. Osmotic stress by 400 mM sorbitol showed less effect compared to the high salinity condition as the degree of root skewing by the sorbitol treatment was not significant from the control treatment. Consistent with the results from other parameters of root growth, *Atann2* degree of root skewing did not differ significantly from the Col-0 in all the three different growth media (Figure 5.6 D).

The overall fresh weight of the seedlings might also be affected by salinity stress since it proved to interfere with the primary root growth. Based on statistical analysis carried out, 200 mM NaCl (Col-0 0.016±0.002 g; *Atann2* 0.015±0.003 g) and 400 mM Sorbitol (Col-0 0.018±0.002 g; *Atann2* 0.016±0.002 g) caused significant loss of fresh weight compared to the control medium (Col-0 0.029±0.003 g; *Atann2* 0.030±0.003 g) in both Col-0 and *Atann2* mutant. There was however no significant differences in fresh weight between genotypes effected by treatment with NaCl or sorbitol (Figure 5.6 E).

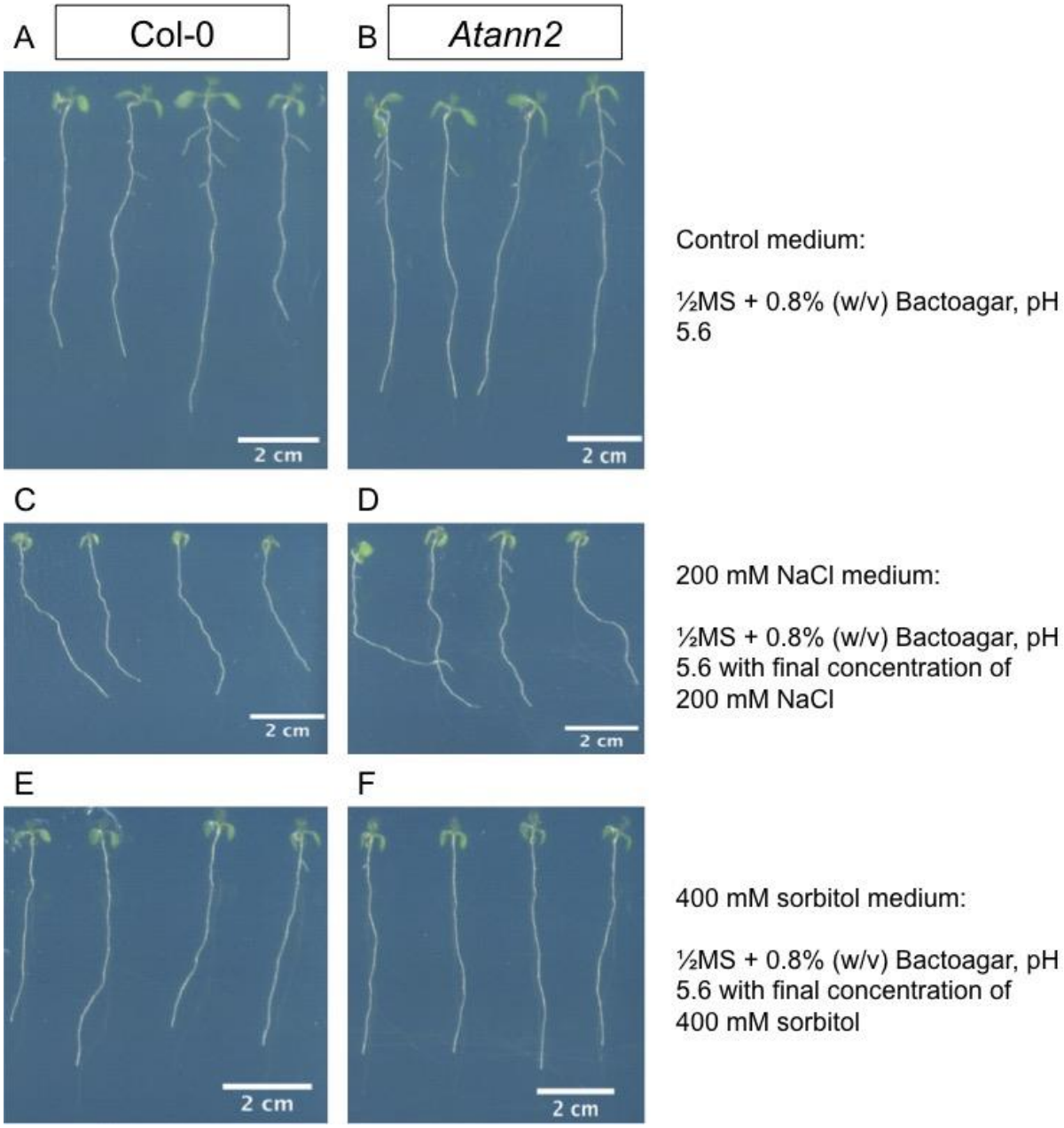

Figure 5.5: **Growth inhibition and roots right skewing caused by 200 mM NaCl treatment.** Col-0 and *Atann2* were grown on either control medium (A, B), 200 mM NaCl-containing medium (C, D) or on the 400 mM sorbitol-containing medium (E, F). All seeds were germinated on control medium for 3 days before being transferred to the different growth medium. Scan images were taken on the 6th day after transfer. Images shown were the representative of each treatment.

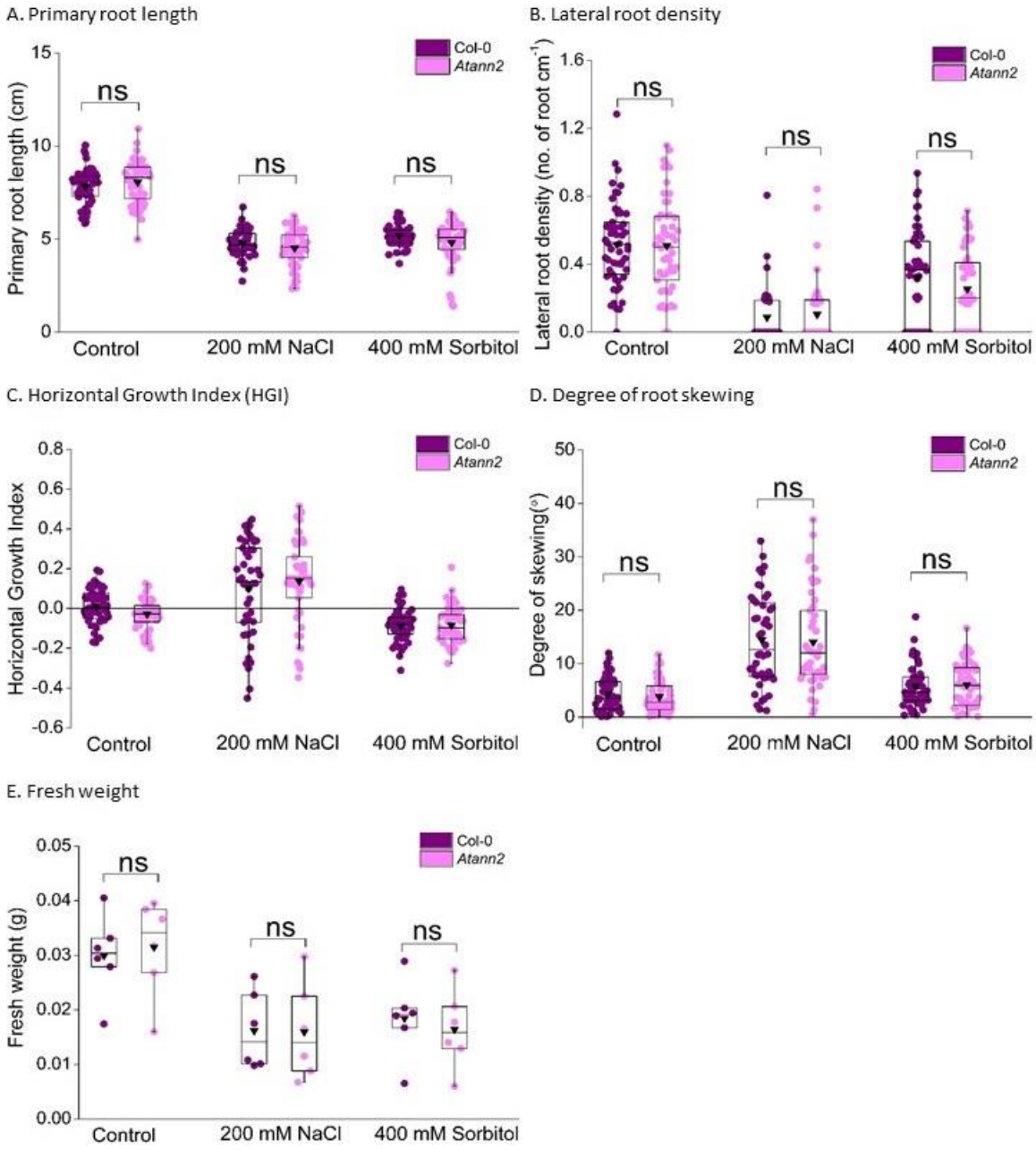

Figure 5.6: **Both Col-0 and *Atann2* growth were affected by the presence of 200 mM NaCl.** The effect of 200 mM NaCl contained in ½ MS growth medium for Col-0 and *Atann2* was observed through changes in the primary root length (A), lateral root density (B), horizontal growth index (C), degree of root skewing (D) and the seedling fresh weight (E). Growth medium containing 400 mM sorbitol acted as the osmotic control to the salinity stress tested whereas control treatment represent normal ½ MS growth medium. All seeds were germinated on normal growth medium (½ MS medium) for 3 days before being transferred onto treatment-containing medium. Measurements were taken at the 6th day after being transferred. These data were from the means ± SEM of 3 independent trials, with n = 15 - 20 seedlings per genotype and treatment. Middle line of the boxplot represents the median whereas the inverted triangle represents the mean. p-values: ns (p>0.05), * (p<0.05), ** (p<0.01),*** (p< 0.001); Analysis of Variance (ANOVA) with Tukey's test.

5.2.5 Role of AtANN2 in producing calcium response at whole root level in the presence of flg22.

In Chapter 4.2.2, we have focused on the role of AtANN2 in mediating eATP-induced $[Ca^{2+}]_{cyt}$ elevation possibly as a calcium channel. Past studies have demonstrated that biotic stress PAMP elicitors evoked eATP production (Kim *et al.*, 2006; Wu *et al.*, 2008). Since flg22 is one of the PAMP elicitors, we hypothesised that eATP could be the signalling molecule that governs stress responses in plants including biotic stresses. Discovering the role of AtANN2 under flg22 stress would be helpful in order to relate the eATP signalling molecule to the downstream responses in biotic stress conditions. Flg22 elicitor has previously been shown to induce $[Ca^{2+}]_{cyt}$ elevation, production of ROS burst and inhibition of growth and development (Ranf *et al.*, 2011). In this chapter we tested the changes in the $[Ca^{2+}]_{cyt}$ elevation in *Atann2* loss-of-function mutant when subjected to 1 μM flg22 treatment. *Atfls2* loss of function mutant of the flg22 receptor was also included in these tests as a control for the flg22 perception (Gómez-Gómez and Boller, 2000)

Figure 5.7 A shows the $[Ca^{2+}]_{cyt}$ traces from whole seedlings in response to control treatment (2 mM MES/Tris-HCl; 10 mM $CaCl_2$; 0.1 mM KCl) where Col-0, *Atann2* and *Atfls2* produced a familiar single touch peak before returning to basal level for 250 intervals (6 seconds per measurement). Analysis of the touch peak (Col-0 0.18±0.02 μM; *Atann2* 0.09±0.03 μM*; Atfls2* 0.18±0.05 μM) and the total $[Ca^{2+}]_{cyt}$ accumulation (Col-0 0.30±0.82 μM; *Atann2* 2.23±0.66 μM; *Atfls2* 0.5±0.40 μM) showed no significant difference between Col-0 and *Atann2* or *Atfls2* (Figure 5.7 B, C).

Replacing the control treatment with 1 μM flg22 solution caused Col-0, *Atann2* but not *atfls2* to evoke a single $[Ca^{2+}]_{cyt}$ peak after the touch peak that lasted until the end of measurement (Figure 5.7 D). Detailed statistical analysis of the touch peak revealed no significant difference in terms of $[Ca^{2+}]_{cyt}$ touch peak value between Col-0 (0.06±0.01 μM) and *Atann2* (0.11±0.02 μM) or *Atfls2* (0.05±0.01 μM). *Atann2* however produced a significantly higher touch response than *Atfls2* (Figure 5.7 E). First peak $[Ca^{2+}]_{cyt}$ value due to the flg22 treatment demonstrated that Col-0 (0.09±0.01 μM) first peak was not significantly different from *Atann2* (0.1±0.05 μM). Absence of AtFLS2 proved to be effective in inhibiting the flg22 response as the $[Ca^{2+}]_{cyt}$ first peak value of *Atfls2* (0.02±0.007 μM) was significantly impaired compared to Col-0 and *Atann2* (Figure 5.7 F). Consistent with the first peak, the total $[Ca^{2+}]_{cyt}$ accumulated in the flg22 treatment of *Atfls2* (0.5±0.1 μM) was

significantly lower compared to the Col-0 (12.55±0.87 µM) and *Atann2* (13.4±0.6 µM). There was however no significant difference between Col-0 and *Atann2* in the total accumulation of $[Ca^{2+}]_{cyt}$ in the flg22 treatment (Figure 5.7 G).

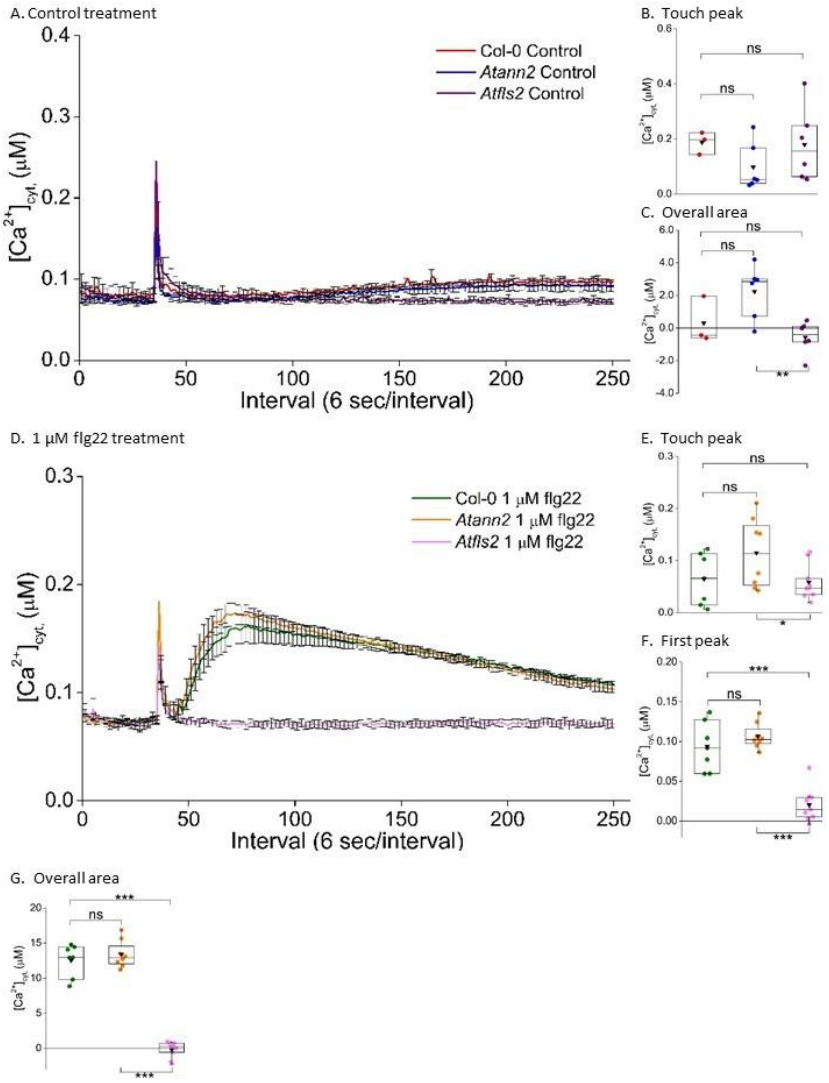

Figure 5.7: **Both Col-0 and *Atann2* produced $[Ca^{2+}]_{cyt}$ increase due to 1 µM flg22 treatment.** Col-0, *Atann2* and *Atfls2* (knock-out mutant of flg22 receptor) 7-day-old whole seedlings used contained cytosolic apo-aequorin. The $[Ca^{2+}]_{cyt}$ response for the control treatment (A) and 1 µM flg22 (D) were recorded for 250 intervals (6 s $[Ca^{2+}]_{cyt}$ measurement per interval) where each treatment was added at the 35th interval. Background measurement was taken for the first 35 intervals (1 s per interval for 35 intervals). The data are from the means ± SEM of 6 independent trials, with n = 5 - 11 seedlings per genotype and treatment. Touch peak (B) represents the highest value of the touch response (35 - 43 intervals) whereas the overall area (C) is the total area under the curve extracted from the line graph of the control treatment (35 - 250 intervals). Interval course analysis of the 1 µM flg22 treatment is split up into the touch peak (E) (35 - 43 intervals) and the first peak (F) (43 - 250 intervals) responses. The total accumulation of $[Ca^{2+}]_{cyt}$ of Col-0, *Atann2* and *Atfls2* were determined through the overall

area under the curve (G) (35 - 250 intervals). All calculations were carried out with the baseline (the first 35 intervals of measurement) subtracted. Middle line of the boxplot represents the median whereas the inverted triangle represents the mean. *p*-values: ns ($p>0.05$), * ($p<0.05$), ** ($p<0.01$),*** ($p< 0.001$), Welch's *t*-test for parametric test and Wilcoxon rank-sum test for non-parametric test.

5.2.6 ROS burst due to flg22 treatment might not require AtANN2

One of the hallmarks of flg22 elicitor perception is the production of an ROS burst (Yi *et al.*, 2014). Other than looking at the calcium response, we also observed the ROS production to find out whether AtANN2 was involved in mediating the flg22-induced ROS response. ROS measurement was carried out by using luminol dye with horseradish peroxidase (HRP) on leaf discs prepared from 21-day-old leaves of Col-0, *Atann2* and *Atfls2*. The measurement was recorded for 250 intervals with 6 seconds period per interval (method as in Chapter 2.9.2). The unit of measurement used was RLU (Relative Light Unit), which represents the raw data obtained from the recording device (plate reader, FLUOstar OPTIMA; BMG Labtech).

All the samples were first treated with control solution (2 mM MES/Tris-HCl; 10 mM $CaCl_2$; 0.1 mM KCl) to determine the baseline level of ROS in all the genotypes. Upon addition of the control solution, a sharp peak of ROS was produced by Col-0, *Atann2* and *Atfls2*, which would be labelled as the touch peak. The ROS level then plummeted and remained low until the end of recording (Figure 5.8 A). Analysis of the touch peak revealed that the ROS burst at the touch peak was not significantly different between Col-0 (495±445 RLU) and *Atann2* (556±375 RLU) or *Atfls2* (23±7.7 RLU) (Figure 5.8 B). Total ROS production in control treatment also showed no significant difference between the three genotypes although the ROS value of Col-0 (2613±8201 RLU) and *Atfls2* (150.9±309 RLU) seemed to be lower than that of *Atann2* (2064±1192) (Figure 5.8 C).

The test was then done by adding 1 μM flg22 solution as treatment at the 35^{th} interval. Similar touch peak was produced by all three genotypes immediately after the addition of flg22 before the formation of another bigger ROS burst. The ROS burst lasted the entire recording before going down at the end of the measurement (Figure 5.8 D). Detailed analysis done on the ROS value of the touch peak induced by flg22 showed a lower ROS value of both *Atann2* (222±115 RLU) and *Atfls2* (228±123 RLU) compared to Col-0 (639±348 RLU) although not statistically significant (Figure 5.8 E). The importance of flg22 perception in the production of ROS burst was confirmed when the total ROS formation by *Atfls2*

(303±348 RLU) was significantly impaired compared to the Col-0 (92177±28800 RLU) and *Atann2*. Although the mean ROS burst value of *Atann2* (239200±71670 RLU) sample was higher than the Col-0, it was not statistically significant suggesting that the flg22-induced ROS burst does not require AtANN2 (Figure 5.8 F).

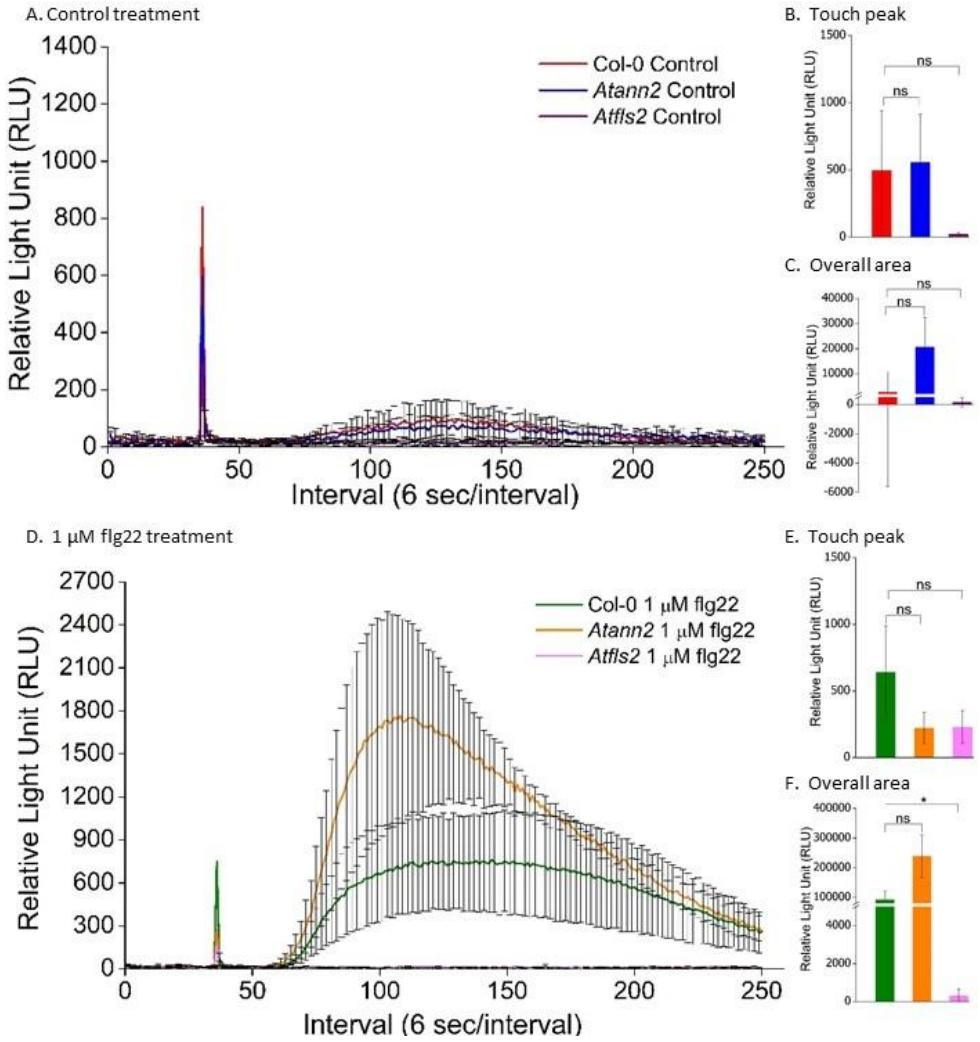

Figure 5.8: **flg22-induced ROS production by both Col-0 and *Atann2*.** Leaf discs were prepared from 21-day-old Col-0, *Atann2* and *Atfls2* leaves. The ROS production for the control treatment (A) and 1 µM flg22 (D) were recorded for 250 intervals (6 s per interval) where each treatment was added at the 35th interval. Background measurements were taken for the first 35 intervals (1 s per interval for 35 intervals). The data are from the means ± SEM of 4 independent trials, with n = 6 - 7 leaf discs per genotype and treatment. Touch peak (B) represents the highest value of the touch response (35 - 45 intervals) whereas the overall area (C) is the total area under the curve extracted from the data of the control treatment (35 - 250 intervals). Analysis of the 1 µM flg22 treatment is split up into the touch peak (E) (35 - 45 intervals) and the overall area. The total accumulation of $[Ca^{2+}]_{cyt}$ of Col-0, *Atann2* and *Atfls2* was determined through the overall area under the curve (H) (35 - 250 intervals). All calculations carried out were with the baseline (the first 35 intervals of measurement) subtracted. *p*-

values: ns (p>0.05), * (p<0.05), ** (p<0.01),*** (p< 0.001), Welch's *t*-test for parametric test and Wilcoxon rank-sum test for non-parametric test.

5.2.7 flg22 treatment might be affecting the primary root length of *Atann2* only

In past studies, flg22 elicitor inhibited the growth of plants (Ranf *et al.*, 2011). In order to determine whether AtANN2 was involved in the regulation of growth under biotic stress, we observed the growth of Col-0 and *Atann2* loss-of-function mutant when grown in the presence of 1 μM flg22 elicitor. All the seeds were germinated on normal control medium (½ MS, no sucrose, pH 5.6) for 3 days before being transferred to either control medium or flg22-containing medium (½ MS + 1 μM flg22, no sucrose, pH 5.6). Primary root length, lateral root density and the horizontal growth index were the parameters that were used to monitor the growth of both Col-0 and *Atann2* seedlings. Representative images of seedlings grown on either control medium or the 1 μM flg22 medium are as shown in Figure 5.9 (A, B) and Figure 5.9 (C, D) respectively.

The presence of 1 μM flg22 in the growth medium had no effect on Col-0 as the primary root length of Col-0 grown in control medium (4.34±0.16 cm) was similar to the Col-0 grown in flg22-containing medium (4.26±0.13 cm). Flg22 however seemed effective in inhibiting the primary root length of *Atann2* as the *Atann2* grown in 1 μM flg22 medium (4.39±0.14 cm) had significantly shorter primary root than the one grown in control medium (4.97±0.18 cm). However, no significant differences were found between Col-0 and *Atann2* in both control medium and the flg22-containing medium (Figure 5.10 A).

In contrast to primary root length, 1 μM flg22 failed to reduce the lateral root density as both Col-0 (control 0.81±0.07; flg22 0.81±0.10) and *Atann2* (control 1.22±0.10; flg22 1.0±0.09) bore statistically similar lateral root density in both control medium and the flg22 growth medium. Mutation of *AtANN2* however caused reduction in lateral root density as *Atann2* grown in both control medium and flg22-containing medium exhibited significantly lower lateral root density compared to the Col-0 (Figure 5.10 B). As explained in the Chapter 2.8.2, horizontal growth index (HGI) value is used as a tool to measure the direction of root skewing from horizontal growth. In this test, we found that addition of 1 μM flg22 did not cause any primary root skewing as both genotypes grown in either control (Col-0 0.10±0.01; *Atann2* 0.13±0.02) or flg22-containing medium (Col-0 0.22±0.12; *Atann2* 0.04±0.01) showed HGI value close to zero indicating straight horizontal growth. The absence of AtANN2 also

seemed to not be affecting the direction of the primary root growth as the HGI values of *Atann2* in both treatments were not different from the Col-0 (Figure 5.10 C).

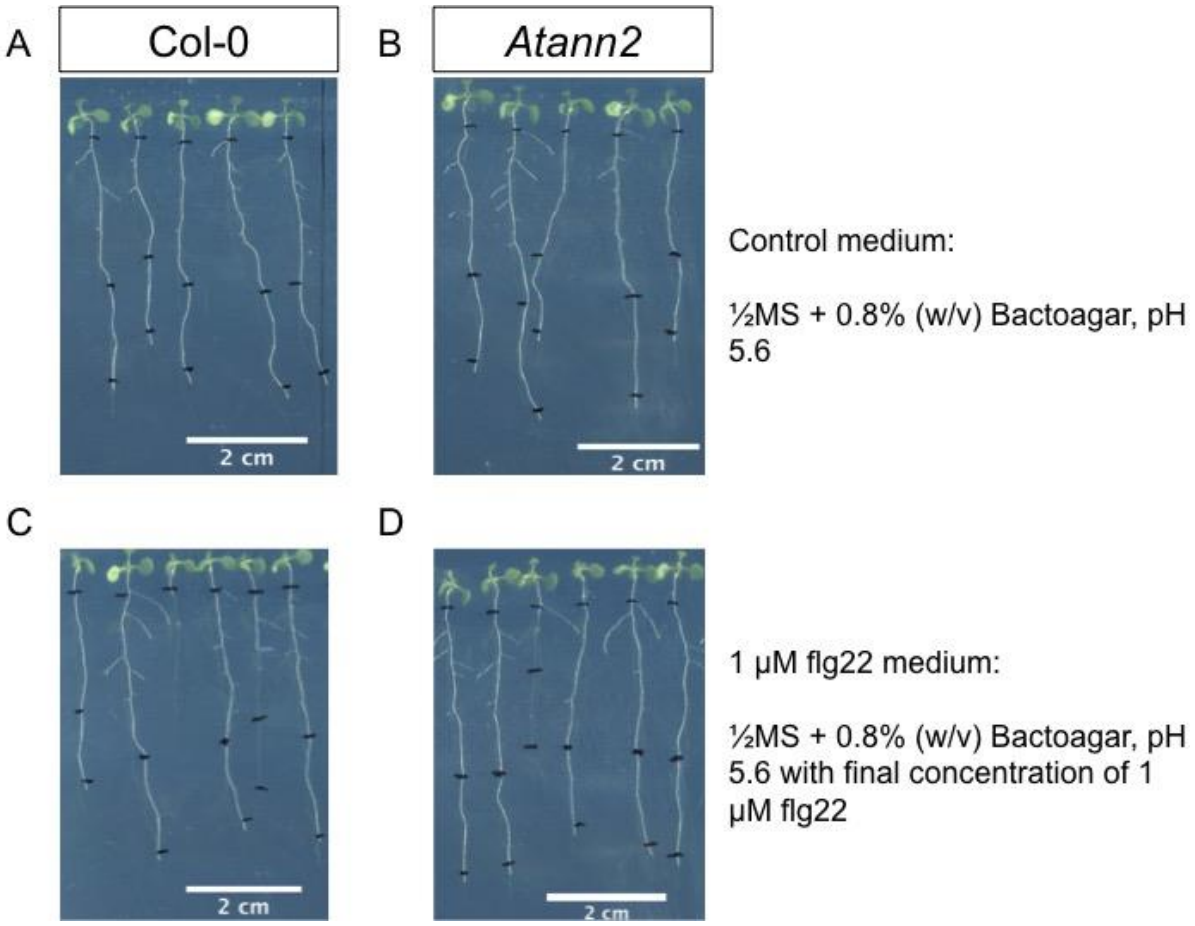

Figure 5.9: **1 µM flg22 was not effective in inhibiting root growth.** Images shown are the Col-0 and *Atann2* grown on either control medium (A,B) or the 1 µM flg22 medium (C,D). All seeds were germinated on normal control medium for 3 days before being transferred onto respective treatment plates and the images were taken after 6 days of transfer. Images are the representative of each treatment.

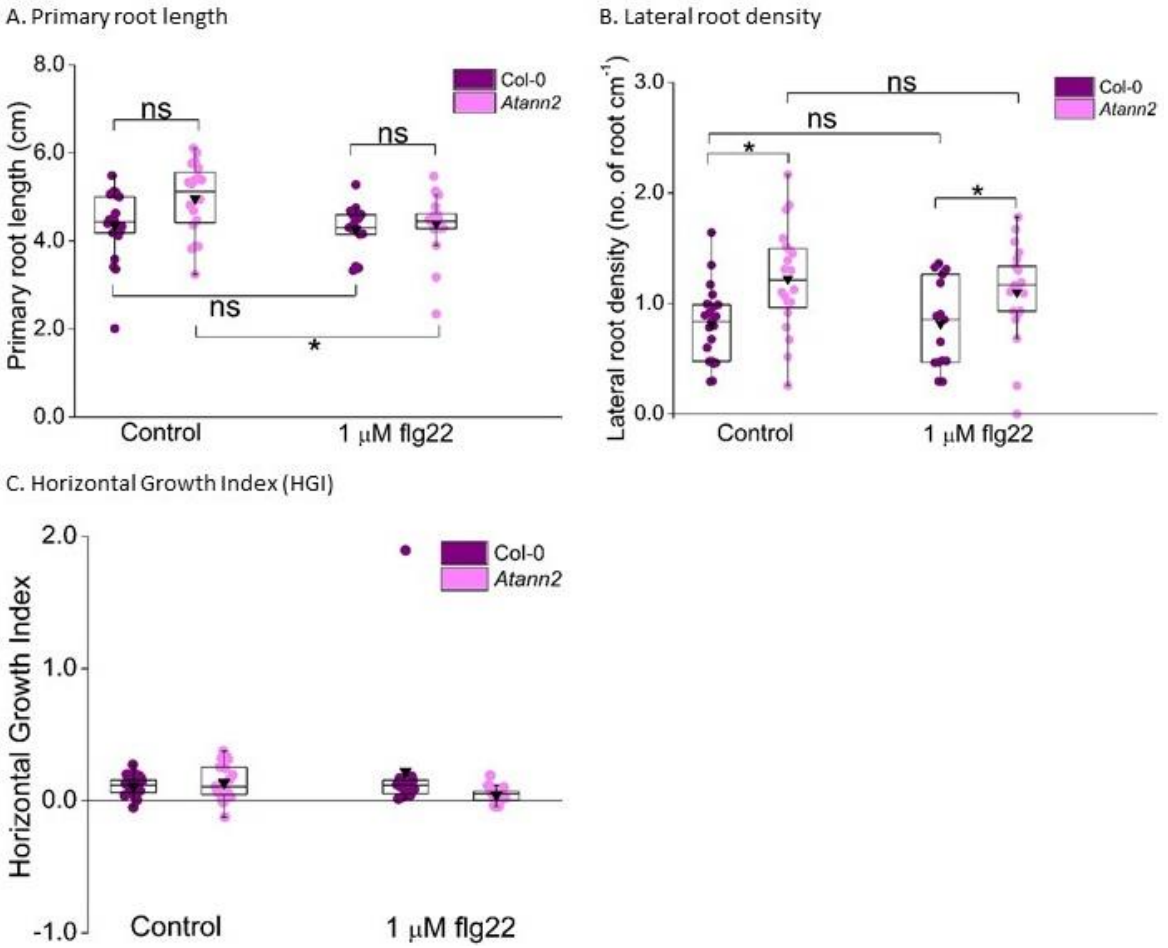

Figure 5.10: **flg22 affects the primary root length of *Atann2*.** The effect of flg22 on the growth of Col-0 and *Atann2* in ½ MS growth medium containing 1 μM flg22 was observed through changes in the primary root length (A), lateral root density (B), and horizontal growth index (C). Control treatment represents normal ½ MS growth medium and the Atfls2 acted as a control for the flg22 perception. All seeds were germinated on normal growth medium (½ MS medium) for 3 days before being transferred onto treatment-containing medium. Measurements were taken at the 6th day after being transferred. These data were from the means ± SEM of 2 independent trials, with n = 8 - 12 seedlings per genotype and treatment. Middle line of the boxplot represents the median whereas the inverted triangle represents the mean. p-values: ns (p>0.05), * (p<0.05), ** (p<0.01),*** (p< 0.001); Analysis of Variance (ANOVA) with Tukey's test.

5.2.8 Production of stable *Atann2/AtANN2* mutant complementary lines

Based on previous findings (Chapter 4.2.2 and Chapter 5.2.2), AtANN2 might be involved in mediating the $[Ca^{2+}]_{cyt}$ elevation in the presence of eATP (whole root) and also under high salinity conditions (whole seedling). This could support the hypothesis that eATP might be the initial signalling molecule that is upstream of the plant response towards stress conditions such as high salinity and AtANN2 might be one of the components involved in

this pathway possibly as a calcium channel. In order to complete the test carried out previously on the loss-of-function *Atann2* mutant, another set of tests with complemented *Atann2* mutant line (*Atann2/AtANN2*) is needed. In this chapter, we describe the outcomes from the production of stable *Atann2/AtANN2* complemented mutant line for future use.

a. AtANN2 gene amplification

AtANN2 gene with its native promoter was amplified first before the subsequent cloning process is done as explained in Chapter 2.12.1. Figure 5.11 shows the successful amplification of the *AtANN2* gene. The first 3 wells consist of Col-0 gDNA samples amplified by using the *AtANN2* with 2 kb native promoter primer (Pann2_ANN2). Based on the primer analysis done on NCBI Primer-Blast programme, the expected size of the PCR product is 3683 bp. The PCR products formed had the size of approximately ~3683 bp which showed that the correct *AtANN2* gene was amplified during the PCR reaction.

Since the PCR product formed based on the gel electrophoresis showed faint bands with different size to *AtANN2* and possible formation of primer dimer, the bands with the desired size (*AtANN2* gene) were excised from the gel and subjected to gel purification to obtain the pure PCR product. Gel purification was carried out by using QIAquick Gel Extraction kit (Qiagen). The method of extraction was as explained by the manufacturer. The concentration and purity of the amplified *AtANN2* gene PCR product were measured by using a nanodrop spectrophotometer.

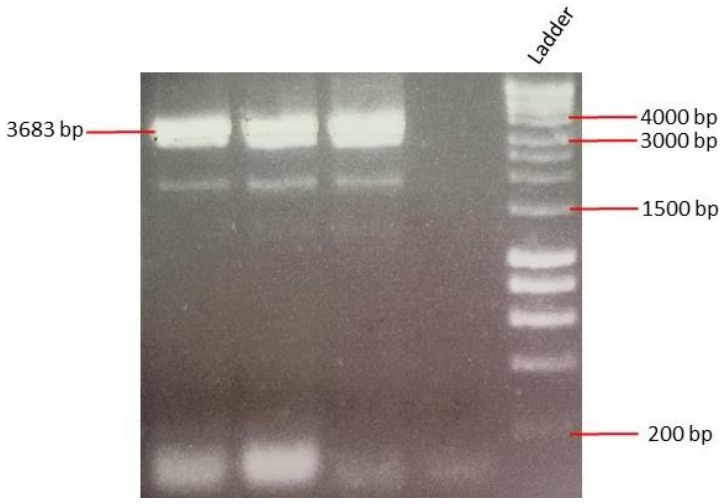

Figure 5.11: **Gel image from gel electrophoresis of PCR product of *AtANN2* gene amplification.** The first 3 wells contained the PCR product from the *AtANN2* with 2 kb native promoter primer pairs (Pann2_ANN2). The fourth well from the left contained the negative control PCR product (no template control). DNA ladder used for the gel electrophoresis was the 1 kb hyperladder (Bioline).

b. BP Cloning of AtANN2 construct into pDONR221 entry vector

The BP cloning reaction and the *E. coli* transformation was done as previously described in chapter 2.12.2. The transformations were successful as the colony PCR (method in chapter 2.12.3, Table 2.9 and Table 2.10) carried out showed one of the colonies amplified the correct PCR product size (~683 bp) indicating that it might carry the *AtANN2* construct (Figure 5.12).

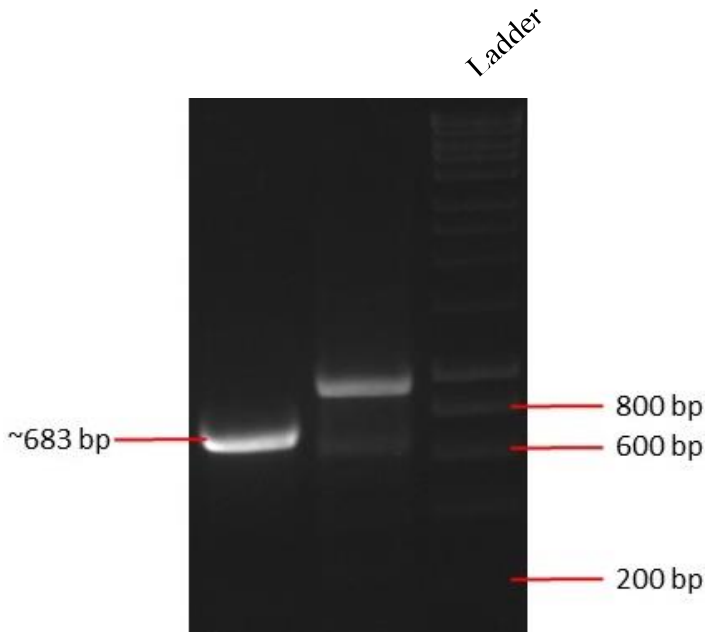

Figure 5.12: **Gel image of product from colony PCR obtained after *E. coli* transformation with BP cloning reaction product.** The first well from the left showed the colony with the correct expected size product (~683 bp). The ladder used was the 1 kb hyperladder (Bioline).

In order to make sure that the full construct of *AtANN2* with its native promoter was cloned into the entry vector, plasmid PCR by using the 6 parts primer pairs making up the whole construct (as explained in chapter 2.12.3) was carried out to screen for the successful cloning. The primer pairs used and the expected PCR product was as shown in Table 2.11 (chapter 2.12.3). The reagents and parameters used for the plasmid PCR was as in Table 2.12 and Table 2.10 (with modifications in the annealing temperature as explained in chapter 2.12.3) respectively.

BP cloning was proved to be successful in the plasmid PCR when the PCR product from each primer pair showed the correct size of expected product (Figure 5.13). Part_2 primer pair was expected to produce 586 bp of PCR product. The gel electrophoresis revealed

that the plasmid from colonies formed had the size of ~586 bp hinting for it to be the correct second part of the *AtANN2* construct (Figure 5.13 A). As described in Table 2.11 (chapter 2.12.3), part_3, 4, 5 and 6 of the primer pair should be producing PCR product of the size 840 bp, 603 bp, 557 bp, and 646 bp respectively. The plasmid PCR product formed from these primer pair proved the correct size of *AtANN2* construct cloned into the entry vector as part_3, part_4, part_6 and part_5 primers each produced the expected PCR product of ~840 bp, ~603 bp, 557 bp and 646 bp respectively (Figure 5.12 B, C).

Based on gel electrophoresis, we can only estimate the correct inserted *AtANN2* sequence based on the size of the amplified construct. In order to further confirm that the correct sequence with the right orientation had been inserted, the purified plasmid from the colonies formed were subjected to Sanger sequencing. Sanger sequencing service was carried out by Source Bioscience (U.K). Alignment of the 6 parts of the plasmid sequence obtained from Sanger sequencing with the desired *AtANN2* construct was done by using the Pairwise Sequence Alignment tool provided by the EMBL-EBI (https://www.ebi.ac.uk/Tools/psa). Based on the outcomes of the alignment, the insertion of correct *AtANN2* construct into pDONR221 entry clone with the correct orientation was confirmed (Appendix III).

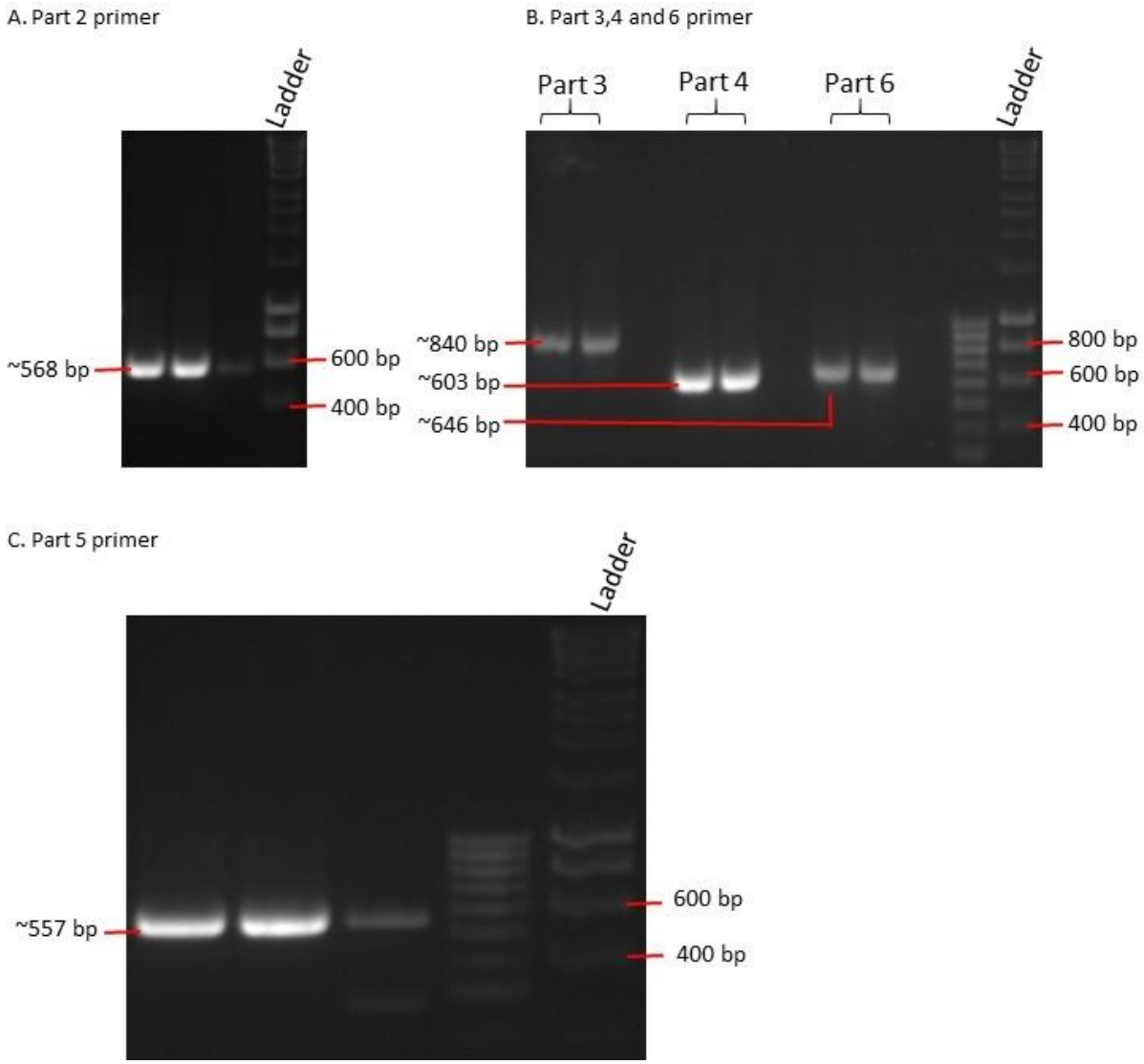

Figure 5.13: **Successful BP cloning showed correct plasmid PCR product size**. Part_2 primer pair (A), Part_3;Part_4;Part_6 primer pair (B) and Part_5 primer pair (C) were used to get smaller PCR product size for sequencing reason. The bands formed from each primer pair showed correct size indicating successful BP cloning into entry vector. Ladder used during gel electrophoresis is the 1 kb hyperladder (Bioline).

c. LR Cloning of AtANN2 construct into destination vector impGWB604

The entry vector containing the the desired *AtANN2* construct was then cloned into the destination vector impGWB604 as described in chapter 2.12.4. Screening of the successful cloning was done via colony PCR as shown in chapter 2.12.3. Figure 5.14 shows the gel image from gel electrophoresis of the colony PCR product. The last well on the right contained the ladder used to determine the size of product. The first six wells from the left were assigned to the colony PCR product whereas the seventh well contained the negative control for the PCR (no template control). A single band of the size ~664 bp formed in all the

wells assigned for the PCR product sample and no band was formed by the negative control sample. Since the size of the colony PCR product formed was similar to the expected size of product from the primers used, this indicated that the *AtANN2* construct managed to be integrated into the destination vector.

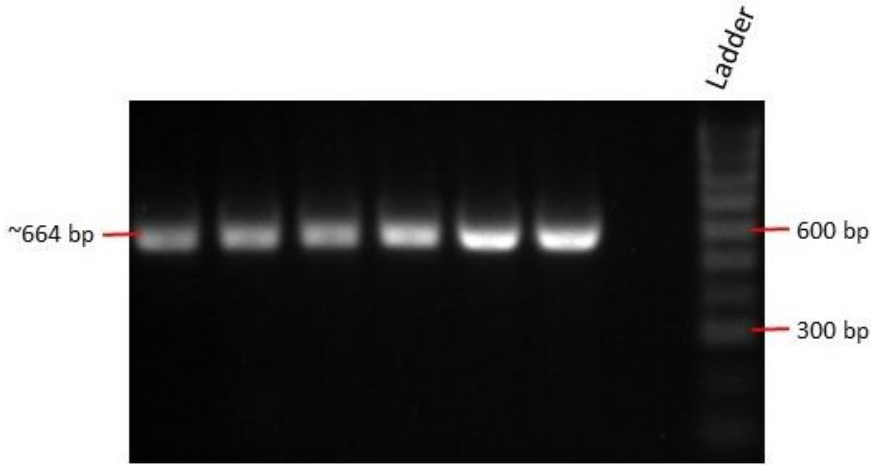

Figure 5.14: **Gel image of the colony PCR product.** The primer pair that was used is attB forward primer with Part_1 reverse primer to determine the correct first part of *AtANN2* construct. The first 6 wells from the left contained the PCR product of the primers mentioned whereas the seventh well contained no template negative control for the PCR. A 100 bp hyperladder (Bioline) was used as size indicator.

Colonies with the desired *AtANN2* construct were grown for plasmid extraction and extracted via Qiaprep Spin Miniprep kit (Qiagen) and the method used was as described by the manufacturer. Plasmids extracted were then examined for the presence of the *AtANN2* construct via plasmid PCR with different sets of primers to obtain small size of PCR product as explained in chapter 2.12.3. The primer sequences and expected product size were as described in Table 2.11 (Chapter 2.12.3). Plasmid PCR reagents and programme that was used is as shown in Table 2.12 and 2.10 (with modification in annealing temperatures; refer chapter 2.12.3) respectively.

Gel electrophoresis was carried out to check the plasmid PCR product from each pair of primers. In Figure 5.15 A, the first well contained the ladder used as a size indicator. The same figure shows the first seven wells after the ladder assigned for the plasmid PCR product of the Part_2 primers contained a single band of about ~568 bp. The ninth well until the fourteenth well contained the PCR product from Part_3 primer pair also contained a single band with the size of ~840 bp. As the size of PCR product of both Part_2 and Part_3 primers

were close to the expected product size, it could be confirmed that the second and third part of the *AtANN2* construct were successfully transferred into the destination vector. Part_4 and Part_5 primer pairs were expected to form a single band with the size of 603 bp and 557 bp respectively. Based on Figure 5.15 B, the fourth and the fifth part of the *AtANN2* construct were present in the destination vector as the wells assigned to the PCR product sample of Part_4 primer (well 2 to well 6) and Part_5 primer (well 8 to well 13) contained a single band that was similar to the expected PCR product of Part_4 primer (~603 bp) and Part_5 primer (~557 bp). Part_6 primer tested also produced a single band of PCR product in each well (well 1 until well 7) with the size similar to the expected product size of about ~646 bp which again confirmed that the *AtANN2* construct successfully inserted into the destination vector during the LR reaction (Figure 5.15 C).

Based on the plasmid PCR results, the purified plasmid with the size of desired construct was sent for Sanger sequencing at Source Bioscience (U.K). Sequencing was carried out with the primer pair shown in Table 2.11 (replacing M13 primer with *att*B forward primer; Chapter 2.12.3) as a crucial step to make sure the right construct was present in the destination vector before subsequent agrobacterium transformation was carried out. Alignment of the sequencing results of each primer pair (Part_1 until Part_6) with the desired *AtANN2* construct verified that the sequence that was inserted into the destination vector was the *AtANN2* construct (Appendix V). Sequence alignment was done by using Pairwise Sequence Alignment tool (EMBL-EBI).

d. ***Agrobacterium transformation of Atann2 with AtANN2 with its native promoter construct.***

Agrobacterium transformation of *Atann2* plants with destination vector containing the desired AtANN2 construct was carried out as explained in subchapter 2.12.5. The lines of *Atann2/AtANN2* complementary mutant are currently at the second generation of propagation. Further confirmation of the presence of *AtANN2* construct with PCR will need to be carried out after the stable lines of third generation are ready. Besides that, verification of the *AtANN2* expression will also be needed *via* qRT-PCR approach.

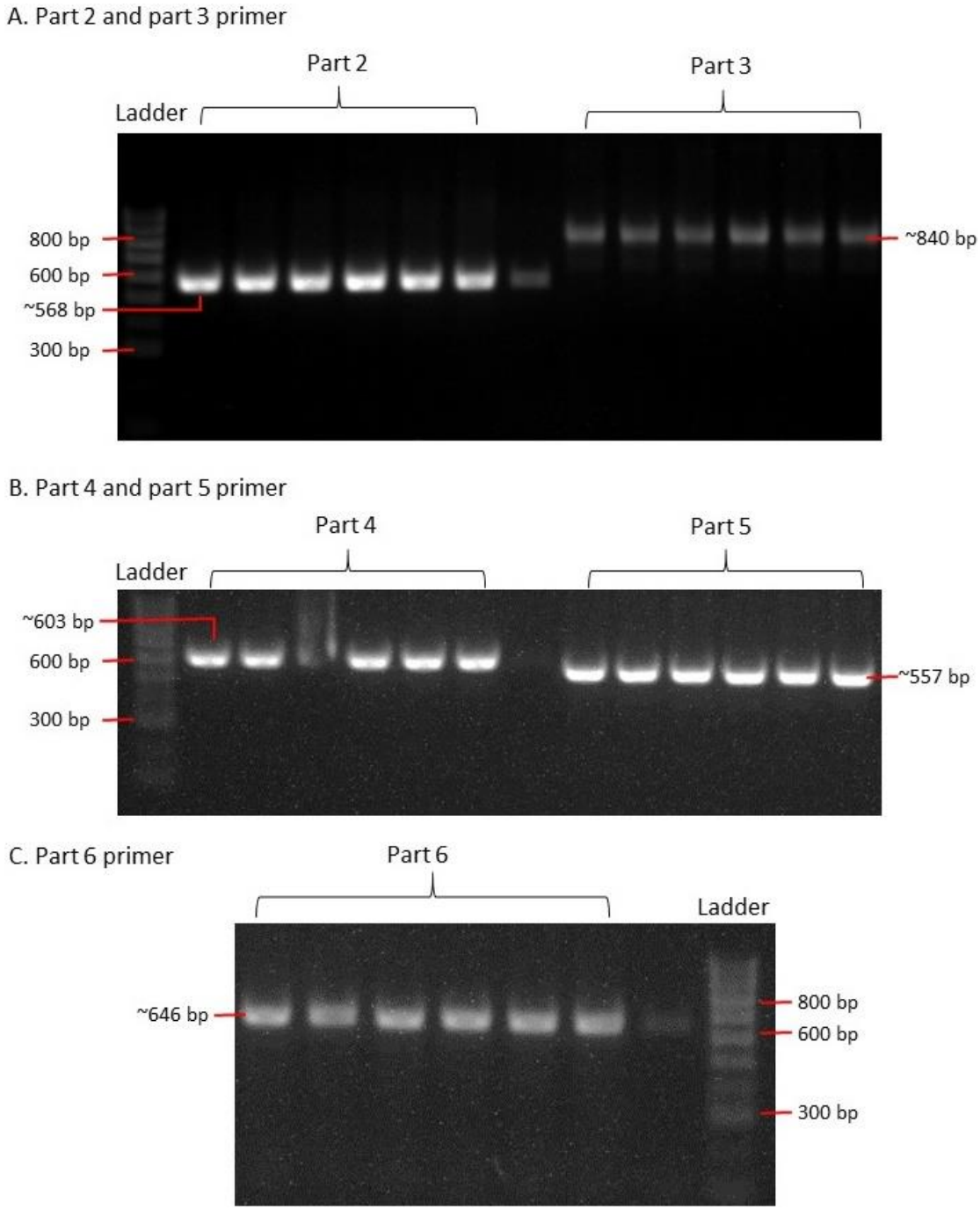

Figure 5.15: **Gel images of plasmid PCR product from different pairs of primers to detect the presence of *AtANN2* construct in impGWB604 destination vector.** Primers were designed to split the *AtANN2* construct into 6 parts with smaller size product. The first part of the construct was determined through previous colony PCR, the second and third part of the construct via plasmid PCR with Part_2 and Part_3 primers (A); the fourth and fifth part of the construct via Part_4 and Part_5 primer pair (B) and the end part of the AtANN2 construct via Part_6 primer pair (C). The DNA ladder used was the 100 bp hyperladder (Bioline).

5.3 Discussion

5.3.1 AtANN2 might not be involved in mediating H_2O_2-induced $[Ca^{2+}]_{cyt}$ accumulation.

H_2O_2 is one of the ROS species with the most stable state and longest shelf life compared to other ROS species. In a low concentration, it has been associated with growth and development in plants. Higher concentrations of H_2O_2 however could generate oxidative stress toward plants that could damage membrane and protein function (Demidchik, 2015). Previously it was found that exogenous application of H_2O_2 could trigger an increase in $[Ca^{2+}]_{cyt}$ in *Arabidopsis* (Richards *et al.*, 2014). In the same study, the authors reported that AtANN1 was involved in mediating the $[Ca^{2+}]_{cyt}$ increase at whole root level but there is the possibility of other channels working as the response was not completely abolished in the absence of AtANN1. In a study carried out by Wang *et al.* (2015), both AtANN1 and AtANN2 were found to be participating in heat stress response in *A. thaliana.* Thus it is feasible that AtANN2 could work alongside AtANN1 in stress responses.

AtMYB30 is a transcription factor that was envisaged to control the expression of *AtANN1*, *AtANN2*, *AtANN3* as well as *AtANN4* (Liao *et al.*, 2017). Loss of function of this AtMYB30 transcription factor caused an increase of $[Ca^{2+}]_{cyt}$ higher than the wild type under oxidative stress and heat stress and also exhibiting hypersensitive responses towards these stimuli. The authors found that both AtANN1 and AtANN4 help mediate the $[Ca^{2+}]_{cyt}$ under these stresses with the control of MYB30 transcription factor. In the same study, AtMYB30 was also found to regulate the expression of *AtANN2* although no further test of the role of AtANN2 in oxidative stress or heat stress was done. Based on this evidence, we hypothesised that AtANN2 (which is under AtMYB30 transcription factor control) might be involved possibly as a calcium channel working alongside AtANN1 and AtANN4 under the H_2O_2 stimulus. In this chapter, we tested AtANN2's involvement in mediating $[Ca^{2+}]_{cyt}$ response by comparing the changes in calcium response between wild type Col-0 and *Atann2* loss-of-function mutant at whole root level.

Based on the results shown in Figure 5.1 D, the interval time course displayed lower $[Ca^{2+}]_{cyt}$ in *Atann2* compared to the Col-0 whole roots when supplied with 5 mM H_2O_2 as hypothesised. Detailed analysis however revealed *Atann2* peak value and the total accumulated $[Ca^{2+}]_{cyt}$ were not significantly different when compared to the Col-0 (Figure 5.1

E, F, G, H). As the absence of *AtANN2* brought no significant effect towards the $[Ca^{2+}]_{cyt}$ response, it could be that AtANN2 is not involved in mediating $[Ca^{2+}]_{cyt}$ response in H_2O_2 in contrast to AtANN1. Although both AtANN1 and AtANN2 shared certain structural similarities, this could prove that AtANN1 and AtANN2 might play different roles under different conditions. A gene expression study by Richards *et al.*, (2014) discovered that *AtANN2* transcript was down-regulated in *A. thaliana* seedlings treated with 10 mM H_2O_2 similar to the result found in the Liao *et al.*, (2017) study. It could be that since the *AtANN2* gene in wild type was down-regulated in the presence of H_2O_2, mutating the gene might not yield any difference from the wild type. It could be interesting to test the response of plants with overexpressed *AtANN2* as they might be exhibiting hypersensitive response towards H_2O_2 based on this result.

The insignificant effect of the *AtANN2* mutation in this test could also be due to the lower number of samples resulting in the high standard error of measurement. Unlike stimuli such as eATP or high salinity, H_2O_2 triggers slower increase of $[Ca^{2+}]_{cyt}$ taking up to about 20 to 30 minutes to produce $[Ca^{2+}]_{cyt}$ peaks (Richards *et al.*, 2014). The temperature of the instrument used for the $[Ca^{2+}]_{cyt}$ measurement in this test could not be controlled and longer periods of measurement could lead to rise in temperature of the instrument. As a precaution, limited number of samples were measured for each test to make sure the $[Ca^{2+}]_{cyt}$ response recorded was due to H_2O_2 stimulus and not heat stress. Other than that, the concentration of H_2O_2 treatment used in this study (5 mM) might be too low to induce high enough $[Ca^{2+}]_{cyt}$ in order to see the significance. The previous studies mentioned (Richards *et al.*, 2014; Liao *et al.*, 2017) used higher concentration of H_2O_2 (10 mM) thus making direct comparison to be less accurate. AtANN2 might also be involved in mediating the H_2O_2 response in a cell-specific manner. This study was performed at whole root level thus differences occurred at cell-specific level might be masked by the average $[Ca^{2+}]_{cyt}$ of the whole roots. It may also be the case that AtANN2 may have a role to play in leaves and this now needs to be tested.

5.3.2 *Atann2* mutant might be important in mediating $[Ca^{2+}]_{cyt}$ elevation due to salinity stress at whole seedling level

Previous studies showed interrelation between oxidative stress and salinity stress (Jiang *et al.*, 2013). The role of AtANN1 in salinity stress has been extensively studied. AtANN1 has been found to be involved in mediating $[Ca^{2+}]_{cyt}$ response under saline conditions (Laohavisit *et al.*, 2013). *AtANN1* gene transcript was also up-regulated in salt-

treated samples (Cantero *et al.*, 2006). However, AtANN1 was not the only calcium channel that is involved in salinity stress response as mutation of *AtANN1* did not completely abolish the $[Ca^{2+}]_{cyt}$ response. *AtANN2* gene transcript regulation was also significantly down-regulated when treated with high NaCl concentration (Cantero *et al.*, 2006). This finding and as AtANN2 shared almost similar protein structure as AtANN1, raises question whether AtANN2 could also be involved in regulating salt stress response. In this chapter, we tested AtANN2's role in mediating the $[Ca^{2+}]_{cyt}$ response under high 200 mM NaCl concentration at both whole seedling and whole root level. Other than $[Ca^{2+}]_{cyt}$ measurement, we also looked at changes in growth and development under high saline condition via determining germination rate and root growth assay.

$[Ca^{2+}]_{cyt}$ assay at whole seedling level of Col-0 and *Atann2* showed an interesting pattern as each individual seedling exhibited calcium oscillation at distinct time points (Figure 5.2 A, B). This occurrence was also reported by Schmöckel *et al.* (2015) where individual Col-0 seedlings formed calcium oscillations. This oscillation signature might be specific towards salt stimulus as previously tested whole seedlings with different stimului such as eATP (Chapter 4.2.2, Figure 4.2) and eADP (Chapter 4.2.2, Figure 4.3) did not show the calcium oscillation pattern. The mechanism behind the formation of this oscillation however is not yet known. Because of this oscillation pattern, we can only analyse the touch peak and the total $[Ca^{2+}]_{cyt}$ accumulation (35 s - 155 s) as it was not practical to analyse the peaks formed by each individual seedling after the touch peak at different time points. Analysis of the touch peak response showed the *Atann2* mutant to have total $[Ca^{2+}]_{cyt}$ accumulation lower than Col-0 in control treatment. This showed that AtANN2 might be important in the touch or mechanical response in *A. thaliana.* This is however might not be confirmed as we found contrasting results with control treatment carried out previously in eATP tests showing similar $[Ca^{2+}]_{cyt}$ accumulation between Col-0 and *Atann2* (Chapter 4.2.2, Figure 4.2 C).

In the 200 mM NaCl treatment, *Atann2* again showed lower touch peak value compared to the Col-0, which might indicate involvement in mechanical response (Figure 5.2 E). This pattern was also shown in the total $[Ca^{2+}]_{cyt}$ accumulation where *Atann2* accumulated significantly lower total $[Ca^{2+}]_{cyt}$ compared to the Col-0 (Figure 5.2 F). Based on this result, we could say that AtANN2 might be important in transporting NaCl-induced calcium influx across plasma membrane. However, since $[Ca^{2+}]_{cyt}$ accumulation of *Atann2* in control

treatment also showed impairment compared to the Col-0, it could be that the initial $[Ca^{2+}]_{cyt}$ in *Atann2* was already low thus making comparison between treatment to be inaccurate. Sorbitol treatment as a control for the osmotic stimulus showed lower $[Ca^{2+}]_{cyt}$ than the NaCl treatment. Col-0 and *Atann2* response towards osmotic stress also was similar showing that lower *Atann2* response in NaCl treatment was due to ionic stress (Figure 5.2 G, H).

AtANN2 is abundant in root compared to the shoot region of young seedlings (Clark *et al.*, 2001). The root also is the organ that has higher risk of exposure towards salinity stress, especially in the soil. Thus, a similar test was repeated at whole root level in order to capture the root-specific response of AtANN2 in saline conditions. In contrast to the outcome at whole seedling level, no significant differences were found between Col-0 and *Atann2* in touch peak and overall $[Ca^{2+}]_{cyt}$ response by control treatment. Although the time course in Figure 5.3 D showed lower $[Ca^{2+}]_{cyt}$ response by *Atann2* in 200 mM NaCl treatment,Col-0 and *Atann2* bore no statistically significant difference in both touch peak and the total $[Ca^{2+}]_{cyt}$ accumulation. Similar result with AtANN1 was found by Laohavisit *et al.* (2013) where *Atann1* loss-of-function mutant failed to show significant difference with Col-0 in NaCl treatment when tested at whole root level. In the same study however *Atann1* managed to show significant impairment compared to Col-0 when the test was carried out at root epidermal protoplast level. This could mean that the response mediated by AtANN2 might also occur in certain types of tissues or cells, thus recording the response at whole root level might not capture the effect of the absence of AtANN2.

Other than that, it could also be that the NaCl concentration used was not high enough to be able to reach all the layers of tissues of the root. However, using NaCl concentration of more than 300 mM NaCl would instead cause salinity shock instead of salinity stress (Shavrukov, 2013), which could affect the viability of the samples and might trigger a different response pathway. Thus a lower concentration of 200 mM was used in thus study to avoid salinity shock.

Since the absence of AtANN2 could not show a clear effect in terms of $[Ca^{2+}]_{cyt}$ response, we also observed the germination and root growth alongside the calcium assay to investigate whether AtANN2 might play a role in the NaCl-induced growth retardation. Germination assay was first carried out to examine the effect of NaCl on the rate of germination before moving on to the growth assay as a precaution step. We hypothesised that 200 mM NaCl supplied in the growth medium for germination would inhibit the germination

of Col-0 seeds but might not have an effect on *Atann2* mutant seeds since AtANN2 was found to be significantly down-regulated in young seedlings under salinity stress (Clark *et al.*, 2001).

We tested Col-0 and *Atann2* germination on control medium, 200 mM NaCl and 400 mM sorbitol-containing media. Based on Figure 5.4, 200 mM NaCl exerted an obvious effect on germination rate as both Col-0 and *Atann2* rate of germination was lower than the control and sorbitol media and the germination was also delayed. Rate of germination of *Atann2* however was on par with the Col-0 suggesting that AtANN2 might not be related to the salinity induced germination inhibition. This observation was in contrast to a previous study that found *Atann2* lacked the delayed or inhibition of germination as in *Atann1* or *Atann4* mutant seeds (Lee *et al.*, 2004). The author also mentioned some *Atann2* seeds showed enhanced germination compared to the Col-0 seeds as we hypothesised. The study however was done with lower 75 mM NaCl concentration compared to the 200 mM NaCl used in the test we carried out. This showed that AtANN2 might be involved in the germination process under low salt concentration. Salt-induced $[Ca^{2+}]_{cyt}$ increase has been shown to be concentration-dependent. It could be that higher 200 mM NaCl concentration evoked higher $[Ca^{2+}]_{cyt}$ increase thus activating a different pathway which does not involve AtANN2.

Since we have determined that 200 mM NaCl could affect germination of both Col-0 and *Atann2*, the seeds that were used in the subsequent growth assay were germinated on control medium for 3 days before being transferred onto either control medium, 200 mM NaCl or 400 mM sorbitol-containing media. Measurement of growth was done on the 6^{th} day after being transferred. Primary root length as shown in Figure 5.5 A showed the length of Col-0 and *Atann2* roots grown in control medium were longer compared to the roots grown in either 200 mM NaCl or 400 mM sorbitol-containing media. Similar observation was found in the lateral root density measurement (Figure 5.5 B) and the fresh weight (Figure 5.5 E) where NaCl and sorbitol treatment caused impairment in growth compared to the control medium. Since no differences could be observed in terms of primary root length and the lateral root density between seedlings grown on 200 mM NaCl and 400 mM sorbitol, we could assume that the root inhibition was caused by both osmotic stress and the Na^+ ionic stress.

Both ionic and water stress was proven to cause growth retardation based on previous studies. In a study conducted by Valenzuela *et al.* (2016), Jasmonic Acid (JA) was postulated to be involved partially in inhibiting root growth especially in the elongation zone under both

salt stress and osmotic stress. The same study also discovered increase in JA-responsive genes under salinity stress in a gene expression test. Another study carried out on maize also found exposure of NaCl imposed both salt stress and osmotic stress on the fresh weight of the maize treated (Zhao *et al.*, 2010). This occurrence however was in contrast to the $[Ca^{2+}]_{cyt}$ measurement carried out in our test (Figure 5.2;5.3) as similar concentration of 200 mM NaCl used imposed salt stress more than water stress. It is possible that Na^+ ionic stress would have more effect on the level of $[Ca^{2+}]_{cyt}$ than the water stress as Na^+ could easily disturbed the plasma membrane potential thus interfering with voltage-dependent calcium channels leading to changes in $[Ca^{2+}]_{cyt}$ increase.

NaCl treatment however does not cause consistent root growth inhibition. According to a study published by Geng *et al.* (2013), root growth inhibition was pronounced in the first 8 hours of exposure to the NaCl stimulus and the root growth recovery phase started from 8 to 13 hours of exposure to the NaCl stimulus. This growth recovery process depends on ABA and was inhibited by JA. Another study focusing on the effect of the osmotic stress part of the NaCl found that ABA curbs ethylene biosynthesis, which was found to promote root retardation under osmotic stress (Spollen *et al.*, 2000). In the root growth assay that was done in this chapter, no significant differences were found between Col-0 and *Atann2* in all treatments whereas in a previous study done by Laohavisit *et al.* (2013), *Atann1* secondary root growth was impaired compared to the Col-0 in the presence of 250 mM NaCl. The distinction found between these two studies could be attributed to the role of ABA. AtANN1 was previously found to be involved in mediating ABA response in osmotic stress (Lee *et al.*, 2004). It is possible that the absence of AtANN1 interferes with the ABA-mediated growth recovery period thus causing the inhibition of the root growth. AtANN2 on the other hand might not be implicated with ABA response thus the absence did not interfere with the ABA-mediated root growth recovery.

Horizontal Growth Index (HGI) was the other parameter of growth that was recorded. Seedlings assigned on control medium grew straight vertically as expected whereas seedlings in the NaCl treatment skewed slightly to the right (Figure 5.5 C). On the other hand the seedlings that were exposed to the osmotic control sorbitol grew slightly towards the left (Figure 5.5 C). Lower concentration of 75 mM NaCl used in a previous study showed a similar pattern of skewing where Col-0 skewed to the right (Van der Does *et al.*, 2017). In the same study, a mutant of a LRR-kinase, which is thought to perceive cues from the

environment via sensing interrupted cell wall, exhibited a higher degree of skewing than the Col-0 when grown on 75 mM NaCl. The relation between the function of this receptor and AtANN2 however remains unclear. *AtANN2* was previously found to be highly expressed in *Atpin2* mutant root columella and root cap cells when placed in horizontal rotation (Tan *et al.*, 2011). This could relate AtANN2 with the auxin transport across the root thus possibly regulating root skewing. Based on Figure 5.5 C, root skewing was similar between Col-0 and *Atann2* in control, 200 mM NaCl or 400 mM sorbitol. This confirmed that AtANN2 might not play a crucial role in causing the different skewing caused by NaCl or sorbitol exposure.

5.3.3 AtANN2 might not be involved in mediating flg22-induced response

Extracellular ATP has been found to be tightly associates with PAMPs (Kim *et al.*, 2006, Wu *et al.*, 2008). In the previous chapter we have shown that AtANN2 played an important role in mediating the calcium response in eATP signalling pathway (Chapter 4). If the flg22 elicitor response were downstream of eATP signalling, AtANN2 could also indirectly be involved in governing the flg22 pathway response. A previous study on flg22 elicitor showed its ability to evoke an increase in $[Ca^{2+}]_{cyt,}$ produce an ROS burst and also reduction in growth (Ranf *et al.*, 2011). In this chapter, we applied the same parameters in order to determine the involvement of AtANN2 in mediating the flg22 response. Comparison between Col-0 and *Atann2* loss-of-function mutant seedlings was done during $[Ca^{2+}]_{cyt}$ measurement, ROS measurement and growth assay in the presence of flg22 elicitor. *Atfls2* which is the loss-of-function mutant for the flg22 receptor was also tested to serve as a control for the flg22-induced response.

Figure 5.6 shows the outcomes of the $[Ca^{2+}]_{cyt}$ measurement when Col-0 and *Atann2* were treated with 1 μM flg22. Both Col-0 and *Atann2* produced similar levels of $[Ca^{2+}]_{cyt}$ increase whereas the *Atfls2* was completely impaired in inducing the $[Ca^{2+}]_{cyt}$ response. This observation was in contrast to what we hypothesised and showed that AtANN2 might not be needed for the flg22-induced $[Ca^{2+}]_{cyt}$ response. In this experiment, whole seedlings were used instead of whole roots as in a preliminary test carried out, roots gave very low signal to flg22 treatment, thus making it hard to be measured. AtANN2 has been shown to be highly expressed in roots and less in shoot thus it is possible that the effect of the absence of AtANN2 could not be detected, as the level of the protein was initially low to begin with.

ROS burst is one of the hallmarks of PAMP-induced response. A preliminary study carried out by a previous member of Davies laboratory revealed a distinct *Atann2* ROS burst

compared to the Col-0. Here we tested again to determine whether AtANN2 is required for the flg22-induced ROS accumulation. Leaf discs from 21-day-old leaves were used during the measurement. According to past studies, AtANN1 was proven to be an ROS-activated calcium channel (Laohavisit *et al.*, 2013). Since AtANN2 maintained a close amino acid sequence similarity with AtANN1, we hypothesised that the AtANN2 might also be a ROS-activated calcium channel in the presence of flg22 elicitor.

The time-course of ROS accumulation in Figure 5.7 showed *Atann2* mutant evoked a higher level of ROS accumulation compared to the Col-0. A study on the sequence of AtANN2 showed potential peroxidase activity based on the conserved His40 residue (Mortimer *et al.*, 2008). It is possible that the absence of functional AtANN2 as a peroxidase failed to alleviate the ROS accumulation caused by flg22 elicitor. Statistical analysis however showed the total ROS accumulated by *Atann2* was not significantly higher than the Col-0. *Atfls2* samples showed significantly impaired ROS production as expected confirming that the ROS measured was due to flg22 elicitor treatment. This could confirm the hypothesis that AtANN2 might be downstream of ROS production thus mutation on AtANN2 did not have any effect on the ROS measured. However, measurement of $[Ca^{2+}]_{cyt}$ response by flg22 elicitor previously (Figure 5.6) showed AtANN2 to possibly not be involved in mediating flg22 response $[Ca^{2+}]_{cyt}$ increase.

It is also possible that because the time taken to measure each sample was quite long, fewer samples can be tested thus making the standard error of measurement to be huge causing the indifference between Col-0 and *Atann2* during statistical analysis. Other than that, leaf disc preparation has the potential to introduce physical damage thus causing more ROS released and possibly skewed data points. We have previously tested measuring ROS by using less destructive whole roots and whole seedlings but the signal produced was too low to get a reliable measurement. The underlying reason behind this difference between leaf disc and whole root or whole seedling when tested with flg22 elicitor however is not known. It is also interesting that during the ROS measurement, ROS touch response due to the addition of treatment also formed. This has not been reported in previous studies executing flg22-induced ROS measurement in *A. thaliana*. A study by Li and Gong (2011) however reported the ability of mechanical stimulus to trigger production of H_2O_2 in tobacco suspension cells, which could be the underlying reason of the touch response.

Both calcium assay measurement and ROS accumulation measurement seems to show that AtANN2 might not be involved in flg22-induced response. In this chapter we also tested another aspect of flg22-induced response, which is growth and development. Exogenously applied flg22 elicitor has been shown to cause growth retardation. We tested both Col-0 and *Atann2* root growth by growing them on either control medium or 1 μM flg22-containing medium before measurements were taken at the 9th day. All the seeds were germinated on control medium first for 3 days before being transferred onto each treatment plate to rule out possible delayed germination caused by the different treatments. If AtANN2 were involved in regulation of growth under the influence of flg22, we hypothesised that the AtANN2 mutation might cause root resistance phenotype towards the flg22.

Measurement of the primary root length showed both Col-0 and *Atann2* grew similar root lengths in either control treatment or the flg22 elicitor treatment (Figure 5.8 A). This again portrayed the notion that AtANN2 might not be one of the components of flg22-induced response. It is interesting to note that *Atann2* that were grown on flg22-containing medium showed lower primary root length than the ones that were grown on control medium. This is however not true for Col-0, which showed that flg22 failed to inhibit root growth of the Col-0. Previous publications that managed to prove that 1uM flg22 could cause reduction in primary root growth used sucrose in the media (Gómez-Gómez *et al.*, 1999; Ranf *et al.*, 2011). Growth medium that was used in this test was not supplied with sucrose as sucrose was reported to be able to induce a stress response (Bolouri Moghaddam and Van den Ende , 2012). A different study that managed to exhibit the inhibition of growth by flg22 used 10 μμM flg22 concentration instead of just 1 μM (Bethke *et al.*, 2009). Other than that, Poncini *et al.*, (2017) in their publication reported that growth inhibition elicited by 1 μM flg22 without sucrose addition is weak compared to 1 μM Atpep elicitor. The authors suggested that the abundance of flg22 in the rhizosphere could be the underlying reason of the root weak response towards flg22. *Atann2* however showed hypersensitivity towards 1 μM flg22, which might indicate the possibility of AtANN2 as a positive regulator in flg22-induced root growth inhibition. AtANN2 has been implicated in growth and development as it was previously found localised to the periphery of highly secretory cells (Clark *et al.*, 2005a). AtANN2 was also involved in sugar transport (Wang *et al.*, 2018b) making it possible that exposure to flg22 elicitor in the absence of AtANN2 might impair the root growth.

Similar observation was found with lateral root density where flg22 medium did not cause any difference compared to the control medium for both Col-0 and *Atann2*. This again could be caused by lower concentration of flg22 used this test. *Atann2* however formed statistically higher lateral root density than the Col-0 in both treatments. Formation of denser lateral roots is one of the phenotype of stressed seedlings. As observed in the primary root growth, the hypersensitive *Atann2* might have formed denser lateral root density in response to flg22. Although this is true, the phenotype was not specific towards flg22 treatment as *Atann2* also produced denser lateral roots than Col-0 in control conditions, which indicates that the *Atann2* seedlings were under stress even in control medium. As AtANN2 has a possible role in sugar transport in roots, it could be that the absence of AtANN2 interfered with sugar distribution causing root starvation thus the formation of denser lateral roots.

5.4 Summary and future work

Based on the results and discussion presented earlier, AtANN2 might not be involved in mediating the calcium transport under H_2O_2 stimulus. Since the time-course showed lower $[Ca^{2+}]_{cyt}$ response of *Atann2* than Col-0 although insignificant, repeating the experiments with bigger number of samples and with a higher concentration of 10 mM H_2O_2 might yield a better response. As mentioned before, *AtANN2* gene expression was down-regulated in the presence of H_2O_2 which could suggest possible function of AtANN2 as a negative regulator. This test could only be completed by repeating the experiment with overexpression of *AtANN2* (*35S::AtANN2*) alongside the *Atann2* mutant and the wild type Col-0 in order to delineate the possible function of AtANN2 as a negative regulator. If AtANN2 functions as a negative regulator in the presence of H_2O_2, the *35S::AtANN2* would yield much lower $[Ca^{2+}]_{cyt}$ than the Col-0. Another downstream response such as monitoring the H_2O_2-induced transcript accumulation might help explain function of AtANN2 in the H_2O_2 response. Other ROS such as the hydroxyl radical should also now be tested.

When challenged with 200 mM NaCl treatment in the $[Ca^{2+}]_{cyt}$ assay at whole seedling level, AtANN2 might be needed in mediating the $[Ca^{2+}]_{cyt}$ increase however more samples might be needed to confirm this. At whole roots level, *Atann2* failed to produce similar phenotype as in whole seedlings test thus it might also be that AtANN2 did not play any role in mediating the root NaCl-induced $[Ca^{2+}]_{cyt}$ response. Carrying out the experiment at protoplast level might help solved this inconsistency in the $[Ca^{2+}]_{cyt}$ response in *Atann2* mutant. Shoot tissue should also now be tested. Another aspect of the NaCl test, which is

germination and growth assay, confirmed that mutation of *AtANN2* did not have any effect on the germination or the root system architecture under salinity stress. However, it would be interesting to determine if overexpression of *AtANN2* would cause hypersensitivity towards both salt stress and water stress thus causing growth arrest. This would again shed light on the possible function of AtANN2 as a negative regulator in mediating this response.

Other than abiotic stress, we also tested biotic stress by using the established flg22 elicitor. Based on the $[Ca^{2+}]_{cyt}$ assay measurement, it was clear that AtANN2 was not involved in mediating the calcium influx under the influence of flg22 elicitor. However, ROS accumulation might show a different side of the involvement of AtANN2. Time-course of the ROS accumulation showed *Atann2* to produce higher ROS than the Col-0 although not significantly, possibly due to too high a standard error of measurement. Increasing the number of samples tested could solve this problem. Other ROS probes such as CMH_2DCFDA could also be used to replace the luminol-HRP ROS probe in order to measure the total ROS accumulation. An advantage of using the CMH_2DCFDA dye is that younger samples such as 7-day-old whole roots or whole seedlings could be used instead of 21-day-old leaf discs. This could minimise sample handling and introducing wounding to the samples. Furthermore, *AtANN2* was reported to be highly expressed in the root of young seedlings compared to older leaves. This could also link the results of $[Ca^{2+}]_{cyt}$ accumulation and ROS accumulation as the samples used were of the same age. However, CMH_2DCFDA dye is a cumulative dye thus the monitoring could not be done in real time. The higher ROS production by *Atann2* could suggest possible negative regulation by AtANN2. Again, repeating the experiment with overexpressed AtANN2 might be helpful in confirming the negative regulation of AtANN2.

In terms of growth and development in the presence of flg22 elicitor, we could not deduce that AtANN2 was involved in the growth regulation as we failed to see the root inhibition effect of flg22 elicitor even in the wild type Col-0. However, we could not rule out the possibility of the involvement of AtANN2 in the growth regulation. The experiment could be repeated by using higher concentration of 10 μM flg22 to possibly get a discernible wild type response. In order to test for the specificity of the flg22 response, we carried out several experiments with Atpep1 elicitor. Unfortunately we could not present the data in this chapter due to problems with contamination. Possible tests with Atpep1 and chitin should be carried out in the future for specificity purpose.

In the final section of this chapter, we managed to produce a stable line of *Atann2/AtANN2* complemented mutant. However, due to time constraint, we have not yet use the complemented mutant alongside the loss-of-function mutant in the test to confirm the role of AtANN2 in mediating both abiotic and biotic stress responses. We also have designed the primer CDSann2_ANN2 to amplify *AtANN2* gene for the production of a 35S::*AtANN2* overexpression line in the future. This chapter served as preliminary screening to help point to the right direction of the next step to better understand the function of AtANN2.

Chapter 6

Discussion

6.1 AtANN1, AtANN2 and AtANN4 play a role in mediating eATP-induced $[Ca^{2+}]_{cyt}$ increase in *A. thaliana*

An increase in $[Ca^{2+}]_{cyt}$ is one of the earliest responses to an eATP signal besides ROS, NO and PA production. In this thesis we have shown that 1 mM eATP treatment instantly evoked a biphasic $[Ca^{2+}]_{cyt}$ increase in *A. thaliana* whole seedlings, whole roots and 1 cm excised root tips. This biphasic increase followed a monophasic mechanical stimulus-induced $[Ca^{2+}]_{cyt}$ accumulation that was not affected by mutation of any of the genes of interest. This increase indicates the involvement of mechanosensitive channels during the experiments. There are a few groups of mechanosensitive channels identified in plants such as MSL channels (MscS-Like) that are activated upon membrane pressure (Maksaev and Haswell 2012), TPK channels (Two Pore Domain K^+) involved in osmosensing (Maathuis, 2011) and MCA channels (Mid1-Complementing Activity; Nakagawa *et al.*, 2007) possibly involved in root mechanosensing. Most of these channels are assigned to protect plants against cells bursting due to pressure under hypo-osmotic shock (Basu and Haswell, 2017). A structural and electrophysiological study on the recently discovered mechanosensitive plasma membrane AtOSCA channels (AtOSCA1.1 and AtOSCA3.1; *Arabidopsis thaliana* reduced hyperosmolality induced $[Ca^{2+}]_i$ increase 1) has helped in understanding the working

mechanism of this group of channels. It was envisaged that upon mechanical pressure such as osmotic shock, a contorted plasma membrane would change the conformation of the mechanosensitive channel thus opening the calcium pore (Zhang *et al.*, 2018). AtDEK1 (Defective Kernel1) is involved in development but its structure means that it is likely to be a mechanosensitive Ca^{2+} channel regulator rather than a channel sub-unit (Tran *et al.*, 2017). It seems to be unlikely that the mechanosensitive channels are in the same pathway as the AtDORN1 eATP-perception pathway since our test with *Atdorn1* still produced a $[Ca^{2+}]_{cyt}$ touch peak. However, the possibility of eATP regulating mechanosensitive channels cannot completely be ruled out as eATP was found to be released under touch mechanical force and osmotic stress in a previous report (Jeter *et al.*, 2004).

The identity of the calcium channels involved in the biphasic eATP-induced $[Ca^{2+}]_{cyt}$ elevation is not yet known. Based on the tests that we have done in Chapters 3 and 4 with *Atann1, Atann2* and *Atann1/2* T-DNA insertion mutants, we found that both AtANN1 and AtANN2 are required (possibly as calcium channels) for the normal eATP-induced $[Ca^{2+}]_{cyt}$ accumulation. As eATP was perceived by the AtDORN1 purinoreceptor at whole root level (Choi *et al.*, 2014b), we also showed that the function of AtANN1 possibly as a calcium channel might be in the same pathway as the AtDORN1 from the test carried out with the *Atdorn1-3/ann1* double mutant.

In our study, *Atdorn1-3/ann1* was tested at whole root level. Matthus *et al.*, (2019a) showed that *Atdorn1-3* mutant leaves exposed to eATP treatment were still able to produce $[Ca^{2+}]_{cyt}$ accumulation, showing a possible function of another receptor in leaf tissues. The ancestor of photosynthetic plants, a type of green alga *Ostreococcus tauri* has a vacuolar purinoreceptor OtP2X with 28% homology to human P2X receptors (Burnstock, 2018). Based on a genomic sequence study of *O. tauri*, there are four other open reading frames related to P2X receptors (Fountain *et al.*, 2008). Thus, it is not impossible in higher plants for *A. thaliana* to comprise more than one P2K receptor, possibly localised in different tissues or organs. Comparison of transcriptomic data between *A. thaliana, O. tauri* and *C. reinhardtii* showed a quarter of *A. thaliana* genes with Gene Ontology term "Cell communication", "Cell wall organisation" and "Multiorganism reproductive process" are specific and not present in the other two organisms (de los Reyes *et al.*, 2017). What is perhaps more remarkable is why, through evolution, higher plants appear to have lost the P2X homologues evident in their single-celled ancestor.

AtANN1 has the ability to transport Ca^{2+} across a planar lipid bilayer (Laohavisit *et al.*, 2013). In terms of ROS production, it could be likely from what we discovered that AtANN1 could be downstream of ROS production in the eATP signalling pathway (Chapter 3). This was previously suggested to be the case under salt stress by Laohavisit *et al.* (2013) as AtANN1 was shown to be a ROS-driven Ca^{2+} channel. Salt stress itself causes transient increase of eATP around *A. thaliana* roots (Dark *et al.*, 2011), suggesting that the involvement of AtANN1 in eATP signalling can be an intermediate in the salinity stress pathway.

Although there is no evidence to date showing a similar ability of AtANN2 to form a channel, the amino acid sequence of AtANN2 is highly similar to AtANN1 (Clark *et al.*, 2001). It might also be that AtANN2 is downstream of ROS production in eATP signalling. This would however need further tests with *Atann2* mutant ROS measurement under eATP treatment. The double mutant *Atann1/2* showed additive impairment in the $[Ca^{2+}]_{cyt}$ accumulation compared to the single mutant, giving the idea of possible interaction between AtANN1 and AtANN2 in the eATP signalling pathway. It will be interesting in the future to study the localisation of these two annexins upon eATP treatment as it is not clear in which compartment they operate in this signalling pathway. As both have been found in the apoplast, it may be that they act at the extracellular face of the plasma membrane (Kwon *et al.*, 2005; Laohavisit *et al.*, 2009). Certainly, their interaction needs to be tested. Interaction studies can be done through the co-immunoprecipitation (Co-IP) method. Beads with antibody specific against AtANN1 that interacted and co-precipitated with AtANN2 could be detected through western blot. This method has previously been used in detecting interaction between AtANN1 and AtANN4 (Huh *et al.*, 2010). Chinchilla *et al.* (2007) employed this method successfully to find interaction between the flg22 receptor AtFLS2 with its co-receptor AtBAK1. Co-IP however is an *in vitro* method and does not take into account the native environment of the proteins of interest, which could influence the interaction process. Thus, it would be preferable to couple this method with the Bimolecular Fluorescence Complementation (BIFC) assay which is an *in planta* method that could be carried out in protoplasts or epidermal cells. Fluorescence protein separated between the N-terminal and C-terminal could be tagged to AtANN1 and AtANN2 proteins respectively. Interaction between AtANN1 and AtANN2 causing the N and C-terminal of this fluorescence protein to come into close proximity and fuse with each other forming a functional protein from which

fluorescence could be observed. An advantage of using this method is to be able to detect the subcellular localisation of the proteins interacting (Hu *et al.*, 2002).

Additionally, recombinant AtANN2 needs to be tested for Ca^{2+} transport ability in a planar lipid bilayer. These two *A. thaliana* annexins however are not the only possible channels in eATP signalling as the treatment with the channel blocker $GdCl_3$ still managed to produce a $[Ca^{2+}]_{cyt}$ response, suggesting possible intracellular calcium channel involvement. AtTPC1 would be a prime candidate and the mutant now needs to be tested.

Huh *et al.* (2010) reported the interaction between AtANN1 and AtANN4 and that both proteins were needed for the $[Ca^{2+}]_{cyt}$ response under salinity stress. Here we anticipated that both AtANN1 and AtANN4 would also mediate $[Ca^{2+}]_{cyt}$ accumulation. Interestingly we found that instead of exhibiting additive impairment of the eATP-induced $[Ca^{2+}]_{cyt}$ increase, the *Atann1/4* double mutant accumulated a similar level of $[Ca^{2+}]_{cyt}$ to the Col-0 wild type. The test done with *Atann1/2/4* triple mutant whole roots with 1 mM ATP also showed a similar level of $[Ca^{2+}]_{cyt}$ as *Atann1/2.* This could indicate that AtANN4 acts as a negative regulator of AtANN1 or other potential calcium channels as the absence of AtANN4 might activate AtANN1 or the potential calcium channels to elevate $[Ca^{2+}]_{cyt}$, even masking the absence of AtANN1.

This observation was in contrast to the study by Ma *et al.*, (2019) which showed the ability of AtANN4 to mediate Ca^{2+} influx when challenged with 1 μM ATP. The study however was not done *in planta* but rather with AtANN4 expressed in HEK293 cells. Thus, it is intriguing that whole roots of the *Atann1/4* double mutant exhibited normal wild type $[Ca^{2+}]_{cyt}$ response instead. Jewell *et al.* (2019) listed AtANN4 as one of the eATP-regulated genes suggesting its importance in the eATP signalling pathway. The possible reason that the *Atann1/4* showed a normal response is the probable post-translational modification that occurs *in planta* during eATP signalling. The same study by Ma *et al.* (2019) reported that phosphorylation of AtANN4 could affect its ability to transfer Ca^{2+}. It was found that AtANN4 functioned in mediating $[Ca^{2+}]_{cyt}$ increase in the early response towards NaCl and interacted with the SOS3-like calcium-binding protein 8 (AtSCaBP8) as well as being phosphorylated by the protein kinase SOS2 leading to the recruitment of Na^+/H^+ antiporter AtSOS1 in the process of Na^+ exclusion (Ma *et al.*, 2019). AtANN4 was found to be phosphorylated by AtSOS2 protein kinase at the Ser46 residue of its N-terminus. The phosphorylated form of AtANN4 tested for ability to increase $[Ca^{2+}]_{cyt}$ showed impairment

compared to the non-phosphorylated form (Ma *et al.*, 2019). Thus, in this case it could be that *in planta*, under the eATP signal the AtANN4 undergoes phosphorylation thus causing less $[Ca^{2+}]_{cyt}$ accumulation. Since AtANN4 was previously shown to interact with AtANN1 under salt stress (Huh *et al.*, 2010), it was also possible that the binding of the phosphorylated form of AtANN4 with AtANN1 somehow negatively regulates AtANN1 function and may be acting as a negative feedback regulator to end the eATP signal.

Post-translational modification of annexins such as phosphorylation, S-glutathionylation, and S-nitrosylation under various stress conditions could be the underlying reason for the multi-functionality of these proteins in plant cells. *A. thaliana* annexins contain residues such as lysine and histidine which could be involved in membrane binding and change of conformation after post-translational modifications (Clark *et al.*, 2012). AtANN1 was listed as one of the S-nitrosylated proteins under the influence of NO (Lindermayr *et al.*, 2005). Konopka-Postupolska *et al.* (2009) in their effort to look at AtANN1 function under drought stress discovered that ROS-induced S-glutathionylation of AtANN1 could jeopardise its Ca^{2+}-binding ability in *planta*. As eATP signalling produces NO and ROS, it may be that such modifications curtail the activity of AtANN1 in $[Ca^{2+}]_{cyt}$ elevation. Similarly, AtANN4 showed potential for post-translational modification as the RNA transcript was highly up-regulated in salinity stress but protein level remained the same (Huh *et al.*, 2010).

The results showing the possibility of AtANN1, AtANN2 and AtANN4 involvement in mediating Ca^{2+} movements under eATP and eADP as shown in chapter 3 and chapter 4 however were obtained from experiments using (apo)aequorin reporter and luminometry. There were some variables of the $[Ca^{2+}]_{cyt}$ measurements using this method in terms of peak values especially the touch peak. As explained in Chapter 3.3.1, there are some disadvantages of using luminometry that should be taken into considerations when analysing the results. Besides this, making sure that other possible factors that could affect the experiments such as maintaining constant speed of treatment injection, preparing samples and taking measurements at similar time of the day are crucial in order to get a constant outcomes. This method however is very high-throughput which makes it a great tool in initial screening of possible Ca^{2+} channels when there are more than one candidates. This screening using luminometry method managed to previously identify the purinoreceptor DORN1 (Choi *et al.*, 2014b) and the possible Na^{2+} sensor (MOCA1) in *A.thaliana* (Jiang *et al.*, 2019). Based on the results we obtained with AtANN1, AtANN2 and AtANN4; the next step is to use a higher resolution Ca^{2+} measurement methods such as YC3.6 reporter with confocal microscopy to

further confirm the involvement of these proteins at whole roots or root tips level. This method would also allows visualisation of Ca^{2+} propagation upon eATP perception (Matthus *et al*., 2019b) and might resolved the possibility of these annexins working in different tissues of the root.

Other than that, the concentration of ATP used as agonist in this study (1 mM and 0.1 mM) is higher than the nM concentration previously found released by plant cells (Weerasinghe *et al*., 2009; Dark *et al*., 2011). Although this did not mimics the physiological effects of eATP, higher concentration is used here in order to get the most Ca^{2+} response to identify the possible components involved. Initial test with different concentrations of non-hydrolysable ATP analogue found that the total $[Ca^{2+}]_{cyt}$ accumulated increases as the treatment concentration increased (Appendix VI) and that 1 mM concentration showed the highest total $[Ca^{2+}]_{cyt}$ accumulation. Furthermore, as whole roots and root tips were tested here, higher 1 mM ATP concentration is used to induce more response as the time taken for the treatment to be fully perceived by different layers of root tissues might be longer. Another study of AtANN1, AtANN2 and AtANN4 with higher Ca^{2+} reporter resolution together with lower concentration of ATP needs to be tested in the future to confirm the role of these annexins in the eATP signalling pathway.

Figure 6.1 shows the proposed model of the eATP signalling pathway. Upon stimulation with wounding, biotic or abiotic stresses, ATP will be released through an ABC transporter, unknown anion channel or through membrane damage (Kim *et al.*, 2006; Song *et al.*, 2006; Weerasinghe *et al.*, 2009; Dark *et al.*, 2011) and accumulates in the extracellular matrix (ECM). Accumulation of this eATP becomes a signal that is perceived by the purinoreceptor AtDORN1 (Choi *et al.*, 2014b) that phosphorylates (P) (AtRBOHD) NADPH oxidase (Chen *et al.*, 2017) to activate the production of ROS. Unknown proteins could cause transient elevation of $[Ca^{2+}]_{cyt}$. This Ca^{2+} flux could originate from the apoplast or from the intracellular Ca^{2+} stores such as vacuole through AtTPC1 or unknown channels that might be needed for ROS production. These extracellular ROS could activate AtANN1 which then also allows the transient increase in $[Ca^{2+}]_{cyt.}$ AtANN1 might be working together with AtANN2 and also might be negatively regulated by AtANN4. Increase in intracellular ROS could also occur due to influx of ROS through aquaporins (AQP) (Rodrigues *et al.*, 2017). The binding of Ca^{2+} sensors such as Calmodulin (CaM), CBL (Calcineurin B-Like), CDPKs helps bring $[Ca^{2+}]_{cyt}$ back to the basal level. This would be aided by the activation of AtACA8 at the plasma membrane to export Ca^{2+} to the apoplast (Costa *et al.*, 2017; Behera *et al.*,

2018). The activated Ca^{2+} sensors eventually lead to downstream responses such as transcriptional changes. To date, these involve AtCAMTA3 (Jewell *et al.*, 2019).

The model presented however is at the cellular level. DeFalco *et al.* (2017) and Matthus *et al.* (2019a) demonstrated the production of $[Ca^{2+}]_{cyt}$ waves by eATP in *N. benthamiana* and *A. thaliana* respectively. A $[Ca^{2+}]_{cyt}$ wave has the characteristic of starting at the point of stimulus induction and then travelling in the vascular tissue such as in wounding (Vincent *et al.*, 2017) and salt stress (Choi *et al.*, 2014a). Other than $[Ca^{2+}]_{cyt}$, ROS have been shown to be producing waves in *A. thaliana* under abiotic stresses. The ROS wave acting as a systemic signal depends on the function of the NADPH Oxidase encoded by AtRBOHD and the propagation was at the speed of (8.4 cm min^{-1}). The AtRBOHD generated ROS at the apoplast of each cell from the local point of stimulation and propagating away from it. This wave was also independent of hormone treatment but could be activated by abiotic stresses such as wounding, temperature stress and salinity (Miller *et al.*, 2009). Salt stress has been shown to produce a $[Ca^{2+}]_{cyt}$ wave as a long-distance systemic signalling molecule from the root to the shoot. This involves AtRBOHD and the vacuolar Ca^{2+} channel AtTPC1 (Two Pore Channel 1) (Choi *et al.*, 2014a; Evans *et al.*, 2016).

Our proposed model of the eATP signalling pathway could be hypothetically incorporated into the $[Ca^{2+}]_{cyt}$ and ROS wave phenomena in plant cells as an overall picture. Upon exposure towards biotic or abiotic stresses, plants produce eATP as a danger signal which upon perception causes accumulation of $[Ca^{2+}]_{cyt,}$ production of ROS and NO. The ROS produced in the extracellular space (probably sourced by AtRBOHD) activate Ca^{2+} channels of the neighbouring cells causing the accumulation of $[Ca^{2+}]_{cyt}$ in neighbouring cells to occur thus forming the $[Ca^{2+}]_{cyt}$ wave as part of ROS-induced calcium release (RICR). The $[Ca^{2+}]_{cyt}$ accumulation in the neighbouring cells induces the activation of NADPH Oxidase and accumulation of more ROS in the extracellular space forming the ROS wave. This would solve the problem of ROS scavengers present ubiquitously as each plant cell would produce ROS to form the wave. It is fitting that the hormone treatments in the study by Miller *et al.* (2009) would not produce the ROS wave, as the eATP-induced $[Ca^{2+}]_{cyt}$ and ROS wave could be the components of an early response towards stresses whereas the hormone defence response could be downstream. It is tempting to put AtANN1 as one of the candidates of Ca^{2+} channel that is involved in this systemic signalling under salt stress or in response to eATP. Another way to determine the possible role of AtANN1 in the systemic signalling is by

studying the transcriptional response in the leaves of seedlings when the roots are treated with eATP.

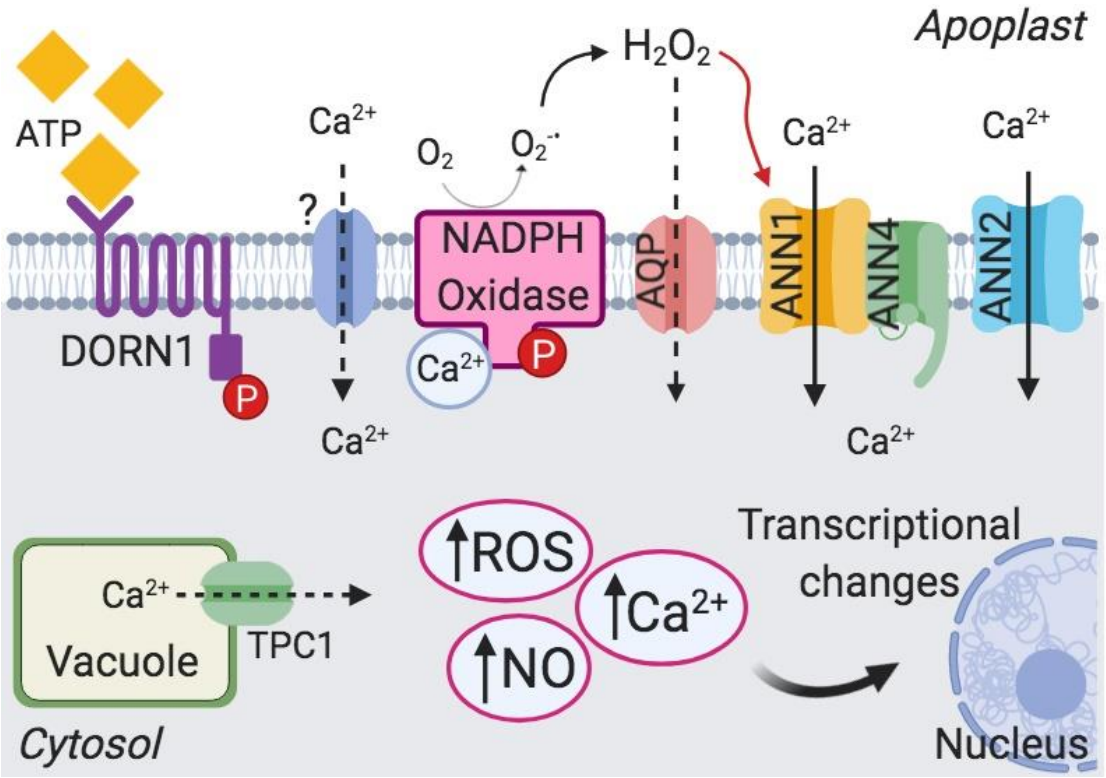

Figure 6.1: **Proposed model of the eATP signalling pathway.** The proposed model is based on the outcome of this study and previous reported studies. Components that involved are AtDORN1 (purinoreceptor), AtRBOHD (as NADPH Oxidase) to produce ROS, and AtANNs as calcium channels downstream of the AtDORN1 producing overall increase in free $[Ca^{2+}]_{cyt}$, ROS production and NO. Dashed arrow (--->) shows putative calcium channels not yet identified in the eATP-signalling pathway. Model is created by using Biorender (www.biorender.com).

6.2 Extracellular ATP signalling might be upstream of hormone-related stress responses in *A. thaliana* but the mechanism is unclear

Extracellular ATP was envisaged as the signalling molecule that governs both biotic and abiotic stresses in plants. Exposure to stress conditions such as salinity stress (Dark *et al.*, 2011), wounding (Jeter *et al.*, 2004; Dark *et al.*, 2011), osmotic stress (Dark *et al.*, 2011), and PAMP elicitors (Wu *et al.*, 2008) showed accumulation of eATP in the extracellular space. Most of these stress conditions and eATP exposure evoked a similar early response; elevation of $[Ca^{2+}]_{cyt}$ (Demidchik *et al.*, 2003a; Jeter *et al.*, 2004; Ranf *et al.*,2011; Sun *et al.*, 2012), production of ROS (Demidchik *et al.*, 2009, 2011; Sun *et al.*, 2012; Ranf *et al.*, 2011), and

NO (Foresi *et al.*, 2007) leading to downstream responses such as induction of stress-related genes (Demidchik *et al.*, 2009; Choi *et al.*, 2014a; Jewell *et al.*, 2019). The incorporation of an eATP signal in the stress-signalling pathways however is not yet secured. Whether eATP acts as the earlier signal molecule or downstream of the stress signalling pathway is still a question. Most of the stress-signalling pathways in plant cells involve the action of phytohormones such as ABA, ethylene, salicylic acid or jasmonic acid. These would be another factor to consider when discussing the action of the eATP signal.

In most studies, ABA has been implicated with stomatal aperture regulation in a water-deprived state such as drought or salinity stress (Wilkinson and Davies, 2010) as well as during pathogen attacks to counter the entry of pathogens. Chen *et al.*, (2017) reported that eATP induced stomatal closure dependent on the function of AtDORN1 and AtRBOHD. The same study however reported that treatment with ABA would cause stomatal closure regardless of the action of AtDORN1 and AtRBOHD. This could suggest that the ABA signalling pathway lies downstream of the eATP signalling pathway thus the mutation of either AtDORN1 or AtRBOHD would not have any effects on the stomatal aperture when the ABA was supplied exogenously. However, in roots, ABA lies upstream of eATP accumulation (Dark *et al.*, 2011). It is also possible that ABA-induced stomatal closure is from a different pathway to the eATP-induced stomatal closure.

AtWRKY40 is a transcription factor that could regulate ABA biosynthesis in plant cells by binding at the promoter region of the genes (Liu *et al.*, 2012b). The same study found that the action of AtWRKY40 together with AtWRKY18 and AtWRKY60 could negatively regulate ABA production. Expression of *AtWRKY40* is upregulated by eATP in an AtDORN1-dependent manner (Choi *et al.*, 2014b). eATP-induced upregulation was also found here (Chapters 3 and 4), suggesting that eATP may help suppress ABA biosynthesis. This seems at odds with the concept of eATP as a danger signal that helps promote survival. However, much would depend on the location and duration of the eATP signal in its possible regulation of ABA. In Chapter 3 and Chapter 4, we carried out the quantification of *AtWRKY40* in eATP-treated *Atann1, Atann2, Atann1/2, Atann1/4* and *Atann1/2/4* mutants. We found that although *AtWRKY40* transcript was up-regulated when the samples were treated with eATP, *AtANN1*, *AtANN2* and *AtANN4* were not involved in the regulation of this gene. As AtANN1, AtANN2 and AtANN4 found involved in eATP-induced $[Ca^{2+}]_{cyt}$ elevation, we anticipated that the loss of function of any of these annexins would possibly alter the *AtWRKY40* expression compared to the wild type. It may be that sufficient $[Ca^{2+}]_{cyt}$

elevation had occurred in the mutants to trigger the response or that another signal had reached its threshold level. Since Choi *et al.* (2014b) found the eATP-induced expression of *AtWRKY40* is dependent on AtDORN1, we would assume that AtWRKY40 would be downstream of AtRBOHD as AtDORN1 interacted with AtRBOHD in the presence of eATP (Chen *et al.*, 2017). However, Zandalinas *et al.*, (2019) listed *AtWRKY40* as one of the genes that were up-regulated in both wild type and *Atrbohd* mutant under light stress which possibly involves an eATP signal (Clark and Roux, 2011). The same study also showed up-regulation of *AtWRKY40* expression in H_2O_2 treatment and the expression was not inhibited by DPI (Diphenyleneiodonium) as an NADPH oxidase inhibitor. This indicates that *AtWRKY40* could be up-regulated under both eATP signal and in the presence of ROS but independently of NADPH Oxidase. Here we hypothesised that AtANN1, AtANN2 and AtANN4 would be downstream of eATP and NADPH Oxidase action; it is possible that the loss-of-function mutant of these annexins has no effect on *AtWRKY40* expression since the annexins are in a different pathway.

Besides *AtWRKY40,* another eATP-induced gene (*AtACS6*) was also tested. *AtACS6* encodes for 1-aminocyclopropane-1-carboxylic acid synthase, which is involved in biosynthesis of ethylene. Ethylene acts as part of the defence mechanism in plants in wounding (Kamiyoshihara *et al.*, 2010), pathogen attacks (specifically necrotrophic pathogens; Han *et al.*, 2010) and also some other abiotic stresses (Li *et al.*, 2018). *AtACS6* was found to be important in elevation of ethylene during *B. cinerea* infection. Based on our study, we found that, unlike the *AtWRKY40* expression, eATP-induced up-regulation of *AtACS6* expression required AtANN1, AtANN2 and AtANN4 (Chapter 3, Chapter 4).

Under the eATP signal from pathogen attack, AtANN1 downstream of AtDORN1 and ROS production possibly with AtANN2 and AtANN4 could help mediate the initial increase in $[Ca^{2+}]_{cyt}$ forming the Ca^{2+} signature. Ca^{2+} sensor proteins such as calmodulin (CaM) and calcium-dependent protein kinases (CDPKs) might decode the Ca^{2+} signature. A transcriptomic study of eATP-treated *A. thaliana* carried out by Jewell *et al.* (2019) listed AtCAMTA3 (Calmodulin binding Transcription Activator3) as the possible component that binds to DNA and regulates the eATP-induced gene expression such as *AtACS6.* This would eventually lead to the production of ethylene in response to eATP as a danger signal. The transcriptomic study also found *AtACS6* as one of the eATP induced genes in the Col-0 wild type, and the expression of this gene was highly up-regulated in overly expressed AtDORN1 (*OXP2K1*) (Jewell *et al.*, 2019). It was expected that the overexpression of the AtDORN1

purinoreceptor would result in up-regulation of *AtACS6,* as more eATP signal perception should lead to increase in AtACS6 activation thus ethylene production.

The action of protein kinases is important in the production of ethylene. Previously, phosphorylation of AtACS6 and AtACS2 was found to strengthen the complex between the two and increase the biosynthesis of ethylene. This has been shown in the Mitogen Activated Protein Kinases MAPK-dependent pathway in *Botrytis cinerea* infection where AtMPK3 and AtMPK6 phosphorylation of AtACS2/AtACS6 is needed for the production of ethylene (Li *et al.,* 2012). Downstream of AtANN1, it might be dependent on a non-MAPK pathway as it could involve $[Ca^{2+}]_{cyt}$ signalling. Protein kinases downstream of AtANN1 in ethylene production have yet to be identified. Both AtACS6 and AtACS2 contain the motif for phosphorylation by CDPKs (Sebastià *et al.,* 2004) making CDPKs suitable candidates. Another study showed the role of AtCPK4 and AtCPK11 in the phosphorylation of AtACS2/AtACS6 in ABA-induced ethylene production (Luo *et al.,* 2014). Other possible CDPK candidates are AtCPK5 and AtCPK6 as the loss-of-function mutant of these two CDPKs altered the expression of *AtACS2* and *AtACS6* leading to reduced ethylene production during wounding (Li *et al.,* 2018). Based on these studies, both CDPKs and AtCAMTA3 might be the divergence point in the eATP-signalling pathway that dictates the stress-related responses.

6.3 AtANNs involvement in eATP-induced root skewing needs further testing

Another component of eATP-induced changes that was examined here was eATP-regulated root growth. Extracellular ATP exposure was previously reported to cause root skewing and interfered with root gravitropism, possibly by disruption of auxin transport (Tang *et al.,* 2003). A protein kinase known as TOR (Target of Rapamycin) is involved in modulating auxin-induced growth in the meristem, dependent on light and glucose in the shoot but dependent only on auxin and glucose in the root (Li *et al.,* 2017). AtYAK1 (Yet Another Kinase 1) which was previously reported to regulate growth under light and ABA signals (Kim *et al.,* 2016; Huang *et al.,* 2017) was recently shown to negatively regulate TOR (Barrada *et al.,* 2019). It is thought that AtYAK1 has to be "switched" off to promote growth (Forzani *et al.,* 2019). AtYAK1 can phosphorylate AtANN1, AtANN2 and AtANN4 (Kim *et al.,* 2015), which suggest that the unphosphorylated form of these annexins promotes growth. AtANN1 and AtANN2 were found to possibly be involved in the transport of sugar in the

phloem (Wang *et al.*, 2018b) as well as possibly functioning in secretion of polysaccharides in growing roots (Clark *et al.*, 2005a). Given the involvement of annexins in root growth, it was hypothesised that *Atann1* may not skew in response to eATP. Here, eATP was found to induce root skewing although AtANN1 might not be involved. Further studies need now to test *Atann2*, *Atann4* and higher order mutants. *AtKAI2* (Karrikin Insensitive 2) and *AtMAX2* (More Axillary Growth 2), which underpin perception of karrikin phytohormone, were found to be some of the genes down-regulated in the presence of eATP (Jewell *et al.*, 2019). Swarbreck *et al.* (2019) reported that AtKAI2 and AtMAX2 were important in maintaining straight vertical growth of roots of *A. thaliana.* Thus it is also possible that the root skewing by eATP involves the action of karrikins and that the down-regulation by eATP caused the skewing to happen.

6.4 Screening of AtANN2 function in salinity stress responses at whole seedling level

Salinity stress responses in plants involve interplay of different components such as ion homeostasis and hormones. In the eATP response, AtANN2 helped mediate $[Ca^{2+}]_{cyt}$ elevation alongside AtANN1 (Chapter 4). However, whether the role of AtANN2 is eATP-specific or could also be involved in salinity stress or hormonal response related to salinity stress is not yet known. Measurement of $[Ca^{2+}]_{cyt}$ under salinity stress (200 mM NaCl) in our study found that AtANN2 is needed for the $[Ca^{2+}]_{cyt}$ response at whole seedling level. Interestingly, the $[Ca^{2+}]_{cyt}$ accumulated in an oscillatory manner in whole seedlings compared to the monophasic response at whole root level. This might indicate that the Ca^{2+} oscillation was likely to originate from the shoot region of the seedlings tested. This is not the first reported case on differences in the Ca^{2+} signature between organs induced by the same stimulus. Matthus *et al.* (2019a) reported monophasic $[Ca^{2+}]_{cyt}$ accumulation in leaves but biphasic $[Ca^{2+}]_{cyt}$ accumulation in root tips by the same eATP treatment. This outcome showed that $[Ca^{2+}]_{cyt}$ increase depends on the different types of tissues responding.

Although the (apo)aequorin reporter captured the oscillatory nature of the $[Ca^{2+}]_{cyt}$ response, it was not adequate to dissect the origin of tissues the $[Ca^{2+}]_{cyt}$ oscillation comes from. Besides the origin on the $[Ca^{2+}]_{cyt}$, the $[Ca^{2+}]_{cyt}$ oscillations for each individual whole seedling temporally differed, further hindering analysis. Development of different Ca^{2+} reporters recently has helped better the resolution of $[Ca^{2+}]_{cyt}$. GFP-based Ca^{2+} sensor Yellow Cameleon (YC) 3.6 under confocal microscopy could be utilised to observe $[Ca^{2+}]_{cyt}$

accumulation at tissue level. Monshausen *et al.*, (2008) employed this reporter in their effort to study $[Ca^{2+}]_{cyt}$ oscillations in root tip growth. They found that the $[Ca^{2+}]_{cyt}$ oscillations in root tips were needed not to accelerate growth but to control growth and prevent root tips from bursting. Under salinity stress however the purpose of the $[Ca^{2+}]_{cyt}$ oscillations is not yet known.

It might be useful in the future to utilise the reporter such as YC3.6 especially in the shoot region to first determine the $[Ca^{2+}]_{cyt}$ oscillation spatially in each seedling. Mapping the $[Ca^{2+}]_{cyt}$ oscillation based on the distance from the tip across the measurement time as done by Monsaushen *et al.* (2008) might be helpful in reducing the variability of oscillation from each seedling making quantification of $[Ca^{2+}]_{cyt}$ measurement to be less complicated and could also be employed at the shoot region. Since chloroplasts produce high levels of intracellular ROS especially in abiotic stresses (Bose *et al.*, 2014) and the oscillation might be mainly happening at the shoot region, it is also worth observing the ROS accumulation whether it is oscillating as well to determine whether the $[Ca^{2+}]_{cyt}$ oscillations are related to ROS production.

6.5 Concluding remarks and future directions

In this thesis, we reported the role of AtANN1, AtANN2 and AtANN4 in mediating the elevation of free $[Ca^{2+}]_{cyt}$ in eATP signalling and the function of these annexins results in the changes at the transcriptional level of ethylene biosynthesis. Experiments with higher resolution reporter should be done as the next step to gather more information regarding these annexins possibly as calcium channels. The possibility of other calcium channels involved was also discussed in this thesis.

Other than in Brassicaceae species such as *A. thaliana,* it would be useful in the future to test for the function of AtANN1, AtANN2 and AtANN4 in mediating $[Ca^{2+}]_{cyt}$ response in other species such as tobacco. DeFalco *et al.* (2017) produced lines of *N. benthamiana* and *N. tabacum* GCAMP3 plants to monitor the $[Ca^{2+}]_{cyt}$ response. In that study, *N. benthamiana* increased its $[Ca^{2+}]_{cyt}$ when tested with eATP, thus showing the possibility of an eATP signalling pathway in a non-Brassica species. Transient expression of *AtANN1, AtANN2* and *AtANN4* in the *N. benthamiana* carrying the GCAMP3 reporter could be useful to test for the function of these annexins as Ca^{2+} channels.

As annexins were heavily implicated in stress responses, production of annexins mutant lines in crop species could possibly help in the long run for application purposes. Rice Annexin 1 (OsANN1) was found to be needed for heat and drought resistance (as the RNAi lines showed hypersensitivity possibly *via* a CDPK24 pathway) and also helps regulate the level of ROS accumulated under these stresses (Qiao *et al.*, 2015). Besides OsANN1, rice Annexin 3 (OsANN3) and Annexin 4 (OsANN4) gene expression was found to be regulated by LecRK-VII.1 involved as negative regulator in salt stress (Zhang *et al.*, 2017). OsANN3 also showed involvement in drought stress when found to be part of the ABA signalling pathway in increasing root length and promoting stomatal closure to reduce water deprivation (Li *et al.*, 2019). Recent development of CRISPR/Cas9 (clustered regularly interspaced short palindromic repeat/CRISPR associated protein 9) as a tool for a precise genome editing could be employed to create loss-of-function mutants of these annexins in rice (Char *et al.*, 2018). Although these rice annexins are not the equivalent of the AtANN1, AtANN3 or AtANN4, the mutant lines could open up possibility of studying eATP signalling in crop species.

Other putative calcium channels especially intracellular calcium channels such as AtTPC1 should be tested in the future. AtCNGC19 was listed as one of the genes that were up-regulated under eATP treatment (Jewell *et al.*, 2019) and was shown to be involved in herbivory responses (Meena *et al.*, 2019) that could relate to eATP signalling in wounding. The (apo)aequorin reporter could be used in screening the function of these putative channels in the eATP signalling pathway (as it is much more high throughput compared to other reporters) before more specific and higher resolution reporters are used.

References

Abdul-Awal, S. M., Hotta, C. T., Davey, M. P., Dodd, A. N., Smith, A. G. and Webb, A. A. R. (2016) 'NO-Mediated $[Ca^{2+}]_{cyt}$ Increases Depend on ADP-Ribosyl Cyclase Activity in Arabidopsis', *Plant Physiology*, 171(1), pp. 623–631. doi: 10.1104/pp.15.01965.

Abe, H., Urao, T., Ito, T., Seki, M., Shinozaki, K. and Yamaguchi-Shinozaki, K. (2003) 'Arabidopsis AtMYC2 (bHLH) and AtMYB2 (MYB) Function as Transcriptional Activators in Abscisic Acid Signaling', *The Plant Cell*, 15(1), pp. 63–78. doi: 10.1105/tpc.006130.

Abràmofff, M. D., Magalhães, P. J. and Ram, S. J. (2005) 'Image processing with ImageJ Part II', *Biophotonics International*, 11(7), pp. 36–43. doi: 10.1117/1.3589100.

Ahlfors, R., Brosché, M., Kollist, H. and Kangasjärvi, J. (2009) 'Nitric oxide modulates ozone-induced cell death, hormone biosynthesis and gene expression in *Arabidopsis thaliana*.', *The Plant journal : for cell and molecular biology*, 58(1), pp. 1–12. doi: 10.1111/j.1365-313X.2008.03756.x.

Ahmad, P., Azooz, M. M. and Prasad, M. N. V (2013) *Ecophysiology and Responses of Plants under Salt Stress*, *Ecophysiology and Responses of Plants under Salt Stress*. Edited by P. Ahmad, M. M. Azooz, and M. N. V. Prasad. New York, NY: Springer New York. doi: 10.1007/978-1-4614-4747-4.

Ali, R., Ma, W., Lemtiri-Chlieh, F., Tsaltas, D., Leng, Q., von Bodman, S. and Berkowitz, G. A. (2007) 'Death don't have no mercy and neither does calcium: Arabidopsis CYCLIC NUCLEOTIDE GATED CHANNEL2 and innate immunity.', *The Plant cell*, 19(3), pp. 1081–95. doi: 10.1105/tpc.106.045096.

Andrej-Nikolai Spiess (2018) 'Package " qpcR ".'

Arispe, N., Rojas, E., Genge, B. R., Wu, L. N. Y. and Wuthier, R. E. (1996) 'Similarity in calcium channel activity of annexin V and matrix vesicles in planar lipid bilayers', *Biophysical Journal*. Elsevier, 71(4), pp. 1764–1775. doi: 10.1016/S0006-3495(96)79377-3.

Arora, P. D., Bibby, K. J. and McCulloch, C. A. G. (1994) 'Slow oscillations of free intracellular calcium ion concentration in human fibroblasts responding to mechanical stretch', *Journal of Cellular Physiology*, 161(2), pp. 187–200. doi: 10.1002/jcp.1041610202.

Asada, K. (2006) 'Production and scavenging of reactive oxygen species in chloroplasts and their functions', *Plant Physiology*, 141(2), pp. 391–396. doi: 10.1104/pp.106.082040.

Ashraf, M. A., Rasheed, R., Hussain, I., Iqbal, M., Haider, M. Z., Parveen, S. and Sajid, M. A. (2015) 'Hydrogen peroxide modulates antioxidant system and nutrient relation in maize (*Zea mays L.*) under water-deficit conditions', *Archives of Agronomy and Soil Science*. Taylor & Francis, 61(4), pp. 507–523. doi: 10.1080/03650340.2014.938644.

Assmann, S. M. (2013) 'Natural Variation in Abiotic Stress and Climate Change Responses in Arabidopsis : Implications for Twenty-First-Century Agriculture', *International Journal of Plant Sciences*, 174(1), pp. 3–26. doi: 10.1086/667798.

Barrada, A., Djendli, M., Desnos, T., Mercier, R., Robaglia, C., Montané, M.-H. and Menand, B. (2019) 'A TOR-YAK1 signaling axis controls cell cycle, meristem activity and plant growth in Arabidopsis', *Development*, 146(3), p. dev171298. doi: 10.1242/dev.171298.

Basu, D. and Haswell, E. S. (2017) 'Plant mechanosensitive ion channels: an ocean of possibilities', *Current Opinion in Plant Biology*, pp. 43–48. doi: 10.1016/j.pbi.2017.07.002.

Beck, M., Wyrsch, I., Strutt, J., Wimalasekera, R., Webb, A., Boller, T. and Robatzek, S. (2014) 'Expression patterns of FLAGELLIN SENSING 2 map to bacterial entry sites in plant shoots and roots', *Journal of Experimental Botany*, 65(22), pp. 6487–6498. doi: 10.1093/jxb/eru366.

Bednarek, P. (2012) 'Chemical warfare or modulators of defence responses - the function of secondary metabolites in plant immunity', *Current Opinion in Plant Biology*. Elsevier Ltd, 15(4), pp. 407–414. doi: 10.1016/j.pbi.2012.03.002.

Behera, S., Xu, Z., Luoni, L., Bonza, M. C., Doccula, F. G., De Michelis, M. I., Morris, R. J., Schwarzländer, M. and Costa, A. (2018) 'Cellular Ca^{2+} signals generate defined pH signatures in plants', *Plant Cell*, 30(11), pp. 2704–2719. doi: 10.1105/tpc.18.00655.

Bethke, G., Unthan, T., Uhrig, J. F., Pöschl, Y., Gust, A. A., Scheel, D. and Lee, J. (2009) 'Flg22 regulates the release of an ethylene response factor substrate from MAP kinase 6 in *Arabidopsis thaliana* via ethylene signaling', *Proceedings of the National Academy of Sciences of the United States of America*, 106(19), pp. 8067–8072. doi: 10.1073/pnas.0810206106.

Bodin, P. and Burnstock, G. (2001) 'Purinergic signalling: ATP release', *Neurochemical Research*, 26(8-9), pp. 959–969. doi: 10.1023/A:1012388618693.

Boller, T. and Felix, G. (2009) 'A Renaissance of Elicitors: Perception of Microbe-Associated Molecular Patterns and Danger Signals by Pattern-Recognition Receptors', *Annual Review of Plant Biology*, 60(1), pp. 379–406. doi: 10.1146/annurev.arplant.57.032905.105346.

Bolouri Moghaddam, M. R. and Van den Ende, W. (2012) 'Sugars and plant innate immunity', *Journal of Experimental Botany*, 63(11), pp. 3989–3998. doi: 10.1093/jxb/ers129.

Bonza, M. C., Morandini, P., Luoni, L., Geisler, M., Palmgren, M. G. and De Michelis, M. I. (2000) 'At-ACA8 encodes a plasma membrane-localized calcium-ATPAse of Arabidopsis with a calmodulin-binding domain at the N terminus', *Plant Physiology*, 123(4), pp. 1495–1505.

Bose, J., Rodrigo-Moreno, A. and Shabala, S. (2014) 'ROS homeostasis in halophytes in the context of salinity stress tolerance', *Journal of Experimental Botany*, 65(5), pp. 1241–1257. doi: 10.1093/jxb/ert430.

Boustead, C. M., Smallwood, M., Small, H., Bowles, D. J. and Walker, J. H. (1989) 'Identification of calcium-dependent phospholipid-binding proteins in higher plant cells', *FEBS Letters*, 244(2), pp. 456–460. doi: 10.1016/0014-5793(89)80582-4.

Bouwmeester, K. and Govers, F. (2009) 'Arabidopsis L-type lectin receptor kinases: Phylogeny, classification, and expression profiles', *Journal of Experimental Botany*, 60(15), pp. 4383–4396. doi: 10.1093/jxb/erp277.

Bouwmeester, K., Han, M., Blanco-Portales, R., Song, W., Weide, R., Guo, L. Y., van der Vossen, E. A. G. and Govers, F. (2014) 'The Arabidopsis lectin receptor kinase LecRK-I.9 enhances resistance to *Phytophthora infestans* in Solanaceous plants', *Plant Biotechnology Journal*, 12(1), pp. 10–16. doi: 10.1111/pbi.12111.

Bouwmeester, K., de Sain, M., Weide, R., Gouget, A., Klamer, S., Canut, H. and Govers, F. (2011) 'The lectin receptor kinase LecRK-I.9 is a novel Phytophthora resistance component and a potential host target for a RXLR effector', *PLoS Pathogens*, 7(3). doi: 10.1371/journal.ppat.1001327.

Brady, S. M., Orlando, D. A., Lee, J.-Y., Wang, J. Y., Koch, J., Dinneny, J. R., Mace, D., Ohler, U. and Benfey, P. N. (2007) 'A High-Resolution Root Spatiotemporal Map Reveals Dominant Expression Patterns', *Science*, 318(5851), pp. 801–806. doi: 10.1126/science.1146265.

Breton, G., Vazquez-Tello, A., Danyluk, J. and Sarhan, F. (2000) 'Two novel intrinsic annexins accumulate in wheat membranes in response to low temperature', *Plant and Cell Physiology*, 41(2), pp. 177–184. doi: 10.1093/pcp/41.2.177.

Buetler, T. M., Krauskopf, A. and Ruegg, U. T. (2004) 'Role of superoxide as a signaling molecule', *News in Physiological Sciences*, 19(3), pp. 120–123. doi: 10.1152/nips.01514.2003.

Burnstock, G. (2006) 'Purinergic signalling', *British Journal of Pharmacology*, 147(SUPPL. 1),

pp. 172–181. doi: 10.1038/sj.bjp.0706429.

Burnstock, G. (2018) 'Purine and purinergic receptors', *Brain and Neuroscience Advances*, 2, p. 239821281881749. doi: 10.1177/2398212818817494.

Burnstock, G., Campbell, G., Satchell, D. and Smythe, A. (1970) 'Evidence that adenosine triphosphate or a related nucleotide is the transmitter substance released by non-adrenergic inhibitory nerves in the gut', *British Journal of Pharmacology*, 40(4), pp. 668–688. doi: 10.1111/j.1476-5381.1970.tb10646.x.

Burnstock, G. and Kennedy, C. (1985) 'Is there a basis for distinguishing two types of P2-purinoceptor?', *General Pharmacology: The Vascular System*, 16(5), pp. 433–440. doi: 10.1016/0306-3623(85)90001-1.

Cantero, a, Barthakur, S., Bushart, T. J., Chou, S., Morgan, R. O., Fernandez, M. P., Clark, G. B. and Roux, S. J. (2006) 'Expression profiling of the Arabidopsis annexin gene family during germination, de-etiolation and abiotic stress', *Plant Physiology and Biochemistry*, 44, pp. 13–24. doi: 10.1016/j.plaphy.2006.02.002.

Cao, Y., Tanaka, K., Nguyen, C. T. and Stacey, G. (2014) 'Extracellular ATP is a central signaling molecule in plant stress responses.', *Current opinion in plant biology*, 20, pp. 82–7. doi: 10.1016/j.pbi.2014.04.009.

Chen, D., Cao, Y., Li, H., Kim, D., Ahsan, N., Thelen, J. and Stacey, G. (2017) 'Extracellular ATP elicits DORN1-mediated RBOHD phosphorylation to regulate stomatal aperture', *Nature Communications*. Springer US, 8(1). doi: 10.1038/s41467-017-02340-3.

Chen, H., Lai, Z., Shi, J., Xiao, Y., Chen, Z. and Xu, X. (2010) 'Roles of arabidopsis WRKY18, WRKY40 and WRKY60 transcription factors in plant responses to abscisic acid and abiotic stress', *BMC Plant Biology*. BioMed Central Ltd, 10(1), p. 281. doi: 10.1186/1471-2229-10-281.

Chen, J., Lalonde, S., Obrdlik, P., Vatani, A. N., Parsa, S. A., Vilarino, C., Revuelta, J. L., Frommer, W. B. and Rhee, S. Y. (2012) 'Uncovering Arabidopsis membrane protein interactome enriched in transporters using mating-based split ubiquitin assays and classification models', *Frontiers in Plant Science*, 3(JUN), pp. 1–14. doi: 10.3389/fpls.2012.00124.

Chen, T. and Fluhr, R. (2018) 'Singlet oxygen plays an essential role in the root's response to osmotic stress', *Plant Physiology*, 177(4), pp. 1717–1727. doi: 10.1104/pp.18.00634.

Cheng, N. H., Pittman, J. K., Shigaki, T., Lachmansingh, J., LeClere, S., Lahner, B., Salt, D.

E. and Hirschi, K. D. (2005) 'Functional association of Arabidopsis CAX1 and CAX3 is required for normal growth and ion homeostasis', *Plant Physiology*, 138(4), pp. 2048–2060. doi: 10.1104/pp.105.061218.

Cheval, C., Aldon, D., Galaud, J.-P. and Ranty, B. (2013) 'Calcium/calmodulin-mediated regulation of plant immunity.', *Biochimica et biophysica acta*. Elsevier B.V., 1833(7), pp. 1766–71. doi: 10.1016/j.bbamcr.2013.01.031.

Chew, O., Whelan, J. and Millar, A. H. (2003) 'Molecular Definition of the Ascorbate-Glutathione Cycle in Arabidopsis Mitochondria Reveals Dual Targeting of Antioxidant Defenses in Plants', *Journal of Biological Chemistry*, 278(47), pp. 46869–46877. doi: 10.1074/jbc.M307525200.

Chinchilla, D., Zipfel, C., Robatzek, S., Kemmerling, B., Nürnberger, T., Jones, J. D. G., Felix, G. and Boller, T. (2007) 'A flagellin-induced complex of the receptor FLS2 and BAK1 initiates plant defence', *Nature*, 448(7152), pp. 497–500. doi: 10.1038/nature05999.

Chivasa, S., Murphy, A. M., Hamilton, J. M., Lindsey, K., Carr, J. P. and Slabas, A. R. (2009) 'Extracellular ATP is a regulator of pathogen defence in plants', *Plant Journal*, 60(3), pp. 436–448. doi: 10.1111/j.1365-313X.2009.03968.x.

Chivasa, S., Ndimba, B. K., Simon, W. J., Lindsey, K. and Slabas, A. R. (2005) 'Extracellular ATP functions as an endogenous external metabolite regulating plant cell viability.', *The Plant cell*, 17(11), pp. 3019–34. doi: 10.1105/tpc.105.036806.

Choi, J., Tanaka, K., Cao, Y., Qi, Y., Qiu, J., Liang, Y., Lee, S. Y. and Stacey, G. (2014b) 'Identification of a plant receptor for extracellular ATP.', *Science (New York, N.Y.)*, 343(6168), pp. 290–4. doi: 10.1126/science.343.6168.290.

Choi, J., Tanaka, K., Liang, Y., Cao, Y., Lee, S. Y. and Stacey, G. (2014c) 'Extracellular ATP, a danger signal, is recognized by DORN1 in Arabidopsis', *Biochemical Journal*, pp. 429–437. doi: 10.1042/BJ20140666.

Choi, W. G., Toyota, M., Kim, S. H., Hilleary, R. and Gilroy, S. (2014a) 'Salt stress-induced Ca^{2+} waves are associated with rapid, long-distance root-to-shoot signaling in plants', *Proceedings of the National Academy of Sciences of the United States of America*, 111(17), pp. 6497–6502. doi: 10.1073/pnas.1319955111.

Chung, J.-S., Zhu, J.-K., Bressan, R. A., Hasegawa, P. M. and Shi, H. (2007) 'Reactive oxygen species mediate Na^{+}-induced SOS1 mRNA stability in Arabidopsis', *The Plant Journal*,

53(3), pp. 554–565. doi: 10.1111/j.1365-313X.2007.03364.x.

Clark, G. B., Lee, D., Dauwalder, M. and Roux, S. J. (2005a) 'Immunolocalization and histochemical evidence for the association of two different Arabidopsis annexins with secretion during early seedling growth and development', *Planta*, 220(4), pp. 621–631. doi: 10.1007/s00425-004-1374-7.

Clark, G. B., Morgan, R. O., Fernandez, M. P. and Roux, S. J. (2012) 'Evolutionary adaptation of plant annexins has diversified their molecular structures, interactions and functional roles', *New Phytologist*, 196(3), pp. 695–712. doi: 10.1111/j.1469-8137.2012.04308.x.

Clark, G., Cantero-Garcia, A., Butterfield, T., Dauwalder, M. and Roux, S. J. (2005b) 'Secretion as a key component of gravitropic growth: implications for annexin involvement in differential growth', *Gravit Space Biol Bull*, 18(2), pp. 113–114.

Clark, G., Fraley, D., Steinebrunner, I., Cervantes, A., Onyirimba, J., Liu, A., Torres, J., Tang, W., Kim, J. and Roux, S. J. (2011) 'Extracellular nucleotides and apyrases regulate stomatal aperture in Arabidopsis', *Plant Physiology*, 156(4), pp. 1740–1753. doi: 10.1104/pp.111.174466

Clark, G. and Roux, S. J. (2011) 'Apyrases, extracellular ATP and the regulation of growth', *Current Opinion in Plant Biology*. Elsevier Ltd, pp. 700–706. doi: 10.1016/j.pbi.2011.07.013.

Clark, G., Torres, J., Herz, N., Wat, N., Ogoti, J., Aranda, G., Blizard, M., Wu, M., Onyirimba, J., Canales, A. A., Pham, T., Gomez, D., Nyberg, T., Roux, S. J., Wu, J. and Terry, A. (2010) 'Both the stimulation and inhibition of root hair growth induced by extracellular nucleotides in Arabidopsis are mediated by nitric oxide and reactive oxygen species', *Plant Molecular Biology*, 74(4-5), pp. 423–435. doi: 10.1007/s11103-010-9683-7.

Clarke, B., Liang, R., Morell, M. K., Bird, A. R., Jenkins, C. L. D. and Li, Z. (2008) 'Gene expression in a starch synthase IIa mutant of barley: Changes in the level of gene transcription and grain composition', *Functional and Integrative Genomics*, 8(3), pp. 211–221. doi: 10.1007/s10142-007-0070-7.

Coca, M. and San Segundo, B. (2010) 'AtCPK1 calcium-dependent protein kinase mediates pathogen resistance in Arabidopsis', *Plant Journal*, 63(3), pp. 526–540. doi: 10.1111/j.1365-313X.2010.04255.x.

Conn, S. and Gilliham, M. (2010) 'Comparative physiology of elemental distributions in plants', *Annals of Botany*, 105(7), pp. 1081–1102. doi: 10.1093/aob/mcq027.

Costa, A., Luoni, L., Marrano, C. A., Hashimoto, K., Köster, P., Giacometti, S., De Michelis, M. I., Kudla, J. and Bonza, M. C. (2017) 'Ca^{2+}-dependent phosphoregulation of the plasma membrane Ca^{2+}-ATPase ACA8 modulates stimulus-induced calcium signatures', *Journal of Experimental Botany*, 68(12), pp. 3215–3230. doi: 10.1093/jxb/erx162.

Dabitz, N., Hu, N. J., Yusof, A. M., Tranter, N., Winter, A., Daley, M., Zschörnig, O., Brisson, A. and Hofmann, A. (2005) 'Structural determinants for plant annexin-membrane interactions', *Biochemistry*, 44(49), pp. 16292–16300. doi: 10.1021/bi0516226.

Dark, A., Demidchik, V., Richards, S. L., Shabala, S. and Davies, J. M. (2011) 'Release of extracellular purines from plant roots and effect on ion fluxes', *Plant Signaling and Behavior*, 6(11), pp. 1855–1857. doi: 10.4161/psb.6.11.17014.

Das, K. and Roychoudhury, A. (2014) 'Reactive oxygen species (ROS) and response of antioxidants as ROS-scavengers during environmental stress in plants', *Frontiers in Environmental Science*, 2(December), p. 53 (1–13). doi: 10.3389/fenvs.2014.00053.

Davies, J. (2014) 'Annexin-Mediated Calcium Signalling in Plants', *Plants*, 3(1), pp. 128–140. doi: 10.3390/plants3010128.

Defalco, T. A., Toyota, M., Phan, V., Karia, P., Moeder, W., Gilroy, S. and Yoshioka, K. (2017) 'Using GCaMP3 to Study Ca^{2+} Signaling in Nicotiana Species', *Plant and Cell Physiology*, 58(7), pp. 1173–1184. doi: 10.1093/pcp/pcx053.

Demidchik, V. (2015) 'Mechanisms of oxidative stress in plants: From classical chemistry to cell biology', *Environmental and Experimental Botany*. Elsevier B.V., 109, pp. 212–228. doi: 10.1016/j.envexpbot.2014.06.021.

Demidchik, V., Bowen, H. C., Maathuis, F. J. M., Shabala, S. N., Tester, M. A., White, P. J. and Davies, J. M. (2002) '*Arabidopsis thaliana* root non-selective cation channels mediate calcium uptake and are involved in growth', *Plant Journal*, 32(5), pp. 799–808. doi: 10.1046/j.1365-313X.2002.01467.x.

Demidchik, V., Nichols, C., Oliynyk, M., Dark, A., Glover, B. J. and Davies, J. M. (2003a) 'Is ATP a Signaling Agent in Plants?', *Plant Physiology*, 133(2), pp. 456–461. doi: 10.1104/pp.103.024091.

Demidchik, V., Shabala, S. N., Coutts, K. B., Tester, M. A. and Davies, J. M. (2003b) 'Free oxygen radicals regulate plasma membrane Ca^{2+}- and K^{+}-permeable channels in plant root cells.', *Journal of cell science*, 116(Pt 1), pp. 81–88. doi: 10.1242/jcs.00201.

Demidchik, V., Shang, Z., Shin, R., Colaço, R., Laohavisit, A., Shabala, S. and Davies, J. M. (2011) 'Receptor-like activity evoked by extracellular ADP in Arabidopsis root epidermal plasma membrane', *Plant Physiology*, 156(3), pp. 1375–1385. doi: 10.1104/pp.111.174722.

Demidchik, V., Shang, Z., Shin, R., Thompson, E., Rubio, L., Laohavisit, A., Mortimer, J. C., Chivasa, S., Slabas, A. R., Glover, B. J., Schachtman, D. P., Shabala, S. N. and Davies, J. M. (2009) 'Plant extracellular ATP signalling by plasma membrane NADPH oxidase and Ca^{2+} channels', *Plant Journal*, 58(6), pp. 903–913. doi: 10.1111/j.1365-313X.2009.03830.x.

Demidchik, V. and Tester, M. (2002) 'Sodium fluxes through nonselective cation channels in the plasma membrane of protoplasts from Arabidopsis roots.', *Plant physiology*, 128(2), pp. 379–387. doi: 10.1104/pp.010524.

Deng, K., Wang, Q., Zeng, J., Guo, X., Zhao, X., Tang, D. and Liu, X. (2009) 'A lectin receptor kinase positively regulates ABA response during seed germination and is involved in salt and osmotic stress response', *Journal of Plant Biology*, 52(6), pp. 493–500. doi: 10.1007/s12374-009-9063-5.

Deng, S., Sun, J., Zhao, R., Ding, M., Zhang, Y., Sun, Y., Wang, W., Tan, Y., Liu, D., Ma, X., Hou, P., Wang, M., Lu, C., Shen, X. and Chen, S. (2015) '*Populus euphratica* APYRASE2 enhances cold tolerance by modulating vesicular trafficking and extracellular ATP in arabidopsis plants', *Plant Physiology*, 169(1), pp. 530–548. doi: 10.1104/pp.15.00581.

Dennison, K. L. and Spalding, E. P. (2000) 'Glutamate-gated calcium fluxes in Arabidopsis', *Plant Physiology*, 124(4), pp. 1511–1514. doi: 10.1104/pp.124.4.1511.

Dietrich, P., Anschütz, U., Kugler, A. and Becker, D. (2010) 'Physiology and biophysics of plant ligand-gated ion channels', *Plant Biology*, 12(SUPPL. 1), pp. 80–93. doi: 10.1111/j.1438-8677.2010.00362.x.

Dodd, A. N., Kudla, J. and Sanders, D. (2010) 'The Language of Calcium Signaling', *Annual Review of Plant Biology*, 61(1), pp. 593–620. doi: 10.1146/annurev-arplant-070109-104628.

Van der Does, D., Boutrot, F., Engelsdorf, T., Rhodes, J., McKenna, J. F., Vernhettes, S., Koevoets, I., Tintor, N., Veerabagu, M., Miedes, E., Segonzac, C., Roux, M., Breda, A. S., Hardtke, C. S., Molina, A., Rep, M., Testerink, C., Mouille, G., Höfte, H., Hamann, T. and Zipfel, C. (2017) 'The Arabidopsis leucine-rich repeat receptor kinase MIK2/LRR-KISS connects cell wall integrity sensing, root growth and response to abiotic and biotic stresses', *PLoS Genetics*, 13(6), pp. 1–27. doi: 10.1371/journal.pgen.1006832.

Doherty, C. J., Van Buskirk, H. A., Myers, S. J. and Thomashow, M. F. (2009) 'Roles for Arabidopsis CAMTA transcription factors in cold-regulated gene expression and freezing tolerance.', *The Plant cell*, 21(3), pp. 972–84. doi: 10.1105/tpc.108.063958.

Dolan, L. and Davies, J. (2004) 'Cell expansion in roots', *Current Opinion in Plant Biology*, 7(1), pp. 33–39. doi: 10.1016/j.pbi.2003.11.006.

Drązkiewicz, M., Skórzyńska-Polit, E. and Krupa, Z. (2004) 'Copper-induced oxidative stress and antioxidant defence in *Arabidopsis thaliana*', *BioMetals*, 17(4), pp. 379–387. doi: 10.1023/B:BIOM.0000029417.18154.22.

Duan, L., Dietrich, D., Ng, C. H., Yeen Chan, P. M., Bhalerao, R., Bennett, M. J. and Dinneny, J. R. (2013) 'Endodermal ABA signaling promotes lateral root quiescence during salt stress in Arabidopsis seedlings', *Plant Cell*, 25(1), pp. 324–341. doi: 10.1105/tpc.112.107227.

Dubouzet, J. G., Sakuma, Y., Ito, Y., Kasuga, M., Dubouzet, E. G., Miura, S., Seki, M., Shinozaki, K. and Yamaguchi-Shinozaki, K. (2003) 'OsDREB genes in rice, *Oryza sativa L.*, encode transcription activators that function in drought-, high-salt- and cold-responsive gene expression', *Plant Journal*, 33(4), pp. 751–763. doi: 10.1046/j.1365-313X.2003.01661.x.

Dunand, C., Crèvecoeur, M. and Penel, C. (2007) 'Distribution of superoxide and hydrogen peroxide in Arabidopsis root and their influence on root development: Possible interaction with peroxidases', *New Phytologist*, 174(2), pp. 332–341. doi: 10.1111/j.1469-8137.2007.01995.x.

Dutta, A. K., Okada, Y. and Sabirov, R. Z. (2002) 'Regulation of an ATP-conductive large-conductance anion channel and swelling-induced ATP release by arachidonic acid.', *The Journal of physiology*, 542(Pt 3), pp. 803–816. doi: 10.1113/jphysiol.2002.019802.

Edel, K. H., Marchadier, E., Brownlee, C., Kudla, J. and Hetherington, A. M. (2017) 'The Evolution of Calcium-Based Signalling in Plants', *Current Biology*, 27(13), pp. R667–R679. doi: 10.1016/j.cub.2017.05.020.

Ermakov, Y. A., Kamaraju, K., Sengupta, K. and Sukharev, S. (2010) 'Gadolinium ions block mechanosensitive channels by altering the packing and lateral pressure of anionic lipids', *Biophysical Journal*. Biophysical Society, 98(6), pp. 1018–1027. doi: 10.1016/j.bpj.2009.11.044.

Ettinger, W. F., Clear, A. M., Fanning, K. J. and Peck, M. Lou (1999) 'Identification of a Ca^{2+}/H^{+} antiport in the plant chloroplast thylakoid membrane', *Plant Physiology*, 119(4), pp. 1379–1385.

Evans, M. J., Choi, W. G., Gilroy, S. and Morris, R. J. (2016) 'A ROS-assisted calcium wave

dependent on the AtRBOHD NADPH oxidase and TPC1 cation channel propagates the systemic response to salt stress', *Plant Physiology*, 171(3), pp. 1771–1784. doi: 10.1104/pp.16.00215.

Evans, N. H., McAinsh, M. R., Hetherington, A. M. and Knight, M. R. (2005) 'ROS perception in Arabidopsis thaliana: The ozone-induced calcium response', *Plant Journal*, 41(4), pp. 615–626. doi: 10.1111/j.1365-313X.2004.02325.x.

Faoland and Water. (2008) 'Drought: a slow, creeping natural disaster', www.fao.org/nr/aboutnr/nrl

Finka, A., Cuendet, A. F. H., Maathuis, F. J. M., Saidi, Y. and Goloubinoff, P. (2012) 'Plasma membrane cyclic nucleotide gated calcium channels control land plant thermal sensing and acquired thermotolerance', *Plant Cell*, 24(8), pp. 3333–3348. doi: 10.1105/tpc.112.095844.

Finkemeier, I., Goodman, M., Lamkemeyer, P., Kandlbinder, A., Sweetlove, L. J. and Dietz, K. J. (2005) 'The mitochondrial type II peroxiredoxin F is essential for redox homeostasis and root growth of *Arabidopsis thaliana* under stress', *Journal of Biological Chemistry*, 280(13), pp. 12168–12180. doi: 10.1074/jbc.M413189200.

Fischer, B. B., Krieger-Liszkay, A., Hideg, É., Šnyrychová, I., Wiesendanger, M. and Eggen, R. I. L. (2007) 'Role of singlet oxygen in chloroplast to nucleus retrograde signaling in *Chlamydomonas reinhardtii*', *FEBS Letters*, 581(29), pp. 5555–5560. doi: 10.1016/j.febslet.2007.11.003.

Fischer, C., Kugler, A., Hoth, S. and Dietrich, P. (2013) 'An IQ domain mediates the interaction with calmodulin in a plant cyclic nucleotide-gated channel', *Plant and Cell Physiology*, 54(4), pp. 573–584. doi: 10.1093/pcp/pct021.

Foreman, J., Demidchik, V., Bothwell, J. H. F., Mylona, P., Miedema, H., Torres, M. A., Linstead, P., Costa, S., Brownlee, C., Jones, J. D. G., Davies, J. M. and Dolan, L. (2003) 'Reactive oxygen species produced by NADPH oxidase regulate plant cell growth.', *Nature*, 422(6930), pp. 442–6. doi: 10.1038/nature01485.

Foresi, N. P., Laxalt, A. M., Tonón, C. V., Casalongué, C. A. and Lamattina, L. (2007) 'Extracellular ATP induces nitric oxide production in tomato cell suspensions', *Plant Physiology*, 145(3), pp. 589–592. doi: 10.1104/pp.107.106518.

Forzani, C., Duarte, G. T., Van Leene, J., Clément, G., Huguet, S., Paysant-Le-Roux, C., Mercier, R., De Jaeger, G., Leprince, A. S. and Meyer, C. (2019) 'Mutations of the AtYAK1 Kinase Suppress TOR Deficiency in Arabidopsis', *Cell Reports*, 27(12), pp. 3696–3708.e5. doi:

10.1016/j.celrep.2019.05.074.

Foster, A. J., Ryder, L. S., Kershaw, M. J. and Talbot, N. J. (2017) 'The role of glycerol in the pathogenic lifestyle of the rice blast fungus *Magnaporthe oryzae*', *Environmental Microbiology*, 19(3), pp. 1008–1016. doi: 10.1111/1462-2920.13688.

Fountain, S. J., Cao, L., Young, M. T. and North, R. A. (2008) 'Permeation properties of a P2X receptor in the green algae *Ostreococcus tauri*', *Journal of Biological Chemistry*, 283(22), pp. 15122–15126. doi: 10.1074/jbc.M801512200.

Frank, J., Happeck, R., Meier, B., Hoang, M. T. T., Stribny, J., Hause, G., Ding, H., Morsomme, P., Baginsky, S. and Peiter, E. (2019) 'Chloroplast-localized BICAT proteins shape stromal calcium signals and are required for efficient photosynthesis', *New Phytologist*, 221(2), pp. 866–880. doi: 10.1111/nph.15407.

Frei Dit Frey, N., Mbengue, M., Kwaaitaal, M., Nitsch, L., Altenbach, D., Haweker, H., Lonzano-Duran, R., Njo, M. F., Beeckman, T., Huettel, B., Borst, J. W., Panstruga, R. and Robatzek, S. (2012) 'Plasma membrane calcium ATPases are important components of receptor-mediated signalling in plant immune responses and development', *Plant Physiology*, 159(2), pp. 798–809. doi: 10.1104/pp.111.192575.

Frietsch, S., Wang, Y.-F. F., Sladek, C., Poulsen, L. R., Romanowsky, S. M., Schroeder, J. I. and Harper, J. F. (2007) 'A cyclic nucleotide-gated channel is essential for polarized tip growth of pollen', *Proceedings of the National Academy of Sciences of the United States of America*, 104(36), pp. 14531–14536. doi: 0701781104 [pii].

Fu, Y., Yang, Y., Chen, S., Ning, N. and Hu, H. (2019) 'Arabidopsis IAR4 modulates primary root growth under salt stress through ros-mediated modulation of auxin distribution', *Frontiers in Plant Science*, 10(April). doi: 10.3389/fpls.2019.00522.

Furuichi, T., Mori, I. C., Takahashi, K. and Muto, S. (2001) 'Sugar-induced increase in cytosolic Ca($^{2+}$) in *Arabidopsis thaliana* whole plants.', *Plant & cell physiology*, 42(10), pp. 1149–1155.

Gao, F., Han, X., Wu, J., Zheng, S., Shang, Z., Sun, D., Zhou, R. and Li, B. (2012) 'A heat-activated calcium-permeable channel - Arabidopsis cyclic nucleotide-gated ion channel 6 - Is involved in heat shock responses', *Plant Journal*, 70(6), pp. 1056–1069. doi: 10.1111/j.1365-313X.2012.04969.x.

Gao, X., Chen, X., Lin, W., Chen, S., Lu, D., Niu, Y., Li, L., Cheng, C., McCormack, M.,

Sheen, J., Shan, L. and He, P. (2013) 'Bifurcation of Arabidopsis NLR Immune Signaling via Ca^{2+}-Dependent Protein Kinases', *PLoS Pathogens*, 9(1). doi: 10.1371/journal.ppat.1003127.

García-Mata, C. and Lamattina, L. (2013) 'Gasotransmitters are emerging as new guard cell signaling molecules and regulators of leaf gas exchange', *Plant Science*. Elsevier Ireland Ltd, 201-202(1), pp. 66–73. doi: 10.1016/j.plantsci.2012.11.007.

Gardner, P. R. (2002) 'Aconitase: Sensitive target and measure of superoxide', *Methods in Enzymology*, 349(1991), pp. 9–23. doi: 10.1016/S0076-6879(02)49317-2.

Geng, Y., Wu, R., Wee, C. W., Xie, F., Wei, X., Chan, P. M. Y., Tham, C., Duan, L. and Dinneny, J. R. (2013) 'A spatio-temporal understanding of growth regulation during the salt stress response in Arabidopsis', *Plant Cell*, 25(6), pp. 2132–2154. doi: 10.1105/tpc.113.112896.

Gilroy, S., Suzuki, N., Miller, G., Choi, W. G., Toyota, M., Devireddy, A. R. and Mittler, R. (2014) 'A tidal wave of signals: Calcium and ROS at the forefront of rapid systemic signaling', *Trends in Plant Science*. Elsevier Ltd, 19(10), pp. 623–630. doi: 10.1016/j.tplants.2014.06.013.

Gobert, A., Park, G., Amtmann, A., Sanders, D. and Maathuis, F. J. M. (2006) '*Arabidopsis thaliana* Cyclic Nucleotide Gated Channel 3 forms a non-selective ion transporter involved in germination and cation transport', *Journal of Experimental Botany*, 57(4), pp. 791–800. doi: 10.1093/jxb/erj064.

Godfray, H. C. J., Beddington, J. R., Crute, I. R., Haddad, L., Lawrence, D., Muir, J. F., Pretty, J., Robinson, S., Thomas, S. M. and Toulmin, C. (2010) 'Food security: The challenge of feeding 9 billion people', *Science*, pp. 812–818. doi: 10.1126/science.1185383.

Gómez-Gómez, L. and Boller, T. (2000) 'FLS2: An LRR receptor-like kinase involved in the perception of the bacterial elicitor flagellin in Arabidopsis', *Molecular Cell*, 5(6), pp. 1003–1011.

Gómez-Gómez, L., Felix, G. and Boller, T. (1999) 'A single locus determines sensitivity to bacterial flagellin in *Arabidopsis thaliana*', *Plant Journal*, 18(3), pp. 277–284. doi: 10.1046/j.1365-313X.1999.00451.x.

Gorecka, K. M., Konopka-Postupolska, D., Hennig, J., Buchet, R. and Pikula, S. (2005) 'Peroxidase activity of annexin 1 from *Arabidopsis thaliana*', *Biochemical and Biophysical Research Communications*, 336(3), pp. 868–875. doi: 10.1016/j.bbrc.2005.08.181.

Gout, E., Bligny, R. and Douce, R. (1992) 'Regulation of intracellular pH values in higher plant cells.', *The Journal of Biological Chemistry*, 267(20), pp. 13903–13909. doi: 10.1111/j.1600-0587.2010.06669.x.

Gout, E., Rébeillé, F., Douce, R. and Bligny, R. (2014) 'Interplay of Mg^{2+}, ADP, and ATP in the cytosol and mitochondria: Unravelling the role of Mg^{2+} in cell respiration', *Proceedings of the National Academy of Sciences of the United States of America*, 111(43), pp. E4560–E4567. doi: 10.1073/pnas.1406251111.

Grabov, a, Ashley, M. K., Rigas, S., Hatzopoulos, P., Dolan, L. and Vicente-Agullo, F. (2005) 'Morphometric analysis of root shape.', *The New phytologist*, 165(2), pp. 641–651. doi: 10.1111/j.1469-8137.2004.01258.x.

Halliwell, B. (2006) 'Reactive Species and Antioxidants. Redox Biology Is a Fundamental Theme of Aerobic Life', *Plant Physiology*, 141(2), pp. 312–322. doi: 10.1104/pp.106.077073.

Hamill, O. P. and Mcbride, D. W. (1996) 'The pharmacology of mechanogated membrane ion channels', *Pharmacological Reviews*, 48(2), pp. 231–252.

Han, L., Li, G. J., Yang, K. Y., Mao, G., Wang, R., Liu, Y. and Zhang, S. (2010) 'Mitogen-activated protein kinase 3 and 6 regulate *Botrytis cinerea*-induced ethylene production in Arabidopsis', *Plant Journal*, 64(1), pp. 114–127. doi: 10.1111/j.1365-313X.2010.04318.x.

Harper, J. F., Hong, B., Hwang, I., Guo, H. Q., Stoddard, R., Huang, J. F., Palmgren, M. G. and Sze, H. (1998) 'A novel calmodulin-regulated Ca^{2+}-ATPase (ACA2) from Arabidopsis with an N-terminal autoinhibitory domain', *Journal of Biological Chemistry*, 273(2), pp. 1099–1106. doi: 10.1074/jbc.273.2.1099.

Hartung, W. (1983) 'The site of action of abscisic acid at the guard cell plasmalemma of *Valerianella locusta*', *Plant, Cell & Environment*, 6(5), pp. 427–428. doi: 10.1111/j.1365-3040.1983.tb01276.x.

Hocking, B., Conn, S. J., Manohar, M., Xu, B., Athman, A., Stancombe, M. A., Webb, A. R., Hirschi, K. D. and Gilliham, M. (2017) 'Heterodimerization of Arabidopsis calcium/proton exchangers contributes to regulation of guard cell dynamics and plant defense responses', *Journal of Experimental Botany*, 68(15), pp. 4171–4183. doi: 10.1093/jxb/erx209.

Hofmann A. (2004) Annexins in the plant kingdom: perspectives and potentials. *Annexins* 1:51–61

Hofmann, A., Ruvinov, S., Hess, S., Schantz, R., Delmer, D. P. and Wlodawer, A. (2002) 'Plant annexins form calcium-independent oligomers in solution', *Protein Science*, 11(8), pp. 2033–2040. doi: 10.1110/ps.4770102.

Höglund, A., Dönnes, P., Blum, T., Adolph, H. W. and Kohlbacher, O. (2006) 'MultiLoc:

Prediction of protein subcellular localization using N-terminal targeting sequences, sequence motifs and amino acid composition', *Bioinformatics*, 22(10), pp. 1158–1165. doi: 10.1093/bioinformatics/btl002.

Hooper, C. M., Stevens, T. J., Saukkonen, A., Castleden, I. R., Singh, P., Mann, G. W., Fabre, B., Ito, J., Deery, M. J., Lilley, K. S., Petzold, C. J., Millar, A. H., Heazlewood, J. L. and Parsons, H. T. (2017) 'Multiple marker abundance profiling: combining selected reaction monitoring and data-dependent acquisition for rapid estimation of organelle abundance in subcellular samples', *Plant Journal*, 92(6), pp. 1202–1217. doi: 10.1111/tpj.13743.

Hoyle, C. H. V., Knight, G. E. and Burnstock, G. (1990) 'Suramin antagonizes responses to P2-purinoceptor agonists and purinergic nerve stimulation in the guinea-pig urinary bladder and *taenia coli*', *British Journal of Pharmacology*, 99(3), pp. 617–621. doi: 10.1111/j.1476-5381.1990.tb12979.x.

Hu, C. D., Chinenov, Y. and Kerppola, T. K. (2002) 'Visualization of interactions among bZIP and Rel family proteins in living cells using bimolecular fluorescence complementation', *Molecular Cell*, 9(4), pp. 789–798. doi: 10.1016/S1097-2765(02)00496-3.

Hu, H., You, J., Fang, Y., Zhu, X., Qi, Z. and Xiong, L. (2008) 'Characterization of transcription factor gene SNAC2 conferring cold and salt tolerance in rice', *Plant Molecular Biology*, 67(1-2), pp. 169–181. doi: 10.1007/s11103-008-9309-5.

Hu, X., Jiang, M., Zhang, J., Zhang, A., Lin, F. and Tan, M. (2007) 'Calcium-calmodulin is required for abscisic acid-induced antioxidant defense and functions both upstream and downstream of H_2O_2 production in leaves of maize (*Zea mays*) plants', *New Phytologist*, 173(1), pp. 27–38. doi: 10.1111/j.1469-8137.2006.01888.x.

Huang, L., Berkelman, T., Franklin, A. E. and Hoffman, N. E. (1993) 'Characterization of a gene encoding a Ca^{2+}-ATPase-like protein in the plastid envelope', *Proceedings of the National Academy of Sciences of the United States of America*, 90(21), pp. 10066–10070. doi: 10.1073/pnas.90.21.10066.

Huang, W. Y., Wu, Y. C., Pu, H. Y., Wang, Y., Jang, G. J. and Wu, S. H. (2017) 'Plant dual-specificity tyrosine phosphorylation-regulated kinase optimizes light-regulated growth and development in Arabidopsis', *Plant Cell and Environment*, 40(9), pp. 1735–1747. doi: 10.1111/pce.12977.

Huang, X. S., Liu, J. H. and Chen, X. J. (2010) 'Overexpression of PtrABF gene, a bZIP transcription factor isolated from Poncirus trifoliata, enhances dehydration and drought tolerance

in tobacco via scavenging ROS and modulating expression of stress-responsive genes', *BMC Plant Biology*. BioMed Central Ltd, 10(1), p. 230. doi: 10.1186/1471-2229-10-230.

Huang, Y., Wang, J., Zhang, L. and Zuo, K. (2013) 'A Cotton Annexin Protein AnxGb6 Regulates Fiber Elongation through Its Interaction with Actin 1', *PLoS ONE*, 8(6), pp. 1–14. doi: 10.1371/journal.pone.0066160.

Huh, S. M., Noh, E. K., Kim, H. G., Jeon, B. W., Bae, K., Hu, H. C., Kwak, J. M. and Park, O. K. (2010) 'Arabidopsis annexins AnnAt1 and AnnAt4 interact with each other and regulate drought and salt stress responses', *Plant and Cell Physiology*, 51(9), pp. 1499–1514. doi: 10.1093/pcp/pcq111.

Hyodo, K., Suzuki, N., Mise, K. and Okuno, T. (2017) 'Roles of superoxide anion and hydrogen peroxide during replication of two unrelated plant RNA viruses in *Nicotiana benthamiana*', *Plant Signaling and Behavior*. Taylor & Francis, 12(6), pp. 1–4. doi: 10.1080/15592324.2017.1338223.

Ito, J., Heazlewood, J. L. and Millar, A. H. (2006) 'Analysis of the soluble ATP-binding proteome of plant mitochondria identifies new proteins and nucleotide triphosphate interactions within the matrix', *Journal of Proteome Research*, 5(12), pp. 3459–3469. doi: 10.1021/pr060403j.

Jacobson, K. A., Jarvis, M. F. and Williams, M. (2002) 'Purine and pyrimidine (P2) receptors as drug targets', *Journal of Medicinal Chemistry*, 45(19), pp. 4057–4093. doi: 10.1021/jm020046y.

Jami, S. K., Clark, G. B., Ayele, B. T., Roux, S. J. and Kirti, P. B. (2012) 'Identification and characterization of annexin gene family in rice', *Plant Cell Reports*, 31(5), pp. 813–825. doi: 10.1007/s00299-011-1201-0.

Jeon, B. W., Acharya, B. R. and Assmann, S. M. (2019) 'The Arabidopsis heterotrimeric G-protein β subunit, AGB1, is required for guard cell calcium sensing and calcium-induced calcium release', *Plant Journal*, 99(2), pp. 231–244. doi: 10.1111/tpj.14318.

Jeter, C. R. and Roux, S. J. (2006) 'Plant responses to extracellular nucleotides: Cellular processes and biological effects', *Purinergic Signalling*, 2(3), pp. 443–449. doi: 10.1007/s11302-005-3981-6.

Jeter, C. R., Tang, W., Henaff, E., Butterfield, T. and Roux, S. J. (2004) 'Evidence of a novel cell signaling role for extracellular adenosine triphosphates and diphosphates in Arabidopsis',

Plant Cell, 16(10), pp. 2652–2664. doi: 10.1105/tpc.104.023945.

Jewell, J. B., Sowders, J. M., He, R., Willis, M. A., Gang, D. R. and Tanaka, K. (2019) 'Extracellular ATP shapes a defense-related transcriptome both independently and along with other defense signaling pathways', *Plant Physiology*, 179(3), pp. 1144–1158. doi: 10.1104/pp.18.01301.

Jeworutzki, E., Roelfsema, M. R. G., Anschütz, U., Krol, E., Elzenga, J. T. M., Felix, G., Boller, T., Hedrich, R. and Becker, D. (2010) 'Early signaling through the arabidopsis pattern recognition receptors FLS2 and EFR involves Ca^{2+}-associated opening of plasma membrane anion channels', *Plant Journal*, 62(3), pp. 367–378. doi: 10.1111/j.1365-313X.2010.04155.x.

Jia, L. Y., Bai, J. Y., Sun, K., Wang, R. fang and Feng, H. Q. (2019) 'Extracellular ATP released by copper stress could act as diffusible signal in alleviating the copper stress-induced cell death', *Protoplasma*. Protoplasma, 256(2), pp. 491–501. doi: 10.1007/s00709-018-1309-y.

Jiang, Y. and Deyholos, M. K. (2009) 'Functional characterization of Arabidopsis NaCl-inducible WRKY25 and WRKY33 transcription factors in abiotic stresses', *Plant Molecular Biology*, 69(1-2), pp. 91–105. doi: 10.1007/s11103-008-9408-3.

Jiang, Z., Zhou, X., Tao, M., Yuan, F., Liu, L., Wu, F., Wu, X., Xiang, Y., Niu, Y., Liu, F., Li, C., Ye, R., Byeon, B., Xue, Y., Zhao, H., Wang, H.-N., Crawford, B. M., Johnson, D. M., Hu, C., Pei, C., Zhou, W., Swift, G. B., Zhang, H., Vo-Dinh, T., Hu, Z., Siedow, J. N. and Pei, Z.-M. (2019) 'Plant cell-surface GIPC sphingolipids sense salt to trigger Ca^{2+} influx', *Nature*. Springer US, 572(7769), pp. 341–346. doi: 10.1038/s41586-019-1449-z.

Jiang, Z., Zhu, S., Ye, R., Xue, Y., Chen, A., An, L. and Pei, Z. M. (2013) 'Relationship between NaCl- and H_2O_2-Induced Cytosolic Ca^{2+} Increases in Response to Stress in Arabidopsis', *PLoS ONE*, 8(10), pp. 1–10. doi: 10.1371/journal.pone.0076130.

Kamiyoshihara, Y., Iwata, M., Fukaya, T., Tatsuki, M. and Mori, H. (2010) 'Turnover of LeACS2, a wound-inducible 1-aminocyclopropane-1-carboxylic acid synthase in tomato, is regulated by phosphorylation/dephosphorylation', *Plant Journal*, 64(1), pp. 140–150. doi: 10.1111/j.1365-313X.2010.04316.x.

Kasai, M. and Muto, S. (1990) 'Ca^{2+} pump and Ca^{2+}/H^{+} antiporter in plasma membrane vesicles isolated by aqueous two-phase partitioning from corn leaves', *The Journal of Membrane Biology*, 114(2), pp. 133–142. doi: 10.1007/BF01869094.

Kiep, V., Vadassery, J., Lattke, J., Maaß, J. P., Boland, W., Peiter, E. and Mithöfer, A.

(2015) ‘Systemic cytosolic Ca^{2+} elevation is activated upon wounding and herbivory in Arabidopsis’, *New Phytologist*, 207(4), pp. 996–1004. doi: 10.1111/nph.13493.

Kim, D., Ntui, V. O. and Xiong, L. (2016) ‘Arabidopsis YAK1 regulates abscisic acid response and drought resistance’, *FEBS Letters*, 590, pp. 2201–2209. doi: 10.1002/1873-3468.12234.

Kim, D., Ntui, V. O., Zhang, N. and Xiong, L. (2015) ‘Arabidopsis Yak1 protein (AtYak1) is a dual specificity protein kinase’, *FEBS Letters*. Federation of European Biochemical Societies, 589(21), pp. 3321–3327. doi: 10.1016/j.febslet.2015.09.025.

Kim, J. and Kim, H.-Y. (2006) ‘Functional analysis of a calcium-binding transcription factor involved in plant salt stress signaling.’, *FEBS letters*, 580, pp. 5251–5256. doi: 10.1016/j.febslet.2006.08.050.

Kim, M. C., Chung, W. S., Yun, D.-J. and Cho, M. J. (2009) ‘Calcium and calmodulin-mediated regulation of gene expression in plants.’, *Molecular plant*, 2(1), pp. 13–21. doi: 10.1093/mp/ssn091.

Kim, S. A., Kwak, J. M., Jae, S. K., Wang, M. H. and Nam, H. G. (2001) ‘Overexpression of the AtGluR2 gene encoding an Arabidopsis homolog of mammalian glutamate receptors impairs calcium utilization and sensitivity to ionic stress in transgenic plants’, *Plant and Cell Physiology*, 42(1), pp. 74–84. doi: 10.1093/pcp/pce008.

Kim, S. Y., Sivaguru, M. and Stacey, G. (2006) ‘Extracellular ATP in plants. Visualization, localization, and analysis of physiological significance in growth and signaling’, *Plant Physiology*, 142(3), pp. 984–992. doi: 10.1104/pp.106.085670.

Knight, H., Trewavas, a J. and Knight, M. R. (1997) ‘Calcium signalling in Arabidopsis thaliana responding to drought and salinity’, *The Plant journal : for cell and molecular biology*, 12(5), pp. 1067–1078. doi: 10.1046/j.1365-313X.1997.12051067.x.

Knight, M. R., Smith, S. M. and Trewavas, a J. (1992) ‘Wind-induced plant motion immediately increases cytosolic calcium’, *Proceedings of the National Academy of Sciences of the United States of America*, 89(11), pp. 4967–4971. doi: 10.1073/pnas.89.11.4967.

Konopka-Postupolska, D., Clark, G., Goch, G., Debski, J., Floras, K., Cantero, A., Fijolek, B., Roux, S. and Hennig, J. (2009) ‘The role of annexin 1 in drought stress in Arabidopsis.’, *Plant physiology*, 150(3), pp. 1394–410. doi: 10.1104/pp.109.135228.

Kosová, K., Prášil, I. and Vítámvás, P. (2013) ‘Protein Contribution to Plant Salinity Response and Tolerance Acquisition’, *International Journal of Molecular Sciences*, 14(4), pp. 6757–6789.

doi: 10.3390/ijms14046757.

Kovács, I., Ayaydin, F., Oberschall, A., Ipacs, L., Bottka, S., Pongor, S., Dudits, D. and Tóth, É. C. (1998) 'Immunolocalization of a novel annexin-like protein encoded by a stress and abscisic acid responsive gene in alfalfa', *Plant Journal*, 15(2), pp. 185–197. doi: 10.1046/j.1365-313X.1998.00194.x.

Kovtun, Y., Chiu, W. L., Tena, G. and Sheen, J. (2000) 'Functional analysis of oxidative stress-activated mitogen-activated protein kinase cascade in plants', *Proceedings of the National Academy of Sciences of the United States of America*, 97(6), pp. 2940–2945. doi: 10.1073/pnas.97.6.2940.

Krebs, M., Held, K., Binder, A., Hashimoto, K., Den Herder, G., Parniske, M., Kudla, J. and Schumacher, K. (2012) 'FRET-based genetically encoded sensors allow high-resolution live cell imaging of Ca^{2+} dynamics', *Plant Journal*, 69(1), pp. 181–192. doi: 10.1111/j.1365-313X.2011.04780.x.

De Kreij, C., Janse, J., Van Goor, B. J. and Van Doesburg, J. D. J. (1992) 'The incidence of calcium oxalate crystals in fruit walls of tomato (*Lycopersicon esculentum Mill.*) as affected by humidity, phosphate and calcium supply', *Journal of Horticultural Science*. Taylor & Francis, 67(1), pp. 45–50. doi: 10.1080/00221589.1992.11516219.

Krieger-Liszkay, A., Fufezan, C. and Trebst, A. (2008) 'Singlet oxygen production in photosystem II and related protection mechanism', *Photosynthesis Research*, 98(1-3), pp. 551–564. doi: 10.1007/s11120-008-9349-3.

Krieger-Liszkay, A. and Trebst, A. (2006) 'Tocopherol is the scavenger of singlet oxygen produced by the triplet states of chlorophyll in the PSII reaction centre', *Journal of Experimental Botany*, 57(8), pp. 1677–1684. doi: 10.1093/jxb/erl002.

Kukavica, B., Mojović, M., Vučinić, Ž., Maksimović, V., Takahama, U. and Jovanović, S. V. (2009) 'Generation of hydroxyl radical in isolated pea root cell wall, and the role of cell wall-bound peroxidase, Mn-SOD and phenolics in their production', *Plant and Cell Physiology*, 50(2), pp. 304–317. doi: 10.1093/pcp/pcn199.

Kumar, J., Singh, S., Singh, M., Srivastava, P. K., Mishra, R. K., Singh, V. P. and Prasad, S. M. (2017) 'Transcriptional regulation of salinity stress in plants: A short review', *Plant Gene*. Elsevier, 11(April), pp. 160–169. doi: 10.1016/j.plgene.2017.04.001.

Kwaaitaal, M., Huisman, R., Maintz, J., Reinstaẗler, A. and Panstruga, R. (2011)

'Ionotropic glutamate receptor (iGluR)-like channels mediate MAMP-induced calcium influx in *Arabidopsis thaliana*', *Biochemical Journal*, 440(3), pp. 355–365. doi: 10.1042/BJ20111112.

Kwak, J. M., Mori, I. C., Pei, Z. M., Leonhard, N., Angel Torres, M., Dangl, J. L., Bloom, R. E., Bodde, S., Jones, J. D. G. and Schroeder, J. I. (2003) 'NADPH oxidase AtrbohD and AtrbohF genes function in ROS-dependent ABA signaling in arabidopsis', *EMBO Journal*, 22(11), pp. 2623–2633. doi: 10.1093/emboj/cdg277.

Kwon, H. K., Yokoyama, R. and Nishitani, K. (2005) 'A proteomic approach to apoplastic proteins involved in cell wall regeneration in protoplasts of Arabidopsis suspension-cultured cells', *Plant and Cell Physiology*, 46(6), pp. 843–857. doi: 10.1093/pcp/pci089.

Laloi, C., Apel, K. and Danon, A. (2004) 'Reactive oxygen signalling: The latest news', *Current Opinion in Plant Biology*, 7(3), pp. 323–328. doi: 10.1016/j.pbi.2004.03.005.

Lam, H.-M., Chiu, J., Hsieh, M.-H., Meisel, L., Oliveira, I. C., Shin, M. and Coruzzi, G. (1998) 'Glutamate-receptor genes in plants.', *Nature*, 396(6707), pp. 125–126. doi: 10.1038/24066.

Laohavisit, A., Brown, A. T., Cicuta, P. and Davies, J. M. (2010) 'Annexins: Components of the Calcium and Reactive Oxygen Signaling Network', *Plant Physiology*, 152(4), pp. 1824–1829. doi: 10.1104/pp.109.145458.

Laohavisit, A. and Davies, J. M. (2011) 'Annexins', *New Phytol*, 189(1), pp. 40–53. doi: 10.1111/j.1469-8137.2010.03533.x.

Laohavisit, A., Mortimer, J. C., Demidchik, V., Coxon, K. M., Stancombe, M. A., Macpherson, N., Brownlee, C., Hofmann, A., Webb, A. A. R., Miedema, H., Battey, N. H. and Davies, J. M. (2009) '*Zea mays* Annexins Modulate Cytosolic Free Ca^{2+} and Generate a Ca^{2+}-Permeable Conductance', *Plant signaling & behavior*, 21(5), pp. 479–493. doi: 10.1105/tpc.108.059550.

Laohavisit, A., Richards, S. L., Shabala, L., Chen, C., Colaco, R. D. D. R., Swarbreck, S. M., Shaw, E., Dark, A., Shabala, S., Shang, Z. and Davies, J. M. (2013) 'Salinity-Induced Calcium Signaling and Root Adaptation in Arabidopsis Require the Calcium Regulatory Protein Annexin1', *Plant Physiology*, 163(1), pp. 253–262. doi: 10.1104/pp.113.217810.

Larkindale, J. and Knight, M. (2002) 'Protection against heat stress-induced oxidative damage in Arabidopsis involves calcium, abscisic acid, ethylene, and salicylic acid', *Plant physiology*, 128(2), pp. 682–695. doi: 10.1104/pp.010320.682.

Laxa, M., Liebthal, M., Telman, W., Chibani, K. and Dietz, K.-J. (2019) 'The Role of the Plant Antioxidant System in Drought Tolerance', *Antioxidants*, 8(4), p. 94. doi: 10.3390/antiox8040094.

Laxalt, A. M., Raho, N., Ten Have, A. and Lamattina, L. (2007) 'Nitric oxide is critical for inducing phosphatidic acid accumulation in xylanase-elicited tomato cells', *Journal of Biological Chemistry*, 282(29), pp. 21160–21168. doi: 10.1074/jbc.M701212200.

Lazarowski, E. R., Boucher, R. C. and Harden, T. K. (2003) 'Mechanisms of Release of Nucleotides and Integration of Their Action as P2X- and P2Y-Receptor Activating Molecules', *Molecular Pharmacology*, 64(4), pp. 785–795. doi: 10.1124/mol.64.4.785.

Ledford, H. K., Chin, B. L. and Niyogi, K. K. (2007) 'Acclimation to singlet oxygen stress in Chlamydomonas reinhardtii', *Eukaryotic Cell*, 6(6), pp. 919–930. doi: 10.1128/EC.00207-06.

Lee, S., Hirt, H. and Lee, Y. (2001) 'Phosphatidic acid activates a wound-activated MAPK in *Glycine max*', *Plant Journal*, 26(5), pp. 479–486. doi: 10.1046/j.1365-313X.2001.01037.x.

Lee, S., Lee, E. J., Yang, E. J., Lee, J. E., Park, A. R., Song, W. H. and Park, O. K. (2004) 'Proteomic of identification of annexins, calcium-dependent membrane binding proteins that mediate osmotic stress and abscisic acid signal transduction in arabidopsis', *Plant Cell*, 16(6), pp. 1378–1391. doi: 10.1105/tpc.021683.

León, J., Rojo, E. and Sánchez-Serrano, J. J. (2001) 'Wound signalling in plants.', *Journal of experimental botany*, 52(354), pp. 1–9. doi: 10.1093/jexbot/52.354.1.

Lew, R. R. and Dearnaley, J. D. W. (2000) 'Extracellular nucleotide effects on the electrical properties of growing *Arabidopsis thaliana* root hairs', *Plant Science*, 153(1), pp. 1–6. doi: 10.1016/S0168-9452(99)00242-3.

Lewandowski (2015) United Nations, Department of Economic and Social Affairs, Population Division. World Population Prospects: The 2015 Revision, Volume I: Comprehensive Tables. ST/ESA/SER.A/379.

Li, G., Meng, X., Wang, R., Mao, G., Han, L., Liu, Y. and Zhang, S. (2012) 'Dual-level regulation of ACC synthase activity by MPK3/MPK6 cascade and its downstream WRKY transcription factor during ethylene induction in Arabidopsis', *PLoS Genetics*, 8(6). doi: 10.1371/journal.pgen.1002767.

Li, L., Li, M., Yu, L., Zhou, Z., Liang, X., Liu, Z., Cai, G., Gao, L., Zhang, X., Wang, Y., Chen, S. and Zhou, J. M. (2014) 'The FLS2-associated kinase BIK1 directly phosphorylates the

NADPH oxidase RbohD to control plant immunity', *Cell Host and Microbe*. Elsevier Inc., 15(3), pp. 329–338. doi: 10.1016/j.chom.2014.02.009.

Li, S., Han, X., Yang, L., Deng, X., Wu, H., Zhang, M., Liu, Y., Zhang, S. and Xu, J. (2018) 'Mitogen-activated protein kinases and calcium-dependent protein kinases are involved in wounding-induced ethylene biosynthesis in *Arabidopsis thaliana*', *Plant Cell and Environment*, 41(1), pp. 134–147. doi: 10.1111/pce.12984.

Li, X., Cai, W., Liu, Y., Li, H., Fu, L., Liu, Z., Xu, L., Liu, H., Xu, T. and Xiong, Y. (2017) 'Differential TOR activation and cell proliferation in Arabidopsis root and shoot apexes', *Proceedings of the National Academy of Sciences of the United States of America*, 114(10), pp. 2765–2770. doi: 10.1073/pnas.1618782114.

Li, X., Zhang, Q., Yang, X., Han, J. and Zhu, Z. (2019) 'OsANN3, a calcium-dependent lipid binding annexin is a positive regulator of ABA-dependent stress tolerance in rice', *Plant Science*. Elsevier, 284(April), pp. 212–220. doi: 10.1016/j.plantsci.2019.04.019.

Li, Z. G. and Gong, M. (2011) 'Mechanical Stimulation-Induced Cross-Adaptation in Plants: An Overview', *Journal of Plant Biology*, 54(6), pp. 358–364. doi: 10.1007/s12374-011-9178-3.

Li, Z. G., Luo, L. J. and Sun, Y. F. (2015) 'Signal crosstalk between nitric oxide and hydrogen sulfide may be involved in hydrogen peroxide-induced thermotolerance in maize seedlings', *Russian Journal of Plant Physiology*, 62(4), pp. 507–514. doi: 10.1134/S1021443715030127.

Liao, C., Zheng, Y. and Guo, Y. (2017) 'MYB30 transcription factor regulates oxidative and heat stress responses through ANNEXIN-mediated cytosolic calcium signaling in *Arabidopsis*', *New Phytologist*, pp. 163–177. doi: 10.1111/nph.14679.

Lichocka, M., Rymaszewski, W., Morgiewicz, K., Barymow-Filoniuk, I., Chlebowski, A., Sobczak, M., Samuel, M. A., Schmelzer, E., Krzymowska, M. and Hennig, J. (2018) 'Nucleus- and plastid-targeted annexin 5 promotes reproductive development in Arabidopsis and is essential for pollen and embryo formation', *BMC Plant Biology*. BMC Plant Biology, 18(1), pp. 1–15. doi: 10.1186/s12870-018-1405-3.

Liemann, S., Benz, J., Burger, A., Voges, D., Hofmann, A., Huber, R. and Gottig, P. (1996) 'Structural and functional characterisation of the voltage sensor in the ion channel human annexin V', *J.Mol.Biol.*, 258, pp. 555–561. doi: 0022-2836/96/190555-07.

Lindermayr, C., Saalbach, G. and Durner, J. (2005) 'Proteomic identification of S-nitrosylated proteins in arabidopsis', *Plant Physiology*, 137(3), pp. 921–930. doi:

10.1104/pp.104.058719.

Liszkay, A., Van Der Zalm, E. and Schopfer, P. (2004) 'Production of reactive oxygen intermediates ($O_2^{\cdot-}$, H_2O_2, and .OH) by maize roots and their role in wall loosening and elongation growth', *Plant Physiology*, 136(2), pp. 3114–3123. doi: 10.1104/pp.104.044784.

Liu, H. T., Gao, F., Li, G. L., Han, J. L., Liu, D. L., Sun, D. Y. and Zhou, R. G. (2008) 'The calmodulin-binding protein kinase 3 is part of heat-shock signal transduction in *Arabidopsis thaliana*', *Plant Journal*, 55(5), pp. 760–773. doi: 10.1111/j.1365-313X.2008.03544.x.

Liu, J., Macarisin, D., Wisniewski, M., Sui, Y., Droby, S., Norelli, J. and Hershkovitz, V. (2013) 'Production of hydrogen peroxide and expression of ROS-generating genes in peach flower petals in response to host and non-host fungal pathogens', *Plant Pathology*, 62(4), pp. 820–828. doi: 10.1111/j.1365-3059.2012.02683.x.

Liu, X., Wu, J., Clark, G., Lundy, S., Lim, M., Arnold, D., Chan, J., Tang, W., Muday, G. K., Gardner, G. and Roux, S. J. (2012a) 'Role for apyrases in polar auxin transport in Arabidopsis.', *Plant physiology*, 160(4), pp. 1985–95. doi: 10.1104/pp.112.202887.

Liu, Z. Q., Yan, L., Wu, Z., Mei, C., Lu, K., Yu, Y. T., Liang, S., Zhang, X. F., Wang, X. F. and Zhang, D. P. (2012b) 'Cooperation of three WRKY-domain transcription factors WRKY18, WRKY40, and WRKY60 in repressing two ABA-responsive genes ABI4 and ABI5 in Arabidopsis', *Journal of Experimental Botany*, 63(18), pp. 6371–6392. doi: 10.1093/jxb/ers293.

Loro, G., Drago, I., Pozzan, T., Schiavo, F. Lo, Zottini, M. and Costa, A. (2012) 'Targeting of Cameleons to various subcellular compartments reveals a strict cytoplasmic/mitochondrial Ca^{2+} handling relationship in plant cells', *Plant Journal*, 71(1), pp. 1–13. doi: 10.1111/j.1365-313X.2012.04968.x.

Loro, G., Wagner, S., Doccula, F. G., Behera, S., Weinl, S., Kudla, J., Schwarzländer, M., Costa, A. and Zottini, M. (2016) 'Chloroplast-specific in vivo Ca^{2+} imaging using Yellow Cameleon fluorescent protein sensors reveals organelle-autonomous Ca^{2+} signatures in the stroma', *Plant Physiology*, p. pp.00652.2016. doi: 10.1104/pp.16.00652.

de los Reyes, P., Romero-Campero, F. J., Teresa Ruiz, M., Romero, J. M. and Valverde, F. (2017) 'Evolution of daily gene co-expression patterns from algae to plants', *Frontiers in Plant Science*, 8(July), pp. 1–22. doi: 10.3389/fpls.2017.01217.

Van der Luit, A. H., Piatti, T., Van Doorn, A., Musgrave, A., Felix, G., Boller, T. and Munnik, T. (2000) 'Elicitation of suspension-cultured tomato cells triggers the formation of

phosphatidic acid and diacylglycerol pyrophosphate', *Plant Physiology*, 123(4), pp. 1507–1515.

Luo, L., Zhang, P., Zhu, R., Fu, J., Su, J., Zheng, J., Wang, Z., Wang, D. and Gong, Q. (2017) 'Autophagy is rapidly induced by salt stress and is required for salt tolerance in Arabidopsis', *Frontiers in Plant Science*, 8(August), pp. 1–13. doi: 10.3389/fpls.2017.01459.

Luo, X., Chen, Z., Gao, J. and Gong, Z. (2014) 'Abscisic acid inhibits root growth in Arabidopsis through ethylene biosynthesis', *Plant Journal*, 79(1), pp. 44–55. doi: 10.1111/tpj.12534.

Ma, L., Ye, J., Yang, Y., Lin, H., Yue, L., Luo, J., Long, Y., Fu, H., Liu, X., Zhang, Y., Wang, Y., Chen, L., Kudla, J., Wang, Y., Han, S., Song, C. P. and Guo, Y. (2019) 'The SOS2-SCaBP8 Complex Generates and Fine-Tunes an AtANN4-Dependent Calcium Signature under Salt Stress', *Developmental Cell*. Elsevier Inc., 48(5), pp. 697–709.e5. doi: 10.1016/j.devcel.2019.02.010.

Maathuis, F. J. M. (2011) 'Vacuolar two-pore K^+ channels act as vacuolar osmosensors', *New Phytologist*, 191(1), pp. 84–91. doi: 10.1111/j.1469-8137.2011.03664.x.

Maksaev, G. and Haswell, E. S. (2012) 'MscS-Like10 is a stretch-activated ion channel from *Arabidopsis thaliana* with a preference for anions', *Proceedings of the National Academy of Sciences of the United States of America*, 109(46), pp. 19015–19020. doi: 10.1073/pnas.1213931109.

Malasics, A., Boda, D., Valiskó, M., Henderson, D. and Gillespie, D. (2010) 'Simulations of calcium channel block by trivalent cations: Gd^{3+} competes with permeant ions for the selectivity filter', *Biochimica et Biophysica Acta (BBA) - Biomembranes*, 1798(11), pp. 2013–2021. doi: 10.1016/j.bbamem.2010.08.001.

Manzoor, H., Kelloniemi, J., Chiltz, A., Wendehenne, D., Pugin, A., Poinssot, B. and Garcia-Brugger, A. (2013) 'Involvement of the glutamate receptor AtGLR3.3 in plant defense signaling and resistance to Hyaloperonospora arabidopsidis', *Plant Journal*, 76(3), pp. 466–480. doi: 10.1111/tpj.12311.

Mäser, P., Gierth, M. and Schroeder, J. I. (2002) 'Molecular mechanisms of potassium and sodium uptake in plants', *Plant and Soil*, 247(1), pp. 43–54. doi: 10.1023/A:1021159130729.

Matthus, E., Sun, J., Wang, L., Bhat, M. G., Sidik, A. B. M. and Davies, J. M. (2019a) 'DORN1 / P2K1 and purino - calcium signalling in plants ; making waves with extracellular ATP', *Annals of Botany2*. doi: 10.17863/CAM.42662.

Matthus, E., Wilkins, K. A., Swarbreck, S. M., Doddrell, N. H., Doccula, F. G., Costa, A. and Davies, J. M. (2019b) 'Phosphate starvation alters abiotic-stress-induced cytosolic free calcium increases in roots', *Plant Physiology*, 179(4), pp. 1754–1767. doi: 10.1104/pp.18.01469.

McAinsh, M. R. and Pittman, J. K. (2009) 'Shaping the calcium signature', *New Phytologist*, 181(2), pp. 275–294. doi: 10.1111/j.1469-8137.2008.02682.x.

McClung, A. D., Carroll, A. D. and Battey, N. H. (1994) 'Identification and characterization of ATPase activity associated with maize (*Zea mays*) annexins', *Biochemical Journal*, 303(3), pp. 709–712. doi: 10.1042/bj3030709.

McGonigle, T. P. and Grant, C. A. (2015) 'Variation in potassium and calcium uptake with time and root depth', *Canadian Journal of Plant Science*, 95(4), pp. 771–777. doi: 10.4141/cjps-2014-227.

Meena, M. K., Prajapati, R., Krishna, D., Divakaran, K., Pandey, Y., Reichelt, M., Mathew, M. K., Boland, W., Mithöfer, A. and Vadassery, J. (2019) ' The Ca^{2+} Channel CNGC19 Regulates Arabidopsis Defense Against Spodoptera Herbivory ', *The Plant Cell*, 31(7), pp. 1539–1562. doi: 10.1105/tpc.19.00057.

Meijering, E., Jacob, M., Sarria, J. C. F., Steiner, P., Hirling, H. and Unser, M. (2004) 'Design and validation of a tool for neurite tracing and analysis in fluorescence microscopy images', *Cytometry. Part A: The Journal of the International Society for Analytical Cytology*, 58A(2), pp. 167–176. doi: 10.1002/cyto.a.20022.

Melotto, M., Underwood, W., Koczan, J., Nomura, K. and He, S. Y. (2006) 'Plant Stomata Function in Innate Immunity against Bacterial Invasion', *Cell*, 126(5), pp. 969–980. doi: 10.1016/j.cell.2006.06.054.

Meyerhoff, O., Müller, K., Roelfsema, M. R. G., Latz, A., Lacombe, B., Hedrich, R., Dietrich, P. and Becker, D. (2005) 'AtGLR3.4, a glutamate receptor channel-like gene is sensitive to touch and cold', *Planta*, 222(3), pp. 418–427. doi: 10.1007/s00425-005-1551-3.

Michard, E., Lima, P. T., Borges, F., Silva, A. C., Portes, M. T., Carvalho, J. E., Gilliham, M., Liu, L.-H., Obermeyer, G. and Feijó, J. a (2011) 'Glutamate receptor-like genes form Ca^{2+} channels in pollen tubes and are regulated by pistil D-serine.', *Science (New York, N.Y.)*, 332(6028), pp. 434–437. doi: 10.1126/science.1201101.

Miedema, H., Bothwell, J. H. F., Brownlee, C. and Davies, J. M. (2001) 'Calcium uptake by plant cells-channels and pumps acting in concert', *Trends in Plant Science*, 6(11), pp. 514–519.

doi: 10.1016/S1360-1385(01)02124-0.

Miller, G., Schlauch, K., Tam, R., Cortes, D., Torres, M. A., Shulaev, V., Dangl, J. L. and Mittler, R. (2009) 'The plant NADPH oxidase RBOHD mediates rapid systemic signaling in response to diverse stimuli', *Science Signaling*, 2(84), pp. 1–11. doi: 10.1126/scisignal.2000448.

Mills, R. F., Doherty, M. L., López-Marqués, R. L., Weimar, T., Dupree, P., Palmgren, M. G., Pittman, J. K. and Williams, L. E. (2008) 'ECA3, a golgi-localized P2A-type ATPase, plays a crucial role in manganese nutrition in arabidopsis', *Plant Physiology*, 146(1), pp. 116–128. doi: 10.1104/pp.107.110817.

Monshausen, G. B., Messerli, M. a and Gilroy, S. (2008) 'Imaging of the Yellow Cameleon 3.6 indicator reveals that elevations in cytosolic Ca^{2+} follow oscillating increases in growth in root hairs of Arabidopsis.', *Plant physiology*, 147(4), pp. 1690–1698. doi: 10.1104/pp.108.123638.

Mortimer, J. C., Laohavisit, A., Miedema, H. and Davies, J. M. (2008) 'Voltage , reactive oxygen species and the influx of calcium', *Plant Physiology*, 3(April), pp. 698–699. doi: 10.1111/j.1469-8137.2008.02465.x.7.

Moss, S. E. and Morgan, R. O. (2004) 'The annexins', *Genome Biology*, 5(4), pp. 1–8. doi: 10.1186/gb-2004-5-4-219.

Muller, K., Linkies, A., Vreeburg, R. A. M., Fry, S. C., Krieger-Liszkay, A. and Leubner-Metzger, G. (2009) 'In vivo cell wall loosening by hydroxyl radicals during cress seed germination and elongation growth', *Plant Physiology*, 150(4), pp. 1855–1865. doi: 10.1104/pp.109.139204.

Munns, R. (2005) 'Genes and salt tolerance: Bringing them together', *New Phytologist*, 167(3), pp. 645–663. doi: 10.1111/j.1469-8137.2005.01487.x.

Nakagawa, Y., Katagiri, T., Shinozaki, K., Qi, Z., Tatsumi, H., Furuichi, T., Kishigami, A., Sokabe, M., Kojima, I., Sato, S., Kato, T., Tabata, S., Iida, K., Terashima, A., Nakano, M., Ikeda, M., Yamanaka, T. and Iida, H. (2007) 'Arabidopsis plasma membrane protein crucial for Ca^{2+} influx and touch sensing in roots', *Proceedings of the National Academy of Sciences of the United States of America*, 104(9), pp. 3639–3644. doi: 10.1073/pnas.0607703104.

Naranjo, M. A., Romero, C., Bellés, J. M., Montesinos, C., Vicente, O. and Serrano, R. (2003) 'Lithium treatment induces a hypersensitive-like response in tobacco', *Planta*, 217(3), pp. 417–424. doi: 10.1007/s00425-003-1017-4.

Navazio, L., Mariani, P. and Sanders, D. (2001) 'Mobilization of Ca^{2+} by cyclic ADP-ribose

from the endoplasmic reticulum of cauliflower florets', *Plant Physiology*, 125(4), pp. 2129–2138. doi: 10.1104/pp.125.4.2129.

Nguyen, C. T., Kurenda, A., Stolz, S., Chételat, A. and Farmer, E. E. (2018) 'Identification of cell populations necessary for leaf-toleaf electrical signaling in a wounded plant', *Proceedings of the National Academy of Sciences of the United States of America*, 115(40), pp. 10178–10183. doi: 10.1073/pnas.1807049115.

Niu, L. and Liao, W. (2016) 'Hydrogen peroxide signaling in plant development and abiotic responses: Crosstalk with nitric oxide and calcium', *Frontiers in Plant Science*, 7(MAR2016), pp. 1–14. doi: 10.3389/fpls.2016.00230.

Noctor, G., Veljovic-Jovanovic, S., Driscoll, S., Novitskaya, L. and Foyer, C. H. (2002) 'Drought and oxidative load in the leaves of C3 plants: A predominant role for photorespiration?', *Annals of Botany*, 89(SPEC. ISS.), pp. 841–850. doi: 10.1093/aob/mcf096.

North, R. A. and Jarvis, M. F. (2013) 'P2X receptors as drug targets', *Molecular Pharmacology*, 83(4), pp. 759–769. doi: 10.1124/mol.112.083758.

Ogasawara, Y., Kaya, H., Hiraoka, G., Yumoto, F., Kimura, S., Kadota, Y., Hishinuma, H., Senzaki, E., Yamagoe, S., Nagata, K., Nara, M., Suzuki, K., Tanokura, M. and Kuchitsu, K. (2008) 'Synergistic activation of the arabidopsis NADPH oxidase AtrbohD by Ca^{2+} and phosphorylation', *Journal of Biological Chemistry*, 283(14), pp. 8885–8892. doi: 10.1074/jbc.M708106200.

Ogawa, K., Kanematsu, S. and Asada, K. (1997) 'Generation of superoxide anion and localization of CuZn-superoxide dismutase in the vascular tissue of spinach hypocotyls: Their association with lignification', *Plant and Cell Physiology*, 38(10), pp. 1118–1126. doi: 10.1093/oxfordjournals.pcp.a029096.

Oh, D. H., Zahir, A., Yun, D. J., Bressan, R. A. and Bohnert, H. J. (2009) 'SOS1 and halophytism.', *Plant signaling & behavior*, 4(11), pp. 1081–1083. doi: 10.4161/psb.4.11.9786.

Olle, M. and Bender, I. (2009) 'Causes and control of calcium deficiency disorders in vegetables: A review', *Journal of Horticultural Science and Biotechnology*, 84(6), pp. 577–584. doi: 10.1080/14620316.2009.11512568.

op den Camp, R. G. L. (2003) 'Rapid Induction of Distinct Stress Responses after the Release of Singlet Oxygen in Arabidopsis', *THE PLANT CELL ONLINE*, 15(10), pp. 2320–2332. doi: 10.1105/tpc.014662.

Pan, Y., Chai, X., Gao, Q., Zhou, L., Zhang, S., Li, L. and Luan, S. (2019) 'Dynamic Interactions of Plant CNGC Subunits and Calmodulins Drive Oscillatory Ca^{2+} Channel Activities', *Developmental Cell*. Elsevier Inc., 48(5), pp. 710–725.e5. doi: 10.1016/j.devcel.2018.12.025.

Pei, Z.-M., Murata, Y., Benning, G., Thomine, S., Klüsener, B., Allen, G. J., Grill, E. and Schroeder, J. I. (2000) 'Calcium channels activated by hydrogen peroxide mediate abscisic acidsignalling in guard cells', *Nature*, 406(6797), pp. 731–734. doi: 10.1038/35021067.

Peiter, E., Maathuis, F. J. M., Mills, L. N., Knight, H., Pelloux, J., Hetherington, A. M. and Sanders, D. (2005) 'The vacuolar Ca^{2+}-activated channel TPC1 regulates germination and stomatal movement', *Nature*, 434(7031), pp. 404–408. doi: 10.1038/nature03381.

Plieth, C. and Trewavas, A. J. (2002) 'Reorientation of seedlings in the earth's gravitational field induces cytosolic calcium transients', *Plant Physiology*, 129(2), pp. 786–796. doi: 10.1104/pp.011007.

Poncini, L., Wyrsch, I., Tendon, V. D., Vorley, T., Boller, T., Geldner, N., Métraux, J. P. and Lehmann, S. (2017) 'In roots of *Arabidopsis thaliana*, the damage-associated molecular pattern AtPep1 is a stronger elicitor of immune signalling than flg22 or the chitin heptamer', *PLoS ONE*, 12(10), pp. 1–21. doi: 10.1371/journal.pone.0185808.

Pottosin, I., Wherrett, T. and Shabala, S. (2009) 'SV channels dominate the vacuolar Ca2+ release during intracellular signaling', *FEBS Letters*. Federation of European Biochemical Societies, 583(5), pp. 921–926. doi: 10.1016/j.febslet.2009.02.009.

Prieß, M., Göddeke, H., Groenhof, G. and Schäfer, L. V. (2018) 'Molecular Mechanism of ATP Hydrolysis in an ABC Transporter', *ACS Central Science*, 4(10), pp. 1334–1343. doi: 10.1021/acscentsci.8b00369.

Qia, Z., Verma, R., Gehring, C., Yamaguchi, Y., Zhao, Y., Ryan, C. A. and Berkowitz, G. A. (2010) 'Ca^{2+} signaling by plant *Arabidopsis thaliana* Pep peptides depends on AtPepR1, a receptor with guanylyl cyclase activity, and cGMP-activated Ca^{2+} channels', *Proceedings of the National Academy of Sciences of the United States of America*, 107(49), pp. 21193–21198. doi: 10.1073/pnas.1000191107.

Qiao, B., Zhang, Q., Liu, D., Wang, H., Yin, J., Wang, R., He, M., Cui, M., Shang, Z., Wang, D. and Zhu, Z. (2015) 'A calcium-binding protein, rice annexin OsANN1, enhances heat stress tolerance by modulating the production of H 2 O 2', *Journal of Experimental Botany*, 66(19), pp. 5853–5866. doi: 10.1093/jxb/erv294.

Qiu, Q. S., Guo, Y., Quintero, F. J., Pardo, J. M., Schumaker, K. S. and Zhu, J. K. (2004) 'Regulation of Vacuolar Na^+/H^+ Exchange in *Arabidopsis thaliana* by the Salt-Overly-Sensitive (SOS) Pathway', *Journal of Biological Chemistry*, 279(1), pp. 207–215. doi: 10.1074/jbc.M307982200.

Raho, N., Ramirez, L., Lanteri, M. L., Gonorazky, G., Lamattina, L., ten Have, A. and Laxalt, A. M. (2011) 'Phosphatidic acid production in chitosan-elicited tomato cells, via both phospholipase D and phospholipase C/diacylglycerol kinase, requires nitric oxide', *Journal of Plant Physiology*, 168(6), pp. 534–539. doi: 10.1016/j.jplph.2010.09.004.

Ramel, F., Birtic, S., Cuiné, S., Triantaphylidès, C., Ravanat, J. L. and Havaux, M. (2012b) 'Chemical quenching of singlet oxygen by carotenoids in plants', *Plant Physiology*, 158(3), pp. 1267–1278. doi: 10.1104/pp.111.182394.

Ramel, F., Birtic, S., Ginies, C., Soubigou-Taconnat, L., Triantaphylidès, C. and Havaux, M. (2012a) 'Carotenoid oxidation products are stress signals that mediate gene responses to singlet oxygen in plants', *Proceedings of the National Academy of Sciences of the United States of America*, 109(14), pp. 5535–5540. doi: 10.1073/pnas.1115982109.

Ranf, S., Eschen-Lippold, L., Pecher, P., Lee, J. and Scheel, D. (2011) 'Interplay between calcium signalling and early signalling elements during defence responses to microbe- or damage-associated molecular patterns', *Plant Journal*, 68(1), pp. 100–113. doi: 10.1111/j.1365-313X.2011.04671.x.

Rentel, M. C., Knight, M. R. and Kingdom, U. (2004) 'Oxidative Stress-Induced Calcium Signaling', *Plant Physiology*, 135(July), pp. 1471–1479. doi: 10.1104/pp.104.042663.1.

Reyt, G., Boudouf, S., Boucherez, J., Gaymard, F. and Briat, J. F. (2015) 'Iron- and ferritin-dependent reactive oxygen species distribution: Impact on arabidopsis root system architecture', *Molecular Plant*, 8(3), pp. 439–453. doi: 10.1016/j.molp.2014.11.014.

Richards, S. L., Laohavisit, A., Mortimer, J. C., Shabala, L., Swarbreck, S. M., Shabala, S. and Davies, J. M. (2014) 'Annexin 1 regulates the H_2O_2-induced calcium signature in *Arabidopsis thaliana* roots', *Plant Journal*, 77(1), pp. 136–145. doi: 10.1111/tpj.12372.

Richards, S. L., Wilkins, K. A., Swarbreck, S. M., Anderson, A. A., Habib, N., Smith, A. G., McAinsh, M. and Davies, J. M. (2015) 'The hydroxyl radical in plants: From seed to seed', *Journal of Experimental Botany*, 66(1), pp. 37–46. doi: 10.1093/jxb/eru398.

Riewe, D., Grosman, L., Fernie, A. R., Wucke, C. and Geigenberger, P. (2008a) 'The potato-

specific apyrase is apoplastically localized and has influence on gene expression, growth, and development', *Plant Physiology*, 147(3), pp. 1092–1109. doi: 10.1104/pp.108.117564.

Riewe, D., Grosman, L., Fernie, A. R., Zauber, H., Wucke, C. and Geigenberger, P. (2008b) 'A cell wall-bound adenosine nucleosidase is involved in the salvage of extracellular ATP in *Solanum tuberosum*', *Plant and Cell Physiology*, 49(10), pp. 1572–1579. doi: 10.1093/pcp/pcn127.

Rinalducci, S., Pedersen, J. Z. and Zolla, L. (2004) 'Formation of radicals from singlet oxygen produced during photoinhibition of isolated light-harvesting proteins of photosystem II', *Biochimica et Biophysica Acta - Bioenergetics*, 1608(1), pp. 63–73. doi: 10.1016/j.bbabio.2003.10.009.

Del Río, L. A. and López-Huertas, E. (2016) 'ROS generation in peroxisomes and its role in cell signaling', *Plant and Cell Physiology*, 57(7), pp. 1364–1376. doi: 10.1093/pcp/pcw076.

Rodrigues, O., Reshetnyak, G., Grondin, A., Saijo, Y., Leonhardt, N., Maurel, C. and Verdoucq, L. (2017) 'Aquaporins facilitate hydrogen peroxide entry into guard cells to mediate ABA- and pathogen-triggered stomatal closure', *Proceedings of the National Academy of Sciences of the United States of America*, 114(34), pp. 9200–9205. doi: 10.1073/pnas.1704754114.

Rossi, A. E. and Dirksen, R. T. (2006) 'Sarcoplasmic reticulum: The dynamic calcium governor of muscle', *Muscle & Nerve*, 33(6), pp. 715–731. doi: 10.1002/mus.20512.

Roux, S. J. and Steinebrunner, I. (2007) 'Extracellular ATP: an unexpected role as a signaler in plants', *Trends in Plant Science*, pp. 522–527. doi: 10.1016/j.tplants.2007.09.003.

Sauer, H., Hescheler, J. and Wartenberg, M. (2000) 'Mechanical strain-induced Ca^{2+} waves are propagated via ATP release and purinergic receptor activation', *American Journal of Physiology - Cell Physiology*, 279(2 48-2), pp. 295–307.

Savary, S., Willocquet, L., Pethybridge, S. J., Esker, P., McRoberts, N. and Nelson, A. (2019) 'The global burden of pathogens and pests on major food crops', *Nature Ecology and Evolution*. Springer US, 3(3), pp. 430–439. doi: 10.1038/s41559-018-0793-y.

Sawinski, K., Mersmann, S., Robatzek, S. and Böhmer, M. (2013) 'Guarding the Green: Pathways to Stomatal Immunity', *Molecular Plant-Microbe Interactions*, 26(6), pp. 626–632. doi: 10.1094/MPMI-12-12-0288-CR.

Schmöckel, S. M., Garcia, A. F., Berger, B., Tester, M., Webb, A. A. R. and Roy, S. J. (2015)

'Different NaCl-induced calcium signatures in the *Arabidopsis thaliana* ecotypes Col-0 and C24', *PLoS ONE*, 10(2), pp. 1–9. doi: 10.1371/journal.pone.0117564.

Schön, M., Töller, A., Diezel, C., Roth, C., Westphal, L., Wiermer, M. and Somssich, I. E. (2013) 'Analyses of wrky18 wrky40 plants reveal critical roles of SA/EDS1 signaling and indole-glucosinolate biosynthesis for *Golovinomyces orontii* resistance and a loss-of resistance towards Pseudomonas syringae pv. tomato AvrRPS4', *Molecular Plant-Microbe Interactions*, 26(7), pp. 758–767. doi: 10.1094/MPMI-11-12-0265-R.

Schopfer, P., Liszkay, A., Bechtold, M., Frahry, G. and Wagner, A. (2002) 'Evidence that hydroxyl radicals mediate auxin-induced extension growth', *Planta*, 214(6), pp. 821–828. doi: 10.1007/s00425-001-0699-8.

Schulze-Lefert, P. and Robatzek, S. (2006) 'Plant Pathogens Trick Guard Cells into Opening the Gates', *Cell*, 126(5), pp. 831–834. doi: 10.1016/j.cell.2006.08.020.

Sebastià, C. H., Hardin, S. C., Clouse, S. D., Kieber, J. J. and Huber, S. C. (2004) 'Identification of a new motif for CDPK phosphorylation in vitro that suggests ACC synthase may be a CDPK substrate', *Archives of Biochemistry and Biophysics*, 428(1), pp. 81–91. doi: 10.1016/j.abb.2004.04.025.

Shabala, S., Wu, H. and Bose, J. (2015) 'Salt stress sensing and early signalling events in plant roots: Current knowledge and hypothesis', *Plant Science*. Elsevier Ireland Ltd, 241, pp. 109–119. doi: 10.1016/j.plantsci.2015.10.003.

Shang, Z., Laohavisit, A. and Davies, J. M. (2009) 'Extracellular ATP activates an Arabidopsis plasma membrane Ca($^{2+}$)-permeable conductance.', *Plant signaling & behavior*, 4(10), pp. 989–91. doi: 10.1111/j.1365-313X.2009.03830.x.xtracellular.

Shavrukov, Y. (2013) 'Salt stress or salt shock: which genes are we studying?', *Journal of Experimental Botany*, 64(1), pp. 119–127. doi: 10.1093/jxb/ers316.

Shen, C., Que, Z., Xia, Y., Tang, N., Li, D., He, R. and Cao, M. (2017) 'Knock out of the annexin gene OsAnn3 via CRISPR/Cas9-mediated genome editing decreased cold tolerance in rice', *Journal of Plant Biology*, 60(6), pp. 539–547. doi: 10.1007/s12374-016-0400-1.

Shi, H., Ishitani, M., Kim, C. and Zhu, J.-K. (2000) 'The *Arabidopsis thaliana* salt tolerance gene SOS1 encodes a putative Na^+/H^+ antiporter', *Proceedings of the National Academy of Sciences*, 97(12), pp. 6896–6901. doi: 10.1073/pnas.120170197.

Shi, K., Li, X., Zhang, H., Zhang, G., Liu, Y., Zhou, Y., Xia, X., Chen, Z. and Yu, J. (2015)

'Guard cell hydrogen peroxide and nitric oxide mediate elevated CO_2-induced stomatal movement in tomato', *New Phytologist*, 208(2), pp. 342–353. doi: 10.1111/nph.13621.

Shigaki, T. and Hirschi, K. (2000) 'Characterization of CAX-like genes in plants: Implications for functional diversity', *Gene*, 257(2), pp. 291–298. doi: 10.1016/S0378-1119(00)00390-5.

Shih, H. W., Depew, C. L., Miller, N. D. and Monshausen, G. B. (2015) 'The cyclic nucleotide-gated channel CNGC14 regulates root gravitropism in *arabidopsis thaliana*', *Current Biology*. Elsevier Ltd, 25(23), pp. 3119–3125. doi: 10.1016/j.cub.2015.10.025.

Short, E. F., North, K. A., Roberts, M. R., Hetherington, A. M., Shirras, A. D. and McAinsh, M. R. (2012) 'A stress-specific calcium signature regulating an ozone-responsive gene expression network in Arabidopsis', *Plant Journal*, 71(6), pp. 948–961. doi: 10.1111/j.1365-313X.2012.05043.x.

Smirnoff, N. and Arnaud, D. (2019) 'Hydrogen peroxide metabolism and functions in plants', *New Phytologist*, 221(3), pp. 1197–1214. doi: 10.1111/nph.15488.

Smirnova, A. V., Matveyeva, N. P. and Yermakov, I. P. (2014) 'Reactive oxygen species are involved in regulation of pollen wall cytomechanics', *Plant Biology*, 16(1), pp. 252–257. doi: 10.1111/plb.12004.

Song, C. J. (2006) 'Extracellular ATP Induces the Accumulation of Superoxide via NADPH Oxidases in Arabidopsis', *Plant Physiology*, 140(4), pp. 1222–1232. doi: 10.1104/pp.105.073072.

Song, S. Y., Chen, Y., Chen, J., Dai, X. Y. and Zhang, W. H. (2011) 'Physiological mechanisms underlying OsNAC5-dependent tolerance of rice plants to abiotic stress', *Planta*, 234(2), pp. 331–345. doi: 10.1007/s00425-011-1403-2.

Spollen, W. G., Lenoble, M. E., Samuels, T. D., Bernstein, N. and Sharp, R. E. (2000) 'Abscisic acid accumulation maintains maize primary root elongation at low water potentials by restricting ethylene production', *Plant Physiology*, 122(3), pp. 967–976. doi: 10.1104/pp.122.3.967.

Stratmann, J., Scheer, J. and Ryan, C. A. (2000) 'Suramin inhibits initiation of defense signaling by systemin, chitosan, and a beta-glucan elicitor in suspension-cultured Lycopersicon peruvianum cells', *Proc Natl Acad Sci U S A*, 97(16), pp. 8862–8867. doi: 97/16/8862 [pii].

Sueldo, D. J., Foresi, N. P., Casalongué, C. A., Lamattina, L. and Laxalt, A. M. (2010) 'Phosphatidic acid formation is required for extracellular ATP-mediated nitric oxide production in suspension-cultured tomato cells', *New Phytologist*, 185(4), pp. 909–916. doi: 10.1111/j.1469-

8137.2009.03165.x.

Sun, J., Zhang, X., Deng, S., Zhang, C., Wang, M., Ding, M., Zhao, R., Shen, X., Zhou, X., Lu, C. and Chen, S. (2012) 'Extracellular ATP Signaling Is Mediated by H_2O_2 and Cytosolic Ca^{2+} in the Salt Response of *Populus euphratica* Cells', *PLoS ONE*, 7(12). doi: 10.1371/journal.pone.0053136.

Sun, Y., Li, L., Macho, A. P., Han, Z., Hu, Z., Zipfel, C., Zhou, J. M. and Chai, J. (2013) 'Structural basis for flg22-induced activation of the Arabidopsis FLS2-BAK1 immune complex', *Science*, 342(6158), pp. 624–628. doi: 10.1126/science.1243825.

Swarbreck, S. M., Guerringue, Y., Matthus, E., Jamieson, F. J. C. and Davies, J. M. (2019) 'Impairment in karrikin but not strigolactone sensing enhances root skewing in *Arabidopsis thaliana*', *Plant Journal*, 98(4), pp. 607–621. doi: 10.1111/tpj.14233.

Takahashi, F., Mizoguchi, T., Yoshida, R., Ichimura, K. and Shinozaki, K. (2011) 'Calmodulin-Dependent Activation of MAP Kinase for ROS Homeostasis in Arabidopsis', *Molecular Cell*. Elsevier Inc., 41(6), pp. 649–660. doi: 10.1016/j.molcel.2011.02.029.

Talke, I. N., Blaudez, D., Maathuis, F. J. M. and Sanders, D. (2003) 'CNGCs: Prime targets of plant cyclic nucleotide signalling?', *Trends in Plant Science*, 8(6), pp. 286–293. doi: 10.1016/S1360-1385(03)00099-2.

Tan, C., Wang, H., Zhang, Y., Qi, B., Xu, G. and Zheng, H. (2011) 'A proteomic approach to analyzing responses of *Arabidopsis thaliana* root cells to different gravitational conditions using an agravitropic mutant, pin2 and its wild type', *Proteome Science*. BioMed Central Ltd, 9(1), p. 72. doi: 10.1186/1477-5956-9-72.

Tanaka, K., Choi, J., Cao, Y. and Stacey, G. (2014) 'Extracellular ATP acts as a damage-associated molecular pattern (DAMP) signal in plants', *Frontiers in Plant Science*, pp. 1–9. doi: 10.3389/fpls.2014.00446.

Tanaka, K., Swanson, S. J., Gilroy, S. and Stacey, G. (2010) 'Extracellular Nucleotides Elicit Cytosolic Free Calcium Oscillations in Arabidopsis', *Plant Physiology*, 154(2), pp. 705–719. doi: 10.1104/pp.110.162503.

Tang, W., Brady, S. R., Sun, Y., Muday, G. K. and Roux, S. J. (2003) 'Extracellular ATP inhibits root gravitropism at concentrations that inhibit polar auxin transport.', *Plant physiology*, 131(January), pp. 147–154. doi: 10.1104/pp.013672.

Tapken, D. and Hollmann, M. (2008) '*Arabidopsis thaliana* Glutamate Receptor Ion Channel

Function Demonstrated by Ion Pore Transplantation', *Journal of Molecular Biology*, 383(1), pp. 36–48. doi: 10.1016/j.jmb.2008.06.076.

Teardo, E., Carraretto, L., Moscatiello, R., Cortese, E., Vicario, M., Festa, M., Maso, L., De Bortoli, S., Calì, T., Vothknecht, U. C., Formentin, E., Cendron, L., Navazio, L. and Szabo, I. (2019) 'A chloroplast-localized mitochondrial calcium uniporter transduces osmotic stress in Arabidopsis', *Nature Plants*. Springer US, 5(6), pp. 581–588. doi: 10.1038/s41477-019-0434-8.

Teardo, E., Carraretto, L., Wagner, S., Formentin, E., Behera, S., De Bortoli, S., Larosa, V., Fuchs, P., Lo Schiavo, F., Raffaello, A., Rizzuto, R., Costa, A., Schwarzländer, M. and Szabò, I. (2017) 'Physiological characterization of a plant mitochondrial Calcium uniporter in Vitro and in Vivo', *Plant Physiology*, 173(2), pp. 1355–1370. doi: 10.1104/pp.16.01359.

Terrile, M. C., Tonoń, C. V., Iglesias, M. J., Lamattina, L. and Casalongué, C. A. (2010) 'Extracellular ATP and nitric oxide signaling pathways regulate redox-dependent responses associated to root hair growth in etiolated Arabidopsis seedlings', *Plant Signaling and Behavior*, 5(6), pp. 698–701. doi: 10.4161/psb.5.6.11579.

Thomas, C., Rajagopal, A., Windsor, B., Dudler, R., Lloyd, A. and Roux, S. J. (2000) 'A role for ectophosphatase in xenobiotic resistance', *The Plant cell*, 12(April), pp. 519–533. doi: 10.1105/tpc.12.4.519.

Tian, W., Hou, C., Ren, Z., Wang, C., Zhao, F., Dahlbeck, D., Hu, S., Zhang, L., Niu, Q., Li, L., Staskawicz, B. J. and Luan, S. (2019) 'A calmodulin-gated calcium channel links pathogen patterns to plant immunity', *Nature*. Springer US, 572(7767), pp. 131–135. doi: 10.1038/s41586-019-1413-y.

Tonón, C., Cecilia Terrile, M., José Iglesias, M., Lamattina, L. and Casalongué, C. (2010) 'Extracellular ATP, nitric oxide and superoxide act coordinately to regulate hypocotyl growth in etiolated Arabidopsis seedlings', *Journal of Plant Physiology*, 167(7), pp. 540–546. doi: 10.1016/j.jplph.2009.11.002.

Torres, M. A., Dangl, J. L. and Jones, J. D. G. (2002) 'Arabidopsis gp91phox homologues Atrbohd and Atrbohf are required for accumulation of reactive oxygen intermediates in the plant defense response', *Proceedings of the National Academy of Sciences of the United States of America*, 99(1), pp. 517–522. doi: 10.1073/pnas.012452499.

Toyota, M., Spencer, D., Sawai-Toyota, S., Jiaqi, W., Zhang, T., Koo, A. J., Howe, G. A. and Gilroy, S. (2018) 'Glutamate triggers long-distance, calcium-based plant defense signaling', *Science*, 361(6407), pp. 1112–1115. doi: 10.1126/science.aat7744.

Tracy, F. E., Gilliham, M., Dodd, A. N., Webb, A. A. R. and Tester, M. (2008) 'NaCl-induced changes in cytosolic free Ca^{2+} in *Arabidopsis thaliana* are heterogeneous and modified by external ionic composition', *Plant, Cell and Environment*, 31(8), pp. 1063–1073. doi: 10.1111/j.1365-3040.2008.01817.x.

Tran, D., Galletti, R., Neumann, E. D., Dubois, A., Sharif-Naeini, R., Geitmann, A., Frachisse, J. M., Hamant, O. and Ingram, G. C. (2017) 'A mechanosensitive Ca^{2+} channel activity is dependent on the developmental regulator DEK1', *Nature Communications*. Springer US, 8(1), pp. 1–7. doi: 10.1038/s41467-017-00878-w.

Tripathi, D., Zhang, T., Koo, A. J., Stacey, G. and Tanaka, K. (2017) 'Extracellular ATP acts on jasmonate signaling to reinforce plant defense', *Plant Physiology*, 176(January), p. pp.01477.2017. doi: 10.1104/pp.17.01477.

Tsukagoshi, H., Busch, W. and Benfey, P. N. (2010) 'Transcriptional regulation of ROS controls transition from proliferation to differentiation in the root', *Cell*. Elsevier Ltd, 143(4), pp. 606–616. doi: 10.1016/j.cell.2010.10.020.

Tunc-Ozdemir, M., Rato, C., Brown, E., Rogers, S., Mooneyham, A., Frietsch, S., Myers, C. T., Poulsen, L. R., Malhó, R. and Harper, J. F. (2013a) 'Cyclic Nucleotide Gated Channels 7 and 8 Are Essential for Male Reproductive Fertility', *PLoS ONE*, 8(2). doi: 10.1371/journal.pone.0055277.

Tunc-Ozdemir, M., Tang, C., Ishka, M. R., Brown, E., Groves, N. R., Myers, C. T., Rato, C., Poulsen, L. R., McDowell, S., Miller, G., Mittler, R. and Harper, J. F. (2013b) 'A cyclic nucleotide-gated channel (CNGC16) in pollen is critical for stress tolerance in pollen reproductive development', *Plant Physiology*, 161(2), pp. 1010–1020. doi: 10.1104/pp.112.206888.

Turrens, J. F. (2003) 'Mitochondrial formation of reactive oxygen species', *Journal of Physiology*, 552(2), pp. 335–344. doi: 10.1113/jphysiol.2003.049478.

Valenzuela, C. E., Acevedo-Acevedo, O., Miranda, G. S., Vergara-Barros, P., Holuigue, L., Figueroa, C. R. and Figueroa, P. M. (2016) 'Salt stress response triggers activation of the jasmonate signaling pathway leading to inhibition of cell elongation in Arabidopsis primary root', *Journal of Experimental Botany*, 67(14), pp. 4209–4220. doi: 10.1093/jxb/erw202.

Vanderauwera, S., Suzuki, N., Miller, G., Van De Cotte, B., Morsa, S., Ravanat, J. L., Hegie, A., Triantaphylidès, C., Shulaev, V., Van Montagu, M. C. E., Van Breusegem, F. and Mittler, R. (2011) 'Extranuclear protection of chromosomal DNA from oxidative stress',

Proceedings of the National Academy of Sciences of the United States of America, 108(4), pp. 1711–1716. doi: 10.1073/pnas.1018359108.

Vatsa, P., Chiltz, A., Bourque, S., Wendehenne, D., Garcia-Brugger, A. and Pugin, A. (2011) 'Involvement of putative glutamate receptors in plant defence signaling and NO production', *Biochimie*. Elsevier Masson SAS, 93(12), pp. 2095–2101. doi: 10.1016/j.biochi.2011.04.006.

Verbelen, J.-P., Cnodder, T. De, Le, J., Vissenberg, K. and Baluška, F. (2006) 'The Root Apex of *Arabidopsis thaliana* Consists of Four Distinct Zones of Growth Activities', *Plant Signaling & Behavior*, 1(6), pp. 296–304. doi: 10.4161/psb.1.6.3511.

Verkhratsky, A. and Burnstock, G. (2014) 'Biology of purinergic signalling: Its ancient evolutionary roots, its omnipresence and its multiple functional significance', *BioEssays*, 36(7), pp. 697–705. doi: 10.1002/bies.201400024.

Vincent, T. R., Avramova, M., Canham, J., Higgins, P., Bilkey, N., Mugford, S. T., Pitino, M., Toyota, M., Gilroy, S., Miller, A. J., Hogenhout, S. A. and Sanders, D. (2017) 'Interplay of plasma membrane and vacuolar ion channels, together with BAK1, elicits rapid cytosolic calcium elevations in Arabidopsis during aphid feeding', *Plant Cell*, 29(6), pp. 1460–1479. doi: 10.1105/tpc.17.00136.

Vincill, E. D., Bieck, A. M. and Spalding, E. P. (2012) 'Ca^{2+} Conduction by an Amino Acid-Gated Ion Channel Related to Glutamate Receptors', *Plant Physiology*, 159(1), pp. 40–46. doi: 10.1104/pp.112.197509.

Vincill, E. D., Clarin, A. E., Molenda, J. N. and Spalding, E. P. (2013) 'Interacting glutamate receptor-like proteins in phloem regulate lateral root initiation in Arabidopsis', *Plant Cell*, 25(4), pp. 1304–1313. doi: 10.1105/tpc.113.110668.

Wagner, D., Przybyla, D., Op Den Camp, R., Kim, C., Landgraf, F., Keun, P. L., Würsch, M., Laloi, C., Nater, M., Hideg, E. and Apel, K. (2004) 'The genetic basis of singlet oxygen-induced stress response of *Arabidopsis thaliana*', *Science*, 306(5699), pp. 1183–1185. doi: 10.1126/science.1103178.

Wang, C., Xu, W., Jin, H., Zhang, T., Lai, J., Zhou, X., Zhang, S., Liu, S., Duan, X., Wang, H., Peng, C. and Yang, C. (2016) 'A Putative Chloroplast-Localized Ca^{2+}/H^{+} Antiporter CCHA1 Is Involved in Calcium and pH Homeostasis and Required for PSII Function in Arabidopsis', *Molecular Plant*. Elsevier Ltd, 9(8), pp. 1183–1196. doi: 10.1016/j.molp.2016.05.015.

Wang, F., Jia, J., Wang, Y., Wang, W., Chen, Y., Liu, T. and Shang, Z. (2014) 'Hyperpolization-activated Ca^{2+} channels in guard cell plasma membrane are involved in extracellular ATP-promoted stomatal opening in Vicia faba', *Journal of Plant Physiology*. Elsevier GmbH., 171(14), pp. 1241–1247. doi: 10.1016/j.jplph.2014.05.007.

Wang, J., Song, J., Clark, G. and Roux, S. J. (2018b) 'ANN1 and ANN2 function in post-phloem sugar transport in root tips to affect primary root growth', *Plant Physiology*, 178(1), pp. 390–401. doi: 10.1104/pp.18.00713.

Wang, K. L. C., Li, H. and Ecker, J. R. (2002) 'Ethylene biosynthesis and signaling networks', *Plant Cell*, 14(SUPPL.), pp. 131–151. doi: 10.1105/tpc.001768.S-.

Wang, K., Senthil-Kumar, M., Ryu, C. M., Kang, L. and Mysore, K. S. (2012) 'Phytosterols play a key role in plant innate immunity against bacterial pathogens by regulating nutrient efflux into the apoplast', *Plant Physiology*, 158(4), pp. 1789–1802. doi: 10.1104/pp.111.189217.

Wang, L., Stacey, G., Leblanc-Fournier, N., Legué, V., Moulia, B. and Davies, J. M. (2019) 'Early Extracellular ATP Signaling in Arabidopsis Root Epidermis: A Multi-Conductance Process', *Frontiers in Plant Science*, 10(September). doi: 10.3389/fpls.2019.01064.

Wang, L., Wilkins, K. A. and Davies, J. M. (2018a) 'Arabidopsis DORN1 extracellular ATP receptor; activation of plasma membrane K^+-and Ca^{2+}-permeable conductances', *New Phytologist*, 218(4), pp. 1301–1304. doi: 10.1111/nph.15111.

Wang, X., Ma, X., Wang, H., Li, B., Clark, G., Guo, Y., Roux, S., Sun, D. and Tang, W. (2015) 'Proteomic study of microsomal proteins reveals a key role for Arabidopsis annexin 1 in mediating heat stress-induced increase in intracellular calcium levels.', *Molecular & cellular proteomics : MCP*, 14(3), pp. 686–94. doi: 10.1074/mcp.M114.042697.

Weerasinghe, R. R., Swanson, S. J., Okada, S. F., Garrett, M. B., Kim, S. Y., Stacey, G., Boucher, R. C., Gilroy, S. and Jones, A. M. (2009) 'Touch induces ATP release in Arabidopsis roots that is modulated by the heterotrimeric G-protein complex', *FEBS Letters*. Federation of European Biochemical Societies, 583(15), pp. 2521–2526. doi: 10.1016/j.febslet.2009.07.007.

Whalley, H. J. and Knight, M. R. (2013) 'Calcium signatures are decoded by plants to give specific gene responses', *New Phytologist*, 197(3), pp. 690–693. doi: 10.1111/nph.12087.

Whitaker, C., Beckett, R. P., Minibayeva, F. V. and Kranner, I. (2010) 'Alleviation of dormancy by reactive oxygen species in Bidens pilosa L. seeds', *South African Journal of Botany*. Elsevier B.V., 76(3), pp. 601–605. doi: 10.1016/j.sajb.2010.04.014.

White, P. J. (2001) 'The pathways of calcium movement to the xylem', *Journal of Experimental Botany*, pp. 891–899. doi: 10.1093/jexbot/52.358.891.

White, P. J. and Broadley, M. R. (2003) 'Calcium in plants', *Annals of Botany*, 92(4), pp. 487–511. doi: 10.1093/aob/mcg164.

Wilkinson, S. and Davies, W. J. (2010) 'Drought, ozone, ABA and ethylene: new insights from cell to plant to community', *Plant, Cell and Environment*, 33(4), pp. 510–525. doi: 10.1111/j.1365-3040.2009.02052.x.

Wu, S.-J., Liu, Y.-S. and Wu, J.-Y. (2008) 'The signaling role of extracellular ATP and its dependence on Ca^{2+} flux in elicitation of Salvia miltiorrhiza hairy root cultures.', *Plant & cell physiology*, 49(4), pp. 617–624. doi: 10.1093/pcp/pcn033.

Wu, Z., Liang, F., Hong, B., Young, J. C., Sussman, M. R., Harper, J. F. and Sze, H. (2002) 'An Endoplasmic Reticulum-Bound Ca^{2+}/Mn^{2+} Pump, ECA1, Supports Plant Growth and Confers Tolerance to Mn^{2+} Stress', *Plant Physiology*, 130(1), pp. 128–137. doi: 10.1104/pp.004440.

Yadav, D., Ahmed, I., Shukla, P., Boyidi, P. and Kirti, P. B. (2016) 'Overexpression of Arabidopsis AnnAt8 alleviates abiotic stress in transgenic Arabidopsis and tobacco', *Plants*, 5(2), pp. 1–14. doi: 10.3390/plants5020018.

Yang, A., Dai, X. and Zhang, W. H. (2012) 'A R2R3-type MYB gene, OsMYB2, is involved in salt, cold, and dehydration tolerance in rice', *Journal of Experimental Botany*, 63(7), pp. 2541–2556. doi: 10.1093/jxb/err431.

Yang, X., Wang, B., Farris, B., Clark, G. and Roux, S. J. (2015) 'Modulation of Root Skewing in Arabidopsis by Apyrases and Extracellular ATP', *Plant and Cell Physiology*, 56(11), pp. 2197–2206. doi: 10.1093/pcp/pcv134.

Yang, Y. W., Bian, S. M., Yao, Y. and Liu, J. Y. (2008) 'Comparative proteomic analysis provides new insights into the fiber elongating process in cotton', *Journal of Proteome Research*, 7(11), pp. 4623–4637. doi: 10.1021/pr800550q.

Yi, S. Y., Shirasu, K., Moon, J. S., Lee, S. G. and Kwon, S. Y. (2014) 'The activated SA and JA signaling pathways have an influence on flg22-triggered oxidative burst and callose deposition', *PLoS ONE*, 9(2). doi: 10.1371/journal.pone.0088951.

Yoshida, K., Ohnishi, M., Fukao, Y., Okazaki, Y., Fujiwara, M., Song, C., Nakanishi, Y., Saito, K., Shimmen, T., Suzaki, T., Hayashi, F., Fukaki, H., Maeshima, M. and Mimura, T. (2013) 'Studies on vacuolar membrane microdomains isolated from arabidopsis suspension-

cultured cells: Local distribution of vacuolar membrane proteins', *Plant and Cell Physiology*, 54(10), pp. 1571–1584. doi: 10.1093/pcp/pct107.

Zambrano Leal, A. (2014) *Climate Change 2013 - The Physical Science Basis*, *Antimicrobial Agents and Chemotherapy*. Edited by Intergovernmental Panel on Climate Change. Cambridge: Cambridge University Press. doi: 10.1017/CBO9781107415324.

Zandalinas, S. I., Balfagón, D., Arbona, V. and Gómez-Cadenas, A. (2017) 'Modulation of antioxidant defense system is associated with combined drought and heat stress tolerance in citrus', *Frontiers in Plant Science*, 8(June), pp. 1–10. doi: 10.3389/fpls.2017.00953.

Zandalinas, S. I., Sengupta, S., Burks, D., Azad, R. K. and Mittler, R. (2019) 'Identification and characterization of a core set of ROS wave-associated transcripts involved in the systemic acquired acclimation response of Arabidopsis to excess light', *Plant Journal*, 98(1), pp. 126–141. doi: 10.1111/tpj.14205.

Zhang, C., Li, J., Guo, X., Zhu, B., Xiao, W., Wang, P., Jiang, M., Hu, S., Lu, X., He, Z. and Chen, P. (2017b) 'LecRK-VII.1, a Lectin Receptor-Like Kinase, Mediates the Regulation of Salt Stress and Jasmonic Acid Response in Arabidopsis', *Journal of Plant Growth Regulation*. Springer US, 36(2), pp. 385–401. doi: 10.1007/s00344-016-9647-5.

Zhang, M., Wang, D., Kang, Y., Wu, J. X., Yao, F., Pan, C., Yan, Z., Song, C. and Chen, L. (2018) 'Structure of the mechanosensitive OSCA channels', *Nature Structural and Molecular Biology*. Springer US, 25(9), pp. 850–858. doi: 10.1038/s41594-018-0117-6.

Zhang, S., Pan, Y., Tian, W., Dong, M., Zhu, H., Luan, S. and Li, L. (2017a) 'Arabidopsis CNGC14 Mediates Calcium Influx Required for Tip Growth in Root Hairs', *Molecular Plant*, 10(7), pp. 1004–1006. doi: 10.1016/j.molp.2017.02.007.

Zhang, Y., Zhu, H., Zhang, Q., Li, M., Yan, M., Wang, R., Wang, L., Welti, R., Zhang, W. and Wang, X. (2009) 'Phospholipase Dα1 and phosphatidic acid regulate NADPH oxidase activity and production of reactive oxygen species in ABA-mediated stomatal closure in arabidopsis', *Plant Cell*, 21(8), pp. 2357–2377. doi: 10.1105/tpc.108.062992.

Zhao, K. F., Song, J., Fan, H., Zhou, S. and Zhao, M. (2010) 'Growth response to ionic and osmotic stress of NaCl in salt-tolerant and salt-sensitive maize', *Journal of Integrative Plant Biology*, 52(5), pp. 468–475. doi: 10.1111/j.1744-7909.2010.00947.x.

Zhu, J., Wu, X., Yuan, S., Qian, D., Nan, Q., An, L. and Xiang, Y. (2014a) 'Annexin5 Plays a Vital Role in Arabidopsis Pollen Development via Ca^{2+}-Dependent Membrane Trafficking',

PLoS ONE, 9(7), p. e102407. doi: 10.1371/journal.pone.0102407.

Zhu, J., Yuan, S., Wei, G., Qian, D., Wu, X., Jia, H., Gui, M., Liu, W., An, L. and Xiang, Y. (2014b) 'Annexin5 Is Essential for Pollen Development in Arabidopsis', *Molecular Plant*, 7(4), pp. 751–754. doi: 10.1093/mp/sst171.

Zhu, R., Dong, X., Hao, W., Gao, W., Zhang, W., Xia, S., Liu, T. and Shang, Z. (2017) 'Heterotrimeric G Protein-Regulated Ca^{2+} Influx and PIN2 Asymmetric Distribution Are Involved in *Arabidopsis thaliana* Roots' Avoidance Response to Extracellular ATP', *Frontiers in Plant Science*, 8(September), pp. 1–17. doi: 10.3389/fpls.2017.01522.

Zonia, L. and Munnik, T. (2004) 'Osmotically Induced Cell Swelling versus Cell Shrinking Elicits Specific Changes in Phospholipid Signals in Tobacco Pollen Tubes', *Plant Physiology*, 134(2), pp. 813–823. doi: 10.1104/pp.103.029454.

Appendices

Appendix I

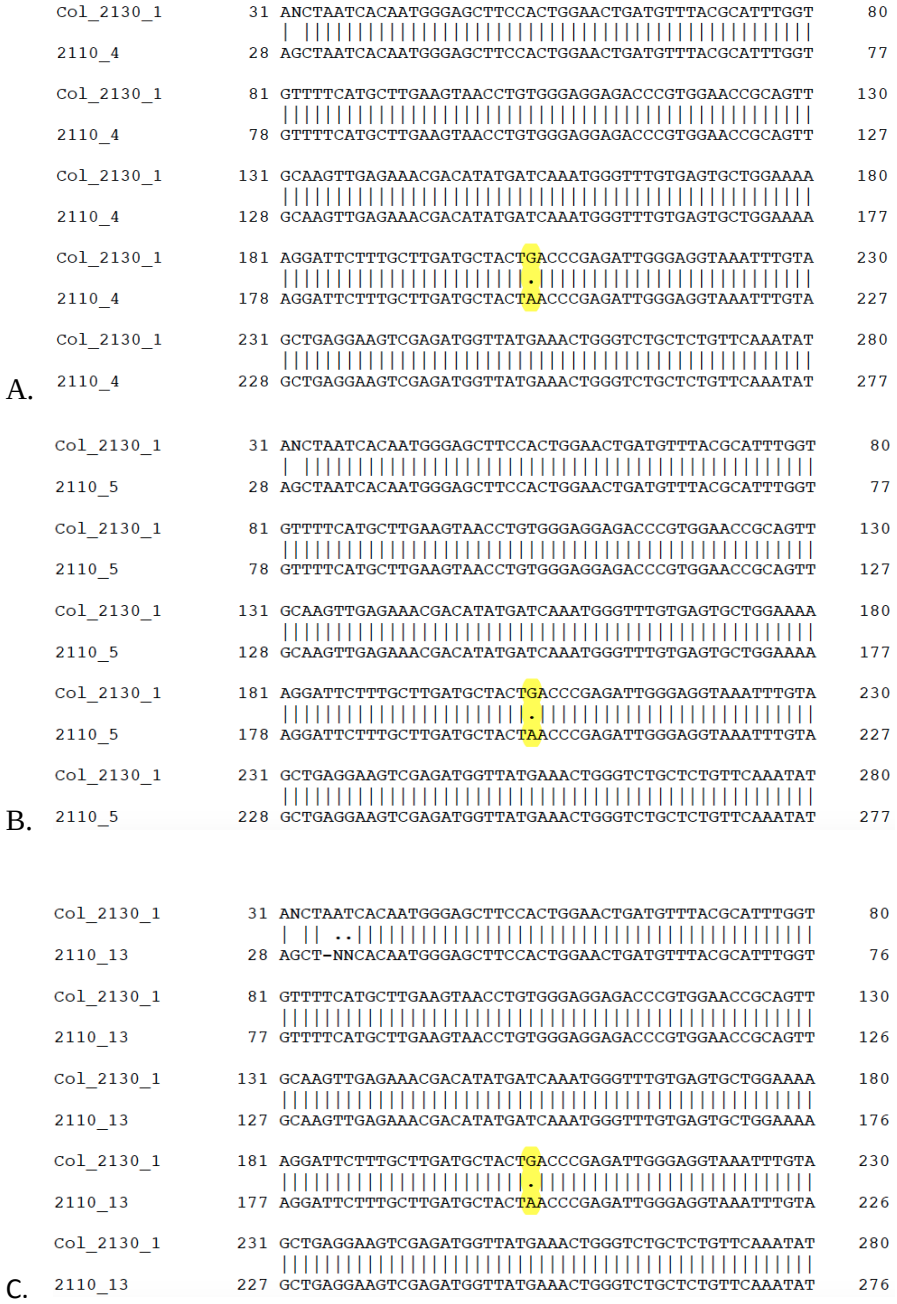

Figure 7.1: This is the representative alignment between wild type Col-0 (sample 2130) and *Atdorn1-1/ann1* (sample 2110) by using the Pairwise Sequence Alignment tool provided by the EMBL-EBI (https://www.ebi.ac.uk/Tools/psa/). Single point mutation of nucleotide in *Atdorn1-1/ann1* samples from G to A is shown in yellow highlight

Appendix II

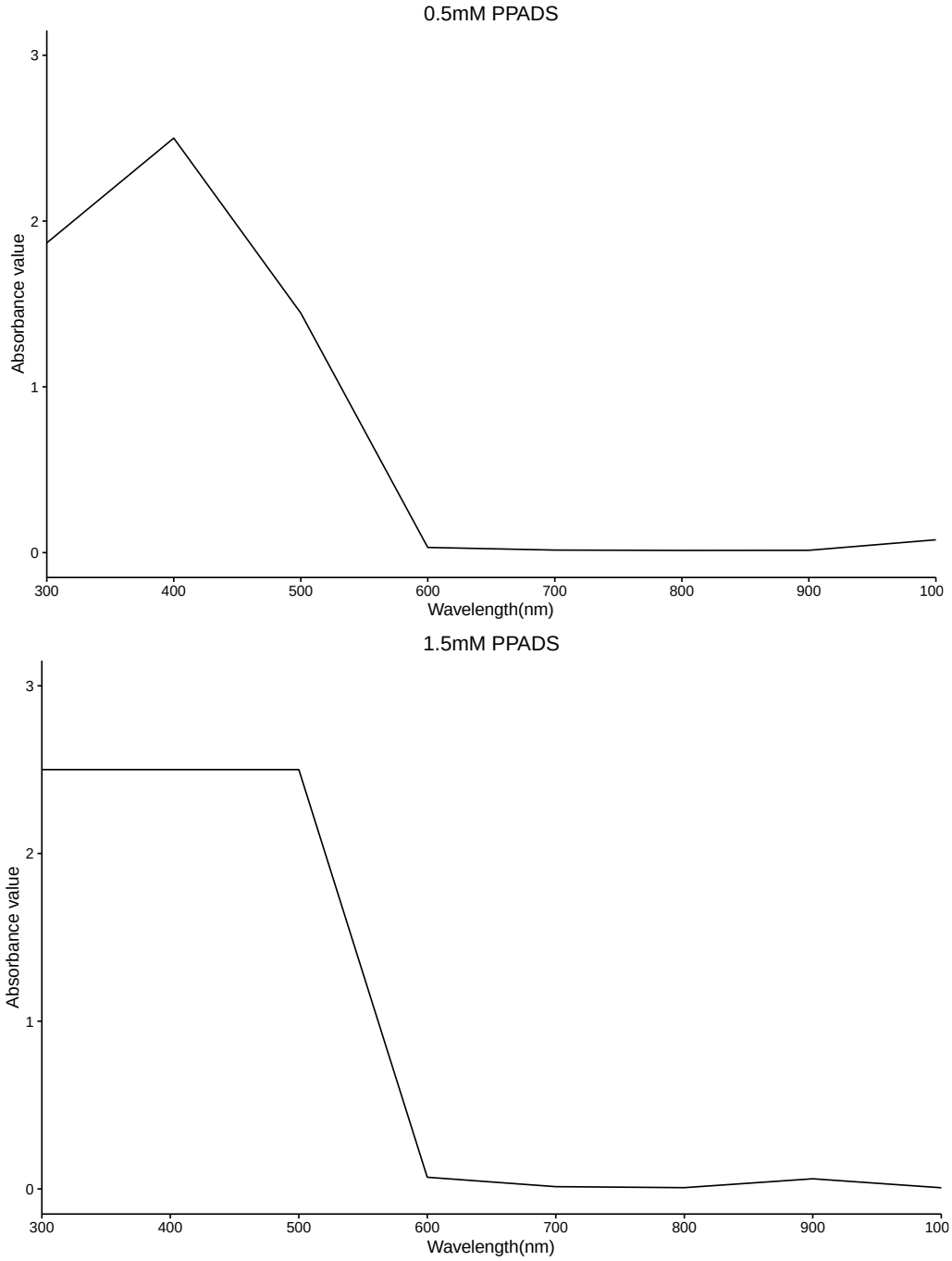

Figure 7.2: Spectrum analysis of the orange colour of 0.5 mM and 1.5 mM PPADS inhibitor (Pyridoxalphosphate-6-azophenyl-2',4'-disulfonic acid) was carried out with a spectrophotometer. The absorbance values of the PPADS at 400 nm wavelength for both concentrations were high enough to mask the luminescence value of (apo)aequorin reporter; which is also in the wavelength of range 300 - 400 nm.

Appendix III

```
M13Part1          1 ACCTGTTCGTTGCAACAAATTGATGAGCAATGCTTTTTTATAATGCCAAC     50

Template          1 --------------------------------------------------      0

M13Part1         51 TTTGTACAAAAAAGCAGGCTGGTCTCTGATACTATGCTGTCAAACGCAAG    100
                                    ||||||||||||||||||||||||||||||||
Template          1 --------------------ggtctctgatactatgctgtcaaacgcaag     30

M13Part1        101 CTTTGTCTTCCCGGATAACACACCTCTGACAAAAGAAGCGTACTACTACA    150
                    ||||||||||||||||||||||||||||||||||||||||||||||||||||
Template         31 ctttgtcttcccggataacacacctctgacaaaagaagcgtactactaca     80

M13Part1        151 GAACCATCTTCGAGAAGTTCTTCCCGAAGGTAATAAAATGCCATAAATTT    200
                    ||||||||||||||||||||||||||||||||||||||||||||||||||||
Template         81 gaaccatcttcgagaagttcttcccgaaggtaataaaatgccataaattt    130

M13Part1        201 TCAAAATCTCACATAAACGTCTCTGCTTTGCTGATTTGTTTTGTTGTATT    250
                    ||||||||||||||||||||||||||||||||||||||||||||||||||||
Template        131 tcaaaatctcacataaacgtctctgctttgctgatttgttttgttgtatt    180

M13Part1        251 TCCTGAGCAGAGTGCTGCTAGAGCGACTGTACCAGGAGGTCCAAGTATAG    300
                    ||||||||||||||||||||||||||||||||||||||||||||||||||||
Template        181 tcctgagcagagtgctgctagagcgactgtaccaggaggtccaagtatag    230

M13Part1        301 CTTGCAGTACCGCGAAAGCTGTAGAATGGGATGCAACTTGGTCAAAGAAT    350
                    ||||||||||||||||||||||||||||||||||||||||||||||||||||
Template        231 cttgcagtaccgcgaaagctgtagaatgggatgcaacttggtcaaagaat    280

M13Part1        351 CTTGATCCGTCAGGCCGTGCGGCTCTTGGAGTTCATGTTGCAGCTTATGA    400
                    ||||||||||||||||||||||||||||||||||||||||||||||||||||
Template        281 cttgatccgtcaggccgtgcggctcttggagttcatgttgcagcttatga    330

M13Part1        401 AGAGGATAAAGCAGCTGCTGCTGCTAAGGCTGGATCGGATTTAGTAGATC    450
                    ||||||||||||||||||||||||||||||||||||||||||||||||||||
Template        331 agaggataaagcagctgctgctgctaaggctggatcggatttagtagatc    380

M13Part1        451 CTCTTCCTAAGAATGGAACATAAGAGAACAACACTACAGGCATTGAGGAT    500
                    ||||||||||||||||||||||||||||||||||||||||||||||||||||
Template        381 ctcttcctaagaatggaacataagagaacaacactacaggcattgaggat    430

M13Part1        501 ATAAGCAAATGTTTTATTCTTCTACACAGAGAGATCGTTATCTTCTAGAG    550
                    ||||||||||||||||||||||||||||||||||||||||||||||||||||
Template        431 ataagcaaatgttttattcttctacacagagagatcgttatcttctagag    480

M13Part1        551 GGATCAATGAATAAAAGCTTCGTCCATTTCTAGCTGGAGATTCCATGGAT    600
                    ||||||||||||||||||||||||||||||||||||||||||||||||||||
Template        481 ggatcaatgaataaaagcttcgtccatttctagctggagattccatggat    530

M13Part1        601 CTCCAGTTAGTGCAAGTGATACACGTTGTCTACATTTGTACCTAAGTTTC    650
                    ||||||||||||||||||||||||||||||||||
Template        531 ctccagttagtgcaagtgatacacgttgtctaca----------------    564
```

Figure 7.3: Sequence alignment of the PCR product between M13 forward primer and Part 1 reverse primer. Sequencing product is labelled as 'M13Part1' whereas the *AtANN2* sequence from database is labelled as 'Template' for reference. Alignment was done to confirm that the correct sequence of *AtANN2* construct was inserted into the entry vector pDONR221 during BP reaction. Pairwise Sequence Alignment tool provided by the EMBL-EBI (https://www.ebi.ac.uk/Tools/psa/) was used for the alignment. The PCR was expected to produce a 683 bp size product.

```
Part2              1 --------------------------------------------------      0

Template           1 agtgcaagtgatacacgttgtctacatttgtacctaagtttctgcatttt     50

Part2              1 -----------------TAGACAAGTCTTGGACCCTAGATGATACTTCAG     33
                                       |||||||||||||||||||||||||||||||||
Template          51 ttgtcgttcttttgtgttagacaagtcttggaccctagatgatacttcag    100

Part2             34 TTTCTTAGACGTTAAATTTGATGAATCCGAACTTGTTTGATTTCAAAGCC     83
                     ||||||||||||||||||||||||||||||||||||||||||||||||||||
Template         101 tttcttagacgttaaatttgatgaatccgaacttgtttgatttcaaagcc    150

Part2             84 TGGCCTTTCTGCAATGTGTTTTTGTGCATGTTCTGGCTTGTTTGTTGTTA    133
                     ||||||||||||||||||||||||||||||||||||||||||||||||||||
Template         151 tggcctttctgcaatgtgtttttgtgcatgttctggcttgtttgttgtta    200

Part2            134 CTCAACGCAGGATTTGTTATAATATGTACAATATATCTAGTACACACATA    183
                     ||||||||||||||||||||||||||||||||||||||||||||||||||||
Template         201 ctcaacgcaggatttgttataatatgtacaatatatctagtacacacata    250

Part2            184 AGTCAAGCAAGTAAGACTCCGTGGCCCAATGGATAAGGCGCTGGTCTACG    233
                     ||||||||||||||||||||||||||||||||||||||||||||||||||||
Template         251 agtcaagcaagtaagactccgtggcccaatggataaggcgctggtctacg    300

Part2            234 AAACCAGAGATTCTGGGTTCGATCCCCAGCGGAGTCGCTCTTCATCTACT    283
                     ||||||||||||||||||||||||||||||||||||||||||||||||||||
Template         301 aaaccagagattctgggttcgatccccagcggagtcgctcttcatctact    350

Part2            284 ATTTTTATTTTTCTTACGCGCATTGCTTATAAAAGTTTTTTAATGAACGT    333
                     ||||||||||||||||||||||||||||||||||||||||||||||||||||
Template         351 atttttatttttcttacgcgcattgcttataaaagtttttttaatgaacgt    400

Part2            334 GGGATAAAAGTTTTCAGATTCGTATTTATTATTTCAAAAAGACAGATGAC    383
                     ||||||||||||||||||||||||||||||||||||||||||||||||||||
Template         401 gggataaaagttttcagattcgtatttattatttcaaaaagacagatgac    450

Part2            384 CTAACCTCATTACTCGTGTATGGACTTTTTTTTCCTTCAAATTATATTTT    433
                     ||||||||||||||||||||||||||||||||||||||||||||||||||||
Template         451 ctaacctcattactcgtgtatggacttttttttccttcaaattatatttt    500

Part2            434 ATGAAATTTGAGTAGACGAAGTAACTGCTCCCCTTCAGATTTAGCTAAAG    483
                     ||||||||||||||||||||||||||||||||||||||||||||||||||||
Template         501 atgaaatttgagtagacgaagtaactgctccccttcagatttagctaaag    550

Part2            484 AGCCAACCACGTGAAGTCGTGAATCCTCTCTGTCGTTTTCGTATTAACAA    533
                     ||||||||||||||||||
Template         551 agccaaccacgtgaagtcgt----------------------------    570
```

Figure 7.4: Sequence alignment of the PCR product using the Part 2 primer pairs. Sequencing product is labelled as 'Part2' whereas the *AtANN2* sequence from database is labelled as 'Template' for reference. Alignment was done to confirm that the correct sequence of *AtANN2* construct was inserted into the entry vector pDONR221 during BP reaction. Pairwise Sequence Alignment tool provided by the EMBL-EBI (https://www.ebi.ac.uk/Tools/psa/) was used for the alignment. Expected PCR product from the primer pair was 568 bp.

```
Part3              1 -------------CTTATGTATAATTGTTTTATATCGATCACCGGTTTCT     37
                                  |||||||||||||||||||||||||||||||||||||
Template3         51 aaaatctcgttttcttatgtataattgttttatatcgatcaccggtttct    100

Part3             38 CTAGGTCTAGGTATAGCTGTTCCAATATCATGATTTTTAAGTTTAGTTTT     87
                     ||||||||||||||||||||||||||||||||||||||||||||||||||||
Template3        101 ctaggtctaggtatagctgttccaatatcatgattttaagtttagtttt    150

Part3             88 CAACATCATTAAGTAAAAGTGTGAACTCATTATCATCATCGCTTTCCCTT    137
                     ||||||||||||||||||||||||||||||||||||||||||||||||||||
Template3        151 caacatcattaagtaaaagtgtgaactcattatcatcatcgctttccctt    200

Part3            138 TAGAATTTTTGCAAACACACGAAAATAAATAAATTGTTTGGACATATTAT    187
                     ||||||||||||||||||||||||||||||||||||||||||||||||||||
Template3        201 tagaatttttgcaaacacacgaaaataaataaattgtttggacatattat    250

Part3            188 TGAGAAACATAGTCAAATGAGCCCGTTCACATTCTGAATCATATAAGTTA    237
                     ||||||||||||||||||||||||||||||||||||||||||||||||||||
Template3        251 tgagaaacatagtcaaatgagcccgttcacattctgaatcatataagtta    300

Part3            238 CAGTCCCAAACCCACGTTTTATTAAAAATGTACTACTAGTCAATAATTTA    287
                     ||||||||||||||||||||||||||||||||||||||||||||||||||||
Template3        301 cagtcccaaacccacgttttattaaaaatgtactactagtcaataattta    350

Part3            288 TGTTGAGTCATATTTATTTATTTTGACACAGTTGGTTTTCGCAGTTTCTT    337
                     ||||||||||||||||||||||||||||||||||||||||||||||||||||
Template3        351 tgttgagtcatatttatttatttgacacagttggttttcgcagtttctt    400

Part3            338 GTTTATTAGTTTCAAATTGCACTTATTAGTTTTAAAAACAATTTAATTTG    387
                     ||||||||||||||||||||||||||||||||||||||||||||||||||||
Template3        401 gtttattagtttcaaattgcacttattagttttaaaaacaatttaatttg    450

Part3            388 ATATTTGGTATAATATCTCTTTTGAATTATTTACAAACTTTATTACAGCC    437
                     ||||||||||||||||||||||||||||||||||||||||||||||||||||
Template3        451 atatttggtataatatctctttgaattatttacaaactttattacagcc    500

Part3            438 TGGTTTTGAAAAAAAAAAAATACTTTGCATAATTGCTACTTTGCTAGGAT    487
                     ||||||||||||||||||||||||||||||||||||||||||||||||||||
Template3        501 tggttttgaaaaaaaaaaaatactttgcataattgctactttgctaggat    550

Part3            488 TACTTTATAAACTTTTTCAGCTTTGATTCATTTAACATTAAACCCAATTA    537
                     ||||||||||||||||||||||||||||||||||||||||||||||||||||
Template3        551 tactttataaacttttcagctttgattcatttaacattaaacccaatta    600

Part3            538 AAATATTTTATTCATTTTAGCATAAAAGGGGAAAAAAAAGAAATATATAT    587
                     ||||||||||||||||||||||||||||||||||||||||||||||||||||
Template3        601 aaatattttattcattttagcataaaaggggaaaaaaaagaaatatatat    650

Part3            588 ATATATATATATATATTTCCTCTTTTCAATTAAATCAGCTGTTAAAAG    637
                     ||||||||||||||||||||||||||||||||||||||||||||||||||||
Template3        651 atatatatatatatatatttcctcttttcaattaaatcagctgttaaaag    700

Part3            638 TGGAAAAAAATCAAAGAGATATCAAAATATTGATTAGAAGAATATGTCCAT    687
                     ||||||||||||||||||||||||||||||||||||||||||||||||||||
Template3        701 tggaaaaaatcaaagagatatcaaaatattgattagaagaatatgtccat    750

Part3            688 ATTCAATTATTTTATATTATCTTTATTAAATGCTTTACCTTACAACAATA    737
                     ||||||||||||||||||||||||||||||||||||||||||||||||||||
Template3        751 attcaattattttatattatctttattaaatgctttaccttacaacaata    800

Part3            738 ACTTAAATAAATTTTTGGGATTCCCGTTACATTACTTAAGTAGGACGACG    787
                     |||||||||||||||||||||||||||||||||||||||||
Template3        801 acttaaataaatttttgggattcccgttacattacttaag----------    840
```

Figure 7.5: Sequence alignment of the PCR product using the Part 3 primer pairs. Sequencing product is labelled as 'Part3' whereas the *AtANN2* sequence from database is labelled as 'Template' for reference. Alignment was done to confirm that the correct sequence of *AtANN2* construct was inserted into the entry vector pDONR221 during BP reaction. Pairwise Sequence Alignment tool provided by the EMBL-EBI (https://www.ebi.ac.uk/Tools/psa/) was used for the alignment. Expected PCR product from the primer pair was 840 bp.

```
Part4              1 ----------------------------AGGCAGAGATCTTAAGAGTTAA     22
                                                  ||||||||||||||||||||||
Template4         51 cattacaaagcagaagaaacacaaacagaggcagagatcttaagagttaa    100

Part4             23 AGACTAATCCCAACAATGGCGTCTCTCAAAGTCCCAAGCAATGTTCCTCT     72
                     ||||||||||||||||||||||||||||||||||||||||||||||||||||
Template4        101 agactaatcccaacaatggcgtctctcaaagtcccaagcaatgttcctct    150

Part4             73 TCCCGAAGATGACGCCGAGCAACTCCACAAGGCTTTTTCAGGTCTCTCTC    122
                     ||||||||||||||||||||||||||||||||||||||||||||||||||||
Template4        151 tcccgaagatgacgccgagcaactccacaaggctttttcaggtctctctc    200

Part4            123 TTTTTTTTTCATCACTTGATCGGGATTTAGTTTCTTCTTATACGATCTCT    172
                     ||||||||||||||||||||||||||||||||||||||||||||||||||||
Template4        201 ttttttttcatcacttgatcgggatttagtttcttcttatacgatctct    250

Part4            173 AATCTGTAATCGGTTTCGTTAATCACAAGATTAATCATTTTTGATATCTT    222
                     ||||||||||||||||||||||||||||||||||||||||||||||||||||
Template4        251 aatctgtaatcggtttcgttaatcacaagattaatcatttttgatatctt    300

Part4            223 AAGTACTCTCCTATACTCATCGTTGAGTATTATTTAGTTTGTTGATTTAA    272
                     ||||||||||||||||||||||||||||||||||||||||||||||||||||
Template4        301 aagtactctcctatactcatcgttgagtattatttagtttgttgatttaa    350

Part4            273 TCACAACTACATTGGTGATTCGGGATTTACTCTTGTTTGACCTGATCTGT    322
                     ||||||||||||||||||||||||||||||||||||||||||||||||||||
Template4        351 tcacaactacattggtgattcgggatttactcttgtttgacctgatctgt    400

Part4            323 GTTCTGTGTCCCACCACAAGATCAGGATCATGTCTTCTTATATTAGATAC    372
                     ||||||||||||||||||||||||||||||||||||||||||||||||||||
Template4        401 gttctgtgtcccaccacaagatcaggatcatgtcttcttatattagatac    450

Part4            373 AGTCCGATGATGTCCTAATTGATTGATTATAATGAAAATATGTTTCTTTT    422
                     ||||||||||||||||||||||||||||||||||||||||||||||||||||
Template4        451 agtccgatgatgtcctaattgattgattataatgaaaatatgtttctttt    500

Part4            423 TGTTCTTTAGTGAACCAAGATTATGCTTGTTTTGTGTTCTCCTTGGGAGA    472
                     ||||||||||||||||||||||||||||||||||||||||||||||||||||
Template4        501 tgttctttagtgaaccaagattatgcttgttttgtgttctccttgggaga    550

Part4            473 TTTGTGACATGACAAAATGTTTGTTTTTTGGGTTTGGTCTGAAACAGGAT    522
                     ||||||||||||||||||||||||||||||||||||||||||||||||||||
Template4        551 tttgtgacatgacaaaatgtttgtttttgggtttggtctgaaacaggat    600

Part4            523 GGGGTACCAACGAGAAGCTGATCATATCAATACTAGCTCACAGGAACGCA    572
                     |||
Template4        601 ggg--------------------------------------------    603
```

Figure 7.6: Sequence alignment of the PCR product using the Part 4 primer pairs. Sequencing product is labelled as 'Part4' whereas the *AtANN2* sequence from database is labelled as 'Template' for reference. Alignment was done to confirm that the correct sequence of *AtANN2* construct was inserted into the entry vector pDONR221 during BP reaction. Pairwise Sequence Alignment tool provided by the EMBL-EBI (https://www.ebi.ac.uk/Tools/psa/) was used for the alignment. Expected PCR product from the primer pair was 603 bp.

```
Part5              1 ----------------------CAACGCAGCTTGATCCGCAGCGTTTATG     28
                                            ||||||||||||||||||||||||||||
Template5         51 actagctcacaggaacgcagcacaacgcagcttgatccgcagcgtttatg    100

Part5             29 CAGCTACCTACAATGAGGATCTTCTCAAAGCATTAGACAAAGAGCTTTCT     78
                     ||||||||||||||||||||||||||||||||||||||||||||||||||||
Template5        101 cagctacctacaatgaggatcttctcaaagcattagacaaagagctttct    150

Part5             79 AGCGACTTTGAGGTATTTTTAACTCTTTTCTTTCTTTCTTTCTTTTGGGG    128
                     ||||||||||||||||||||||||||||||||||||||||||||||||||||
Template5        151 agcgactttgaggtattttaactcttttctttctttctttctttgggg    200

Part5            129 GTCTCTGAAATGATATAGTGACTGATTTAGGATTGTGAAACTGTTGTATT    178
                     ||||||||||||||||||||||||||||||||||||||||||||||||||||
Template5        201 gtctctgaaatgatatagtgactgatttaggattgtgaaactgttgtatt    250

Part5            179 TGGTGTTTTTTTGTAACAGAGAGCTGTGATGTTGTGGACTCTTGATCCAC    228
                     ||||||||||||||||||||||||||||||||||||||||||||||||||||
Template5        251 tggtgttttttgtaacagagagctgtgatgttgtggactcttgatccac    300

Part5            229 CAGAGAGAGATGCTTATTTGGCTAAAGAATCCACCAAGATGTTCACCAAG    278
                     ||||||||||||||||||||||||||||||||||||||||||||||||||||
Template5        301 cagagagagatgcttatttggctaaagaatccaccaagatgttcaccaag    350

Part5            279 AACAATTGGGTTCTTGTTGAAATCGCTTGCACAAGGCCTGCTCTTGAGCT    328
                     ||||||||||||||||||||||||||||||||||||||||||||||||||||
Template5        351 aacaattgggttcttgttgaaatcgcttgcacaaggcctgctcttgagct    400

Part5            329 TATCAAGGTCAAGCAAGCTTACCAAGCTCGATACAAGAAATCAATCGAGG    378
                     ||||||||||||||||||||||||||||||||||||||||||||||||||||
Template5        401 tatcaaggtcaagcaagcttaccaagctcgatacaagaaatcaatcgagg    450

Part5            379 AAGATGTCGCGCAACACACATCTGGTGACCTTCGTAAGGTAATCATTCAA    428
                     ||||||||||||||||||||||||||||||||||||||||||||||||||||
Template5        451 aagatgtcgcgcaacacacatctggtgaccttcgtaaggtaatcattcaa    500

Part5            429 TAAACCAAATCTTGCTTGTTTGTTTTGTATTTGGGACACATGTTTCTGAC    478
                     ||||||||||||||||||||||||||||||||||||||||||||||||||||
Template5        501 taaaccaaatcttgcttgtttgttttgtatttgggacacatgtttctgac    550
```

Figure 7.7: Sequence alignment of the PCR product using the Part 5 primer pairs. Sequencing product is labelled as 'Part5' whereas the *AtANN2* sequence from database is labelled as 'Template' for reference. Alignment was done to confirm that the correct sequence of *AtANN2* construct was inserted into the entry vector pDONR221 during BP reaction. Pairwise Sequence Alignment tool provided by the EMBL-EBI (https://www.ebi.ac.uk/Tools/psa/) was used for the alignment. Expected PCR product from the primer pair was 557 bp.

```
Part6              1 -------------------------------------GGAGATGATGTGAA     14
                                                           ||||||||||||||
Template6         51 ctcttgcttcctcttgtgagcactttcaggtatgaaggagatgatgtgaa    100

Part6             15 CATGATGCTTGCAAGATCTGAAGCTAAGATACTTCACGAGAAGGTCTCAG     64
                     ||||||||||||||||||||||||||||||||||||||||||||||||||||
Template6        101 catgatgcttgcaagatctgaagctaagatacttcacgagaaggtctcag    150

Part6             65 AGAAATCTTACAGTGACGATGACTTCATCAGAATCTTGACAACAAGAAGC    114
                     ||||||||||||||||||||||||||||||||||||||||||||||||||||
Template6        151 agaaatcttacagtgacgatgacttcatcagaatcttgacaacaagaagc    200

Part6            115 AAAGCACAGCTCGGTGCAACACTCAACCACTACAACAACGAGTATGGAAA    164
                     ||||||||||||||||||||||||||||||||||||||||||||||||||||
Template6        201 aaagcacagctcggtgcaacactcaaccactacaacaacgagtatggaaa    250

Part6            165 CGCCATTAACAAGGTTAGCTTAACCACCAACTGCTTTTTCATTTGATGTT    214
                     ||||||||||||||||||||||||||||||||||||||||||||||||||||
Template6        251 cgccattaacaaggttagcttaaccaccaactgctttttcatttgatgtt    300

Part6            215 ACAAAATCTTGTTCGGAAAGCTTATTATATGAAGTGAAATTTTTGCAGAA    264
                     ||||||||||||||||||||||||||||||||||||||||||||||||||||
Template6        301 acaaaatcttgttcggaaagcttattatatgaagtgaaatttttgcagaa    350

Part6            265 CTTGAAGGAAGAGTCGGACGACAATGACTACATGAAACTACTAAGAGCTG    314
                     ||||||||||||||||||||||||||||||||||||||||||||||||||||
Template6        351 cttgaaggaagagtcggacgacaatgactacatgaaactactaagagctg    400

Part6            315 TAATCACATGTTTGACATACCCTGAGAAGCATTTTGAGAAGGTTCTTCGT    364
                     ||||||||||||||||||||||||||||||||||||||||||||||||||||
Template6        401 taatcacatgtttgacataccctgagaagcattttgagaaggttcttcgt    450

Part6            365 CTATCAATCAACAAAATGGGAACAGACGAATGGGGACTAACCCGAGTCGT    414
                     ||||||||||||||||||||||||||||||||||||||||||||||||||||
Template6        451 ctatcaatcaacaaaatgggaacagacgaatggggactaacccgagtcgt    500

Part6            415 GACTACACGAACTGAAGTTGACATGGAACGCATCAAAGAGGAATATCAGC    464
                     ||||||||||||||||||||||||||||||||||||||||||||||||||||
Template6        501 gactacacgaactgaagttgacatggaacgcatcaaagaggaatatcagc    550

Part6            465 GAAGAAACAGCATTCCTTTGGACCGTGCTATCGCCAAAGACACTTCTGGT    514
                     ||||||||||||||||||||||||||||||||||||||||||||||||||||
Template6        551 gaagaaacagcattcctttggaccgtgctatcgccaaagacacttctggt    600

Part6            515 GACTATGAGGACATGCTTGTTGCTCTTCTCGGACATGGCGATGCTTGAAA    564
                     ||||||||||||||||||||||||||||||||||||||||||||||||
Template6        601 gactatgaggacatgcttgttgctcttctcggacatggcgatgctt----    646
```

Figure 7.8: Sequence alignment of the PCR product using the Part 6 primer pairs. Sequencing product is labelled as 'Part6' whereas the *AtANN2* sequence from database is labelled as 'Template' for reference. Alignment was done to confirm that the correct sequence of *AtANN2* construct was inserted into the entry vector pDONR221 during BP reaction. Pairwise Sequence Alignment tool provided by the EMBL-EBI (https://www.ebi.ac.uk/Tools/psa/) was used for the alignment. Expected PCR product from the primer pair was 646 bp.

Appendix IV

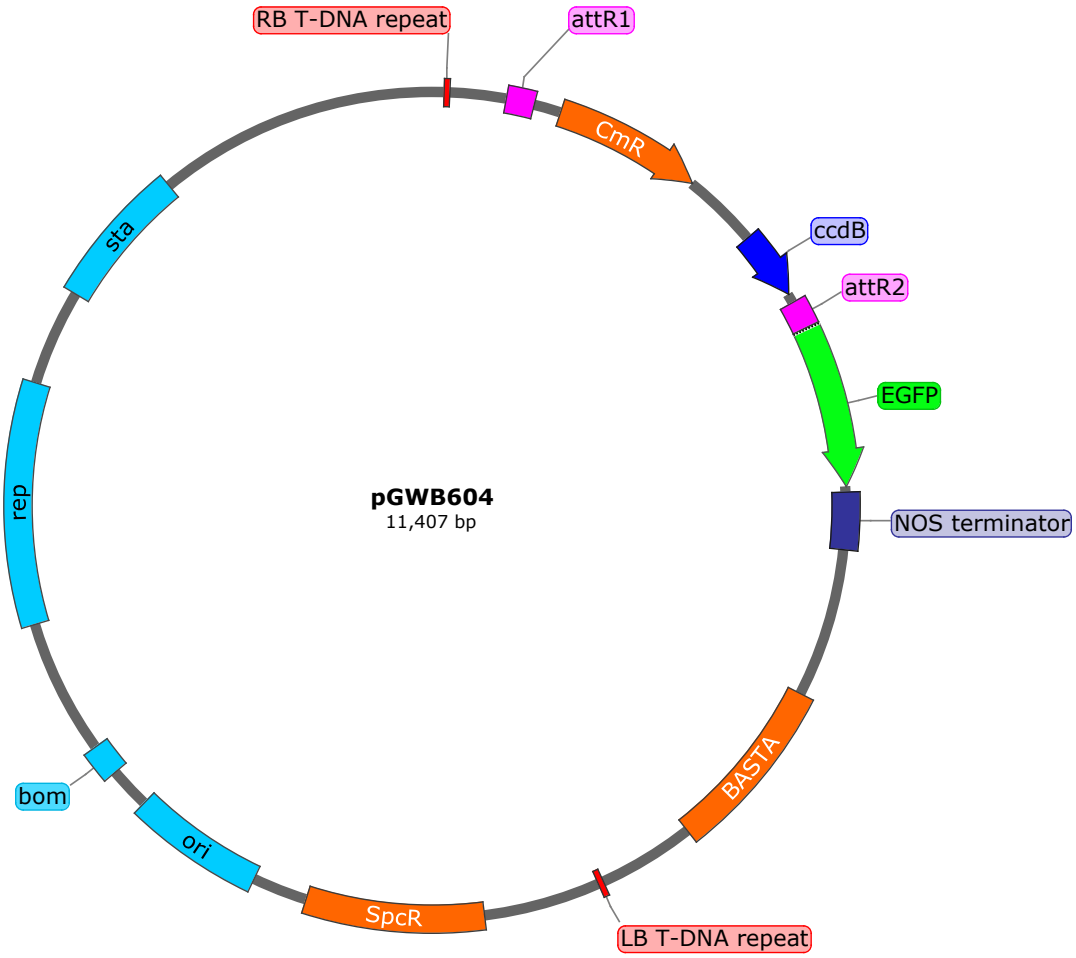

Figure 7.9: Diagram shows some of the features included in the impGWB604 destination vector (http://shimane-u.org/nakagawa/gbv.htm; Nakamura *et al.*, 2010) that was used during Gateway cloning to produce *Atann2/AtANN2* complemented mutant line. Image was created by using SnapGene Viewer.

Appendix V

```
attB1_Part1        1 ggtctctgatactatgctgtcaaacgcaagctttgtcttcccggataaca     50
                                          || |||||||||| |||||||.||
attB1_part1_L      1 -------------------------GC-AGCTTTGTCTT-CCGGATANCA     23

attB1_Part1       51 cacctctgacaaaagaagcgtactactacagaaccatcttcgagaagttc    100
                     |||||||||||||||||||||||||||||||||||...|..|.||||
attB1_part1_L     24 CACCTCTGACAAAAGAAGCGTACTACTACAGAACCATCNCNGNNANGTTC     73

attB1_Part1      101 ttcccgaaggtaataaaatgccataaattttcaaaatctcacataaacgt    150
                     ||||||||||||||||||||||||||||||||||||||||||||||||||
attB1_part1_L     74 TTCCCGAAGGTAATAAAATGCCATAAATTTTCAAAATCTCACATAAACGT    123

attB1_Part1      151 ctctgctttgctgatttgttttgttgtatttcctgagcagagtgctgcta    200
                     ||||||||||||||||||||||||||||||||||||||||||||||||||
attB1_part1_L    124 CTCTGCTTTGCTGATTTGTTTTGTTGTATTTCCTGAGCAGAGTGCTGCTA    173

attB1_Part1      201 gagcgactgtaccaggaggtccaagtatagcttgcagtaccgcgaaagct    250
                     ||||||||||||||||||||||||||||||||||||||||||||||||||
attB1_part1_L    174 GAGCGACTGTACCAGGAGGTCCAAGTATAGCTTGCAGTACCGCGAAAGCT    223

attB1_Part1      251 gtagaatgggatgcaacttggtcaaagaatcttgatccgtcaggccgtgc    300
                     ||||||||||||||||||||||||||||||||||||||||||||||||||
attB1_part1_L    224 GTAGAATGGGATGCAACTTGGTCAAAGAATCTTGATCCGTCAGGCCGTGC    273

attB1_Part1      301 ggctcttggagttcatgttgcagcttatgaagaggataaagcagctgctg    350
                     ||||||||||||||||||||||||||||||||||||||||||||||||||
attB1_part1_L    274 GGCTCTTGGAGTTCATGTTGCAGCTTATGAAGAGGATAAAGCAGCTGCTG    323

attB1_Part1      351 ctgctaaggctggatcggatttagtagatcctcttcctaagaatggaaca    400
                     ||||||||||||||||||||||||||||||||||||||||||||||||||
attB1_part1_L    324 CTGCTAAGGCTGGATCGGATTTAGTAGATCCTCTTCCTAAGAATGGAACA    373

attB1_Part1      401 taagagaacaacactacaggcattgaggatataagcaaatgttttattct    450
                     ||||||||||||||||||||||||||||||||||||||||||||||||||
attB1_part1_L    374 TAAGAGAACAACACTACAGGCATTGAGGATATAAGCAAATGTTTTATTCT    423

attB1_Part1      451 tctacacagagagatcgttatcttctagagggatcaatgaataaaagctt    500
                     ||||||||||||||||||||||||||||||||||||||||||||||||||
attB1_part1_L    424 TCTACACAGAGAGATCGTTATCTTCTAGAGGGATCAATGAATAAAAGCTT    473

attB1_Part1      501 cgtccatttctagctggagattccatggatctccagttagtgcaagtgat    550
                     ||||||||||||||||||||||||||||||||||||||||||||||||||
attB1_part1_L    474 CGTCCATTTCTAGCTGGAGATTCCATGGATCTCCAGTTAGTGCAAGTGAT    523

attB1_Part1      551 acacgttgtctaca-----------------------------------    564
                     |||||||||||||
attB1_part1_L    524 ACACGTTGTCTACATTTGTACCTAAGTTTCTGCATTTTTTGTCGTTCTTT    573
```

Figure 7.10: Sequence alignment of the PCR product using the part attB1 forward primer and Part 1 reverse primer pairs. Sequencing product is labelled as 'attB1_Part1_L' whereas the *AtANN2* sequence from database is labelled as 'attB1_Part1' for reference. Alignment was done to confirm that the correct sequence of *AtANN2* construct was inserted into the destination vector impGWB604 during LR reaction. Pairwise Sequence Alignment tool provided by the EMBL-EBI (https://www.ebi.ac.uk/Tools/psa/) was used for the alignment. Expected PCR product from the primer pair was 664 bp.

```
part2              1 agtgcaagtgatacacgttgtctacatttgtacctaagtttctgcatttt     50
                                                                 ||||
part2_LR           1 -----------------------------------------------TTTT      4

part2             51 ttgtcgttcttttgtgttagacaagtcttggaccctagatgatacttcag    100
                     |||.||||||||||||||||||||||||||||||||||||||||||||||
part2_LR           5 TTGNCGTTCTTTTGTGTTAGACAAGTCTTGGACCCTAGATGATACTTCAG     54

part2            101 tttcttagacgttaaatttgatgaatccgaacttgtttgatttcaaagcc    150
                     |||||||...||||||||||||||||||||||||||||||||||||||||
part2_LR          55 TTTCTTNNNCGTTAAATTTGATGAATCCGAACTTGTTTGATTTCAAAGCC    104

part2            151 tggcctttctgcaatgtgtttttgtgcatgttctggcttgtttgttgtta    200
                     ||||||||||||||||||||||||||||||||||||||||||||||||||||
part2_LR         105 TGGCCTTTCTGCAATGTGTTTTTGTGCATGTTCTGGCTTGTTTGTTGTTA    154

part2            201 ctcaacgcaggatttgttataatatgtacaatatatctagtacacacata    250
                     ||||||||||||||||||||||||||||||||||||||||||||||||||||
part2_LR         155 CTCAACGCAGGATTTGTTATAATATGTACAATATATCTAGTACACACATA    204

part2            251 agtcaagcaagtaagactccgtggcccaatggataaggcgctggtctacg    300
                     ||||||||||||||||||||||||||||||||||||||||||||||||||||
part2_LR         205 AGTCAAGCAAGTAAGACTCCGTGGCCCAATGGATAAGGCGCTGGTCTACG    254

part2            301 aaaccagagattctgggttcgatccccagcggagtcgctcttcatctact    350
                     ||||||||||||||||||||||||||||||||||||||||||||||||||||
part2_LR         255 AAACCAGAGATTCTGGGTTCGATCCCCAGCGGAGTCGCTCTTCATCTACT    304

part2            351 atttttatttttcttacgcgcattgcttataaaagtttttttaatgaacgt    400
                     ||||||||||||||||||||||||||||||||||||||||||||||||||||
part2_LR         305 ATTTTTATTTTTCTTACGCGCATTGCTTATAAAAGTTTTTTAATGAACGT    354

part2            401 gggataaaagttttcagattcgtatttattatttcaaaaagacagatgac    450
                     ||||||||||||||||||||||||||||||||||||||||||||||||||||
part2_LR         355 GGGATAAAAGTTTTCAGATTCGTATTTATTATTTCAAAAAGACAGATGAC    404

part2            451 ctaacctcattactcgtgtatggacttttttttccttcaaattatatttt    500
                     ||||||||||||||||||||||||||||||||||||||||||||||||||||
part2_LR         405 CTAACCTCATTACTCGTGTATGGACTTTTTTTTCCTTCAAATTATATTTT    454

part2            501 atgaaatttgagtagacgaagtaactgctccccttcagatttagctaaag    550
                     ||||||||||||||||||||||||||||||||||||||||||||||||||||
part2_LR         455 ATGAAATTTGAGTAGACGAAGTAACTGCTCCCCTTCAGATTTAGCTAAAG    504

part2            551 agccaaccacgtgaagtc----------------------------------    568
                     ||||||||||||||||||
part2_LR         505 AGCCAACCACGTGAAGTCGTGAATCCTCTCTGTCGTTTTCGTATTAACAA    554
```

Figure 7.11: Sequence alignment of the PCR product using the Part 2 primer pairs. Sequencing product is labelled as 'part2_LR' whereas the *AtANN2* sequence from database is labelled as 'part2' for reference. Alignment was done to confirm that the correct sequence of *AtANN2* construct was inserted into the destination vector impGWB604 during LR reaction. Pairwise Sequence Alignment tool provided by the EMBL-EBI (https://www.ebi.ac.uk/Tools/psa/) was used for the alignment. Expected PCR product from the primer pair was 568 bp.

```
part3             1 gaatcctctctgtcgttttcgtattaacaaacataagaaattaagaaatg     50

part3_LR          1 --------------------------------------------------      0

part3            51 aaaatctcgttttcttatgtataattgttttatatcgatcaccggtttct    100
                        ||||||||||||||||||.||||||||||||||||||||||||||||
part3_LR          1 ----TCTCGTTTTCTTATGTATANTTGTTTTATATCGATCACCGGTTTCT     46

part3           101 ctaggtctaggtatagctgttccaatatcatgatttttaagtttagtttt    150
                     |||||.||..||||||||||||||||||||||||||||||||||||||||
part3_LR         47 CTAGGCCTTTGTATAGCTGTTCCAATATCATGATTTTTAAGTTTAGTTTT     96

part3           151 caacatcattaagtaaaagtgtgaactcattatcatcatcgctttccctt    200
                     ||||||||||||||||||||||||||||||||||||||||||||||||||||
part3_LR         97 CAACATCATTAAGTAAAAGTGTGAACTCATTATCATCATCGCTTTCCCTT    146

part3           201 tagaatttttgcaaacacacgaaaataaataaattgtttggacatattat    250
                     ||||||||||||||||||||||||||||||||||||||||||||||||||||
part3_LR        147 TAGAATTTTTGCAAACACACGAAAATAAATAAATTGTTTGGACATATTAT    196

part3           251 tgagaaacatagtcaaatgagcccgttcacattctgaatcatataagtta    300
                     ||||||||||||||||||||||||||||||||||||||||||||||||||||
part3_LR        197 TGAGAAACATAGTCAAATGAGCCCGTTCACATTCTGAATCATATAAGTTA    246

part3           301 cagtcccaaacccacgttttattaaaaatgtactactagtcaataattta    350
                     ||||||||||||||||||||||||||||||||||||||||||||||||||||
part3_LR        247 CAGTCCCAAACCCACGTTTTATTAAAAATGTACTACTAGTCAATAATTTA    296

part3           351 tgttgagtcatatttatttattttgacacagttggttttcgcagtttctt    400
                     ||||||||||||||||||||||||||||||||||||||||||||||||||||
part3_LR        297 TGTTGAGTCATATTTATTTATTTTGACACAGTTGGTTTTCGCAGTTTCTT    346

part3           401 gtttattagtttcaaattgcacttattagttttaaaaacaatttaatttg    450
                     ||||||||||||||||||||||||||||||||||||||||||||||||||||
part3_LR        347 GTTTATTAGTTTCAAATTGCACTTATTAGTTTTAAAAACAATTTAATTTG    396

part3           451 atatttggtataatatctcttttgaattatttacaaactttattacagcc    500
                     ||||||||||||||||||||||||||||||||||||||||||||||||||||
part3_LR        397 ATATTTGGTATAATATCTCTTTTGAATTATTTACAAACTTTATTACAGCC    446

part3           501 tggttttgaaaaaaaaaaaatactttgcataattgctactttgctaggat    550
                     ||||||||||||||||||||||||||||||||||||||||||||||||||||
part3_LR        447 TGGTTTTGAAAAAAAAAAAATACTTTGCATAATTGCTACTTTGCTAGGAT    496

part3           551 tactttataaacttttttcagctttgattcatttaacattaaacccaatta    600
                     ||||||||||||||||||||||||||||||||||||||||||||||||||||
part3_LR        497 TACTTTATAAACTTTTTCAGCTTTGATTCATTTAACATTAAACCCAATTA    546

part3           601 aaatattttattcattttagcataaaaggggaaaaaaaagaaatatatat    650
                     ||||||||||||||||||||||||||||||||||||||||||||||||||||
part3_LR        547 AAATATTTTATTCATTTTAGCATAAAAGGGGAAAAAAAAGAAATATATAT    596

part3           651 atatatatatatatatatttcctcttttcaattaaatcagctgttaaaag    700
                     ||||||||||||||||||||||||||||||||||||||||||||||||||||
part3_LR        597 ATATATATATATATATATTTCCTCTTTTCAATTAAATCAGCTGTTAAAAG    646

part3           701 tggaaaaaatcaaagagatatcaaaatattgattagaagaatatgtccat    750
                     ||||||||||||||||||||||||||||||||||||||||||||||||||||
part3_LR        647 TGGAAAAAATCAAAGAGATATCAAAATATTGATTAGAAGAATATGTCCAT    696

part3           751 attcaattatttttatattatctttattaaatgctttaccttacaacaata    800
                     ||||||||||||||||||||||||||||||||||||||||||||||||||||
part3_LR        697 ATTCAATTATTTTATATTATCTTTATTAAATGCTTTACCTTACAACAATA    746

part3           801 acttaaataaatttttgggattcccgttacattacttaag----------    840
                     |||||||||||||||||||||||||||||||||||||||||
part3_LR        747 ACTTAAATAAATTTTTGGGATTCCCGTTACATTACTTAAGTAGGACGACG    796
```

Figure 7.12: Sequence alignment of the PCR product using the Part 3 primer pairs. Sequencing product is labelled as 'part3_LR' whereas the *AtANN2* sequence from database is labelled as 'part3' for reference. Alignment was done to confirm that the correct sequence of *AtANN2* construct was inserted into the destination vector impGWB604 during LR reaction. Pairwise Sequence Alignment tool provided by the EMBL-EBI (https://www.ebi.ac.uk/Tools/psa/) was used for the alignment. Expected PCR product from the primer pair was 840 bp.

```
part4             1 gggattcccgttacattacttaagtaggacgacgtgcgtctgcttcgtct     50
                                                      |||||.|||||
part4_LR          1 ---------------------------------------CTGCTNCGTCT     11

part4            51 cattacaaagcagaagaaacacaaacagaggcagagatcttaagagttaa    100
                    |.|||| |||||||  .||||||||||||||||||||||||||||||||
part4_LR         12 CNTTAC-AAGCAGA--NAACACAAACAGAGGCAGAGATCTTAAGAGTTAA     58

part4           101 agactaatcccaacaatggcgtctctcaaagtcccaagcaatgttcctct    150
                    |||||......|||||||||||||||||||||||||||||||||||||||
part4_LR         59 AGACTNNNNTTAACAATGGCGTCTCTCAAAGTCCCAAGCAATGTTCCTCT    108

part4           151 tcccgaagatgacgccgagcaactccacaaggctttttcaggtctctctc    200
                    ||||||||||||||||||||||||||||||||||||||||||||||||||
part4_LR        109 TCCCGAAGATGACGCCGAGCAACTCCACAAGGCTTTTTCAGGTCTCTCTC    158

part4           201 ttttttttttcatcacttgatcgggatttagtttcttcttatacgatctct    250
                    ||||||||||||||||||||||||||||||||||||||||||||||||||
part4_LR        159 TTTTTTTTTCATCACTTGATCGGGATTTAGTTTCTTCTTATACGATCTCT    208

part4           251 aatctgtaatcggtttcgttaatcacaagattaatcatttttgatatctt    300
                    ||||||||||||||||||||||||||||||||||||||||||||||||||
part4_LR        209 AATCTGTAATCGGTTTCGTTAATCACAAGATTAATCATTTTTGATATCTT    258

part4           301 aagtactctcctatactcatcgttgagtattatttagtttgttgatttaa    350
                    ||||||||||||||||||||||||||||||||||||||||||||||||||
part4_LR        259 AAGTACTCTCCTATACTCATCGTTGAGTATTATTTAGTTTGTTGATTTAA    308

part4           351 tcacaactacattggtgattcgggatttactcttgtttgacctgatctgt    400
                    ||||||||||||||||||||||||||||||||||||||||||||||||||
part4_LR        309 TCACAACTACATTGGTGATTCGGGATTTACTCTTGTTTGACCTGATCTGT    358

part4           401 gttctgtgtcccaccacaagatcaggatcatgtcttcttatattagatac    450
                    ||||||||||||||||||||||||||||||||||||||||||||||||||
part4_LR        359 GTTCTGTGTCCCACCACAAGATCAGGATCATGTCTTCTTATATTAGATAC    408

part4           451 agtccgatgatgtcctaattgattgattataatgaaaatatgtttctttt    500
                    ||||||||||||||||||||||||||||||||||||||||||||||||||
part4_LR        409 AGTCCGATGATGTCCTAATTGATTGATTATAATGAAAATATGTTTCTTTT    458

part4           501 tgttctttagtgaaccaagattatgcttgttttgtgttctccttgggaga    550
                    ||||||||||||||||||||||||||||||||||||||||||||||||||
part4_LR        459 TGTTCTTTAGTGAACCAAGATTATGCTTGTTTTGTGTTCTCCTTGGGAGA    508

part4           551 tttgtgacatgacaaaatgtttgttttttgggtttggtctgaaacaggat    600
                    ||||||||||||||||||||||||||||||||||||||||||||||||||
part4_LR        509 TTTGTGACATGACAAAATGTTTGTTTTTTGGGTTTGGTCTGAAACAGGAT    558

part4           601 ggg-----------------------------------------------    603
                    |||
part4_LR        559 GGGGTACCAACGAGAAGCTGATCATATCAATACTAGCTCACAGGAACGCA    608
```

Figure 7.13: Sequence alignment of the PCR product using the Part 4 primer pairs. Sequencing product is labelled as 'part4_LR' whereas the *AtANN2* sequence from database is labelled as 'part4' for reference. Alignment was done to confirm that the correct sequence of *AtANN2* construct was inserted into the destination vector impGWB604 during LR reaction. Pairwise Sequence Alignment tool provided by the EMBL-EBI (https://www.ebi.ac.uk/Tools/psa/) was used for the alignment. Expected PCR product from the primer pair was 603 bp.

```
part5             1 gtttggtctgaaacaggatggggtaccaacgagaagctgatcatatcaat     50
                                                                 |
part5_LR          1 -------------------------------------------------T      1

part5            51 actagctcacaggaacgcagcacaacgcagcttgatccgcagcgtttatg    100
                    ||||||||||||||||||||||||||||||||||||||||||||||||||||
part5_LR          2 ACTAGCTCACAGGAACGCAGCACAACGCAGCTTGATCCGCAGCGTTTATG     51

part5           101 cagctacctacaatgaggatcttctcaaagcattagacaaagagctttct    150
                    ||||||.....||||||||||||||||||||||||||||||||||||||||||
part5_LR         52 CAGCTANNNNNAATGAGGATCTTCTCAAAGCATTAGACAAAGAGCTTTCT    101

part5           151 agcgactttgaggtatttttaactcttttctttctttctttctttttgggg    200
                    ..||||||||||||||||||||||||||||||||||||||||||||||||||
part5_LR        102 NTCGACTTTGAGGTATTTTTAACTCTTTTCTTTCTTTCTTTCTTTTGGGG    151

part5           201 gtctctgaaatgatatagtgactgatttaggattgtgaaactgttgtatt    250
                    ||||||||||||||||||||||||||||||||||||||||||||||||||||
part5_LR        152 GTCTCTGAAATGATATAGTGACTGATTTAGGATTGTGAAACTGTTGTATT    201

part5           251 tggtgtttttttgtaacagagagctgtgatgttgtggactcttgatccac    300
                    ||||||||||||||||||||||||||||||||||||||||||||||||||||
part5_LR        202 TGGTGTTTTTTTGTAACAGAGAGCTGTGATGTTGTGGACTCTTGATCCAC    251

part5           301 cagagagagatgcttatttggctaaagaatccaccaagatgttcaccaag    350
                    ||||||||||||||||||||||||||||||||||||||||||||||||||||
part5_LR        252 CAGAGAGAGATGCTTATTTGGCTAAAGAATCCACCAAGATGTTCACCAAG    301

part5           351 aacaattgggttcttgttgaaatcgcttgcacaaggcctgctcttgagct    400
                    ||||||||||||||||||||||||||||||||||||||||||||||||||||
part5_LR        302 AACAATTGGGTTCTTGTTGAAATCGCTTGCACAAGGCCTGCTCTTGAGCT    351

part5           401 tatcaaggtcaagcaagcttaccaagctcgatacaagaaatcaatcgagg    450
                    ||||||||||||||||||||||||||||||||||||||||||||||||||||
part5_LR        352 TATCAAGGTCAAGCAAGCTTACCAAGCTCGATACAAGAAATCAATCGAGG    401

part5           451 aagatgtcgcgcaacacacatctggtgaccttcgtaaggtaatcattcaa    500
                    ||||||||||||||||||||||||||||||||||||||||||||||||||||
part5_LR        402 AAGATGTCGCGCAACACACATCTGGTGACCTTCGTAAGGTAATCATTCAA    451

part5           501 taaaccaaatcttgcttgtttgttttgtatttgggacacatgtttctgac    550
                    ||||||||||||||||||||||||||||||||||||||||||||||||||||
part5_LR        452 TAAACCAAATCTTGCTTGTTTGTTTTGTATTTGGGACACATGTTTCTGAC    501

part5           551 a----------------------------------------------------    551
                    |
part5_LR        502 ATATTTGTGTGTCCTCTTTTGTATAGCTCTTGCTTCCTCTTGTGAGCACT    551
```

Figure 7.14: Sequence alignment of the PCR product using the Part 5 primer pairs. Sequencing product is labelled as 'part5_LR' whereas the *AtANN2* sequence from database is labelled as 'part5' for reference. Alignment was done to confirm that the correct sequence of *AtANN2* construct was inserted into the destination vector impGWB604 during LR reaction. Pairwise Sequence Alignment tool provided by the EMBL-EBI (https://www.ebi.ac.uk/Tools/psa/) was used for the alignment. Expected PCR product from the primer pair was 557 bp.

```
part6             1 gtatttgggacacatgtttctgacatatttgtgtgtcctcttttgtatag     50
                                                                  |
part6_LR          1 -------------------------------------------------G      1

part6            51 ctcttgcttcctcttgtgagcactttcaggtatgaaggagatgatgtgaa    100
                    ||||||||||||||||||||||||||||||||||||||||||||||||||||
part6_LR          2 CTCTTGCTTCCTCTTGTGAGCACTTTCAGGTATGAAGGAGATGATGTGAA     51

part6           101 catgatgcttgcaagatctgaagctaagatacttcacgagaaggtctcag    150
                    |||.......||||||||||||||||||||||||||||||||||||||..
part6_LR         52 CATNNNNNNNGCAAGATCTGAAGCTAAGATACTTCACGAGAAGGTCTCNN    101

part6           151 agaaatcttacagtgacgatgacttcatcagaatcttgacaacaagaagc    200
                    .||||||||||||||||||||||||||||||||||||||||||||||||||||
part6_LR        102 NGAAATCTTACAGTGACGATGACTTCATCAGAATCTTGACAACAAGAAGC    151

part6           201 aaagcacagctcggtgcaacactcaaccactacaacaacgagtatggaaa    250
                    ||||||||||||||||||||||||||||||||||||||||||||||||||||
part6_LR        152 AAAGCACAGCTCGGTGCAACACTCAACCACTACAACAACGAGTATGGAAA    201

part6           251 cgccattaacaaggttagcttaaccaccaactgctttttcatttgatgtt    300
                    ||||||||||||||||||||||||||||||||||||||||||||||||||||
part6_LR        202 CGCCATTAACAAGGTTAGCTTAACCACCAACTGCTTTTTCATTTGATGTT    251

part6           301 acaaaatcttgttcggaaagcttattatatgaagtgaaatttttgcagaa    350
                    ||||||||||||||||||||||||||||||||||||||||||||||||||||
part6_LR        252 ACAAAATCTTGTTCGGAAAGCTTATTATATGAAGTGAAATTTTTGCAGAA    301

part6           351 cttgaaggaagagtcggacgacaatgactacatgaaactactaagagctg    400
                    ||||||||||||||||||||||||||||||||||||||||||||||||||||
part6_LR        302 CTTGAAGGAAGAGTCGGACGACAATGACTACATGAAACTACTAAGAGCTG    351

part6           401 taatcacatgtttgacataccctgagaagcattttgagaaggttcttcgt    450
                    ||||||||||||||||||||||||||||||||||||||||||||||||||||
part6_LR        352 TAATCACATGTTTGACATACCCTGAGAAGCATTTTGAGAAGGTTCTTCGT    401

part6           451 ctatcaatcaacaaaatgggaacagacgaatggggactaacccgagtcgt    500
                    ||||||||||||||||||||||||||||||||||||||||||||||||||||
part6_LR        402 CTATCAATCAACAAAATGGGAACAGACGAATGGGGACTAACCCGAGTCGT    451

part6           501 gactacacgaactgaagttgacatggaacgcatcaaagaggaatatcagc    550
                    ||||||||||||||||||||||||||||||||||||||||||||||||||||
part6_LR        452 GACTACACGAACTGAAGTTGACATGGAACGCATCAAAGAGGAATATCAGC    501

part6           551 gaagaaacagcattccttggaccgtgctatcgccaaagacacttctggt    600
                    ||||||||||||||||||||||||||||||||||||||||||||||||||||
part6_LR        502 GAAGAAACAGCATTCCTTTGGACCGTGCTATCGCCAAAGACACTTCTGGT    551

part6           601 gactatgaggacatgcttgttgctcttctcggacatggcgatgcttgaaa    650
                    ||||||||||||||||||||||||||||||||||||||||||||||||||||
part6_LR        552 GACTATGAGGACATGCTTGTTGCTCTTCTCGGACATGGCGATGCTTGAAA    601

part6           651 ct----------------------------------------------    652
                    ||
part6_LR        602 CTACCCAGCTTTCTTGTACAAAGTGGTGATCATGGTGAGCAAGGGCGAGG    651
```

Figure 7.15: Sequence alignment of the PCR product using the Part 6 primer pairs. Sequencing product is labelled as 'part6_LR' whereas the *AtANN2* sequence from database is labelled as 'part6' for reference. Alignment was done to confirm that the correct sequence of *AtANN2* construct was inserted into the destination vector impGWB604 during LR reaction. Pairwise Sequence Alignment tool provided by the EMBL-EBI (https://www.ebi.ac.uk/Tools/psa/) was used for the alignment. Expected PCR product from the primer pair was 646 bp.

Appendix VI

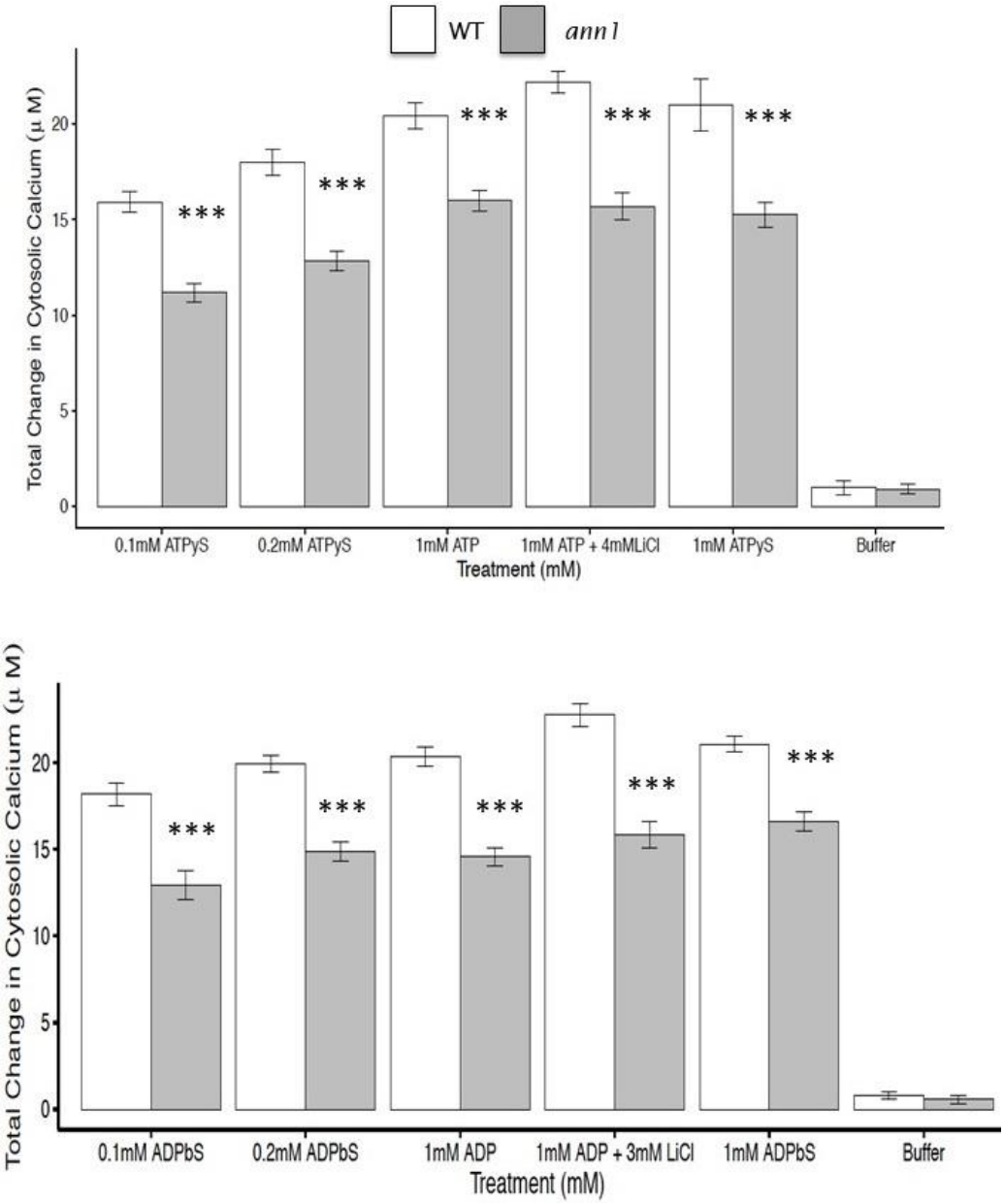

Figure 7.16: Total $[Ca^{2+}]_{cyt}$ accumulation by Col-0 and *Atann1* under different concentrations of ATPɣS and ADPβS. Both Col-0 and *Atann1* were tested with 0.1 mM, 0.2 mM and 1 mM concentration of ATPɣS and ADPβS. The total $[Ca^{2+}]_{cyt}$ accumulation increases as the concentration of agonist increases. The buffer was the control solution treatment (2 mM Bis-Tris Propane; 10 mM $CaCl_2$; 0. 1mM KCl, pH 5.8) whereas the 4 mM LiCl (for ATPɣS) and 3 mM LiCl treatment (for ADPβS) acted as a control to test for the effect of Li^+ contained in the non-hydrolysable analogues.